TRANSPORTATION RESEARCH

RECORD

No. 1290

Volume 1

Bridges and Structures

Third Bridge Engineering Conference

Papers presented at the Third Bridge Engineering Conference March 10–13, 1991 Denver, Colorado

A peer-reviewed publication of the Transportation Research Board

TRANSPORTATION RESEARCH BOARD
NATIONAL RESEARCH COUNCIL
WASHINGTON, D.C. 1991

Transportation Research Record 1290
Price: $70.00

Subscriber Category
IIC bridges and structures

TRB Publications Staff
Director of Publications: Nancy A. Ackerman
Senior Editor: Naomi C. Kassabian
Associate Editor: Alison G. Tobias
Assistant Editors: Luanne Crayton, Kathleen Solomon, Norman Solomon
Graphics Coordinator: Diane L. Ross
Production Coordinator: Karen S. Waugh
Office Manager: Phyllis D. Barber
Production Assistant: Betty L. Hawkins

Printed in the United States of America

Library of Congress Cataloging-in-Publication Data
National Research Council. Transportation Research Board.

Third Bridge Engineering Conference
Papers presented at the Third Bridge Engineering Conference, March 10-13, 1991, Denver, Colorado.
p. cm.--(Transportation research record ISSN 0361-1981 ; no. 1290)
ISBN 0-309-05067-7
1. Bridges—Congresses. I. National Research Council (U.S.). Transportation Research Board. II. Title. III. Series: Transportation research record ; 1290.
TE7.H5 no. 1290
[TG5]
388 s—dc20
[624'.2]
90-28843
CIP

Sponsorship of Transportation Research Record

GROUP 2—DESIGN AND CONSTRUCTION OF TRANSPORTATION FACILITIES
Chairman: Raymond A. Forsyth, Sacramento, California

General Design Section
Chairman: Jarvis D. Michie, Dynatech Engineering Inc.

Committee on Hydrology, Hydraulics and Water Quality
Chairman: J. Sterling Jones, Federal Highway Administration
Secretary: Lawrence J. Harrison, Federal Highway Administration
Dennis Athayde, Charles W. Boning, Stanley R. Davis, David J. Flavell, Thomas L. Hart, John Owen Hurd, S. Bennett P. John, Kenneth D. Kerri, M. Dean Knighton, Floyd J. Laumann, Norman Miller, Johnny L. Morris, Jerome M. Normann, Glenn A. Pickering, Don L. Potter, Jean Reichert, Everett V. Richardson, H. Earl Shaver, Corwin L. Tracy, E. L. Walker, Jr., Ken Young, Michael E. Zeller

Structures Section
Chairman: Robert C. Cassano, Imbsen & Associates Inc.

Committee on General Structures
Chairman: John J. Ahlskog, Federal Highway Administration
Dan S. Bechly, Neal H. Bettigole, Amar Bhajandas, Charles H. Bryant, Edwin G. Burdette, Martin P. Burke, Jr., Paul F. Csagoly, Donald J. Flemming, Theodore V. Galambos, Frederick Gottemoeller, Richard P. Knight, Andrew Lally, Clellon Lewis Loveall, Dennis R. Mertz, Roy L. Mion, Andrzej S. Nowak, Richard V. Nutt, Andrew E. N. Osborn, William J. Rogers, Arunprakash M. Shirole, Michael S. Stenko, Stanley W. Woods

Committee on Steel Bridges
Chairman: Charles W. Roeder, University of Washington
John J. Ahlskog, David R. Anderson, Charles J. Arnold, Alfred G. Bishara, William G. Byers, William F. Crozier, Donald J. Flemming, Dan M. Frangopol, Geerhard Haaiger, Ray W. James, Theodore H. Karasopoulos, Michael J. Koob, Andrew Lally, Albert D. M. Lewis, Ayaz H. Malik, Richard A. Parmelee, Charles G. Schmidt, Charles Seim, Robert A. P. Sweeney, John A. Van Lund, Ivan M. Viest, Gerald M. White, Stanley W. Woods

Committee on Concrete Bridges
Chairman: Wayne Henneberger, Figg & Muller Engineers Inc.
J. C. Beauchamp, Robert N. Bruce, Jr., George A. Christian, John H. Clark, Anthony Ralph Cusens, C. Stewart Gloyd, H. Henrie Henson, James J. Hill, Roy A. Imbsen, John M. Kulicki, Charles M. Minervino, Mrutyunjaya Pani, Richard A. Parmelee, Philip C. Perdikaris, Walter Podolny, Jr., Henry G. Russell, Alex C. Scordelis, S. Srinivasan, John F. Stanton, Holger S. Svensson, Robert A. P. Sweeney, Man-Chung Tang, Julius F. J. Volgyi, Jr., Allan H. Walley

Committee on Dynamics and Field Testing of Bridges
Chairman: David B. Beal, New York State Department of Transportation
Secretary: Harold R. Bosch, Federal Highway Administration
Baidar Bakht, James W. Baldwin, Jr., Ian G. Buckle, C. B. Crouse, Bruce M. Douglas, Thomas E. Fenske, Dan M. Frangopol, Hota V. S. Gangarao, David William Goodpasture, Ramankutty Kannankutty, F. Wayne Klaiber, Michael J. Koob, Albert N. Lin, Fred Moses, Andrzej S. Nowak, Suresh G. Pinjarkar, Kwok-Nam Shiu, Robert A. P. Sweeney, Ivan M. Viest, Robert C. Y. Young

Committee on Culverts and Hydraulic Structures
Chairman: A. P. Moser, Utah State University
Gordon A. Alison, James D. Arnoult, A. E. Bacher, Kenneth J. Boedecker, Jr., Thomas K. Breitfuss, Dennis L. Bunke, Bernard E. Butler, James E. Cowgill, William D. Drake, J. Michael Duncan, James B. Goddard, James J. Hill, Jey K. Jeyapalan, Iraj I. Kaspar, Michael G. Katona, Timothy J. McGrath, John C. Potterk Russell B. Preuit, Jr., Harold R. Sandberg, James C. Schluter, David C. Thomas, Corwin L. Tracy, Robert P. Walker, Jr.

Task Force on Structural Applications of Fiber Reinforced Plastic
Chairman: Craig A. Ballinger, Wilbur Smith Associates
Robert J. Bailey, Andrew L. Bastone, Albert F. Dorris, Hota V. S. Gangarao, Andrew Green, Frank J. Heger, Srinivasa L. Iyer, Fred C. McCormick, Urs Meier, J. M. Plecnik, Winston Renoud, Ferdinand S. Rostasy, Alvin Smith, Wayne W. Stinchcomb, Jerry Stone, Alan Webb, Kenneth H. Wechsler, Dick J. Wilkins, Charles H. Wilson

Construction Section
Chairman: Charles T. Edson, New Jersey DOT

Committee on Construction of Bridges and Structures
Chairman: Robert M. Barnoff, R. M. Barnoff & Associates Inc.
Ernest V. Acree, Jr., Ostap Bender, Neal H. Bettigole, D. Stephen Brown, Bruce M. Douglas, Jackson L. Durkee, Allan C. Harwood, James R. Hoblitzell, Ramankutty Kannankutty, Jai B. Kim, Thomas P. McCarthy, William T. Peckham, Charles H. Quandel, John P. Rutter, Charles V. Slavis, Michael S. Stenko, Francis E. Ward, James R. Wilder, Kenneth C. Wilson, Luis Ybanez

Soil Mechanics Section
Chairman: Michael G. Katona, Air Force Engineering and Services

Committee on Foundations of Bridges and Other Structures
Chairman: Richard S. Cheney, Federal Highway Administration
Secretary: Richard P. Long, University of Connecticut
Gregg Batchelder Adams, Roy H. Borden, Jean-Louis Briaud, Joseph A. Caliendo, Ronald G. Chassie, Murty S. Devata, Albert F. Dimillio, Victor Elias, Richard L. Engel, George G. Goble, Robert C. Houghton, Alan P. Kilian, John F. Ledbetter, Jr., Larry Lockett, James H. Long, Randolph W. Losch, Thomas Neff, Peter J. Nicholson, Gary M. Norris, Michael Wayne O'Neill, John L. Walkinshaw, Gdalyah Wiseman, James L. Withiam

Planning Committee for the Third Bridge Engineering Conference
Chairman: Robert C. Cassano, Imbsen & Associates Inc.
Robert M. Barnoff, David B. Beal, John M. Hanson, Wayne Henneberger, J. Sterling Jones, Robert N. Kamp, John M. Kulicki, Albert D. M. Lewis, Clellon Lewis Loveall, Fred Moses, John P. Rutter, Charles F. Scheffey, A. J. Siccardi, Robert A. P. Sweeney, Robert L. Nickerson

George W. Ring III, Transportation Research Board staff
The organizational units, officers, and members are as of December 31, 1990.

Transportation Research Record 1290

Contents—Volume 1

Contents — Volume 2

Foreword

The most recent national bridge inventory of deficient bridges conducted by the Federal Highway Administration (FHWA), U.S. Department of Transportation, indicates that an alarming number of the nation's bridges are classified as structurally deficient or functionally obsolete. Forty-two percent of the 575,607 bridges in the national system are so classified. Twenty-eight percent of the 271,300 bridges in the federal-aid highway system fall in the same category.

The problem is widely recognized, and increasing federal, state, and operating agency appropriations are being made available for bridge research, design, maintenance, and rehabilitation. The Transportation Research Board addressed this problem at the First Bridge Engineering Conference, held in St. Louis, Missouri, September 1978, and again at the Second Bridge Engineering Conference, held in Minneapolis, Minnesota, September 1984. Proceedings of these conferences were published in *Transportation Research Records 664*, *665*, and *950*, Volumes 1 and 2. This Record contains the papers prepared for the Third Bridge Engineering Conference, to be held in Denver, Colorado, March 10–13, 1991.

The papers in this Record highlight research and practice resulting from bridge studies performed by the National Cooperative Highway Research Program and sponsored by the American Association of State Highway and Transportation Officials as well as from federal, state, and other research agency programs. Areas addressed include safety and vulnerability of bridge structures; bridge maintenance; repair and rehabilitation; bridge inspection, testing, and evaluation; concrete and steel bridge design; segmental and cable-stayed bridges; seismic design and retrofit; bridge management; and scour prediction and countermeasures. The conference program includes working sessions on bridge specifications for the future. The proceedings of these sessions are not published in this Record because of space limitations.

Organization and direction of the conference were the responsibilities of the Planning Committee listed on the reverse side of the title page. Committees listed on the same page conducted technical reviews of the papers.

FHWA partially funded the Bridge Conference. The following organizations cooperated to make the conference possible:

COSPONSOR

Federal Highway Administration

COOPERATING AGENCIES

American Road and Transportation Builders Assoc.
Colorado Department of Highways
International Road Federation

Pedro Albrecht
Department of Civil Engineering
University of Maryland
College Park, Md. 20742

John H. Allen
Allen Research and Development Inc.
3300 Arapahoe Ave.
Suite 221
Boulder, Colo. 80303

T. T. Baber
Department of Civil Engineering
University of Virginia
Charlottesville, Va. 22903

Furman W. Barton
Department of Civil Engineering
University of Virginia
Charlottesville, Va. 22903

Fred R. Beckmann
American Institute of Steel Construction, Inc.
Suite 3100
One East Wacker Drive
Chicago, Ill. 60601

Chad Clancy
College of Engineering
University of Wyoming
Laramie, Wyo. 20418

D. N. Corda
Greiner, Inc.
2219 York Road
Timonium, Md. 21093

J. Hartley Daniels
Department of Civil Engineering
Fritz Engineering Laboratory
Lehigh University
Bethlehem, Pa. 18015

Charles W. Dolan
Department of Civil Engineering
University of Delaware
137 DuPont Hall
Newark, Del. 19716

P. S. Duemmel
Department of Civil Engineering
University of Virginia
Charlottesville, Va. 22903

John W. Fisher
Center for Advanced Technology For Large Structural Systems
117 ATLSS Drive, H Building
Lehigh University
Bethlehem, Pa. 18015

Dan M. Frangopol
Department of Civil, Environmental, and Architectural Engineering
University of Colorado at Boulder
Boulder, Colo. 80309

Gongkang Fu
New York State
Department of Transportation
Building 5, State Office Campus
Albany, N.Y. 12232

Verne A. Geidl
Department of Civil Engineering
University of Idaho
Moscow, Idaho 83843

John M. Hanson
Wiss, Janney, Elstner Associates, Inc.
330 Pfingsten Road
Northbrook, Ill. 60062

Robert C. Holt
New York State
Department of Transportation
1220 Washington Ave.
State Office Campus Building 5
Albany, N.Y. 12232

Young-Kyun Hong
Department of Civil Engineering
University of Michigan
Ann Arbor, Mich. 48109

Frank W. Huber
Edwards and Kelcey Engineers, Inc.
53 Park Place, Room 1200
New York, N.Y. 10007

Eui-Seung Hwang
Department of Civil Engineering
University of Michigan
2340 GG Brown Building
North Campus
Ann Arbor, Mich. 48109

Rola L. Idriss
New Mexico State University
Department of Civil, Agricultural, and Geological Engineering
Box 30001
Las Cruces, N.Mex. 88003

Roy A. Imbsen
Imbsen & Associates, Inc.
9833 Horn Road, Suite C
Sacramento, Calif. 95827

Michael J. Koob
Wiss, Janney, Elstner Associates, Inc.
330 Pfingsten Road
Northbrook, Ill. 60062

Kosalram Krishnan
Department of Applied Mechanics and Engineering Science
University of California, San Diego
LaJolla, Calif. 92093

R. W. Kritzler
Raths, Raths & Johnson, Inc.
835 Midway Drive
Willowbrook, Ill.

P. O. McCarthy
H. W. Lochner, Inc.
20 N. Wacker Dr.
Chicago, Ill. 60606

Laurie G. McGinnis
Howard Needles Tammen & Bergendoff
6700 France Ave.
Minneapolis, Minn. 55435

W. T. McKeel, Jr.
Virginia Transportation Research Council
Box 3817 University Station
Charlottesville, Va. 22903

Shashi Moorty
Department of Civil Engineering
University of Washington
Seattle, Wash. 98195

Fred Moses
Department of Civil Engineering
Case Western Reserve University
Cleveland, Ohio 44106

Rachid Nakib
Department of Civil and Environmental Engineering
Washington State University
Pullman, Wash. 99164

Ahmad H. Namini
Department of Civil and Architectural Engineering
University of Miami
Coral Gables, Fla. 33124

Andrzej S. Nowak
Department of Civil Engineering
University of Michigan
2340 GG Brown Building
North Campus
Ann Arbor, Mich. 48109

Oscar A. Oliden
Parsons Brinckerhoff Quade & Douglas
1501 W. Fountainhead Parkway
Suite 400
Tempe, Ariz. 85282

Timothy A. Osterkamp
Imbsen & Associates, Inc.
9833 Horn Road, Suite C
Sacramento, Calif. 95827

R. B. Peel
Greiner, Inc.
2219 York Road
Timonium, Md. 21093

Philip Perdikaris
Department of Civil Engineering
Case Western Reserve University
Cleveland, Ohio 44106

Michael Petrou
Department of Civil Engineering
Case Western Reserve University
Cleveland, Ohio 44106

S. G. Pinjarkar
Raths, Raths & Johnson, Inc.
835 Midway Drive
Willowbrook, Ill. 60521

Dale E. Poorman
Burgess & Niple, Limited
5085 Reed Road
Columbus, Ohio 43220

David Pope
Wyoming State Highway Department
P.O. Box 1708
Cheyenne, Wyo. 82002

M. J. Nigel Priestley
Department of Applied Mechanics and Engineering Sciences
University of California, San Diego
LaJolla, Calif. 92093

J. A. Puckett
Department of Civil Engineering
University of Wyoming
Laramie, Wyo. 82071

Ronald L. Purvis
Wilbur Smith Associates
2921 Telestar Court
Falls Church, Va. 22042

Seetha V. Ramaiah
Parsons Brinckerhoff Quade & Douglas
1501 W. Fountainhead Parkway
Suite 400
Tempe, Ariz. 85282

Stephen J. Ressler
Department of Civil Engineering
Fritz Engineering Laboratory
Lehigh University
Bethlehem, Pa. 18015

E. V. Richardson
Resource Consultants Inc.
402 West Mountain Ave.
P.O. Box Q
Ft. Collins, Colo. 80522

Charles W. Roeder
Department of Civil Engineering
University of Washington
233-More Hall FX-10
Seattle, Wash. 98195

R. A. Rolsing
McDonough Associates, Inc.
224 S. Michigan Ave.
Chicago, Ill. 60604

Frieder Seible
Department of Applied Mechanics and Engineering Science
University of California, San Diego
LaJolla, Calif. 92093

N. Ali Seyedmadani
Parsons Brinckerhoff Quade & Douglas
1501 W. Fountainhead Parkway
Suite 400
Tempe, Ariz. 85285

Arunprakash M. Shirole
New York State
Department of Transportation
1220 Washington Ave.
Building 5, State Office Campus
Albany, N.Y. 12232

Peter Sluszka
Steinman Boynton Gronquist & Birdsall
110 William Street
New York, N.Y. 10038

Michael M. Sprinkel
Virginia Transportation Research Council
Box 3817 University Station
Charlottesville, Va. 22903

Thomas W. Stelmack
Figg Engineers, Inc.
Western Regional Office
4601 DTC Blvd., Suite 680
Denver, Colo. 80237

Ralph J. Trapani
Colorado Department of Highways
Glenwood Canyon Project
P.O. Box 1430
201 Centennial St.
Glenwood Springs, Colo. 81602

A. M. Vaysburd
Greiner, Inc.
2219 York Road
Timonium, Md. 21093

Krishna K. Verma
U.S. Department of Transportation
Federal Highway Administration
HNG-32 400 7th St. S.W., Room 3117
Washington, D.C. 20590

Dayi Wang
Center for Advanced Technology For Large Structural Systems
117 ATLSS Drive, H Building
Lehigh University
Bethlehem, Pa. 18015

Kenneth R. White
Department of Civil, Agricultural, and Geological Engineering
Box 30001
New Mexico State University
Las Cruces, N. Mex. 88003

William J. Wright
U.S. Department of Transportation
Federal Highway Administration
Turner-Fairbank Highway Research Center
6300 Georgetown Pike
McLean, Va. 22101

Ben T. Yen
Center for Advanced Technology For Large Structural Systems
117 ATLSS Drive, H Building
Lehigh University
Bethlehem, Pa. 18015

Toorak Zokaie
Imbsen & Associates, Inc.
9833 Horn Road, Suite C
Sacramento, Calif. 95827

Jack L. Abcarius
California Department of Transportation
1120 N Street
P.O. Box 942874
Sacramento, Calif. 94274

L. Abed
Resource Consultants Inc.
402 West Mountain Ave.
P.O. Box Q
Ft. Collins, Colo. 80522

S. G. Arzoumanidis
Steinman Boynton Gronquist & Birdsall
110 William St.
New York, N.Y. 10038

J. B. Atkins
United States Geological Survey
520 19th Ave.
Tuscaloosa, Ala. 35401

Jerry E. Bennett
Transportation Corridor Agencies
345 Clinton St.
Costa Mesa, Calif. 92626

Roger Bligh
Civil Engineering Department and Texas Transportation Institute
Texas A&M University
College Station, Tex. 77843

Ian G. Buckle
Department of Civil Engineering
State University of New York at Buffalo
105 Red Jacket Quadrangle
Buffalo, N.Y. 14261

R. G. Burg
Construction Technology Laboratories, Inc.
5420 Old Orchard Road
Skokie, Ill. 60077

Y. H. Chai
Department of Applied Mechanics and Engineering Sciences
University of California, San Diego
LaJolla, Calif. 92093

York-Kay Chan
DRC Consultants, Inc.
34–36 Union Street
New York, N.Y. 11354

John A. Corven
Figg Engineering Group
424 North Calhoun
Tallahassee, Fla. 32301

Salem S. Faza
Constructed Facilities Center
West Virginia University
Morgantown, W.Va. 26506

David C. Froehlich
Department of Civil Engineering
University of Kentucky
212 Anderson Hall
Lexington, Ky. 40506

Hota V. S. GangaRao
Constructed Facilities Center
West Virginia University
Morgantown, W.Va. 26506

Alberto Garcia-Diaz
Industrial Engineering Department
Texas A&M University
College Station, Tex. 77843

Michel Ghosn
Department of Civil Engineering
The City College of the City University of New York
New York, N.Y. 10031

Stewart Gloyd
Corridor Design Management Group
345 Clinton St.
Costa Mesa, Calif. 92626

Lawrence J. Harrison
U.S. Department of Transportation
Federal Highway Administration
400 7th Street, S.W.
Washington, D.C. 20590

J. J. Hill
New York State
Department of Transportation
Building 5, State Office Campus
Albany, N.Y. 12232

Roy A. Imbsen
Imbsen & Associates, Inc.
9833 Horn Road, Suite C
Sacramento, Calif. 95827

Ray W. James
Civil Engineering Department and Texas Transportation Institute
Texas A&M University
College Station, Tex. 77843

M. E. Jennings
United States Geological Survey
8011 Cameron Road, Building 1
Austin, Tex. 78757

J. S. Jones
U.S. Department of Transportation
Federal Highway Administration
Turner-Fairbank Highway Research Center
6300 Georgetown Pike
McLean, Va. 22101

W. H. Kirby
United States Geological Survey
WGS Mail Stop 415
Reston, Va. 22092

Ivan Kuzyk
Connecticut Department of Transportation
P.O. Box Drawer A
24 Wolcott Hill Rd.
Wethersfield, Conn. 06109

P. F. Lagasse
Resource Consultants Inc.
402 West Mountain Ave.
P.O. Box Q
Ft. Collins, Colo. 80522

Ignatius Po Lam
Earth Mechanics, Inc.
8840 Warner Avenue, Suite 204-E
Fountain Valley, Calif. 92708

Mark Landers
United States Geological Survey
Water Resources Division MS 415
12201 Sunrise Valley Drive
Reston, Va. 22092

Philip J. Lang
DRC Consultants, Inc.
34–36 Union Street
New York, N.Y. 11354

Robert G. Lauzon
Connecticut Department of Transportation
P.O. Box Drawer A
24 Wolcott Hill Rd.
Wethersfield, Conn. 06109

Jon Lea
Imbsen & Associates, Inc.
9833 Horn Road, Suite C
Sacramento, Calif. 95827

Thomas G. Lovett
Greiner Inc.
7650 W. Courtney Campbell Causeway
Tampa, Fla. 33607

Geoffrey R. Martin
Department of Civil Engineering
University of Southern California
Los Angeles, Calif. 90089

Ronald L. Mayes
Computech Engineering Services, Inc.
2855 Telegraph Ave., Suite 410
Berkeley, Calif. 94705

Donald W. Miller
U.S. Department of Transportation
Federal Highway Administration
Eastern Federal Lands Highway Division
21400 Ridgetop Circle
Sterling, Va. 22170

Fred Moses
Department of Civil Engineering
Case Western Reserve University
Cleveland, Ohio 44106

Farid S. Nobari
Imbsen & Associates, Inc.
9833 Horn Road, Suite C
Sacramento, Calif. 95827

C. F. Nordin
Resource Consultants, Inc.
402 West Mountain Ave.
P.O. Box Q
Ft. Collins, Colo. 80522

Nils D. Olsson
DRC Consultants, Inc.
34–36 Union Street
New York, N.Y. 11354

A. C. Parola, Jr.
Civil Engineering Department
University of Louisville
Louisville, Ky. 40292

M. J. Nigel Priestley
Department of Applied Mechanics and
Engineering Sciences
University of California, San Diego
LaJolla, Calif. 92093

E. V. Richardson
Resource Consultants Inc.
402 West Mountain Ave.
P.O. Box Q
Ft. Collins, Colo. 80522

J. R. Richardson
Resource Consultants Inc.
402 West Mountain Ave.
P.O. Box Q
Ft. Collins, Colo. 80522

James E. Roberts
California Department of Transportation
Division of Structures
P.O. Box 942874
Sacramento, Calif. 94274

Charles W. Roeder
Department of Civil Engineering
University of Washington
233-More Hall FX-10
Seattle, Wash. 98195

Walter C. Roehrs
Burgess & Niple, Limited
5085 Reed Road
Columbus, Ohio 43220

G. V. Sabol
Resource Consultants, Inc.
402 West Mountain Ave.
P.O. Box Q
Ft. Collins, Colo. 80522

James D. Schall
Resource Consultants, Inc.
402 West Mountain Ave.
P.O. Box Q
Ft. Collins, Colo. 80522

Robert A. Schamber
Imbsen & Associates, Inc.
9833 Horn Road, Suite C
Sacramento, Calif. 95827

J. Schmid
Steinman Boynton Gronquist & Birdsall
110 William Street
New York, N.Y. 10038

Frieder Seible
Department of Applied Mechanics and
Engineering Science
University of California, San Diego
LaJolla, Calif. 92093

Arunprakash M. Shirole
New York State
Department of Transportation
1220 Washington Ave.
Building 5, State Office Campus
Albany, N.Y. 12232

John Sobanjo
Civil Engineering Department and Texas
Transportation Institute
Texas A&M University
College Station, Tex. 77843

John F. Stanton
Department of Civil Engineering
University of Washington
Seattle, Wash. 98195

George Stukhart
Texas A&M University
Civil Engineering Department and Texas
Transportation Institute
College Station, Tex. 77843

Holger S. Svensson
Leonhardt, Andra und Partner
7000 Stuttgart 10
Germany

Man-Chung Tang
DRC Consultants, Inc.
34–36 Union Street
New York, N.Y. 11354

W. O. Thomas, Jr.
United States Geological Survey
WGS Mail Stop 415
Reston, Va. 22092

Roy E. Trent
Office of Research and Development
U.S. Department of Transportation
Federal Highway Administration
6300 Georgetown Pike
McLean, Va. 22101

W. J. Winkler
New York State
Department of Transportation
Building 5, State Office Campus
Albany, N.Y. 12232

Toorak Zokaie
Imbsen & Associates, Inc.
9833 Horn Road, Suite C
Sacramento, Calif. 95827

William Zuk
Virginia Transportation Research Council
Box 3817 University Station
Charlottesville, Va. 22903

Bridge Safety Inspection Quality Assurance

RONALD L. PURVIS

The National Bridge Inspection Standards (NBIS) were enacted by Congress in 1968 to regulate the inspection of highway bridges. Each highway agency in the U.S. is responsible for the inspection of the bridges in their jurisdiction. The importance of this program is demonstrated every few months with the news of another failure of one of this country's aging structures. Each failure draws the attention of the news media, special interest groups, and lawmakers to the agency responsible for the structure and to the NBIS program in general.

Inevitably, when a bridge collapse is publicized, the responsible agency has to defend policies and procedures that seemed less important before the failure. Questions of negligence and liability are of concern to all associated with the structure. The parties involved learn quickly that it is not enough to update inspection reports at prescribed intervals. The inspection must meet appropriate quality standards. An ongoing quality assurance (QA) program can help provide and document the level of quality necessary to maintain public confidence in the agency. The Federal Highway Administration (FHWA) has recently implemented a program of in-depth reviews to evaluate targeted states' bridge inspection activities. An important element is the ongoing quality control performed by the agency.

This paper describes the considerations in developing a statewide bridge safety inspection QA program. The procedures focus on the accuracy of the inventory and condition data, the uniformity of the condition judgments, and the level of inspection as it corresponds to the criticality of the bridge. The QA procedures are designed to provide objective and quantitative findings that may be used by management to make cost-effective improvements.

IMPORTANCE OF QUALITY BRIDGE INSPECTION

The National Bridge Inspection Standards (NBIS) have been law for over 20 years. They were enacted by Congress because of a lack of uniformity nationwide in monitoring the condition of highway bridges. The incident that prompted the enactment of NBIS was the failure of the Silver Bridge in Point Pleasant, West Virginia, in 1967, where 46 people perished.

Director of the Structures Department, Wilbur Smith Associates, Consulting Engineers, 2921 Telestar Court, Falls Church, VA 22042.

Clearly, the public's expectation for bridge safety is very high. In fact, when human life is at risk, the tolerance for bridge failure is zero. Bridge failures involving human life invariably evoke strong public reaction followed by enhancements in the law or in the specifications. Often the length of time between the catastrophe and the development of new requirements or guidelines tends to obscure the cause/effect relationship. For example, the Sunshine Skyway Bridge over Tampa Bay in Florida was struck by the bulk carrier vessel, Summit Venture, in 1980 which resulted in a catastrophic loss of life and bridge. A guide specification for protection of bridge substructures from impact damage by large ships was completed and recommended for inclusion in the AASHTO Design Manual in 1990. Examples of enhancements in the bridge inspection program prompted by publicized failures have included:

- The development of a Culvert Inspection Manual and Training Course after five people died from a culvert failure in Ohio in 1982.
- The development of a Manual and Training Course for the Inspection of Fracture Critical Bridge Members after the 1983 failure of the Mianus River Bridge in Connecticut where three lives were lost.
- The development of an Underwater Bridge Inspection Demonstration Project and the implementation of Scour Evaluation Criteria after the 1987 Schoharie Creek Bridge failure in New York State where 10 persons were fatally injured.
- The failure of the Cyprus Street Viaduct and other bridge damage associated with California's Loma Prieta Earthquake in 1989 has provided stimulus for more stringent policy to identify potential problems from

seismic damage.

Catastrophic failures not only provide impetus for changes in the standards, they create a significant disturbance within the agency responsible for the failed structure. Attention is immediately focused on the inspection practice; procedures and priorities are scrutinized by attorneys, politicians, and the media. Other serious problems include the loss of service of the structure, the loss of public confidence in the agency, the concern for litigation, and the threat of damage to individual careers.

The basic NBIS inventory condition and appraisal data requirements are standardized nationwide. The inventory data includes types and dimensions of the key elements of the bridge. The condition assessment includes a numerical rating from "0" to "9" that describes primary structural components; for example, "9" means excellent, "4" is poor, and "1" is imminent failure. Numerical appraisal ratings from "0" to "9" are also used to compare various features to current standards. Appraisal ratings might indicate "desirable," "minimum," or intolerable" characteristics. This data is collected or updated by the bridge inspector at each routine inspection. It is coded and incorporated into the Structural Inventory and Appraisal System maintained by the Federal Highway Administration. Eligibility for rehabilitation and replacement funds is established from a sufficiency rating formula that is influenced by the numerical ratings.

The monitoring of quality is an important consideration in managing a bridge inspection program. While this will not guarantee safety it definitely improves safety and can help to ensure that limited resources available for bridge inspection are used efficiently. Certain critical elements should be checked closely each time the bridge is inspected. Other elements do not warrant as much time and attention. The agency that can demonstrate that available resources are used appropriately is in a much better position to defend their program if it is subjected to outside scrutiny.

The diligence and perseverance necessary to be a good bridge inspector is not present in every individual. Inspection involves looking at hundreds of details before finding a serious problem. Close-up inspection of all critical details is necessary. The work is physically demanding and access is difficult. Bridge inspectors often work at remote locations without senior supervision, and the accuracy of their work cannot be measured directly. How can the unit manager determine if an inspector is maintaining the proper level of intensity to identify the flaw that may lead to the fracture that results in the bridge failure? Quality in design or construction is easier to measure than quality in the inspection of an existing structure. With the inspection there are no calculations to check, no drawings to check, no testing reports to serve as documentation; only a report is created. Without reinspecting the bridge, it is impossible to verify the accuracy and thoroughness of the report. Most agencies recognize the need for quality inspections and the need to monitor the quality at more than one level.

The first level of quality is defined as quality control. Quality control (QC) is performed within a work group. (For the purpose of this paper, the work group will be a district bridge inspection unit within a state. It could also be a city, county, toll authority, or any work group within an agency responsible for bridge inspection.) We know that people make mistakes. Mistakes are a part of work. Members of an inspection team check behind each other. They review each other's sketches or descriptions, and they check for consistency of descriptions and measurements. QC is a necessary part of any production process. Quality Assurance (QA) is administered from outside the work group. The objective of QA is not to correct elements of a specific inspection report or load rating calculation. QA measures the quality of the work. The purpose of QA is to monitor and adjust the activity or program to assure ongoing levels of quality consistent with established requirements. Quality assurance can also identify problems with quality control procedures.

Poor quality bridge inspections influence more than the safety of the structures. Maintenance and repair priorities are established based on the inspection reports. Replacement and rehabilitation budgets are influenced by the inspection results. Certain federal money is allocated based on sufficiency ratings which are influenced by condition ratings provided by the inspector. The distribution of state and local funds may also be influenced by these ratings. The fairness and effectiveness of the repair and replacement program is influenced by the uniform interpretation and accuracy of the condition ratings.

Accurate inspection information also can help to maximize the service life of the existing structure. Timely maintenance is cost effective. Activities such as painting, waterproofing, and joint sealing can prevent costly damage to a very expensive structural system. No transportation agency has enough money. Spending should be based on accurate and complete information.

The Federal Highway Administration has recently completed the second year of a program to monitor the quality of state bridge inspection programs nationwide. A team from the FHWA Washington, regional, and state offices visited 18 states to perform an evaluation of the inspection program. Their findings revealed shortcomings in the areas of agency oversight, quality assurance, and follow-up to the inspection. They are

extending the program for the third year where these items will be of primary emphasis. The FHWA findings indicate that the agency responsible for the bridge inspection program should have a formalized procedure to monitor the quality of the inspections. It is also important that the agency monitor their response to the inspection findings when a need is identified for maintenance, repair, or posting.

CURRENT METHODS OF MONITORING BRIDGE INSPECTION QUALITY

The NBIS program has evolved substantially differently in state DOT organizations nationwide. Some like Texas, Florida, Pennsylvania, and Ohio are decentralized with almost independent inspection units relying on the central office only for coordination and instructional guidelines. Others such as New Jersey, Delaware, and Alaska are basically single units responsible for the state inspections. Some units such as California, New Jersey, and New York have all graduate or registered professional engineer inspection team leaders. However, most states do not require "engineer" inspectors or team leaders.

In a few states, bridge inspection and evaluation is an independent DOT department; in others, it is a part of bridge maintenance. In most states, however, bridge inspection is a part of the bridge design department. A few states and most localities do not have full-time bridge inspectors. Their bridges are inspected by private consultants or in-house construction inspectors, designers, technicians, or maintenance employees as time permits. States and localities also differ in use of consultants and commitment of resources to the program.

The original purpose of the NBIS was to classify bridges according to serviceability, safety, and essentiality for public use, and to assign each an appropriate priority for replacement. The basic program was developed to apply to all states. As the program has matured, many states have expanded and enhanced their data collection system to provide additional bridge management needs. Bridge Management Systems (BMS) collect more detailed information on the condition of the bridge components. They prioritize, track, and document maintenance work as it is performed. Some BMS's categorize the structures based on a "level of service" concept. Most systems provide data for future scheduling and budgeting. No matter how complex the system, it is no better than the data provided by the bridge inspectors. QA is an essential part of a BMS.

Bridge inspection QA varies considerably between states. Among the states that place the most emphasis on QA are those that have experienced a catastrophic bridge failure. QA, like any other function, requires a commitment of time and resources. If it is administered as a low priority, "as time permits" function it will invariably be preempted by some other pressing activity.

A common form of bridge inspection QA activity is review of the inspection report by a supervisor. This procedure has limited value since it is not always possible to relate the completeness of the report with the accuracy or thoroughness of the inspection. This is particularly true of follow-up inspections where a prior inspection is being updated. Inspectors have been known to complete a report on an updated inspection without visiting the site. Hopefully this is a rare occurrence. It is more likely that shortcuts would involve a quick look at those problems that were identified during the previous inspection. This is a dangerous practice since critical problems can develop rapidly. There may be only one inspection cycle when the flaw is detectable by visual inspection before failure of the bridge. A QA review of the report can identify omissions or contradictions in the documentation. It may not be a reliable method to determine the quality of the inspection.

Another method of bridge inspection quality assurance often performed is for an observer to accompany the inspection team while they perform the inspection. There are some advantages and disadvantages to this approach. It provides an opportunity to ascertain, by observance, if the inspection team has the knowledge and training to perform the inspection. The observer can ask questions to test the inspector's knowledge. It also provides an opportunity to evaluate the equipment available to the inspection team and if this equipment is used properly. The disadvantage of this approach is that it is unlikely to provide a representative example of the inspector's work. The individuals on the inspection team are unlikely to take shortcuts if they know they are being observed. This type of evaluation also tends to be subjective. The reviewer may be influenced by appearance, by attitude, or by knowledge that may or may not be a gauge of the quality of inspections performed on a day-to-day basis. These type of QA evaluations may be useful but they are not reliable in providing complete and objective results.

Some agencies have a policy of rotating inspection teams between geographical areas to enhance the quality of the program. Presumably, if there is a deficiency on an inspection team, the impact on safety will be reduced if this team does not inspect the same bridge at back to back cycles. When both teams are of equal competence, there may be some advantage in viewing the bridge from another perspective. Rotating teams might also encourage competition among the inspectors to identify problems first. This procedure of

rotating teams to perform routine inspections is a method of QC rather than QA. A standardized peer review by other inspection teams might be incorporated into a QA program; however, if the peer reviews are performed by many different inspectors, it may be difficult to obtain uniform findings that can be quantified and compared.

QA procedures have been implemented in several states. Pennsylvania DOT has a relatively complex QA program to support their BMS and administrative requirements. PennDOT has eleven decentralized districts with bridge inspection units. Counties and townships in Pennsylvania are also responsible for the inspection of their bridges. Currently, the PennDOT QA program monitors the state, local, and Turnpike bridge inspections. Since PennDOT staff was not available, an engineering firm specializing in bridge inspection was selected by the state's established consultant selection process to develop and implement a bridge inspection QA program under the direction of the Bridge Management Systems Division of the Bureau of Bridge and Roadway Technology. The procedures were developed in 1986. 1990 is the fifth year that the program has been in effect. The QA procedures continue to be performed by a consultant under the direction of PennDOT. The QA findings have resulted in several enhancements being made to the state's bridge inspection guidelines and training. There has also been a 5 percent improvement in the correlation between the district and the QA condition ratings since the program began. At the beginning the correlations averaged slightly over 90 percent. They are currently averaging better than 95 percent.

OBJECTIVES OF AN EFFECTIVE QA PROGRAM

For a QA program to be efficient it must include clearly defined procedures. The QA procedures should be performed at regular intervals in the same way each time. The procedures should be understood both by the reviewer and the reviewee. The procedures should be fair and unbiased. The purpose of QA is to improve the bridge inspection program, not to point fingers at individuals. QA should be perceived as a constructive activity to improve the inspection program. For example, if the findings are used to reprimand or punish inspectors, they are likely to be perceived in a negative way. However, if they are used to identify needs for additional training, improved guidelines, or additional resources, they are likely to be perceived in a positive way. This is very important so that the findings will be taken seriously by the inspectors. A quality assurance program developed and presented in a constructive way can improve the quality of the inspections simply because of its existence. It must be perceived as fair in order to accomplish this.

The following components are necessary for a QA procedure to be perceived as fair by the bridge inspectors:

- the procedures are understood and accepted;
- the procedures are objective;
- the procedures provide quantitative results;
- the procedures provide accurate results;
- the procedures are administered uniformly and consistently during each review.

A totally independent field inspection performed by the QA team, where the findings are compared with the findings of the inspection team after the QA condition assessment is made, is more likely to provide objective results than comparing the inspector's current report while performing the QA inspection of the bridge. When a separate inspection is conducted, the QA team is less likely to be influenced by the previous findings. After the QA inspection is complete, the numerical condition ratings should be compared to the latest inspection report and deviations noted. It is suggested that the QA team then verify their decisions on any disagreements with the district's latest inspection report by reexamining the bridge element in question prior to it being reported to ensure that they can defend their findings. Acceptable tolerances should also be clearly defined. For example, on condition ratings greater than 4, a difference of 1 may be considered unimportant.

Procedures should also be clearly defined for the verification of inventory data, load posting data, and implementation of the inspection findings. As much as possible, it is also desirable to have the procedures developed to provide quantitative results. Without quantitative results, it is difficult to compare findings. For example, which elements of the bridge inspection have more deviations between the QA and inspector's findings, or how do the different teams or different districts compare within the state? The quantitative measurements should reflect the number of deviations, the size of each deviation, and a weight factor reflecting the criticality of the item. Quantitative findings permit the inspection teams to measure their own improvement from year to year.

The accuracy of the QA findings is controlled primarily by the knowledge of the individuals performing the review. In other words, the QA reviewer must be very knowledgeable about the inspection standards and guidelines for the results to be credible. The reviewer must also be familiar with the training provided to the

bridge inspectors. Ideally, the person performing the QA review is a registered professional engineer with considerable experience performing bridge related work including routine and comprehensive inspection.

Since many of the condition ratings involve judgment, it is important that the judgment be as consistent as possible. Funding allocations are influenced by the condition ratings. They should be the same statewide for the same conditions. For example, if a condition rating is in the range of 4, and the inspectors on one side of the state consistently call it a 3 while the other side calls it a 5, more funding is directed to the area that rates lower. If QA judgments are made uniformly, this problem may be identified and corrected. Uniformity and consistency are best attained by using the same QA evaluation team for all the reviews. Some changes are, of course, inevitable. However, they should be minimized, and the QA review team should be large enough to permit a new member to work with others while getting up to speed in providing uniform and consistent judgments.

Skills of diplomacy are also an important consideration in selecting individuals to perform QA. The QA role is to measure and report, not to criticize or direct. QA findings may influence policy and guidelines, but this should happen through the established chain of command. Policy should not be made or distributed by QA team members. QA should be performed in a manner so as to cause minimal interference with ongoing activities within the district.

ELEMENTS OF THE BRIDGE INSPECTION QUALITY ASSURANCE PROGRAM

This section will cover the nuts and bolts of developing and implementing a bridge inspection QA program. The elements of the QA program will be described as follows:

- Planning the evaluation
- QA at the bridge site
- QA at the district office
- Computer edit of SI&A data
- Bridge maintenance evaluation
- District findings
- Annual report

Planning the Evaluation

QA should include reinspections performed independently on a sampling of the bridges. The sample reinspections should accurately represent the bridge inventory. The sample bridges should be selected from those recently inspected.

Each year the districts should be visited in a different sequence to be determined in advance. Sample bridges are selected for QA for each district based on the distribution of bridge types in the district. The recommended sample size is 5% of the bridges inspected by the district teams during that year. The selection process is designed to provide a sampling that is a representative spectrum of all the bridges inspected that year. A profile of all the bridges in the district is developed first for use in selecting the samples. The features that are considered most important in the sample selection process are: type superstructure; total length; sufficiency rating; and district team performing the inspection.

It is important that the QA bridge inspection be performed soon after the district inspection is completed. Therefore, the sample bridges must be selected from those inspected within the last few months. The objective is to match the district's bridge population profile as closely as possible, selecting only from the group that was recently inspected. Beyond that the selection is random. Difficulty of access to the bridge because of size or location should not disqualify a bridge from inclusion in the sample group.

QA at the Bridge Site

The QA at the bridge consists of an independent verification of certain sensitive condition/appraisal items previously identified that remain the same for the annual cycle.

Field QA Review Activities:

- Verify and identify the structure
- Photograph the structure
- Verify inventory data
- Take measurements for load rating check
- Verify traffic safety features and load posting signs
- Perform independent inspection of condition/appraisal items
- Compare with district ratings and reconcile, if possible
- Document findings
- List and prioritize maintenance/repair needs

Assessing the quality of the field inspection is a very important function of QA since deficiencies in this part of the program could impact the safety of the state's bridge system. The QA inspection should be performed with the same degree of thoroughness and intensity that is appropriate for the district's inspection. A hands-on, close-up QA inspection of the sample bridge based on the criticality of the element being inspected is therefore essential.

To save return trips to the field, it is recommended

to compare the QA condition ratings with the inspector's ratings while at the site. It is best for the QA team to prepare an independent inspection report with complete documentation before comparisons are made. An alternative requiring less time is to only document out-of-tolerance findings. This approach involves rating the bridge elements, comparing the QA ratings with the district ratings, and documenting only the QA ratings that are out-of-tolerance. This requires the QA team to be provided with the district ratings prior to the review. The QA team also verifies certain inventory data details and dimensions to check load rating and posting information.

QA at the District Office

QA at the district office consists of verifying the availability and accuracy of the documentation on file.

Office QA Review focuses on the following:

- General file contents
- Inventory documentation
- Inspection documentation
- Proposed improvements
- Load rating analysis
- Compliance with posting policy

The details obtained in the field are confirmed in the office. The file is also evaluated to determine how the inspection data is used. For example, were recommendations implemented, or was a new load rating analysis necessary? The QA teams should use a standard format to rate each item and comment as necessary. Each element of the office QA review is rated for completeness and accuracy.

A questionnaire is also completed during the office visit. This questionnaire is intended to monitor the district procedures. Often there are no specific procedural requirements, provided overall standards are met. However, it is helpful in evaluating the results to relate the effectiveness of procedures to the unique organizational structure of the district under review.

Computer Edit of Data

The system may be programmed to identify certain data items for consistency and conformance with guidelines. It identifies erroneous entries; for example, codes that do not apply. It identifies inspections that are overdue. Omitted items are also flagged.

The system may also be programmed to select the sample bridges to receive QA based on prescribed selection criteria using data input as district inspections are completed.

Bridge Maintenance Evaluation

An important purpose of bridge safety inspection is to identify maintenance/repair needs and priorities. Part of the QA evaluation should focus on the accuracy of maintenance/repair needs identified by the districts and the procedures and documentation for implementing the work. If the agency has a bridge management system, the QA review should verify the utilization of this information in accomplishing and tracking maintenance/repair needs identified by the inspection.

Ideally, the inspection documentation identifies immediate problems, potential problems, and necessary maintenance to avoid future problems. The bridge safety inspection data base should include documentation that indicates the recommended improvements, a priority for each, and the dates that the work is scheduled and completed.

QA Review Report

The district is provided a report after each district QA evaluation that provides the details of the findings. The district report is designed to provide a quantitative evaluation of the QA findings based on the accepted QA procedures. The same data is documented in the same order on each bridge review. The report provides a statistical correlation of the data. The data is organized so that areas of high and low correlation between the district and the QA team may be readily identified. The rating correlation between the district and the QA team is presented graphically with bar charts as shown in Exhibit 1. Unique findings are also listed. The report contains a section for a summary and conclusions. After the report is submitted and reviewed, a close-out meeting is held to discuss the findings and resolve any problems. If, after the close-out, the district does not agree with certain findings or conclusions they may respond with an addendum which is filed with the final report. Addenda by several districts on the same subject suggest a need to reevaluate the QA interpretation of the item in question and/or modify training course material.

Annual Report

The annual report contains a summary of all QA activities performed for a given year and a comparison of these findings statewide. In this report bar charts for each inspection item are arranged so that all the district results are listed side by side. An example of this is included in Exhibit 2. This format is helpful in identifying inspection items that have received a wide range of ratings for a given condition. This information is helpful in identifying possible needed enhancements in the

inspector's training information or the guidelines. If deviations are experienced for a particular item in just one district, it is more likely an internal problem. Exhibit 3 shows how the QA results can be evaluated over a period of several years.

The annual report also includes a narrative summary of the findings per district with details of their resolution at the close-out meetings. There is a section on conclusions that identifies areas of concern based on the overall findings.

There is also a section on recommendations for the next year. This section proposes modifications in the program based on the annual findings. If there are improvements warranted in the QA procedures these are also recommended. This section might also contain suggestions for improvements in the statewide bridge inspection guidelines or inspector's training.

PURPOSE OF EXHIBITS

Bar graphs are useful in comparing differences in the numerical condition and appraisal ratings between the QA team and the district bridge inspection teams. QA evaluations were performed on 30 bridge inspections in each district. The vertical bars on the graphs represent the frequency of agreement and magnitude of difference.

Exhibit 1 illustrates the correlation in all the numerical condition and appraisal ratings for a single district QA review. Exhibit 2 illustrates the correlation with the QA team for all the districts in the state for the same inspection item. Exhibit 3 illustrates the average statewide correlation on one inspection item with the QA team per year for a five-year span.

EXHIBIT 1

DIFFERENCE BETWEEN QUALITY ASSURANCE REVIEW AND DISTRICT A RATINGS 1989

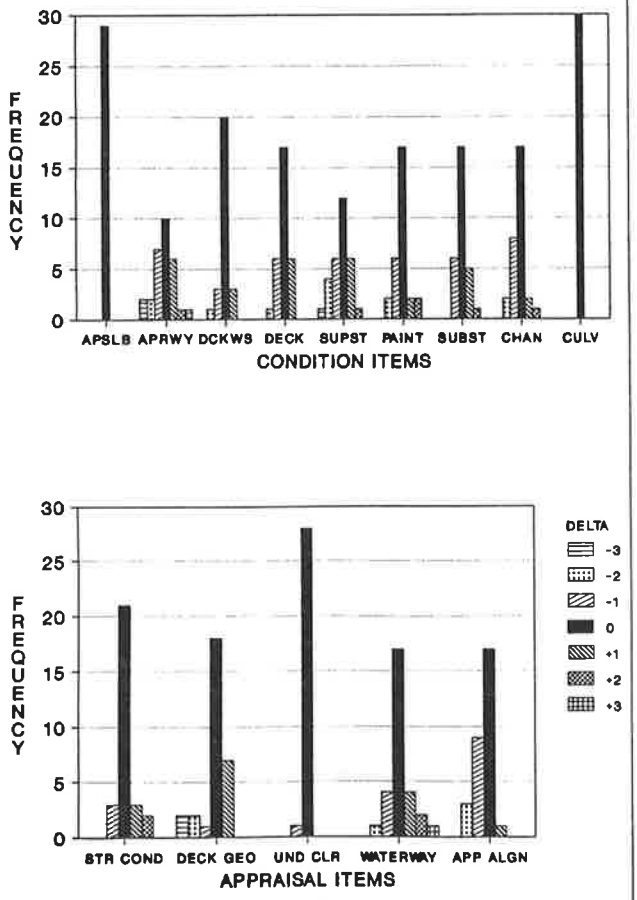

NOTE:+ Indicates District rating greater than review

EXHIBIT 2

'86 DIFFERENCE BETWEEN QUALITY ASSURANCE REVIEW AND DISTRICT RATINGS STATEWIDE STRUCTURAL EVALUATION

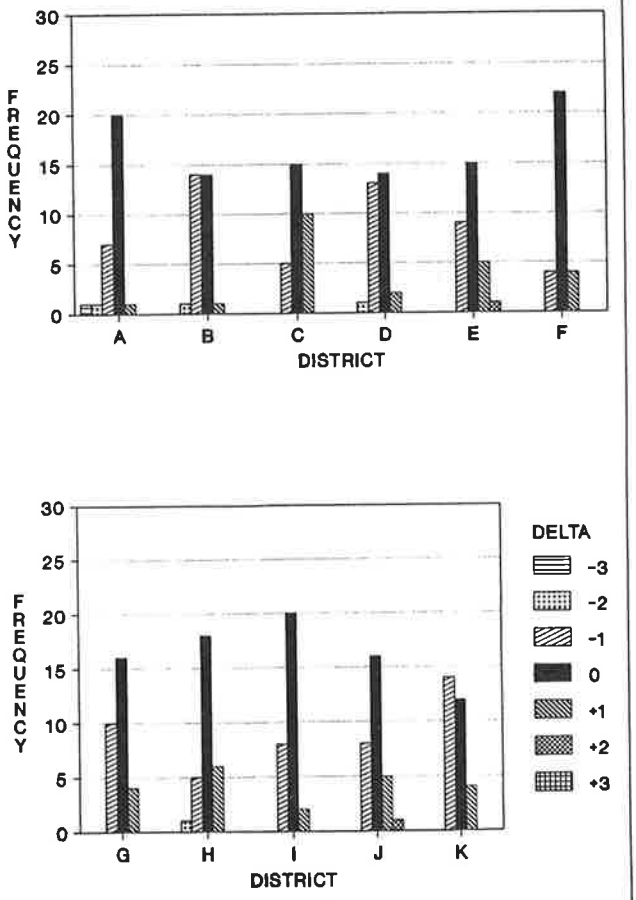

NOTE:+ Indicates District rating greater than review

EXHIBIT 3
DIFFERENCE BETWEEN QUALITY ASSURANCE REVIEW AND DISTRICT RATINGS

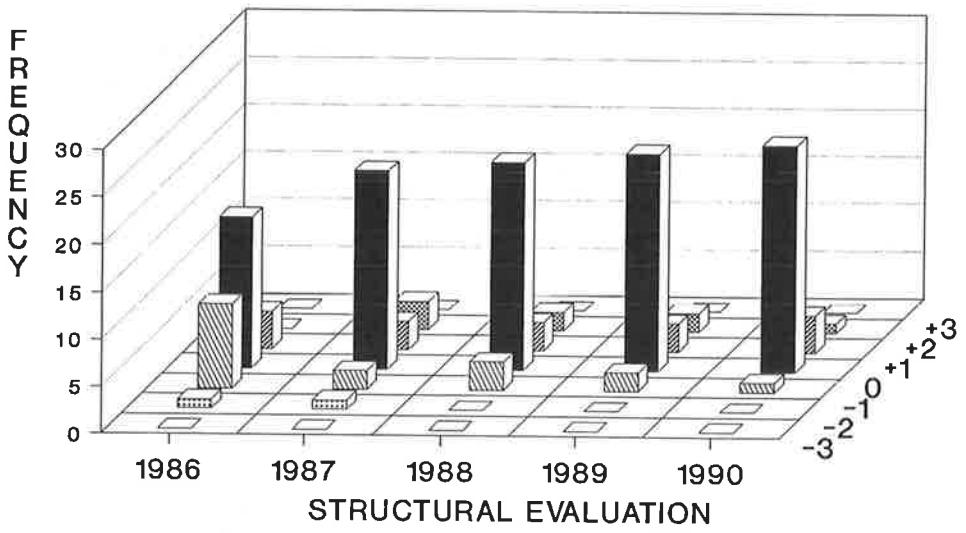

NOTE:+ Indicates District rating greater than review

Effects of Damage and Redundancy on the Safety of Existing Bridges

DAN M. FRANGOPOL AND RACHID NAKIB

Many existing bridges are damaged. The older these bridges are, the higher their probability of being damaged. Yet, they continue to function and exhibit higher capacities than those associated with their designed vehicular loads. This may be the result of several factors, but the prevalent explanation among researchers today is that the existing bridges have a much greater amount of reserve strength than that anticipated by the original bridge designer. This indicates a need for determining an effective means for modeling and evaluating existing bridges, particularly for those exceeding their design life. The present study primarily reviews definitions of deterministic and probabilistic system redundancy measures which could be used in the design and evaluation of highway bridges. Some of these measures are used to evaluate the redundancy of an existing steel girder bridge. In this context, corrosion and accidental damages are simulated and the bridge redundancy is evaluated by using three-dimensional nonlinear finite element and probabilistic system analyses. The bridge damage - redundancy - reliability interaction is also studied.

INTRODUCTION

Despite the fact that the need for redundancy ability in highway bridges has already been recognized by AASHTO*(1)*, no criteria pertaining to quantify redundancy are explicitly specified within current bridge design codes. With heavier loads on existing bridges and increasing allowable stresses in newly designed structures, logical procedures would be required to determine the load carrying capacity and the redundancy level in bridge structures.

The need for redundancy in highway bridges can also be seen from a survey by the ASCE-AASHTO Committee on Redundancy of Flexural Systems*(2)* conducted on damaged bridges, which indicated that few bridge structures have collapsed when redundancy was present. Many of the reported collapses involved truss bridges with essentially no redundancy.

Dan M. Frangopol, Department of Civil, Environmental, and Architectural Engineering, University of Colorado at Boulder, Boulder, Colorado 80309-0428. Rachid Nakib, Department of Civil and Environmental Engineering, Washington State University, Pullman, Washington 99164-2910.

Additionally, with the expanding usage of reliability theory in structural engineering, probabilistic procedures for bridge design and evaluation are gaining wide acceptance in the structural engineering community*(3,4)*. In the past, most structural analysis studies were directed toward single component deterministic analysis. Today, the need to introduce system redundancy and reliability measures in structural analysis and design is obvious*(5)*. However, while there has been much research into the safety of structures and the development of probabilistic design codes*(6-9)*, little work has yet been done on quantifying the level of redundancy and its impact on bridge reliability*(10-13)*.

In view of the above, the need for a method which quantifies structural redundancy levels in the design and evaluation of highway bridge systems is evident. This paper primarily reviews definitions of deterministic and probabilistic bridge redundancy measures. It also reports analytical investigations into the redundancy evaluation of an existing steel girder bridge using three-dimensional nonlinear finite element analysis and damage scenarios. In this context, corrosion and accidental damages are simulated. The redundancy measures used in evaluating the existing bridge offer useful information to quantify the effects of various damage states on bridge reliability and the availability of warning before total bridge collapse occurs.

BRIDGE REDUNDANCY MEASURES

Redundancy in a bridge system is generally defined as the ability of other members to help carry load when a member becomes weak or fails. The AASHTO Guide Specification for Fracture Critical Bridge Members penalizes nonredundant steel members. The bridge engineer is assigned the responsibilities of determining which members of the bridge must be classified as nonredundant and if the bridge system is sufficiently redundant. These are extremely difficult tasks, since no guidance is given in the AASHTO specifications concerning bridge redundancy evaluation. Presently, there are considerable differences of opinion about the definition of structural redundancy.

A review of both the deterministic and probabilistic system redundancy measures available in the literature is given in the following two subsections.

Deterministic Redundancy Measures

There are a number of definitions of deterministic measures of system redundancy*(14-17)*. These include:

- *Degree of indeterminacy,* (i.e., classical definition of indeterminacy used in structural analysis), I, defined as

$$I = F - E \tag{1}$$

in which F and E are the numbers of unknown reactive forces and of independent equilibrium equations, respectively. Unfortunately, this definition has no applicability in assessing the overall redundancy of a structural system which refers to the capability of the structure to carry load after one or more of its members have failed.

- *Reserve strength factor,* $R_{reserve}$, defined as

$$R_{reserve} = Q_{intact} / Q_{nominal} \tag{2}$$

in which Q_{intact} and $Q_{nominal}$ are the ultimate strength of the undamaged structural system and the nominal applied load on this system, respectively. However, to evaluate system redundancy one needs to cover the complete range of structural behavior from damage initiation until total collapse.

- *Residual strength factor,* $R_{residual}$, defined as

$$R_{residual} = Q_{damaged} / Q_{intact} \tag{3}$$

in which $Q_{damaged}$ is the ultimate strength of the damaged structural system.

A statically determinate structure would have no residual strength, $R_{residual} = 0$, after failure of any single component. On the other hand, failure of one component of a statically indeterminate structure will not necessarily constitute a complete loss of the load-carrying capacity for the structure (i.e., $R_{residual} > 0$).

- *Redundancy factor,* R, defined as

$$R = Q_{intact} / (Q_{intact} - Q_{damaged}) = 1 / (1 - R_{residual}) \tag{4}$$

The redundancy factor R depends on the loading, the damaged members, the amount of damage in each member, and the material behavior of the damaged as well as of the intact members. The bridge redundancy factor correlates directly with the overall bridge strength in a damaged condition *(16,17)*. In general, the redundancy measure (R) ranges from a value of 1, when the structure has completely lost its strength (i.e., collapse), to ∞, when structural damage has no effect on the residual strength of the structure. It is interesting to note that in some cases of brittle behavior a damaged structure could have a higher ultimate strength than that of the intact structure (i.e., $Q_{damaged} > Q_{intact}$). In these particular cases of unexpected favorable behavior in the presence of damage, the redundancy factor R is negative. Examples of such cases were reported by Nakib*(18)*.

Probabilistic Redundancy Measures

The redundancy of a system has also a probabilistic nature. The availability of warning before total collapse occurs (i.e., system redundancy) depends also on the uncertainties in loads and strengths, correlations between member capacities and between loads, individual member failure probability levels, and structure configurations*(19)*. Several probabilistic measures of the redundancy of a system have been suggested in the literature *(16,20-23)*. These include:

- *Redundancy factor with respect to failure of the weakest member*

$$R_1 = (\beta_{collapse} - \beta_{weakestmember}) / \beta_{collapse} \tag{5a}$$

or, alternatively,

$$R_2 = (P_{weakestmember} - P_{collapse}) / P_{collapse} \tag{5b}$$

in which $\beta_{weakestmember}$ = reliability index of the weakest member = min $(\beta_1, \beta_2, \ldots, \beta_i, \ldots, \beta_m)$ where m is the number of bridge members, $\beta_{collapse}$ = reliability index of the intact system with respect to collapse, $P_{collapse}$ = probability of collapse of the intact system, and $P_{weakestmember}$ = probability of failure of the weakest member.

- *Redundancy factor with respect to any first-member-failure*

$$R_3 = (\beta_{collapse} - \beta_{firstfailure}) / \beta_{collapse} \tag{6a}$$

or, alternatively,

$$R_4 = (P_{firstfailure} - P_{collapse}) / P_{collapse} \tag{6b}$$

in which $\beta_{first\,failure}$ = reliability index of the intact system with respect to any first-member-failure, and $P_{first\,failure}$ = probability that any first-member-failure occurs in the intact system.

- *Redundancy factor with respect to a given damaged state of the system*

$$R_5 = \beta_{collapse} / (\beta_{collapse} - \beta_{damaged}) \quad (7a)$$

or, alternatively,

$$R_6 = (P_{damaged} - P_{collapse}) / P_{collapse} \quad (7b)$$

in which $\beta_{damaged}$ = reliability index of the damaged system with respect to collapse, and $P_{damaged}$ = probability of failure of the damaged system.

Observations

The computations of reliability indices in Equations 5a, 6a and 7a and probabilities in Equations 5b, 6b and 7b could be done by using modern system reliability techniques*(5)*. For the case of normal distributed variables

$$P_f = \Phi(-\beta) \quad (8)$$

where P_f is the probability of failure with respect to a given limit state, β is the reliability index with respect to the occurrence of the same limit state, and $\Phi(\cdot)$ is the normal cumulative probability distribution function.

It is interesting to note that

$$\beta_{first\,failure} \leq \beta_{weakest\,member} \quad (9a)$$

or, alternatively,

$$P_{first\,failure} \geq P_{weakest\,member} \quad (9b)$$

because initial failure can occur in any of the several bridge members. Consequently, for nonnegative reliability indices with respect to all limit states considered (i.e., $P_f < 0.5$) we have $R_1 \leq R_3$ and $R_2 \leq R_4$. For a statically determinate system the probability that any first-member-failure occurs is equivalent to the probability of system collapse (i.e., $R_3 = R_4 = 0$). The probabilistic redundancy measure R_5 varies within the range between zero and ∞, with $R_5 = 0$ indicating catastrophic effect of damage (i.e., $\beta_{damaged} = -\infty$ or, alternatively, $P_{damaged} = 1$) and $R_5 = \infty$ (i.e., $R_6 = 0$) indicating no effect of damage on the reliability of the structure (i.e., $\beta_{damaged} = \beta_{collapse}$ or, alternatively, $P_{damaged} = P_{collapse}$).

The redundancy measures R_1, R_2, R_3, and R_4, could be used in bridge design and R, R_5, and R_6, in bridge evaluation. It is important to note that these latter factors could also be used in damage tolerant bridge design, where redundancy is desired to ensure an acceptable bridge residual reliability level in case of unexpected damages.

AN APPLICATION EXAMPLE: COLORADO STATE BRIDGE E-15-AF

Bridge Description and Modeling

The example bridge used for this study is the Colorado State Bridge E-15-AF described by Nakib*(18)*. This bridge is a 90ft single span structure with a width of 36ft. It consists of a concrete deck with a thickness of 8.5in supported by four steel girders spaced at 9ft apart. Concrete and steel stress-strain relationships are given in Nakib*(18)*. The bridge is analyzed until failure using the Abaqus Multipurpose Finite Element Program*(25)*. The concrete deck is modeled using 143 quadrilateral shell elements, while each of the four girders of the bridge is modeled using 39 two-noded beam elements (i.e., 13 elements for the bottom flange, 13 for the web, and 13 for the top flange). The total number of degrees of freedom within the finite element bridge model equals 1794. The interaction between girders and deck is accounted for through the three-dimensional finite element modeling. The applied loads include dead loads D (weight of concrete deck and girders), live loads L (two HS-20 trucks applied side by side on the deck in order to induce maximum stresses in the bridge) and impact loads, I.

The detailed description of the geometrical and mechanical properties of the bridge, the finite element modeling, the uncertainties in loads and strengths, and the side-by-side position of the two HS-20 trucks which induce maximum stresses in the bridge are given in Nakib*(18)*. The live and impact loads are incremented progressively by the factor λ until reaching collapse.

Damage Models

The effects of damage on the redundancy of the Colorado State Bridge E-15-AF were evaluated using two damage models: (a) corrosion damage, and (b) accidental damage. In modeling corrosion damage a uniform loss of material in the exposed surface of the girders is considered. A uniform corrosion damage factor is defined as

$$D.F. = (A_i - A_d)/A_d \quad (10)$$

in which A_i and A_d are the cross sectional areas of the intact and damaged (i.e., corroded) girders, respectively. In modeling accidental damage one or two girders are completely removed from the bridge system. The program Abaqus(*25*) is used to determine the response of the bridge at different corrosion and accidental damage levels by increasing progressively the live and impact loads until total collapse of the bridge. Both the redundancy and reliability of this bridge were calculated for each damage scenario considered.

Deterministic Results

Inelastic load-deflection bridge responses under dead (D) and incremental (i.e., λ) live (L) and impact (I) loads, for various corrosion damage factors and accidental damage scenarios were obtained and the results are shown in Figures 1 and 2. Figure 1 illustrates the effect of corrosion damage, while Figure 2 shows how the removal of one or two girders affects the response of the bridge system. Deterministic bridge redundancy factors (see Equation (*4*))

$$R = \lambda_{intact}/(\lambda_{intact} - \lambda_{damaged}) \quad (11)$$

were calculated for both damage models. In Equation (11) λ_{intact} and $\lambda_{damaged}$ are the ultimate load increment factors for the intact and damaged bridge, respectively. The redundancy factors R for corrosion and accidental damage states are indicated in Tables 1 and 2, respectively. The effects of corrosion on bridge redundancy depend on the rate of girder section loss. For example, a corrosion increase from 25 to 50% decreases the bridge redundancy factor from 3.13 to 1.54. A further increase in corrosion to 75% results in R = 1.02 (see Table 1). On the other hand, the damage caused by removal of one internal girder results in the redundancy factor R = 2.43, while removal of the two internal girders reduces drastically this redundancy factor to R = 1.34 (see Table 2).

Probabilistic Results

The effects of both damage and mean load multiplier (i.e., λ) on the bridge reliability index β are shown in Figures 3 and 4. For example, for λ = 1, Figure 3 shows that a 25% corrosion damage factor results in shifting the bridge reliability index from β_{intact} = 4.75 to $\beta_{damaged}$ = 3.40 and, consequently, the probabilistic bridge redundancy factor from $R_S = \infty$ to R_S = 4.75/(4.75 - 3.40) = 3.52, whereas 50% corrosion results in a lower bridge reliability, $\beta_{damaged}$ = 1.35, and, consequently, a lower probabilistic bridge redundancy factor, R_S = 4.75/(4.75 - 1.35) = 1.40. On the other hand, also for λ = 1, Figure 4 shows that removal of one internal girder shifts the bridge reliability index from β_{intact} = 4.75 to $\beta_{damaged}$ = 2.60 and, consequently, the probabilistic bridge redundancy factor from $R_S = \infty$ to R_S = 4.75/(4.75 - 2.60) = 2.21, whereas removal of the two internal girders results in a lower bridge reliability, $\beta_{damaged}$ = 0.71, and a lower probabilistic bridge redundancy factor, R_S = 4.75/(4.75 - 0.71) = 1.18.

CONCLUSIONS

Bridge redundancy is desired to ensure an acceptable level of residual reliability in case of unexpected damages. There are a number of definitions for structural redundancy in highway bridges, ranging from that implied by the traditional degree of structural indeterminacy to more rational measures that take into account the complete range of nondeterministic bridge behavior from damage initiation to total collapse.

In this paper, both deterministic and probabilistic system redundancy measures are reviewed. These redundancy measures deserve more attention in the design and evaluation of highway bridges. Further research efforts must be made towards establishing qualitative and quantitative provisions for designing sufficiently redundant bridge structures. The measures of bridge redundancy reviewed in this paper and the damage- redundancy- reliability interaction demonstrated in the numerical example should contribute to assist designers and inspectors in determining redundancy in highway bridges.

ACKNOWLEDGEMENT

Support of this work by the National Science Foundation (NSF Grant ECE-8609894), with Dr. J.B. Scalzi as Program Director, is gratefully acknowledged. The authors are also grateful to Dr. Geerhard Haaijer, Vice President, Technology and Research for American Institute of Steel Structures (AISC) who, during the 69th TRB annual meeting, encouraged them to submit their bridge redundancy research results for publication in the AISC Engineering Journal(*26*).

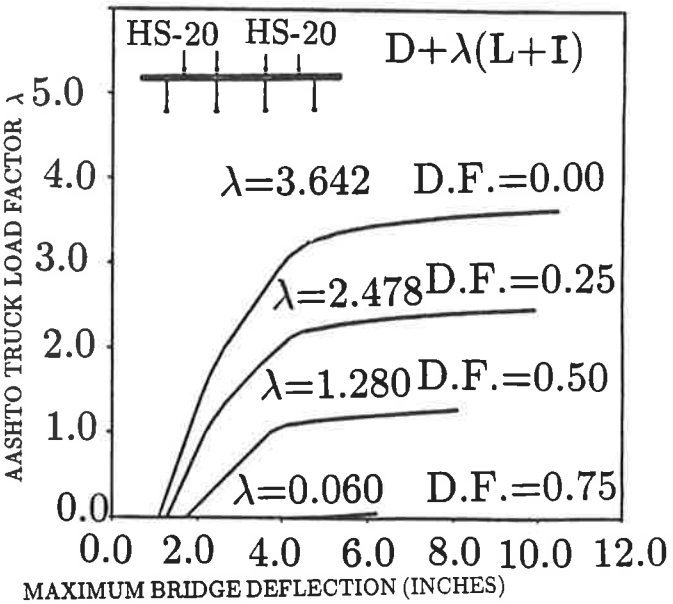

FIGURE 1 Load deflection response for corrosion damaged states.

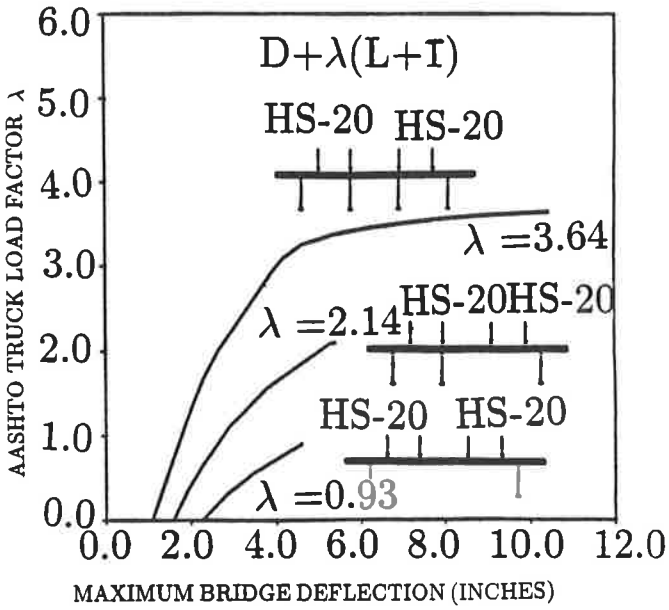

FIGURE 2 Load-deflection response for accidental damage scenarios.

TABLE 1 REDUNDANCY FACTORS UNDER CORROSION DAMAGE

Corrosion Damage Factor, D.F.	Load Increment Factors		Redundancy Factor, R
	λ_{intact}	$\lambda_{damaged}$	0
0.00	3.64	3.64	∞
0.25		2.48	3.13
0.50		1.28	1.54
0.75		0.06	1.02

TABLE 2 REDUNDANCY FACTORS UNDER ACCIDENTAL DAMAGE

Accidental Damage Scenario	Load Increment Factors		Redundancy Factor, R
	λ_{intact}	$\lambda_{damaged}$	0
Intact Bridge	3.64	3.64	∞
One Internal Girder Removed		2.14	2.43
Both Internal Girders Removed		0.93	1.34

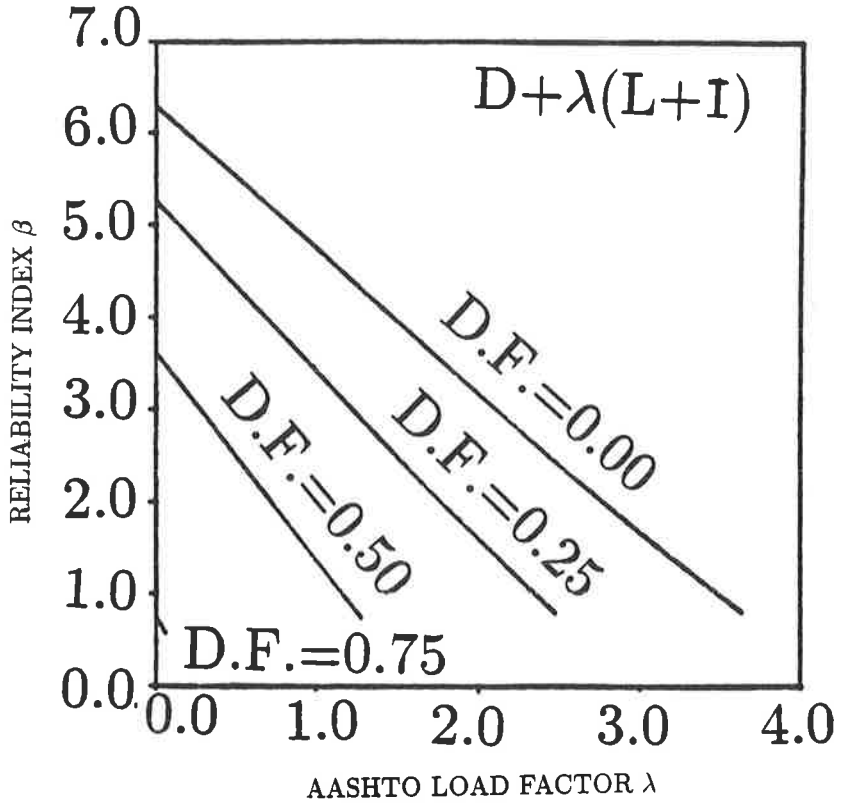

FIGURE 3 Bridge reliability index under incremental loading and corrosion damage states.

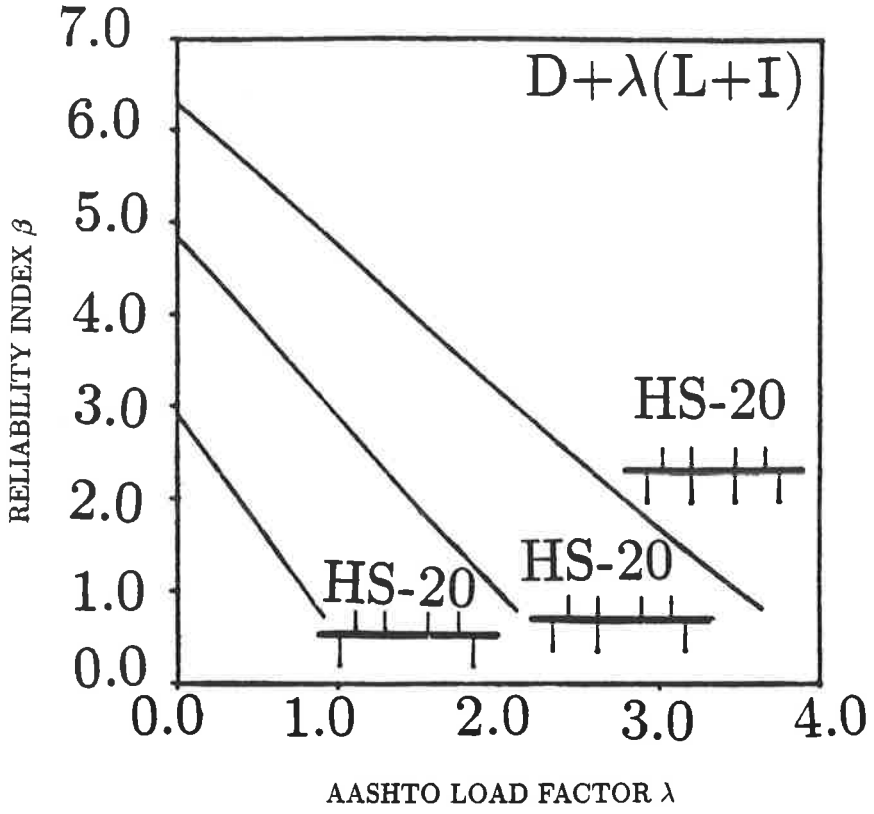

FIGURE 4 Bridge reliability index under incremental loading and accidental damage scenarios

REFERENCES

1. American Association of State Highway and Transportation Officials (AASHTO). *Standard Specifications for Highway Bridges.* Fourteenth Edition. Washington, D.C., 1989.
2. Task Committee on Redundancy of Flexural Systems of the ASCE-AASHTO Committee on Flexural Members of the Committee on Metals of the Structural Division. *State-of-the-Art Report on Redundant Bridge Systems.* Journal of Structural Engineering. ASCE, Vol. 111, No. 12, 1985.
3. R. A. Imbsen, D. H. Liu, R. A. Schamber, and R. V. Nutt. *Strength Evaluation of Existing Reinforced Concrete Bridges. NCHRP* Report 292. Washington, D.C., 1987.
4. F. Moses, and D. Verma. *Load Capacity Evaluation of Existing Bridges,* NCHRP Report 301, Washington, D.C., 1987.
5. D. M. Frangopol, (Editor). *New Directions in Structural System Reliability.* University of Colorado, Boulder, Colorado, 1989.
6. R. B. Corotis. *Probability-Based Design Codes.* Concrete International. Vol. 7, No. 4, Detroit, April 1985.
7. B. Ellingwood, T. V. Galambos, J. G. MacGregor, and C. A. Cornell. *Development of a Probability-Based Load Criterion for American National Standard A58.* NBS Special Publication 577. U.S. Dept. of Commerce. Washington, D.C., 1980.
8. American Institute of Steel Construction, Inc. *Manual of Steel Construction; Load and Resistance Factor Design.* First Edition, Chicago, Illinois, 1986.
9. T. V. Galambos. *Systems Reliability and Structural Design.* New Directions in Structural System Reliability. University of Colorado, Boulder, Colorado, 1989.
10. H. R. Sandberg, and R. A. Parmelee. *Redundancy by Design - Its Implications.* 3rd Annual International Bridge Conference. Paper Number IBC-86--28. Pittsburg, Pennsylvania, 1986.
11. R. A. Parmelee, and H. R. Sandberg. *If it's redundant, prove it.* Civil Engineering, ASCE, New York, Oct. 1987.
12. D. M. Frangopol, and G. G. Goble. *Development of a Redundancy Measure for Existing Bridges.* Bridge Evaluation, Repair and Rehabilitation. The University of Michigan, Ann Arbor, Michigan, 1987.
13. D. M. Frangopol, G. G. Goble, J. J. Trautner, and M. M. Scholfield. *Redundancy Evaluation of Existing Bridges.* Materials and Member Behavior, ASCE, New York, 1987.
14. J. R. Lloyd, and W. C. Clawson. *Reserve and Residual Strength of Pile Founded Offshore Platforms.* The Role of Design, Inspection, and Redundancy in Marine Structural Reliability. National Research Council, Washington, D.C, 1984.
15. J.P. Tang, and J.T.P. Yao. *Evaluation of Structural Damage and Redundancy.* Effects of Damage and Redundancy on Structural Performance. ASCE, New York, 1987.
16. D. M. Frangopol, and J. P. Curley. *Damage States, Redundancy and System Strength.* Effects of Damage and Redundancy on Structural Performance. ASCE, New York, 1987.
17. D. M. Frangopol, and R. Nakib. *Redundancy Evaluation of Steel Girder Bridges.* Structural Safety and Reliability. Vol. III, ASCE, New York, 1990.
18. R. Nakib, *Reliability Analysis and Optimization of Multistate Structural Systems.* Ph.D. Thesis. University of Colorado, Boulder, Colorado, 1988.
19. F. Moses, *New Directions and Research Needs in System Reliability Research.* New Directions in Structural System Reliability. University of Colorado, Boulder, Colorado, 1989.
20. D. M. Frangopol, and R. Nakib. *Effects of Redundancy on Bridge Reliability.* 69th Annual Meeting of the Transportation Research Board. Presentation CP 036, Washington, D.C, 1990.
21. R. S. De, A. Karamchandani, and C. A. Cornell. *Study of Redundancy in Near-Ideal Parallel Structural Systems.* Structural Safety and Reliability. ASCE, Vol. II, New York, 1990.
22. C. Paliou, M. Shinozuka, and Y.-N. Chen. *Reliability and Redundancy of Offshore Structures.* Journal of Engineering Mechanics. ASCE, Vol. 116, No. 2, New York, 1990.
23. G. Fu, and F. Moses. *Probabilistic Concepts of Redundancy and Damage Tolerability for Structural Systems.* Structural Safety and Reliability. ASCE, Vol. II, New York, 1990.
24. D. M. Frangopol, R. Nakib, and G. Fu. *Bridge Reliability Evaluation Using 3-D Analysis and Damage Scenarios.* Probabilistic Methods in Civil Engineering. ASCE, New York, 1988.
25. Hibbit, Karlsson, and Sorensen, Inc. *The Abaqus Multipurpose Finite Element Program,* 1987.
26. D. M. Frangopol, and R. Nakib. *Redundancy in Highway Bridges,* AISC Engineering Journal, AISC, Chicago, 1991.

Vulnerability Assessment and Ranking of Steel Bridges

J. HARTLEY DANIELS, STEPHEN J. RESSLER, AND JOHN W. FISHER

Failure of Connecticut's Mianus River bridge in 1983, the New York State Thruway's bridge over the Schoharie Creek in 1987 and the recent failure of the US 51 bridge in Covington, Tennessee, have underscored the importance of inspection, evaluation and maintenance in achieving bridge safety. However the magnitude and cost of arbitrary bridge safety assurance actions can be prohibitive. Since budgetary restraints limit even safety actions a prioritizing system is needed which can identify the most vulnerable bridges for remedial project work. The system must distinguish between rather benign local failures and catastrophic failures resulting in a significant hazard to the lives of the travelling public which may include total collapse of a bridge or bridge span. This paper presents the essential details of such a system which provides a practical and immediately implementable method of identifying the most vulnerable bridges or spans within a given population. It is being reviewed for inclusion in a comprehensive bridge management program currently being implemented by the New York State Department of Transportation.

Reference 1 presents a probabilistic model for the vulnerability assessment and ranking of steel highway bridges or bridge spans and discusses some practical applications. Vulnerability ranking is a means of prioritizing the repair, retrofit, rehabilitation, and replacement of in-service bridges. In order to perform vulnerability ranking of a group of bridges or spans, the degree of vulnerability of each bridge or span in the group must first be determined. This process is vulnerability assessment. The term "bridge" will refer to either a complete bridge or an individual span.

Vulnerability assessment and ranking is being reviewed for inclusion in a comprehensive bridge management program currently being implemented by the New York State Department of Transportation (NYSDOT). As part of that program, the procedures described herein were developed and proposed by the NYSDOT Bridge Safety Assurance Task Force (BSATF), an independent committee formed to review New York State's safety assurance measures (2, 3).

DEFINITION OF VULNERABILITY

The model is based on fundamental structural reliability and risk assessment concepts, both of which are applications of the mathematical theory of probability. Because probabilistic methods attempt to deal rationally with uncertainty, they are well suited to studies of bridge safety. Vulnerability is the relative probability that a given bridge will fail within a given period of time, say, the next two years. The two year time period is practical because it corresponds to the federally-mandated inspection interval. The term "relative probability" is a quantitative measure of the relative likelihood of an event, defined on an arbitrary numerical scale. To rank a group of bridges according to their vulnerability, the "true" failure probability for a given bridge is not needed; rather it is only necessary to know whether a given bridge is more or less likely to fail than the other bridges in the group.

In the vulnerability assessment model, relative failure probabilities are, for the most part, subjectively defined. Use of subjective probabilities as the basis for engineering decision-making has been well established in basic Bayesian Decision Theory (4).

In the definition of vulnerability, "failure" is any major change in the geometry of the bridge which creates a significant hazard to the lives of the traveling public. This definition is a direct reflection of New York State bridge management program's emphasis on public safety. Note that, as used here, the term "failure" encompasses a wide range of limit states. For the purpose of vulnerability assessment, a bridge has "failed" if, for example:

- The entire bridge has collapsed.
- One or more spans have collapsed.
- The floor system fails, resulting in severe injury or loss of life.
- Failure of a main member (e.g. girder fracture) causes large deck deformations which result in severe injury or loss of life.

Note that the model is designed to ignore rather benign local failures and to identify potential catastrophic failures.

THE VULNERABILITY ASSESSMENT MODEL

Formulation of the vulnerability assessment model is accomplished in four steps, as follows:

(1) Six significant failure modes are identified for steel bridges. These are based primarily on the observed performance of in-service bridges (5). Types of failure observed most often are considered to be the most significant.

(2) Each failure mode is analyzed to determine specific structural characteristics, conditions, and events which might

Department of Civil Engineering, Fritz Engineering Laboratory, No. 13, Lehigh University, Bethlehem, Pennsylvania 18015-3191

contribute to the failure.
(3) These characteristics, conditions, and events are incorporated into a single logic network, called the Vulnerability Assessment Flowchart. The flowchart, which is shown in Figure 1, is designed to generate a quantitative vulnerability assessment for a given bridge. To achieve a vulnerability assessment, the flowchart guides the user through a series of decision points, the outcomes of which depend on the general characteristics and condition of the bridge being assessed.
(4) Specific guidelines for the use of the flowchart are prepared. These guidelines provide standard criteria for selection of outcomes at decision points.

Definitions

The formulation of the vulnerability assessment model includes a number of key terms. They are as follows:

MEMBER - A major structural element requiring separate design consideration; e.g., girder, floor beam, stringer.
COMPONENT - A discrete part of a member; e.g., flange plate, web plate, flange angle (in a riveted plate girder).
INTERNAL REDUNDANCY - Capacity of a member to carry load following the fracture of a single component of that member. Riveted plate girders and multiple eyebar truss members have a high degree of internal redundancy (6). Welded plate girders and rolled sections have no internal redundancy.
STRUCTURAL REDUNDANCY - Capacity of a structure to carry load following the fracture of a single member. Multi-girder bridges have high structural redundancy (7). The structural redundancy of two- and three-girder bridges can range from low to moderate, depending on the configuration of their secondary or redundant bracing systems (8).
DETECTABLE DECK DEFORMATION - After-fracture deformation of the bridge deck which is clearly noticeable to occupants of crossing vehicles, but is not large enough to constitute a significant safety hazard. If detectable deck deformation occurs following a member fracture, traffic is likely to be quickly halted. If detectable deck deformations do not occur after a fracture, traffic will continue to cross the bridge, and the intact portion of the structure will continue to accumulate fatigue damage; and the likelihood of catastrophic failure will increase. For example, detectable deck deformation did not occur after near full depth fracture of the girder of the I79 and Lafayette St. bridges (9).
FATIGUE RESISTANCE - Characteristics of structural members, components and connections which affect its susceptibility to fatigue cracking (9). These characteristics include design details and workmanship.
MATERIAL TOUGHNESS - Capacity of a metallic material to resist fracture.
ADTT - Average Daily Truck Traffic for a given bridge.
WATER CONTROL - Existence of well-maintained expansion joints, drains, and gutters, which carry water and dissolved salts off of the deck surface without allowing contact with the steel superstructure.

Significant Failure Modes

As shown in Figure 1, six significant failure modes are identified for steel bridges. They are as follows:

- Failure Model 1: Fatigue cracking occurs in primary members, such as plate-girders, tie-girders, floor beams, truss members or their connections. Cracking may lead to brittle fracture.
- Failure Mode 2: Collision of a vehicle or vessel with a member causing loss of load-carrying capacity.
- Failure Mode 3: Fatigue cracking in hangers, pins, or seats of a suspended span. Cracking may lead to brittle fracture.
- Failure Mode 4: Hangers supporting a suspended span fail due to "pack out" of retainers on the hanger pins (Mianus).
- Failure Mode 5: Fatigue cracking occurs in a steel pier cap or other steel substructure member(s).
- Failure Model 6: Corrosion of primary members causes loss of load-carrying capacity.

Although these failure modes are not all inclusive, they are applicable to short-and medium-span bridges (with or without floor systems) and to the floor systems of long-span bridges. They are not fully applicable to the main load-carrying members (truss members, arch ribs, or cables) of long-span structures. This is because Failure Modes 1, 3, and 5 are primarily concerned with fatigue effects caused by vehicular loading. These effects are quite significant for short- and medium-span bridges and for the floor systems of long-span bridges. For the main load-carrying members of long-span structures, however, the dead load-to-live load ratio is so large that fatigue effects are rarely significant. Vulnerability of these members is expected to be governed by other failure modes which are beyond the scope of this paper.

Vulnerability Assessment Flowchart

The Vulnerability Assessment Flowchart shown in Figure 1 is organized such that the six failure modes are considered in sequence. A vulnerability assessment must consider all six failure modes.

The purpose of the Vulnerability Assessment Flowchart is to determine a relative probability of failure for a given bridge, based on its general characteristics and current condition. The formulation of the flowchart consists of two distinct elements: the logic network and the relative failure probabilities.

LOGIC NETWORK

The logic network follows directly from a "fault tree" analysis which is described in Reference 1. Referring to Figure 1 the network consists of a series of decision points, which are designated with diamond-shaped boxes. For reference, each decision point is labeled with a letter in parentheses; e.g., (a). Each decision point has two or three possible outcomes. Selection of the appropriate outcome at each decision point depends on the general characteristics and condition of the bridge being assessed. Decision points are interconnected with

(a) Failure Mode 1

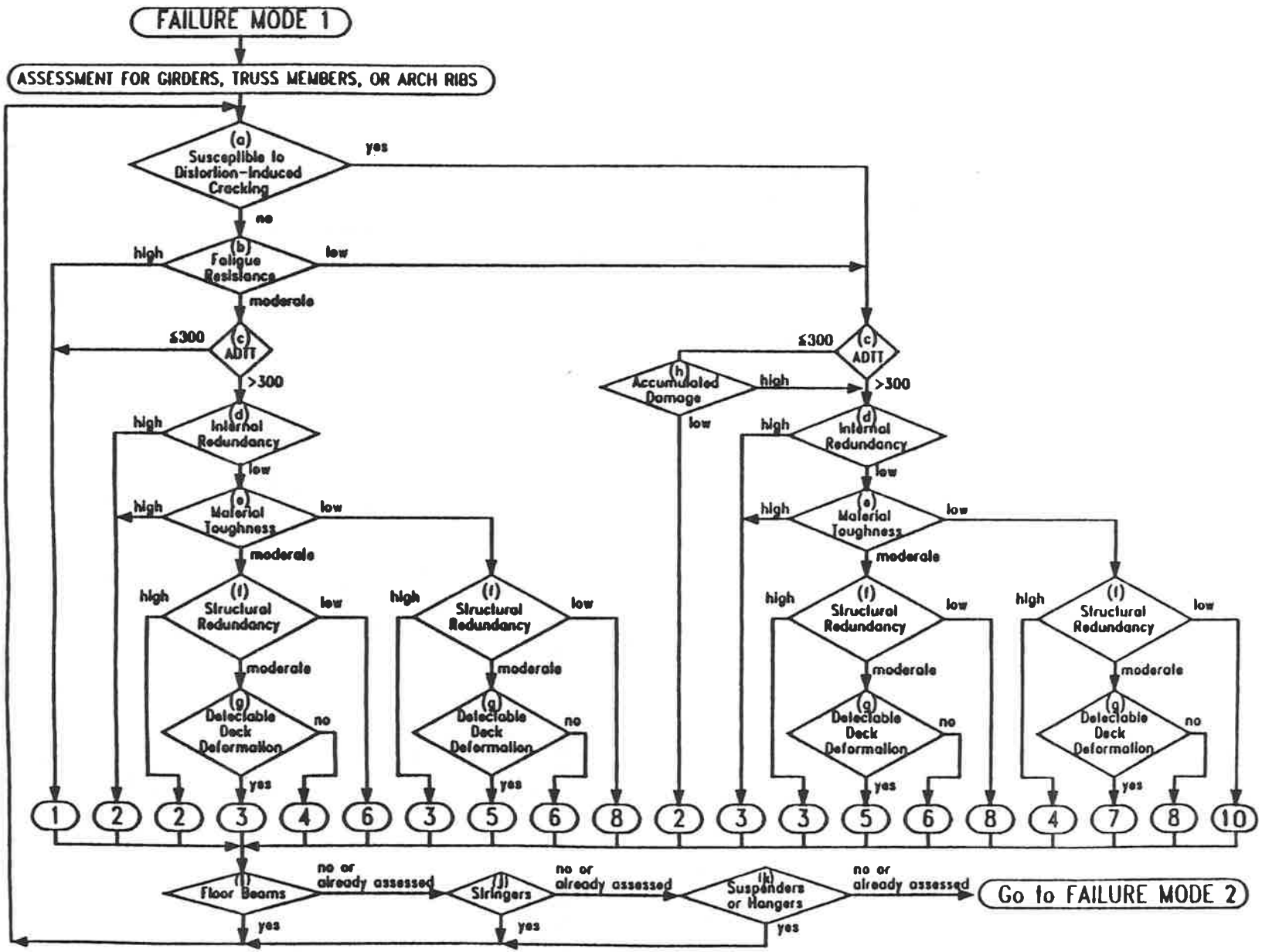

Figure 1. Vulnerability Assessment Flowchart

(b) **Failure Modes 2, 3, and 4**

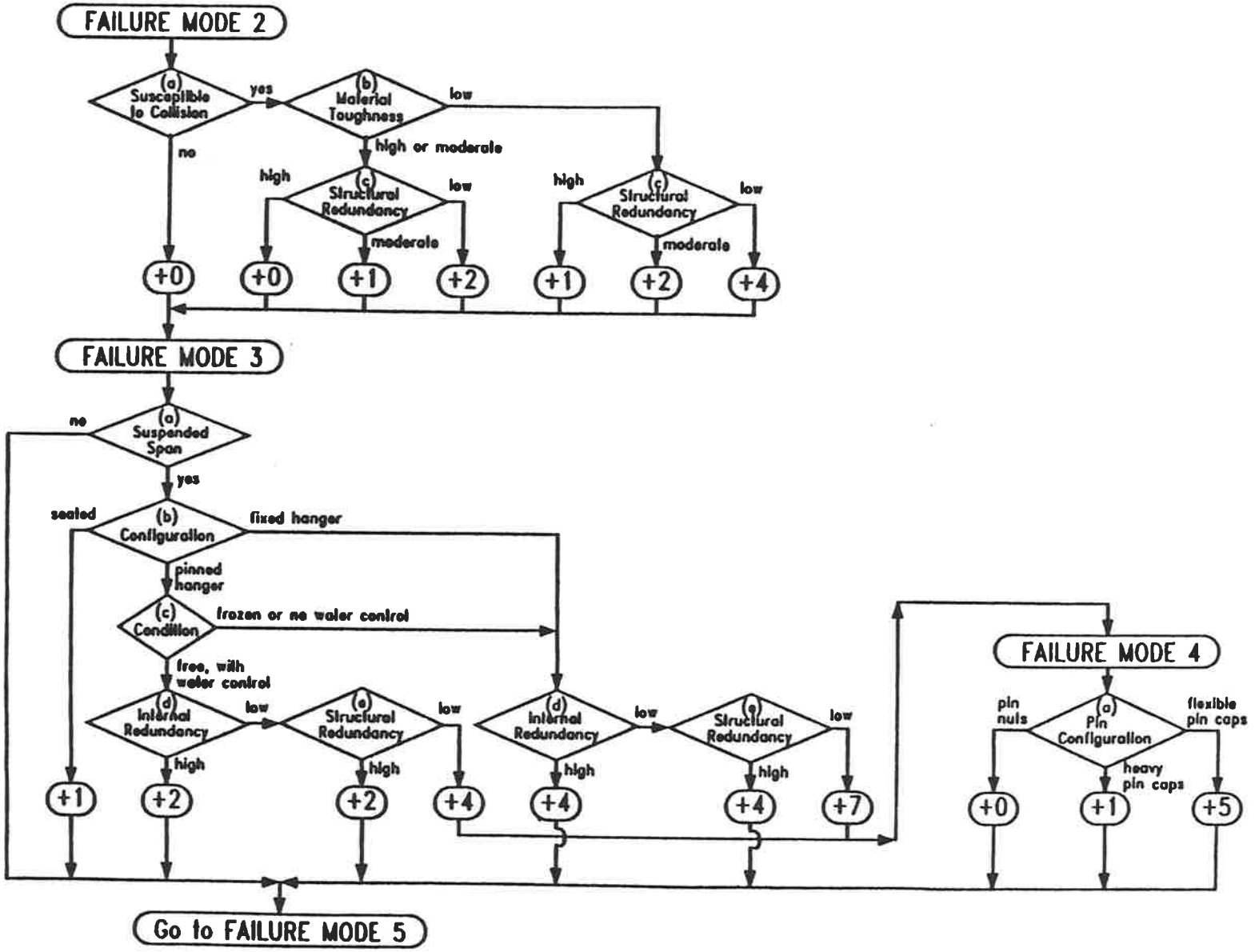

Figure 1. Vulnerability Assessment Flowchart (Continued)

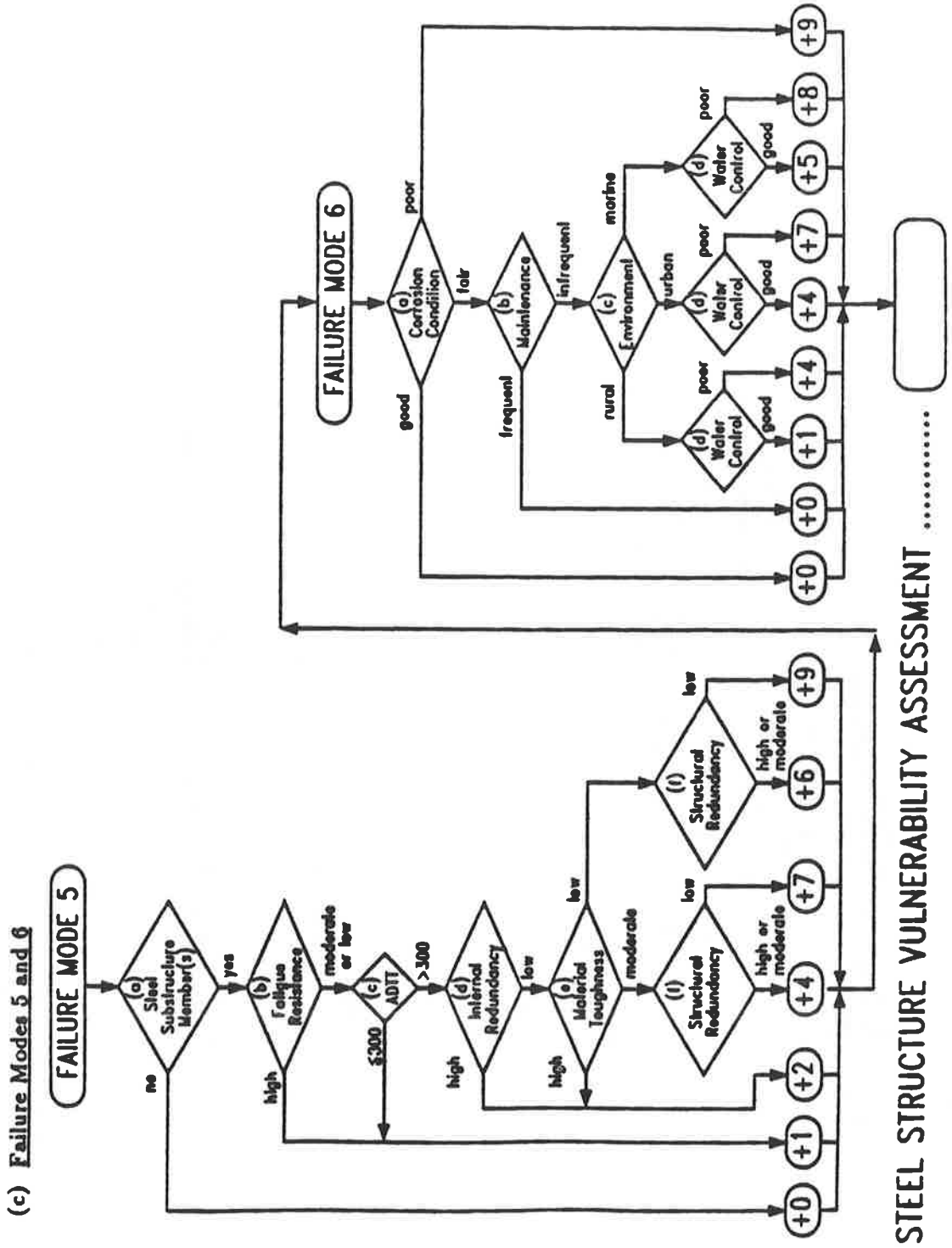

Figure 1. Vulnerability Assessment Flowchart (Continued)

lines, to form the logic network. Arrowheads are placed on the lines to show the direction of logical flow. Each possible path through the network yields a relative failure probability for each failure mode. The relative probabilities are contained in small ovals. The **TOTAL VULNERABILITY ASSESSMENT** (Figure 1(c)) is the sum of the six failure mode probabilities.

The logic network for Failure Mode 1, Figure 1(a), also contains a "loop" - a path which returns the user to the first decision point for certain types of bridges. The loop dictates that the vulnerability assessment for Failure Mode 1 must be performed more than once for any bridge which has floor beams, stringers, suspenders and/or hangers. Note that the vulnerability assessment for Failure Mode 1 may be performed as many as four times. The assessments for all passes through flowchart must be added together to obtain the total relative failure probability for Failure Mode 1. Thus the vulnerability assessment for Failure Mode 1 can take on any value from 1 to 40.

The loop in Failure Mode 1 is used because bridges with floor beams, stringers, suspenders, and/or hangers have additional significant failure modes. On a given bridge, main load-carrying members, floor beams, stringers, and hangers generally have very different characteristics. They are likely to have different susceptibilities to distortion-induced cracking, different fatigue resistances, and different degrees of internal and structural redundancy. They are also subject to different numbers of load cycles and somewhat different magnitudes of live load. Though the total vulnerability assessment for Failure Mode 1 can potentially be as high as 40, it is highly unlikely that the total will exceed 25 for an actual bridge. The reason is that floor beams, stringers, suspenders and/or hangers tend to have high or moderate structural redundancy. If one of these members fractures, numerous alternate load paths generally exist. Thus the individual vulnerability assessments of these three types of members will rarely, if ever, exceed 5 each, for a total of 15, which when added to the 10 from the first loop gives and overall total of 25.

It is acknowledged that fracture or fatigue failure of, say, a floor beam is not likely to be as serious as fracture of a main girder. A floor beam fracture may only result in a local deck failure, while a main girder fracture might well result in collapse of the structure. Note, however, that the definition of failure used in this paper does not discriminate between local failure and catastrophic failure. The significant point is that if a floor beam failure and a main member failure both constitute a "hazard to the traveling public", then they are, in effect, equally weighted failures, and the local failure is not a benign failure in this case.

RELATIVE FAILURE PROBABILITIES

The relative failure probabilities shown in the small ovals on the Vulnerability Assessment Flowchart are defined via a simple "calibration" process. Based on the observed frequency of distress in in-service steel bridges, Failure Model 1 is judged to be the predominant failure mode. For this reason, the maximum possible failure probability for Failure Mode 1 is used to calibrate the remainder of this flowchart. The maximum value for one pass through the Failure Mode 1 network is arbitrarily assigned a value of 10, and all other numbers in the flowchart are defined with respect to that value. For example, a value of 5 indicates that the corresponding path through the flowchart represents a probability of failure which is one-half that of the worst-case path for Failure Mode 1.

The total vulnerability assessment for all six Failure Modes can potentially take on any value from 1 to 74. The maximum value of 74 has no particular significance, since it is a relative probability. Experience using Figure 1 for vulnerability assessments of actual bridges indicates that the total vulnerability assessment will rarely exceed about 40 or 50 (2,3).

Though the relative failure probabilities indicated in the flowchart have been developed rationally, they are primarily the product of the experience and judgement of the authors and NYSDOT engineers. As such, they are subject to modification, based on future experience and observations of distress in steel bridges.

LEVEL OF SIMPLIFICATION

A deliberate attempt has been made to keep the flow chart as simple as possible. This is accomplished in two ways: (1) Only those decision points which are considered to have a significant influence on bridge vulnerability are included. (2) No more than three outcomes are defined for each decision point.

This level of simplification is judged to be appropriate, given the nature and intended use of the flowchart. It has been found that the addition of decision points or outcomes tends to cause a disproportionately large increase in the complexity of the logic network. As the logic network becomes more complex, subjective calibration of the relative likelihoods of failure becomes considerably more difficult. Large increases in complexity also render the flowchart too unwieldy for manual use.

Given that the Vulnerability Assessment Flowchart is simply a logical algorithm, it can be easily converted to a computer program or for use with an expert system. Such a program would not necessarily be constrained to any particular level of simplicity.

GUIDELINES FOR USE OF THE VULNERABILITY ASSESSMENT FLOWCHART

In order to ensure that vulnerability assessment is performed in a consistent manner, it is necessary to establish guidelines for selection of each possible outcome at each decision point in the Vulnerability Assessment Flowchart. A recommended set of decision criteria has been developed and is included in References 1, 2 and 3.

These guidelines are very specific in nature. As an example, consider the first two decision points in **FAILURE MODE 1**. Decision Point (a) is an assessment of "Susceptibility to Distortion-Induced Cracking". The guidelines specify that this decision point is to be answered with "yes" if any one of the following conditions exist:

- Narrow web gaps exist at transverse stiffeners, floor beam connection plates, or diaphragm connection plates. For

example, webs are susceptible to out-of-plane bending (9).

- Cantilever brackets or outriggers have tie plates which are connected to girder flanges. Tie plates are susceptible to high inplane bending stresses (9).
- Floor beams or stringers are coped. (Coped webs are susceptible to high bending stresses caused by excessive restraint at connection (9).

As another example the guidelines specify that Decision Point (b), "Fatigue Resistance", is to be answered with "low" if any of the following are true:

- One or more primary members are flagged because of known fatigue cracks.
- One or more primary members have large fabrication defects of poor welding workmanship, as evidenced by visual inspection; e.g., lack of fusion or cold cracking.
- Primary members have category E or E' details.
- Tack welds, plug welds, or other non-standard welds are present.

The complete guidelines establish similar criteria for selection of outcomes at all decision points in the flowchart which is shown in Figure 1.

APPLICATION OF THE VULNERABILITY ASSESSMENT MODEL

The vulnerability assessment model described above is applicable to a wide range of structural configurations, to include deck-girder, through-girder, box-girder, truss, and tied-arch bridges.

The model can be used to assess simply-supported spans, continuous spans, and suspended-span configurations. It is applicable to bridges with short and medium span lengths and to the floor systems of long-span structures.

Though the vulnerability assessment model has been developed principally for use by NYSDOT, its applicability is by no means limited to New York State bridges. The logic network of the flowchart is expected to be fully applicable to steel bridges in other states. The relative probabilities and guidelines may require minor modifications, based on local experience. For example, in those southern states where salt is not applied to roads in the winter, corrosion may be less significant and thus may warrant lower relative probabilities for Failure Mode 6. Similarly, the guidelines may require modification or augmentation as a result of differences in local design and inspection codes.

EXAMPLE VULNERABILITY ASSESSMENTS

As part of the development of the vulnerability assessment model, example vulnerability assessments have been performed for seven in-service bridges. Of these, six are New York State bridges. The seventh is the I-95 Bridge over the Mianus River near Greenwich, Connecticut, which failed catastrophically in 1983.

The results of these example vulnerability assessments are summarized in Table 1. The seven subject bridges are identified in column (a); a general description of each is provided in columns (b) through (h), and the corresponding vulnerability assessment is indicated in column (i). Bridges are ranked in order of decreasing vulnerability. The detailed information required for vulnerability assessments of the New York State bridges was readily available from NYSDOT's bridge inspection (BIN) files, construction drawings, and bridge management data base. Information on the I-95 Bridge was obtained from other sources. Step-by-step descriptions of the seven vulnerability assessments, which include the justifications for selection of outcomes at all decision points, are included in References 2 and 3.

In comparing the vulnerability assessments shown in Table 1, several interesting observations can be made:

- It is not surprising that the Mianus River Bridge is assessed as the most vulnerable of the seven bridges considered; however, the characteristics of the bridge which contributed to its collapse (suspended span supported by non-redundant pin-and-hanger assemblies with flexible pin caps) account for only a portion of its vulnerability assessment of 37. The Mianus River Bridge is assessed as highly vulnerable because it has a number of adverse characteristics which independently increase its probability of failure. These include low fatigue resistance of girders, floor beams, and stringers, a non-redundant superstructure configuration, and an adverse combination of fair corrosion condition, infrequent maintenance, and poor water control. The implication is that the pin and hanger detail which failed was only the weakest link in a chain with many weak links.
- Because it is a multi-girder bridge, the Harlem River Drive Viaduct might not be expected to be a highly vulnerable structure. Nonetheless, the vulnerability assessment model assigns it a relatively high vulnerability, primarily because it has a highly nonredundant steel pier cap with poor fatigue resistance.
- The Route 20A and Route 971V Bridges have relatively low vulnerability assessments, despite the fact that they are both two-girder bridges with suspended spans. The reason is that their riveted girders are internally redundant.
- The Route 971V Bridge is somewhat less vulnerable than the Route 20A Bridge because its pin-and-hanger details have been retrofitted with steel rods, to improve their internal redundancy.
- The Ramp from CR 80 is the least vulnerable of the seven subject bridges, for two reasons: First, it is simply configured, with no suspended spans, floor beams, stringers, or steel substructure members. Second, the bridge has a heavy bracing system designed to stiffen its curved girders torsionally; this bracing system greatly improves the structural redundancy of the superstructure.

Note that the relative vulnerability of each bridge is controlled by a different set of contributing factors. Thus these examples serve to illustrate the fundamental concept of the vulnerability assessment model - that no single structural characteristic or condition rating can be used to consistently assess the vulnerability of every bridge. Rather, bridge vulnerability is a function of many contributing factors.

TABLE 1 – SUMMARY OF EXAMPLE VULNERABILITY ASSESSMENTS

a. BRIDGE	b. SUPERSTRUCTURE TYPE	c. SPANS	d. MAIN MEMBERS	e. FLOOR BEAMS	f. STRINGERS	g. HANGERS/ SUSPENDERS	h. SUB STRUCTURE	i. VULNERABILITY ASSESSMENT
1. I-95 Bridge over Mianus River	Deck Girder	3-Anchor 2 Suspended	2 Welded Plate Girders	Welded	Rolled	None	Concrete Piers	37
2. Water Ford Mechanicville Bridge over D & H R.R.	Through Girder	2 Continuous	2 Welded Plate Girders	Rolled w/Welded C.PLs	None	None	Concrete Piers and Abutments	21
3. Harlem River Drive Vidaduct	Deck Girder	Multiple Simply Supported	4 or 5 Rolled Sections with Welded C.PLs	None	None	None	Concrete and Steel Piers	21
4. Robert Moses Causeway Bridge over Great South Bay	Through Truss	2 Anchor 1 Suspended (Tied Arch)	Riveted Truss Box Sections	Welded	Rolled	Riveted Box Sections	Concrete Piers	16
5. Rt. 20A Bridge over Cazenovia Creek	Deck Gider	2 Anchor 1 Suspended	2 Riveted Plate Girders	None	None	None	Concrete Piers and Abutments	11
6. Rt. 971V Bridge over Black River	Deck Girder	2 Anchor 1 Suspended	2 Riveted Plate Girders	Rolled	None	None	Concrete Piers and Abutments	8
7. Ramp from CR 80	Deck Girder	2 Simply Supported	3 Welded Plate Girders (Curved)	None	None	None	Concrete Piers	5

CONCLUSION

Vulnerability assessment and ranking constitute only one step in a comprehensive bridge safety assurance program. They should be followed by more detailed analyses of bridges identified as vulnerable. They should also be supplemented by traditional methods of assessment, such as load and condition rating.

The consequences of failure should also be used to set priorities for bridges having equal or near equal high vulnerability assessments. For example, a bridge in a densely populated area, where detouring of traffic may result in a major disruption of commerce and severe economic impact has a high consequence of failure and should receive higher priority for repair, retrofit or rehabilitation.

Failure modes not included in the model can be considered separately as NYSDOT is currently doing with scour, earthquake, and other failure modes (2, 3). The severity of a given failure mode (within the broad definition of failure) might also serve as a useful "discriminator" in the vulnerability ranking of bridges with approximately equal vulnerability assessments.

The vulnerability assessment model is only a tool - one of many already available to bridge engineers. Its true value is that it fulfills a particular need which cannot be satisfied by any of the existing tools.

REFERENCES

1. Ressler, S.J. and Daniels, J. Hartley, VULNERABILITY ASSESSMENT OF STEEL HIGHWAY BRIDGES: A PROBABILISTIC MODEL, Advanced Technology for Large Structural Systems (ATLSS) Report No. 90-01, Lehigh University, Bethlehem, PA 18015, January 1990.

2. Bridge Safety Assurance Task Force, SAFER BRIDGES FOR NEW YORK-VOLUME I, Final Report of the Bridge Safety Assurance Task Force to the New York State Commissioner of Transportation, 1990.

3. Bridge Safety Assurance Task Force, SAFER BRIDGES FOR NEW YORK-VOLUME II (APPENDICES), Final Report of the Bridge Safety Assurance Task Force to the New York State Commissioner of Transportation, 1990.

4. Benjamin, J.R. and Cornell, C.A., PROBABILITY, STATISTICS, AND DECISION FOR CIVIL ENGINEERS, McGraw-Hill, New York, 1970.

5. Demers, C.E. and Fisher, J.W., A SURVEY OF LOCALIZED CRACKING IN STEEL BRIDGES, 1981 to 1988, Advanced Technology for Large Structural Systems (ATLSS) Report No. 89-01, Lehigh University, Bethlehem, PA 18015, July 1989.

6. Fisher, J.W., Yen, B.T., Wang, D. and Mann, J.E., FATIGUE AND FRACTURE EVALUATION FOR RATING RIVETED BRIDGES (Final Report), Fritz Engineering Laboratory Report No. 499-3(87), Lehigh University, Bethlehem, PA 18015, December 1987.

7. Lenox, T.A. and Kostem, C.N., THE OVERLOADING BEHAVIOR OF DAMAGED MULTIGIRDER STEEL BRIDGES, Fritz Engineering Laboratory Report No. 432.11, Lehigh University, Bethlehem, PA 18015, March 1988.

8. Daniels, J.H., Kim, W. and Wilson, J.L., GUIDELINES FOR REDUNDANCY DESIGN AND RATING OF TWO-GIRDER STEEL BRIDGES, National Cooperative Highway Research Program Report 319, Transportation Research Board, Washington, D.C., 1989.

9. Fisher, J.W., FATIGUE AND FRACTURE IN STEEL BRIDGES: CASE STUDIES, John Wiley and Sons, New York 1984.

Evaluation of Bridge Vulnerability to Hydraulic Forces, Stream Instability, and Scour

E. V. RICHARDSON AND FRANK W. HUBER

The principal causes of failure of bridges over rivers and streams are scour at the foundations, channel movement and hydraulic forces. Scour is the removal of material from around piers and abutments due to extreme flows, ice jams or debris which destroy the foundation support and result in excessive settlement or movement and loss of support for the superstructure. Channel movement is the natural realignment of the river channel so that the stream encroaches on a pier, abutment or bent, resulting in failure from scour as described above. In addition, channel movement can erode the approaches to the bridge. Hydraulic forces from the impact of ice or debris against a pier, abutment or superstructure can cause dislocation of the bridge elements. Buoyancy and flotation, as the result of submergence, can also dislodge bridge decks off of their supports. A procedure for conducting a comprehensive hydraulic evaluation of existing bridges to determine their vulnerability to scour, stream instability, and hydraulic forces is given in this paper. The procedure is based on the five step process recommended in the September 1988 FHWA Technical Advisory on Scour (1).

The September 1988 FHWA Technical Advisory titled "Scour at Bridges" (1) recommended that the states develop and implement a program to evaluate every bridge over a stream, whether existing or under design, to determine its vulnerability to floods in order to determine prudent measures to be taken for its protection. The Advisory stated:

"Most waterways can be expected to experience scour over a bridge's service life (which is now approaching 100 years). Exceptions might include waterways in massive, competent rock formations where scour and erosion occur on a scale that is measured in centuries..... The added cost of making a bridge less vulnerable to scour is small when compared to the total cost of a failure which can easily be two or three times the original cost of the bridge itself. Moreover, the need to ensure public safety and to minimize the adverse effects stemming from bridge closures requires our best effort to improve the state-of-practice of designing and maintaining bridge foundations to resist the effects of scour."

The Advisory and accompanying document titled "Interim Procedures for Evaluating Scour at Bridges" further recommended that the evaluation of existing bridges should be carried out by an interdisciplinary team comprised of structural, hydraulic, and geotechnical engineers. The risk of failure should be determined for scour resulting from a superflood with a recurrence interval of once in 500 years. The five step procedure contained in the Interim Procedures should be used by the states to identify bridges most susceptible to scour damage, establish a priority list for evaluation, and develop a plan of action for those bridges determined to be scour critical. The plan of action "should include instructions regarding the type and frequency of inspections to be made at the bridge, particularly in regard to monitoring the performance and closing of the bridge, if necessary, during and after flood events. ...The plan of action should include a schedule for timely design and construction of scour countermeasures determined to be needed for the protection of the bridge." It was left to the states to develop their own procedures for evaluating the vulnerability of existing bridges to scour. A procedure developed by the Minnesota Department of Transportation was given in the Interim Procedures.

This paper presents a procedure that was developed for the New York State Department of Transportation and the Colorado Highway Department to evaluate and categorize the scour vulnerability of their existing bridges.(2,3) Methods of calculating scour, or scour countermeasures, are not given in the paper as these were given in the Interim Procedures (1), HEC 18 (4), HEC 20 (5) and Highways in the River Environment (6).

OVERVIEW

All the bridges over water are to be evaluated. However it is crucial that the

Resource Consultants, Inc., Ft. Collins, Co.
Edwards and Kelcey Engineers, Inc.,N. Y., N. Y.

most scour critical bridges be identified first and either replaced or provided with interim protection. To do this it was decided to divide all bridges over water into four categories on the basis of their scour susceptibility and then rank them in each category by their scour vulnerability. The four categories are 1) MOST SCOUR CRITICAL, 2) MEDIUM SCOUR CRITICAL, 3) LOW SCOUR CRITICAL, and 4) NOT SCOUR CRITICAL. Bridges in category 1 would be replaced or receive interim protection first. Then the next category and so on. Flow charts were developed to help in evaluating the bridges as to their scour susceptibility and to rank the bridges in each category. The ranking is based only on scour susceptibility.The evaluation is a five step procedure. The steps are as follows:

- Step 1. Screening the entire bridge population to compile a list of those bridges with actual or potential scour vulnerability.
- Step 2. Establish priorities, by conducting a preliminary office and field examination to categorize the bridges identified in step 1 as to scour susceptibility and then ranking the bridges in each category as to scour vulnerability. The following factors are to be used as a guide:
  (a) The potential for bridge collapse or for damage to the bridge in the event of a major flood.
  (b) The functional classification of the highway on which the bridge is located, and the effect of a bridge collapse on the safety of the travelling public and on the operation of the overall transportation system for the area or region.
- Step 3. Determine a plan of action and interim protection for correcting the scour problem for bridges identified as most scour critical in step 2 (Category 1).
- Step 4. Perform a detailed hydraulic, structural and geotechnical evaluation of the most scour critical bridges as determined in step 2 to determine final action to repair or replace the bridge and design appropriate scour countermeasures. This detailed evaluation is to be done taking in consideration the developed priority list.
- Step 5. Evaluate the bridges in the other categories in accordance with the priority list.

Note 1. In the above procedure, some of the activities can be conducted concurrently.
Note 2. The above procedure should be carried out for all bridges, regardless of ownership.

DETAILED PROCEDURE

I. Step 1. Compile a list of potential scour vulnerable bridges.

Determine all bridges that are over water on the basis of the bridge inventory data.

II. Step 2. Prioritize the list determined in step 1.

The priorities would be established in a two part process. Part one would categorize the bridges as to scour vulnerability and Part two would rank the bridges as to scour vulnerability in each category.

Part One

Divide the list derived in Step 1 into four categories. (1) MOST SCOUR CRITICAL, 2) MEDIUM SCOUR CRITICAL, 3) LOW SCOUR CRITICAL, and 4) NOT SCOUR CRITICAL.)

The procedure consists of the following:

1. Office review of the data base to divide the bridges into the four scour susceptibility categories.
2. Field inspection of bridges in the medium scour category or indeterminate from the office review.

Office Review

The office review would divide the bridges into the four categories on the basis of the following criteria.

1. Bridges over water with piers whose foundations are on spread footing without piles and not on solid rock.
2. Bridges with piers in water with foundations on shallow piles.
3. Bridges over water with vertical wall abutments with foundations on spread footing without piles and not on solid rock.
4. Bridges over water with vertical wall abutments with foundations on shallow piles.
5. Bridges over streams with lateral movement that may erode abutments, piers or bents.
6. Bridges with piers in water with foundations on wood piles.
7. Bridges over water with vertical wall abutments with foundations on wooden piles.
8. Bridges over water with spill-through or stub abutments with foundations on spread footing without piles and not on solid rock or have shallow or wooden piles.
9. Bridges over water where the water is a lake, canal, ditch or other slow

moving water that will not cause scour.

10. Bridges over water with abutments and piers with foundations on solid rock or with adequate piles.

Category 1 bridges are those that fall in classifications 1, 2 and 3.
Category 2 bridges are those that fall in classifications 4, 5, 6 and 7.
Category 3 bridges are those that fall in classification 8 and 9.
Category 4 bridges are all others.

The office review would also compile the following data on the bridges.

1. Bridge over water or relief bridge subject to water.
2. Type of water and name.
   a. River
   b. Canal
   c. Estuary
   d. Lake
   e. Swamp
3. Geologic area or region.
4. Stream Slope at bridge. From USGS map.
5. Pier or piers in the flow.
6. Abutment in flow or subject to flow. (yes, no)
7. Abutment Type
8. Foundations
   a. Piers on piles. (yes, no) Depth _____
   b. Abutments on piles. (yes, no) Depth _____
   c. Scour countermeasures. (yes, no) Type _____
9. Debris possible problem. (yes, no)
10. Ice possible problem. (yes, no)
11. Channel movement possible problem. (yes, no)
12. River characteristics.
    a. Slope.Steep (S > .0015 ft/ft)_____ Medium (.0015< S <.0004)_____ or Mild (S <.0004)_____
    b. Flash floods (peaks in hours not days).
    c. Meandering, straight or braided.
    d. Incised, floodplain.
    e. Size (Use Drainage Area).
    f. Stream bed (rock, glacial till, or alluvium).
13. Floods.
    a. Q_{50}
    b. Q_{100}
    c. Largest observed Q and date.
    d. Next Largest observed Q and date.
    e. Flood studies. Who?
14. Traffic volume.

Field Review

Examine in the field those bridges identified as category 2 scour susceptible or bridges for which the office review does not provide sufficient data to clearly determine the proper category. On some of the bridges, this examination could determine the interim scour protection asked for in step 3.

The field review should be made by staff knowledgeable about hydraulics and river mechanics. In some cases (bridges) it may be necessary for the Geotechnical and/or Structural Engineers to examine the site. An example of the latter would be if the Hydraulic Engineers were not sure of the resistance to scour of the rock the foundation is set in.

The criteria for the classification into most, medium, least and not scour critical would be the same as in the office review.

The field review would examine each site to determine the following:

1. Is there evidence of scour or deposition at the piers or abutments?
2. Are there channel conditions, such as a bend, that increases the scour risk?
3. Is there deposition in part of the bridge section that decreases the flow area?
4. Does the angle of attack of the flow on a pier or abutment increase the scour risk?
5. Are there conditions at the bridge that decrease its vulnerability to scour? For example, local aggradation of the bed, downstream controls that decrease scour, foundations in bed rock, etc.
6. What is the potential for contraction scour? That is, are the overbank flow area and the natural banks so vegetated that the discharge and the velocity of the returning flow would be small? Or do the conditions represent the laboratory conditions from which the equations were developed.
7. What is the potential for long term scour or deposition?
8. What is the potential for local scour at the abutments?
9. What is the potential for local scour at the piers?
10. What is the potential for movement undermining abutments, piers or bents in the channel or floodplains.

The field examination could also determine the type and extent of field data measurement needed for the detailed evaluation called for in step 4. In addition, the type of intermediate scour protection could be decided. It is estimated that this field examination would take about a few hours per bridge. To aid in this office and field review, scour susceptibility flow charts are given in the next section.

Scour Susceptibility Flow Charts

The scour susceptibility of bridges is to be evaluated by the use of two flow charts: The Office Review Flow Chart, followed by the Field Review Flow Chart.

It is expected that information required to complete the Office Review Flow Chart is available in the bridge data base. The primary function of the Office Review Flow Chart is to quickly identify those bridges that are clearly the most scour susceptible, as well as those which are clearly not scour prone. For bridges identified as the most susceptible (Category 1) and least susceptible (Category 3) to scour, proceed to the Vulnerability Ranking Flow Chart following the Office Review. For bridges identified with medium susceptibility to scour (Category 2) proceed to the Field Review prior to the Vulnerability Ranking Flow Chart. The purpose of the Field Review is to refine the Office Review to identify bridges in Category 2 that should be placed in Category 1, 2 or 4.

Office Review Screening Flow Chart The Office Review Flow Chart eliminates from further consideration structures that are not over water, structures that do not have a pier or abutment in the floodplain, those bridges that lateral movement of the stream would not scour abutments, piers or bents and those whose foundations are placed on non-scourable foundation material. Non-scourable material is considered to be durable rock that is not susceptible to significant deterioration due to weathering and that scours at such a slow rate that changes occur over a long period of time, measured in centuries. If the response to all of these parameters is other than above or unknown, the path proceeds to evaluation of stream velocity.

Structures that are concrete box culverts with bottom slabs and structures that experience predominately static flow conditions or slow velocities, such as expected for a lake, canal or ditch, etc., warrant additional evaluation to identify scour prone facilities, primarily based on historic scour problems.

It is expected that the bi-annual inspection, underwater reports and bridge folders will provide the required information. A scour rating above 5, with no notes describing previous scour or potential scour producing problems, eliminates the structure from further consideration. However, a rating below 5 or the presence of notes describing scour history or potential, yields the need for further evaluation. For bridges, the evaluation proceeds to the assessment of pier and abutment foundations. Culverts requiring further evaluation are placed in category 3 and ranked at the highest priority in this category.

Bridges with foundations (abutments, piers or bents) that are not in the channel or floodplain and not subject to scour from lateral movement of the stream are eliminated from consideration. If the above is not true then proceed with the office review.

Recognizing that scour susceptibility is primarily a function of the foundation type, evaluation of pier and abutment foundation data expected to be contained in the data base and bridge folder permits separation of the bridges into the three scour susceptibility categories. Pier foundations with spread or unknown footing conditions and vertical wall abutments on spread or unknown footings or with piles less than 20 feet long are considered most susceptible to scour. This is because the worst case pier scour depth is approximately 2.3 times the pier width, accounting for debris and ice jams, and is, therefore, usually greater than the normal depth of spread footings, and usually exceeds five feet. Similarly, piles less than twenty feet long are considered scour prone because the embedment remaining subsequent to scour may be inadequate to provide the required support.

Pier foundations on solid wood piles greater than 20 feet long and vertical wall abutments on long piles are considered to be of medium scour susceptibility because the additional embedment is expected to provide adequate support during a flood and inspection after will determine if countermeasures are needed prior to the next flood. Spill-through abutments with spread or unknown footing conditions or short or wooden piles are included in the medium category because the expected scour is approximately one half the amount experienced at vertical wall abutments. All other pier and abutment configurations are considered to be the least susceptible to scour.

Bridges classified as having medium susceptibility to scour are further evaluated using the bi-annual inspection report and scour notes, in a manner similar to that previously described for streams with slow velocity, to identify locations that should be in the most susceptible category because of historic or potential scour problems. Bridges considered the least susceptible to scour are similarly evaluated. The bridges that are thus elevated to the next higher susceptibility category will, therefore, receive a more detailed vulnerability ranking earlier than otherwise.

OFFICE REVIEW
SCREENING FLOWCHART TO DETERMINE SCOUR SUSCEPTIBILITY OF EXISTING BRIDGES

BRIDGE # _____ FEATURE CARRIED _____ STREAM _____

COMMUNITY _____ COUNTY _____

BRIDGE TYPE _____ SPANS _____

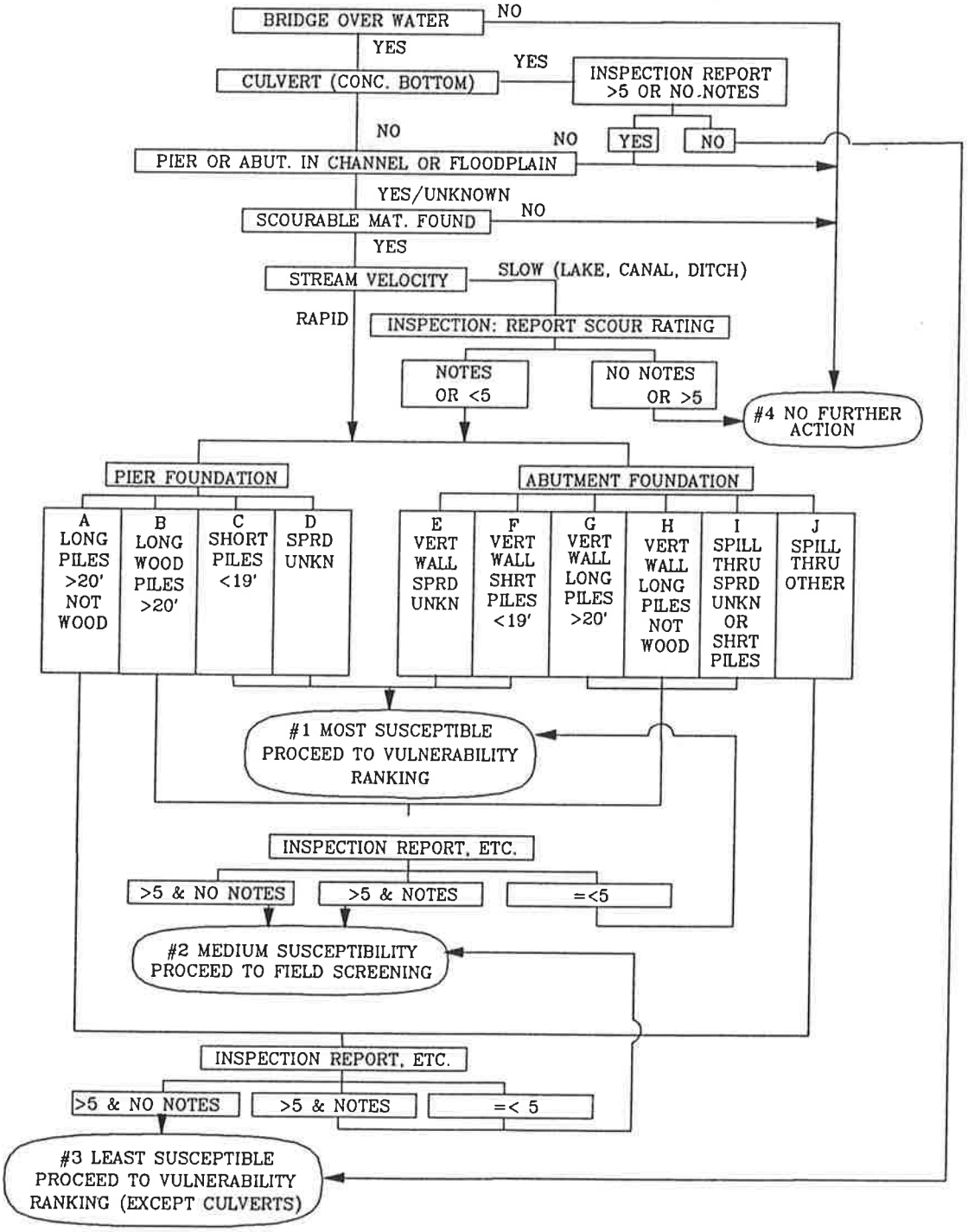

It is expected that the detailed vulnerability ranking will be performed for the most susceptible bridges as soon as possible after their identification in this category. Similarly, the field Screening and vulnerability ranking of bridges with medium susceptibility should proceed as soon as possible after their identification in this category. Vulnerability ranking of the least susceptible bridges (Category 3) may be postponed until the ranking of the other two categories is complete.

Field Review Screening Flow Charts The Field Review Screening Flow Chart for bridges with medium susceptibility to scour provides an intermediate step for these bridges prior to the detailed vulnerability ranking to identify bridges in this category that should be elevated to the most susceptible category. The field review will permit the identification of bridges whose abutments and piers are located beyond the floodplain, have abutments, piers or bents not subject to scour by lateral stream movement or whose foundation is on non-scourable material and, therefore, do not warrant further consideration. Presence of the other parameters warrants leaving the structure in category 2 or elevating it to the most scour susceptible category.

Evidence of a limited amount of previous scour or deposition of material does not warrant a change in the category. However, evidence of one foot or more of scour warrants elevation to the higher category because the actual scour depth is probably larger, although the magnitude is uncertain. Similarly, extensive deposition, particularly where it appears to restrict flow, warrants elevation.

Intensification of the potential for scour as a result of the following parameters warrants elevation to the most susceptible category for the following reasons:

1. Angle of Attack - The pier scour equation includes the angle of attack that clearly increases the expected scour depth.
2. River Bend - The abutment or pier on the outside of a bend clearly experiences higher velocity and resultant potential scour depth.
3. Potential Pier Scour - The maximum expected scour can be approximated using the method developed by Chang (1) from a study of all relevant data and equations.
4. Recognizing that spread footings are normally approximately three or four feet below the stream bed, potential pier scour exceeding this amount is a concern. Similarly, pile supported structures that experience material removed from the majority of the pile length are a concern.
5. Potential for Abutment Scour - Extensive vegetation on the encroachment embankment and on the stream overbank, particularly at the top of bank parallel to the direction of stream flow, limits potential abutment scour.
6. Potential for Contraction Scour - Severe restriction of the floodplain, particularly where relief is not possible through a structure or by overtopping, is a concern.
7. Stream movement that could undermine abutments, piers or bents.

Completion of the Field Review Screening Flow Chart increases confidence in the division of structures into the three scour susceptibility categories. It is recommended that the field data required for the scour vulnerability ranking should be gathered concurrently with the data for the Field Review Flow Chart to maximize the value of the field evaluation.

Part Two

Ranking the bridges in each category as to scour vulnerability.

Scour Vulnerability Ranking Flow Charts

The ranking of the scour vulnerability of bridges in each scour category is obtained by flow charts that evaluate the vulnerability on the basis of the bridges geologic, hydraulic and river conditions as well as the conditions of the bridges foundation (abutments and piers).

The purpose of the Vulnerability Ranking Flow Charts is to provide a procedure to prioritize the list of scour susceptible bridges by determining the relative scour vulnerability of all bridges in each scour susceptibility category. The numerical values included in the flow charts were selected to give the relative effect of each parameter on the potential to produce scour. For example, the river slope/ velocity parameter for steep, medium and mild conditions is valued at "2," "1" and "0" respectively because a steep slope will produce deeper scour than a medium slope, which is more likely to have deeper scour than a mild slope. The values in each parameter are such that the most scour vulnerable bridge will have the largest value. More than one bridge can have the same value of vulnerability.

The value of the vulnerability ranking is that it orders a bridge relative to other scour vulnerable bridges, and other things being equal (traffic counts for example)

FIELD REVIEW
SCREENING FLOWCHART TO DETERMINE SCOUR SUSCEPTIBILITY OF EXISTING BRIDGES

BRIDGE # _____ FEATURE CARRIED _____ STREAM _____

COMMUNITY _____ COUNTY _____

BRIDGE TYPE _____ SPANS _____

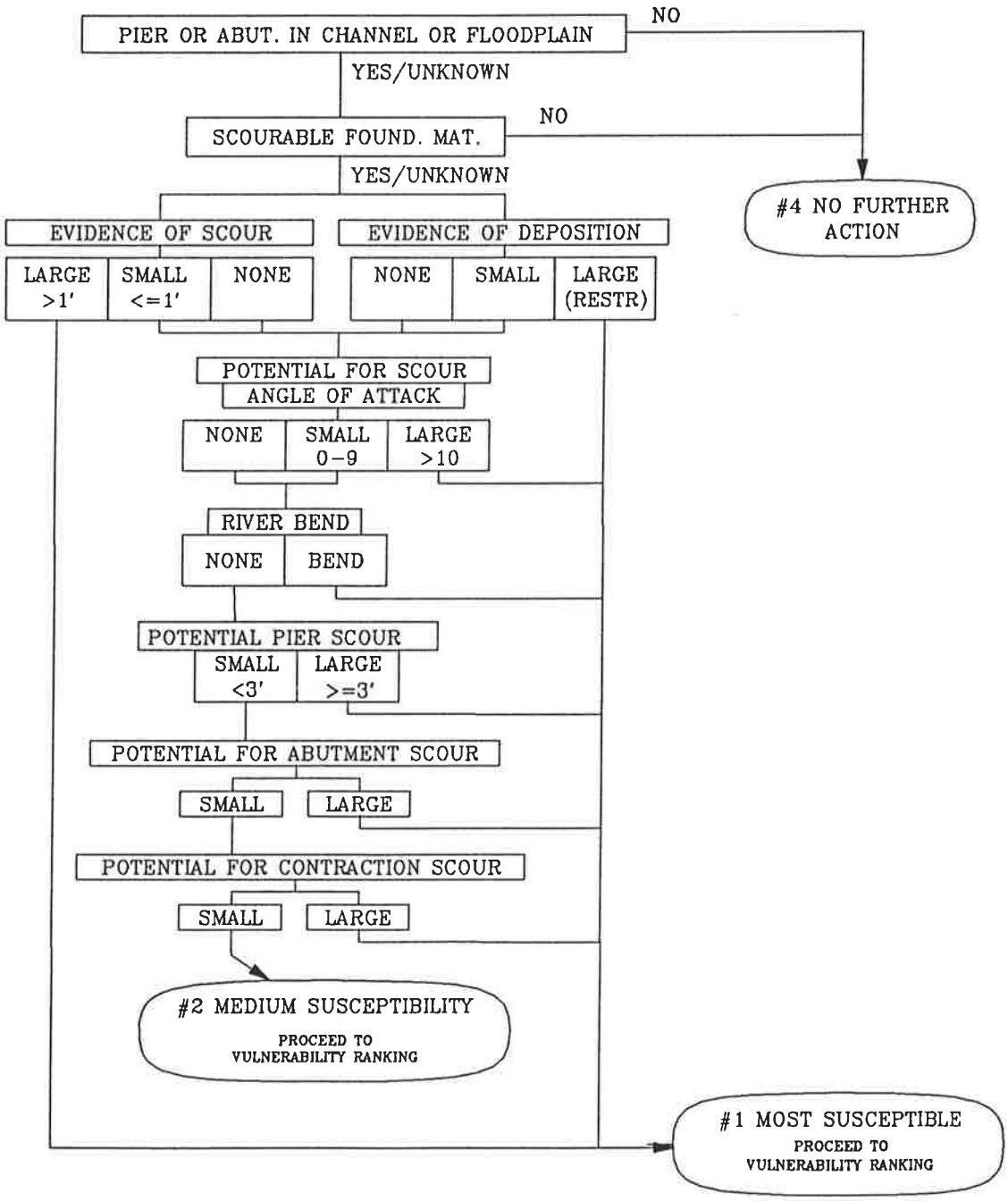

determines what bridge should be repaired or replaced first.

The Scour Vulnerability Ranking has three flow charts. They consider: 1) General Considerations, 2) Abutments and 3) Piers, which proceed sequentially. It is possible that field evaluation of the bridge may be required to complete the ranking.

General Conditions Flow Chart The General Conditions Flow Chart addresses parameters that have a general impact on the potential scour depth. The need for intermediate scour countermeasures is included in the flow chart to remind the evaluator to identify this need. No vulnerability ranking value is assigned to this parameter because it is expected that the countermeasures will be implemented before the detailed scour evaluation and installation of remedial measure is complete. The intermediate scour countermeasures are intended to protect the bridge from catastrophic failure until the design and construction of remedial measures is completed.

The remaining parameters are included for the following reasons:

1. River Slope/Velocity - A steeper/faster flowing stream is expected to experience more severe scour than one with a medium or mild slope. The stream slope is defined as follows:
   a. Steep $S > 0.0015$ ft/ft
   b. Medium $0.0015 < S > 0.0004$ ft/ft
   c. Mild $S < 0.0004$ ft/ft
2. Channel Bottom - An agrading condition is given a value of 0 because the slight deposition represented reflects a decrease in scour potential. Severe deposition that restricts capacity is addressed later in the flow chart. A stable channel condition is, therefore, given a value of 1 because it represents a more scour-prone condition than aggradation. Similarly, a degrading channel is given a value of 2.
3. The channel bed material is ranked because rock would take more time to erode to maximum scour than sand. The other materials indicated also would take more time to erode. Thus, in ranking bridges to scour vulnerability, the bridge that takes longer for scour to reach its maximum value would be less vulnerable.
4. Channel Configuration - A meandering channel is given a value of 2 and a braided channel is given a value of 3 to reflect the relative scour potential of each. A straight channel, defined as exhibiting a sinuosity of less than 1.5, is given a value of 0, because it is the least likely to affect scour. However, if a straight channel has bar formations that shift the thalweg, it should be given a value of 1.0.
5. Channel Migration - Channel migration can undermine abutments, piers or bents in the channel, on the floodplain or near the floodplain and thus warrant a 3.
6. Debris/Ice Problem - Watershed, river conditions or pier and abutment configurations that promote debris and ice accumulation, primarily as indicated by historic records or field observations, warrant a value of 1 because the accumulation increases potential scour depth by either reducing the conveyance area or by increasing the effective pier width.
7. Near River Confluence - The potential for increased flow and river velocity near a river confluence and the resultant scour potential, warrants use of the value of 1 for this condition.
8. Affected by Backwater - Locations affected by backwater for all flow conditions, primarily resulting from proximity to a dam, warrants use of a value of 0. For this condition backwater from a downstream waterway should not be considered because it may not occur concurrently with peak flow and velocity on the tributary and at the location being studied.
9. Historic Scour Depth - Historic scour indicates a clear potential for continued and increased scour activity. Historic scour depths in excess of 3 feet are a concern because spread footings are seldom deeper than this.
10. Historic Maximum Flood Depth - Flow depth is a parameter in the scour prediction equations. Deeper flow is expected to produce greater scour.
11. Adequate Opening - An inadequate opening is expected to produce greater scour than an adequate one, therefore, a value of 2 is assigned to this condition. This parameter also addresses the deposition of material in the channel at the structure to the point that the capacity of the bridge opening is restricted. Bridges that experience overtopping and thus have pressure flow should also be given a 2.
12. Overflow/Relief Available - The ability of the design flow to proceed downstream by a means other than through the structure, usually by way of a relief structure or by overtopping the roadway embankment,

GENERAL CONDITIONS
SCOUR VULNERABILITY RANKING FLOW CHART

BRIDGE # _____ FEATURE CARRIED _____ STREAM _____

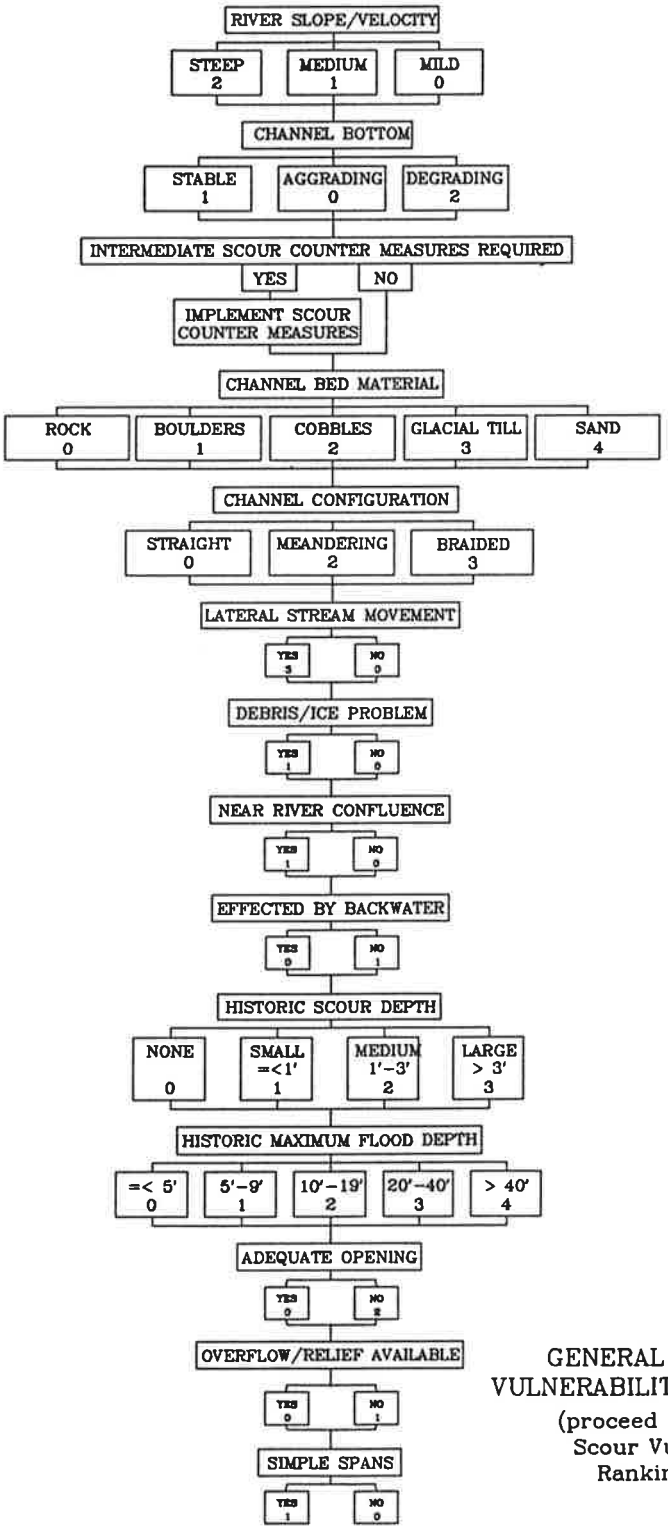

GENERAL CONDITION VULNERABILITY SCORE_____

(proceed to Abutment Scour Vulnerability Ranking Chart)

reduces the scour potential at the structure being evaluated because the resultant discharge and velocity are less than would otherwise be the case.

13. Simple Spans - This parameter recognizes that the ramifications of scour at simple span structures is more severe than would occur for structures with alternate load paths. Structures with alternate load paths probably would not experience catastrophic failure due to the loss of some foundation material.

The sum of the vulnerability ranking scores is tabulated at the bottom of the form before proceeding to the abutment vulnerability ranking flow chart.

Abutment Vulnerability Flow Chart The Abutment Vulnerability flow chart is intended to evaluate the relative vulnerability of a bridge to scour considering factors that affect abutment scour. A separate evaluation is provided for each abutment because the scour producing parameters may vary at each one, although it is expected that the abutment foundation configuration will remain the same. The left and right directions are established looking downstream. The parameters evaluated in the Abutment Vulnerability Ranking Flow Chart reflect their relative effect on scour vulnerability as discussed for the office review flow chart. The rationale for their use follow:

1. Scour Countermeasures - Installation of a wall or spur dike (guide bank)represent a relatively permanent countermeasure and are, therefore, provided the lowest value. Riprap and other countermeasures are considered temporary and are, therefore, given a higher value. The absence of scour countermeasures warrants assignment of the highest value. Locations that do not require scour countermeasures, as indicated in the general conditions flow chart, should be given a value of 0 for this parameter.
2. Abutment Foundation - The value assigned to each classification of abutment configuration and foundation type reflects their relative susceptibility to scour as discussed for the office review flow chart.
3. Abutment Location on River Bend - An abutment located on the outside of a bend is more susceptible to scour than one on the inside of the bend or one on a straight channel and is, therefore, given a higher value than the other conditions.
4. Angle of Inclination - The angle of inclination is determined in accordance with Figure 4.11 of the Technical Advisory (1). Relative values are assigned to each range of angles.
5. Embankment Encroachment - The magnitude of the scour encroachment is reflected in most of the abutment scour equations, therefore, this parameter is included in the chart. A large encroachment would be considered one that substantially reduces the overbank flow area available for the conveyance of peak discharges. A small encroachment would be considered one that impacts less than 10 percent of the total discharge for the design discharge.

The abutment vulnerability score for each abutment is tabulated and summarized at the bottom of the form. The intermediate vulnerability score from the general conditions flow chart is also tabulated and added to the total abutment score to yield the subtotal, which is the final score, if the bridge does not have any piers. The presence of piers necessitates continuation of the evaluation by proceeding to the pier vulnerability ranking flow chart.

Pier Vulnerability Flow Chart The Pier Vulnerability Flow chart is intended to evaluate the relative vulnerability of a bridge to scour considering factors that affect pier scour. A separate evaluation is provided for each pier because the scour producing parameters may vary at each one. The piers are numbered sequentially from the left abutment, with the left side established looking downstream.

The parameters evaluated in the pier vulnerability ranking flow chart reflect their relative effect on scour. The rationale for their use follows:

1. Scour Countermeasures - The rationale is the same as presented for the abutment flow chart.
2. Pier Foundation - A spread footing or unknown foundation condition warrants a higher value than a pile foundation.
3. Skew Angle - The skew angle ranges reflect the relative effect on scour potential as indicated in Table 4.3 of the Technical Advisory.(1)
4. Pier/Pile Bottom Below Streambed - This parameter reflects the relative susceptibility to scour based on the depth of the footing or pile bottom to the streambed elevation. The highest value is assigned to a depth of three feet or less because this is the normal depth of spread footings. Deeper footing or pile bottom elevations warrant lower ranking

ABUTMENT SCOUR VULNERABILITY RANKING FLOW CHART

BRIDGE # _____ FEATURE CARRIED _____ STREAM _____

COMMUNITY _____ COUNTY _____

BRIDGE TYPE _____ SPANS _____

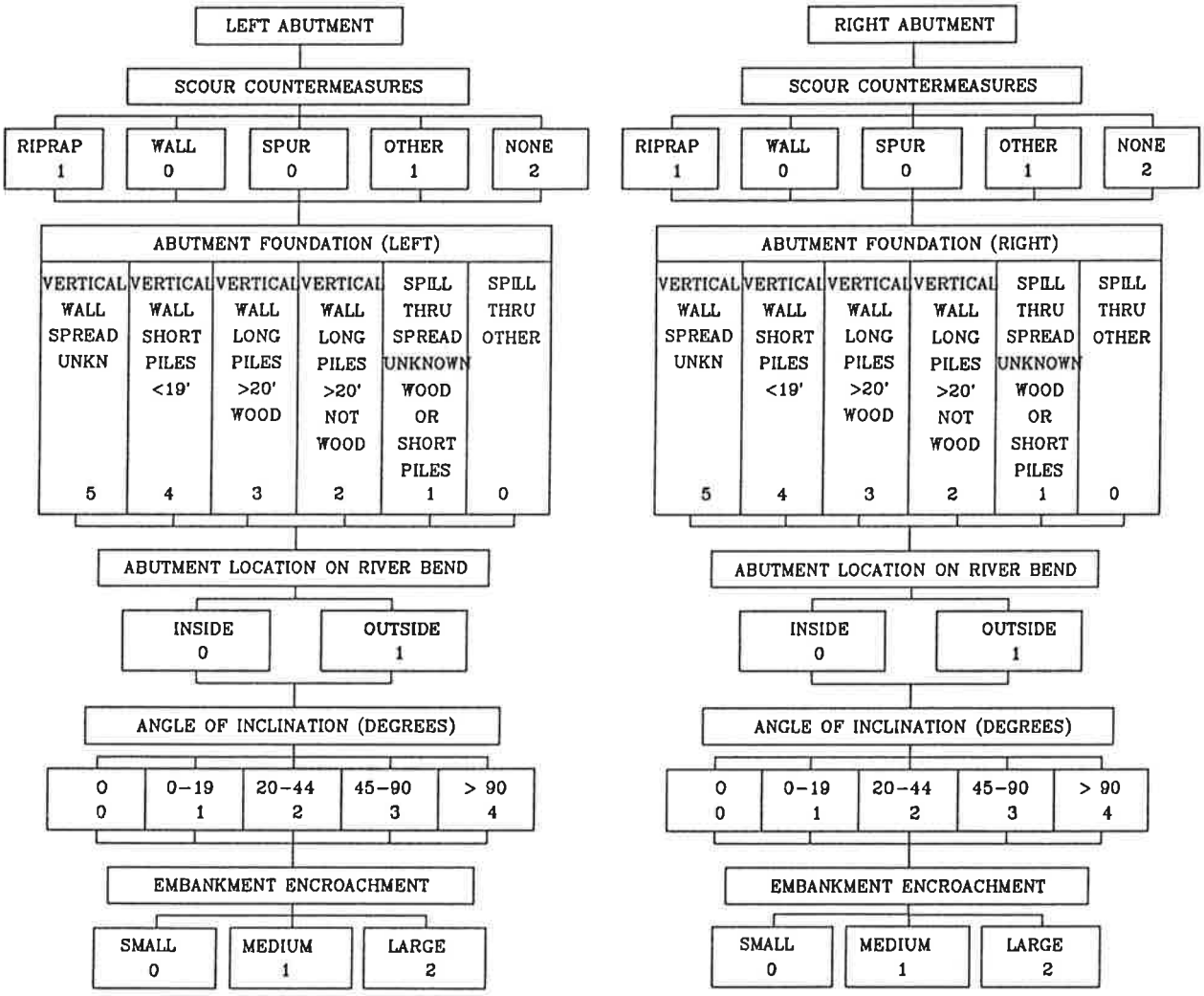

LEFT ABUTMENT VULNERABILITY

SCORE: _____

RIGHT ABUTMENT VULNERABILITY

SCORE: _____

* LEFT AND RIGHT ARE ESTABLISHED LOOKING DOWNSTREAM

ABUTMENT SCOUR VULNERABILTIY

LEFT ABUTMENT_____ RIGHT ABUTMENT_____ TOTAL_____

GENERAL CONDITIONS VULNERABILITY SCORE TOTAL_____

SUB TOTAL:

(FINAL SCORE IF THERE ARE NO PIERS) _____

[PROCEED TO PIER VULNERABILITY RANKING FLOW CHART, IF NECESSARY]

PIER VULNERABILITY RANKING FLOW CHART

BRIDGE # _____ FEATURE CARRIED _____ STREAM _____

COMMUNITY _____ COUNTY _____

BRIDGE TYPE _____ SPANS _____

PIER #1

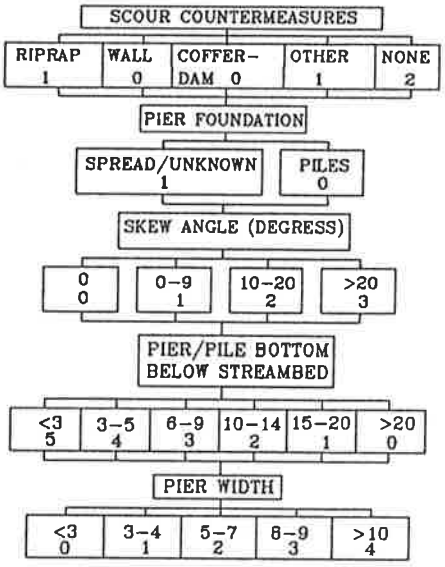

PIER #1 VULNERABILITY SCORE: _____

PIER #2

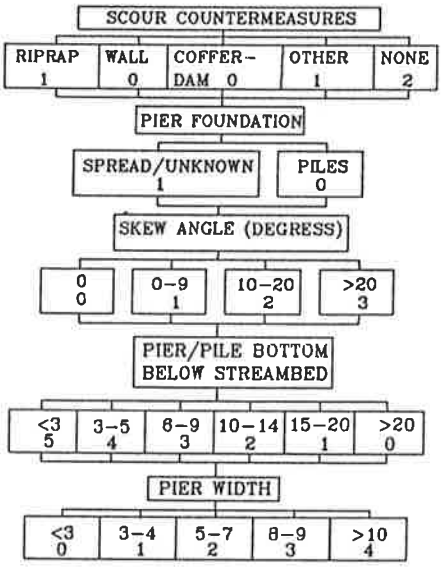

PIER #2 VULNERABILITY SCORE: _____

PIER #3

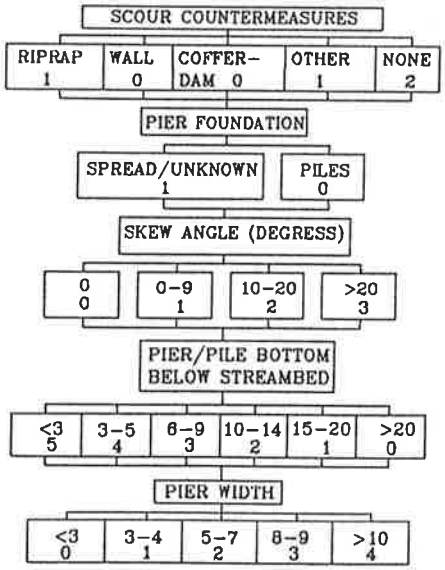

PIER #3 VULNERABILITY SCORE: _____

PIER #4

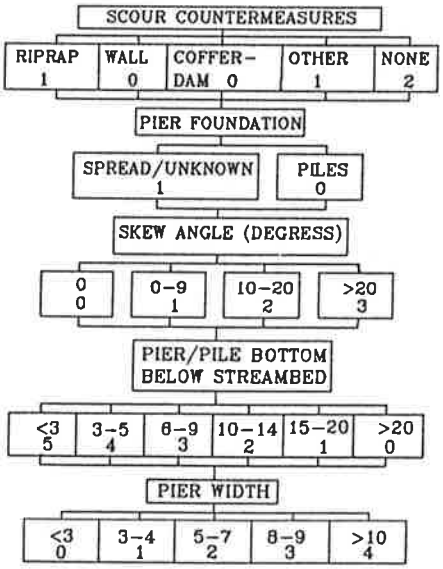

PIER #4 VULNERABILITY SCORE: _____

PIER VULNERABILITY RANKING SCORE SUMMARY

PIER #1____ PIER #2____ PIER #3____ PIER #4____

PIER WITH MAXIMUM SCORE: PIER #____ _____

SUBTOTAL FROM ABUTMENT SCOUR VULNERABILITY: _____

TOTAL VULNERABILITY SCORE: _____

values. Depths greater than twenty feet are arbitrarily assigned the lowest value.

5. Pier Width - The pier width reflects the maximum expected scour in accordance with pier scour questions as indicated in the Technical Advisory. The range of three to five feet in the pier width represents the normal dimensions expected. No adjustment for debris or ice accumulation is used here because it is reflected in the general conditions flow chart.

The pier vulnerability score is tabulated for each pier evaluated. The values are summarized and the value of the most vulnerable pier added to the subtotal from the abutment vulnerability flow chart to determine the total vulnerability score.

III. **Step 3. Plan of action and interim countermeasures.**

The plan of action for correcting the scour problem includes the following:

1. Interim protection for scour critical bridges until countermeasures are designed and constructed or the bridge is replaced. This could include:
   a. Timely installation of interim scour countermeasures such as riprap.
   b. Plans for monitoring scour critical bridges during and inspection after flood events and for blocking traffic if need be until scour countermeasures are installed.
   c. Immediate bridge replacement or the installation of permanent scour countermeasures.
2. Establishing a time table for step 4 below.

Note. Monitoring a bridge during a flood can not at this time determine if the bridge is about to collapse. Thus, the need to provide scour protection (riprap, grade control, etc) on an interim basis if the bridge cannot be closed during high water. Many bridges could be closed during high flow without disrupting traffic too much because the traffic volume is low, there are alternate routes or both.

IV. **Step 4. Detailed evaluation and design of scour countermeasure.**

In the detailed evaluation the following are recommended:

1. THE PROCEDURES AND EQUATIONS GIVEN IN FHWA SEPT. 1988 TA (1) BE FOLLOWED, EXCEPT IN THE CASE OF ABUTMENT SCOUR.
2. FOR ABUTMENT SCOUR, USE RIPRAP OR CONSTRUCT A SPUR DIKE TO PROTECT ABUTMENTS THAT STEP 2 HAS IDENTIFIED AS SCOUR CRITICAL.

   The reason for this recommendation is that equations for predicting scour depths at abutments are based on laboratory studies with no field verification. The conditions of the experiments do not represent field conditions. The experiments were for abutments projecting into a channel with no vegetation on the banks, the elevation of the bed in the overbank area was the same as the channel in the experiments and the velocity in the experimental overbank area was almost the same as in the main experimental channel. Also, only recently has the volume of flow in the overbank area, rather than the encroachment length, been considered in the equations. (7,8)

   ONE FACTOR THAT THE EXPERIMENTS DO SHOW IS THAT SCOUR DEPTHS AT VERTICAL WALL ABUTMENTS ARE TWICE THAT OF SPILL THROUGH ABUTMENTS.

   Use Froehlich's live-bed abutment scour equation to calculate scour depths, if it is desired to calculate potential scour depths in the design of foundations or countermeasures.(4, 6)
3. SIMPLE SPANS WITHOUT ALTERNATE LOAD PATHS (WITHOUT REDUNDANCY)SHOULD BE ELIMINATED IN THE REPAIR OR REPLACEMENT OF SCOUR CRITICAL BRIDGES. THIS WOULD ELIMINATE INSTANTANEOUS COLLAPSE IF A PIER OR ABUTMENT SHIFTED.

V. **Step 5. Evaluate the other bridges over water in the inventory.**

The procedure would be to evaluate the most scour critical bridges, then the medium scour critical bridges and last the least scour critical bridges. However, in Step 2 many of the bridges identified in Step 1 would be eliminated from further evaluation and would depend on the inspection program to determine problems.

SUMMARY

This paper presents a method for screening and placing in priority bridge vulnerability to hydraulic forces, stream instability and scour.

ACKNOWLEDGEMENTS

The writers wish to acknowledge the help and advice given in the development of this scour vulnerability assessment method by the Staff of the New York State Department of Transportation, in particular Mike Cuddey, Richard Simberg, Aron Shirole, Steve Georgopoulis and Kenneth Dodge; the Colorado Highway Department, in particular A. Joe Siccardi, Walt Mystkowski, Mike Best and Del Roupp; and the members of the New York Bridge Safety Assurance Task Force, John Kozak, John W Fisher, J. Hartley Daniels, Kenneth Hover, Clarence Mosher and Victor E. Taylor.

LITERATURE CITED

1. *Technical Advisory, "Interim Procedures for Evaluating Scour at Bridges"*. FHWA, Department of Transportation, Washington, D. C., September, 1988.
2. *Safer Bridges for New York*. Report by the New York Bridge Safety Assurance Task Force, New York State Department of Transportation, Albany, N. Y., 1990.
3. *Colorado Bridge Safety Evaluation*. Report to Colorado Highway Department by Resources Consultants, Inc. Ft. Collins, Colo., 1990.
4. *Scour at Bridges*. Hydraulic Engineering Circular No. 18, FHWA, Department of Transportation, Washington, D. C. (Draft), 1990.
5. *Stream Stability at Highway Crossings*. Hydraulic Engineering. Circular No. 20, FHWA, Department of Transportation, Washington, D. C. (Draft), 1990.
6. E. V. Richardson, D. B. Simons, and P. Julien. Highways in the River Environment: (Revision of 1975 edition), FHWA, Department of Transportation, Washington, D.C., 1990.
7. E. M. Laursen. Predicting Scour at Bridge Piers and Abutments: General Report No. 3, Arizona DOT, 1980.
8. D. C. Froehlich. Abutment Scour Prediction: Paper presented at the 68 TRB Annual Meeting, Washington D. C., 1989.

Planning for a Comprehensive Bridge Safety Assurance Program

A. M. SHIROLE AND R. C. HOLT

With the increasing number of structurally deficient and functionally obsolete bridges and recent catastrophic bridge failures in the United States, the need to strengthen bridge safety has become pronounced. This paper presents considerations in planning a comprehensive bridge safety assurance progam, including identification of potential causes and modes of bridge failures based on review of failures, imminent failures and actual closures. As these causes and modes of failure are identified, they are prioritized in terms of their potential impact on the structures for which an agency is responsible. The paper discusses steps to develop a rating system that categorizes and ranks bridges by their relative vulnerability to the various failure modes. Further, it presents a method of preparing initial screening lists based on characteristics of the site and structure, verifying such lists, and then categorizing them according to appropriate action-needed categories. Preparation of short and long-term strategies to reduce or eliminate vulnerability of bridge failures is also discussed.

INTRODUCTION

Since the catastrophic bridge collapse at Point Pleasant, W.V., in 1967, most agencies responsible for bridges have initiated systematic inspection and inventory programs. These were later followed by structural capacity rating and load posting programs as well as improved maintenance practices. Failure of Connecticut's Mianus River Bridge in 1983, the New York State Thruway Bridge over Schoharie Creek in 1987, and that of the US 51 Bridge in Covington, Tennessee, in 1989, have further underscored the importance of inspection, evaluation and maintenance in achieving bridge safety. Bridge engineers have responded to these failures by initiating upgrades of pin and hanger, fracture critical, and scour susceptible structures. These and other efforts have been on a piece-meal basis, in a reactive manner, rather than as a well planned and coordinated proactive strategy. Thus, a strong need exists for agencies responsible for bridges to undertake a systematic program to deal with their vulnerability to all potential modes of failure. A well-planned comprehensive Bridge Safety Assurance (BSA) Program will provide a system to identify, assess, and evaluate vulnerable bridges and then implement actions to prevent these failures.

This paper presents the necessary steps to planning a comprehensive Bridge Safety Assurance program that will facilitate a systematic assessment. It reviews current practices relating to safety assurance and discusses the identification and rating of vulnerability to significant failure modes on the basis of relevant site and structure characteristics. Further, it discusses prioritization of vulnerability reduction needs and formulation of effective strategies to eliminate or reduce failure vulnerabilities of bridges to accomplish short- and long-term objectives.

REVIEW OF CURRENT PRACTICES

Traditionally, bridge safety assurance practices start by complying with design and material standards to assure safe and durable structures. This is followed by construction inspection to assure compliance with the plans and specifications. Bridge conditions are rated and monitored during biennial inspections while the safe load carrying capacity is assured by the load rating and posting programs. Structure deficiencies identified by these programs are addressed through maintenance, rehabilitation and replacement programs. All of these activities, however, are reactions to observed conditions and do not go far enough. This is because most existing structures were not designed in anticipation of the significantly different but more realistic present day design loads and an improved understanding of environmental conditions. Certain design specification requirements and material characteristics once accepted as "state-of-the-art" have been demonstrated with time and further study to be undesirable and ill-advised. Because of previously unexpected loads and implications of environmental conditions, some of these structures have an inherent vulnerability to certain failure modes. Failures of older bridges due to earthquakes or floods demonstrate this vulnerability.

SURVEY OF BRIDGE FAILURES

There does not appear to be a central data base anywhere in the U.S. that can provide comprehensive information about bridge failures, catastrophic or otherwise. The Federal Highway Administration (FHWA) estimates that 50 to 60 bridges fail each year (6), while the U.S. Comptroller General reports that each year an average of 150 U.S. bridges collapse resulting in an average of 12 fatalities (1). For a U.S. bridge population of about 580,000, these two estimates represent an annual failure rate of between 1 in 4,000 and 1 in 10,000.

A study by Harik (2) reviews bridge failures reported in Kentucky as well as nationally. New York State has a database (5) of 823 bridge failures since 1950, 108 of which occurred in the state. Table 1 gives a summary of this database. The Imbsen study (3) reports on bridge failures in 45 states. Failure records are not commonly available, thus individual agencies need to research and review their archives for records and publications in order to determine the failure modes most significant for bridges under their jurisdiction.

TABLE 1. SUMMARY OF BRIDGE FAILURE SURVEY.

U.S. BRIDGE FAILURE SURVEY (Since 1950)

NUMBER OF IDENTIFIED FAILURES 823

NUMBER OF FAILURES DUE TO FAILURE MODE:

HYDRAULICS	= 494
COLLISION	= 108
OVERLOADS	= 84
NATURE	= 24
MISCELLANEOUS	= 39
FIRE	= 24
DETERIORATION	= 36
EARTHQUAKE	= 14

NEW YORK BRIDGE FAILURES (Since 1950)

NUMBER OF IDENTIFIED FAILURES 108

NUMBER OF FAILURES DUE TO FAILURE MODE:

HYDRAULICS	= 43
COLLISION	= 16
OVERLOADS	= 21
NATURE	= 3
MISCELLANEOUS	= 9
FIRE	= 1
DETERIORATION	= 15
EARTHQUAKE	= 0

SIGNIFICANT MODES OF FAILURE

Generally, available data indicates that the majority of bridge failures in the U.S. have occurred on rural, off-system roads and did not generate more than local attention. Harik notes that of 35 bridge failures in Kentucky between 1951 and 1988, only one was widely reported. The Imbsen study and failures in New York State confirm this trend by indicating that over 80 percent of the failures reported in their studies were on local systems.

Because these studies indicate that most bridge failures occur on the local systems, it is important to search for information on such failures through sources knowledgeable about local historical records. Because some states may have unique area characteristics, environmental conditions (e.g., types of loads or geographic peculiarities), or bridge types (e.g., type of construction or material), a study of local historical records is especially beneficial in determining the most significant failure modes for bridges in the area.

Although local bridge failures will indicate most of the significant modes of failure, bridge failures on state and interstate routes may reveal other aspects which cannot be overlooked because of their serious consequences as demonstrated by the Mianus River and Schoharie Creek bridge failures. Thus it would be prudent to identify those failure modes that are significant in terms of their consequences, but are estimated to have a low frequency of occurrence. Earthquake caused failures in the East would be in this category.

As a general rule, the significant bridge failure modes will represent about 90 percent of the area's historical failures. Other failure modes, affecting large geographic areas need to be considered as well. The most significant failure modes can then be prioritized on the basis of their estimated frequency of occurrence and consequences of failure. Although the number of the most significant modes of failure will vary from one area to another, certain modes of failure can be expected to be significant for most areas of the U.S. The State of New York, after extensive study of potential for bridge failures within the state, has identified the six most significant modes of failure for its bridges.

On the basis of available information on bridge failures and closures, the following failure modes appear to be most common:

* Hydraulic: scour/ice/debris
* Overload: design/posted
* Steel Structural Details
* Collision: vehicle/vessel
* Concrete Structrual Details
* Earthquake

Because earthquakes affect a large geographic area and potentially many bridges, they are considered significant. Other failure modes identified but not predominant include failures due to wind, fire, soil conditions, pile deterioration and design/construction errors.

ASSESSING VULNERABILITY TO FAILURE

Vulnerability of a structure to failure is a measure of its susceptibility to failure or collapse because of loads and/or environmental conditions not anticipated in design. To assess bridge vulnerability, it is necessary to describe it in terms of the structure and site characteristics which contribute to the vulnerability. In general, such characteristics will be specific structural, geometric, design, geographic, geologic or hydraulic features. Assessing the vulnerability of a large bridge population to a number of failure modes is very time consuming, but can be simplified by using a multi-level process.

Such a multi-level process starts with screening the entire bridge population based on specific factors or characteristics relevant to individual

failure modes. This is followed by ranking, analyzing, rating, prioritizing and updating. Each level of assessment will successively yield smaller numbers of bridges with higher vulnerability which require a more detailed evaluation. This multi-level assessment process, results in a comprehensive bridge vulnerability rating, and will be discussed in greater detail.

TABLE 2. CORRELATING CHARACTERISTIC FOR BRIDGE FAILURE POTENTIAL.

HYDRAULIC

a. Bridges over water

b. Scour history at site

c. Piers or High Abutments
   - Spread footing on soil.
   - Timber piles.
   - Short piles.

OVERLOAD FAILURES

a. Load Posted

b. Non-Redundant

c. Bridge Width <24'

d. Low Operating Rating

STEEL

a. Pin and Hanger Details

b. Welded Details

c. 2 and 3 girder bridges

d. Built before 1978 (AASHTO Fracture Control Plan)

e. AADTT > 300

COLLISION

a. Bridges over Roadways

b. High Accident History

c. Bridge Geometry
   - Vertical Clearance < 14'
   - Width < 20'

d. Over Navigable Water

e. Barge Traffic

f. Through Structures

CONCRETE

a. Condition Ratings

b. Year Built
   < 1964 (not air entrained)

EARTHQUAKE

a. Built before 1983

b. Multiple Simple Spans

c. High Piers

d. Bearing Type

e. Bridge Seat Support Length

Screening

The specific characteristics needed to assist in easily identifying structures vulnerable to certain modes of failure can be determined. Typical examples of such characteristics are presented in Table 2. The screening process starts with the total bridge population and uses these characteristics to identify structures vulnerable to a failure mode. For example, only bridges crossing waterways would logically be vulnerable to hydraulic failure, those over navigable water would be vulnerable to water vessel collision, and only those with steel superstructures would be vulnerable to steel superstructure failures. Tables 3 and 4 present typical summary results of a screening process in terms of type of material and bridges over water. Figure 1 is an illustration of six bridges on a screen list for scour vulnerability.

These groups of structures identified by the initial screen can be further subdivided into smaller groups according to a particular failure mechanism that would exist within a failure mode. For example, the steel detail failure mode can be subdivided into pin and hanger, fracture-prone weld details, steel pier caps, eye-bar truss or suspension chain, etc. The result of this screening level of assessment will be a list of bridges vulnerable to a specific failure mode or subset, which will be candidates for the next level of assessment.

TABLE 3. COMPOSITION OF NEW YORK STATE BRIDGES.

Characteristic	Number of Bridges			
	State (a)	Non-State (b)	(a)+(b)	% of Total
Steel	5,389	8,840	14,229	74
Concrete	1,722	1,468	3,190	17
Prestressed Concrete	428	606	1,034	5
Timber	12	277	289	2
All Other Types	39	392	431	2
Total	7,590	11,583	19,173	100

TABLE 4. NEW YORK STATE BRIDGES OVER WATER.

Bridge Characteristic	Number of Bridges			
	State (a)	Non-State (b)	(a)+(b)	% of Total
Non-Navigable	3,539	8,015	11,554	60
Navigable	132	238	370	2
NYS Canal	256	109	365	2
Total	3,927	8,362	12,289	64

FIGURE 1. TYPICAL SCREEN CRITERIA AND LIST FOR SCOUR VULNERABILITY.

SCREENING CRITERIA

TYPE SERVICE CROSSED (TS - 2ND DIGIT)
- 5 = WATERWAY
- 6 = HIGHWAY-WATERWAY
- 7 = RAILROAD-WATERWAY
- 8 = HIGHWAY-RAILROAD-WATERWAY

PIER PILE TYPE
- * = UNKNOWN
- 1 = NO PILES
- 8 = TIMBER PILES

SCREEN LIST OF BRIDGES OVER WATER WITH TIMBER PILES, NO PILES OR UNKNOWN FOUNDATIONS.

R	C	BIN	SP#	TS	FEATURE CARRIED	FEATURE CROSSED	[PIER] TY	HGT	F	P	AB PL
1	2	1060240	001	15	73 12011521	EBR AUSABLE RV	02	***	6	1	11
1	3	1041250	001	15	214 13021008	STONY COVER CREEK	02	008	0	1	11
1	4	1017000	001	56	22 14071322	WALLOOMSAC RIVER	02	012	6	1	11
1	4	1017000	002	56	22 14071322	WALLOOMSAC RIVER	02	025	7	8	11
1	4	1017000	003	56	22 14407322	WALLOOMSAC RIVER	02	035	7	8	11
1	4	1017000	004	56	22 14407322	WALLOOMSAC RIVER	02	002	1	1	11
1	5	1026350	001	15	50 15021083	KAYADEROSSERAS CR	02	***	*	*	11
1	6	1054370	001	15	20 16191001	SCHOHARIE CR	02	033	7	1	11
1	6	4038360	001	15	146 16033040	ERIE CANAL	02	030	3	1	22
1	6	4038360	002	15	146 16033040	ERIE CANAL	02	034	3	1	22
1	6	4038360	003	15	146 16033040	ERIE CANAL	02	032	9	2	22

INVENTORY & INSPECTION DATABASE KEY

- R = REGION
- C = COUNTY
- SP# = SPAN NUMBER
- TS = TYPE SERVICE
  - 1ST DIGIT = CARRIED
  - 2ND DIGIT = UNDER
- TY = TYPE
- HGT = HEIGHT
- F = FOOTING TYPE
- P = PILE TYPE
- AB = ABUTMENT
- PL = PILES
  - 1ST DIGIT = BEGIN ABUTMENT
  - 2ND DIGIT = END ABUTMENT

Ranking

Bridges on the list produced by the screening will not be organized in any order based on their relative extent of vulnerability to the particular failure mode. This can be accomplished by weighting the characteristic indicators according to their relative importance and degree to which they contribute to the vulnerability of an individual bridge. Figure 2 shows an example of the scour vulnerability ranking indicators and their weights. Selecting the indicators and assigning them their relative weights requires experience and good engineering judgement. The Delphi technique (7) can be effectively used for this purpose.

FIGURE 2. SCOUR VULNERABILITY RANKING.

Scour Vulnerability Ranking = Sum of Waterway, Critical Abutment and Critical Pier Vulnerability Ranking Scores = Range of 0-48 points

Ranking Factor	Choices	Score
A. Waterway -		
River Slope/Velocity	(steep, medium, mild)	0-2 points
Channel Bottom	(stable, aggrading, degrading)	0-2 points
Channel Configuration	(straight, meandering, braided)	0-2 points
Debris Ice Problem	(yes, no)	0-1 point
Near River Confluence	(yes, no)	0-1 point
Effected by Backwater	(yes, no)	0-1 point
Historic Scour Depth	(none, <1 ft., 1-3 ft., >3 ft.)	0-3 points
Historic Maximum Flood Depth	(<5 ft., 5-10 ft., 10-20 ft., 20-40 ft., >40 ft.)	0-4 points
Adequate Opening	(yes, no)	0-1 point
Overflow/Relief Available	(yes, no)	0-1 point
Simple Spans	(yes, no)	0-1 point
	Range of Score =	0-19 points
B. Abutment -		
Scour Countermeasures	(rip rap, wall, cofferdam, not req'd, other, none)	0-2 points
Abutment Foundation	(type of footings and length of piles)	0-5 points
Abutment Location on River Bend	(inside, outside)	0-1 points
Angle of Inclination (Degrees)	(0, 0-20, 20-45, 45-90, >90)	0-4 points
Embankment Encroachment	(small, medium, large)	0-2 points
	Range of Score =	0-14 points
C. Pier -		
Scour Countermeasures	(rip rap, wall, cofferdam, other, none)	0-2 points
Pile Foundation	(spread/unknown, piles)	0-1 points
Skew-Angle (Degrees)	(0, 0-20, 20-45, 45-90)	0-3 points
Pier/Pile Bottom Below Streambed	(<4, 4-7, 7-10, 10-15, 15-20, >20)	0-5 points
Pier Width	(<3. 3-5, 5-8, 8-10, >10)	0-4 points
	Range of Score =	0-15 points

The result of this ranking level of assessment will be a screen-list organized in order of the extent of the vulnerability to an individual mode of failure. There will be a separate ranked list of bridges for each significant failure mode.

Analysis

Using the ranked order of bridges in each failure mode, an engineering analysis will be performed. This will specifically address the vulnerability being assessed. The following are some examples of the types of analyses associated with the failure modes:

Hydraulic - hydrologic, hydraulic and scour analysis
Overload - load rating
Collision - impact analysis
Structural Details - remaining fatigue life or load rating
Earthquake - seismic analysis

The analysis is only necessary where the risk or consequence of failure warrants it. Thus, at least initially, an acceptable level of risk within each ranking list must be determined. As the analyses progress down the ranking lists, the results of the successive analyses will define an acceptable level of risk.

The results of these analyses will be used to determine the final vulnerability rating for each bridge in each failure mode.

Rating

Each list produced by the ranking level of assessment pertains to only one significant mode of failure. All failure modes must be considered, however, in formulating a comprehensive plan for bridge safety assurance. Factors contributing to different failure modes are generally so unique and diverse that no meaningful relationship may exist between them. For example, Pier angle of attack (Hydraulic), frequency of barge traffic (Collision) and bridge seat width (Earthquake). As a result, the ranking values for one failure mode cannot be directly compared with the ranking values for another failure mode. All

TABLE 5. VULNERABILITY RATING SYSTEM

1. **High Priority** - Reasonable expectation of an event which may cause a catastrophic or life-threatening failure. Remedial work desired within 12 months.

2. **Medium Priority** - Possible but unlikely expectation of an event which may cause catastrophic or life-threatening failure. Remedial work desired within three years.

3. **Capital Program Priority** - Reasonable expectation of a failure that could cause traffic disruptions. Remedial work desired to be programmed within five years.

4. **Inspection Action** - Possible but unlikely expectation of a failure that could cause traffic disruptions. Inspection monitoring desired to assure adequate load resistance.

5. **Not Vulnerable** - Adequate structural resistance to this type of vulnerability failure unlikely.

6. **Not Applicable** - No exposure to this type of failure vulnerability.

failure modes have inherently associated with them a certain degree of risk based on frequency of occurrence and consequence of failure causing events. Further, associated with the degree of risk is a consequent requirement for priority of prudent action needed to preclude the possibility of failure. It is possible, thus, to develop a scale/system to rate bridges for vulnerability across different failure modes based on the type and urgency of needed action. Table 5 presents one approach to such a vulnerability rating system. It translates individual failure mode ranking using the related analyses into a common rating scale for purposes of prioritizing actions across the spectrum of all significant modes of failure. The rating scale identifies the urgency for needed action and ties it to the type of action. Figure 3 illustrates a typical six-digit comprehensive vulnerability rating code for a bridge, in a rating system for six significant modes of failure. The result of this rating level of assessment will be ratings of all bridges vulnerable to any of the significant modes of failure.

Prioritizing

The list produced by the rating level assessment will include all bridges and the degree of vulnerability they have to each mode of failure. There will generally be inadequate resources during a fiscal year, to initiate needed actions for all of the bridges in any one of the rating categories. Thus, it will be necessary to prioritize the bridges based on the rating code. Since there is a desired completion time associated with the first three rating categories, those bridges that have a rating of "1" will take precedent. The list is prioritized by the rating number and then its' position (starting from the left) in the vulnerability rating code. Thus, all bridges with a rating of "1" in the left position (Hydraulic) is given the highest priority followed by the second and so on. The remainder of the bridges, which will have no ratings of "1", will be prioritized by the position of the "2" rating in a similar manner and so on through all six digits of the rating categories. For example, a bridge with the vulnerability rating code of 512365 will have precedence over

FIGURE 3. BRIDGE VULNERABILITY RATING CODE.

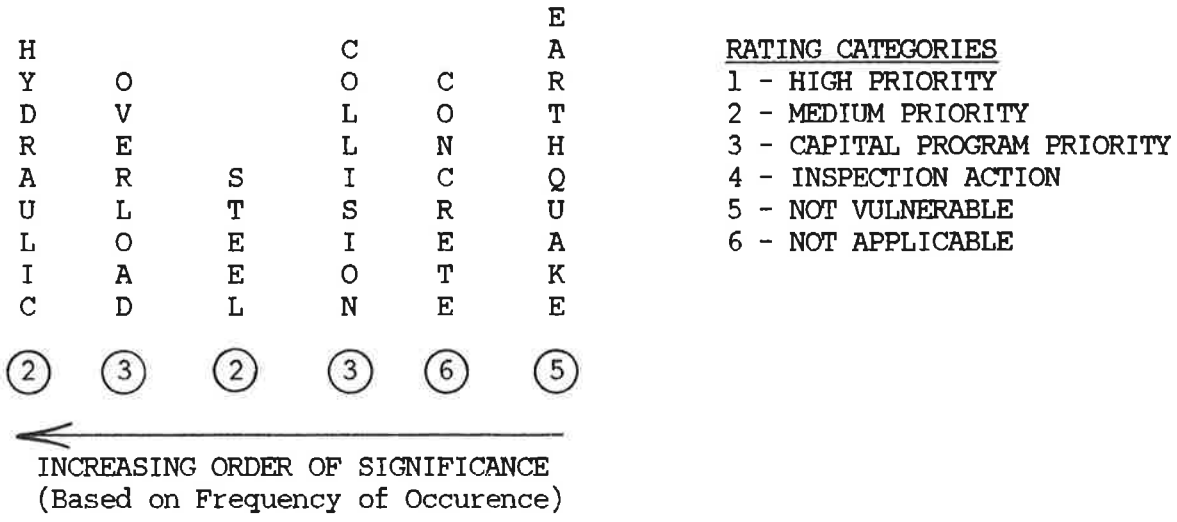

a bridge with a rating of 222115. This process will result in a prioritized list of all bridges in order of their extent of vulnerability to any significant mode of failure.

Updating

The final prioritized rating list of bridges produced in this assessment process must be periodically updated. As the characteristics of the site or bridge can change over time, the vulnerability rating may be affected requiring a new assessment of that bridge, and repositioning it in the prioritized rating list. The frequency of this updating process will depend on local circumstances and resources. Similarly, provision must be made to reassess a bridge after a corrective action has been completed. This updating of the vulnerability assessment will result in a reasonably current prioritized rating list.

EVALUATION

Bridges on the prioritized list will need to be evaluated in the order of their priority. This will consider the overall structural integrity of a bridge subject to all failure modes. The basis of such evaluation will be consideration of current design codes, existing condition, structural capacity, adequacy of structure, vulnerability to all modes of failure, estimate of remaining life, and life cycle costs of rehabilitation alternatives. This level of assessment will result in a structural integrity evaluation report for individual bridges. It will include a discussion of available vulnerability reduction strategies, recommended actions with cost estimates, and a required time schedule for implementation.

IMPLEMENTATION OF RECOMMENDATIONS

The implementation phase of the program will use the prioritized rating list of bridges as well as structural integrity evaluation reports to program, plan, design and construct projects to eliminate or reduce identified failure vulnerabilities. To achieve both short- and long-term goals, it is essential to identify and program the necessary resources estimated in the evaluation phase. The short term goal should be to implement the priority actions for all bridges with a rating of "1". This will satisfy the need for a prompt response to mitigate the vulnerability of the high risk bridges. The result will be to reclassify the repaired/retrofitted bridges to a reduced or no vulnerability category. Due to the prompt nature of the response, these actions could be of an interim or temporary corrective nature. In such cases, these retrofitted bridges along with those rated with lower urgency of action will be included in the long term goal to further reduce or ideally eliminate the vulnerability. Because long term efforts will be a programmed response, with a permanent corrective action, more time will be needed to design and construct this type of project. This work may be initiated as part of a separate vulnerability reduction program or can be incorporated into the next scheduled rehabilitation or replacement project, depending on the rating and urgency of the corrective action.

As the BSA program is implemented it will be necessary to monitor and report progress. This will provide an overview of the scope and progress of the vulnerability reduction projects. It will also provide information for updating or modifying the program to become more responsive to the dynamic problem of failure vulnerability. The Figure 4 flowchart shows implementation of the BSA program.

FIGURE 4. BRIDGE SAFETY ASSURANCE IMPLEMENTATION FLOWCHART.

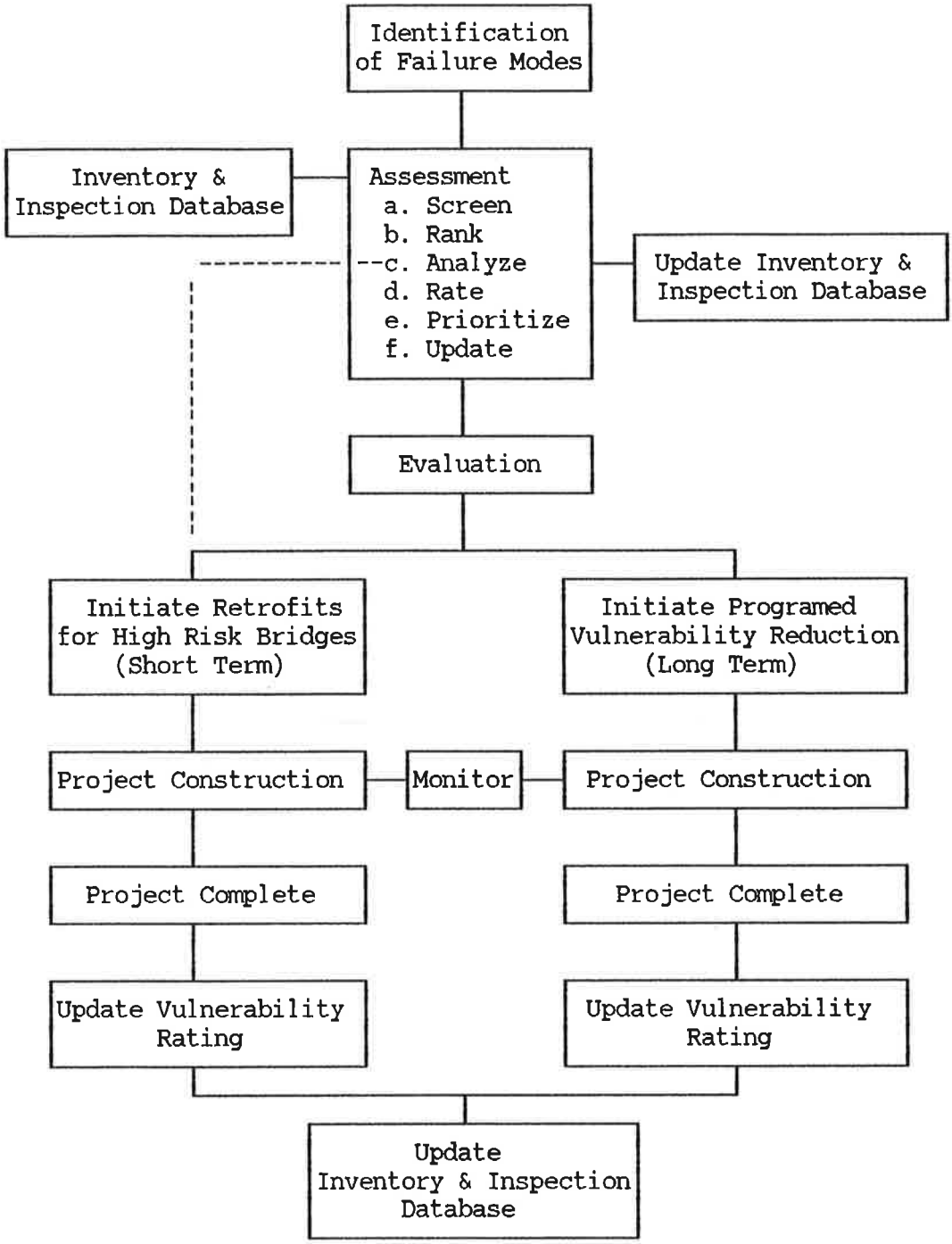

CONCLUSION

Bridges are generally built using state-of-the-art knowledge in design, materials and construction practices. Over time, unanticipated loads and implications of environmental events as well as site condition changes may make a bridge more vulnerable to failure. A comprehensive BSA program will assess this changing vulnerability, and evaluate the structural integrity, and initiate a corrective action on a priority basis to reduce the vulnerability to failure.

The Comprehensive Bridge Safety Assurance Program when fully operational, will permit evaluation of all bridges in a given jurisdiction on a regular basis and provide the current status of the bridge network vulnerability to the significant modes of failure relevant for that area. This program will consist of four phases:

1. Identification of significant failure modes,
2. Assessment of vulnerability of bridges to failure modes,
3. Evaluation of vulnerable bridges, and
4. Implementation of vulnerability reduction recommendations.

Bridge Safety Assurance will become an on-going program with planned periodic updates to account for changing site and bridge conditions. If systematically planned and managed, a comprehensive BSA program will significantly lower the risk of catastrophic bridge failures.

REFERENCES

1. "Better Targeting of Federal Funds Needed to Eliminate Unsafe Bridges.", Report to Hon. James R. Sasser, U.S. Senate, USGAI, U.S. Comptroller General, (August 11, 1981), p.11.
2. "Bridge Failures in the U.S. from 1951 to 1988.", Harik I.E., al., U. Kentucky, Unpublished ASCE Journal Article, 1989.
3. "Bridge Weight-Limit Posting Practice in the United States.", Imbsen, P.A., Butt., R.V., TRR 950, TRB, (1984).
4. "Comprehensive Program For Bridge Safety Assurance Work Plan", Structures Division NYSDOT, June 1990.
5. NYSDOT Survey of Bridge Failures in U.S. - Unpublished Survey, 1989-90.
6. Phone conversation with John Ahlskog, Chief of Bridge Management Division, FHWA, (Aug. 1989), (202) 366-4618.
7. "The Delphi Method: Techniques and Applications", ed. Harold A. Linstone & Murray Turoff, pub. Addison-Wesley, 1975.

Techniques for Increasing the Skid Resistance of Bridge Decks

MICHAEL M. SPRINKEL

ABSTRACT

Prior to 1970 many bridge decks in Virginia were constructed with aggregates that polish when subjected to traffic. In the seventies many decks were constructed with insufficient macrotexture to provide a good bald tire skid number. To provide adequate macrotexture, a tined texture has been applied to most decks constructed in the eighties. Because of problems with achieving a uniform texture with tining, grooves were being sawcut on new decks constructed in the latter part of 1989. Other techniques that have been used experimentally to increase the skid resistance of decks include shotblasting and sealing, application of a latex modified slag slurry and application of thin polymer overlays. The paper describes the techniques and compares them from the standpoint of skid number, the permeability to chloride ion of the top 2 in of the deck, cost, and application requirements.

INTRODUCTION

To provide good skid resistance bridge decks must have adequate microtexture and macrotexture (*1*). A sharp microtexture is required to provide friction between the tire and the surface. A deep macrotexture is required to drain the water from the surface so that friction can occur between the tire and the high points of the surface and hydroplaning can be avoided.

In Virginia prior to 1970, many bridge decks were constructed with aggregates such as limestone and dolomite that polish when subjected to traffic. In the seventies, new decks were constructed with nonpolishing aggregates such as siliceous, basalt, and granite or constructed with a 1.25 inch minimum thickness latex modified concrete overlay that contained nonpolishing aggregates. Older decks were rehabilitated with a 1.25 inch minimum thickness latex modified concrete overlay that contained nonpolishing aggregates that provide adequate microtexture.

In the late seventies it was recognized that new decks and overlays should be grooved to provide adequate macrotexture (*2*). Grooves approximately 1/8 in wide by 1/8 in deep and spaced at approximately 3/4 in on center were applied to the deck by dragging a tining device across the surface of the plastic concrete prior to placing the curing materials (*3*). In the latter part of 1989, because of problems with obtaining a uniform texture and because the tining operation delayed the application of the curing materials, causing an increase in the incidence of plastic shrinkage cracking, grooves were sawcut into the surface of decks and overlays after the concrete had cured for a minimum of 14 days (*4*). Other techniques that have been used experimentally in the eighties to increase the skid resistance of decks constructed with insufficient microtexture and macrotexture include shotblasting and application of a penetrating sealer, application of a latex modified slag slurry, and application of thin polymer concrete overlays (*5*).

Virginia Transportation Research Council, Box 3817 University Station, Charlottesville, Va. 22903

OBJECTIVE

The objective of this paper is to describe the techniques used in Virginia to increase the skid resistance of bridge decks and to compare the techniques from the standpoint of skid number, permeability to chloride ion of the top 2 in of the deck, cost and application requirements.

DESCRIPTION OF TECHNIQUES

Tining Plastic Concrete

Grooves 1/8 in wide by 1/8 in deep and spaced at approximately 3/4 in on centers are placed in the plastic concrete by dragging a tining device over the surface prior to placing the curing materials (see Figure 1) (*3*). The technique is limited to use on freshly placed concrete. Uniform textures can be achieved when the concrete on the surface is workable and uniform at the time the tining is done. However, the degree of macrotexture usually varies over the surface of most decks because the concrete tends to vary over the surface due to the differences in the physical properties between batches, the location of the batches on the surface, and the time between adding water to the mixture and the placing, consolidation, striking off and tining of the concrete. The variability of the concrete on the surface is greatest for decks constructed with long longitudinal screed spans, slow concrete placement methods, and long concrete haul distances; for decks constructed when the evaporation rate from the freshly placed concrete surface is high; and for decks constructed with mixtures that have a low water to cement ratio. These factors increase the chance that the concrete on the surface will have insufficient workability at the time it is struckoff and textured to provide a suitable texture. The cost of tining is negligible since it is done as the concrete is placed. There may be a hidden cost associated with tining if contractors are required to repair areas that are not textured properly or to repair areas that contain plastic shrinkage cracks caused by the delay in application of curing material to accommodate the tining operation. Tined surfaces constructed with polishing aggregates will not have adequate microtexture once the aggregates polish.

Sawcut Grooves

Adequate macrotexture can be obtained by sawcutting grooves in the hardened concrete in the transverse direction 3/16 in deep by 1/8 in wide and approximately 3/4 in on center (see Figure 2) (*2*). Although VDOT specifications require a depth of 3/16 in + 1/16 in, it is difficult to meet the requirement on some decks because the tolerance to which decks are constructed is 1/8 in 10 ft (*3*, *4*). An area that is 1/8 in low may get a groove that is 1/16 in deep if the sawcut is set for 3/16 in. The sharp corners left by the sawcut will usually spall at a angle of 45 degrees and leave a land area as little as 1/4 in wide. Groove spacings up to 1 1/2 in on center can provide adequate skid numbers and are being examined to

increase the land area left after corner spalling occurs (2). The grooves cause some reduction in cover over the rebar and the technique may not be suitable for decks that have less than 2 in of cover (less than 1.25 in for latex modified concrete). Also, sawcutting grooves in decks constructed with polishing aggregate would not provide adequate microtexture. New concretes should have a strength suitable for traffic prior to grooving. The VDOT requires a 14–day cure prior to grooving (*4*). An advantage is that once grooved, the surface can be opened to traffic immediately.

Shotblasting and Sealing

On the afternoon of May 18, 1989, the travel lane and passing lane of a 3–span bridge, 113 ft long, located on the southbound lane of I–81 in Botetourt County, Virginia was shotblasted to increase the skid resistance. The surfaces were blasted at the rate of 1.4 yd^2/min. Because of concern about reducing the cover over the rebar and increasing the permeability of the concrete to chloride ion by removing approximately 1/8 to 1/4 in of the top surface mortar, two penetrating sealers were applied to spans B & C of the bridge. A 30% solids synthetic gum resin was applied to the travel lane of span B at the rate of 140 ft^2/gal. A poly–siloxane resin was applied at the rates of 162 ft^2/gal (span C of travel lane) and 192 ft^2/gal (spans B and C of passing lane). It was sunny and 85°F at the time of the applications. The gum resin was still tacky when opened to traffic after 3 hours of cure. The siloxane was tack free in 30–60 minutes.

A sand patch test (ASTM E965) was used to measure the macrotexture depth of the shotblasted surfaces (*6*). Prior to shotblasting the average diameter of the sand patch was 12.8 in. After shotblasting it was 7.4 in. After application of the penetrating sealers average sand patch diameters of 7.2 in and 7.5 in were measured for the gum resin and siloxane treated surfaces, respectively. The shotblasting increased the macrotexture by removing the mortar between the coarse aggregates and increased the microtexture by abrading the surface of the coarse aggregate (see Figure 3). It is believed the improvement in microtexture will be lost as the aggregates polish. An advantage of the technique is that once the sealers are tack free the surface can be opened to traffic.

Latex Modified Portland Cement Slag Slurry

On May 17, 1989, two 300–ft sections, one in the passing lane and one in the travel lane, of the northbound lane of I–81 in Botetourt County were shotblasted to increase the skid resistance. Another 300–ft section in the travel lane was shotblasted on the morning of May 18. Because of a concern that the microtexture applied to the polishing coarse aggregate would be lost in several years, a latex modified portland cement slag slurry was applied to the first section blasted in the travel lane. The latex modified slag slurry was placed between 3:30 and 4:30 p.m. on May 17. It was sunny and 82°F at the time of the application. The lane was opened to traffic on May 19 after 42 hours of cure.

On October 31, 1989 the passing lane of structure 2016 located on the northbound lane of I–81 in Rockbridge County (over Rte. 679 south of milepost 184 and Buffalo Creek) was shotblasted and overlaid with a latex modified slag slurry. The average tensile rupture strength (ACI 503R) of the overlay was measured on November 13 at an age of 13 days and found to be 260 lb/in^2 (*7*). The overlay was opened to traffic at an age of approximately 4 weeks. On April 26, 1990 the travel lane of the same structure was shotblasted at the rate of 11.5 yd^2/min and overlaid with a latex modified slag slurry (see Figure 4). The slurry was placed between 10:00 and 11:30 a.m. The temperature was 86°F at noon. The slurry was opened to traffic after 48 hours of cure.

The 300–ft pavement application and the two 204–ft bridge deck plus approach slab applications illustrate that a latex modified slag slurry can be placed on decks to provide adequate surface texture. The surface was shotblasted prior to placing the slurry to remove dirt, oil, weak surface mortar and materials that can interfere with the bonding or curing of the slurry. The slurry was batched with a concrete mobile and brooms were used to brush the binder into the surface. Gage rakes set at 3/16 to 1/4 in were used to strikeoff the slurry placed on the bridge deck. Gage rakes were not used on the 300–ft pavement application and the surface was very uneven and not pleasing to the eye. Slag having a gradation similar to an ASTM C33 concrete sand (see Table 1) was used in the slurry mixture. However, the slag used on the bridge deck was first passed through a No. 8 sieve. Material that passed the sieve was used in the mixture (see Table 2) and material that was retained was broadcast onto the freshly placed slurry at the rate of 5 lb/yd^2 to provide additional microtexture and macrotexture. A liquid membrane curing material was applied to prevent water from evaporating from the slurry. The slag was obtained from Ducan Slag Products Company in Pittsburgh, Pennsylvania.

The slurry must cure for about 48 hours to obtain adequate strength for traffic (1,500 psi compressive strength) (See Table 3). Advantages of the slag slurry include increased cover over the top mat of rebar, high micro–texture and adequate macrotexture at a very low cost compared to 2–in thick portland cement concrete overlays, 1.25–in thick latex modified concrete overlays and 0.25–in thick polymer overlays. A slag slurry mixture made with a high early strength special blended cement should be evaluated for use when a short lane closure time is required.

Multiple Layer Polymer Overlays

Multiple layer polymer concrete overlays have been installed on portland cement concrete bridge decks in Virginia and several other states to increase the skid resistance of the surface and to protect the concrete from the infiltration of chloride ion (*5*). The overlay consists of two layers of epoxy, polyester with a methacrylate prime coat, or epoxy urethane and clean, dry, angular–grained, silica or basalt aggregate applied to the top of a portland cement concrete deck to provide a 0.25–in thick wearing surface. Typically, the polymer is applied with brooms or squeegees uniformly over the surface of the deck and before it gels is covered to excess with broadcasted fine aggregate (see Figure 5). Usually, within the first hour, a layer cures sufficiently to permit vacuuming the excess aggregate preparatory to placing a subsequent layer. The polymer concrete overlay has an advantage over other deck protective systems in that it can be constructed in stages during off–peak traffic periods. The first layer of resin and aggregate can be applied to a lane that has been closed and shotblasted, and after a minimum of three hours of cure, the lane can be opened to traffic. The second layer can be placed on the next day or night off–peak traffic period.

An additional advantage of overlays such as latex modified slag slurry and polymer is that new decks can be constructed with polishing aggregates, thereby extending our diminishing supplies of aggregates, and the thin overlays can be applied to provide adequate skid resistance.

RESULTS

Skid Numbers at 40 mph

Table 4 shows the results of skid tests conducted at 40 mph using a smooth tire (ASTM E524–88) (*8*). The minimum

acceptable number in Virginia is 20. New surfaces should have numbers much higher than 20 because the numbers decline as the cumulative traffic over the surfaces increases (*5*).

As can be seen from Table 4 the bridge deck and pavement constructed with polishing limestone aggregate and a screeded surface in the sixties were in need of corrective action. Table 4 shows that the highest numbers were obtained with the latex slag slurry pavement application and the polymer overlays and the lowest numbers were obtained with shotblasting and sealing and the latex slag slurry bridge deck application. The numbers shown in Table 4 were measured within several months after the techniques were applied. All the techniques provide adequate skid numbers.

With the exception of the polymer overlays, skid numbers at later ages are not available because the experimental techniques were first applied in Virginia in 1989. Polymer overlays have been shown to exhibit skid numbers of 35 after 7 years in service (*5*). The skid numbers should be measured at later ages to allow the service life to be estimated.

Permeability to Chloride Ion

A rapid permeability test (AASHTO T277) was used to measure the permeability to chloride ion of the top 2 in of 4–in diameter cores taken from selected bridge decks and the pavement on I–81. The cores were taken within several weeks after the textures were applied with the exception that the cores taken to represent the sawcutting of grooves were textured in the laboratory several days prior to testing. The results are reported in Table 5 in coulombs where <100 = negligible; 100–1,000 = very low; 1,000 – 2,000 = low; and 2,000 – 4,000 = moderate permeability. It can be seen from Table 5 that all the techniques with the exception of the polymer overlay increase the permeability of the top 2 in of the concrete. However, the application of the penetrating sealers to the shotblasted surface brings the permeability back in line with that of the unblasted surface. The application of the latex modified slag slurry also increases the cover over the rebar and should provide additional protection. The protection is not apparent from the test results because the test requires a 2–in thick specimen. In new construction additional cover can be added to account for the cover that will be lost by tining, sawcutting grooves or shotblasting.

The permeability of portland cement concrete surfaces usually decreases with age as the surfaces are sealed by road dirt, oil and carbonation as the portland cement concrete ages. The permeability of the polymer overlays increases with age (*5*). The permeability to chloride ion can be a significant factor when selecting the texturing technique for bridge decks with less than 2 in of cover over the rebar and rebar that is not epoxy coated.

Cost

Table 6 shows the initial cost of the texturing techniques. It is obvious that tining is the most economical technique and the polymer overlay is the most expensive. The other techniques cost about $\$6/yd^2$ with the exception that shotblasting with no sealing costs about $\$2.50/yd^2$. The life cycle cost of the techniques cannot be computed because the life of the surfaces is not known.

Subjective Rating of Techniques

Any one of the five techniques can be used to increase the skid resistance of a deck and the most effective technique is the one that best meets the needs of the deck. A subjective rating as shown in Table 7 can be used to select the optimum alternative in a given situation. The analysis in Table 7 shows that tining is the optimum technique when all factors are given equal weight. However, tining is not an option on old decks and some high quality concretes do not lend themselves to tining. When lane closure time is important sawcutting grooves, shotblasting and polymer overlays can be used. When decks are constructed with polishing aggregates, overlays such as the latex modified slag slurry or the polymer can be used.

CONCLUSIONS

1. At least five techniques can be used to increase the skid resistance of bridge decks and the most effective technique is the one that best meets the needs of the deck.
2. Tining the plastic concrete is the most economical technique for increasing macrotexture but its use is limited to new decks or overlays that are constructed with nonpolishing aggregates and with mixtures and construction procedures that provide for good surface workability at the time the texture is applied.
3. Sawcutting grooves and shotblasting and sealing are economical techniques for increasing the macrotexture of hardened concrete surfaces constructed with nonpolishing aggregates. Both techniques reduce the cover over the rebar and the protection provided by the concrete. Traffic can be applied to the sawcut surface immediately and to sealed surfaces after about 1 hour of cure time.
4. Decks constructed with polishing aggregates would have to be shotblasted on a regular basis, depending on the volume of traffic, to maintain an adequate microtexture.
5. The application of a latex modified portland cement slag slurry is an economical technique for increasing the microtexture and macrotexture of hardened concrete surfaces constructed with polishing or nonpolishing aggregates. The technique also increases the cover over the rebar but is limited to decks that can be closed for two days to allow for proper cure. A slag slurry mixture made with a high early strength special blended cement should be evaluated for use when a short lane closure time is necessary.
6. The application of a multiple layer polymer overlay is a more expensive technique for increasing the microtexture and macrotexture of hardened concrete surfaces constructed with polishing or nonpolishing aggregates. The higher cost can be justified when additional protection against the infiltration of chloride ion is needed and a short lane closure time is necessary.

REFERENCES

1. "Standard Definition of Terms Relating to Traveled Surface Characteristics," *ASTM E867–89*, American Society for Testing and Materials, 1990, Philadelphia Pennsylvania, p. 644.
2. Mahone, David, McGhee, K. H., McGhee, Guy, and Galloway, J. E., Jr. "Texturing New Concrete Pavements," *VTRC 77–R25*, Virginia Transportation Research Council, Charlottesville, Virginia, November 1976, p. 13.
3. Virginia Department of Transportation Road and Bridge Specifications, January 1987, Richmond, Virginia, p. 433.
4. Virginia Department of Transportation Road and Bridge Specifications, January 1987, Richmond, Virginia (as Revised 1989).
5. Sprinkel, Michael M., "Performance of Multiple Layer Polymer Concrete Overlays on Bridge Decks," *Polymers in Concrete: Advances and Applications SP116–5*, American Concrete Institute, 1989, pp. 61–95.
6. "Standard Test Method for Measuring Surface Macrotexture Depth Using a Volumetric Technique," *ASTM E965–87*, American Society for Testing and Materials, Philadelphia, Pennsylvania, 1990, p. 650.

7. "Field Test for Surface Soundness and Adhesion, Appendix A – Test Methods," *ACI Manual of Concrete Practice, Part 5*, American Concrete Institute, Detroit, Michigan, 1982, p. 503R30–31

8. "Standard Specification for Standard Smooth Tire for Pavement Skid–Resistance Tests," *ASTM E524–88*, American Society for Testing and Materials, Philadelphia, Pennsylvania, 1990, p. 612.

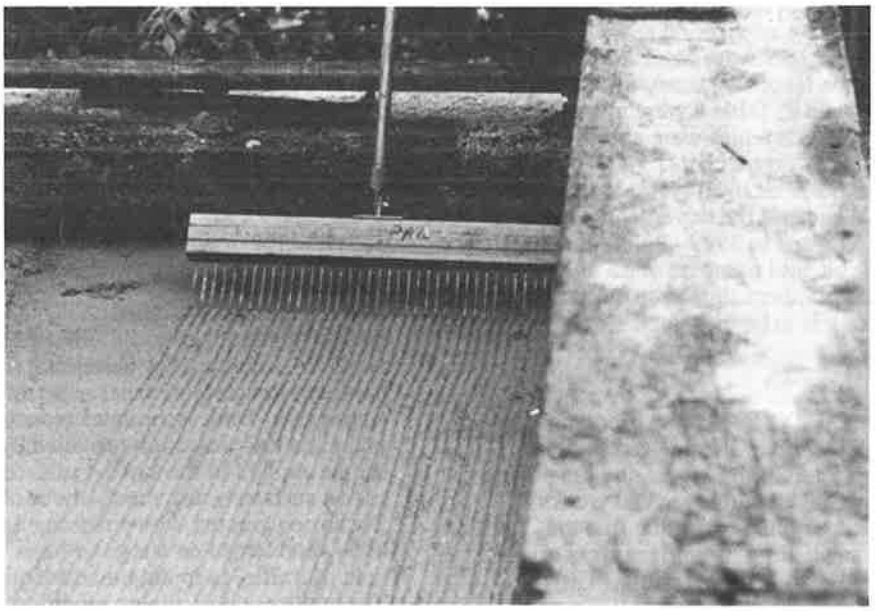

FIGURE 1 A tining device should be pulled across the surface as soon as possible after the finishing operation is complete to produce grooves that are approximately 1/8 in wide and 1/8 in deep and 3/4 in on center to produce a surface with a high skid resistance.

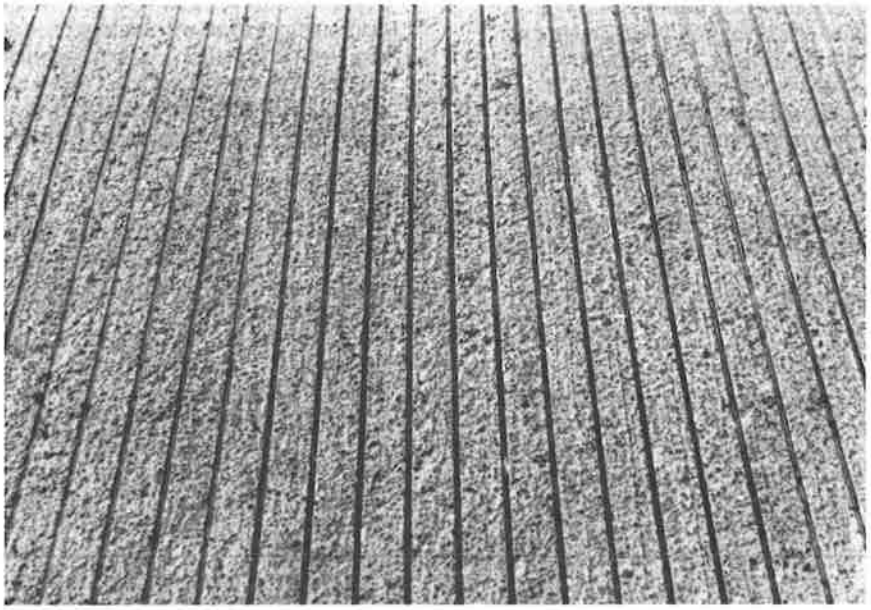

FIGURE 2 The hardened concrete may be sawed to produce grooves approximately 1/8 in wide by 3/16 in deep and 3/4 to 1 1/2 in on centers. The grooves shown here are spaced 1 1/4 in on centers.

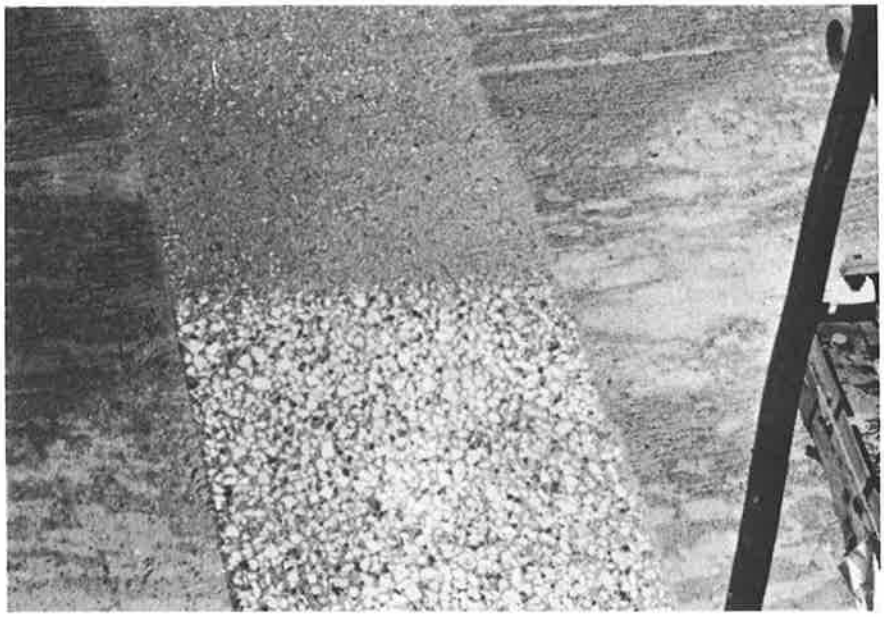

FIGURE 3 The degree of cleaning obtained with shotblast equipment is a function of the forward speed, the number of passes, the size of the shot, and the gate opening. Once the proper setting is identified, the entire surface should be cleaned at that setting. A slow speed or multiple passes are required to obtain the exposed aggregate surface shown above. The lighter cleaning (top of figure) was obtained by increasing the forward speed of the blaster. It is usually necessary to expose the coarse aggregate to obtain adequate bond strength and to provide good skid resistance.

FIGURE 4 A latex modified slag slurry overlay is here applied to a bridge deck to increase the skid resistance. Brooms should be used to brush the slurry into the shotblasted surface and the slurry should be struck off and pulled forward with gage rakes set to provide a 3/16 in to 1/4 in thick slurry. For increased skid resistance slag should be broadcast onto the struck off surface, and a liquid curing material should be applied to prevent the evaporation of water. The slurry can be opened to traffic in two to three days.

FIGURE 5 An epoxy urethane mixture is here spread over the deck with notched squeegees. Basalt aggregate is here broadcast to excess from the back of a dump truck. Polymer overlays constructed with epoxy, polyester, methacrylate, and epoxy urethane can be used to increase the skid resistance of bridge decks.

TABLE 1 Sieve Analysis of Slag, % Passing Indicated Sieve

Sieve	Slag	ASTM C33
-3/8	100	100
—4	95	95–100
—8	63	80–100
—16	39	50–85
—30	24	25–60
—50	16	10–30
-100	9	2–10
-200	4	

TABLE 2 Mixture Proportions for Latex Modified Portland Cement Slag Slurry, lb/yd^3

	Design	Actual**
Cement*	911	874
Slag	2,375	2,279
Latex emulsion	368	353
Water	213	272
W/C	0.44	0.52

* Type III portland

** The slag was assumed to have an 8% moisture content, but was found to have an 11% moisture content.

TABLE 3 Compressive Strength, lb/in^2, Vs Age*

Technique Test section	Latex Modified Slag Slurry I-81 NBTL pavement	 I-81 NBTL bridge deck	Polymer Overlay Typical for modified epoxy
3 hr	—	—	2,800
18 hr	370	—	—
24 hr	—	1,050	8,100
40 hr	1,970	—	—
48 hr	—	1,590	8,500
28 day	4,100	2,680	—

* Results based on average of three tests on 2-in field cured mortar cube specimens.

TABLE 4 Smooth Tire Skid Numbers at 40 mph

Technique	Test Section	Skid Numbers
None (12.8 in dia. sand patch)	I–81 SBTL bridge deck	17
None (10.1 in dia. sand patch)	I–81 NBTL pavement	27
Tining plastic concrete	Latex modified concrete overlay Rte. 340 over Hawksbill Creek	41
Tining plastic concrete	Bridge deck Rte. 161 over North Run	42
Sawcutting grooves 3/4 in on center	International Blvd. pavement [2]	47
Sawcutting grooves 1 1/2 in on center	International Blvd. pavement [2]	41
Shotblast (5.5 in dia. sand patch)	I–81 NBTL pavement	45
Shotblast (7.4 in dia. sand patch)	I–81 SBTL bridge deck	37
Shotblast and seal with gum resin (7.2 in dia. sand patch)	I–81 SBTL bridge deck	36
Shotblast and seal with siloxane (7.5 in dia. sand patch)	I–81 SBTL bridge deck	40
Latex modified slag slurry	I–81 NBTL pavement	65
Latex modified slag slurry	I–81 NBTL bridge deck	39
Polymer overlay	I–64 EBTL bridge deck	63

TABLE 5 Permeability to Chloride Ion, Coulombs

Technique	Test Section	Permeability
None	I–81 SBPL bridge deck	1,866
None	I–81 NBTL pavement	2,100
Tining plastic concrete	Latex modified concrete overlay Rte. 340 over Hawksbill Creek	1,464
Tining plastic concrete	Bridge deck Rte. 161 over North Run	3,385
Sawcutting grooves 3/4 in on center	Latex modified portland cement concrete overlay (16 yr old)	146*
Sawcuttings grooves 3/4 in on center	Portland cement cencrete concrete overlay (16 yr old)	2,147**
Shotblast (8.0 in dia. sand patch)	I–81 NBTL pavement	2.925
Shotblast (7.4 in dia. sand patch)	I–81 SBTL bridge deck	2,731
Shotblast and seal with gum resin (7.2 in dia. sand patch)	I–81 SBTL bridge deck	1,480
Shotblast and seal with siloxane (7.5 in dia. sand patch)	I–81 SBTL bridge deck	1,975
Latex modified slag slurry	I–81 NBTL pavement	2,879
Polymer overlay	I–64 EBTL bridge deck	12

* 102 before saw cuts made.
** 1,305 before saw cuts made.

TABLE 6 Cost, $/yd^2

Technique	Test Section	Cost
Tining plastic conrete	Typical	0
Sawcutting grooves 3/4 in on center	Average for nine bridge decks in Staunton District in 1989 (10,450 yd^2)	6.15
Shotblast (5.5 in dia. sand patch)	I–81 NBTL pavement	2.50
Shotblast and seal with gum resin (7.2 in dia. sand patch)	I–81 SBTL bridge deck	5.25
Shotblast and seal with siloxane (7.5 in dia. sand patch)	I–81 SBTL bridge deck	5.85
Latex modified slag slurry	I–81 NBTL pavement	5.90
Polymer overlay	Typical cost in 1989	30.00

TABLE 7 Subjective Rating of Techniques.

Technique	Tining	Sawcut Grooves	Shotblast and Seal	Latex Modifited Slag Slurry	Polymer Overlay
Cost	5	3	3	3	1
Lane closure time	5	3	3	1	3
Wear	3	3	2	3	3
Surface appearance	3	3	3	2	4
Chloride ion protection	2	2	2	3	5
Total	18	14	13	12	16

1 = low rating for disadvantage.
5 = high rating for advantage.

Bridge Superstructure Rehabilitation and Strengthening

FRIEDER SEIBLE, M. J. NIGEL PRIESTLEY, AND KOSALRAM KRISHNAN

Increased demand for higher legal loads and permit overloads on the nation's highway system necessitates the strengthening of a large number of existing short and medium span bridge structures. Frequently, the strengthening of bridge superstructures goes hand in hand with rehabilitation measures of the bridge deck and the road surface, such as structural concrete overlays or widening measures to accommodate additional traffic lanes. As part of an ongoing research project with the California State Department of Transportation, a 12 ft. wide, 60 ft. long section of an existing 25 year old cast-in-place reinforced concrete T-girder bridge was brought from near Fresno, California to the Charles Lee Powell Structural Systems Laboratory at the University of California, San Diego, for full scale investigation of different repair and strengthening measures.

The bridge deck was rehabilitated by a full depth structural concrete overlay and tested under simulated service and overloads. Upon completion of the overlay tests to the flexural yield limit state, the flexural cracks of the bridge girder were repaired by epoxy injection. Two types of strengthening measures were subsequently investigated, namely the more popular external post- tensioning and a new innovative approach in which a prestressed high strength precast concrete panel was added to the existing bridge girder in the form of a thin bottom soffit. Prior and subsequent to the implementation of the repair and strengthening measures, forced vibration tests as well as centric and eccentric working load level tests were conducted to monitor the change in the structural response characteristics. A brief description of the implementation of the repair and strengthening measures is provided together with experimental behavioral data and a discussion on the effectiveness of the various strengthening measures.

INTRODUCTION

General

There is a growing need for rehabilitation, repair and strengthening of a large number of aging short and medium span bridge structures on the nation's highway system. Increased demand for higher legal loads and permit overloads, changes in design specifications, corrosion of existing reinforcement and the need for significant deck resurfacing or overlays necessitates strengthening of existing reinforced concrete bridge structures. Frequently, the strengthening of bridge superstructures goes hand in hand with rehabilitation measures of the bridge deck and the road surface or widening measures to accommodate additional traffic lanes.

The design of rehabilitation measures is commonly based on design experience or available empirical field data. Frequently, repair or strengthening measures replace or add structural components in an existing bridge structure in a composite fashion. However, few design guidelines or specifications based on comprehensive research exist to ensure monolithic composite behavior. With a large number of bridge structures in need of rehabilitation, a systematic and research oriented approach to the design of the rehabilitation measures is essential to ensure an effective and reliable structural systems behavior.

Small-scale laboratory experiments on repair and strengthening measures are only of limited use, since the connection detail between the existing bridge and the rehabilitation measure does not allow for scaling without loss of accuracy for various behavior limit states. Thus, basic data on the effectiveness of repair and strengthening measures can either be obtained from low level nondestructive field tests, destructive field tests or full scale laboratory experiments.

As part of an ongoing research project with the California State Department of Transportation, an 11 ft-6 in. wide, 56 ft long section of an existing 25 year old cast-in-place reinforced concrete T-girder bridge was brought from Fresno, California, to the Charles Lee Powell Structural Systems Laboratory at the University of California, San Diego, for full scale repair and testing of a structural concrete overlay [1]. A basic overview of the bridge geometry is given in Fig. 1(a), together with an outline of the section which was removed and brought to San Diego for full scale laboratory testing. The principal dimensions of the test section are shown in Fig. 1(b). After 25 years of service, the Gepford Overhead became obsolete since the railroad line it crossed was abandoned and Caltrans decided to remove the bridge structure eliminating continuous maintenance. Upon completion of the overlay tests which are summarized in the following section and reported in detail in [2], the fully instrumented bridge section presented a unique opportunity to investigate the effectiveness of strengthening measures for existing bridge superstructures under controlled laboratory conditions. First, the flexural cracks in the bridge girders were sealed by epoxy injection. Subsequently, two types of strengthening measures were investigated, namely, the more popular external post-tensioning and a new innovative approach in which prestressed high strength precast concrete panels were added to the existing bridge girder in the form of a thin bottom soffit. The bottom soffit panel was positioned with galvanized dowel bolts and epoxy grouted to the girder bottom. The panel not only increases the longitudinal flexural capacity, but also improves the transverse load distribution characteristics and bridge aesthetics through a closed bottom soffit. Prior and subsequent to the implementation of the repair and strengthening measures, forced vibration tests as well as centric and eccentric working load level tests were conducted to monitor the change in the structural response characteristics.

A brief overview of the overlay research and a description of the implementation and effectiveness of the

Department of Applied Mechanics and Engineering Sciences, University of California-San Diego, La Jolla, CA 92093-0411.

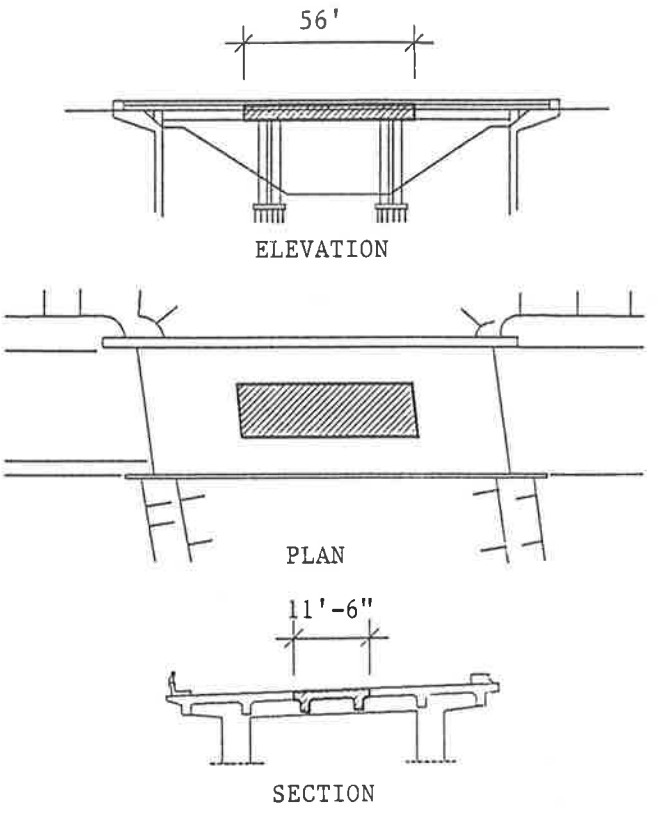

(a) Prototype from Calif. Hwy. 41, Fresno

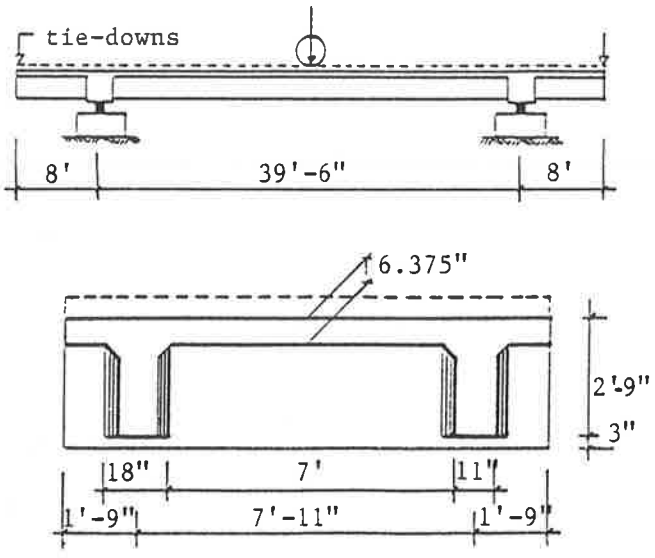

(b) Full-Scale Test Section Dimensions

FIGURE 1 Gepford Overhead bridge section

repair and strengthening measures together with behavioral data is presented in the ensuing sections.

Structural Concrete Overlay

Repair of individual potholes or scaled-off concrete bridge deck areas typically has limited longevity, and hence prompted the use of full depth structural concrete overlays placed on top of the existing damaged bridge deck in the State of California. Since the contribution of the existing damaged deck is difficult to assess, the full depth overlay is typically fully reinforced. However, this fully reinforced overlay can only be considered effective if horizontal shear transfer between the old deck and the overlay ensures monolithic flexural action. Reinforcing dowels placed across the horizontal construction joint to provide monolithic flexural action are very costly and labor intensive. Moreover, their effectiveness to provide horizontal shear transfer in conjunction with various interface surface preparations is questionable.

The Gepford Overhead bridge section was repaired with a full depth (6 in.) structural (reinforced) concrete overlay in accordance with the design recommendations developed in [1,3] which are based on horizontal shear transfer without dowels [4] for most practical applications. The full depth overlay was placed on a dry and clean surface without any interface dowels for horizontal shear transfer. The surface was sandblasted over one-half the span and scarified over the other half of the span. The overlaid test section is depicted in Fig. 2, together with the vertical loading arrangement and the inflection point tie-downs to effectuate continuous bridge action. The overlay implementation was substantially simplified with the omission of interface dowels and no interface delamination was observed during the overload tests to the flexural yield limit state or after 200,000 dynamic cyclic (5 Hz frequency) wheel load tests at the quarter span points.

A detailed account of the overlay application and the associated test results are presented in [1] and [2]. In the following, the repair and strengthening measures are described first in general, followed by a section on specific behavioral results.

STRENGTHENING MEASURES

Epoxy Injection of the Flexural Cracks

The Gepford Overhead bridge section upon removal from State Highway 41, already exhibited substantial flexural cracking in the positive moment region. The midspan flexural cracks extended through the girders almost to the top deck slab.The yield limit state tests, subsequent to the full depth overlay application clearly amplified and propagated this flexural crack pattern. The presence of nearly forty flexural full penetration cracks in each girder presented an unique opportunity to investigate the effectiveness of epoxy injection of flexural cracks under controlled laboratory conditions.

The tie-downs at the inflection points were released to investigate the grouting of fully open flexural cracks. In preparation for epoxy injection, loose material was blown from the cracks with compressed air. Injection ports were

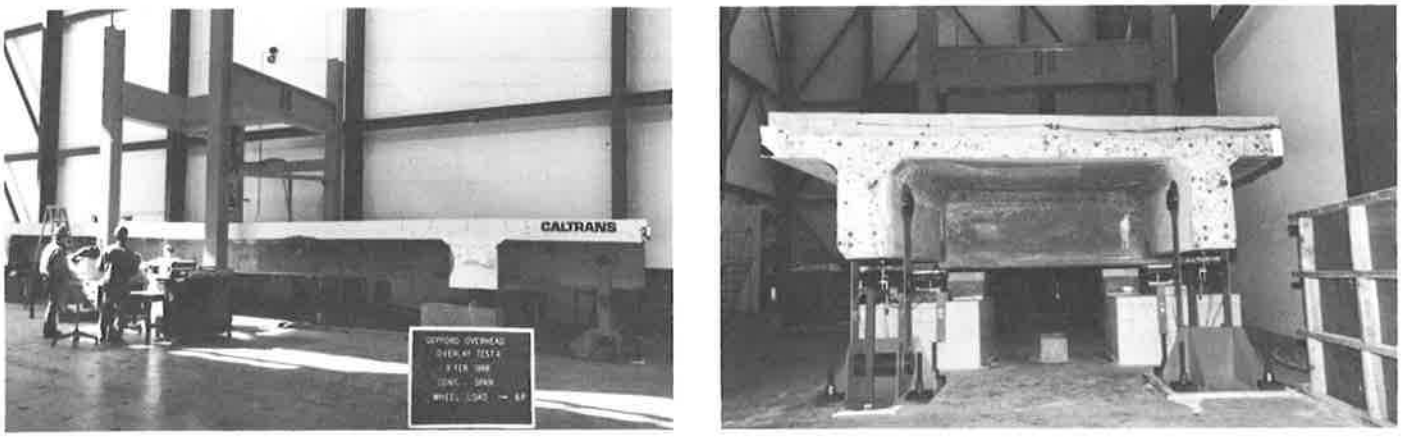

FIGURE 2 Gepford overhead bridge section laboratory setup

placed every 10 to 12 inches along the length of the crack, as shown in Fig. 3(a). The port spacing corresponds approximately to the web thickness to ensure adequate epoxy penetration through the cracks. A two component, rapid curing, smooth paste epoxy gel was used to seal the cracks and secure the injection ports to the cracks prior to pressure grouting. Upon curing of the epoxy seal (approximately two hours), a two component, low viscosity, high strength epoxy adhesive was used for pressure injection of the flexural cracks. Injection started at the lowermost injection port on each crack and progressed from port to port, as soon as epoxy emerged from the next higher port along the crack or a pressure of 100-150 psi was sustained at one port for 30 seconds without the flow of epoxy. Injection was not essential at all ports; if the resin flow was good, the interim ports were only used to monitor penetration. Upon curing of the epoxy adhesive (approximately 1-2 days), the epoxy seal around the cracks was burnt off with a gas torch and the residues scraped off leaving a smooth but discolored surface as indicated in Figs. 3(b) and 3(c).

Low level forced vibration tests performed before and after the epoxy injection of the flexural cracks, showed a 15% increase in the first natural frequency, from 8.8 Hz to 10.42 Hz. This 15% fundamental frequency increase corresponds to a 40% stiffness increase in an equivalent generalized single degree of freedom bridge deck model. Subsequent overload tests showed the development of new flexural cracks in the bridge girders, independent of the existing epoxy sealed cracks.

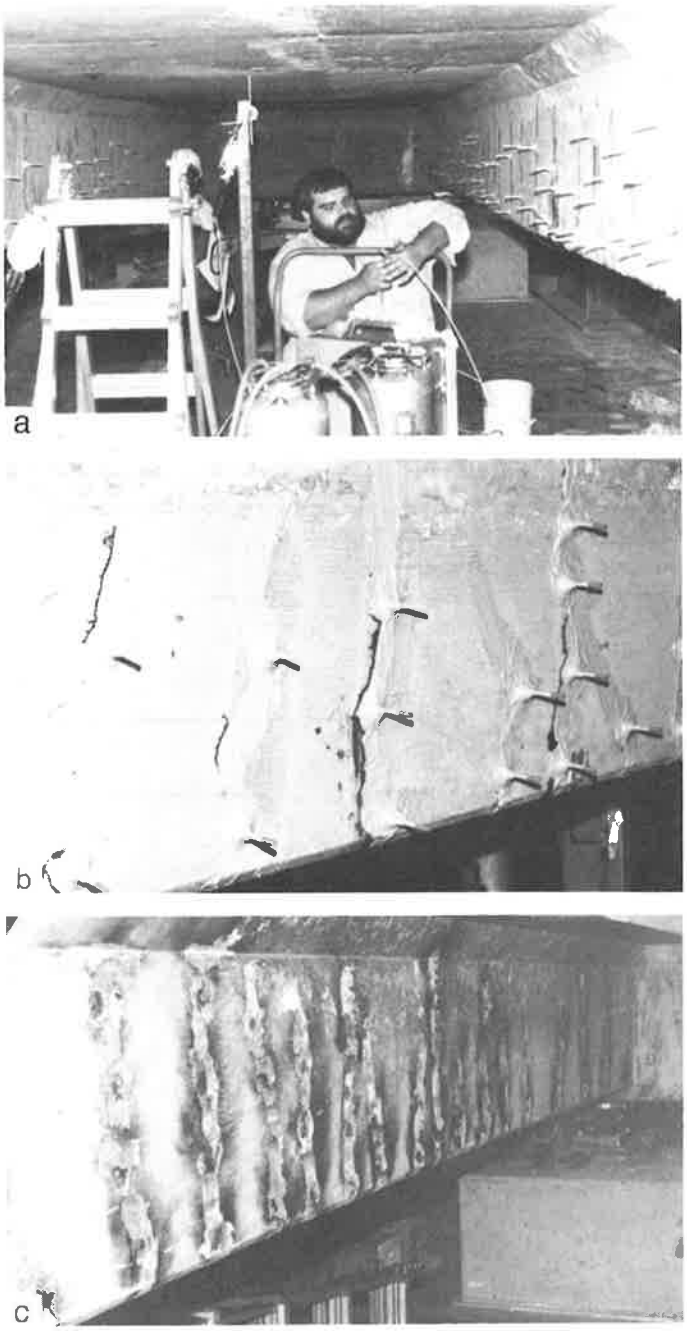

FIGURE 3 Epoxy injection of flexural cracks

External Prestressing

The bridge section was tied to the test floor after epoxy injection of the flexural cracks to effectuate continuous bridge action. External prestressing tendons were added at the bottom of the webs to increase the flexural midspan capacity. The external post-tensioning was designed to balance the increased negative moment capacity at the bents due to the full depth structural concrete overlay. Two #8 Grade 150 thread bars were placed along the sides of each girder, see Fig. 4(a), and anchored to the bridge section through the anchor blocks in the webs on one end and through the intermediate diaphragm at the other end of the bridge span.

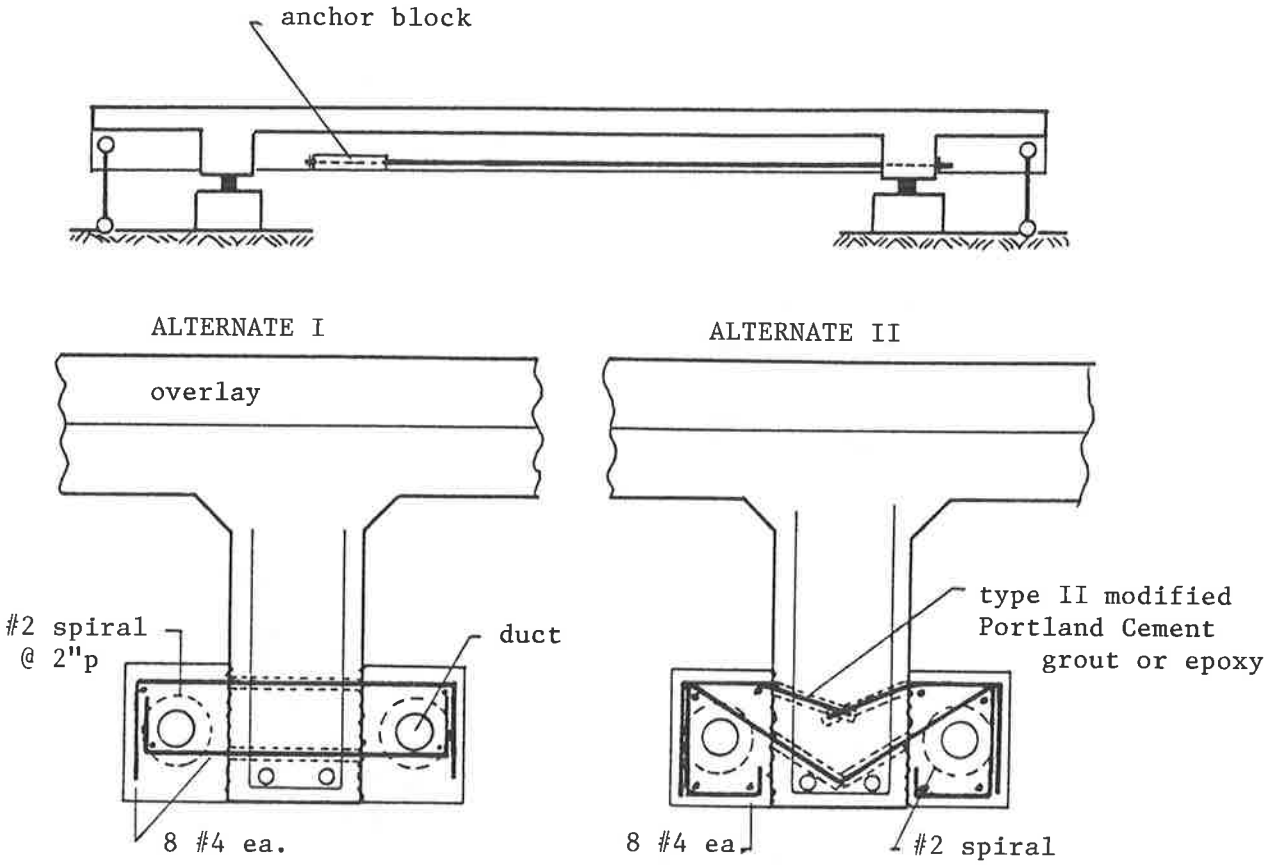

(a) External Tendon Strengthening Measure

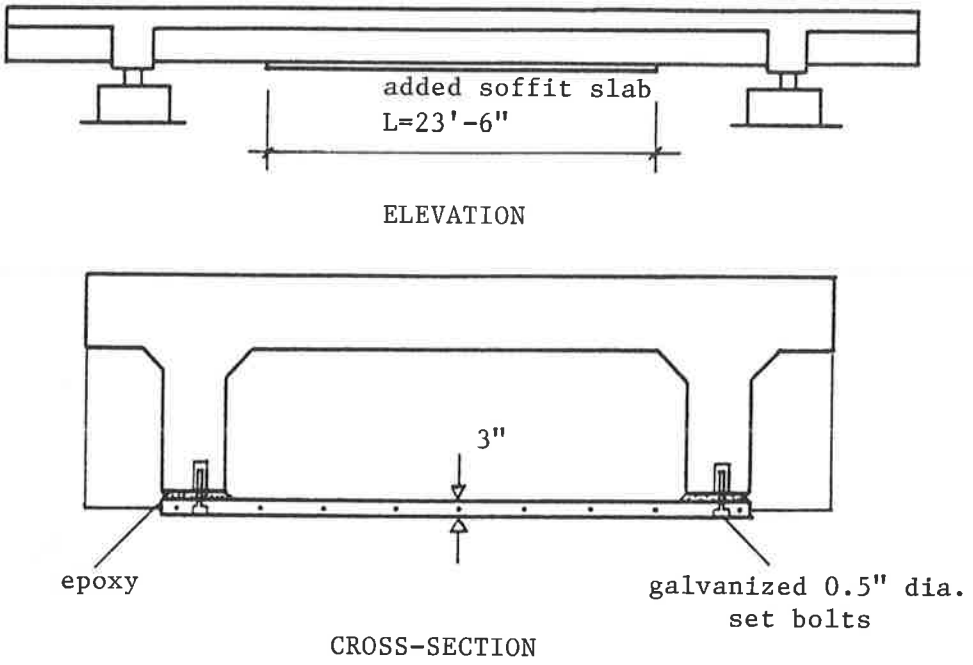

(b) Bottom Soffit Slab Panel Addition

FIGURE 4 External strengthening measures

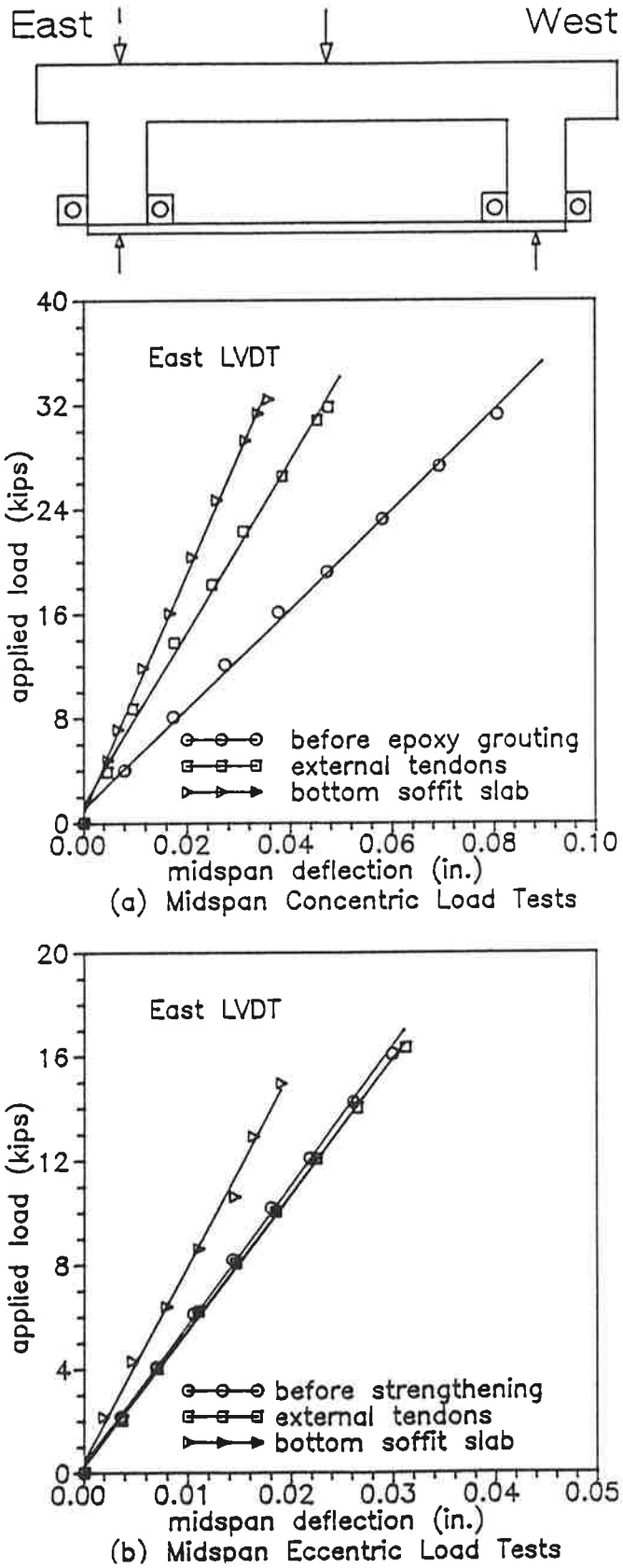

FIGURE 5 Stiffness characteristics of the test section

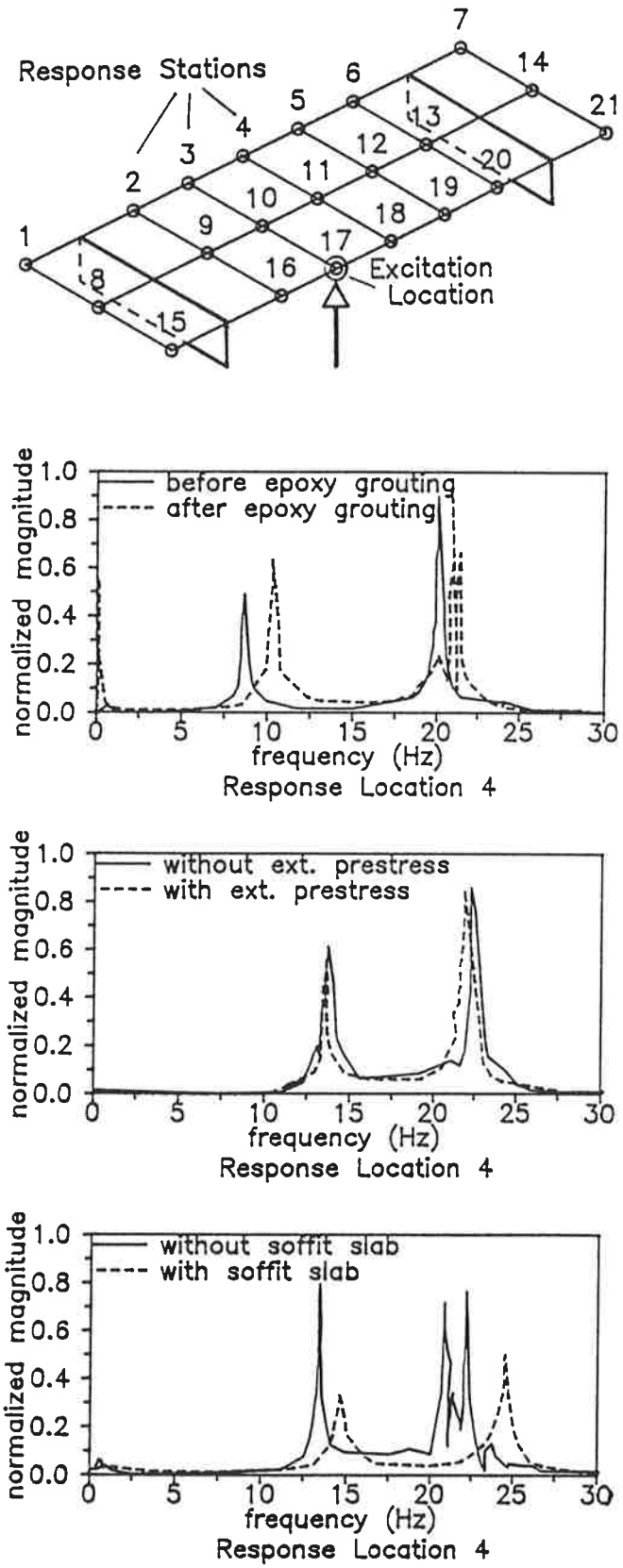

FIGURE 6 Change in dynamic response characteristics

The amount of anchor block reinforcement was based on ACI 318-83, shear friction criteria. Three different ways to anchor and develop the shear friction reinforcement were investigated, namely, through dowels grouted with epoxy in horizontally drilled holes, using the previously described epoxy injection process, and alternatively, individual dowels set in 6 in. deep drilled inclined holes with Type II modified Portland cement grout on one side and epoxy gel on the other side of the girder, respectively, as depicted in Fig. 4(a). All dowel reinforcement consisted of #4 Grade 60 bars pre-bent or bent-in-place depending on the application. The contact surface between the girder face and the anchor block was scarified. The anchor blocks were cast with 5,000 psi concrete and the #8 post-tensioning bars were placed in galvanized pipes for protection. The bars were tensioned to a force level of about 80 kips per bar after the anchor block concrete had reached 80% of its design strength. The galvanized pipes were grouted using Portland cement grout with an expansive grout aid. For post-tensioning, all the anchor blocks were instrumented with Linear Variation Displacement Transducers (LVDT's) in addition to strain gage instrumentation on selected shear friction dowels. No separation or sliding between the anchor block and the bridge girder was observed, which indicates that all three dowel bonding methods were effective.

Service load tests and forced vibration tests indicated virtually no increase in stiffness due to the external post-tensioning. This is again an indication that all flexural cracks were effectively sealed during the epoxy injection process. The bridge section behaved as a typical prestressed concrete structure with no significant flexural cracking even at a load level of 208 kips applied centric between the girder lines at midspan.

Bottom Soffit Panel

The final strengthening measure investigated consisted of the addition of a thin prestressed, high strength precast concrete soffit slab, see Fig. 4(b), after the external tendons were cut. The prestress level in the panel was designed to match the midspan flexural capacity of the external tendon strengthening measure. The panel was manufactured in a 200 ft. long casting bed where nine 0.5 in. ϕ Grade 270 strands were pre-tensioned to 60% f_{pu} prior to the casting of the high strength concrete.

The horizontal load transfer between the new bottom soffit panel and the existing bridge section was designed to be achieved through epoxy bonding, while the self weight of the panel was supported by ten 1/2 in. ϕ threaded rods which were also used to position and clamp the soffit panel in place during installation and the curing of the epoxy. Two different epoxy bonding procedures were employed, namely the gel process where the soffit slab was buttered with 1/2 in. thick epoxy gel along one girder, and the epoxy injection process, where the joint between the soffit panel and the bridge girder was first sealed with epoxy gel and subsequently injected with a low viscosity, high strength epoxy adhesive. In both cases, the bottom of the girder was roughened with a jack hammer and cleaned with compressed air and the surface of the precast soffit slab panel was sandblasted prior to installation.

The addition of the bottom soffit panel resulted in a significant increase in flexural stiffness and improved transverse load distribution characteristics. Overload tests with a midspan point load between the girder lines initiated horizontal shear failure of the girder concrete cover adjacent to the epoxy joint at the south-western corner of the precast bottom soffit panel, at a load level of 176 kips and an estimated horizontal shear stress level of 350 psi.

SYSTEMS EVALUATION

Load Tests

Each structural repair or strengthening measure was evaluated by a series of tests which were performed prior and subsequent to the structural modification. First, forced vibration tests were conducted to evaluate the effectiveness of low level experimental modal analysis techniques to predict the change in the dynamic response characteristics due to various repair and strengthening measures. Subsequent to the forced vibration tests, the test program consisted of midspan point loads applied both centrically between and eccentrically over the girder lines. These loads represented wheel loads at various service load limit states. Finally, these same point loads were used to investigate overload limit states, in some cases, up to the flexural yield limit state in the midspan girder reinforcement.

Point loads were applied at midspan with a MTS servo controlled actuator reacted against a four column load frame depicted in Fig. 2. The load was applied in increments of the AASHTO-83 [5] HS-20 basic maximum wheel load of P_{20} = 16,000 lbs. without impact allowance. The 8 inch by 20 inch loading area was based on AASHTO-83, Section 3.3 tire contact area of $A = 0.01\ P_{20}$ [in^2] or 160 in^2 with a 1:2.5 aspect ratio. At full multiples of the P_{20} load, three cycles of unloading and reloading were performed to simulate three traffic cycles at that particular load. The point load tests were primarily used to establish comparative load deformation or stiffness characteristics between adjacent girders.

The longitudinal stiffness increases due to the overlay application and continuous support conditions were expected but the most striking result was obtained from the epoxy injection of the flexural cracks, where a substantial stiffness increase was noticed, see Fig. 5(a). This stiffness increase can be completely attributed to the epoxy injection since no additional stiffness increase resulted from the external post-tensioning as is evident from Fig. 5(b).

Forced Vibration Tests

Full scale field tests with known service loads are very involved and often prohibited by continued service requirements. Moreover, overload load tests can introduce additional cracking and with it progressive and cumulative structural deterioration. Thus, there is a need for nondestructive field testing to identify the current state of the bridge structure and assess the changes in the structural response due to the various repair or strengthening measures.

Experimental modal analysis with a low level random excitation from a seismic shaker is one such nondestructive testing technique used for systems identification of the bridge section at various stages of the research program. The frequency response was obtained at a number of discrete,

Table 1 - Summary of Response Characteristics of Gepford Overhead Section

Test No.	Bridge Condition	Support Condition	Mode	Frequency (Hz)	Mode Shape Characteristic
(1)	Simply supported	simple	1 2	8.80 20.24	Main span & overhang flexure Main span torsion
(2)	(1) + epoxy grouted cracks	simple	1 2	10.42 20.90	Main span & overhang flexure Main span torsion
(3)	(2) + continuous support	continuos	1 2	14.04 22.70	Main span flexure Main span torsion
(4)	(3) + external post-tensioning	continuous	1 2	13.85 22.00	Main span flexure Main span torsion
(5)	(4) + after traffic load tests	continuous	1 2	13.56 21.66	Main span flexure Main span torsion
(6)	(5) + removal of external tendons	continuous	1 2	13.23 20.90	Main span flexure Main span torsion
(7)	(6) + bottom soffit panel	continuous	1 2	14.50 24.40	Main span flexure Main span torsion
(8)	(7) - continuous support	simple	1 2	10.65 21.80	Main span & overhang flexure Main span torsion

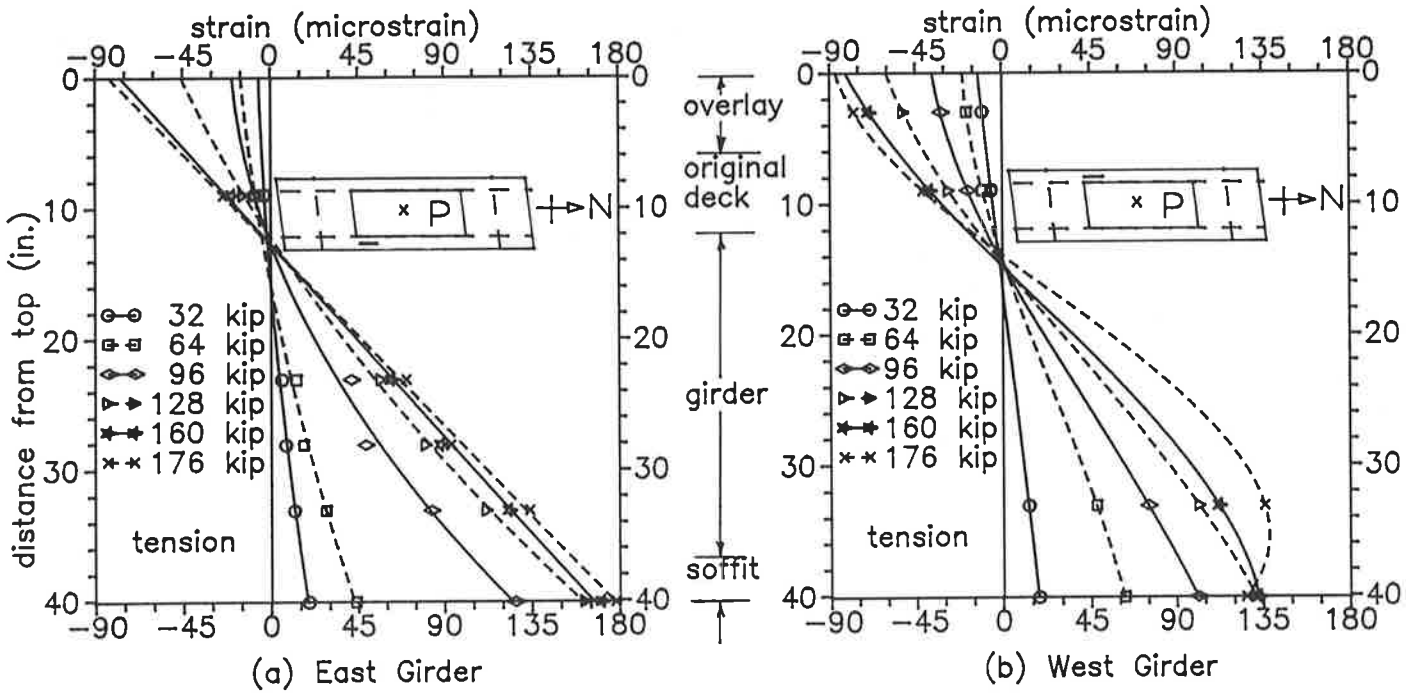

FIGURE 7 Strain profile on the girder at the south quarter span

strategic locations in the structure to an excitation from a 30 lb. Acoustic Power System vertical shaker. An analysis band of 50 Hz was chosen to capture changes in the fundamental modes of the bridge structure due to the various strengthening procedures.

A numerical evaluation of the first two natural frequencies obtained from the forced vibration tests conducted and the various support conditions are presented in Table 1. The most striking result can be found in a 15% frequency increase in the first mode of the simply supported bridge structure due to epoxy grouting of the flexural cracks, from 8.80 Hz to 10.42 Hz, whereas virtually no additional stiffness increase was observed due to external prestressing. Gluing a thin precast slab panel to the bottom of the double-Tee bridge section increased the fundamental frequency from 13.23 Hz to 14.5 Hz, thereby indicating an increased longitudinal stiffness. A significant increase in the transverse load distribution characteristic was also noted by the change in the second mode frequency from 20.9 Hz to 24.4 Hz on the addition of the precast bottom soffit panel, since the transverse flexible T-girder deck was transformed into a stiff box girder with highly improved torsional characteristics. However, no transverse stiffness increase was noticed due to the epoxy injection of the flexural girder cracks or external prestressing. The shift in the natural frequency is graphically depicted for a midspan response station in Fig. 6. These low level dynamic systems identification results are currently correlated to service and overload test results as well as comprehensive analytical modeling to quantify the effectiveness of rehabilitation measures based on nondestructive systems evaluation.

Overload and Ultimate Load Tests

Midspan point load overload tests were performed subsequent to each strengthening measure up to the flexural yield limit state to correlate low level nondestructive test characteristics with subsequent limit state behavior and to investigate the onset and development of possible failure modes. One such failure mode characteristic for the precast bottom soffit strengthening measure is graphically depicted in Fig. 7 where the strain profiles at a section 10 ft. from the left (South) support are plotted at subsequent overload levels. The nonlinear strain profile in the west girder at higher load levels, see Fig. 7, indicates a force reduction in the bottom soffit panel. This force reduction on the west side of the soffit panel was caused by a horizontal shear failure, see Fig. 8, in the cover concrete of the bridge girder parallel to the epoxy joint at a calculated horizontal shear stress level of 350 psi. Thus, while the epoxy bonding of the bottom soffit panel proved adequate for the overload tests, the necessity to anchor the added soffit panel mechanically through dowels into the core of the bridge girder became obvious for the ultimate limit state. The overload tests were repeated after the horizontal failure crack was sealed again by epoxy injection and the tie-downs detensioned to provide a simple support condition for the bridge section. In the subsequent final ultimate limit state test with an increasing midspan point load the bridge section exhibited a similar horizontal shear failure of the girder concrete cover parallel to the epoxy joint.

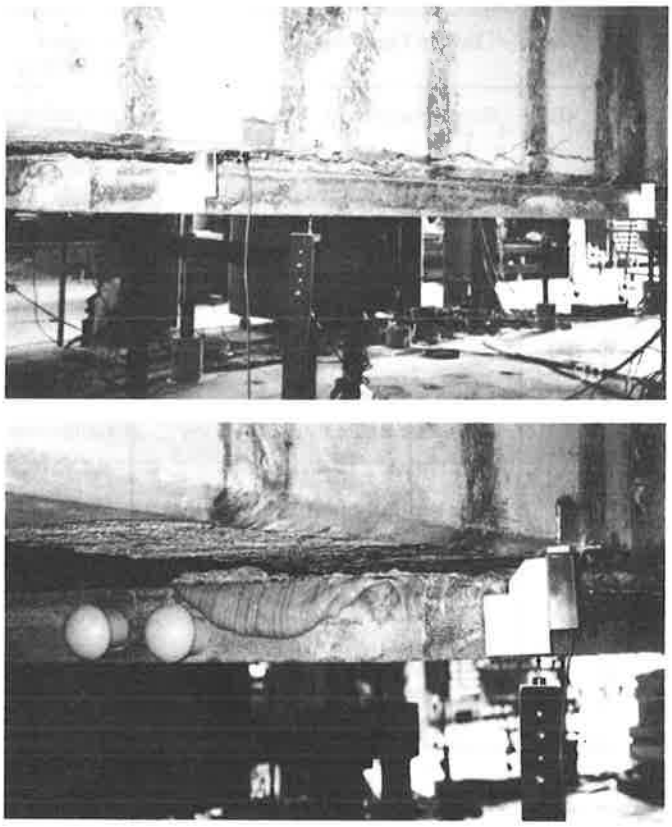

FIGURE 8 Shear failure on the west girder

Finally, ultimate load tests were conducted on the west and east exterior anchor blocks added for the external post-tensioning strengthening measure, see Fig. 4(a), to investigate ultimate limit state characteristics for different anchoring procedures. The west exterior anchor block had 16 # 4 dowels anchored in 6 in. deep inclined holes and grouted with Type II modified Portland cement grout. The east exterior anchor block had 16 # 4 through dowels anchored in horizontally drilled holes, grouted by epoxy injection. The anchor blocks were sheared off with calibrated hollow core jacks and the horizontal anchor block movement as well as the dowel strains were monitored. Fig. 9 depicts the load versus horizontal displacement relationship obtained for the two different anchoring procedures together with the ACI shear friction design level. It is evident that the anchor blocks performed adequate with respect to the shear friction design value. However, the through dowels exhibited a ductile behavior while the set dowels resulted in anchor block slip with significant capacity loss, see Fig. 9, due to slip in the dowel anchorage.

CONCLUSIONS

The repair and strengthening measures investigated were: (1) bridge deck repair with a full depth structural concrete overlay; (2) repair of flexurally cracked bridge superstructures by epoxy injection; (3) strengthening with external post-tensioning tendons; and (4) strengthening with the addition of a thin high strength prestressed bottom soffit panel to the

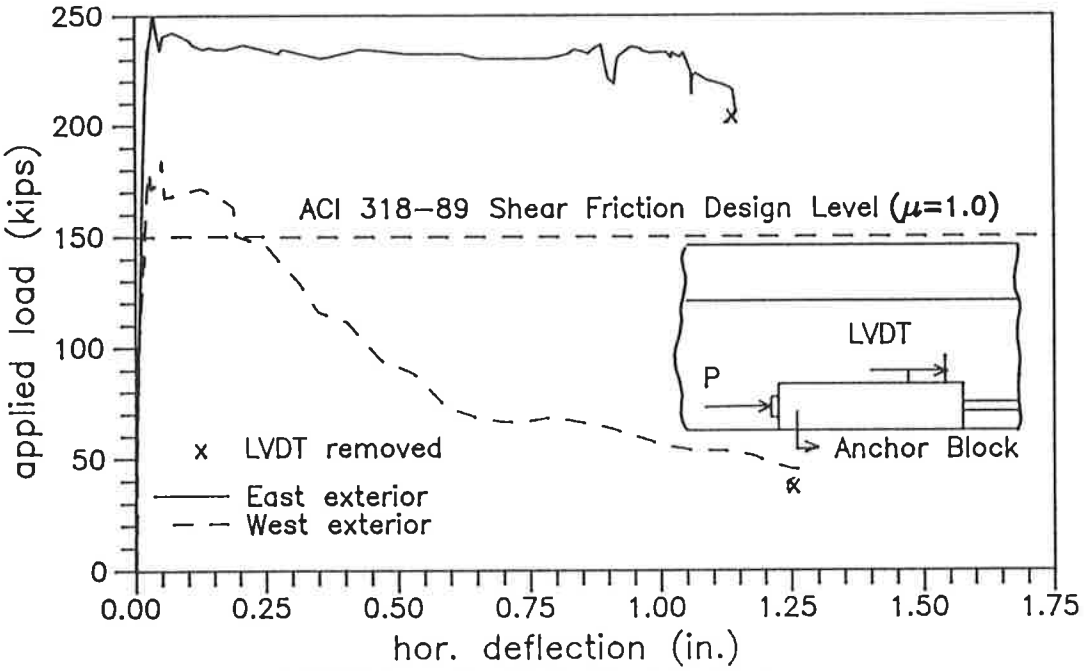

FIGURE 9 Anchor block-ultimate load test response

implementation of the other repair and strengthening measures was furnished together with experimental behavioral data.

The dowel reinforcement was found to be ineffective for full depth structural concrete overlays in conjunction with a rough and clean interface if horizontal shear stress levels did not exceed $2\sqrt{f'_c}$. Forced Vibration systems identification of the Gepford Overhead test section at various stages of the research program showed a significant change in the structural response characteristics due to epoxy injection of the flexural cracks and the addition of the bottom soffit panel, whereas external post-tensioning had virtually no impact on the structural stiffness. Both centric and eccentric working load level tests confirmed the above inference thereby proving low level forced vibration testing as an effective nondestructive systems identification tool. Overload tests to the onset of flexural yield in the main longitudinal rebars, with the external post- tensioning exhibited the excellent performance of the anchor blocks and the bridge structure with virtually no new flexural cracks. Ultimate limit state tests on the anchor blocks investigated the differences in the failure characteristics due to the different anchorage procedures. The two different epoxy bonding procedures for the bottom soffit panel performed satisfactorily and the bridge section behaved as a monolithic unit. The horizontal shear failure of the girder concrete demonstrates the need for additional edge bonding (e.g. dowels) by mechanical means into the core of the bridge girder.

ACKNOWLEDGEMENTS

The presented research was co-sponsored under the Presidential Young Investigators research program by the National Science Foundation and by Caltrans, Office of Structures Design. The National Science Foundation participated under Grant Number CES 85-52672 and the Federal Highway Administration under Contract Number F85SD19 and Agency Grant Number RTA 1294-53D408.

Epoxy injection of the flexural cracks and epoxy bonding of the anchor block dowels and the precast bottom soffit panel was performed and donated to the project by Slater Waterproofing Inc., Montclair, California, in cooperation with Sika Corporation. Post-tensioning hardware equipment was provided by Dywidag Systems International, U.S.A. Inc., Long Beach, California. The precast prestressed bottom soffit panel was manufactured at Tru Span, San Diego, a subsidiary of Spancrete.

REFERENCES

1. Seible, F., Latham, C. and Krishnan, K., *"Structural Concrete Overlays in Bridge Deck Rehabilitation – Summary of Experimental Results, Analytical Studies and Design Recommendations,"* University of California, San Diego, Structural Systems Research Project, Report No. SSRP-88/04, June 1988.
2. Seible, F., Latham, C. and Krishnan, K., *"Structural Concrete Overlays in Bridge Deck Rehabilitation – Experimental Program,"* University of California, San Diego, Structural Systems Research Project, Report No. SSRP-88/02, May 1988.
3. Seible, F., and Latham, C., "*Analysis and Des*ign Models for Structural Concrete Bridge Deck Overlays," Journal of Structural Engineering, ASCE, Vol. 116, No. 10, October 1990, pp. 2711-2728.
4. Seible, F., and Latham, C., *"Horizontal Load Transfer in Structural Concrete Bridge Deck Overlays,"* Journal of Structural Engineering, ASCE, Vol. 116, No. 10, October 1990, pp. 2691-2710.
5. American Association of State Highway and Transportation Officials, *"Standard Specifications for Highway Bridges,"* Thirteenth Edition, Washington D.C., 1983.

Kevlar Reinforced Prestressing for Bridge Decks

CHARLES W. DOLAN

Kevlar reinforced composites show considerable promise for use as prestressing tendons. Their high strength, low relaxation properties and resistance to chloride induced corrosion make them attractive for the design of prestressed concrete bridge decks and for rehabilitation or strengthening of existing bridge decks. Experimental work using Kevlar reinforced tendons for slab structures is presented and the design guidelines for using brittle materials in post-tensioning tendons are discussed. Structural issues of anchorage and reliance on resin socketed terminations and research necessary to develop composites to construction grade standards are addressed.

Substantial research has been conducted examining the use of composite materials for structural applications. Among the research has been an examination of both glass reinforced plastics and aramid reinforced plastics for prestressing applications (*1*). The primary motivation for the examination of these composites is their inherent resistance to corrosive conditions found in many structures. While both glass and aramids have some reactivity with alkali environments, they remain relatively impervious to sodium or calcium chloride solutions. The ability to reliably prestress bridge decks with these composites could enhance the durability of the bridge.

The issue of the cost of composites is of some concern. Glass fiber composites will cost in excess of $2.00 per pound. Aramid fibers, Kevlar being the most common in the United States, can cost in excess of $12.00 per pound. Even when corrected for their lower specific gravities and for their higher strengths, these materials will not compete with traditional prestressing steel on a first cost basis. If, however, the materials can extend the service life of a structure, or if they prevent the need to reconstruct a bridge deck, then they may become cost competitive. Current research and prototype installations are providing long term performance data which will assist engineers to determine the effectiveness of these materials.

C.W. Dolan, Associate Professor, Department of Civil Engineering, University of Delaware, Newark, DE, 19716

Three synthetic materials are currently available for use as prestressing tendons. They are glass, aramid, and carbon. Typical stress strain curves for these fibers are shown in Figure 1 along with the stress strain curve for ASTM 416 - 270 ksi (1.20 GPa) seven wire prestressing strand. In addition to their high tensile capacity, the fibers are nearly linearly elastic to failure. The lack of a yield region creates significant concerns about the ductility of the structure and the method of design.

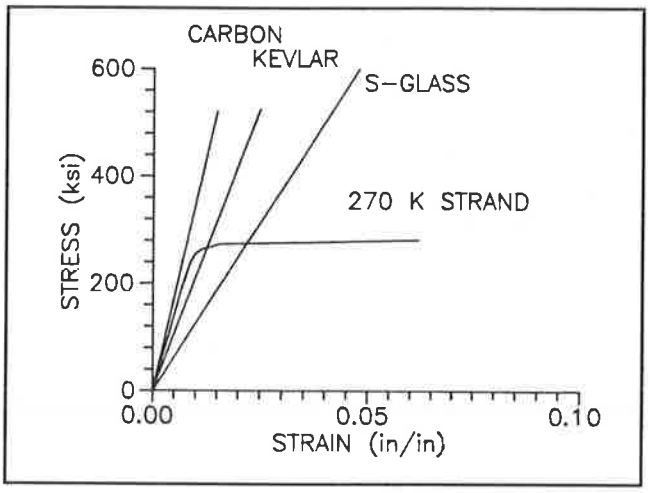

FIGURE 1 Sample Stress Strain Curves

This paper focus on the use of aramid fibers as reinforcing for prestressing tendons. The rationale for examining aramids is twofold. First, carbon fibers, while having a very high strength, also have a low strain to failure. When allocating the strain capacity of the fibers, as will be discussed later, there is little ductility reserve in carbon tendons used for prestressing applications. Glass fibers have the initial advantage of lower cost. E-Glass has been the focus of most development work in glass tendons. E-Glass has a lower strain to failure than S-Glass. E-Glass resistance to fatigue conditions which may be encountered in bridge decks suggests that aramids may be a superior choice for tendons.

Aramid is the generic name for polyparaphenylene-terepthalamine. It is most commonly recognized by the trade name Kevlar, an E.I. duPont product. Other commercial aramid fibers are Twaron, manufactured by ENKA in Europe and Technora, made by Teijin Industries in Japan. Three grades of aramid fibers are available. Kevlar serves to differentiate these grades. Kevlar 29 has an elastic modulus of about 9.0 x 10^6 psi (62 GPa) and a strain to failure of about 3.8 percent. Kevlar 49 has an elastic modulus of about 17 x 10^6 psi (117 GPa) and a strain to failure of about 2.5 percent. Kevlar 149 has a modulus of 21.1 x 10^6 psi (146 GPa) and a strain to failure of 1.4-1.5 percent (*2*). Kevlar 29 and Kevlar 49 both have tensile fiber strengths of 525 ksi (2.3 GPa) and Kevlar 149 has a slightly lower tensile stress. Twaron is similar to Kevlar 49 while Technora has properties between Kevlar 29 and Kevlar 49.

CHARACTERISTICS OF ARAMID MATERIALS

Individual fiber strength, fiber strength capacity under sustained loads, durability in moist, alkali and chloride environments, fatigue resistance, and relaxation properties of aramid fibers are examined to determine the suitability of the fibers for prestressing applications.

Tendon strength

The strength of a composite tendon must be examined from three viewpoints. First the strength of a single fiber must be considered, then the behavior of a fiber bundle assessed, and lastly the strength of a resin coated fiber bundle ascertained. The high strength of an individual fiber cannot be realized in a design application. Like a chain, a long fiber may be considered to be no stronger than its weakest segment. Probability theory indicates that the longer the fiber is, the lower its strength will be. This behavior has been demonstrated in laboratory experiments (*3*).

When many fibers are assembled into a parallel system, the reliability of the resulting tendon increases. The parallel fibers act as a redundant structural system, and the load carried by the weakest fiber is transferred to the stronger fibers when the weakest fibers fail. Providing that the strength of the remaining fibers is greater than the applied load, the tendon will continue to function, however the apparent strength of the fibers will be less than single fiber strength. This scenario assumes that the load is free to search out the weakest fiber. In actual bundles of twisted or resin coated fibers, once a fiber breaks, the load is transferred by friction, or by the matrix resin, to the adjacent fibers. Thus, the load does not have the opportunity to search out the next weakest fiber. Thus friction or resins increase the strength and the reliability of the tendon.

Extensive probability analysis by Phoenix and others (*4*) provide some guidance to the behavior of fiber bundles. Applying this theory to a Kevlar reinforced tendon, and using a probability of failure of 1 in 1000 for prestressing tendons, the theoretical tensile capacity of the tendon is about 315 ksi (2.2 GPa) based on the total fiber area. Glass and carbon fiber bundles undergo similar strength reductions. Glass is slightly more sensitive to strength loss with length than is Kevlar or Carbon.

If the fibers in the tendon are bound together with a resin, then the average strength of the tendon is determined by the volume fraction of the rod which is Kevlar. A typical Kevlar reinforced tendon will be 60 - 70 percent fiber and the remaining cross section will be resin. The resin strength contributes little to the total strength. Thus, based on the stresses predicted from probability theory and a volume fraction of 60 - 70 percent, the expected tendon strength is 190 - 214 ksi (1.3 to 1.5 GPa) using the total composite cross section. The DuPont Data Manual for Kevlar 49 (*5*) gives a tensile strength of 200 ksi (1.4 GPa) for a unidirectional Kevlar composite with a volume fraction of 60 percent fiber. This is consistent with the predictions based on probability theory. Since prestressing represents a proof load condition, stressing the tendons to 70 percent of their tensile capacity assures that the short term strength of the tendon is adequate. Using the DuPont guideline of 200 ksi (1.4 GPa), a jacking stress of 140 ksi (965 MPa) may be considered for prestressing applications.

Sustained Load Capacity

Aramid fibers have a lower long term strength than the short term strength determined by static testing. This behavior is similar to concrete. A concrete cylinder will fail at 75 - 85 percent of its short term strength if left under a sustained high load. Test data indicates that Kevlar fibers have a 50 percent probability of failure after 100,000 hours if they are stressed above 70 percent of their short term fiber strength. S-Glass in comparison has a 50 percent probability of failure after 10,000 hours if stressed above 50 percent of its short term tensile strength (*5*). Thus Kevlar is superior to S-Glass for sustained load capacity and may be initially stressed to a slightly higher prestress level.

Seventy percent of the short term Kevlar strength is about 220 ksi (1.5 GPa) in a resin impregnated rod. The long term strength mechanics of sustained load capacity of resin reinforced rods with many fibers is not fully understood. However, allowing a jacking stress of 140 ksi (965 MPa) appears to be within the allowable range for long term strength retention. In order to increase the sustained strength capacity of the tendon a slightly lower jacking stress may be considered.

Environmental Durability

Environmental durability addresses the performance of aramids in their working state. Specifically, three conditions are examined. They are normal and elevated temperature properties, moist environments, and alkali and chloride environments. The behavior of Kevlar 49 under static load at normal room temperature and at 250 °F (121 °C) are given in Table 1.

TABLE 1 STATIC LOAD DATA FOR KEVLAR 49

Properties at Room Temperature	U.S. Units	S.I.
Axial Modulus	18 x 10^6 psi	124 GPa
Axial Tensile Strength	525 x 10^3 psi	3.6 GPa
Coefficient of Thermal Expansion	-2.9 x 10^{-6} in/in/°F	-5.2 x 10^{-6}m/m/°C
Axial Strain at Break	2.9 %	2.9%
Properties at 250 °F (121 °C)		
Axial Modulus	15.4 x 10^6 psi	114 GPa
Axial Tensile Strength	460 x 10^3 psi	3.2 GPa
Coefficient of Thermal Expansion	-2.9 x 10^{-6} in/in/°F	-5.2 x 10^{-6}m/m/°C
Axial Strain at Break	2.8%	2.8%

Data from Reference 5.

The loss of properties at elevated temperature is a concern, however, this magnitude of temperature increase is unlikely to occur in a bridge deck. The larger concern is the loss of strength associated with the resins used to bind the fibers. These resins are typically epoxies or vinylesters, and will have strength losses greater than the aramid fibers at elevated temperatures. The effects of strength loss in the resins is quite similar to the concerns about strength loss in epoxy coated strands and glass fiber reinforced tendons. The resin behavior suggest that the primary mode of failure at elevated temperature is likely to be debonding of the tendon at the resin interface.

The behavior of aramids in moist and alkali environments is a concern. The primary tensile strength of aramid fibers is generated by Van der Waals forces. Moisture can penetrate these bonds and cause a strength and modulus loss. Exposure tests of single fibers to water and to 5% salt water solutions have indicated no loss of strength and about an 8% loss of modulus in a 24 hour test at room temperature (*5*). Tests of Kevlar fibers in a cement matrix and increasing the temperature to 80 °C (180 °F) indicated a 30 percent strength loss after 30 days exposure (*6*). This loss is a combination of moisture, alkali, and elevated temperature effects. The surface to volume ratio of the individual fibers is very high, thereby maximizing the chemical reactivity. Glass fibers also display deterioration when exposed to the alkali environments found in concrete. Encasing the fibers in a resin may substantially change the response to this moisture. Glass reinforced tendons in prototype bridge structures have used an epoxy mortar grout in the tendon to assure bond and further protect the tendon (*7*). No long term durability tests of resin encased aramids were found in the literature.

Fatigue Resistance

Fatigue tests were performed in England on tendons made of 64 small diameter composite rods (*8*). Tests were performed on composite rods made of fiber and epoxy resin, anchored in a steel socket using and epoxy. These tests indicated that the fatigue strength of aramids and carbons was superior to steel and that glass was more susceptible to fatigue damage than steel. The fatigue tests are summarized in Table 2.

TABLE 2 FATIGUE RESULTS OF COMPOSITE TENDONS

Material	Number of Samples	Base Load % break strength	Load Range % strength	Average number cycles	Number of rods broken
E-Glass	3	15-31	6-8	.17 x10^6	15
Kevlar 49	3	50-55	7-10	2.08 x10^6	0
Carbon	7	45-55	7-10	2.24 x10^6	0
HS Steel	2	35	5-7.5	2.04 x10^6	0-5

Data based on results given in Reference 8. The actual test programs contained additional tests outside the load ranges summarized in this table. The composite rods had a volume fraction of about 63 percent.

Relaxation

Tests at Delft Technical University in the Netherlands and by Enka examined the long term relaxation characteristics of aramid tendons. They concluded that the relaxation losses for 100 years were about 20 percent (*9,10*). An independent relaxation test was undertaken to confirm these claims for a Kevlar aramid.

A four foot long (1.22 m) tendon comprised of 4 - 1/8 inch (3.2 mm) rods was secured in an epoxy socket anchor. The tendon was stressed to 70 percent of the tensile capacity in a double extra strong steel pipe. A load cell was installed under the dead end anchor, Figure 2. The resulting loads, normalized to the jacking stress equal to 1.0, are given in

Figure 3. Two phenomenon occur concurrently. First, there is movement of the epoxy plugs in the anchors. This accounts for much of the initial stress loss and resulted in the tendon being restressed shortly after the initiation of the tests. After restressing, dial gages were placed on the epoxy plugs to allow separation of the anchor movement from the tendon relaxation. Creep in the epoxy of the anchor continued during the test. Secondly, the tendon continued to relax, but at a lower rate for the test duration. The top line corresponds to the relaxation losses if effects of the anchor movement are removed from the test results. Test data was recorded for over 5000 hours. The corrected relaxation data at 5000 hours was about 11 percent. This agreed well with the european data.

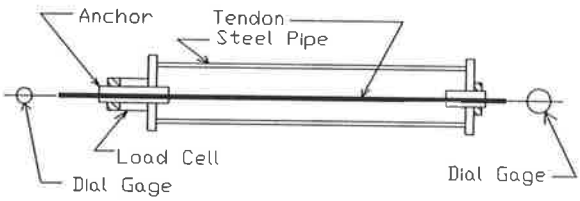

FIGURE 2 Relaxation Test Assembly

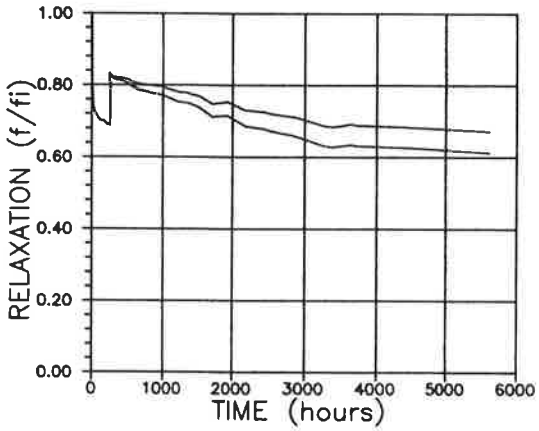

Unity of the graph represents 143 ksi (20.7 MPa) and corresponds to a load of 7.0 kips (31 kN).

FIGURE 3. Tendon Stress Versus Time

STRUCTURAL BEHAVIOR

To investigate the short term behavior of concrete prestressed with Kevlar reinforced tendons, six prototype slab elements were constructed. Four tests examined the behavior of unbonded tendons and two tests were conducted using bonded tendons. The slab test was a 6 inch wide by 4 inch deep (152 x 100 mm) segment reinforced with a single tendon, Figure 4. The tendon consisted of a series of smooth 1/8 inch (3.2 mm) diameter rods. The rods were 68 percent Kevlar 49 in a vinylester resin. Tendons consisted of either 4 or 6 rods. The tendons were stressed to 120 ksi (830 MPa).

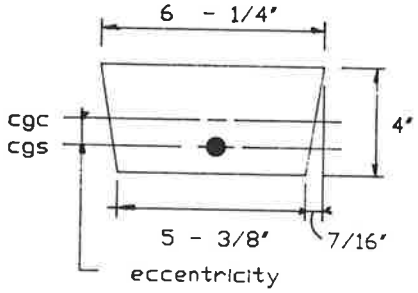

FIGURE 4 Test Cross Section

The beams were tests were conducted with a two point loading system. Beams were tested montonically to failure using a hydraulic jacking system. Data was recorded either with dial gages or with an automatic data acquisition system, Figure 5.

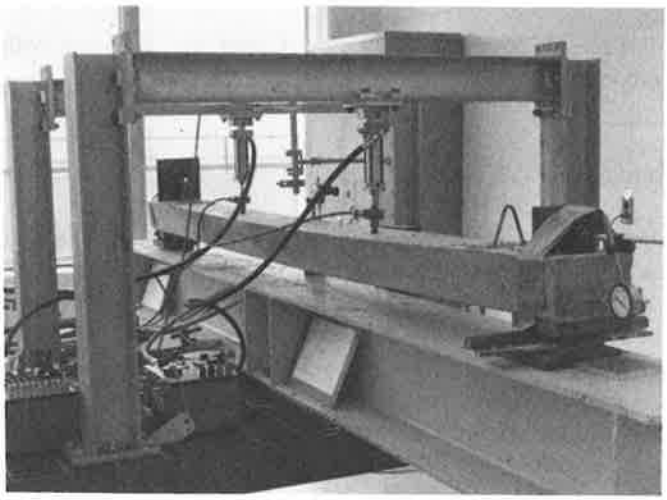

FIGURE 5 Test Arrangement

Unbonded Tendon Results

The unbonded tendons specimens failed when the concrete exceeded its ultimate strain capacity. After initial crushing of the concrete, the sections continued to carry load, although the initial moment capacities were never regained. The test frame limited the total beam deflection, therefore it was not possible to strain the tendons to failure. Figure 6 shows a typical moment deflection curve for a six rod unbonded tendon system. The section was cycled several times after the initial failure. Deterioration of the section is evident by the gradual loss of deflection and strength capacity.

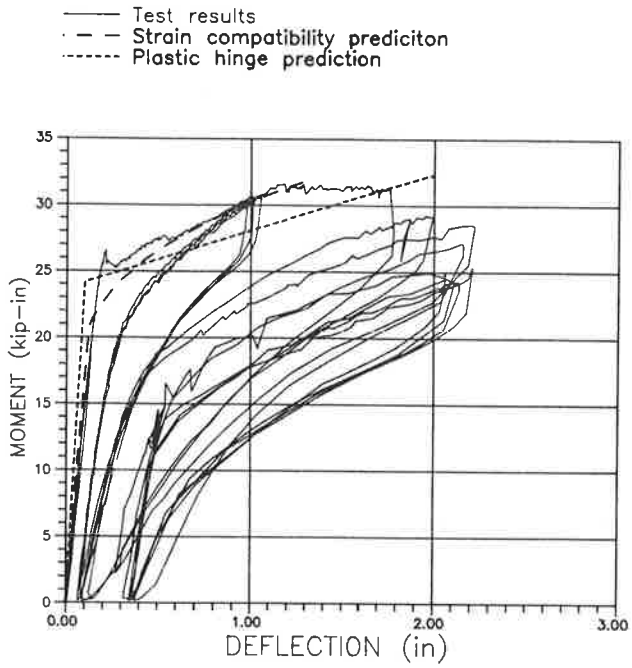

FIGURE 6 Moment Deflection Curve for a Beam with Unbonded Tendons

Bonded Tendon Results

The bonded tendons failed by pullout of the tendon. The rods used in this research were originally intended for post-tensioning applications. As a consequence, the surfaces were not roughened to improve the bond with the concrete. The surface texture has the smoothness of a fiberglass fishing pole, and loss of bond was not unexpected. Furthermore, the test setup allowed only 27 inches (.69 m) between the end of the beam and the point of application of the load. For a 6 rod tendon, this is about 60 tendon diameters. Steel tendons have similar difficulties developing their capacity in that length. Figure 7 provides the moment deflection results for a six rod pretensioned beam. The sharp drop in moment capacity, followed by a quick recovery, represents the formation of cracks in the concrete. The jump in recovered deflection following the first maximum load cycle is a direct result of the tendon slipping. When the moment was controlled so that the tendon was not allowed to slip, the beam showed virtually complete deflection recovery. A uniform pattern of flexural cracks formed at about 6 inches (150 mm) on center.

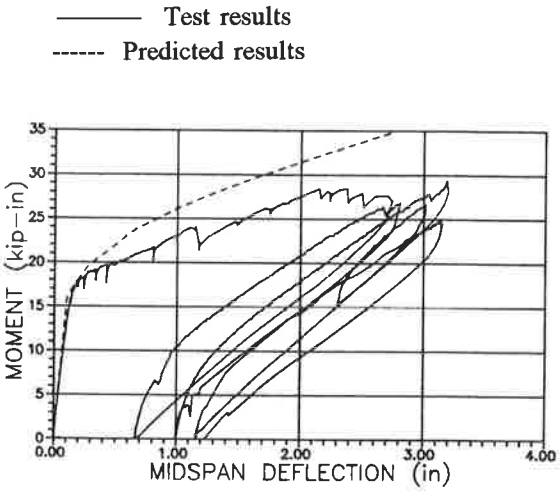

The permanent deflection of about 0.7 inches (18 mm) is associated with the slip of the tendon.

FIGURE 7 Moment Deflection Results for a Beam with Bonded Tendons

Test Implications

These tests lead to several short term conclusions. First, Kevlar reinforced tendons did provide the strength required for load carrying capacity on a short term basis. Second, the structures displayed substantial ductility during loading. The failure to rupture a tendon is a function of the shallow cross section and the inability to develop large tensile strains in the tendon. A deeper beam would may less ductility depending upon the prestressing reinforcement ratio.

One post-tensioned beam failed when one of the rods pulled out of the anchor. This confirms the concern regarding the long term reliance on epoxy bonded anchor systems. Tendon grouting is preferable to assure long term strength development.

DESIGN IMPLICATIONS

The slab tests indicated that aramid prestressing materials are satisfactory for short term applications. Several questions arise on the actual application of Kevlar reinforced tendons in a design situation. These include the combined effects of using resin reinforced composites in wet, chloride environments, the long term strength degradation, anchorage of the tendons, and the reliability of brittle materials. These concerns lead to consideration of the tendon strain condition as a basis for strength and serviceability design.

Combined Material Effects

While the individual components performed satisfactorily in short term tests, the combined effects of moisture on resin coated fibers, fatigue and sustained high load are not yet defined. Tests at the University of Delaware are currently investigating the long term effects of Kevlar reinforced tendons in pretensioned concrete. Two tests of importance are underway. The first test is examining flexural fatigue of a thin plank pretensioned with Kevlar reinforced tendons. The plank is being fatigue tested in a salt water bath. The second test is examining the long term strength, relaxation and bond development length of small bars pretensioned with Kevlar reinforced tendons. For these tests, the surface texture of the rods are modified to assess the bond effects. Improved bond will assist not only the behavior in pretensioned concrete, but may also improve the resin socketed anchor strength.

One of the most important issues to be addressed is the mechanism of strength deterioration under sustained load. Is the strength reduction a stress phenomenon, or is it accompanied by a reduction of strain capacity? A stress reduction may be accompanied by reduction in apparent modulus of elasticity. This will lead to a softening of the structure and increased deflections. A loss of strain capacity can lead directly to rupture of the tendon and reduced ductility in the structure. Tests on concrete sections which have been cured for several months or years will provide some illumination of this behavior.

Anchorage Issues

The tests reported above have depended upon epoxy socketed anchors for post-tensioning applications and for initially anchoring the pretensioned tendons. A mechanical anchor is desirable for pretensioning operations and for single strand post-tensioning systems. A reliable mechanical anchor could reduce the need to grout single strand tendons. Figure 9 shows several of the anchors commonly used with composite tendons. The Enka anchor uses plastic wedges, however, their system is primarily intended to hold the aramid reinforced tape during pretensioning operations and are not relied on to carry the service loads. The Japanese are conducting tests using a modified steel strand vice, but the details are not available.

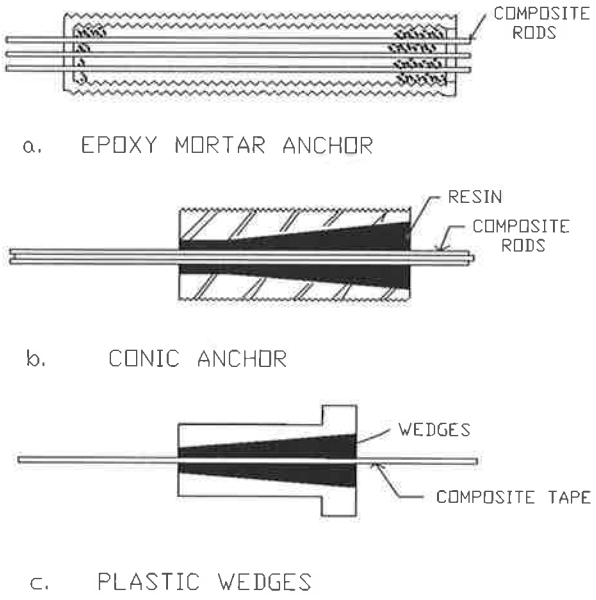

a. Polystal anchor for glass reinforced composite tendons from reference 1.

b. Conical anchor used for beam tests described in the preceding sections

c. Plastic wedges used in the Enka pretensioning systems from reference 10.

FIGURE 8 Representative Composite Tendon Anchor Systems

Strain Compatible Design

The concept of strain compatibility has been prevalent in concrete design for decades. The brittle nature of composite tendons suggests that strain compatibility must be extended to the design of the tension reinforcement in addition to the limitations imposed on the concrete compressive strain. This is a direct result of the lack of an extended yield zone to provide a large tensile strain capacity. The highly uniform strain to failure behavior of composites suggests that a strain approach to strength prediction is desirable. Depending upon the location of the neutral axis, the depth of the structure and the structural configuration, the tendon may remain elastic, or it may exceed its ultimate strain capacity. Figure 9 indicates the possible stress and strain conditions which may occur in a concrete section reinforced with a composite tendon.

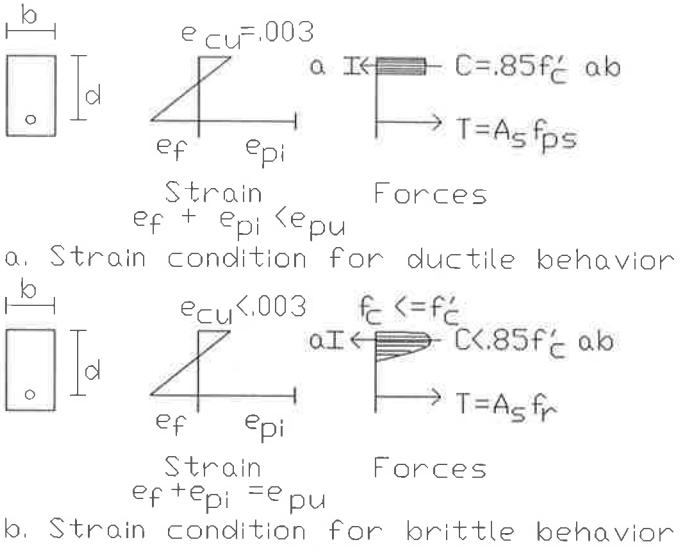

b = width of compression block
d = depth to prestressing tendon from compressive face
a = depth of equivalent compression
ϵ_{cu} = ultimate concrete strain
f'c = concrete compressive strength
ϵ_f = strain due to flexure
ϵ_{pe} = strain due to prestress and decompression
ϵ_r = rupture strain of the tendon
A_s = area of prestressing strands
f_{pe} = stress of prestressing strands
f_r = stress of strands at rupture

FIGURE 9 Schematic representation of the strain compatibility of composite tendons in prestressed flexural member design.

The possibility of a brittle failure of the tendon suggests that sections designed with composite tendons should be treated differently than those with steel prestressing materials. Design modifications could address the capacity reduction factor, ϕ, the load factor, or both. One option may be to substantially reduce the ϕ factor. Since the ϕ factor is supposed to account for variability of material property and construction tolerances, adjusting the ϕ factor does not directly address the issue of ductility. ϕ factors have yet to be developed for composite tendons, but their development should be consistent with other materials.

An alternative approach could be to define a supplemental load factor which is used in conjunction with the nominal capacity of the section based on the tensile strain capacity of the tendon. An increased load factor would then be applied to those conditions which may result in a tendon failure. The result is analogous to designing a prestressed concrete section which has a cracking moment close to its strength capacity. An additional margin of safety against failure is provided to assure that cracking does not lead to a brittle failure.

Appendix A develops a brittle reinforcement ratio for composite prestressing tendons. The brittle ratio uses the initial strain resulting from prestressing instead of attempting to combine the strain changes due to losses and to decompression of the tendon during flexural loading. Use of the prestressing strain is expedient because it represents a well defined condition while the losses are generally estimated values.

An important difference between composite tendons and steel tendons is that the rupture condition may be solved for directly. The resulting brittle reinforcement ratio is then dependent upon the initial prestressing strain and the flexural strain. The need to apportion the strain between prestressing and flexure indicates why the low strain to failure of carbon fibers makes them less likely candidates for prestressing applications.

Examining the brittle reinforcement ratio provides an interpretation of the difference between steel and composite tendons. Structures with actual reinforcement ratios less than the brittle reinforcement ratio will require tensile strains in excess of the tendon capacity. These tendons will rupture before the concrete compressive capacity is attained. Prestressing reinforcement ratios in excess of the brittle ratio will develop the concrete capacity before the tendon capacity is reached.

The brittle ratio is different than the balanced ratio associated with reinforced concrete. The balanced ratio defines the simultaneous yielding for the reinforcement and the compressive failure of the concrete. Sections with reinforcement ratios in excess of the balance ratio may fail suddenly since the reinforcement remains elastic when the concrete compressive strain is reached. The tensile strain for a balanced condition is generally less than 0.2 %. Composite tendons will strain to 1 to 1.5 % prior to rupture. This is in addition to the 1% strain used during prestressing. Consequently, while the tendons remain elastic, substantial deflection and cracking precedes failure. This ductility has been observed in the beam tests described earlier.

Design Recommendations

Until more complete data is available, sections with prestress reinforcement ratios less than the brittle reinforcement ratio should be designed to have nominal capacity of 20 percent greater than the required ultimate capacity. The 20 percent recommendation follows from section 18 of the ACI building code provisions for prestressed concrete sections having cracking moments near to the strength requirements of the section (*11*). These sections require a strength capacity 20 percent greater than the cracking load to assure proper behavior. The strain reserve generated from this condition will provide assurance that the tendon does not rupture at less than the required strength.

CONCLUSIONS

The body of knowledge regarding the behavior of composite prestressing tendons is growing rapidly. Glass fiber tendons have been used in prototypical bridges and aramid prestressing has been demonstrated in europe. The flexural strength of bonded tendons may be predicted using the same principles now available for prestressed concrete.

Short term tests have indicated that the aramid reinforced tendons are satisfactory for prestressing applications. The long term strength characteristics of aramid tendons appear satisfactory based on limited testing. Long term durability tests are being conducted. Shear performance of members prestressed with composite tendons has not been addressed. Mechanical anchors need to be developed to support commercial pretensioning operations for reliable post-tensioning applications.

Attention must be paid to the mode of failure of the tendon and supplemental load factors applied when tendon rupture is a possibility.

ACKNOWLEDGEMENTS

Beam tests and relaxations tests reported in this paper were part of the author's PhD research at Cornell University. This research was sponsored by the Precast/Prestressed Concrete Institute and by E. I. duPont de Nemours Company, Inc. Their support is gratefully acknowledged.

REFERENCES

1. Dolan, C. W., "Developments in Non-Metallic Prestressing Tendons", Journal of the Precast/Prestressed Concrete Institute, Vol 35, No. 5 September/October 1990.

2. Riewald, P.G., Dingra, A.K., and Chern, T.S., "Recent Advances in Aramid Fiber Technology", Proceedings of the 6th International Conference in Composite Materials, Mathews, F.L., Buskell, N.C.R., Hodgkinson, J.M., and Morton, J., eds., Elseviner Applied Sciences, London, 1987.

3. Wagner, H.D., Schwartz, P., and Phoenix, S.L., "Lifetime Statistics for Single Kevlar 49 Filaments in Creep-Rupture", Journal of Material Science (21), 1986, pages 1868-1878.

4. Phoenix, S. L., "Statistical Theory for the Strength of Twisted Fiber Bundles with Applications to Yarns and Cables", Textile Research Journal, Vol. 49, No. 7, July 1979, pages 407-423.

5. DATA MANUAL FOR KEVLAR 49 ARAMID, E.I. DuPont Company, Chestnut Run Building 702, Wilmington, DE, May 1986.

6. Gale, D.M., Riewald, P.G. and Champion, A.R., "Cement Reinforcement with Man-Made Fibers", International Man-Made Fibers Congress, Dornbirn, Austria, 24-26 Sept, 1986.

7. Wolff, R. and Miesser, H-J. "New Materials for Prestressing and Monitoring Heavy Structures", Concrete International, Detroit, MI., vol 11, no. 9, September 1989, pages 86-89.

8. Walton, J.M., and Yeung, Y.T.C., "The Fatigue Performance of Structural Strands of Pultruded Composite Rods", Journal of the Institute of Mechanical Engineers, London, C286/86, 1986, pages 315-320.

9. "Relaxation of Aramid Tendons", Research Activities, Faculty of Civil Engineering, Delft University of Technology, Delft, TUDelft, 1985-86, page 71.

10. Gerritse, A., Schurhoff, H.J., and Maatjes, E., "Prestressed Concrete Structures with Arapree; Relaxation", contribution to IABSE Symposium, Paris, 1987. (Available from Hollandsche Beton Groep nv, R&D Department, Rijswijk, The Netherlands)

11. Building Code Requirements for Reinforced Concrete (ACI -318-86), American Concrete Institute, Detroit, MI, 1986.

APPENDIX A
Derivation of Brittle Reinforcement Condition for Bonded Composite Tendons

A brittle condition exists when the tensile capacity of the tendon occurs simultaneously with the compression failure of the concrete. In the case of concrete reinforced with a composite prestressing tendon, the tensile capacity of the tendon is also the rupture strength of the tendon. Figure A.1 shows the strain and stress state at the simultaneous occurrence of brittle failure of the tendon and compressive failure of the concrete.

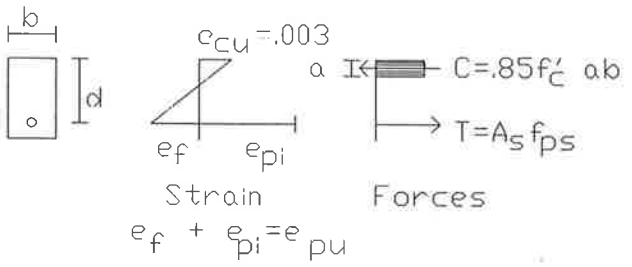

Figure A.1 Stress and Strain at Brittle Conditions

Examining Horizontal equilibrium

$$A_p f_{pu} = .85 f'_c \beta_1 c b \quad (1)$$

Define

$$\rho_p = \frac{A_p}{b d} \quad (2)$$

Then

$$\rho_p \frac{f_{pu}}{f'_c} = .85 \beta_1 \frac{c}{d} \quad (3)$$

$$\rho_{pbr} = .85 \beta_1 \frac{c}{d} \frac{f'_c}{f_{pu}} \quad (4)$$

By strain compatibility

$$\frac{c}{d} = \frac{\epsilon_{cu}}{\epsilon_{cu} + \epsilon_f} \quad (5)$$

And the constitutive behavior of composite tendons

$$\epsilon_f + \epsilon_{pi} = \epsilon_{pu} \quad (6)$$

Therefore

$$\rho_{pbr} = .85 \beta_1 \frac{\epsilon_{cu}}{\epsilon_{cu} + \epsilon_{pu} - \epsilon_{pi}} \frac{f'_c}{f_{pu}} \quad (7)$$

Definition of Terms

A_p	Area of prestressed reinforcement
b	Width of compression face of the member
c	Depth from compression face to the neutral axis
d	Depth from the compression face to the prestressing centroid
f'_c	Specified strength of concrete
f_{pu}	Tensile capacity of the composite tendon
β_1	Concrete strength reduction factor equal to 0.85 for $f'_c \leq 4000$ psi (27 MPa) and reduced .05 for every 1000 psi (6.9 MPa), but not less than 0.65.
ϵ_{cu}	Concrete compressive strain at failure, generally taken as 0.003
ϵ_f	Strain in tendon due to flexure
ϵ_{pi}	Strain due to initial prestress
ρ_p	Ratio of prestressed tension reinforcement $= A_p/bd$
ρ_{pbr}	Brittle reinforcement ratio when concrete reached ϵ_{cu} as the tendon reached e_{pu}

Design Provisions for a Replaceable Segmental Bridge Deck

THOMAS W. STELMACK AND RALPH J. TRAPANI

A major precast concrete segmental bridge located in Glenwood Canyon, Colorado, was mandated by the Federal Highway Administration and, the Colorado Department of Highways to have the capability of full depth deck replacement. A simple procedure for replacement of the top slab of the box girder was developed and integrated into the final design of the structure. Although erected by the balanced cantilever method, no compromises were required of the design and replacement capability was satisfied with little initial cost impact to the construction of the viaduct. The deck replacement procedure, the special design features and the analysis method and results are presented. It is concluded that full depth deck replacement capability is economically feasible for a precast segmental bridge, ensuring the owner of a durable concrete structure for many years of service.

The Hanging Lake Viaduct in Glenwood Canyon, Colorado, is part of the last link to complete the I-70 route through Western Colorado. The project site is located within an extremely steep and narrow portion of the environmentally sensitive canyon. There is no reasonable alternate route capable of handling the traffic from I-70 at either end of the canyon and, therefore, maintenance of traffic during construction is of equal importance as preserving the environment. Thus, the design requirements of the viaduct included that the superstructure be completely erected from the bridge itself and prohibited the use of falsework or temporary bents during construction in areas where traffic or the environment would be affected.

Figg Engineers, Inc., Western Regional Office
Denver, Colorado

Colorado Department of Highways
Glenwood Canyon, Colorado

Based on those construction limitations, the Bidding Documents were prepared for both a precast, concrete segmental box girder alternate and a steel box girder alternate. In August of 1989, a joint venture of Flatiron Structures Company and The Prescon Corporation submitted a low bid of $34,091,925 for the concrete alternate and construction of the project began in the Fall of 1989.

The project consists of approximately 8,400 lineal feet of bridge with a typical span length of 200 feet and twin 300 foot spans crossing the Colorado River. To meet the construction requirements described above, the structure was designed to be built using the balanced cantilever method. The segments are trucked over the completed portion of the bridge and then placed in cantilever on either side of the pier using a piece of erection equipment called a launching gantry (see Figure 1). The gantry is self-launching and can be advanced from the previous cantilever to the following pier without the aid of additional ground or structure based equipment.

Prior to work beginning on the conceptual design of the project, the Federal Highway Administration (FHWA) and the structure's owner, the Colorado Department of Highways (CDOH), mandated that the concrete alternate be designed and constructed so as to allow for complete replacement of the entire deck.

It is worth noting, however, that while deterioration of reinforced concrete decks has been a serious problem for both concrete and steel bridges, concrete segmental bridges have not experienced the same problem. A recent survey, by the author's firm of existing segmental bridges, both in the United States and Europe, showed that major bridge deck deterioration is virtually non-existant, with some of the structures 25 years old. This is particularly true for structures built using precast segments with decks prestressed in the transverse direction. One particular example is the segmental bridge in Maine, crossing the

Sheepscot River at Wiscasset. Recent inspection by Maine DOT, both interior and exterior, revealed no deterioration in the deck of the seven year old structure. Other than 5,000 psi concrete and transverse post-tensioning of the deck, the only additional protection provided for the severe weather conditions was a 1-1/4" latex modified wearing surface. The main reasons that this and other segmental bridge decks are so durable are that the segments are typically cast with high strength concrete under controlled, factory conditions and are prestressed in both the transverse and longitudinal directions. This results in high quality decks which are designed to be essentially free of cracks under typical service conditions.

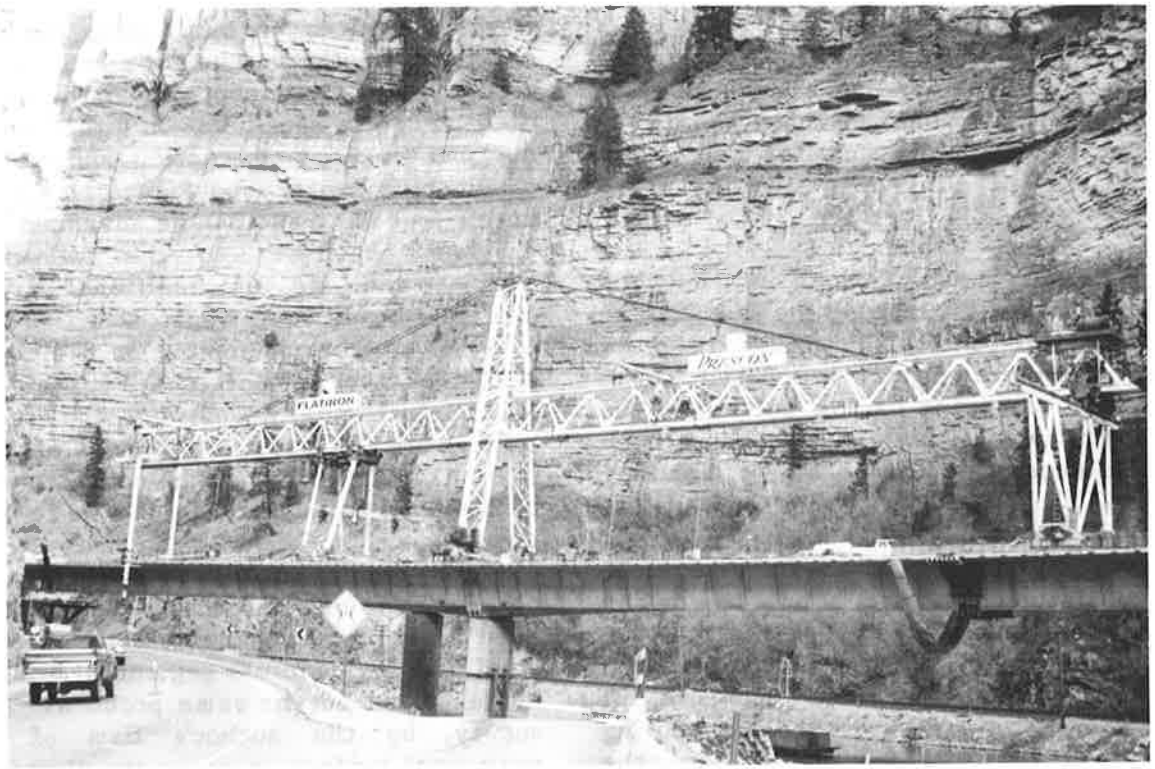

FIGURE 1 Overhead launching gantry.

Further evidence of the performance of this deck system can be found in the research by Poston, et al (1), who studied deck deterioration under harsh evnironmental conditions. The testing consisted of subjecting both prestressed and conventionally reinforced concrete slabs to an aggressive deicing salt exposure. Another variable used in the study was crack width and three cases were studied for both slab types - uncracked, .002" and .015". The results showed that chloride penetration occurred primarily at crack locations, and although the prestressing greatly reduced the penetration at crack locations in which the crack width was limited to .002", the chloride concentration was above the chloride-corrosion threshold at the reinforcement level. The uncracked sections, both prestressed and non-prestressed, had chloride values below the widely accepted chloride-corrison threshold. Thus, the researchers concluded that the primary benefit and goal of prestressing is to eliminate and to control greatly cracking so as to restrict the chloride and oxygen penetration into the concrete.

Therefore, the probability of deterioration of a segmental bridge deck to the point of complete replacement is highly unlikely. With proper inspection and maintenance, two repair options exist which require little, if any, special design considerations. The first is a concrete or asphalt wearing surface placed above a waterproof membrane adhered to the bridge deck. This protects the structural concrete deck and can be easily replaced as necessary. Second, if the deterioration extends into the concrete deck, the top 3 to 4, inches including the top mat of reinforcing steel, may be replaced and leaving the remainder of the deck intact.

However, should deterioration of the deck become so great, or damage occur to the deck by some other means, the consideration of complete deck replacement by the bridge designer provides the owner with the security of knowing that the option will always exist in the future. Based on that philosophy, the primary objectives of the design requirement were as follows:

1. Develop conceptual deck replacement scheme and associated details.
2. Incorporate into the final design of the structure the necessary details and structural capacities to allow for the deck replacement scheme.
3. Complete a structural analysis of a typical span through all stages of the deck replacement operation to verify the feasibility of the replacement scheme.

Each of the three objectives are discussed in more detail below.

Deck Replacement Scheme

In developing a conceptual scheme for the complete deck replacement of a prestressed concrete segmental box girder, several important factors were kept in mind:

- As previously discussed, the procedure may never by necessary; therefore, the initial cost to the owner for the required details provided in the design of the structure should be kept to a minimum. The initial serviceability and economy of the structure should not be sacrificed to decrease the actual replacement costs.
- The restrictions due to the sensitive environment required during construction will also apply during the deck replacement. Therefore, no intermediate temporary bents or falsework will be allowed.
- The scheme should be as simple as possible and minimize the requirement for special construction equipment.

For this project there was no economic analysis required by the owner to determine if the deck replacement capability would be a final design requirement; this was previously decided by the owner and the deck replaceability was not an option to be studied. Therefore, no life cycle cost analyses of the structure including initial costs and deck replacement costs were done. However, the special design provisions proved to have minimal negative impact on the cost of initial construction and in fact may have had a slight positive impact. Also, although no actual cost estimates and comparisons were made, the cost of the developed deck replacement procedure should not be much different from that for a typical reinforced concrete deck on steel or concrete girders.

The scheme which was developed for the deck replacement of an entire span is illustrated fully in Figures 2 and 3 and the

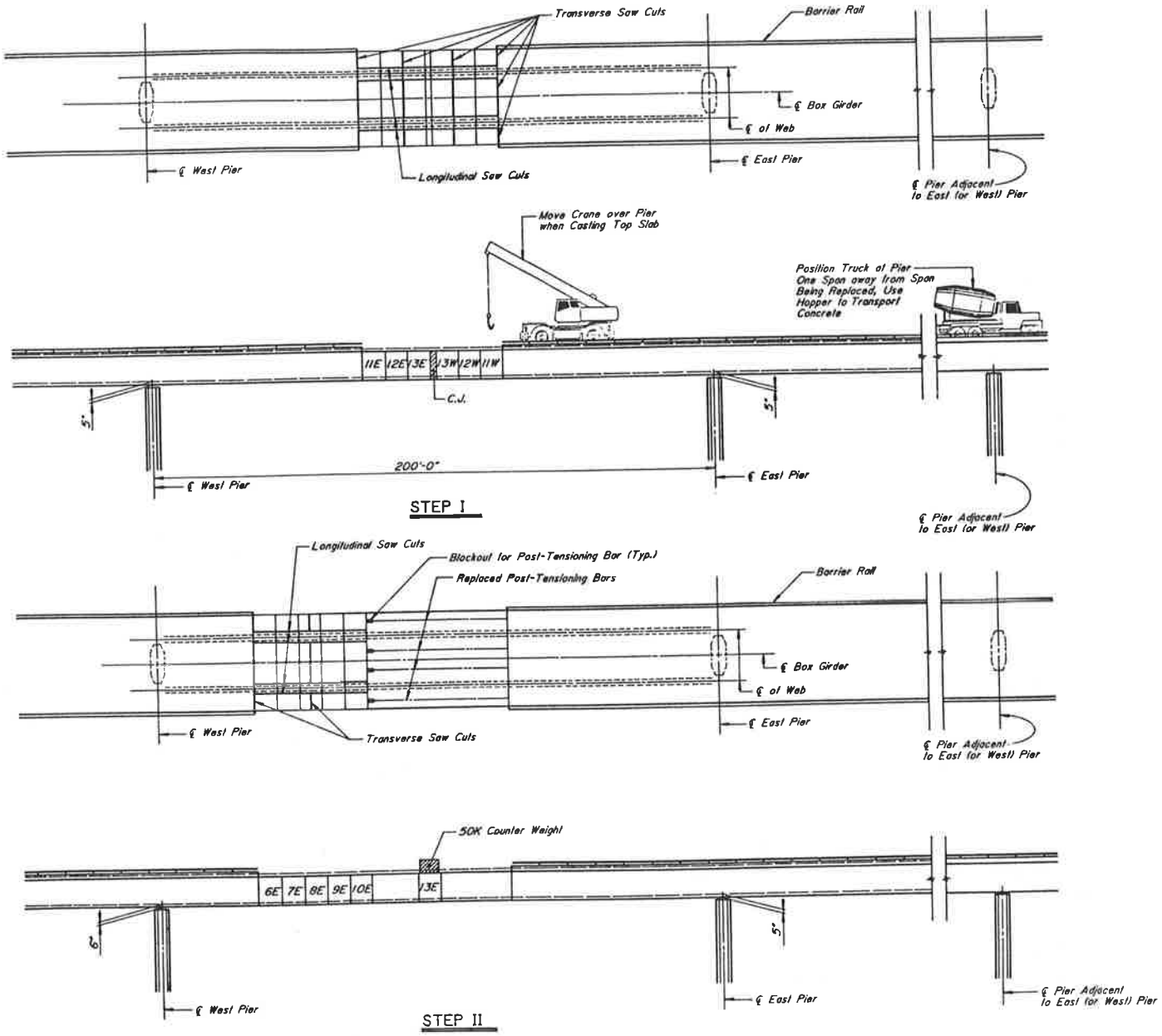

REPLACEMENT SEQUENCE

STEP I

1. Jack up deck 5" at piers adjacent to span being replaced.
2. Remove barriers from Segments 11E to 11W.
3. Cut post-tensioning bars in top slab at each transverse saw cut.
4. Make longitudinal and transverse saw cuts in deck and remove top slab.
5. Jack hammer area above and beside head of web to leave a rough surface.
6. Replace reinforcing, transverse post-tensioning and longitudinal post-tensioning bars.
7. Clean exposed concrete surfaces of all loose material.
8. Cast top slab in Segments 11E to 11W.
9. Stress transverse tendons in top slab.
10. Stress 4 longitudinal post-tensioning bars in top slab.

NOTE: Blockout may be left in slab to accommodate stressing jack for bars.

STEP II

1. Place 50^{k} counterweight over webs of segment 13E.
2. Jack up an additional 1" at west pier (to 6" total).
3. Remove barriers from Segments 6E to 10E.
4. Replace top slab in Segments 6E to 10E (Steps I.3 to I.8).
5. Couple post-tensioning bars to those in previously replaced portion and stress.

FIGURE 2 Deck replacement procedures, Steps I and II.

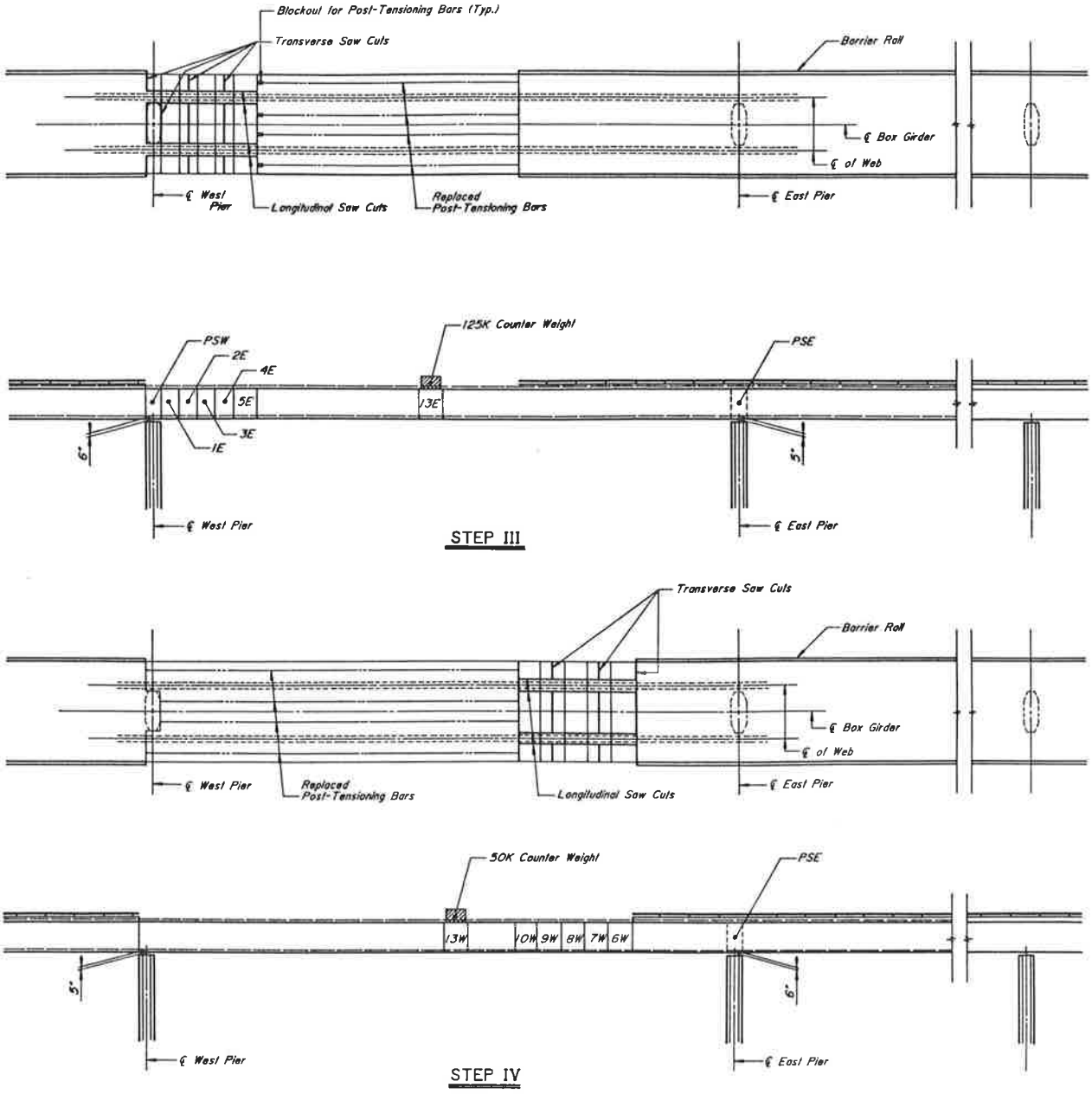

STEP III

1. Place an additional 75^{k} counterweight over webs of Segment 13E. (To 125^{k} total).
2. Remove barriers from Segments PSW, 1E to 5E.
3. Replace top slab in segments PSW, 1E to 5E (Steps I.3 to I.9).
   NOTE: Replace only top 6" of deck between webs over the pier segment diaphragm.
4. Couple post-tensioning bars to those in previously replaced portion and stress.

STEP IV

1. Lower deck 1" at west pier and raise deck an additional 1" at east pier (to 6" total).
2. Remove 125^{k} counterweight from segment 13E and place 50^{k} counterweight over webs of segment 13W.
3. Remove barriers from segments 6W to 10W.
4. Replace top slab in segments 6W to 10W (Steps I.3 to I.9).
5. Couple post-tensioning bars to those in previously replaced section and stress.

STEP V

1. Replace top slab in Segments PSE, 1W to 5W, using same procedure as Step III.

STEP VI

1. Lower deck to grade at east and west piers.
2. Cast barriers and wearing surface.
3. Stress the contingency tendons in the replacement span.
4. Return bridge to service.

FIGURE 3 Deck replacement procedure Steps III through VI.

important features are discussed below.

As stated earlier, the deck in a typical segmental bridge is under compression in both the longitudinal and transverse directions under service conditions. Therefore, prior to removing the deck, this compression must be removed. Transversally, this compression is provided only by the transverse post-tensioning and can be eliminated simply by making a series of saw cuts in the longitudinal direction through the concrete and the post-tensioning tendons. Longitudinally, the compression is due to a combination of post-tensioning and structure dead load. The most straight forward method of removing the compression is by raising the structure vertically at the piers adjacent to span under consideration. This induces a constant negative moment in the span and thus a constant decompression of the top slab. The structure is raised enough to nearly provide a state of zero stress down to the level of concrete to be removed. For the typical 200 foot span, this was found to be 5 inches. Once the compression has been removed, the concrete can then also be safely cut in the transverse direction in the area being replaced. The 6 inches of concrete over the webs is removed down to the level of the cantilever tendons by using a jackhammer.

The section of the span replaced at one time was limited for two reasons. First, it allows for replacement of a limited section of the top slab if the damage is local. Second, it provides more stability by limiting the length of span having the decreased torsional stiffness. Once the concrete has been removed in the section under repair, the new reinforcement and transverse post-tensioning is placed. Figure 4 depicts in detail the portions of the deck which are replaced and the overall cross-section remaining once the replaceable deck sections have been removed. As discussed more fully in the next section, no main longitudinal post-tensioning is located within the replaceable deck area; however, there are longitudinal post-tensioning bars which are replaced and connected to the existing bars by using standard coupling devices. Once the concrete has been cast and reaches the necessary strength, the new post-tensioning is stressed and work may proceed to the next section if necessary, or the span is lowered if no additional deck needs replacing.

Special Design Provisions

Once the scheme has been developed for the deck replacement procedure, provisions had to be made in the design of the structure to make the scheme feasible. By choosing jacking of the span to induce a constant negative moment to remove top slab compression, the final stress state of the top slab should be as nearly uniform as possible along the entire span. The typical final top slab compression for a bridge built in balanced cantilever is a minimum at the pier, somewhat higher at midspan and is the largest near the quarter-point of the span. This "bubble" is due to the cantilever post-tensioning being governed by the stresses at the pier during cantilever erection, resulting in an excess amount of post-tensioning near the cantilever midpoint. A stress distribution of this shape would result in either the zero stress point being too low near the piers or excess compression remaining near the quarter-point of the span when applying the constant negative moment by raising the span.

To solve this problem, the longitudinal post-tensioning layout was optimized to produce as nearly a uniform compression state as possible, while still meeting the allowable stress requirements during construction and service. The result was a layout shown in Figure 5, using both typical cantilever tendons located in the top slab and external draped tendons anchoring in blocks above the bottom slab on either side of the pier. The addition of the draped tendons, as seen in Figure 6, provides the negative moment capacity at the piers, while reducing the excess top slab compression away from the pier.

The external draped tendons solved other problems as well. First, the drape of the tendon provides additional shear resistance near the pier. This is important when replacing the deck near the pier when the section properties are reduced. Second, it helped reduce the problem of where to locate the cantilever tendons such that they are not within the replaceable top slab. The draped tendons reduced the number of typical cantilever tendons required and enabled all of them to be placed above the web as shown in Figure 4. The typical 200 foot span required only 6 19-0.6 inch diameter strand cantilever tendons per web, although their efficiency was reduced by their lower placement in the top slab. FHWA and CDOH agreed to limiting the replaceable concrete to a depth of

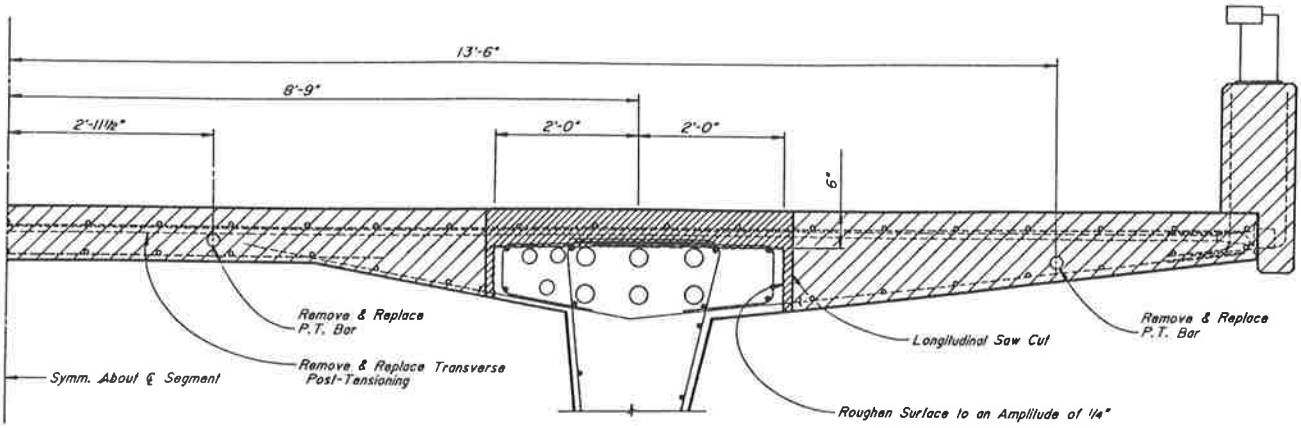

TYPICAL CROSS SECTION
(Top Slab)

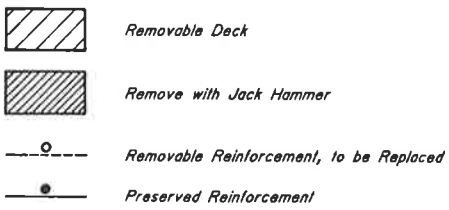

CROSS SECTION DURING DECK REPLACEMENT OPERATIONS

FIGURE 4 Typical cross-sections during replacement.

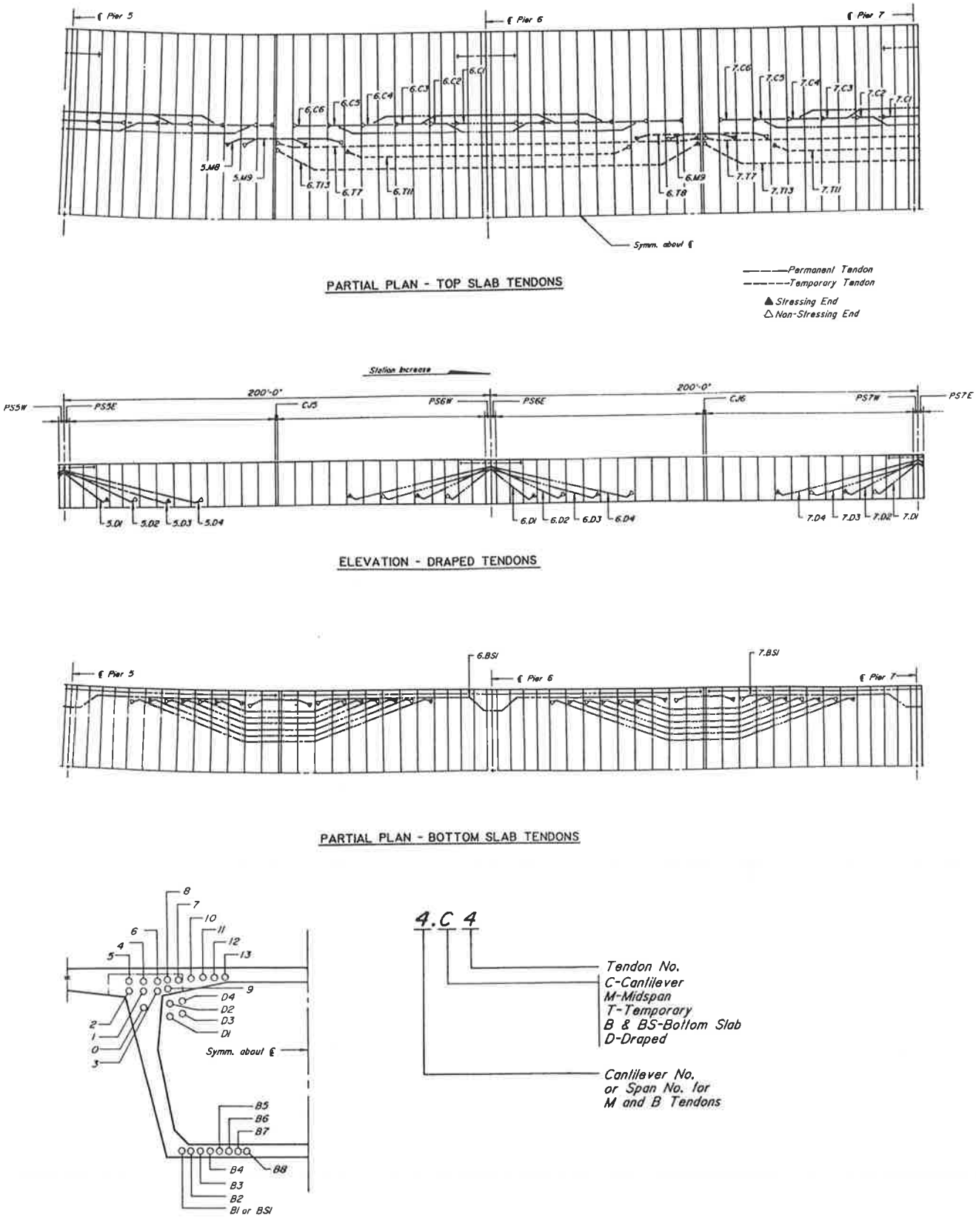

FIGURE 5 Typical post-tensioning layout.

approximately 5-1/2 inches in this area. The three tendons shown in Figure 4 outside of the web reinforcement are top slab continuity tendons located at midspan.

The area containing the 6 cantilever tendons was specially reinforced for the deck replacement condition. The hammerhead left at the top of web also provides additional transverse stiffness to the top of web when the top slab is removed. The area above the web is typically where the cantilever tendon achorages are located. Since the tendons are located in this area, the anchorages were forced to be lowered into the web resulting in a necessary thickening of the top portion of the web. This is basically the only change to the box girder cross-section necessitated by the deck replacement scheme. A typical full box girder cross-section is shown in Figure 7 just after casting. The duct locations in the top slab outside of the hammerhead are temporary tendons used only during construction and are not a part of the permanent post-tensioning.

Figure 8 shows a plan view of a typical pier cap and the placement of the jacks for lifting the span. The pier cap and the superstructure were specially reinforced for the relocated bearing reactions while jacking. However, the jack locations shown are also used for lifting the bridge approximately 1/2 inch to replace the pot bearing assemblies, if necessary.

Deck Replacement Analysis

The structural changes occurring within the bridge during the deck replacement procedure are complex due to the change in stiffness, the change in dead load, the change in the internal post-tensioning moments and the resulting change in moments due to redistribution. The analysis required to accurately and completely include all of the above behavior was beyond the scope of the work requested by the owner. Therefore, the analysis completed at this time was preliminary in nature and intended only to verify that the scheme was feasible and accounted for in the structure design. Should deck replacement ever be required, a more complete and exact analysis would be necessary at that time. Therefore, the level and methods of analysis used were determined by the following primary objectives:

- The analysis and information shown in the contract documents would be only for a typical, interior 200 foot span.
- The bridge must be stable during all phases of replacement.
- The superstructure stresses must be within allowable limits during deck replacement and upon return to service.
- Local stresses in the transition area at each end of the section to be replaced must not be critical.

The global longitudinal analysis was completed by using the same two-dimensional, plane frame analysis computer program used to design the superstructure. The program is capable of time-dependent analysis of prestressed concrete; however, that feature was not used for the deck replacement analysis. It was assumed that all time-dependent behavior of the initial structure would be complete at the time of replacement and that the new concrete deck is not stressed high enough to cause a significant redistribution of moments after replacement. This assumption and the effects of shrinkage of the new deck should be investigated further in the analysis done at the time of replacement.

The prediction of forces during and after deck replacement was made using the following assumptions:

- The effect of all external loads, including jacking loads, counterweighting, removal of and replacement of top slab, and top slab post-tensioning bars, were evaluated by calculating the change in moments and shears by superposition, using the stiffness of the bridge at the time the load is applied. This stiffness changes as various portions of the top slab are removed and replaced.
- The redistribution of internal loads was calculated by assuming the change in forces to be the difference between the forces in the bridge with the different stiffnesses, both subjected to the same loading. To accurately predict the redistribution, an iterative program would be needed. This procedure would be similar to that used in non-linear finite element codes used to predict redistribution due to material yielding.

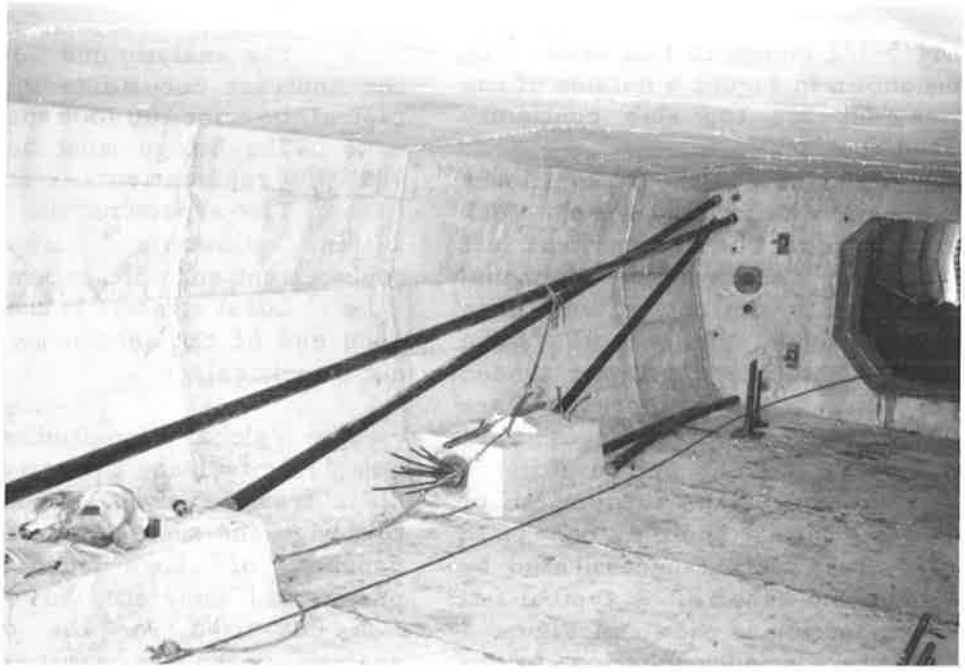

FIGURE 6 Draped external post-tensioning tendons.

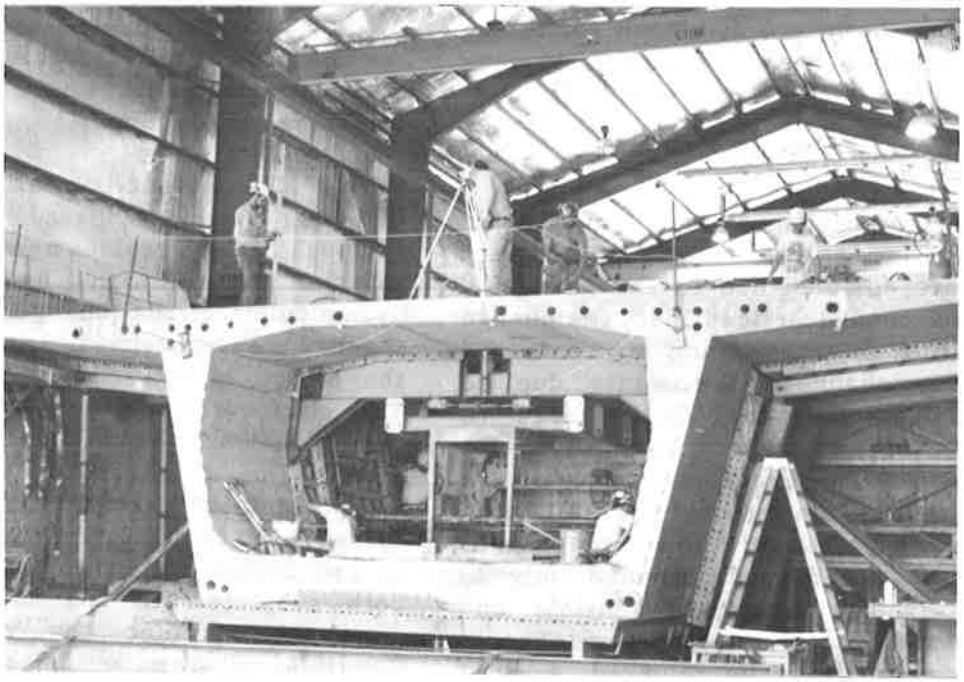

FIGURE 7 Typical box girder section

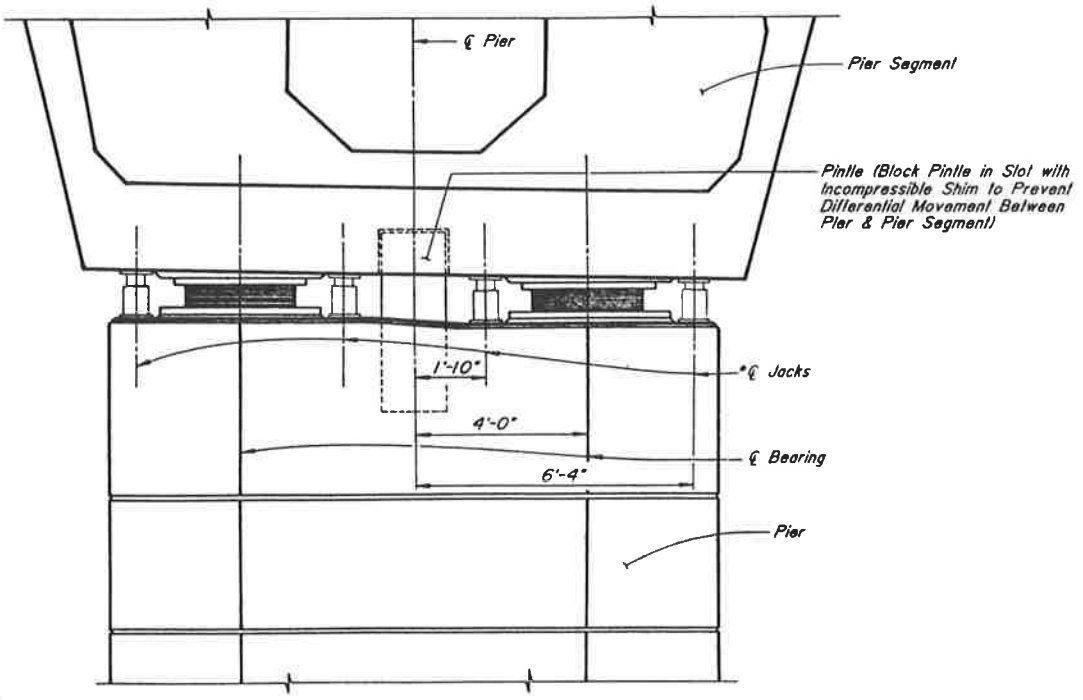

TRANSVERSE ELEVATION

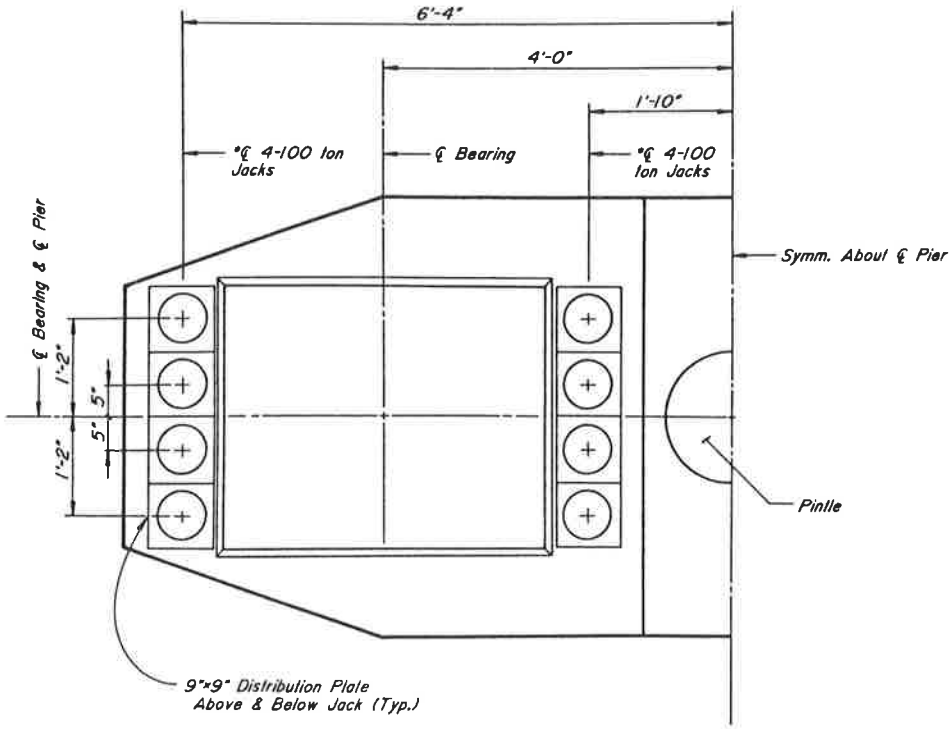

HALF PLAN

FIGURE 8 Jack placement for lifting structure.

To calculate the completed end result of replacing the entire span in sections, the individual changes in forces for each step of each section are simply summed. This results in new moments and shears at each segment joint in span. The stresses must also be calculated in a similar manner by using the flexural stress equation Mc/I at each step of the process. As an example of the process involved, the upper portion of Figure 9shows the moment redistribution in the structure due only to a reduction in stiffness at the center of a span with the deck removed. The increase in negative movement at the piers is due primarily to the span acting more like two cantilevers from the midspan flexural stiffness reduction. During the phase of replacing the deck near the pier the opposite effect is seen, as the span acts more as though it is simply supported at the pier and an increase in positive moment near midspan occurs. The increase in positive moment at midspan for the case of the deck removed at midspan, is due to the change in location of the neutral axis and thus a change in the post-tensioning moment. The lower portion of Figure 9 illustrates the superposition principle used to calculate the changes in stresses. Note the discontinuity which occurs at the bottom of top slab after it has been replaced.

The above step-wise superposition process must be done for each change in stiffness and load for each section replaced. The final result is then the summation of all the steps. The results of the analysis are shown in Figure 10. The structure begins with the top slab stresses in the segments at Day 5000 (time assumed at which long-term effects are finished), which are approximately 75 ksf across the span. The structure is raised 5 inches at each pier and the stresses reduce to approximately 35 ksf. The next three graphs show the stresses after removing the post-tensioning bars (c), then the slab itself from the center section (d), and then with the slab replacd in the center section (e). Finally the last (f) graph shows the final stresses in the top and bottom slabs after all sections in the span have been replaced. Note the elimination of the "spikes" in the top slab stresses due to the cantilever post-tensioning anchorages. The average stress in the top slab is approximately the same as it was prior to the replacement. However, there is a net redistribution of the positive moment in the span after all sections of the deck have replaced in the span (Figure 10(g)). This causes a slight decrease in the bottom slab compression and may require stressing of the contingency tendons within the span. The necessity of stressing these tendons would depend on the stress results obtained in the more accurate analysis done at the time of replacement.

The shear stresses were also checked by using the analysis described above. The final results indicated the following:

- Shear stresses are not critical during the replacement, although no large equipment is allowed on the span during replacement.
- The service shear stresses increase by approximately 5% due to redistribution.
- The service shear capacity increases by 15% due to the redistribution of axial load to the unreplaced concrete (which reduces the principal tensile stress).

A three-dimensional finite element analysis was used to check local stresses a the transition areas and to evaluate torsional stability. The accuracy of the finite element model was checked by comparing the global longitudinal moments with those predicted by the two-dimensional analysis. The correlation between the two analyses was good.

The local stresses at the transition areas were not found to be critical. Stress concentrations were found to be higher at post-tensioning anchorages than at the transition section.

An estimation of the torsional redistribution in horizontally curved spans was made using a procedure analagous to that used in the longitudinal bending analysis. It is found that an increase in torsion in the section with the deck removed can occur. This is counter-intuitive, since the torsional stiffness in these sections decreased dramatically. The reasons for this redistribution are:

1. Torsion alone, does redistribute such that the section with the deck removed carries less torque.
2. However, redistribution of the longitudinal bending moments can increase the net torque due to the component of bending moment "transferred" (due to the curvature) to a torsional moment.

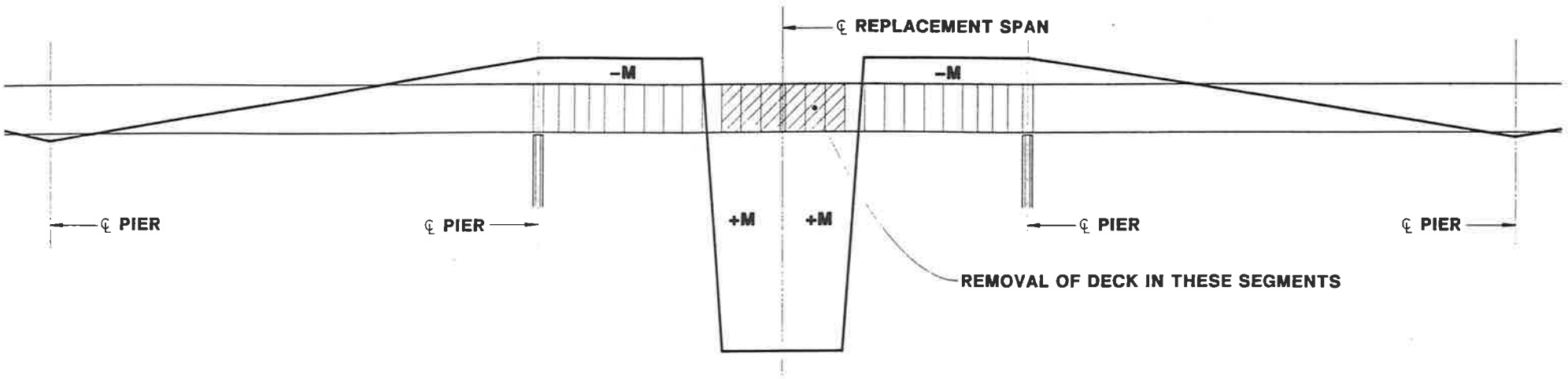

FIGURE 9 Longitudinal bending analysis procedure.

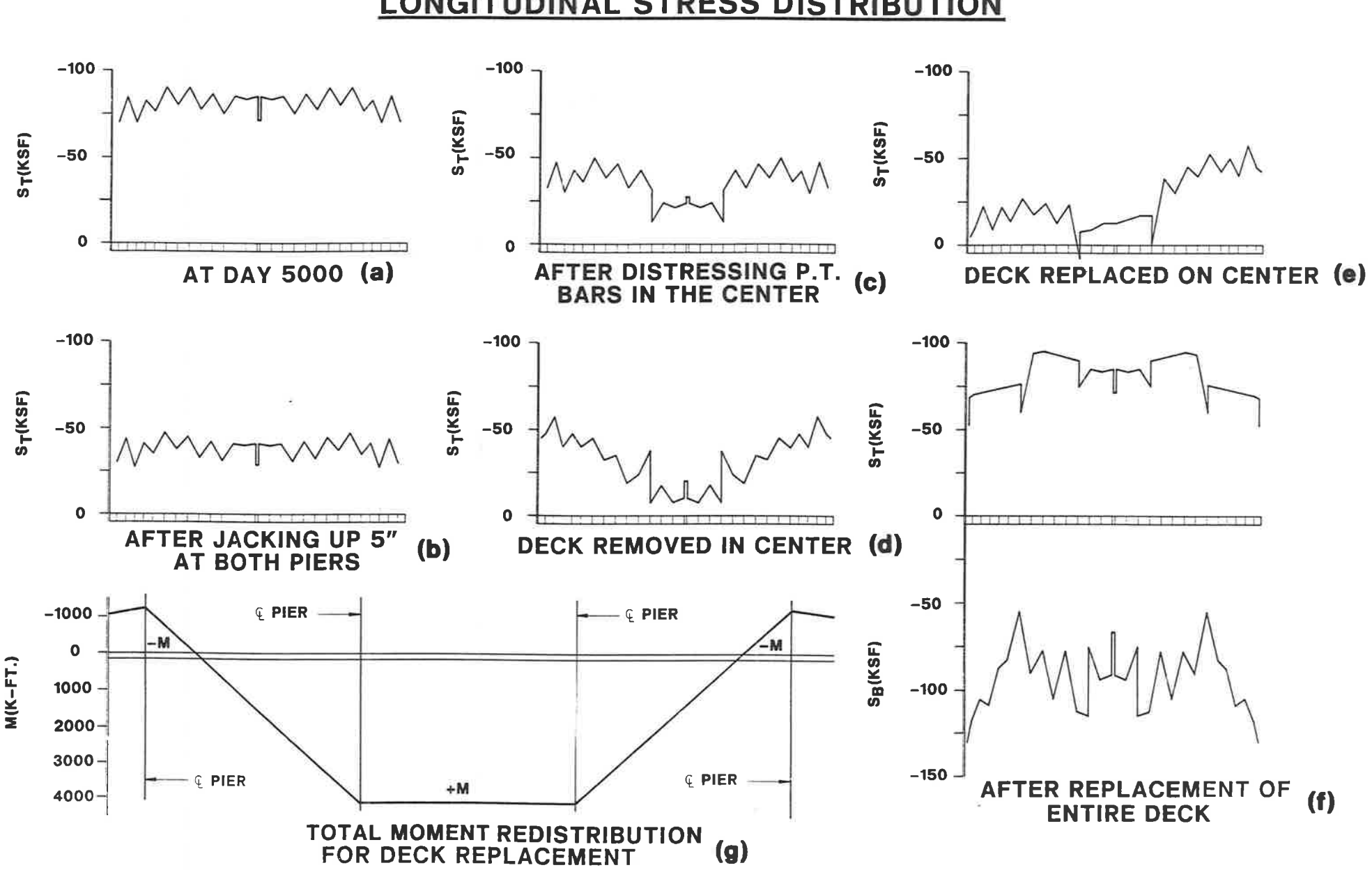

FIGURE 10 Longitudinal bending analysis results.

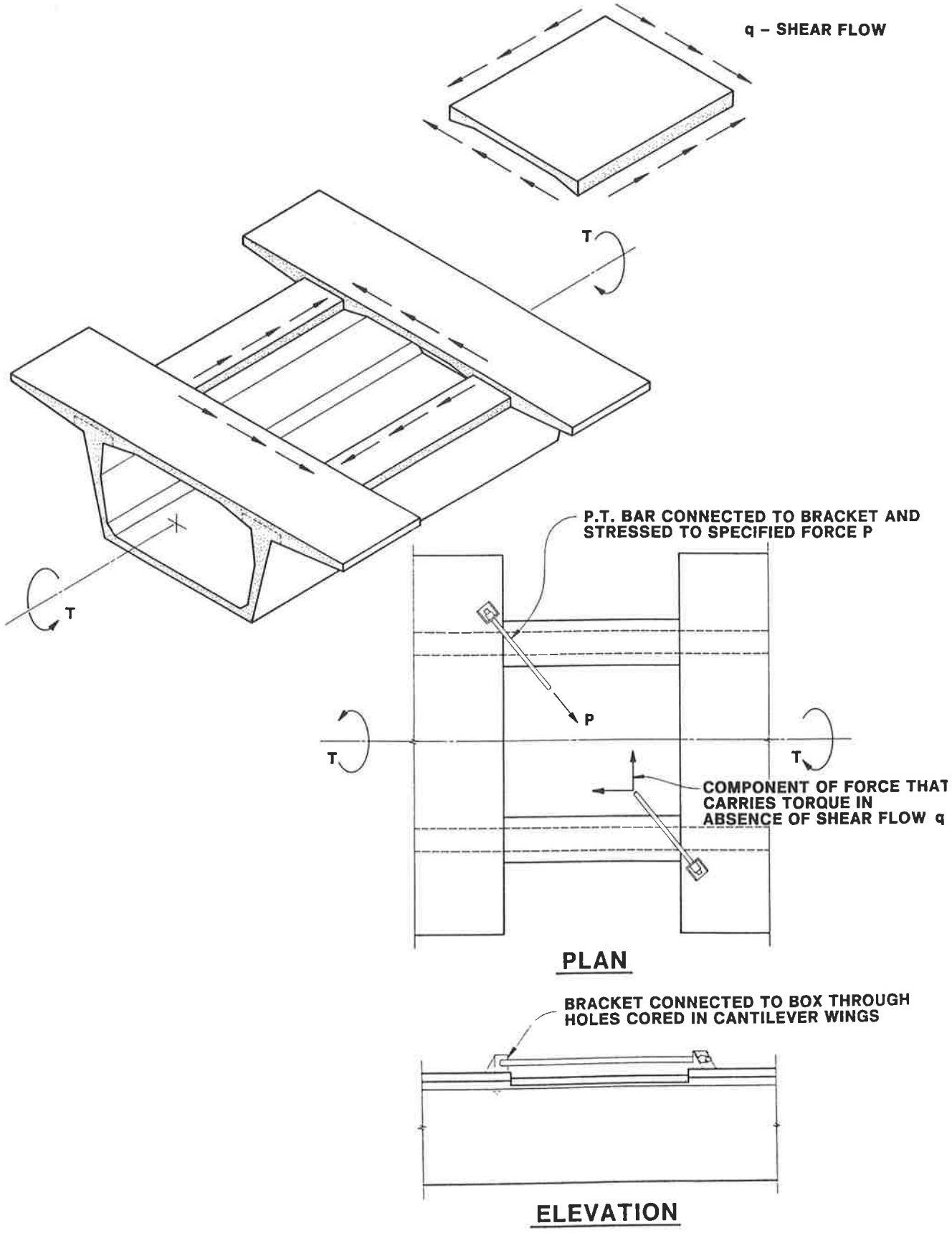

FIGURE 11 Temporary tension tie.

To minimize the effects of the torsional redistribution in the span, the following recommendations were made:

- For straight spans, proceed with the deck replacement procedure as presented.
- For curved spans with radii greater than 1900 ft, limit deck replacement/removal to two segments (16 ft.) at a time. This allows for the development of a diagonal compression strut in the webs.
- For curved spans with radii less than 1990 ft, the stability of each individual span should be checked. A "tension tie" to prevent torsional distress could be used in high curvature spans.

A schematic of the tension tie is illustrated in Figure 11. As the top slab of the box is removed, the section is not able to transfer the torsion through shear flow in the top slab. Therefore, the tension tie, which is simply a post-tensioning bar temporarily anchored to the top slab, is used to carry that shear flow across the gap and warping while the top slab is removed. Again, this simply allows for a simple solution to the problem if it occurs. The final analysis may show that the tie is not needed, or another solution may be developed.

CONCLUSIONS

Although it has been shown that deck deterioration has not yet been a problem in prestressed concrete segmental decks, a simple and feasible deck replacement procedure has been developed for bridges built in balanced cantilever. The procedure can be performed using typical construction practices such as jacking the structure at the piers, concrete sawing and jackhammering. Perhaps the most important feature is that there is relatively little additional cost for necessary details in the initial construction, while still providing the owner with the possibility of complete deck replacement in the future. In summary, it has been shown by this project that prestressed concrete segmental bridges cannot only provide economical solutions to today's bridge requirements, but also to those of the future.

REFERENCES

1. R.W. Poston, R.L. Carrasquillo and J.E. Breen, "durability of Post-Tensioned Bridge Decks", ACI Materials Journal, July-August 1987, pages 315-326.

Underwater Pier Repair

D. N. CORDA, R. B. PEEL, AND A. M. VAYSBURD

The paper describes the extent of concrete deterioration and subsequent repairs performed during 1989 at Pier 2 of the Bayville Bridge over Mill Neck Creek in Nassau County, New York.

The inspection prior to the repairs included visual underwater examination of the concrete and the extraction and testing of concrete cores. The condition of the concrete structure, the degree of erosion damage which had occurred and the process used to select the method of repair are described.

Causes of deterioration of the pier concrete are also discussed.

The use of high-strength water permeable fabric as a forming material for concrete repair is described. Use of fabric-formed concrete is well-suited to underwater repairs where placement of conventionally-formed concrete is both expensive and unreliable.

Concrete mix proportioning and placement in underwater repair are described.

The Bayville Bridge is located in Nassau County, Long Island, New York, between the Villages of Mill Neck and Bayville. The bridge spans Mill Neck Creek at its confluence with Oyster Bay Harbor, an arm of the Long Island Sound. The present Bayville Bridge is the fourth structure located at the same general location. The first bridge was privately built in 1897. In 1907 the bridge was deeded to the Town of Oyster Bay. About this time, the Town started a renovation of the bridge. The third bridge was constructed in 1922 to the east of the previous bridge. The fourth and present bridge was built in 1938 by Nassau County. At first it was the intention to remove the superstructure of the third bridge and reuse the piers and foundations. The footings proved inadequate and a complete new bridge was built several feet east of it.

The present bridge is an eight-span structure, 541-feet (163 m) long and 42-feet (13 m) wide, of which Span 3 is a twin-leaf bascule span. The bridge superstructure is supported on two granite-faced concrete abutments and seven piers.

Approach span piers are resting on concrete footings supported on piles. The bascule piers (No. 2 and No. 3) are pile-supported, reinforced concrete piers, which accommodate machinery and counterweight pits below deck level, and support the masonry buildings (Figure 1). The piers are supported on piles embedded 17 feet (5.1 m) into the creek bottom. The pier stems are encased in granite blocks with mortar joints between courses. The bottom portion is poured flush with granite facing.

There is a 77-foot (23.5 m) wide channel between the timber fenders of the bascule span. The minimum channel depth at mean low water is approximately 9 feet (2.7 m). Mill Neck Creek is a tidal waterway outletting into Oyster Bay harbor which in turn is joined to the Long Island Sound.

Greiner, Inc., 2219 York Road, Suite 200, Timonium, Maryland 21093-3111

FIGURE 1 Bayville Bridge. A view of bascule span.

There is an average tidal range of about 7 feet (2.2 m), from +4.2 (1.3 m) feet to -3.1 feet (0.9 m). Low tide has been known to be as low as -5.1 feet (1.6 m).

Even in the normal tide range there are high velocity currents in the order of 15 feet (4.5 m) per second. The creek bed is sandy and the area west of the bridge is littered with quantities of debris from the demolition of previous bridges.

As part of a scheduled above-water maintenance program, the bridge is inspected semi-annually with an underwater inspection scheduled every five years. During 1984, while conducting an underwater inspection survey of the concrete substructures in preparation for a rehabilitation contract, divers detected several areas of concrete deterioration. In August 1987 a detailed underwater inspection of the bridge was conducted as part of the five-year program.

UNDERWATER INSPECTION

The 1987 underwater inspection covered the area of the bridge from the granite stone facing to the mudline on all of the piers. The inspection was performed by a team of two divers, a tender and a professional engineer. Mortar joints were cleaned prior to inspection. In addition, random stones and portions of the concrete faces were cleaned utilizing wire brushes, water blasters, chisels and scrapers. The marine growth was very heavy and consisted of thick sea grass with oysters and mussels and a well-established layer of barnacles.

All of the underwater inspection was conducted utilizing surface-supplied air systems and continuous communication

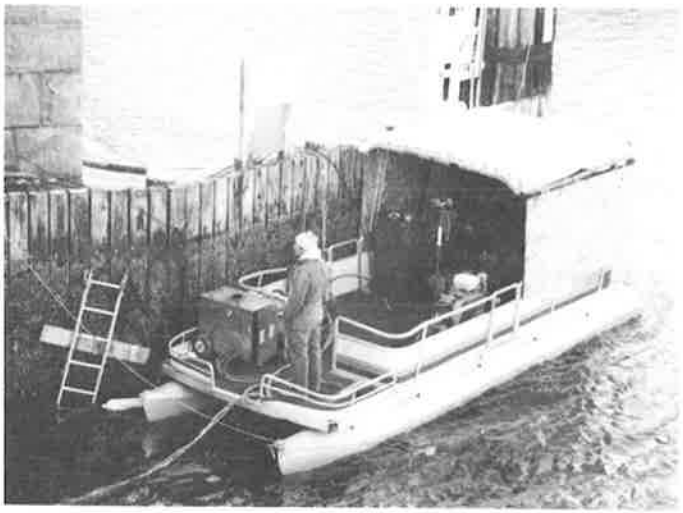

FIGURE 2 Equipment Boat.

between the surface personnel and the diver. An open workboat was used as the surface platform to support the underwater inspection (Figure 2). This boat was also used to perform hydrographic profiling and a fathometer survey.

The turbidity of the water in this area did not allow for acceptable underwater photographs or video taping. Figure 3 shows a diver ready for underwater inspection.

FIGURE 3 Diver ready for underwater inspections.

The mortar joints between the granite stones of the facing on the piers have been seriously eroded and as a result have allowed many of the stones to dislodge and to displace from the protective facing.

In many cases a gap has opened sufficiently wide to allow a visual and tactile inspection of the pier shaft behind the stones. In those locations the concrete appears to be soft and severely disintegrated with exposed coarse aggregate. The space between the stone and concrete of the shaft is between 2 and 3 inches (5 and 7.5 cm). This was verified by using a bent rod that was inserted in the mortar joint and then twisted to determine the extent of the void behind the stones. The inspection revealed that a large number of voids existed between stone facing and concrete, and that some stones had little if any adhesion to the concrete shaft.

The underwater inspection detected larger areas of erosion than in the 1984 survey. Most of these areas were located at the north face of Pier 2, in the footing where deep pockets of laitance and large voids extended under the pier along this face. The erosion reached a maximum depth of 5 feet (1.5 m) and extended about 6 feet (1.8 m) from the existing creek bed (Figure 4). In addition to the observed problems, some deterioration attributed to chemical interaction between the concrete and seawater, was evident.

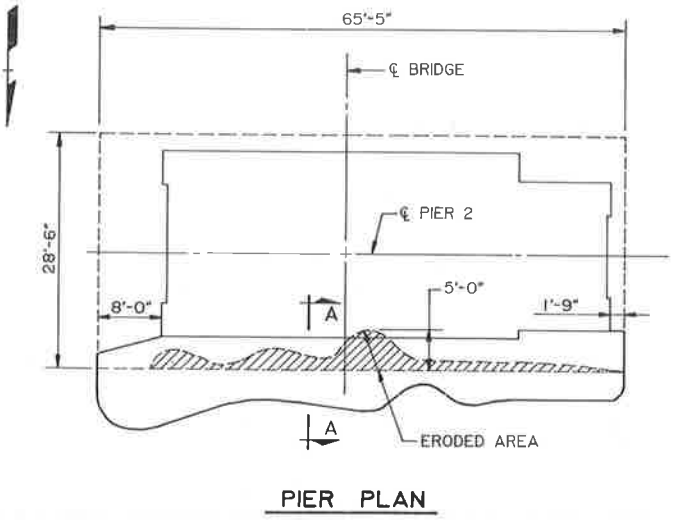

FIGURE 4 Pier 2 showing eroded areas.

TESTING

Based on the 1987 underwater inspection, Greiner, Inc. recommended to expand the testing of the Pier 2 structure. Eight concrete samples were cored at various locations using an electric rig with a nominal 3 inch (76 mm) diameter bit. All concrete cores were visually evaluated and tested for compressive strength. The visual examination and compressive testing are summarized in Tables 1 and 2. A portion of Core No. 8 taken horizontally from the deteriorated footing area of Pier 2 is shown in Figure 5. Core testing revealed zones of non-homogeneous soft material throughout the structure on this face of the pier.

Since the problem with the stone facing of piers was not considered critical, it was not extensively investigated.

Therefore, the remainder of this paper addresses the Pier 2 footing deterioration and repair.

FINDINGS

After the evaluation phase was completed, the next step was to establish the cause or causes of the defects that had been detected. Since many of the symptoms may be caused by more than one mechanism acting upon the concrete, it was necessary to get an understanding of the basic underlying causes of damage and deterioration.

Unfortunately, in the described case, the diagnosis was complicated due to a lack of data, particularly on the history of the structure and such basic data as type of cement, mix, sources of aggregate, climatic conditions during construction, and methods of concrete placement.

The footing concrete was placed by tremie method. The coring program revealed persistent problems in the quality of the concrete. These problems included areas of segregated sand or coarse aggregate, voids, zones of trapped laitance, and zones of honeycombed concrete. Review of the core logs has shown that the areas of poor quality concrete varied horizontally as well as vertically.

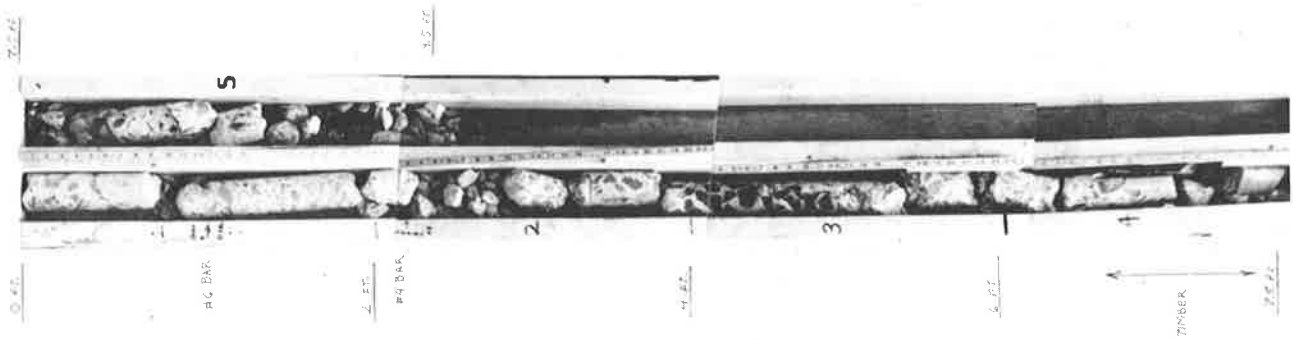

FIGURE 5 Core No. 8 taken horizontally from Pier 2 foundation.

TABLE 1 SUMMARY OF CORE LOG, CORE #8

Distance from Face, ft. (m)		Concrete Description
From	To	
0	2.1 (0.6)	Coarse aggregate segregation 0 to 0.8 ft. (0.25m), at 1.1 ft. (0.35 m) embedded #6 rebar slightly rusted. Test core "A" taken from 1.3 ft. to 1.8 ft. (0.4 m to 0.55 m).
2.1 (0.6)	2.9 (0.9)	Rubble with #4 rebar at 2.3 ft. (0.7 m), slightly rusted.
2.9 (0.9)	4.0 (1.2)	Vertical cracks at 3.2 ft. (1.0 m) and 3.9 ft. (1.2 m). Test core "B" taken from 3.3 ft. to 3.8 ft. (1.0 m to 1.15 m).
4.0 (1.2)	5.9 (1.8)	Honeycombing with random cracking.
5.9 (1.8)	6.5 (2.0)	Short sections of concrete with rubble from 6.3 ft. to 6.5 ft. (1.9 m to 2.0 m)
6.5 (2.0)	7.3 (2.2)	Wood embedded from 6.7 to 7.3 (2.0 m to 2.2 m).
7.3 (2.2)	8.3 (2.5)	Rubble.
8.3 (2.5)	8.9 (2.7)	Sound concrete. Test core "C" taken from 8.6 to 8.9 (2.6 m to 2.7 m).
8.9 (2.7)	10.0 (3.1)	Rubble.

TABLE 2 CONCRETE COMPRESSIVE STRENGTH TESTS (Core #8 Sections)

Core Section	Depth from Face to Top of Section ft. (m)	Compressive Strength psi (MPa)
A	1.3 (0.4)	2,780 (19.2)
B	3.3 (1.0)	4,140 (28.6)
C	8.6 (2.6)	1,760 (12.1)

In our opinion the deterioration of the concrete was caused by the poor quality of the material itself and by the environmental factors. Damage to the foundation concrete was most likely started by the forces of erosion, which are defined in ACI 210R-87 as the progressive disintegration of a solid by cavitation, abrasion, or chemical action.

Ordinarily, properly designed and constructed underwater concrete structures will undergo years of erosion-free service. However, for a variety of reasons such as inadequate design and construction, or environmental changes, erosion does occur in underwater structures. The erosion progresses rapidly after the initial period of exposure roughens the surface with tiny craters and has a tendency to follow the mortar matrix and undermine the aggregate. Once erosion has begun, the rate of erosion increases because protruding pieces of aggregate become new generators of vapor cavities.

Once cavitation damage has substantially altered the flow regime, other mechanisms then begin to act on the concrete, such as abrasion and chemical attack. Abrasion damage results from the abrasive effects of waterborne sand, gravel, silt, and other debris being circulated over a concrete surface. While good quality concrete is capable of resisting destructive forces for many years with little or no damage, poor quality concrete such as the foundation of Pier No. 2, could not withstand the described destructive forces.

This deterioration of the concrete was probably accelerated by chemical attack by the marine water on the compounds present in hardened portland cement. The findings of the underwater inspection clearly indicated the general symptoms of the chemical attack causing concrete disintegration and spalling of the concrete surfaces. The aggregate particles protrude from the matrix, and there is a loss of cementation in the cement matrix. The aggregate, being more inert than the cement-sand matrix, is not attacked and protrudes from the surrounding surface.

Bridge records show that the bridge openings have averaged about 1,500 per year. Fatigue caused by impact and vibration of the bascule pier may also have contributed to the deterioration. Unfortunately there are little reported studies of concrete fatigue caused by vibration and impact.

The inspection also found some scouring of the creek bed under the footing of Pier 2. Along the north edge the scour extended 4 to 6 feet (1.2 to 1.8 m) underneath the footing and was 1 to 2 feet (0.3 to 0.6 m) deep.

Based on the findings of the divers' inspection and test results, plans for repairs were initiated.

REPAIR ALTERNATIVES

A review was carried out to assess alternatives available for underwater repair of large voids. There are two options for performing such repairs: in the dry, or the wet. For the first option, a cofferdam can be installed around the pier, dewatered, and the repair work performed in the dry. The advantages of this method are that conventional above-water repair procedures can be used and construction inspection is easier. The major disadvantage is the high cost of building the cofferdam.

Therefore, underwater concrete repair that does not require dewatering should be an attractive alternative. Several methods can be used to place concrete underwater. The primary concern in placing concrete below water is to prevent washout of the cement. The unhardened concrete should be kept out of direct contact with the water to the extent possible, and protected against fast-flowing water. A number of methods have been developed to accomplish this: tremie concrete, preplaced aggregate concrete, the bottom opening bucket, pumped concrete, and bagged concrete.

In reviewing the tremie concrete method it was learned that while this method of concrete placement is a well established underwater construction technique it is most often used in new construction to place thick sections involving large quantities of concrete. In repair projects, the sections generally are much thinner, making a tremie seal very difficult to maintain (1). Also, concrete mixtures suitable for traditional tremie placement are highly susceptible to washout.

A state-of-the-art report on techniques for underwater repair of concrete (2) indicated that anti-washout and/or silica fume admixtures can eliminate the washout problem. However, it is known that a slightly excessive amount of anti-washout admixture renders the concrete so cohesive as to be unworkable. The key then becomes the successful use of an anti-washout admixture in conjunction with a water-reducing admixture to increase the slump.

In addition to reviewing the state-of-the-art in tremie concrete, the preplaced aggregate method of filling large voids behind forms was also considered.

In reviewing the bagged concrete process it was learned that in recent years, there has been rapid development in this technology. An early use of fabric as a form for concrete was proposed in a patent used in 1922 in Norway (3). The author of this patent, Johann Stere, proposed to build underwater concrete structures such as breakwaters and piers by filling large bags with concrete and placing them with a crane. This method found its practical application in the 1960's, when it became possible to take advantage of the durability and high strength of modern synthetic fibers to produce forms for casting concrete underwater. Fabric forming was introduced in the United States around 1968.

Concrete-filled bags exhibit the high durability required for structures exposed constantly to severe cyclic changes and higher abrasion resistance compared to conventional concrete of similar water/cement ratio (Table 3). The physical properties of fabric-formed concrete are essentially the same as those expected of concrete cast in conventional rigid forms with one important exception. Since the fabric is highly water permeable, excess vehicle water necessary for pump placement will be expelled through the fabric causing a pronounced reduction in the water/cement ratio at and near the surface of the concrete.

It has also generally been found (3) that this reduction of the water/cement ratio is a function only of the permeability and filtering characteristics of the fabric and is essentially independent of the initial water/cement ratio and pumping pressure. Most of this water reduction takes place in the first 5 to 10 minutes after the fabric form is filled.

Having reviewed all the above alternatives it was decided that the requirements of the project could best be met through use of concrete-filled bags for the following reasons:

- More versatile, i.e., not tied to a certain form size.
- Better suited for a small crew and does not involve the use of cranes and handling forms.
- Relatively low cost.
- Durable, high quality repair material can be produced.

The project required the filled bag dimensions to be 10 feet (3 m) long by 45 inches (1.15 m) wide by 25 inches (0.6 m) thick.

From the manufacturer's design and ordering information graphs (5) the bag size had been determined. Bags 11 feet (3.3 m) long by 60 inches (1.5 m) wide, with the volume of the filled bag of approximately 65 cubic feet (1.85 cu. m) requiring 2.44 cubic yards (1.9 cu.m) of concrete were ordered.

The success of concrete repairs depends as much on the thoroughness of preparation as on the quality of the replace ment materials. Project specifications for the repair included a comprehensive section on removal, with the emphasis on full and proper removal of deteriorated concrete. Extensive directions were also provided for preparation of sound substrate, including cleaning and pre-concreting inspection.

Construction requirements included removal of deteriorated concrete and debris, installation of dowels, placement of fabric-formed bags, dowel pins and injection pipes, pumping of concrete into bags, and pumping grout to fill the gap between the existing concrete and fabric-formed concrete.

REPAIR PROCEDURES

The void face was prepared for repair by removal of the deteriorated concrete utilizing chipping hammers in the 30 pounds (14 kg) size range. After concrete removal, the surfaces were cleaned of loose concrete, silt and marine organisms using water jetting techniques. Upon completion of surface preparation an anchorage system was installed utilizing #5 Grade 60 epoxy-coated hooked dowels grouted into drilled 1 inch (25 mm) diameter holes. The holes were air percussion drilled to allow installation of 2-foot (0.6 m) long anchors with a 1-foot (0.3 m) projection on 2-foot (0.6 m) centers. Such spacing is considered sufficient to hold the new repair to the existing concrete surface. Details of the anchor system are shown in Figure 6. The existing streambed was excavated (utilizing an airlift) to a depth of 1'-6" (0.45 m) to provide lateral stability for the initial course of concrete-filled bags.

Fabriform-type bags made of high-strength synthetic fiber, woven into water-permeable fabric were used. Figure 7 shows the diver taking a pack of the bags underwater. Properties of the fabric bag used are shown in Table 4. Each bag was provided with a self-closing inlet valve to accommodate insertion of a concrete pumping hose.

The bags were positioned on a foundation of the undercut existing creek bed and existing concrete.

TABLE 3 COMPARISON OF ABRASION RESISTANCE BETWEEN FABRIC-FORMED MORTAR AND CONVENTIONAL CONCRETE (2)

Fabric-Formed Mortar				Conventional Concrete			
W/C Ratio	Compressive Strength		Abrasion Loss	W/C Ratio	Compressive Strength		Abrasion Loss
	psi	MPa	g		psi	MPa	g
0.41	6,600	46	10	0.36	7,800	54	11
0.45	5,600	39	9	0.40	7,500	52	13
0.50	5,700	39	13	0.55	5,400	37	14

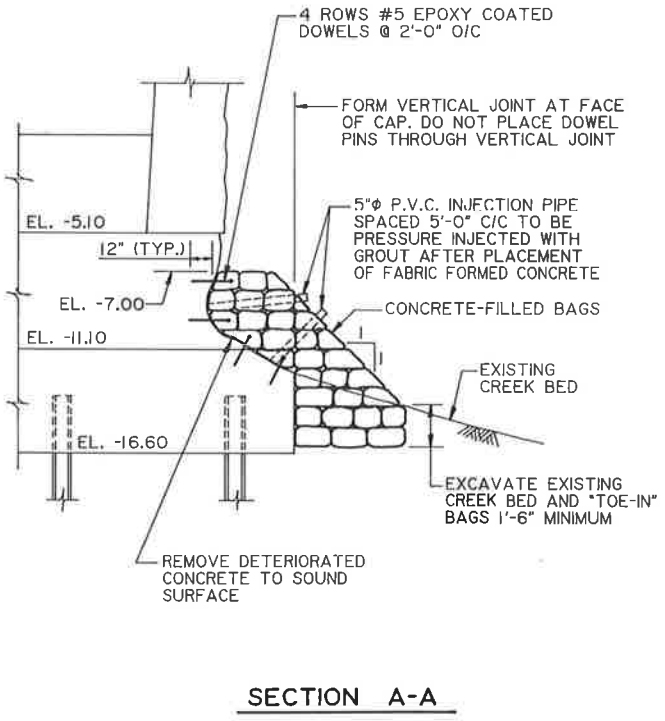

FIGURE 6 Repaired section with concrete-filled bags.

FIGURE 7 Diver taking pack of fabric bags underwater.

A concrete mixture of 3,500 psi at 28 days was used for the project. The mixture proportions are given in Table 5.

PLACING THE UNDERWATER CONCRETE

The concrete was delivered to the jobsite by ready-mix trucks. The delivery system for concrete was a 25 cubic yards (20 cu. m) per hour pump (Figure 8) with a 5-inch (130 mm) diameter output line. This part of the delivery line is a steel pipe in 10 foot (3 m) long sections, coupled with cam action clamps and rubber gaskets. The steel pipe is used to move the concrete close to the actual point of delivery with less friction than is developed in the 2-inch (50 mm) rubber hoses which are used at the end of the line (Figure 9). These hoses are used because of their flexibility, which is necessary for the diver to position the end of the delivery line where it needs to be and move it rapidly from bag to bag. The diver's ability to handle the delivery line is one of the primary factors in the requirement for 2-inch hose. A diver, working underwater sometimes with no place to position or brace himself would not be able to move and maneuver a 5-inch hose.

The length of the hose at the end of the delivery line is important when the time comes to remove the delivery line

TABLE 4 PROPERTIES OF FABRIFORM FIBERS

Property	Standard	Test Data
Weight, oz./yd.^{2}	--	8.0
Tensile Strength, lbs./in. (Ravel Strip Method)	ASTM D 1682	375.0
Tearing Strength, lbs. (Tongue Method)	ASTM D 2262	100.0
Porosity, ft.^{3}/min.	ASTM D 737	105.0

TABLE 5 CONCRETE MIXTURE PROPORTIONS

Material	Mix Proportions lb/yd^3	kg/m^3
Portland Cement (Type II)	752	446
Fine Aggregate (Sand)	1,610	955
Coarse Aggregate (1/2-inch pea gravel)	690	409
Superplasticizer	300	178
Water	3.2	1.9
Water/Cement Ratio	0.40	
Air Entrainment	4 - 6%	

FIGURE 8 Operator at concrete pump.

from the water. With the 25-foot (7.5 m) length of the hoses, it is generally possible to get the ends of the hoses above water before breaking any of the connections. This is very important when the environmental effects of polluting the water are considered.

FIGURE 9 Two-inch hose for pumping concrete.

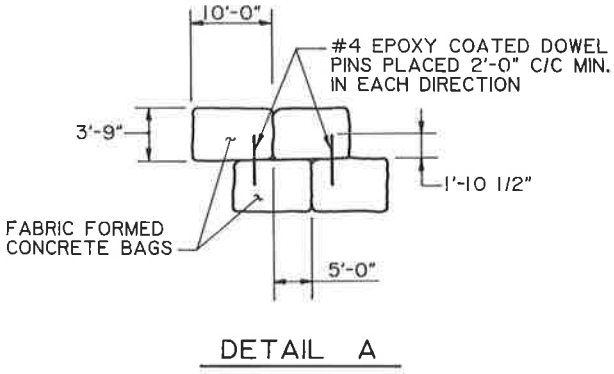

FIGURE 10 Concrete-filled bags with dowel pins.

In order to further prevent the possibility of spilling any cement into the water, the end of the last section of the delivery hose is equipped with a high-pressure quick-acting shut-off valve. Prior to removing the injection line from any one bag, the diver can shut off the flow of concrete through the hose, thus insuring that when he removes the line from the bag inlet, there will be no flow of concrete from the end of the hose.

A diver controlled the end of the hose filling each bag with concrete. Adjacent bags were joined by inserting reinforcing dowels into the freshly filled bag of concrete. The ends of dowels were ground smooth to facilitate penetration through the fabric without tearing (Figure 10).

After a wall of concrete-filled bags was constructed, grouting of the gaps and voids between the existing concrete surface and the wall was started. The grout mixture proportions are given in Table 6.

TABLE 6 INJECTION GROUT MIXTURE PROPORTIONS

Material	Mix Proportions	
	lb/yd^3	kg/m^3
Portland Cement (Type II)	752	446
Fine Aggregate, Sand	2,300	1,363
Water	302	180
Superplasticizer	3.13	1.9

The end of the delivery line shut-off valve was directly coupled to the injection pipe by an Everlock-type coupling. When each void was filled the diver disconnected the delivery hose from the injection pipe and moved to the next injection pipe.

All underwater repair operations were inspected and documented by an independent inspection firm.

CONCLUSIONS

1. Bridges with underwater foundations should be regularly inspected to reduce uncertainty below the waterline. This is a relatively inexpensive form of protection - especially in view of the potential savings through early detection and correction of concrete erosion and deterioration problems.

2. The method of underwater repair with fabric-formed concrete is a relatively simple method, even though continual attention is required to ensure that the specified concrete parameters are met.

3. This method of repair is particularly attractive where strong currents may affect the concrete quality.

4. The success of the described repair project should encourage others to consider such an alternative when underwater repairs are necessary.

ACKNOWLEDGEMENTS

The described repair work was planned and carried out under the supervision of the County of Nassau, Department of Public Works, Division of Highway and General Engineering, Mineola, New York. Construction was performed by Norsea Corporation, Troy, New York. Construction inspection was performed by International Underwater Contractors, New York, New York.

We gratefully acknowledge permission from Nassau County Executive Thomas S. Gulotta, and Nassau County Commissioner of Public Works Ludwig C. Hasl to publish this paper.

REFERENCES

1. T.C. Holland, B.C. Gerwick, Jr., and J.R. Turner. Tremie Concrete Placement, Wolf Creek Damn Cutoff Wall, American Concrete Institute, *Concrete International,* October 1982, Vol. 4, No. 10, pp. 26-34.

2. Gerwick, Ben, Inc., *Review of Technology for Underwater Repair of Concrete subjected to Abrasion Erosion,* U.S. Army Engineer Waterways Experimental Station, Vicksburg, MS.

3. B.A. Lamberton. Fabric Forms for Concrete, American Concrete Institute, *Concrete International,* December 1989, Vol. 11, No. 12, pp. 58-67.

4. E.W. Bindhoff, J.C. King. World's Largest Installation of Fabric-formed Pile Jackets, ASCE, *Civil Engineering,* March 1982, pp. 68-70.

5. Construction Techniques, Inc., *Technical Information, Fabriform Concrete Bags,* Cleveland, Ohio.

Microcomputer-Based Computer-Aided Design of Cable-Stayed Bridges

AHMAD H. NAMINI

This paper describes a software system named LEAF for the computer-aided design (CAD) of cable-stayed bridges. The LEAF system performs the static analysis of three-dimensional cable-stayed bridges with nonlinear effects. Also, the system performs a dynamic analysis for the extraction of pure natural modes of cable-stayed bridges under the undeformed and/or deformed service load configuration. Finally, the LEAF system can determine the lowest wind velocity that initiates aerodynamic flutter instability. The entire LEAF system resides on an IBM or IBM-compatible microcomputing environment with user-friendly features, which include easy-to-use engineering language commands for definition of geometry, structural properties, and loading parameters, while resulting forces, moments, deflections, mode shapes, and flutter profiles can be viewed graphically with multiple-views, zooming, and animation capabilities. As a case study, the LEAF system is applied to the previously built Luling Cable-Stayed Bridge. Though the system's runtime is slower than mainframe-based systems, it has proved itself reliable in accuracy with the added convenience of centralized computing support for cable-stayed bridge designers.

INTRODUCTION

Cable-stayed bridges have become a popular and cost-effective alternative to suspension bridges since World War II. The first modern cable-stayed bridge was the Stromsund Bridge in Sweden, which opened to traffic in 1956. Since then, many cable-stayed bridges have been built throughout the world, with many more being considered. Tada (1) estimates that by the end of the coming year, 90 cable-stayed bridges will be constructed and operational throughout the world. In the United States, eight bridges have been built, seven are under construction, and eight others are in the design and/or consideration process. A cable-stayed bridge consists of components made mainly of steel and concrete. Steel, always used for the cables and sometimes for the deck and pylon, exhibits linear load-deformation behavior below the material's elastic limit. Concrete, used sometimes for the deck and pylon, exhibits nonlinear load-deformation behavior, which is practically linear at low service load levels. In general, a cable-stayed bridge's materials behave in a linear-elastic manner.

Yet, the bridge's overall load-deformation relationship is highly nonlinear. This nonlinearity results from three distinct effects: the nonlinear axial force versus elongation relationship for the inclined cables due to the sag caused under its own weight; the nonlinear axial-flexural interaction in the deck and pylon, which occurs due to the simultaneous effects of large bending moments and axial forces; and the inherently large displacements, which occur due to the structure's high flexibility. Each of the aforementioned nonlinearities change with deformation and level of loading.

Department of Civil and Architectural Engineering, University of Miami, Coral Gables, Florida 33124-0630

To analyze and design a proposed bridge, designers must account for static, dynamic, and aerodynamic behaviors of the fully- and partially-constructed structure. This paper deals exclusively with fully-constructed cable-stayed bridges, and first presents analysis methodologies for the static, dynamic, and flutter analyses of cable-stayed bridges. Then, fundamental principles of a good CAD system are discussed with the important features adopted for cable-stayed bridges. Finally, as a case study, the Luling Cable-Stayed Bridge is analyzed with some of the resulting design information presented.

Static Analysis

As mentioned before, the behavior of cable-stayed bridges is highly nonlinear, and therefore static analysis methodologies must account for such tendencies. Though many methods have been presented in the literature, such as a forced-displacement approach (2,3), a transfer matrix approach (4,5), a finite strip approach (6), and a flexibility approach (7,8), the current pinnacle is the stiffness method (9-15) which is the most favorable method for computer implementation.

In the LEAF system, the use of Lasar's (9) stiffness formulation with load balancing is adopted with the following added features: three-dimensional formulation, cable prestressing, automatic dead loading, member-oriented distributed loading; and global-oriented joint loading. The deck and pylon are modeled with a space frame element allowing for axial-flexural interaction (16). The cables are modeled with an axial rod element, whose nonlinearity is duplicated by the use of Ernst's (17) well-known equivalent modulus of elasticity. Cable arrangements may be of any configuration, lying in a single, double, or inclined plane. All materials are assumed to be linear-elastic.

The load balancing methodology is implemented to reliably climb the static load-deformation curve. The load balancing method first divides the externally applied loads into equal portions, i.e. load steps. Each load step is analyzed using the stiffness method with the stiffness matrix being generated from conditions of geometry and internal loading from the previous load step. An assumption is made that the bridge behaves linearly within a load step. At the end of each load step, internal forces are computed and used to update the stiffness matrix. After all load steps have been traversed, equilibrium is checked at all degrees of freedom. If equilibrium is attained within some small tolerance, the analysis is complete, otherwise the load step method is employed again, this time with the externally applied loads being the negative unbalanced (residual) loads. This process is continued until equilibrium is achieved.

One of the main disadvantages of the load balancing method is that large errors in deformation may accumulate, unless the

externally applied loads are incremented in small steps. Results indicate that improvement in solution accuracy can be made by checking for equilibrium after each load step. The residual load is determined at the end of each load step and applied in addition to the usual load in the next step. With the load balancing method and equilibrium correction, cable-stayed bridges can accurately be analyzed. The methodology described permits the nonlinear static analysis to be used for partially- and fully-constructed bridges. Namini (15) describes in finer detail the nonlinear static analysis methodology.

Dynamic Analysis

The dynamic behavior of cable-stayed bridges involves local and global characteristics. The local behavior pertains to dynamic responses associated with one component of the overall structure. For instance, cables may be excited into violent oscillations due to resonance or galloping. In this case, mechanical dampers are typically installed at the base of the cable to prevent any destructive vibrations. The pylon and deck are generally not susceptible to local oscillations. This paper does not concern itself with local dynamic behavior.

The global behavior pertains to the vibration tendencies associated with the entire structure. In global dynamic behavior, the response motion at the lowest few natural modes of the bridge are of interest. For long span bridges, four predominant types of vibration are of interest: longitudinal, oscillation along the plane of the span; bending, oscillation vertical to the span; sway, oscillation transverse to the span; and torsional, oscillation about the deck cross-section's shear center. For cable-stayed bridges, longitudinal vibration modes are not important, since inclined cables provide horizontal stabilizing forces in the deck. The bending, sway, and torsional modes are typically uncoupled for straight cable-stayed bridges, while coupling between modes occur for horizontally or vertically curved bridges.

To extract cable-stayed bridge modes, previous investigators have developed methods suitable for finite element discretization. Tang (4), Cheung and Kajita (18), and Morris (19) all determined natural modes using a linear-elastic lumped mass formulation, though they did not reveal their solution method. Izyumov et al. (20) also determined natural modes using a lumped mass formulation and also considered the coupling between torsional and sway modes caused by the vertical eccentricity between the deck's center of gravity and shear center. Again, their solution method was not explicitly stated. Fleming and Egeseli (21,22) state that the linear-elastic lumped-mass formulation offers the best discretization model with the solution method being any acceptable eigensystem solution technique. More importantly, they state that linear-elastic assumptions may be assumed for the fully-constructed cable-stayed bridge after the service dead load has been applied. This permits live load analysis to proceed with linear-elastic theory, but the partially-constructed structure must be analyzed with nonlinear effects.

In the LEAF system, extraction of pure natural modes using the well-documented subspace-iteration method with Lanczos generated starting iteration vectors has been adopted. The subspace-iteration method determines the lower natural modes via a Rayleigh-Ritz approximation within an inverse power iteration. Convergence is accelerated, thus decreasing computational effort, when starting iteration vectors are good approximations of the desired modes and are thus generated via the Lanczos method. Namini (23) describes the methodology and implementation onto a microcomputing environment in more detail.

Flutter Analysis

Since the famous Tacoma Narrows Bridge failure of 1940, the bridge engineering community has been faced with the design consideration of aerodynamic flutter. Flutter is the dynamic instability which forms from the mutual interaction of elastic, inertial, damping, and self-excited aerodynamic forces, whereby at some critical wind velocity the bridge oscillates in a divergent, destructive manner. Flutter design consists of analyzing a proposed bridge deck configuration for determination of the lowest wind velocity that initiates instability. The wind velocity at flutter should be higher than meteorological possible wind velocities at the bridge site.

In order to determine the critical wind velocity that initiates flutter, modal analysis is typically employed, with natural modes associated with predominantly torsional motion being the most critical. At present, flutter analysis combines both experimental and analytical procedures. The pioneering free-oscillation method (24) represented self-excited lift and drag forces as well as the aerodynamic moment by so-called flutter derivatives. Flutter derivatives relate forces, per unit span, to the vertical bending, sway, and torsional deformations and associated velocities and are experimentally derived in a controlled wind tunnel environment for a representative portion of the bridge deck over a wide range of wind velocities with the experimental techniques for their extraction described thoroughly by Scanlan (25).

The LEAF system adopts an algorithm, the pK-F method, developed by Namini et al. (26) for the determination of the critical wind velocity that initiates flutter instability. The flutter derivatives are modeled as an aerodynamic element possessing a stiffness and damping component. The solution algorithm is by a determinant search root-finding technique of the complex variable form of the modal equations.

STRUCTURAL ANALYSIS ON A MICROCOMPUTER

On an IBM or IBM-compatible microcomputing environment, the Disk Operating System (DOS) requires individual programs to be no greater than 640 kilobytes when residing in memory. This limit pertains to all portions of a program, i.e. code, data, heap, and stack. This limit on program size directly retards the ability to model large three-dimensional cable-stayed bridges.

For instance, in the static analysis, the assembled global stiffness matrix must be stored, while in the dynamic analysis, the assembled global stiffness and mass matrices must be stored. A cable-stayed bridge modeled with 100 distinct joints with six degrees of freedom per joint, yields each stiffness and mass matrix of order 600. The full matrices each contain 360,000 entries, and if double precision accuracy is used (eight bytes/entry), total storage requirement would be 5.76 Megabytes. Obviously, in-core solution to the governing equations of equilibrium is impossible. There are however techniques to minimize storage requirements and these are discussed in the next section.

Minimizing Program Size

There exist computational techniques for minimizing in-core data storage and manipulation, usually at the expense of computing runtime. Certain attributes of the stiffness and mass matrix are typically employed. Since linear-elastic assumptions are adhered to in their development, the stiffness and mass matrix are both symmetrical, and in the case of the mass matrix may be lumped. A lumped mass matrix contains nonzero elements only along the major diagonal. Thus, only the upper or lower triangular portion of the full matrix need be retained, which effectively reduces the storage requirement to 2.88 Megabytes for the example cable-stayed bridge described in the previous section. This is still too large. More efficient storage techniques retain only the banded portion of the matrices. A banded matrix is stored by rows (or columns) from the major diagonal to the maximum bandwidth (largest number of columns traversing nonzero elements). The efficiency of the banded matrix depends on the joint numbering scheme, which must minimize the difference in a member's near and far joint number. A further refinement of the banded matrix is the skyline matrix. The skyline matrix is stored by rows (or columns) from the major diagonal to the last nonzero element on that row (column).

The other difficulty discussed is the solution method, which goes hand-in-hand with the storage techniques just mentioned. A full matrix is extremely sparse, and therefore standard inverse matrix operations are unstable. The large number of computations needed to invert a matrix by standard inverse procedures propagates roundoff errors, thus producing an ill-conditioned solution. Other methods such as Gaussian Elimination can be easily incorporated, but its effectiveness is reduced since properties of symmetry, positive definiteness, and bandedness are not utilized. The only currently available solution technique permitting three-dimensional cable-stayed bridges to be analyzed on a microcomputer is by the frontal method (27).

Frontal Method

The frontal method, referred also as the wavefront method, is a subset of Gaussian Elimination, but with the strategy of reducing storage by assembling and eliminating degrees of freedom at the same time. As soon as the stiffness coefficients of a particular degree of freedom are completely assembled from the contributions of all members, this particular degree of freedom is eliminated by static condensation. The reduced equation is then stored on peripheral disk. After all degrees of freedom have been traversed, deformations are obtained in the reverse order of static condensation by backward substitution.

An any given moment in the solution algorithm, the computer stores only the upper triangular portion of a square, symmetric matrix containing the equations of the degrees of freedom currently being assembled. Therefore, memory requirements are bound by the constraint of the maximum number of degrees of freedom permitted to be assembled at any one time, termed maximum frontwidth. During the assembly and condensation process, the degrees of freedom are assembled in a prescribed member-by-member order. Maximum frontwidth is not affected by the sequence to which joints are numbered. The frontal method's greatest strength is its stability and reduction of storage. The assembled stiffness matrix is never completely assembled, only portions of it. Its weakness is its increased runtime, since disk input/output during the static condensation and backward substitution stages are slow in comparison to in-core data manipulation.

CABLE-STAYED BRIDGE COMPUTER-AIDED DESIGN

The quality of engineer-computer interaction has often been far from interactive. Rather than simply purchasing new and more powerful computers to solve the problem, by adopting a philosophy of catering to the user's needs, while maintaining computational accuracy, a simulation environment can be developed which is functional, useable, and expandable. There is strong evidence (28,29) that *ease of use* is at least as important as *functionality* in determining the likely success of an application program. This is particularly important when users come from varied backgrounds.

For the LEAF system, it was decided at an early stage of development that the end users would be practicing and research engineers. The practicing engineer would be able to design a new bridge crossing or maintain an existing structure. The research engineer would be able to investigate any aspect of cable-stayed bridge behavior. Also, the scope of problem to solve was limited to fully-constructed bridges with the assumption of linear-elastic behavior after the application of service dead loads. Finally, the microcomputer was chosen as the computing environment since most end users would have access to this facility. This would greatly expand the domain of possible users while eliminating portability problems between different computers. Also, the microcomputer provides the necessary peripheral devices, e.g. monitor, printer, plotter, and mouse for a state-of-the-art CAD system.

After consultation with several cable-stayed bridge engineers, the LEAF system was developed and implemented with the following attributes.

User Interface

To attain a user-friendly environment, the user interface was developed with features common to most well-established general purpose finite element packages. Some of the more important attributes are described next few sections.

Definition of Mesh

One of the most difficult tasks in analyzing a cable-stayed bridge is the process of defining the geometry and associated structural properties. The definition of joints, supports, and connectivity vectors which define members is a laborious chore for any bridge designer. A CAD system's ability to minimize the time and errors in defining the bridge mesh is one the best measures of a program's eventual acceptance or rejection.

In the LEAF system, two different modes of mesh definition are permitted. The first method is by pull-down menu selection windows, while the second is by free-format engineering language commands.

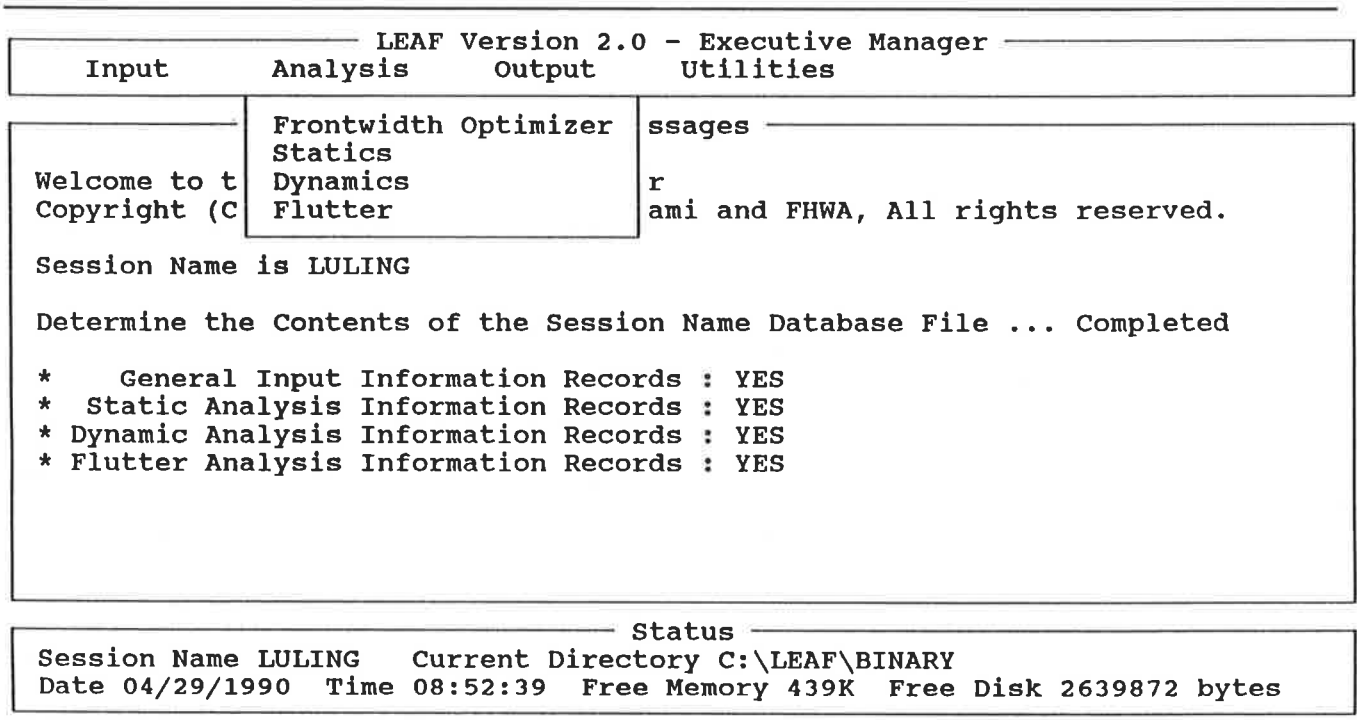

FIGURE 1 Typical pull-down menu selection window

Pull-Down Menu Selection Windows

During the first few exposures to a new CAD system, many users might not remember all the features that the system possesses. Or possibly, a user knows what feature he/she would like to activate, but cannot recall the mechanism. The best user interface attribute to address these scenarios is to permit CAD system features to be activated by pull-down menu selection windows.

Pull-down menu selection windows permit the user to view a CAD system's entire capabilities by using the cursor control keys to scan different features. More importantly, the features can be grouped into different windows by the similarities in scope that the features exhibit with one another. Figure 1 illustrates a typical LEAF pull-down menu selection window.

Free-Format Engineering Language Commands

Many engineers using CAD systems still construct data files to be deciphered by a given data item's column location on a particular line. This technique tends to be tedious in generating a data file, with the resulting file being a large collection of numbers which is difficult to maintain if changes to the mesh need to be made.

The modern and more efficient method for constructing data files is by free-format engineering language commands. In other words, data on a particular line does not have to correspond with predefined column locations. The data is input as a string of numbers separated by one or more blanks. A particular line's data structure is known to the CAD system by words that precede any data. The LEAF system has 45 different commands for complete input generation, with some of the more commonly used for mesh and loading definition shown below.

- *Joint* - The coordinates of a particular joint.
- *Member* - The connectivity vector and structural section for a particular member.
- *Support* - The restraint list for a particular support.
- *Section* - The structural and material properties of a particular section.
- *Initial Cable Force* - An initial prestressing force in a cable stay member before the application of any service loads.
- *Global Joint Load* - A force and/or moment loaded at a particular joint in the global set of axes.
- *Uniform Member Load* - A uniformly distributed load for a particular member in the member set of axes.

A complete list of engineering commands can be found in reference (30). Also, engineering language commands need not always be specified in a data file for batch processing. Instead, a command-line processing environment exists for the user to issue commands interactively. Naturally, a data file for batch processing along with the interactive command-line processing can be used together. Also, the experienced user can use pull-down menu selection windows in conjunction with free-format engineering language commands.

Context-Sensitive Help Windows

No matter how much effort is put into the development of a self-explanatory user interface, users will always have questions because the software system is completely new. Not only do users not know how to converse with the system, but often users are not aware of what the system can and cannot do. Traditionally, this problem is addressed with a printed user's

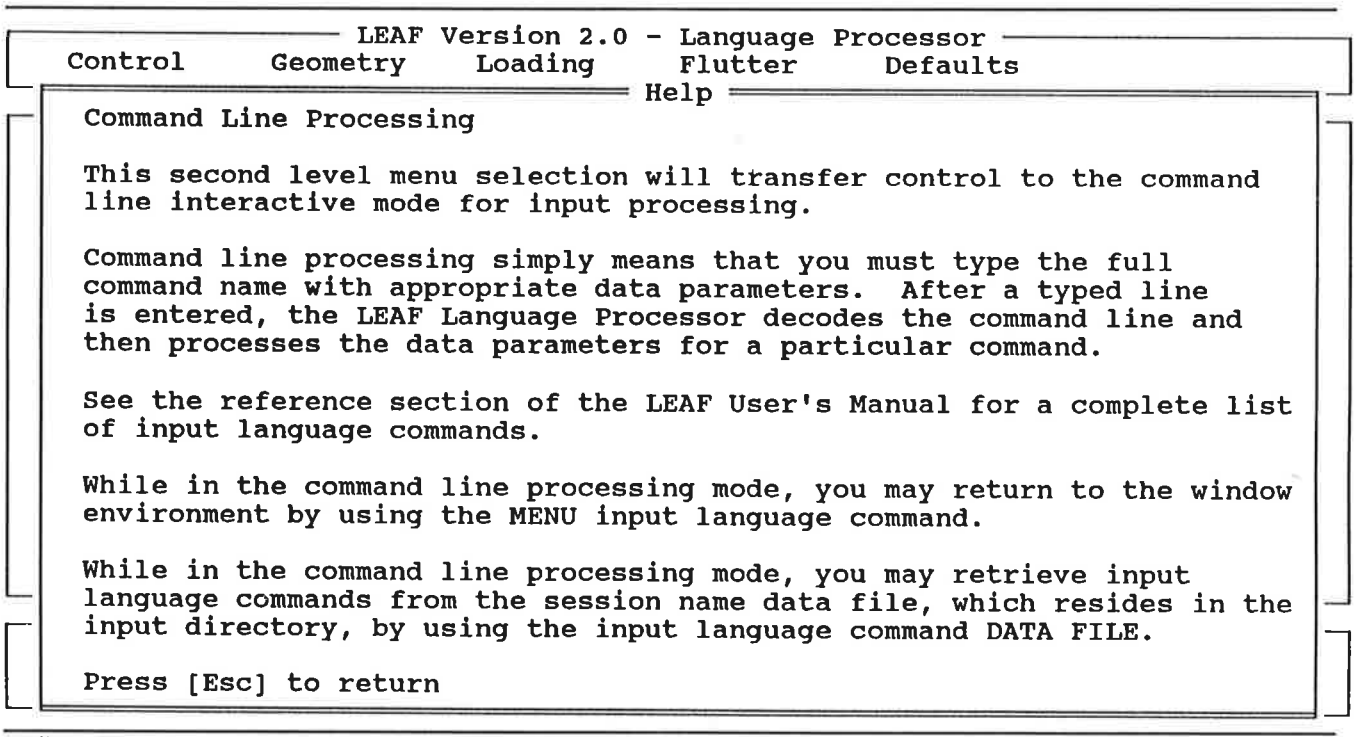

FIGURE 2 Typical context-sensitive help window

manual and perhaps, an automated tutorial. The disadvantage of these solutions is that the user must divert attention from the system to read the manual or run the tutorial. If monitor screens were big enough, a system could maintain a constant display of the user manual. Whenever a user wanted information, the manual would be available. This solution would wear out its welcome, because once a user knows the system, the helpful information is unnecessary and unwanted.

Most interactive systems have a common characteristic: when a user needs help, he/she is looking at the screen and wondering what key to press. It seems only natural that the keystrokes a system will recognize at any time should include a help function key. Press the correct applications key, and the program will perform the appropriate task; press the help function key, and the program will tell the user something about what keys it expects and will happen if the user were to activate them.

Once the help function key is pressed, a help message is displayed to the user. Such a message is best displayed in a pop-up window, in which the window delivers the textual information needed without disturbing the application's use of the screen. A window used for help information is termed a context-sensitive help window. As users operate the program and move from feature to feature, the content of the help window change to reflect the current context of the feature currently highlighted. Figure 2 illustrates a typical LEAF help window.

Graphical-based Examination of Structural Information

The greatest attribute a CAD system can have is the ability to examine structural information in a graphical environment. To illustrate this point, a user viewing a table of numbers that represents a natural mode shape of a three-dimensional bridge would have a difficult time determining what mode type or mode number it represented. However, by graphically superimposing the mode shape on the undeformed structure, one can quickly summize the mode characteristics.

Graphical displays should accommodate a user's preference for viewing structural information. Once such feature is by multiple-views. Currently, the elevation, plan, cross-section, and isometric views may be depicted in the LEAF system. Also, zooming capabilities which allow the user to isolate on a portion of the structure in a view is permitted. Finally, with natural modes being extracted, the use of animation is an ideal means of presentation. Currently, a two frame buffer is used to animate the absolute peaks of the natural mode. Also, displays are permitted to show up to four different windows of information on one screen. This enables users to compare different types of information all at one time. Examples of graphical displays will be shown in the case study section of this paper.

Utility Modules

Utility modules are developed to alleviate the time-consuming process of specifying bridge geometry, structural properties, and general loading conditions. This entailed creating the following modules.

Mesh Generator

A major short coming of many CAD systems is that no mechanisms are available to rapidly describe the bridge geometry and finite element mesh layout. One possibility is to specify joints using a mouse and/or tablet. However, this approach tends

to be slow, and some graphic windows do not have sufficient magnification to ensure adequate modelling precision. Instead, new engineering language commands for multiple joint, member, and support definition are preferred. As an example, the following command as written

Mesh Joint 2 1 0 1000 200 0 400 20 30

would create a rectangular grid of six joints spaced 200 units apart in the x-direction, 21 joint space 20 units apart in the y-direction, and assign a z-coordinate of 30 units to all joints. Every member generated would be assigned structural section number two and flutter section one.

Frontwidth Optimizer

As detailed earlier, the frontal method is used for the solution algorithms of the static, dynamic, and flutter analyses programs. Therefore, a frontwidth optimizer to renumber members for least storage requirements would allow more complex bridge configurations to be readily modelled; and also permit users to not concern themselves with storage requirements.

Though the widely-used reverse Cuthill-McKee (31,32) and Gibbs-King (33,34) methods exist, the Sloan (35) method has recently proved more efficient in frontwidth optimization and is thus adopted by the LEAF system. In essence, the Sloan method determines the minimum frontwidth by the labelling of an undirected graph, where the graph consists of a set of nodes (joints) connected with a set of unordered pairs of distinct nodes called edges (members).

Behavioral Considerations

A good CAD system must be designed with the user's behavior in mind. The measurements of interest, such as execution time, errors and their solution, and learning curve must be addressed.

For instance, the LEAF static, dynamic, and flutter analysis programs will have a high runtime execution, since their solution is, by the nature of the problem, computationally intensive. Benchmark tests on the case study bridge to be discussed showed that: two hours were needed for the nonlinear static analyses under the service dead load condition; 45 minutes were needed to attain two bending modes and one torsional mode in the dynamic analysis program; and the flutter analysis took 30 minutes over a wind velocity range of 10 to 250 miles per hour. Benchmark tests were conducted on a COMPAQ 386/20 microcomputer.

During their execution, on-line descriptions of the task currently being performed are continually being shown. This gives the user a good sense of where the program is in its overall assignment. Also, intermediate results are shown to the user so that he/she can ascertain the effectiveness of the proposed design.

Also, most CAD systems detect user errors in modelling or sequence of program execution. A good CAD system also proposes solutions to these errors. The LEAF system devotes extensive error checking for every modelling parameter. For instance, if a user specifies for a member the same near and far end joint number, the error will be flagged and the user will be told to check one or the other joint connectivity vector.

Finally, a user's learning curve should be carefully confronted. A CAD system that performs every function a user desires but is so difficult to learn will not be adopted. Therefore, great strides are made in the LEAF system for a user-friendly user's manual with an entire chapter devoted to a tutorial. The tutorial leads the user step by step through the use of LEAF. Not only does it show the user how to use the system, it gives practical examples of every operation.

OVERVIEW OF THE CAD SYSTEM CAPABILITIES

The LEAF system is a collection of programs in which each program performs individual tasks in the overall scheme of analyzing and designing a cable-stayed bridge. Table 1 lists the modelling limitations for any cable-stayed bridge analysis and design.

TABLE 1 MODELLING LIMITATIONS

Item	Maximum
Joints	175
Members	250
Frontwidth	150
Structural Sections	30
Flutter Sections	5
Natural Modes of Each Type	4

All analysis programs are written using Microsoft Fortran (36), with all other programs written using Turbo C (37). The LEAF system may be executed on any IBM or IBM-compatible XT, AT, or PS/2 microcomputer with graphical displays being generated on IBM or IBM-compatible CGA, EGA, or VGA device boards. The printer and mouse may be any device that is connected to the computer.

CASE STUDY: LULING CABLE-STAYED BRIDGE

To illustrate the LEAF system's effectiveness in design, the Luling Cable-Stayed Bridge is analyzed for static, dynamic, and flutter effects. The 2,745 ft long, four-lane Luling Bridge on Interstate 310 spans the Mississippi River between the towns of Luling and Destrehan in St. Charles Parish, about 12 miles west of New Orleans, which opened to traffic in October, 1983. The bridge length is subdivided into five spans consisting of a 1222 ft center span between the pylons, two 508 and 495 ft anchor spans, and two 260 ft approach spans. The cables are arranged in a double-plane fan configuration with 12 cables in each plane.

The Luling Bridge was modeled with 24 cable elements, 20 pylon elements, and 119 deck elements, for a total of 163 elements. A total of 660 degrees of freedom at six per joint were used. The pylon consisted of lower and upper strut elements, as well as the main pylon column elements. The deck consisted of box girder, diaphragm, and cross-frame elements. The deck is modeled with two longitudinal rows of elements, with one row per box girder. Each cable corresponded to one element.

The Luling Bridge is analyzed for the resulting internal forces, deformations, and reactions using the nonlinear static analysis

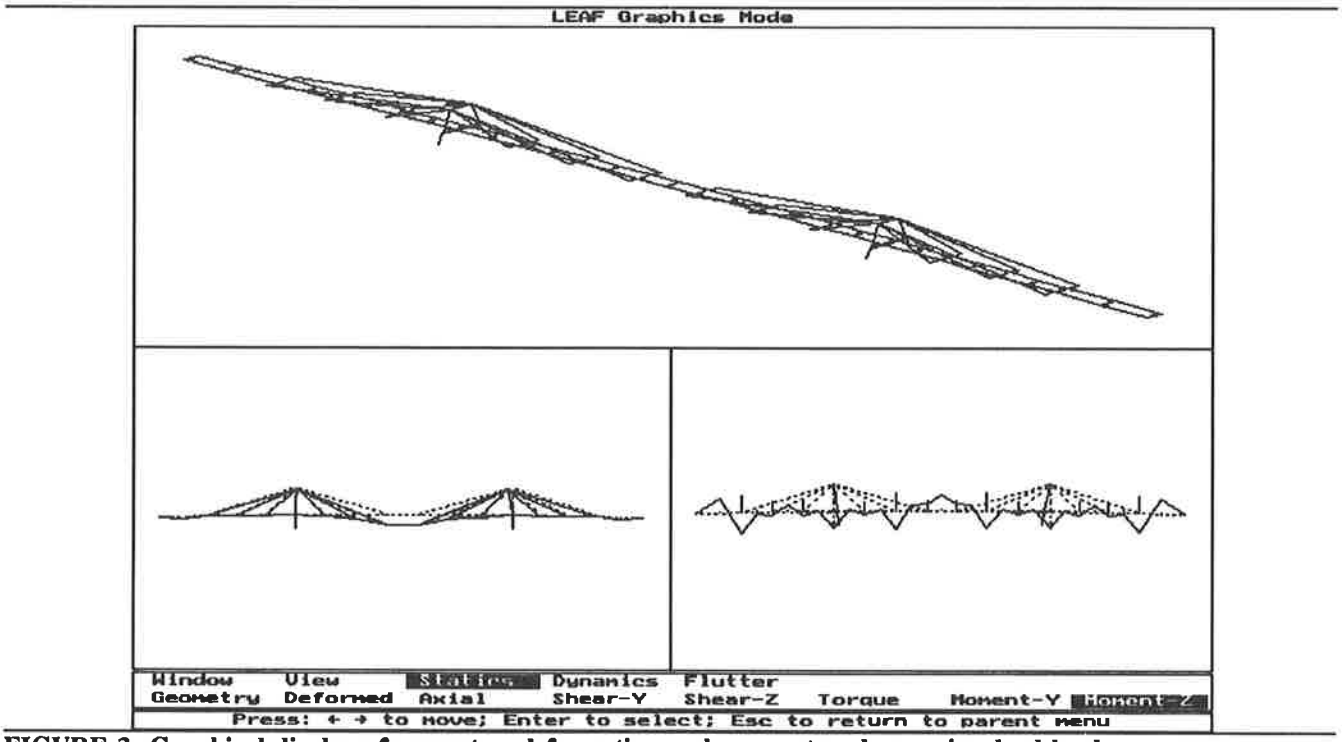

FIGURE 3 Graphical display of geometry, deformation and moment under service dead load

under the service dead load condition. Table 2 lists some of the typical results and the comparison to previous investigations (38). Figure 3 depicts the LEAF systems's graphical display of geometry, deformation, and moment as superimposed on the structure in various views.

TABLE 2 COMPARISON OF STATIC ANALYSES

Item	Present	Previous
Midspan Deflection (ft)	1.872	2.078
Midspan Bending Moment (ft-k)	35290	32550
Pylon-Deck[1] Shearing Force (k)	684	620
Pylon-Deck[1] Axial Force (k)	4844	4450
Maximum Cable Force (k)	3208	3436

[1]In the deck at the junction of pylon and deck.

The consulting engineers previous investigations were conservative compared to that of the present study. This is explained by the fact that the original consultant's analysis was based on a two-dimensional plane frame discretization. Their analysis was unable to model each box girder of the deck as individual elements, as well as not being able to model the three-dimensional A-frame pylon.

Also, the LEAF system extracted the fundamental natural modes of a given mode type, and then determined the critical flutter wind velocity at a six degree angle of incidence. Table 3 lists the results and the comparison to previous investigations (39,40). The previous investigators disregarded the modelling of the approach spans, since originally the bridge was to be only three spans, which eventually was changed to five spans. They did not revise their dynamic analysis since the addition of the approach spans would only increase the overall bridge rigidity, thus their original natural frequencies were conservative. Figure 4 illustrates the LEAF system's graphical displays of fundamental bending and torsional natural modes as overlayed on the undeformed structures, as well as the flutter profile diagrams.

TABLE 3 COMPARISON OF DYNAMIC AND FLUTTER ANALYSES

Item	Present	Previous
1st Bending Mode (Hz)	0.4281	0.3690
1st Torsional Mode (Hz)	1.2490	1.2380
1st Sway Mode (Hz)	0.6966	0.5540
Flutter Wind Velocity (mi/hr)	118.0	115.0

SUMMARY

The LEAF system described within has proved reliable in accuracy with the ability to analyze large three-dimensional cable-stayed bridge configurations on a microcomputing environment. Though the system is slower than commercially available mainframe-based finite element packages, it has centralized the computational algorithms needed for cable-stayed bridges, with the added convenience of user-friendly features for bridge definition and graphical representation of results. The system is easy to learn and use. The LEAF system should permit engineers from varied backgrounds to cost-effectively design and maintain the cable-stayed bridges of the future.

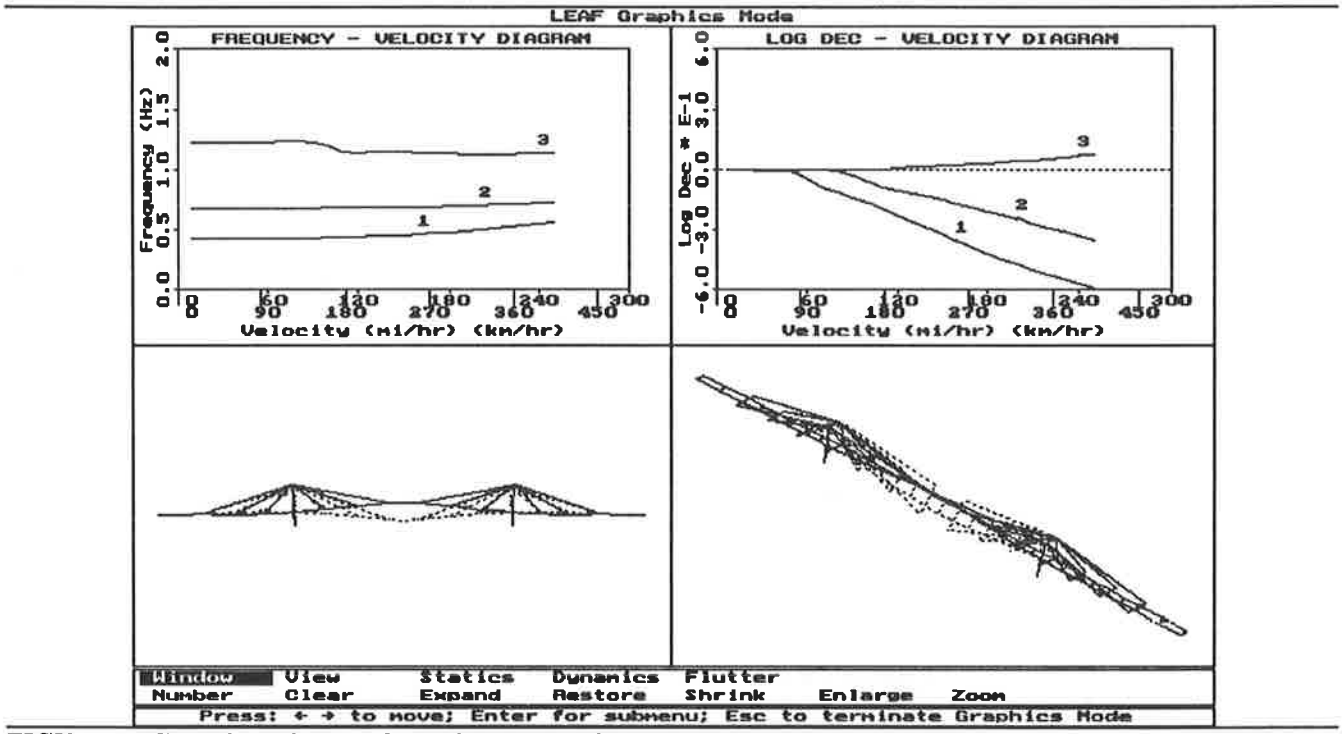

FIGURE 4 Graphical display of bending and torsional natural modes, and flutter profile diagrams

ACKNOWLEDGMENTS

The author wishes to thank Mr. Harold Bosch of FHWA's Turner-Fairbank Highway Research Center, as well as Dr. Walter Podolny and Mr. Huai Wang of FHWA's Bridge Design Section, each for sharing their engineering expertise in cable-stayed bridges and CAD principles as applied to bridges. Also, a special gratitude is made to the National Highway Institute for providing the support to pursue this research topic through a research fellowship.

REFERENCES

1. H. Tada. Recent Trend of Cable-Stayed Bridge Construction Technology. Proceedings of the 19th UJNR Meeting, Panel on Wind and Seismic Effects. National Bureau of Standards, Washington, D.C., 1986.
2. B.S. Smith. The Single Plane Cable-Stayed Girder Bridges, A Method of Analysis Suitable for Computer Use. Proceedings of Institution for Civil Engineers, Paper No. 7040, London, 1968.
3. B.S. Smith. A Linear Method of Analysis for Double-Plane Cable-Stayed Girder Bridges. Proceedings of Institution for Civil Engineers, Paper 7011, London, 1968.
4. M.C. Tang. Analysis of Cable-Stayed Girder Bridges. *Journal of the Structural Division*, ASCE, New York, May 1971.
5. M.C. Tang. Design of Cable-Stayed Girder Bridges. *Journal of the Structural Division*, ASCE, New York, Aug. 1972.
6. M.S. Cheung, W. Li and L.G. Jaeger. Nonlinear Analysis of Cable-Stayed Bridge by Finite Strip Method. *Computers and Structures*, Great Britain, Apr. 1988.
7. M.S. Troitsky and B.E. Lasar. Model Analysis and Design of Cable-Stayed Bridges. Proceedings of Institution for Civil Engineers, Paper No. 7375, London, 1972.
8. B.E. Lazar and M.S. Troitsky. Load Balancing Analysis of Cable-Stayed Bridges. *Journal of the Structural Division*, ASCE, New York, Aug. 1972.
9. B.E. Lazar. Stiffness Analysis of Cable-Stayed Bridges. *Journal of the Structural Division*, ASCE, New York, July 1972.
10. J.F. Fleming. Nonlinear Static Analysis of Cable-Stayed Bridge Structures. *Computers and Structures*, Great Britain, Apr. 1979.
11. W. Podolny. Static Analysis of Cable-Stayed Bridges. Ph.D. Dissertation, Department of Civil Engineering, University of Pittsburgh, 1971.
12. K. Loganathan, N. Raman and A. Ragaraman. The Nonlinear Analysis of Cable-Stayed Bridges. *International Association for Bridge and Structural Engineering*, 1980.
13. J.F. Fleming, J.D. Zenk and R.A. Fabian. Nonlinear Behavior of Cable-Stayed Bridges. *Civil Engineering for Practicing and Design Engineers*, May-June 1983.
14. A.S. Nazmy and A.M. Abdel-Ghaffar. Three-Dimensional Nonlinear Static Analysis of Cable-Stayed Bridges. *Computers and Structures*, Great Britain, Feb. 1990.
15. A.H. Namini. The Aerodynamic Stability of Cable-Stayed Bridges. Ph.D. Dissertation, Department of Civil Engineering, University of Maryland, 1989.
16. Y.K. Cheung and T. Kajita. Finite Element Analysis of Cable-Stayed Bridges. *International Association for Bridge and Structural Engineering*, Paper 33-II, 1973.
17. S.G. Ekhande, M. Selvappalam and M.K.S. Madugula. Stability Functions for Three-Dimensional Beam-Columns.

Journal of Structural Engineering, ASCE, New York, Feb. 1989.

18. J.H. Ernst. Der E-Modul von Seilen unter Berucksichtigung des Durchanges. Der Bauingenieur, Feb. 1965 (in German).
19. N.F. Morris. Dynamic Analysis of Cable-Stiffened Structures. *Journal of the Structural Division*, ASCE, New York, May 1974.
20. N. Izyumov, T. Tschanz and A.G. Davenport. A Study of Wind Action for the Weirton-Steubenville Cable-Stayed Bridge, Boundary Layer Wind Tunnel Laboratory, The University of Western Ontario, 1977.
21. J.F. Fleming and E.A. Egeseli. Dynamic Behavior of Cable-Stayed Bridges. Proceedings of International Symposium of Earthquake Structural Engineering, St. Louis, Missouri, 1976.
22. J.F. Fleming and E.A. Egeseli. Dynamic Behavior of Cable-Stayed Bridges. *International Journal of Earthquake Engineering and Structural Dynamics*, Jan-Feb. 1980.
23. A.H. Namini. Microcomputer-Based Extraction of Cable-Stayed Bridge Natural Modes. Proceedings of the Forth Rail Bridge Centenary Conference, Edinburgh, Scotland, Aug. 1990.
24. R.H. Scanlan and J.J. Tomko. Airfoil and Bridge Deck Flutter Derivatives. *Journal of the Engineering Mechanics Division*, ASCE, New York, 1971.
25. R.H. Scanlan. Recent Methods in the Application of Test Results to the Wind Design of Long, Suspended-Span Bridges. Report No. FHWA-RD-75-115, Federal Highway Administration, Offices of Research and Development, Washington, D.C., 1975.
26. A.H. Namini, P. Albrecht and H. Bosch. Finite Element-Based Flutter Analysis of Cable-Suspended Bridges. Submitted to *Journal of Structural Engineering*, ASCE, New York.
27. B.M. Irons. A Frontal Solution Program for Finite Element Analysis. *International Journal of Numerical Methods in Engineering*, 1970.
28. N.C. Goodwin. Functionality and Usability. *Communications of the ACM*, March, 1987.
29. J.D. Gould and C. Lewis. Designing for Usability: Key Principles and what Designers Think. *Communications of the ACM*, March, 1985.
30. A.H. Namini. LEAF Version 2.0 User's Manual. Department of Civil and Architectural Engineering, University of Miami, Coral Gables, Florida, May 1990.
31. E. Cuthill and J. McKee. Reducing the Bandwidth of Sparse Symmetric Matrices. Proceedings of the ACM National Conference, Association of Computing Machinery, New York, 1969.
32. A. George and J.W.H. Liu. *Computer Solution of Large Sparse Positive Definite Systems*. Prentice-Hall, Englewood Cliffs, New Jersey, 1981.
33. N.E. Gibbs. A Hybrid Profile Reduction Algorithm. *ACM Transactions of Mathematical Software*, 1976.
34. J.G. Lewis. Implementation of the Gibbs-Poole-Stockmeyer and Gibbs-King Algorithms. *ACM Transactions of Mathematical Software*, 1982.
35. S.W. Sloan. An Algorithm for Profile and Wavefront Reduction of Sparse Matrices. *International Journal of Numerical Methods in Engineering*, 1986.
36. Microsoft Fortran Version 5.0, Microsoft Corporation, Seattle, Washington, 1989.
37. Turbo C Version 2.0, Borland International, Scotts Valley, California, 1988.
38. Frankland and Leinhard - Modjeski and Masters, Consulting Engineers. Plans of Proposed State Highway, Mississippi River Bridge (Luling), Main River Crossing - Superstructure. 1977.
39. Frankland and Leinhard - Modjeski and Masters, Consulting Engineers. Section Model Testing - Vibration Analysis - Mississippi River Bridge (Luling), 1974.
40. H.R. Bosch. Aerodynamic Investigations of the Luling, Louisiana Cable-Stayed Bridge. Federal Highway Administration, Washington, D.C., July, 1978.

Modeling Live Load and Dynamic Load for Bridges

ANDRZEJ S. NOWAK, YOUNG-KYUN HONG, AND EUI-SEUNG HWANG

Live load and dynamic load are important load components for highway bridges. Rational load models are needed for the development of LRFD design codes. The paper summarizes the available data base and calculation procedure.

Live load model is based on the truck surveys. Maximum 75 year load effects are derived by extrapolation and simulations. Calculations are performed for single lanes and two lane bridges. For two lanes, the maximum effect is obtained for two trucks side-by-side, with fully correlated weights. For the maximum 75 year moment or shear, each side-by-side truck is represented by the maximum 1.5 month truck. The approach to selection of the design live load is formulated. The acceptance criteria is uniformity of the mean-to-nominal ratio for various spans.

Dynamic load is based on limited test data and special simulations. The major factors influencing dynamic load are the road roughness, bridge dynamics (frequency of vibrations) and vehicle dynamics (suspension system). Tests and analysis indicate that dynamic load (as a fraction of live load) is reduced for heavier trucks. It is also lower for two trucks compared to a single truck. It is recommended to use a uniform dynamic load for all the span lengths larger than 20 ft.

INTRODUCTION

Load model is an important part of the design code development procedure. Calculation of load and resistance factors in LRFD (load and resistance factor design) requires the knowledge of statistical distributions for the considered load components and resistance parameters. Load components for highway bridges include dead load, live load, dynamic load, environmental loads (wind, earthquake, temperature) and special loads (collision). The basic load combination is a simultaneous occurrence of dead load, live load and dynamic load.

Dead load, D, is the gravity load due to the self weight of the structural and nonstructural elements permanently connected to the bridge. Live load covers a range of forces produced by vehicles moving on the bridge. An example of bridge girder deflection under truck loading is shown in Fig. 1. The deflection is plotted as a function of time. Traditionally, the static and dynamic effects are considered separately (D_{sts} and D_{dyn} in Fig. 1). In this study, L covers the static component and the dynamic component is denoted by I.

The objective of this paper is to present the development of static and dynamic load for highway bridges. The developed models can serve as a basis for design code provisions.

DATA BASE FOR LIVE LOAD

The development of live load and dynamic load is based on truck surveys, bridge tests and analytical simulations. There is a need for more data, in particular, for reliable WIM (weigh-in-motion) results.

Extensive truck survey studies have been carried out by the Ontario Ministry of Transportation since early 1970's. The major data base includes 10,000 heavy trucks (only heavily loaded vehicles were measured). Each truck and axle configuration was run on the influence lines to calculate the moments and shears. For shears, for simple spans from 10 to 100 ft, the results are plotted on normal probability paper in Fig. 2 for moments and Fig. 3 for shears (1). Construction and use of the normal probability paper is described in ref. (2). Any normal distribution function is represented by a straight line on normal probability paper and any straight line represents a normal distribution function. In Fig. 2 and 3, the vertical scale, z, is the inverse standard normal distribution. The horizontal scale is the moment (or shear) divided by the HS20 design moment (or shear) specified by AASHTO (3). The maximum values of moments are 1.25 to 1.6 of HS20 moments, and the maximum shears are 1.15 to 1.7 of HS20 shears.

Police citation files provide information about overweight vehicles. Michigan State Police files were reviewed (4). The study covered one year period and 2511 vehicles. According to the Police estimates, these trucks were taken out of a population of 3 million trucks passing through the scales annually. The total

Department of Civil Engineering, University of Michigan, Ann Arbor, MI 48109

annual population of trucks is estimated at 15 million. Moments calculated for these trucks are plotted in Fig. 4. These results can be considered as an indication of the upper tail of the moment distribution.

Processing of the available WIM data is the subject of an ongoing NCHRP Project 12-28(11). However, the validity of some measurements has been recently questioned and the results of final reviews are not published yet. Therefore, in this study, the live load calculations are based on the truck survey data.

DATA BASE FOR DYNAMIC LOAD

Dynamic load model is based on test results and special simulations (6,7). The tests covered 22 bridges and 30 spans, including prestressed concrete girders and slabs, steel girders, trusses and frames. The measurements were taken for four test vehicles (54 to 130 kips) and a normal traffic. The results are summarized in Table 1. Dynamic load is measured as a fraction of the mean live load.

Interpretation of these results is difficult because the observed dynamic loads are separated from the static live loads. It has been observed that the dynamic load, as a fraction of live load, decreases for heavier trucks. It is expected that the largest dynamic load fractions in the tests correspond to light-weight trucks.

To verify these observations, a computer procedure was developed for simulation of the dynamic bridge behavior (6,7). The dynamic load is function of three major parameters: road surface roughness, bridge dynamics (frequency of vibration) and vehicle dynamics (suspension system). The developed numerical procedure includes the effect of these three parameters.

Road surface roughness is one of the major parameters. The quantification of the degree of roughness is very difficult. Road profile is simulated using a Fourier transform of the power spectral density (PSD) function. The PSD function of the road profile has, in general, an exponential form.

The bridge is modeled as a prismatic beam. Modal equations of motion are formulated. Three fundamental modes of vibration are considered. It is assumed that the load is a mixture of 3 axle single trucks and 5 axle tractor-trailers. The axle configurations and weight distributions are shown in Fig. 5. Each truck is composed of a body, suspension system and tires. The body is subjected to a rigid body motion including the vertical displacement and pitching rotation. Suspensions are assumed to be of multi-leaf type springs. In the simulations a nonlinear hysteretic force-deflection equation was used. Tires are assumed as linear elastic springs.

Dynamic load is measured as the maximum dynamic deflection, D_{dyn}, divided by the maximum static deflection, D_{sta}, as shown in Fig. 1. Extensive simulations were carried out using a wide spectrum of parameters (road roughness, truck weight, axle configuration, speed and span length). The obtained dynamic load vs. truck weights is plotted in Fig. 6. Dynamic load turned out to be practically independent of the truck weight.

The simulations were also performed for a simultaneous occurrence of two trucks. For heavily loaded trucks (maximum 75 year load), the mean dynamic loads are plotted vs. span length in Fig. 7. For comparison, the means due to a single truck are also shown. The simulations showed that the dynamic load is lower for two trucks than for a single truck. In general, dynamic load is lower for a larger number of axles. For very heavy trucks, the results are summarized in Table 2. The means and standard deviations are given in terms of the mean live load.

MAXIMUM LIVE LOAD

Let N be the total number of trucks in period of time T. It is assumed that the surveyed trucks represent a two week traffic. Therefore, in T = 75 years the number of trucks, N, will be about 1,500 times larger. This will result in N = 150 million heavy trucks and axle configurations. The probability level corresponding to N is $1/N = 10^{-8}$, which corresponds to z = 5.67 on the vertical scale in Fig. 2 and 3. The distributions can be extrapolated for longer time periods (or larger numbers of trucks) as shown in Fig. 2 and 3. Numbers N, probabilities, 1/N, and inverse normal distribution values, z, corresponding to various time periods T

Table 1 Dynamic Load Factors from Test Results

Type of Structure	Mean	Standard deviation		
	Range	Average	Range	Average
P/C AASHTO girders	0.05-0.10	0.09	0.03-0.07	0.05
P/C box & slabs	0.10-0.15	0.14	0.08-0.40	0.30
Steel girders	0.08-0.20	0.14	0.05-0.20	0.10
Rigid frame, truss	0.10-0.25	0.17	0.12-0.30	0.26

Table 2 Dynamic Load from Simulations

	Mean	Standard deviation
Single truck	0.13	0.10
Two trucks	0.09	0.06

Table 3. Number of Trucks, Time Period and Probability

Time period T	Number of Trucks N	Probability 1/N	Inverse normal z
75 years	150,000,000	7_{10}-9	5.67
50 years	100,000,000	1_{10}-8	5.62
5 years	10,000,000	1_{10}-7	5.19
1 year	2,000,000	5_{10}-7	4.89
6 months	1,000,000	1_{10}-6	4.76
2 months	500,000	2.5_{10}-6	4.56
1 month	200,000	5_{10}-6	4.42
2 weeks	100,000	1_{10}-5	4.26
2 days	20,000	5_{10}-5	3.89
1 day	10,000	1_{10}-4	3.71

from 1 day to 75 years, are shown in Table 3. Horizontal line corresponding to different time periods are also plotted in Fig. 2 and 3.

The mean maximum moments and shears corresponding to various periods of time can be read directly from the graph (Fig. 2 and 3). For example, for 60 ft span and T = 75 years, the mean maximum moment is 1.82 of HS20 moment (3). This is a horizontal coordinate of intersection of the extrapolated distribution and z = 5.67 on the vertical scale. The mean maximum shears are plotted in Fig. 9. For comparison, the means are also plotted for an average truck.

The coefficients of variation for the maximum truck moments and shears can be calculated by transformation of the distribution functions in Fig. 2 and 3. Each function can be raised to a certain power, so that the calculated earlier mean maximum moment (or shear) becomes the mean value after the transformation. The slope of the transformed distribution determines the coefficient of variation. For 75 year period, the coefficients of variation is about 0.11 for 1 month it is about 0.18, and for 1 day it is over 0.20.

Maximum Lane Load (moment or shear) is caused by a single truck or two (or more) trucks following behind each other. For a multiple truck occurrence, the important parameters are the headway distance (from rear axle of one truck to front axle of the other truck) and degree of correlation between truck weights. The maximum lane load is determined by simulations. Several headway distances are considered (15 ft and more).

It is assumed that, on average, about every 10th truck is followed behind by another truck with the headway distance less than 50 ft; about every 50th truck is followed behind by a partially correlated truck; and about every 100th truck is followed behind by a fully correlated truck.

The two trucks are denoted by T_1 and T_2. Three cases of the coefficient of correlation, ρ, are considered.

- $\rho = 0$, no correlation between T_1 and T_2; T_1 is the maximum year truck (10th truck) and T_2 is an average truck.
- $\rho = 0.5$, partial correlation between T_1 and T_2; T_1 is the maximum 1.5 year truck and T_2 is the maximum daily truck.
- $\rho = 1$, full correlation between T_1 and T_2; T_1 and T_2 are both the maximum 9 month trucks.

The results of calculations indicate that single truck governs for spans up to about 100-120 ft for the moment and 90 ft for shear. For longer spans, depending on headway distance, two fully correlated trucks govern.

The minimum headway distance (15 ft) is associated with non-moving vehicles or trucks moving at reduced speeds. This is important in consideration of dynamic loads. In further calculations it is assumed, conservatively, that the headway distance is 15 ft even for normal speeds.

The mean maximum single lane moments are shown by dashed lines in Fig. 8 and 9. For comparison, in Fig. 10, the mean maximum 75 year moments are plotted with HS20 moments and AASHTO factored moments (2.17 times HS20 moment).

The equivalent uniformly distributed loads (UDL) were calculated for the mean maximum 75 year moments and shears. The uniform load, u, as a function of loaded span, x, is plotted in Fig. 11.

Calculation the maximum moments and shears for two lanes involves the determination of the load in each lane and load distribution to girders. The effect of multiple trucks is calculated by superposition. The maximum moments are calculated by simulations. For side-by-side trucks three values of the coefficient of correlations, ρ, are considered: 0, 0.5 and 1.

It has been observed that, about every 50-100th truck is on the bridge simultaneously with another truck (side-by-side). In further calculations it is assumed that every 50th truck occurs on the bridge side-by-side with another truck, which is conservative. For each such a simultaneous occurrence, it is assumed that every 5th time the trucks are partially correlated ($\rho = 0.5$) and every 10th time they are fully correlated with regard to weight ($\rho = 1$). It is also assumed that the transverse distance between two side-by-side trucks is 4 ft (wheel center-to-center).

Two lane loads are denoted by L_1 and L_2. Three cases are considered:

$\rho = 0$, no correlation between L_1 and L_2; L_1 is the maximum 1.5 year lane load and L_2 is an average lane load.

$\rho = 0.5$, partial correlation between L_1 and L_2; L_1 is the maximum 3 month lane load and L_2 is the maximum daily lane load.

$\rho = 1$, full correlation between L_1 and L_2; L_1 and L_2 are both the maximum 1.5 month lane loads.

The structural analysis was performed using an advanced finite element method. The model is based on a linear behavior of girders and slab. Calculations clearly indicate that two fully correlated side-by-side trucks govern. The ratio of the mean maximum 1.5 month lane moment to the mean maximum 7.5 year moment is equal to about 0.85 for all spans.

Girder distribution factors in AASHTO (1989) are linear functions of girder spacing (s/5.5 where s is girder spacing), as shown in Fig. 12. The actual calculated distribution factors are also plotted in Fig. 12.

DESIGN LIVE LOAD AND DYNAMIC LOAD

Criteria considered in the selection of design live load include the uniformity of safety level, simplicity of the code format and tradition (live load model should resemble a real truck). A uniform safety level is an important objective of the LRFD code. To safety this requirement, ratio of the mean maximum 75 year (L + I) to nominal value of (L + I) should be constant. Recommended value of nominal I is 0.25 (for spans larger than 20 ft). Therefore, the mean-to-nominal ratio of L should be constant.

The ratio calculated for the current HS20 load are shown in Fig. 8 and 9, for the moment and shear, respectively. The ratio of the maximum single lane load and the maximum two lane load (per lane) is 0.85. In AASHTO (3) there is no multiple lane reduction factor for two lanes. Therefore for two lane bridges, the ratios of mean-to-nominal (Fig. 8 and 9) can be reduced by 15 percent.

For simply supported spans, for both moments and shears, a perfect fit (constant mean-to-nominal ratio) is obtained by using a uniform load varying with span, u(x), where u is uniform load and x is the span, as shown in Fig. 11.

For continuous spans, the uniform load intensity depends on the loaded length, x, rather than span. The calculation of the moment and shears involves maximization of u(x) and the area under the influence line. For example, in case of influence line shown in Fig. 13, the mean moment, M, is,

$$M = \max [u(\Sigma x_i)\ \Sigma(A_i)] \qquad (1)$$

where the summations are calculated for all combinations of intervals i.

CONCLUSIONS

Models are derived for bridge live load and dynamic load. The calculations are based on the available data base including truck surveys, bridge tests, analysis and simulations. The maximum load parameters are determined for various periods of time. The calculations are performed for single lanes and two lane bridges.

A single lane live load is governed by a truck for spans up to 100-120 ft for moment and 90 ft for shear. For long spans, two (or more) trucks following behind each other produce the maximum effect.

For two lane bridges, a simultaneous occurrence of two side-by-side trucks governs, with perfectly correlated weights. The maximum 75 year moment and shear is modeled by two maximum 1.5 month trucks. The ratio of the mean maximum 1.5 month truck and the mean maximum 75 year truck is about 0.85.

Dynamic load is a function of road roughness, bridge dynamics and vehicle dynamics. Simulations indicate that dynamic load decreases with increasing truck weights. It is also lower for two trucks compared to a single truck.

Design live load should produce a uniform mean-to-nominal ratio. Current HS20 load (3) does not satisfy this requirement. Uniformly distributed load provides a perfect fit. A uniform value of dynamic load, 0.25, is recommended for all spans larger than 20 ft.

REFERENCES

1. Nowak, A.S. and Hong, Y-K., 1990, "Bridge Live Load Models," ASCE Journal of Structural Engineering, submitted.
2. Benjamin, J. R. and Cornell, C. A., 1970, Probability, Statistics, and Decision for Civil Engineers, McGraw-Hill Book Co., p. 684.
3. AASHTO, 1989, "Standard Specifications for Highway Bridges," American Association of State Highway and Transportation Officials, Washington, DC.
4. Nowak, A. S., Al-Zaid, R., Hong, Y-K, Kayser, J. R., Tabsh, S., Tantawi, H. and Zhou, J-H., 1988, "Risk Analysis for Evaluation of Bridges," Report UMCE 88-7, Department of Civil Engineering, University of Michigan, Ann Arbor, MI.
5. Billing, J. R., 1984, "Dynamic Loading and Testing of Bridges in Ontario," Canadian Journal of Civil Engineering, Vol. 11, No. 4, December, pp. 833-843.
6. Hwang, E-S. and Nowak, A. S., 1989, "Dynamic Analysis of Girder Bridges," Transportation Research Record, No. 1223, pp. 85-92.
7. Hwang, E-S. and Nowak, A. S., 1990, "Dynamic Load for Girder Bridges," ASCE Journal of Structural Engineering, submitted.

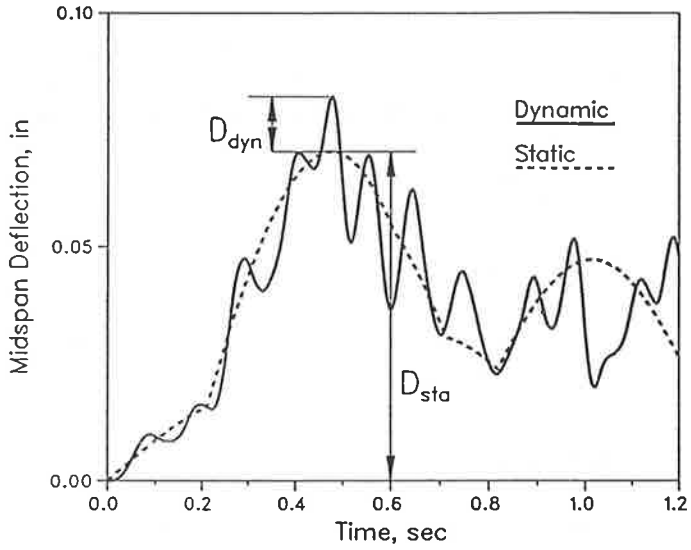

FIGURE 1 Static and Dynamic Deflection of a Bridge Girder.

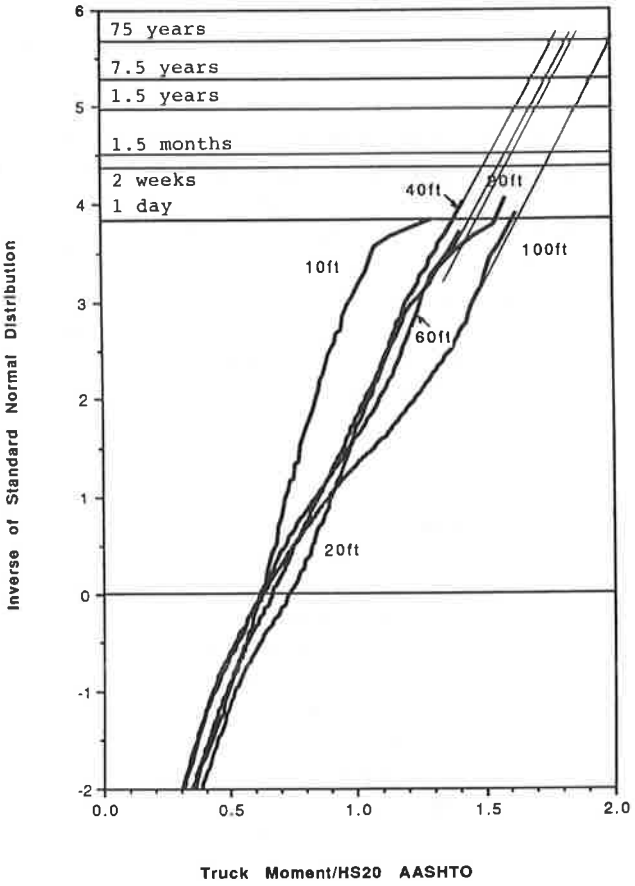

FIGURE 2 Cumulative Distribution Functions for Moments due to Surveyed Trucks.

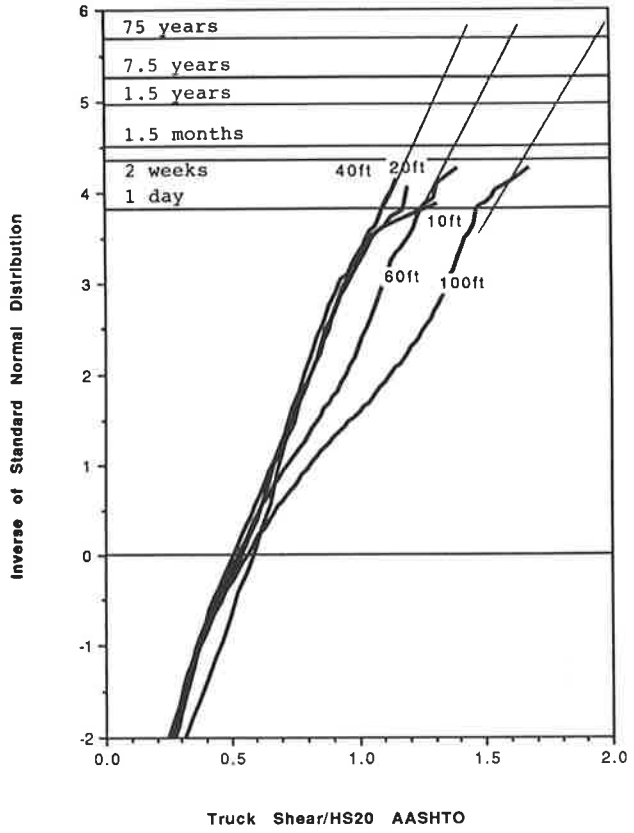

FIGURE 3 Cumulative Distribution Functions for Shears Due to Surveyed Trucks.

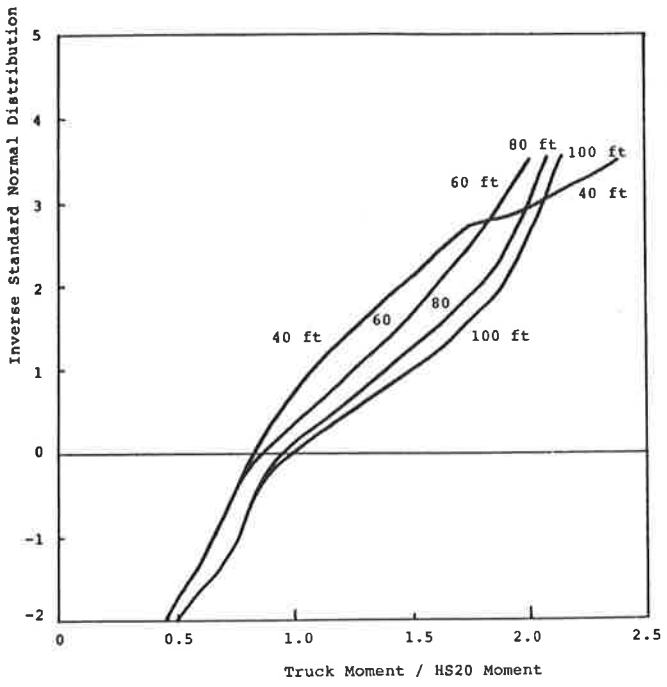

FIGURE 4 Cumulative Distribution Functions for Moment Due to Overloaded Trucks in Michigan (State Police Citation Files).

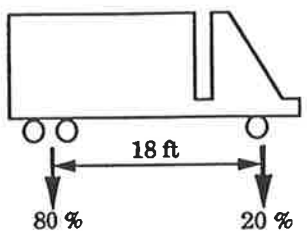

3 Axle Single Truck

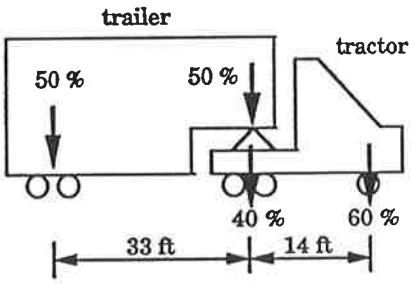

5 Axle Semi Tractor-Trailer

*percentage numbers are the fraction of tractor or trailer weight

FIGURE 5 Truck Configurations Used in Dynamic Simulations.

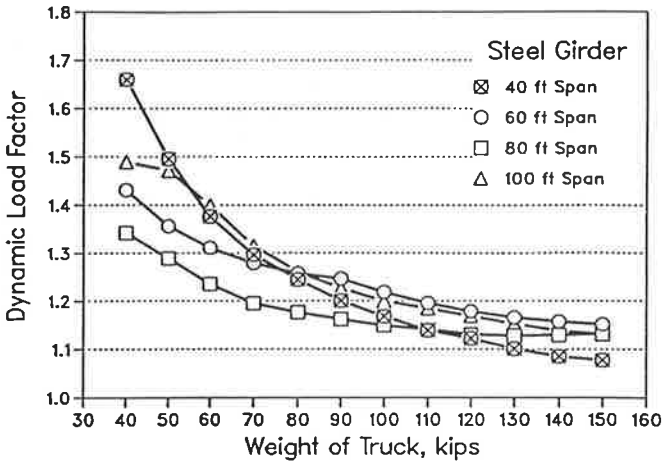

FIGURE 6 Dynamic Load vs. Truck Weight

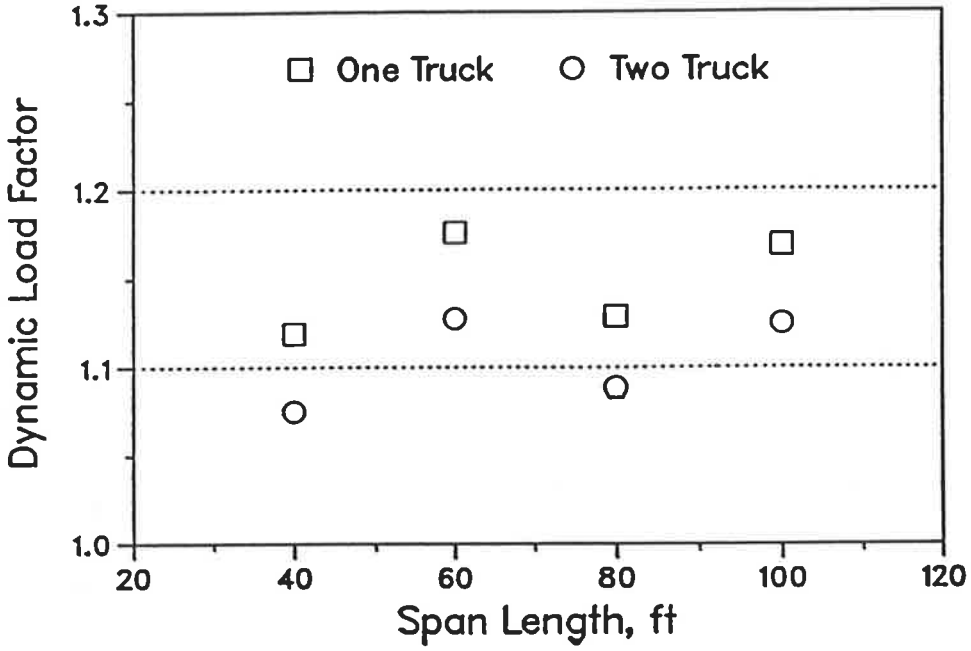

FIGURE 7 Dynamic Load for Single Trucks and Two Trucks.

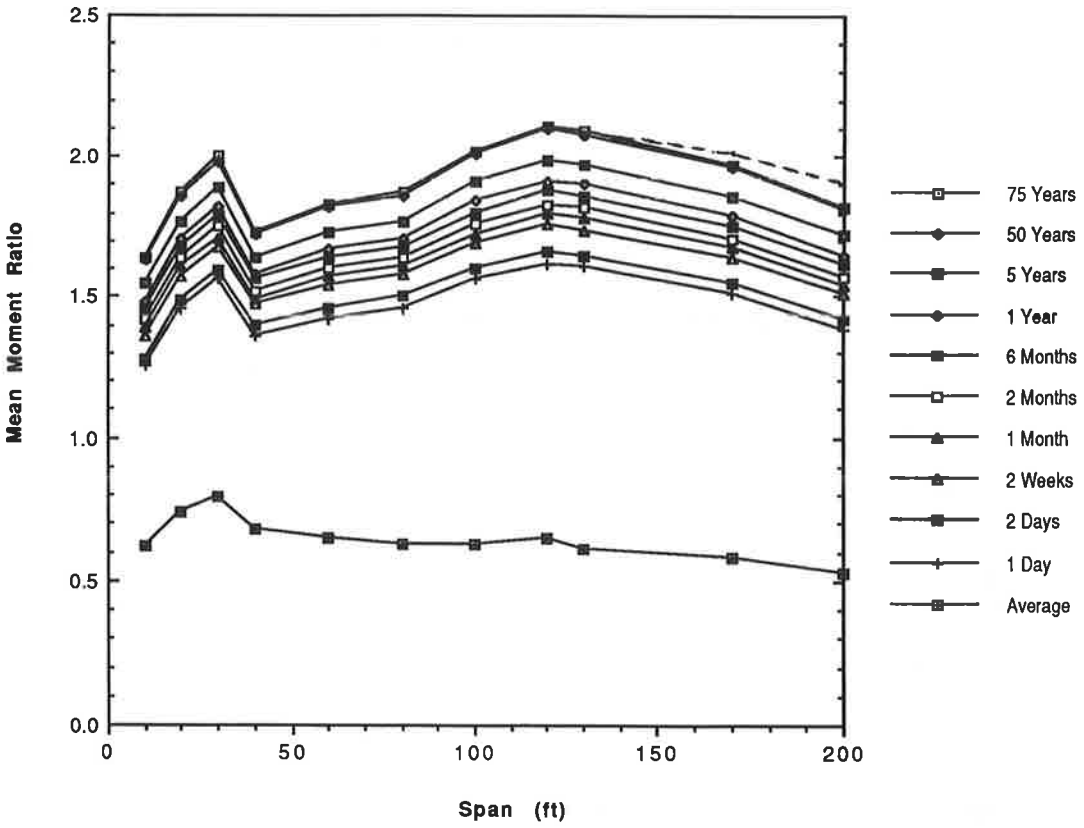

FIGURE 8 Mean Maximum Moments vs. Span Length.

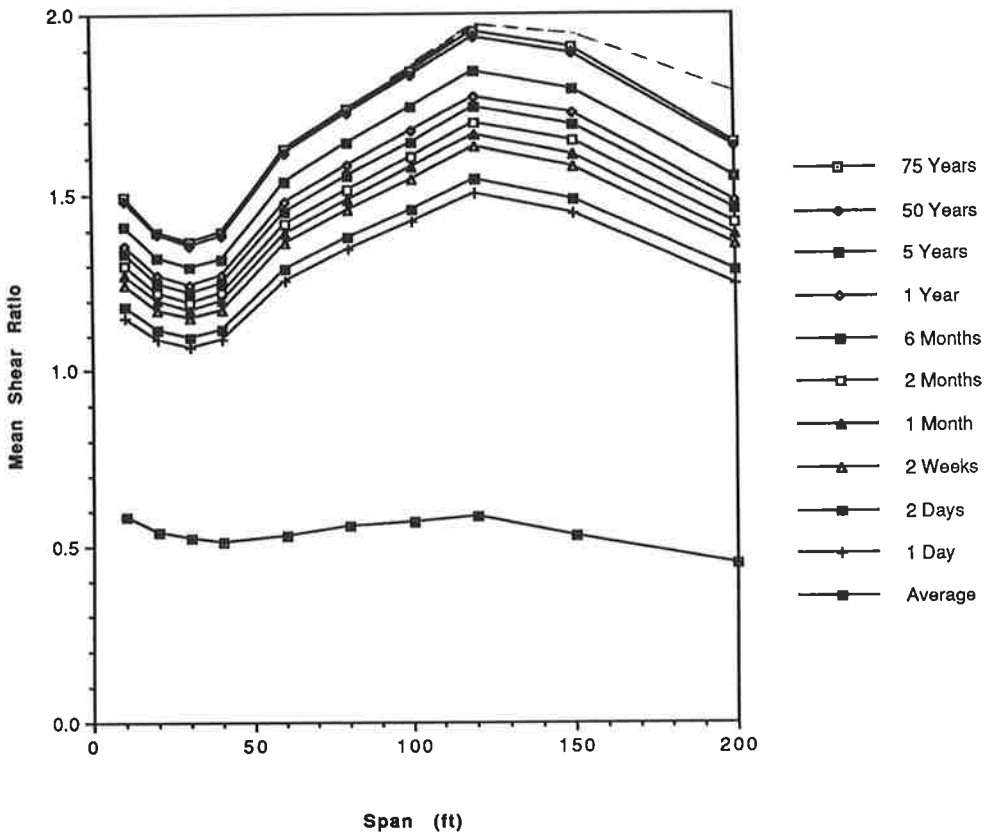

FIGURE 9 Mean Maximum Shears vs. Span Length.

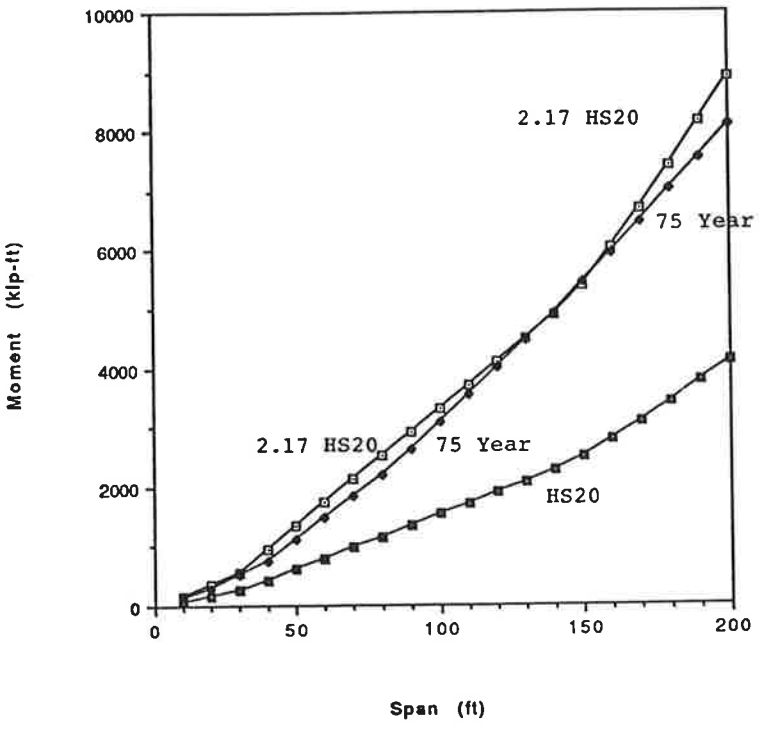

FIGURE 10 Mean Maximum 75 Year Moment, HS20 Moment and 2.17xHS20 Moment.

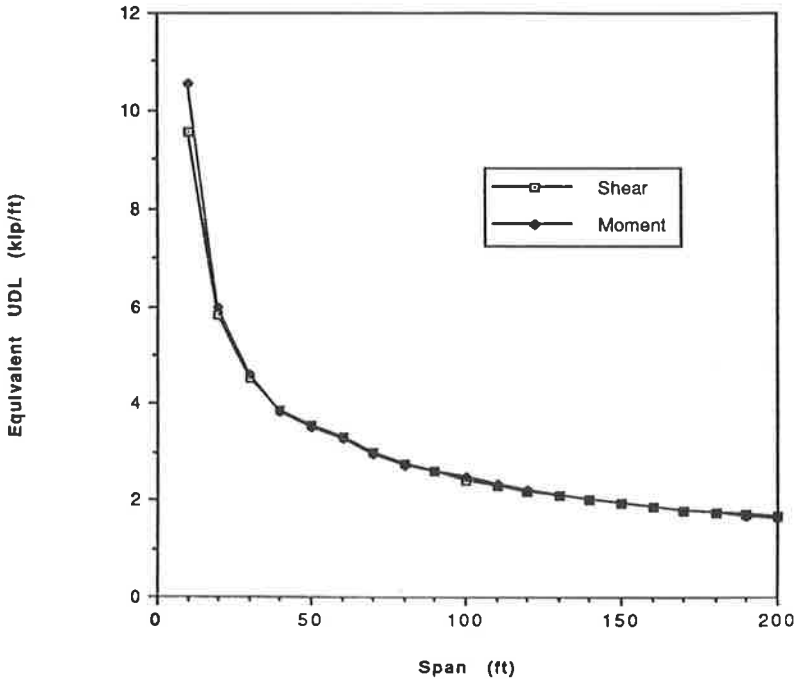

FIGURE 11 Equivalent Uniformly Distributed Load vs. Span Length.

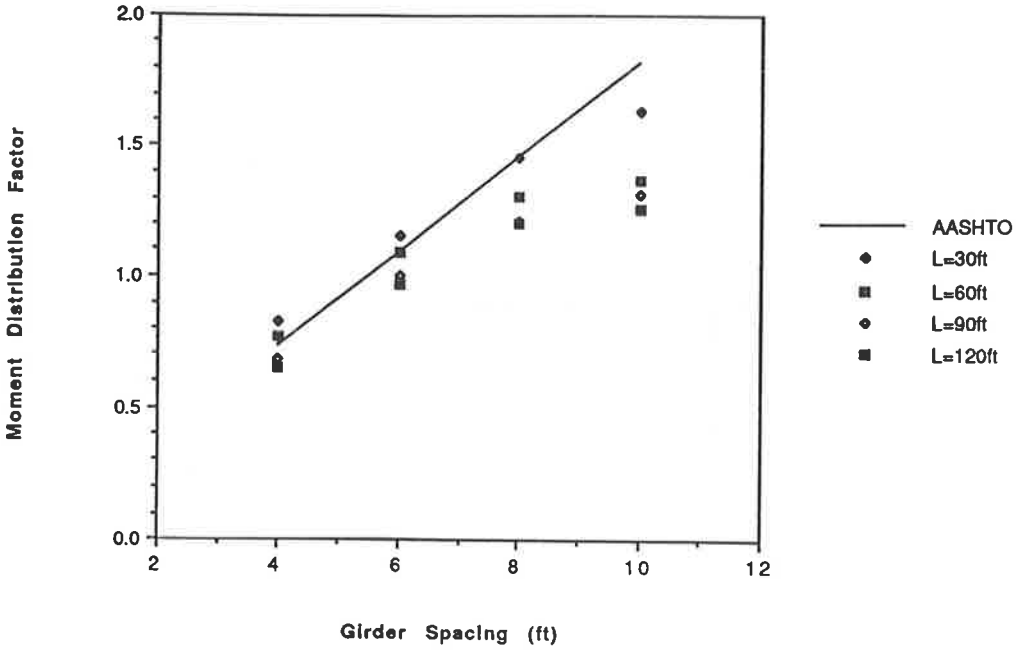

FIGURE 12 Girder Distribution Factors for AASHTO (3) and Calculated.

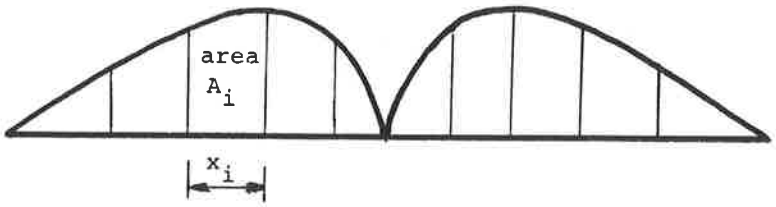

FIGURE 13 Example of an Influence Line.

Distribution of Wheel Loads on Highway Bridges

TOORAK ZOKAIE, ROY A. IMBSEN, AND TIMOTHY A. OSTERKAMP

This report presents the findings of the research performed on distribution of wheel loads on highway bridges under funding from the National Cooperative Highway Research program (NCHRP) . This study was performed in two phases; the first phase (NCHRP 12-26) concentrating on beam and slab, and box girder bridges; and the second phase (NCHRP 12-26/1) concentrating on slab, multi-box beam, and spread box beam bridges.

For each bridge type three levels of analysis are considered. The most accurate level, Level-three, involves detailed modeling of the bridge deck. Level-two includes graphical methods, nomographs, influence surfaces; or simplified computer programs developed to apply such methods. Level-one methods include simple formulae to predict lateral load distribution to various girders using a wheel load distribution factor.

This research has resulted in a number of more accurate formulae for wheel load distribution, and recommendations for use of computer programs to achieve more accurate results. These recommendations focus on use of plane grid analysis as well as detailed finite element analysis.

Also, as a result of this research, a draft specifications is prepared for determination of wheel load distribution factors. This draft specification is recommended to replace the current AASHTO specification.

Wheel load distribution on highway bridges is a function of the magnitude and location of truck wheel loads and the response of the bridge to these loads. This study focuses on the second factor mentioned above; the response of the bridge to a predefined set of wheel loads. The formulae developed herein are based on the standard AASHTO "HS" trucks. Other methods, as described herein, may be applied for the trucks outside the AASHTO family of trucks. Also, a limited study suggests that load distribution factors are not sensitive to truck axle configuration.

Analysis of the response of highway bridges to vehicular live loads is one of the key elements in determining the strength and serviceability of a bridge. It is, therefore, of critical importance, both in the design of new bridges and in the evaluation of the load-carrying capacity of existing bridges, that procedures for calculation of accurate wheel load distribution factors be utilized.

Wheel load distribution factors allow engineers to analyze bridge response by treating the longitudinal and transverse effects of wheel loads as uncoupled phenomena. Empirical distribution factors for stringers and longitudinal beams have been present in the *AASHTO Standard Specifications for Highway Bridges* [1], with only minor changes, since 1931. Recent additions to these specifications have included improved load distribution factors for particular types of superstructures based on tests and mathematical analyses.

Recent research has produced a substantial amount of information on various bridge types indicating a need for revisions of the current AASHTO Bridge Specifications. Methods of distributing wheel loads to individual supporting members, based on the latest information, are also essential in evaluating existing bridges. With the trend to increasing truck and permit loads, the need for reliable criteria becomes more urgent.

The current AASHTO specifications allow for simplified analysis of bridge superstructures utilizing the concept of a wheel load distribution factor for bending moment in interior girders of most types of bridges, i.e. beam and slab, box girder, slab, multi-box beam, and spread box beam.

A major shortcoming of the current specifications is that the piecemeal changes that have taken place over the last 55 years have led to inconsistencies in the load distribution criteria. These include:

1. Inconsistent consideration of a reduction in load intensity for multiple lane loading.
2. Inconsistent changes in distribution factors to reflect the changes in design lane width.
3. Inconsistent verification of accuracy of wheel load distribution factors for various bridge types.

All of the current AASHTO simplified procedures were developed for nonskewed, simply-supported bridges. Although the current specifications state that these procedures apply to the design of normal highway bridges, there are no other guidelines for determining when the procedures are applicable. Because modern highway and bridge design practice requires a large number of bridges to be constructed with skewed supports, on curved alignments and/or continuous over interior supports, it is increasingly important that the limitations of wheel load distribution criteria be fully understood by designers.

The objective of this research is to evaluate the available methods for wheel load distribution in beam and slab, box girder, slab, multi-box beam, and spread box beam bridges. Another objective of this project is to develop additional formulae for wheel load distribution so that a complete and consistent set of formulae can be presented for incorporation into AASHTO specifications. In addition, correction formulae to account for effects of skewed support and continuous structures are developed. This allows more structures to be designed with the simplified method.

Recent developments in computer technology have enabled bridge designers to use grillage or finite element analysis to achieve more accurate results. An objective of this study is to provide guidelines for designers to assist them in selecting applicable computer programs, and developing bridge models to achieve accurate results. The popular computer programs and modeling techniques are evaluated and such guidelines are presented.

SCOPE OF STUDY

This research is focused on the more commonly used bridge types. These types include beam and slab (slab on girder) bridges, multi-cell box girder bridges, slab bridges, multi-box beam bridges, and spread box beam bridges. The beam and slab bridges consist of reinforced concrete T-beam, prestressed concrete I-girder, and both plate girder and rolled beam steel I-girder. Box girder bridges include both reinforced and prestressed concrete multi-cell box girder bridges, but do not include steel box girders. Slab bridges include solid slab bridges with or without a haunch. Slab bridges with circular voids are assumed to act similar to solid slabs. Multi-box beam bridges include side-by-side box-beam bridges which are generally constructed from precast box beams and other closed sections. Multi-beam bridges made of open sections such as double-Tees and bulb-Tees are not included. Spread box-beam bridges include bridges made of box beams connected via structural slab; they are usually constructed from precast box beams and the connection from beam to slab is generally

Imbsen & Associates, Inc., 9833 Horn Road, Suite C
Sacramento, CA 95827

composite. The cross sections of these bridge types are shown in figure 1 schematically.

For each bridge type three levels of analysis are considered. The most accurate level, Level three, involves detailed modeling of the bridge deck. A complete finite element analysis is normally performed for this level of accuracy. Level two includes graphical methods, nomographs, influence surfaces; or simplified computer programs developed to apply such methods. Furthermore, a plane grid analysis utilizing general purpose beam (grid) elements is considered to be a level-two analysis, since the computer programs for this type of analysis are commonly available and do not require high computer resources. Level one methods are the most simple analysis methods. These methods include simple formulae to predict lateral load distribution to various girders using a wheel load distribution factor. These factors are then multiplied by the longitudinal response of a single girder to a truck wheel line (i.e., 1/2 weight of a truck's axle loads) resulting in the total girder response to the truck load on the bridge deck.

The major part of this research is devoted to the study of level one methods because of the ease of application and the surprising good correlation achieved in their application to the majority of bridges. The formulae presented in the current AASHTO specifications are evaluated, and alternate formulae are developed that offer higher accuracy, wider range of applicability, and in some cases easier application than the current AASHTO formulae. These formulas are developed for interior and exterior girder moment and shear load distribution due to single or multiple lane loadings. In addition, correction factors for continuous superstructures and skewed bridges are developed.

Bridges that are less popular and those that are considered special bridge types such as truss, floor beam, arch, and cable supported bridges are outside the scope of this study. The effect of curved girders on wheel load distribution is not studied in this research. One of the most useful findings of this study is new wheel load distribution formulae which offer higher accuracy and are recommended to replace the formulae presented in the current AASHTO specifications. Another outcome of this study is recommendations for computer use, particularly grillage analysis of bridge decks.

RESEARCH APPROACH

Advanced computer technology has become available in recent years which allows detailed finite element analysis of bridge decks. However, many computer programs exist which employ different formulations and techniques. It is important that the computer methodology and formulation that produce the most accurate results be used to predict the behavior of bridge decks. In order to identify the most accurate computer programs, test data from full scale and prototype bridge experiments was compiled. The bridge tests are then modeled by different computer programs and the experimental and computer results are compared. Details of the comparisons and their outcome are presented in the NCHRP Project 12-26/1 draft final report[2]. The programs that produced the most accurate results are then identified and considered as the basis for evaluation of other procedures, i.e. level two and level one procedures.

An important part of the development or evaluation of simplified methods is the range of applicability. In order to make sure that common values of various bridge parameters are considered, a database of actual bridges is compiled. Random bridges from various states were gathered in order to achieve national representation. This bridge database is studied to identify the common values of various parameters such as beam spacing, span length, slab thickness, and so on. Also the range of variation of each parameter is identified. A hypothetical bridge which has all the average properties obtained from the database is referred to as the "Average Bridge". An average bridge for each of the beam and slab, box girder, slab, multi-box beam, and spread box beam bridge types is obtained. For the study of moment responses in box girder bridges, separate reinforced concrete and prestressed concrete box girder average bridges are prepared.

In evaluation of simplified formulae, it is important to understand the effect of various bridge parameters on wheel load distribution. Bridge parameters are varied one at a time in the average bridge for the bridge type under consideration. Wheel load distribution factors for both shear and moment are obtained for all such bridges. Variation of wheel load distribution factors with each parameter shows how important that parameter is. Simplified formulae can be developed to capture the variation of wheel load distribution factors with each of the important parameters. The methodology used in derivation of these formulae consists of identifying the important parameters and using power curves to present their effect on load distribution. This methodology is described in detail in the NCHRP Project 12-26/1 draft final report[2].

Since certain assumptions are made in the derivation of simplified formulae and some bridge parameters are altogether ignored, it is important to verify the accuracy of these formulae when applied to real bridges. The database of actual bridges is used for this purpose. Those bridges that the formula can be applied to are identified and analyzed by an accurate method. The distribution factors found from the accurate analysis are compared to the results of the simplified methods. The ratio of the approximate to accurate distribution factors are calculated and examined to asses the accuracy of the approximate method. Average, standard deviation, minimum, and maximum ratio values are obtained for each formula or simplified method. The method or formula that has the smallest standard deviation is considered to be the most accurate. However it is important that the average be close to unity and slightly greater so that most results are slightly conservative.

In the following some recommendations for each of the three levels of analysis, i.e. detailed bridge deck analysis, graphics and simple computerized methods, and simple formulae are given.

RECOMMENDATIONS FOR DETAILED BRIDGE DECK ANALYSIS

Detailed bridge deck analysis using a finite element computer program may be used to produce accurate results. However extreme care must be taken in preparation of the model, or very inaccurate results will be obtained. Important points to look for are selection of a program capable of accurately modeling responses being investigated, calculation of element properties, mesh density, and support conditions. Every model should be thoroughly checked to make sure that nodes and elements are generated correctly. Detailed recommendations for this level of analysis may be found in the NCHRP Project 12-26/1 draft final report[2].

Another important point is the loading. Truck loads should be placed at positions that produce the maximum response in the components being investigated. In many cases, the truck location is not known before preliminary analysis is performed and therefore many loadings should be investigated. This problem is more pronounced in skewed bridges. Many programs have algorithms which allow loads to be placed at any point on the elements, however if this feature is not present, equivalent nodal loads must be calculated. Distribution of wheel loads to various nodes must also be performed with care, and the mesh should be fine enough to minimize errors which can arise due to load approximations.

Many computer programs, especially the general purpose finite element analysis programs, report stresses and strains, not shear

and moment values. Calculation of shear and moment values from the stresses must be carefully performed, which usually requires some kind of integration over the beam cross section. Some computer programs report stresses at node points rather than gaussian integration points. Integration of stresses reported at nodal points is normally less accurate and may lead to inaccurate results.

Detailed analysis of bridge decks can produce incorrect and inaccurate results if it is not carefully performed. The additional accuracy gained by such an analysis is usually not enough to warrant its use for everyday design practice. However, in some cases, unusual geometry or complex configurations may not allow use of a simplified procedure, and it is recommended to only perform detailed finite element analysis in these cases.

RECOMMENDATIONS FOR GRAPHICAL AND SIMPLIFIED COMPUTER ANALYSIS

Many graphical and computer based methods are available for calculating wheel load distribution. One popular method for such analysis is design charts based on orthotropic plate analogy, similar to those presented in the Ontario Highway Bridge Design Code[3]. As the computers become more and more available to designers, simple computer based methods such as SALOD[4] become more attractive than nomographs and design charts. Also grillage analysis presents a good alternative to other simplified bridge deck analysis methods, and would generally produce more accurate results.

Grillage analogy may be used to model any one of the five bridge types studied in this research. Each bridge type requires special modeling techniques. A major advantage of plane grid analysis is that shear and moment values for girders are directly obtained and integration of stresses is not needed. Loads normally need to be applied at nodal points, and it is recommended that simple beam distribution be used to distribute wheel loads to individual nodes. If the model is generated with care, and the loads are placed in their correct locations, the results will be close to those of detailed finite element analysis. Detailed recommendations for this level of analysis and examples of its application may be found in the NCHRP Project 12-26/1 draft final report[2].

RECOMMENDATIONS FOR SIMPLIFIED FORMULAE

The formulae developed in this study may be used to determine the wheel load distribution factors for moment and shear, in interior and exterior girders of straight or skewed, simply supported or continuous bridges. These formulae are generally more complex than those currently recommended by AASHTO specifications, but they also present a greater degree of accuracy.

The formulae developed in this study are summarized in Tables 1, 2, 3, and 4. Some of these formulae are dependent on stiffness parameters which are not known before the preliminary design. In these cases an approximation of the stiffness parameter may be used to simplify the formulae.

The formulae currently presented in the AASHTO specifications—although simpler—do not present the degree of accuracy demanded by today's bridge engineers. In many cases these formulae can result in highly unconservative results (more than 40%); and in other cases they may be highly conservative (more than 50%). In general, the formulae developed in this study are within 5% of the results of an accurate (i.e., level-three) analysis as measured by the standard deviation of their ratios. Figure 2 shows histogram plots of comparison of the accuracy of current AASHTO formulae and those developed in this study. Each figure shows the accuracy of the distribution factors for moments in one of the five bridge types studied. The accuracy of each formula is measured by comparing it to the accurate (level-three) analysis.

Bridge Design Engineers use the simplified methods and formulae whenever possible because of the efficiency gained by the simplicity of these methods. However, in general, simplified formulae have limitations which should be understood. These limitations apply to the current AASHTO formulae, those presented by other researchers, the ones developed in this study, and any other simplified formulae. These limitations are briefly described below.

The formulae are normally developed for single-lane loading and multi-lane loading. The formulae for multi-lane loading predict the maximum distribution factor for each of two-lane, three-lane, and four-lane loadings and include the multiple presence reduction factors. Therefore, if other reduction factors are to be considered, the formulae developed to date should be reevaluated to assess their accuracy.

The formulae are developed for a specific truck type, normally AASHTO HS family of trucks, and the effect of other truck configurations should be kept in mind. Limited investigation of this matter revealed that if the gauge width is the same and the longitudinal axis positions or loads change, the distribution factors are not affected greatly. However, if two different truck types are considered simultaneously, e.g. one permit truck along with a HS-20 truck, the formulae are not applicable.

The formulae are developed to predict wheel load distribution factors for bridges of common types and dimensions. Therefore, parameters used in the formulae have ranges were valid results may be expected; and if bridge parameters fall outside of those ranges, the accuracy is reduced or the formula may not be applicable.

The simplified formulae have many advantages which should not be overlooked. The most obvious advantage is their simplicity. They are very quick to use, and do not require any special tools other than a calculator. No special computers or computer programs are needed, and no special knowledge of finite element modeling techniques are required. If the simplified formulae are applied in their applicable range and the bridge has a regular geometry, accurate answers will be obtained. Therefore for bridges of regular geometry and properties, simplified formulae present the best alternative.

NUMERICAL EXAMPLE

A typical beam and slab bridge is selected to illustrate the application of the formulas developed in this project. This bridge is made of two continuous spans of 50 and 55 feet. The cross section and plan view of the bridge are shown in figure 3.

The bridge with this configuration is outside the bounds of the current AASHTO specifications. However, the new formulas may be applied as follows to calculate the wheel load distribution factors for moment and shear:

$I = 2850\ in^4$
$A = 24.8\ in^2$
$d = 2.671\ in$
$n = 7.5$
$s = 7.33\ feet$
$t_s = 7.25\ in$

$$e_g = \frac{26.71"}{2} + \frac{8"}{2} = 17.36\ in$$

$$d_e = (3'\text{-}1") - (1'\text{-}5") = 1.67'$$

$$K_g = n(I + Ae_g^2) = 77{,}397\ in^4$$

$\frac{K_g}{Lt^3}$ for 50' span: 0.3385 for 55' span: 0.30773

Moment distribution factor may be calculated as follows:

	50-ft Span		55-ft Span	
Base Distribution Factor	1.157		1.165	
Edge Girder Correction	1.0		1.0	
Skew Correction	0.968		0.970	
Region	A	B	C	D
Continuity Correction	1.05	1.10	1.10	1.05
Design Distribution Factor	1.176	1.232	1.243	1.187

The design Distribution Factors are obtained by applying the skew and continuity correction factors to the base distribution factor. The distribution factor obtained here may be compared to the AASHTO S/5.5 value of 1.333.

The shear distribution factor may be calculated as follows:

	50-ft Span		55-ft Span	
Base Distribution Factor	1.536		1.536	
Edge Girder Correction	0.767		0.767	
Obtuse Corner Skew Correction	1.160		1.164	
Edge Skew Correction	1.0		1.0	
Region	A	B	C	D
Continuity Correction	1.0	1.05	1.05	1.0
Design Distribution Factor	1.536	1.612	1.612	1.536

Note that the reduction due to the edge girder and the increase due to the skew together result in a theorertical reduction. But since all edge girders must be at least as strong as interior girders, this reduction is not applied and the factor is taken as unity. The design distribution factors are obtained by applying the continuity correction to the base distribution factor.

CONCLUSIONS

Three levels of analysis were considered and evaluated in this study. Five bridge types were investigated; namely: beam and slab bridges, box girder bridges, slab bridges, multi-beam bridges, and spread box beam bridges.

Level-three analysis involves detailed bridge deck analysis. The following computer programs were found useful for detailed finite element analysis of different bridge types: GENDEK-5[5] for general beam and slab bridges, CURVBRG[6] for open girder steel bridges, FINITE[7] for all box girder bridges, MUPDI[8] for non-skewed simply supported box girder bridges, GENDEK-5 for slab bridges, FINITE for multi-beam bridges, POWELL[9] for simply supported single span non-skewed multi-beam bridges, FINITE for spread box beam bridges, and MUPDI for non-skewed spread box beam bridges.

Level-two analysis involves use of nomograph, design charts of simple computer methods. It is desirable to have the flexibility to use different truck types and multiple presence factors when these methods are used. Therefore methods such as SALOD[4] and LANELL[10] where influence surfaces are used to calculate wheel load distribution factors, or plane grid analysis are the most useful methods for this level of analysis.

Level-one analysis involves the use of simplified formulas for calculation wheel load distribution factors. This method has some limitations, but is very simple and effective. Simplified formulae presented in AASHTO specifications are found to be inaccurate in some cases. A set of simple formulaes are developed for each one of the bridge types under study. These formulas are evaluated using detailed level-three and level-two analyses and are found to have the same order of accuracy in their ranges of applicability. The formulae developed in this study allow calculation of wheel load distribution factors for moment and shear in the interior girders for single lane and multi-lane loading. Additional formulae are presented to calculate correction factors for the response of edge girder and to account for the effects of skewed supports. Correction factors are also presented to calculate distribution factors in continuous bridges. By using the new set of formulae for load distribution accurate results are obtained from a set of consistent formulae.

In summary, this research project has resulted in a set of formulae for prediction of wheel load distribution factors which are recommended to replace the current AASHTO specifications. Grillage analogy was found to be a good alternate to graphical and simple computer methods for bridges of regular to slightly irregular geometry and guidelines for plane grid analysis are obtained. Some computer programs for detailed analysis of bridge decks are identified and evaluated and the best ones are recommended. It is recommended that this level of analysis be used for highly irregular bridges or truck load configurations.

NOTATION

- A = Area of a stringer
- b = Width of a beam
- c = Correction factor for continuous structures—to be applied to the distribution factor for simple spans.
- d = Depth of a beam or stringer
- d_e = Edge distance of traffic lanes—to be calculated as the distance between the center of the outside roadway stringer web and edge of the exterior lane.
- e = Correction factor for exterior girders—to be applied to the distribution factor for interior girders.
- e_g = Eccentricity of a stringer with respect to the slab—to be calculated as the distance between the geometric centroid of the stringer and mid-depth of the slab.
- g = Distribution factor—i.e., the fraction of wheel loads (front and rear) to be applied to the stringers.
- I = Moment of inertia of a stringer
- J = Torsional inertia of a stringer
- k = $2.5\ (N_b)^{-0.2}$ but not less than 1.5—used in calculation of distribution factor for multi-beam bridges.
- K_g = Longitudinal stiffness parameter = $n\left(I+Ae_g^2\right)$
- L = Span length—to be calculated as the center-to-center spacing between abutments or bents but need not be larger than the clear spacing plus one girder depth.
- L_1 = Span length; but if span length is greater than 60', then L_1 = 60'.
- n = Modular ratio—to be calculated as the ratio of the elastic modulus of stringer to that of the slab.
- N_b = Number of beams or stringers
- N_c = Number of cells in a box girder bridge

N_L = Total number of design traffic lanes.
r = Correction factor for skew—to be applied to the distribution factor for nonskewed (right) bridges.
S = Average stringer spacing
t_s = Slab thickness
W = Bridge width, edge-to-edge
W_1 = Bridge width; but if bridge width is greater than 60', than W_1 = 60'.
W_e = Top slab width—to be measured from the midpoint between girders to the outside edge of the slab. The cantilever dimension of any slab extending beyond the exterior girder shall preferably not exceed half the girder spacing.
θ = Skew angle—to be calculated as the lesser of the skew angles of the two supports for moment, and as the skew angle of the support where shear or reaction is calculated. The angle is measured between the centerline of the bridge and the line perpendicular to the support.

REFERENCES

1. American Association of State Highway Transportation Officials, *Standard Specifications for Highway Bridges*, Thirteenth Edition, 1983.
2. National Cooperative Highway Research Program, "Distribution of Wheel Loads on Highway Bridges," Preliminary Draft Final Report, Project 12-26/1, October, 1990.
3. Ontario Ministry of Transportation and Communications, *Ontario Highway Bridge Design Code*, Second Edition, Downsview, Ontario, Canada, 1983.
4. Hays, C.O. and Berry, A.J., "Further Analytical Studies on Lateral Distribution of Wheel Loads on Highway Bridges", University of Florida Structures and Materials Research Report No. 85-2, August, 1985.
5. Powell, G.H. and Buckle, I.G., "Computer Programs for Bridge Deck Analysis", *Report No. UC SESM 70-6*, Division of Structural Engineering and Structural Mechanics, University of California, Berkeley, April, 1970, 300 pp.
6. Mondkar, D.P. and Powell, G.H., "CURVBRG-A Computer Program for Analysis of Curved Open Girder Bridges", *Report No. UC SESM 74-17*, Division of Structural Engineering and Structural Mechanics, University of California, Berkeley, December, 1974, 166 pp.
7. Lopez, L.A., Rehak, D.R., Dodds, R.H., and Schmidt, R. J., "POLOFINITE, A Structural Mechanics System for Linear and Nonlinear, Static and Dynamic Analysis", Civil Engineering Systems Laboratory, University of Illinois at Urbana-Champaign.
8. Lin, C.S. and Scordelis, A.C., "Computer Program for Bridges on Flexible Bents", *Report No., UC-SESM 71-24*, Structures and Materials Research, College of Engineering, Office of Research Services, University of California, Berkeley, December, 1971.
9. Powell, G.H., Ghose, A., and Buckle, I.G., "Analysis of Multibeam Bridges", *Journal of the Structural Division, Proceedings of the ASCE*, Vol. 95, No. ST9, September, 1969.
10. Davis, R.E., Vu Dinh, B., and Semans, F.M., "Transverse Distribution of Loads in Box Girder Bridges", Volumes 1-8, Office of Structures Design, Division of Transportation Facilities Design, California Department of Transportation, 1980-'86.

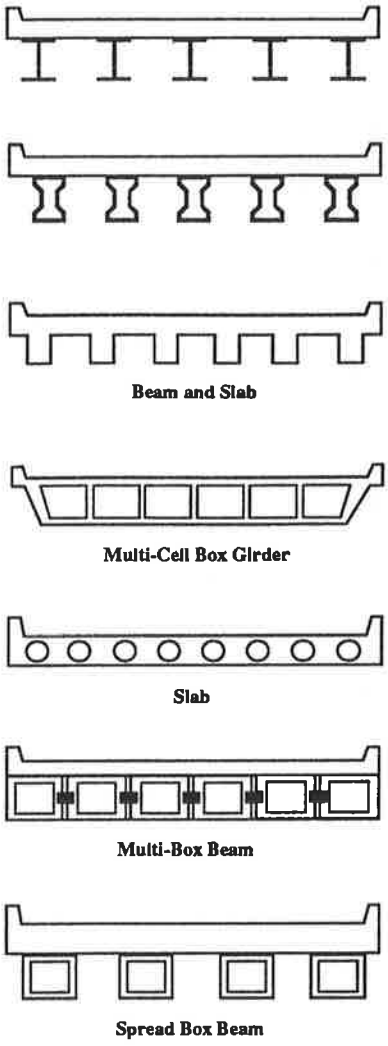

FIGURE 1: Cross Sections of Various Bridge Types

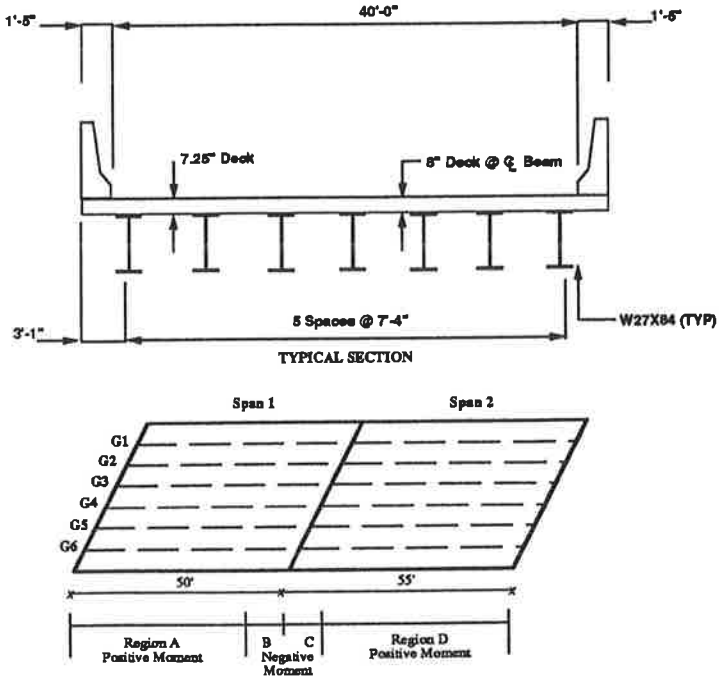

Figure 3: Typical Section and Plan View of Bridge Used For Numerical Example

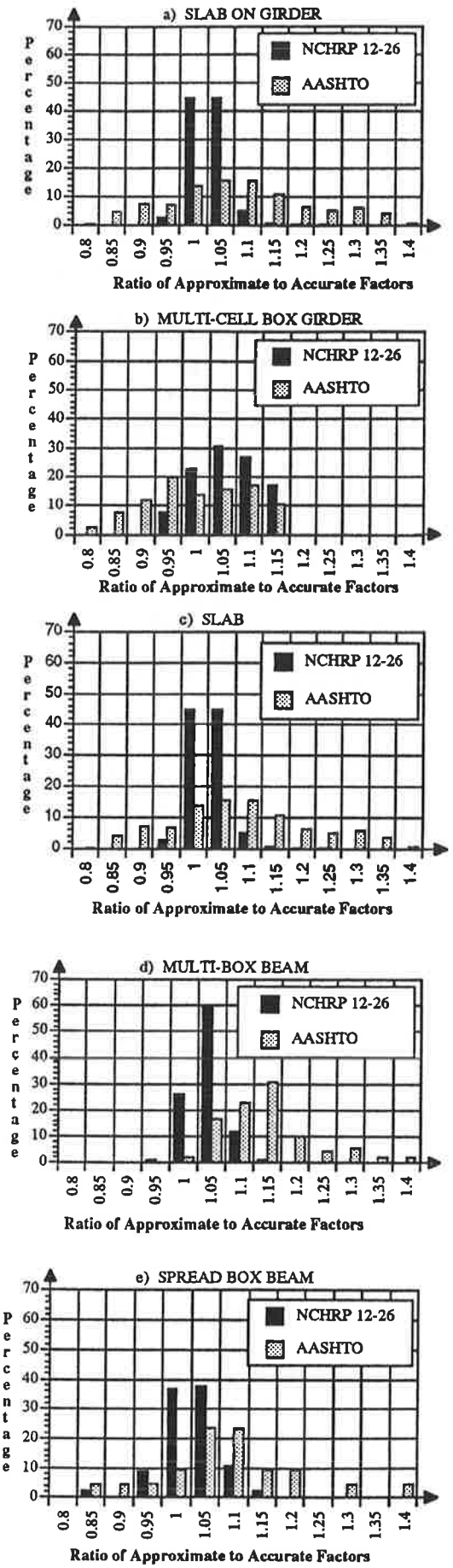

Figure 2: Comparison of AASHTO & NCHRP 12-26 Formulae

TABLE 1: FORMULA FOR MOMENT/SHEAR DISTRIBUTION TO INTERIOR GIRDERS

Bridge Type	Bridge Designed for One Traffic Lane	Bridge Designed for Two or More Traffic Lanes	Range of Applicability
	MOMENT		
Beam and Slab	$0.1 + \left(\frac{S}{4'}\right)^{0.4}\left(\frac{S}{L}\right)^{0.3}\left(\frac{K_g}{Lt_s^3}\right)^{0.1}$	$0.15 + \left(\frac{S}{3'}\right)^{0.6}\left(\frac{S}{L}\right)^{0.2}\left(\frac{K_g}{Lt_s^3}\right)^{0.1}$	3'-6" ≤ S ≤ 16'-0" 20' ≤ L ≤ 200' 4.5" ≤ t ≤ 12.0" 10,000 ≤ K_g ≤ 7,000,000 $N_b \geq 4$
Concrete Box Girders	$\left(3 + \frac{S}{2.2'}\right)\left(\frac{1'}{L}\right)^{0.35}\left(\frac{1}{N_c}\right)^{0.45}$	$\frac{2.5}{Nc} - \frac{1}{NL} + \frac{L}{800'} + \left(\frac{S}{9'}\right)\left(\frac{90'}{L}\right)^{0.25}$	7' ≤ S ≤ 13' 60' ≤ L ≤ 240' Nc>3
Slab	$\frac{2' + \sqrt{L_1 W_1}}{4}$	$3.5' + 0.06\sqrt{L_1\ W_1}$	8' ≤ L ≤ 70' 12' ≤ W ≤ 100'
Spread Box Beams	$2\left(\frac{S}{5'}\right)^{0.35}\left[\left(\frac{S}{L}\right)\left(\frac{d}{L}\right)\right]^{0.25}$	$\left(\frac{S}{2'}\right)^{0.6}\left[\left(\frac{S}{L}\right)\left(\frac{d}{L}\right)\right]^{0.125}$	6' ≤ S ≤ 11'-6" 20' ≤ L ≤ 135' 18" ≤ d ≤ 65" $N_b \geq 3$
Multi-Box Beam Decks	$k\left(\frac{b}{L}\right)^{0.5}\left(\frac{I}{J}\right)^{0.25}$ where: k = 2.5 (Nb)-0.2 ≥ 1.5	$\left(\frac{2b}{3'}\right)^{0.6}\left[\left(\frac{b}{L}\right)\left(\frac{1}{Nb}\right)\right]^{0.2}\left(\frac{I}{J}\right)^{0.06}$	3' ≤ b ≤ 5' 20' ≤ L ≤ 105' 5 ≤ Nb ≤ 20 25,000 ≤ J ≤ 610,000 in^4 40,000 ≤ I ≤ 610,000 in_4
	SHEAR		
Beam and Slab (Slab on Girder)	$0.6 + \frac{S}{15'}$	$0.4 + \frac{S}{6'} - \left(\frac{S}{25'}\right)^2$	3-6" ≤ S ≤ 16'-0" 20' ≤ L ≤ 200' 4.5 ≤ ts ≤12.0" 10,000 ≤ kg ≤ 7,000,000 $N_b \geq 4$
Concrete Box Girder	$\left(\frac{S}{4'}\right)^{0.6}\left(\frac{d}{L}\right)^{0.1}$	$\left(\frac{S}{3.4'}\right)^{0.9}\left(\frac{d}{L}\right)^{0.1}$	6' ≤ S ≤ 13' 20' ≤ L ≤ 240' 3' ≤ d ≤ 9' $N_c \geq 3$
Spread Box Beams	$\left(\frac{S}{4.4'}\right)^{0.6}\left(\frac{d}{L}\right)^{0.1}$	$\left(\frac{S}{3.1'}\right)^{0.8}\left(\frac{d}{L}\right)^{0.1}$	6' ≤ S ≤ 11'-6" 20' ≤ L ≤ 135' 18" ≤ d ≤ 65" $N_b \geq 3$
Multi-Box Beams	$1.15\left(\frac{b}{L}\right)^{0.15}\left(\frac{I}{J}\right)^{0.05}$	$\left(\frac{b}{3.2'}\right)^{0.4}\left(\frac{b}{L}\right)^{0.1}\left(\frac{I}{J}\right)^{0.05}$	35" ≤ b ≤ 60" 20' ≤ L ≤ 105' 5 ≤ N_b ≤ 20 25,000 ≤ J ≤ 610,000 in^4 40,000 ≤ I ≤ 610,000 in^4

TABLE 2: CORRECTION FACTORS FOR CALCULATION OF BENDING MOMENTS AND SHEARS IN CONTINUOUS LONGITUDINAL BEAMS

	MOMENT	
Bridge Type	Correction Factor for Positive Moments	Correction Factor for Negative Moments
Beam and Slab (Slab on Girder)	1.05	1.10
Concrete Box Girders, Slabs, Multi-Box Beams, and Spread Box Beams	1.00	1.10
	SHEAR	
Bridge Type	Correction Factor for Simply-Supported End	Correction Factor for Continuous Bent
Beam and Slab (Slab on Girder)	1.00	1.05
On Concrete Box Girders	1.00	1.00
Multi-Box Beams, and Spread Box Beams	1.00	1.05

TABLE 3: FORMULA/CORRECTION FACTOR FOR MOMENT/SHEAR DISTRIBUTION TO EXTERIOR GIRDERS

Bridge Type	Bridge Designed for One Traffic Lane	Bridge Designed for Two or More Traffic Lanes	Range of Applicability
MOMENT			
Beam and Slab (Slab on Girder)	Use Simple Beam Distribution*	$g = e * g_{interior}$ $e = \frac{7' + d_e}{9.1'} \geq 1.0$	$-1.' \leq d_e \leq 5'\text{-}6"$
Concrete Box Girders	$g = \frac{W_e}{7'}$	$g = \frac{W_e}{7'}$	$W_e \leq S$
Spread Box Beams	Use Simple Beam Distribution*	$g = e * g_{interior}$ $e = \frac{27.7' + d_e}{28.5'}$	$0' \leq d_e \leq 4'\text{-}6"$
Multi-Box Beam	Use Simple Beam Distribution*	$g = e * g_{interior}$ $e = \frac{26' + d_e}{25'}$	$-1 \leq d_e \leq 2'$
SHEAR			
Beam and Slab (Slab on Girder)	Use Simple Beam Distribution*	$g = e * g_{interior}$ $e = \frac{6' + d_e}{10'}$	$-1' \leq d_e \leq 5'\text{-}6"$
Concrete Box Girders	Use Simple Beam Distribution*	$g = e * g_{interior}$ $e = \frac{8' + d_e}{12.5'}$	$-2' \leq d_e \leq 5.0'$
Spread Box Beams	Use Simple Beam Distribution*	$g = e * g_{interior}$ $e = \frac{8' + d_e}{10'}$	$0' \leq d_e, \leq 4'\text{-}6"$
Multi-Box Beam	Use Simple Beam Distribution*	$g = e * g_{interior}$ $e = \frac{51' + d_e}{50'}$	$-1' \leq d_e \leq 2'$

*i.e., distribute the wheel loads to the girder by assuming the slab to act as a simply supported beam between the girders.

TABLE 4: FORMULA/CORRECTION FACTOR FOR CALCULATION OF MOMENT IN INTERIOR GIRDER AND SHEAR IN OBTUSE CORNER FOR SKEWED SUPPORTS

Bridge Type	Bridge Designed for Any Number of Traffic Lanes	Range of Applicability
MOMENT		
Beam and Slab (Slab on Girder)	$1\text{-}c_1 (\tan\theta)^{1.5}$ $c_1 = 0.25 \left(\frac{Kg}{Lt_s^3}\right)^{0.25} \left(\frac{S}{L}\right)^{0.5}$ If θ is less than 30°, $c_1 = 0.0$ If θ is larger than 60° use θ as 60°	$0° \leq \theta \leq 60°$ $3'\text{-}6" \leq S \leq 16'\text{-}0"$ $20' \leq L \leq 200'$ $4.5" \leq t_s \leq 12.0"$ $10{,}000 \leq K_g \leq 7{,}000{,}000$ $N_b \geq 4$
Concrete Box Girders, Slabs, Multi-Box Beams, and Spread Box Beams	$1.05 - 0.25 \tan(\theta) \leq 1.0$ If θ is larger than 60°, use θ as 60°	$0° \leq \theta \leq 60°$
SHEAR		
Beam and Slab (Slab on Girder)	$1.0 + c_1 \tan\theta$ $c1 = \frac{1}{5\left(\frac{k_g}{Lt_s^3}\right)^{0.3}}$	$0° \leq \theta \leq 60°$ $3'\text{-}6" \leq S \leq 16'\text{-}0"$ $20' \leq L \leq 200'$ $4.5" \leq t_s \leq 12.0"$ $10{,}000 \leq k_g \leq 7{,}000{,}000$ $N_b \geq 4$
Concrete Box Girders	$1.0 + c_1 \tan(\theta)$ $c_1 = 0.25 + \frac{L'}{70d}$	$0° < \theta \leq 60°$ $6' \leq S \leq 13'$ $20' \leq L \leq 240'$ $3' \leq d \leq 9'$ $N_c \geq 3$
Spread Box Beams	$1.0 + c_1 \tan(\theta)$ $c_1 = \frac{\sqrt{Ld}}{6S}$	$0° < \theta \leq 60°$ $6' \leq S \leq 11'\text{-}6"$ $20' \leq L \leq 135'$ $18" \leq d \leq 65"$ $N_b \geq 3$
Multi-Box Beams*	$1.0 + c_1 \sqrt{\tan(\theta)}$ $c_1 = \frac{L}{90d}$	$0° < \theta \leq 60°$ $20' \leq L \leq 105'$ $17" \leq d \leq 60"$ $35" \leq b \leq 60"$ $5 \leq N_b \leq 20$

*Apply to all beam (interior and exterior)

Effective Method for Linking Computer-Aided Engineering Procedures with Computer Drafting

J. A. PUCKETT, CHAD CLANCY, AND DAVID POPE

Often a traditional design procedure is used where a designer sketches results which are based on computer applications and transmits this information via hardcopy to a drafter, who reenters it into a CAD system. The inefficiencies are clear and an obvious opportunity exists for productive gain. Recent work by the Wyoming Highway Department (WHD) has shown that productivity ratios can exceed than 20:1 by linking design applications directly with CAD. A graphics library (UWGRAPH) has been developed to facilitate this linkage.

UWGRAPH is used in conjunction with a design application which performs engineering calculations and/or drawing parameterization. Herein, parameterization refers to the determination of the required dimensions to completely define an engineering drawing. UWGRAPH links to three graphic formats commonly used in engineering IGES, IGDS and GKS in one application program. The flexibility and familiarity of FORTRAN is combined with the tools necessary to produce graphics files automatically. The library is based on the graphics entities required for structural drafting. UWGRAPH simplifies and unifies the subroutine calls by combining low-level calls to produce graphical entities useful in engineering drawing, e.g. dimensions, notes, etc. The UWGRAPH scope is directed toward bridge engineering but easily spans other disciplines.

INTRODUCTION

Often a traditional procedure is used where a designer sketches results which are based on computer applications and transmits this information via hardcopy to a drafter, who reenters it into a CAD system. The inefficiencies are clear and an obvious opportunity exists for productive gain. Recent work by the Wyoming Highway Department has shown that productivity ratios can exceed be greater than 20:1 by linking design applications directly with CAD. A graphics library (UWGRAPH) has been developed to facilitate this linkage.

UWGRAPH is used in conjunction with a design application which performs engineering calculations and/or drawing parameterization. The flexibility and familiarity of FORTRAN is combined with the tools necessary to produce graphics files either to the computer screen or to a drafting/design file which can be used by a CAD system. The library is based on the graphical entities required for structural drafting.

The difficulty with many existing graphic systems is they are often difficult to learn and implement. UWGRAPH simplifies and unifies the subroutine calls by using low-level calls, combined with intermediate calculation, to produce graphical entities useful in engineering drawing, e.g. dimensions, notes, etc. Thus, only one call is used in UWGRAPH for each entity, for example, a dimension. All the calculations and decisions involved with leader type and placement, text justification and location, etc. are automatically performed in the desired graphical format. Hence, UWGRAPH performs a great deal of work for the program developer.

Department of Civil Engineering, University of Wyoming - Laramie, WY 82070 & Wyoming Highway Department, Bridge Branch - Cheyenne, WY 82002

STANDARDIZATION EFFORTS AND OBJECTIVES

There has been much effort to standardize computer graphics. CORE, GKS, PHIGS, IGES are examples of standardized graphics library and file formats (6). But the creation of an all-encompassing graphics format that suits every application, type of drawing, and computer system is difficult. Further, a single system which adequately supports the development environment may not support the production environment. For example, a library is used which produces an IGES file which must be interpreted by a CAD system prior to viewing the results. Because the file is converted to the native CAD format, this approach is well suited for production. However, it offers the development engineer an extremely cumbersome approach.

A library based solely on a screen/plot presentation system, like GKS or PHIGS, produces fine screen graphics, almost instantaneously, upon execution of the application. This approach is amenable to both development and the production engineers who wish to rapidly iterate on programs and designs, respectively. However these libraries produce drawing files in formats required by only screen and plotting devices, and can not be easily edited by a drafter for inclusion in a set of plans. This is a major limitation of this programming approach as the greatest productivity potential lies with linking the application to CAD directly.

The intent of the UWGRAPH library is to merge both of the favorable attributes of the screen/presentation libraries with libraries which automate the linkage to CAD. Specifically, the objectives of the UWGRAPH development effort is to develop a graphic library to:

- Produce structural drafting which can be extended to other disciplines.
- Provide an environment for rapid program development.
- Provide an environment fast enough for the design engineer iterating on design solutions.
- Produce a file which can be interpreted or used directly in CAD systems.
- Use existing standardized graphics and CAD formats linked to a common library.

LIBRARY ARCHITECTURE

The UWGRAPH library links to three graphic libraries commonly used in engineering. The purpose of the library is

to allow the use of IGES, IGDS and GKS libraries through one application program. The library architecture is illustrated in Figure 1. Graphics can be created in one or more of these three formats from a single set of subroutine calls. This is helpful in that the graphical output of the application program can be used by one who has the capability of displaying graphics in any or all of the systems. A simple software switch is available to direct the application to the desired format. The application programmer is relieved of the burden of learning more than one graphics system because the initialization, drawing definition, and termination is all consistently defined by the UWGRAPH library. Further, the application developer can use GKS to review drawings in development without accessing the CAD system. This permits program development on inexpensive graphics devices and can help to eliminate scheduling conflicts on the CAD systems.

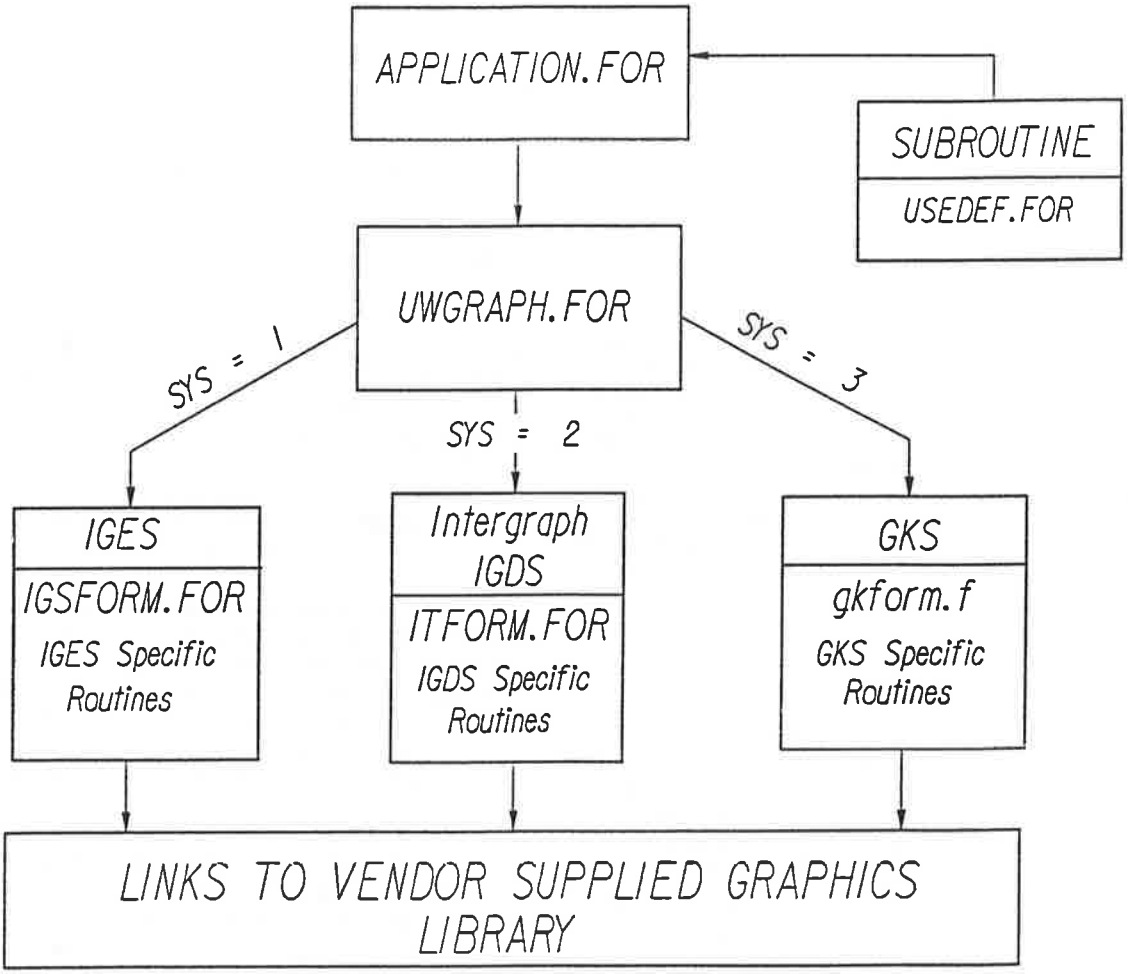

Figure 1. UWGRAPH Architecture

The first link is to the Initial Graphics Exchange Specification (IGES), a standardized file format accepted by the National Bureau of Standards. IGES is expected to be an American National Standards Institute (ANSI) standard after a period of testing and implementation (3). UWGRAPH links to a graphics library to create an ASCII file in the IGES format. Most CAD systems have IGES interpreters to convert the IGES file into their native format. Once in the native format, the drawing can be edited in the usual manner. Thus, atypical and site specific details can be easily added and merged with other drawings as required.

The second link is to a graphics format supported by Intergraph using the Interactive Graphics Design System (IGDS) (4). IGDS is a workstation-based product and used with the Intergraph CAD software. A FORTRAN binding interfaces the capabilities of IGDS. The output from this link to the library is an IGDS design file which can be edited with an Intergraph CAD system. Approximately forty State DOTs, including WHD, use Intergraph systems. Hence, the IGDS was selected for UWGRAPH because of this important constituency.

The third link is to the Graphical Kernel System (GKS)

which was accepted by the *International Organization for Standardization* as a two-dimensional graphics standard in 1985 (4,5). FORTRAN GKS bindings are available for numerous hardware/software platforms including most all engineering workstations and DOS-based computers. GKS is used by some CAD systems to display graphics. GKS is different from the other graphics systems used by UWGRAPH because the output is sent directly to the screen as opposed to an output file. Alternatively, the graphical output can be displayed on the screen, then a metafile can be created and sent to a plotter used in conjunction with a metafile interpreter.

ENTITY SPECIFICS

The UWGRAPH library supports the basic entities needed to create and dimension a drawing. These entities include lines, arcs, multiple point lines, labels, text, and several types of dimensions. In the creation of these entities UWGRAPH does not fully use the capabilities of any one graphical system, but in general uses the capabilities common to all three systems. Extended capabilities have been included by programming within UWGRAPH. For example, the IGES dimension entity is not used but is created using line and text entities common to all systems. This approach results in a practical graphics link between an application and the three graphics libraries. This functionality saves time and simplifies development. Table 1 illustrates the basic entities/procedures available in UWGRAPH.

Other higher level utilities have been developed using the basic entities. These utilities are included and described in Table 2.

It is hopeful that many agencies will use UWGRAPH to develop applications which can be shared. In application development it is inevitable that programmers will develop other high level utilities which can be properly documented and also shared with others.

Table 1. Procedures in UWGRAPH (1)

INITIALIZATION: Initializes the appropriate graphics libraries for subsequent entity calls.
LINE: Creates a two point line.
CIRCULAR ARC: Creates an arc given a center, radius, start angle and an end angle.
MULTIPLE POINT LINE: Draws a line string given more than two points.
GENERAL NOTE: Places strings of text.
GENERAL DIMENSION CALL: Creates a dimension with a break in the leader to place the dimension text. (if there is enough room for the text between witness lines)
SECOND DIMENSION TYPE: Creates a dimension which has a leader arrow drawn from witness line to witness line with no break and a string of text or a numeric dimension placed at user defined coordinates.
SUBSET VERSION OF UWDIM2: Creates a dimension similar to UWDIM2, but allows more than one text string to be placed.
LABEL: Creates a text label with a two segment leader with an arrowhead at the tip and up to three text strings at the leader end. Text justification is controlled in several ways.
SUBSET VERSION OF LABEL: Creates same label as above but automatically draws a bracket around the text associated with the label.
TERMINATION: Terminates all drawing processes.

Table 2. High Level Utilities (1)

DRAWNUT: Uses lines and arcs to draw an elevation of a nut of width NW and of height NH. The nut can be drawn with the flat side down or the flat side up.
DRAWTHR: Uses lines to draw bolt threads of width TW and of height TH. The threads can be drawn with a taper at the top, a taper at the bottom or with no taper. This utility will draw the threads with a vertical axis only.
BOXCOORD: Fills the X and Y arrays with the coordinates to draw a rectangle.
BLDDIM: Builds two or three part dimensions separated by 'x' in a fractional format. For example: 1' -6 3/4" x 10 5/16" x 2".

EXAMPLES

Two examples are presented. The first is a simple example which illustrates the usage of UWGRAPH. The example, called testbox, performs most of the operations required in a typical drawing. The FORTRAN listing of testbox is given in the Appendix and the output is illustrated in Figure 2. The drawing process has three distinct parts: initialization, drawing, and termination. The initialization is performed with a single call of UWINIT. This initializes the target system. The termination is also performed with a call to UWTERM. In between initialization and termination, any drawing entity may be called. The testbox program uses line, text, and dimension entities.

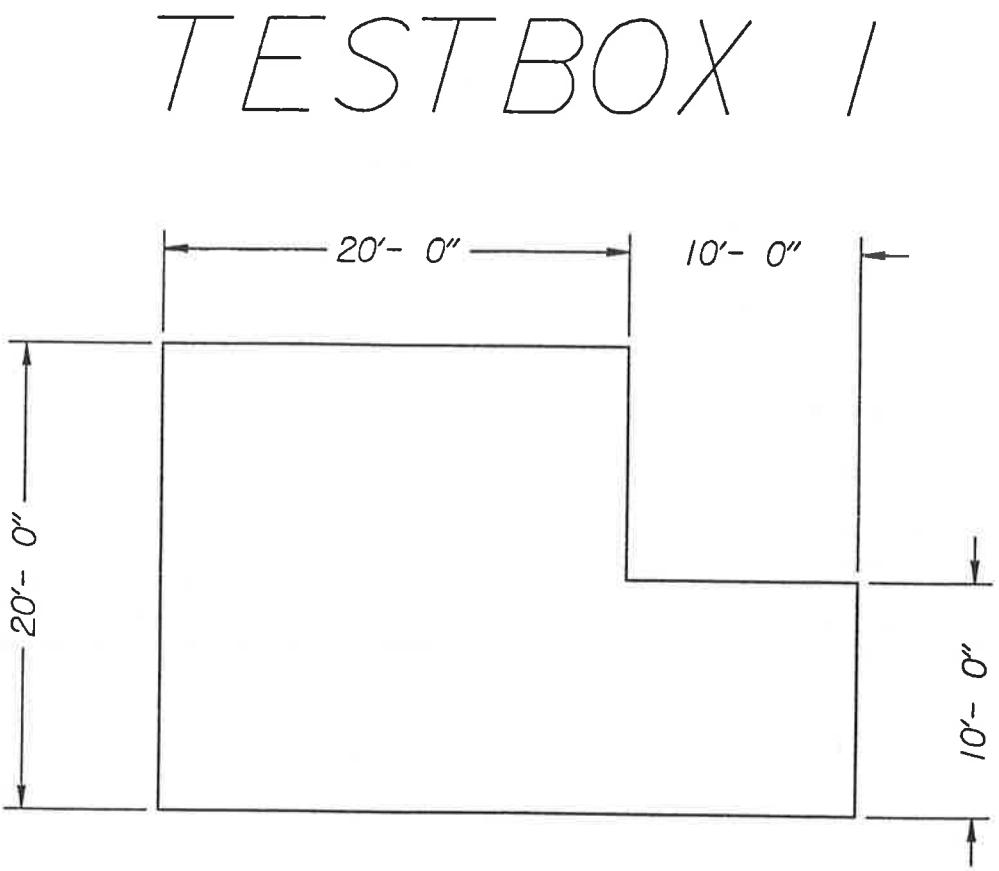

Figure 2. Output From Program Testbox

The second example is the bearing detail shown in Figure 3. This design detail was selected for automation because of its limited scope and the existence of application to perform the design. This was the initial effort to test UWGRAPH in a production environment. In this application, a few design parameters are entered to a design program which generates the details necessary for drafting. The library is used to automatically generate the drafting file. This illustration was developed from an IGDS (Intergraph CAD) file. The generation of the design and drawing took approximately five minutes plus ten minutes for cleanup and merging with the project plans. If the design was performed with the same application but the drawing was "manually" illustrated in the CAD system the time required is approximately 4.5 hours, which gives a productivity ratio of approximately 18.

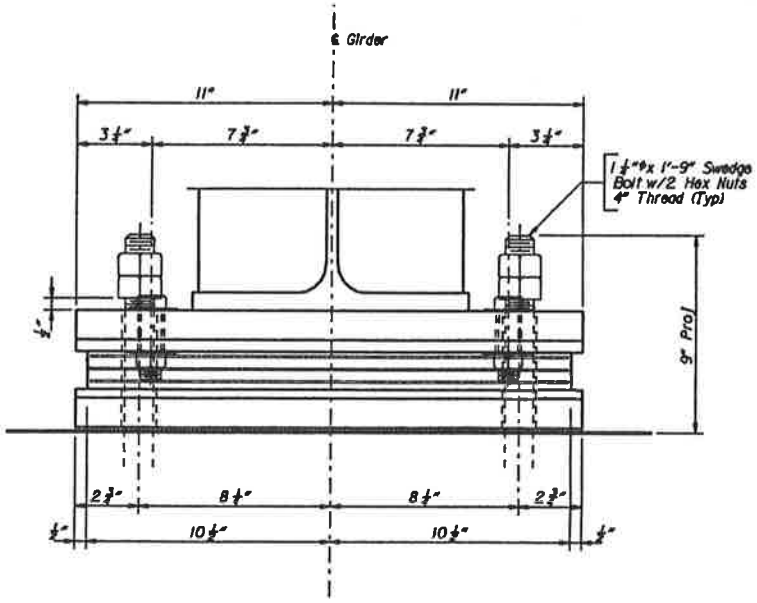

END VIEW

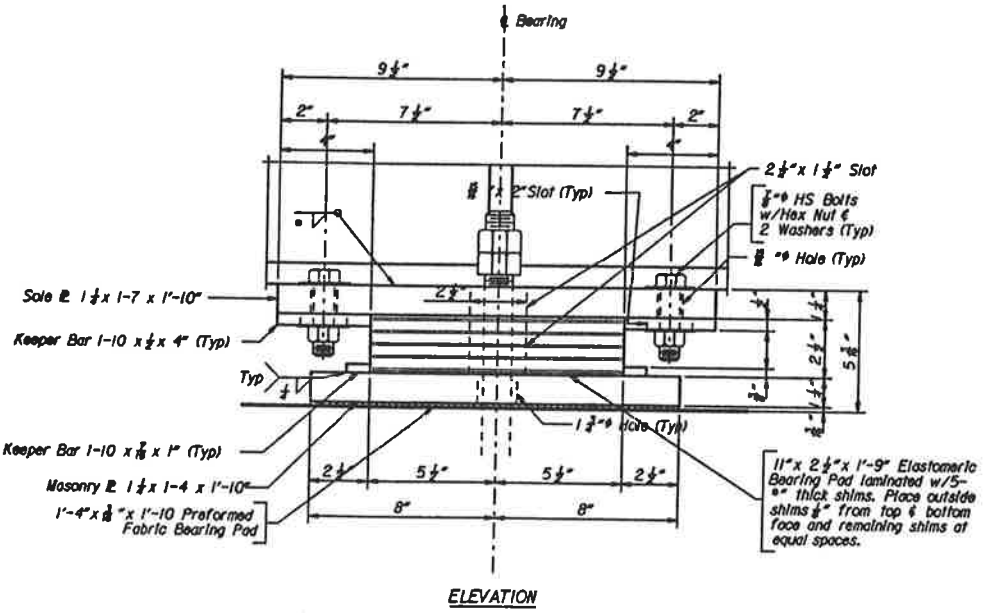

ELEVATION

Figure 3. Bearing Details

PRESENT WORK

Presently UWGRAPH is being used to create design and graphical illustrations for reinforced box culverts and bridge geometry. The initial work on the box culvert application was performed using the IGES format and is implemented in the BRASS system (2). The bridge geometry program is presently under development. Code writing is underway at the time of this writing. This program includes: general plan/elevation drawings and substructure layout.

REFERENCES

1. Clancy, C. and Puckett, J.A., *UWGRAPH Graphics Library*, Wyoming Highway Department, Cheyenne, WY. May 14, 1990.
2. Puckett, J.A. and Guenther, P.W., *Linking Civil Engineering Design and Drafting Software via IGES*, Journal of Computing in Civil Engineering, ASCE, Vol.3, No. 3, July, 1989, pp. 228.
3. National Bureau of Standards, *Initial Graphics Exchange Specification*, Publication PB86-199759, Version 3.0, 1986.
4. Intergraph Corp., *Intergraph GKS/C Reference Manual*, DSYS027, Third Edition, Huntsville, AL, August, 1988.
5. Hopgood, F.R.A., Duce, D.A., Gallop, J.R., and Sutcliffe, D.C., *Introduction to the Graphical Kernal System (GKS)*, Second Edition, Academic Press, Harcourt Brace Jovanovich, London, New York, 1986.
6. Dewey, B.R., *Computer Graphics for Engineers*, Harper and Row, New York, NY, 1988.

APPENDIX -- Program Listing

```
      PROGRAM TESTBOX
C
C     This program draws a box and dimensions it using the
C     UWGRAPH library of graphics calls.
C
C     First, declare the working variables with this include statement.
C
CMSF$INCLUDE:'VARI.FOR'
CVAX      INCLUDE 'VARI.FOR'
CUNX      INCLUDE 'VARI.FOR'
C
C     Now, open up a file to output messages.
C
      OUTNUM=5
      OPEN(UNIT=OUTNUM,FILE='MESSAGE.OUT',STATUS='UNKNOWN')
C
C     Set up the initialization parameters.
C
      OUTNAME = 'BOXOUT'
      NC      = 2
      C(1)    = ' Comments can be entered here, but they'
      C(2)    = 'only show up in the start section of IGES.'
      XWMIN   = 0
      XWMAX   = 90
      YWMIN   = 0
      YWMAX   = 90
      WKSID   = 1
      WSCON   = 1
      WSTYP   = 12
      UNIT    = 'FT'
CIGS      SYS     = 1
CITG      SYS     = 2
CGKS      SYS     = 3
      CALL UWINIT(OUTNAME,NC,C,XWMIN,XWMAX,YWMIN,YWMAX,WKSID,
     1     WSCON,WSTYP,UNIT,SYS)
C
C     Initialize the default flags with this call.
C
      CALL USEDEF(ITYP1,ITYP2,ITYP3,ITYP4,ITYP5,ITYP6,ITYP7,
     1   ILEV1,ILEV2,ILEV3,ILEV4,ILEV5,ILEV6,ILEV7,
     2   ICOL1,ICOL2,ICOL3,ICOL4,ICOL5,ICOL6,ICOL7,
     3   WID1,WID2,WID3,WID4,WID5,WID6,WID7,
     4   SL4,SL5,SL6,SL7,
     5   ROT4,ROT5,ROT6,ROT7,
     6   SW4,SW5,SW6,SW7,
     7   HT4,HT5,HT6,HT7)
C
C     Now, some graphics calls can be made.
C
C     Draw a multiple point line.
C
      POINTS=7
      X(1)=20
      Y(1)=40
      X(2)=50
      Y(2)=40
      X(3)=50
      Y(3)=50
      X(4)=40
      Y(4)=50
      X(5)=40
      Y(5)=60
      X(6)=20
      Y(6)=60
      X(7)=X(1)
      Y(7)=Y(1)
      CALL UWMPLINE(X,Y,POINTS,ITYP3,WID3,ILEV3,ICOL3,SYS)
C
C     Place dimension at left side.
```

```
C
      DNUMX=14
      DNUMY=50
      XPT1=20
      YPT1=40
      XPT2=20
      YPT2=60
      HT5(1)=1
      CALL UWDIM(DNUMX,DNUMY,XPT1,YPT1,XPT2,YPT2,ITYP5,WID5,
     1      ILEV5,ICOL5,SL5,ROT5,HT5,SW5,SYS)
C
C     Place dimension at top-left.
C
      DNUMX=30
      DNUMY=64
      XPT1=20
      YPT1=60
      XPT2=40
      YPT2=60
      CALL UWDIM(DNUMX,DNUMY,XPT1,YPT1,XPT2,YPT2,ITYP5,WID5,
     1      ILEV5,ICOL5,SL5,ROT5,HT5,SW5,SYS)
C
C     Place dimension at top-right.
C
      DNUMX=45
      DNUMY=64
      XPT1=50
      YPT1=60
      XPT2=40
      YPT2=60
      CALL UWDIM(DNUMX,DNUMY,XPT1,YPT1,XPT2,YPT2,ITYP5,WID5,
     1      ILEV5,ICOL5,SL5,ROT5,HT5,SW5,SYS)
C
C     Place dimension on the right side.
C
      DNUMX=55
      DNUMY=45
      XPT1=50
      YPT1=50
      XPT2=50
      YPT2=40
      CALL UWDIM(DNUMX,DNUMY,XPT1,YPT1,XPT2,YPT2,ITYP5,WID5,
     1      ILEV5,ICOL5,SL5,ROT5,HT5,SW5,SYS)
C
C    Place a note.
C
      TCENX(1)=32
      TCENY(1)=72
      TOTCHR(1)=9
      NOSTR=1
      TBUFFR='TESTBOX 1'
      HT4(1)=4
      CALL UWNOTE(TCENX,TCENY,TOTCHR,NOSTR,TBUFFR,ITYP4,WID4,ILEV4,
     1      ICOL4,SL4,ROT4,HT4,SW4,SYS)
C
C     Now, terminate graphics creation.
C
        ID = 'UW ST. GRAPHICS LIB'
        AUTH='CHAD'
        ORG ='DEPT. CIVIL ENGINEER'
        PROG='TESTBOX_1'
        CALL UWTERM(ID,AUTH,ORG,PROG,SYS)
        STOP
        END
```

Thermal Movements in Bridges

CHARLES W. ROEDER AND SHASHI MOORTY

Changes in temperature induce movements in bridges. These movements must be accommodated by bearings or expansion joints, or large internal forces may occur within the structure. These forces may lead to damage and costly repair to the structure if the movements are not properly considered in the design. Present methods for accommodating thermal movements in bridge design are discussed. Experimental results and field observations of thermal movements are summarized, and case studies of bridges which have been damaged by thermal movements are described. A brief overview of recent theoretical research into thermal movements is provided. This leads to conclusions which help bridge engineers better understand thermal movement behavior and may lead to improved performance of bridges under extreme temperatures.

INTRODUCTION

Bridges may be exposed to large variations in temperature. Temperature changes result in expansion or contraction of the bridge, and the resulting movements are accommodated by bridge bearings and expansion joints. Restraint of any component of these movements leads to large internal forces, which must be resisted by the bridge and its substructure. Expansion joints sometimes have serious problems with corrosion and deterioration of the bridge due to water leakage, and as a result bridge engineers frequently minimize the use of these expansion joints and to a lesser extent bridge bearings. In these later applications, they accommodate the movements by deflection or deformation of the bridge piers and abutments. As an alternative, they may design the bridge components very strong to resist the large forces which may result if the movements are restrained.

This paper will review the existing AASHTO (1) design procedures for thermal effects. It will briefly examine the existing evidence regarding temperature effects in bridges, and a number of structures which have developed problems with the existing design methods will be described. These example structures raise questions regarding the accuracy and validity of present design methods, and so the design methods will be briefly compared to more refined analytical results. The comparison will show that the simple design method is very suitable for the vast majority of bridges, but it may be misleading for a few special cases. Guidelines for recognizing these special cases will be discussed, and some factors which must be considered in a more refined analysis will be noted.

AASHTO DESIGN METHOD

Thermal movement design for highway bridges are based on a simple method (1). The United States is divided into two climate zones, and different temperature ranges are used for either steel or concrete bridges within each of these two zones. Metal bridges in the moderate zone vary from 0°F (-18°C) to 120°F (49°C), and in the colder zones, the temperatures vary between -30°F (-34°C) and 120°F (49°C). Concrete bridges use the same two zones, but the temperature range is reduced to approximately 70°F (+30°F and -40°F from the installation temperature) in the moderate zones and 80°F in the colder zones. The smaller temperature range for concrete bridges recognizes the slower rate of heat transfer and greater thermal mass of concrete bridges. Thermal movements are then calculated by a simple uniaxial expansion equation

$$\Delta_T = \alpha L \Delta T , \quad (1)$$

where α is the coefficient of thermal expansion, L is the expansion length, and ΔT is the temperature change. The bridge bearings and expansion joints are designed for these movements. In other cases the bridge piers and abutments may be integrally constructed with the superstructure (2,3,4) and thermal movements may be accommodated by deflection of the piers or movement of the abutment into the backfill. In a few cases, the bridge will restrict all movement (5,6) and the thermal forces will be resisted within the structure. Extremely large forces, F_T, are possible if all movement is restrained. If the movement is restrained in one direction only, the force is

$$F_T = A E (\Delta_T / L) , \quad (2)$$

where A is the cross sectional area of the restrained elements, and E is the elastic modulus. The force may be much larger if the movement is restrained in two dimensions. A few bridges are designed with combinations of these approaches.

In straight bridges, design engineers consider the movement, Δ_T, or the corresponding force, F_T, as longitudinal effects. That is, the bearings and expansion joints are oriented for longitudinal movement, and the restraining forces are longitudinal forces. Curved bridges cause some additional concern with this simple design procedure. Some engineers place the bearings and expansion joints so that they permit tangential movement at the support as illustrated in Fig. 1a. Other engineers believe that this expansion is uniform and that the curved segment assumes a slightly smaller or larger radius under these thermal conditions. They, therefore, place the bearings and expansion joints so that they are oriented on a chord from the point of fixity of the bridge as illustrated in Fig. 1b. Still other engineers use a combination of these approaches, since they place the bearing on a chord while the expansion joints are set for tangential movement.

This simple design procedure has been used for many years, and has generally produced good results. Experimental observations of thermal movements in bridges suggest, however, that there may be reason to question the validity of these methods for some bridges.

EXPERIMENTAL OBSERVATIONS OF THERMAL MOVEMENTS

Thermal movements were measured and studied in some detail for a number of bridges in England by Emerson (7,8,9). This experimental work showed that thermal movements can be

Department of Civil Engineering, University of Washington, Seattle, WA 98195.

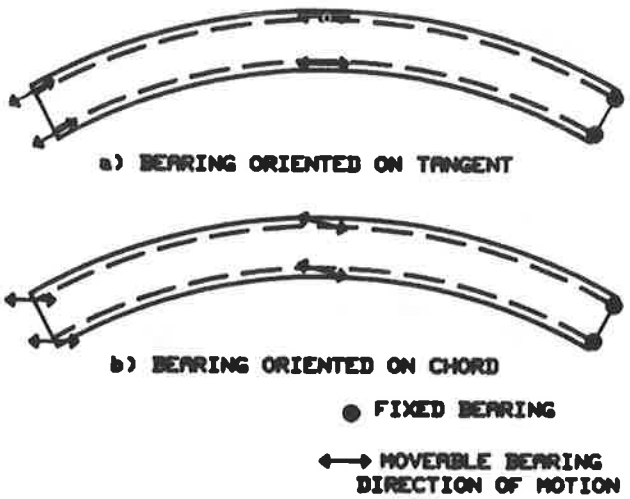

FIGURE 1 Typical orientation and placement of bridge bearings on a curved bridge

divided into two parts. First, there is a daily temperature cycle and the movements associated with this cycle. These daily movements tend to be much larger for steel bridges than concrete bridges, because the steel may experience the full daily range of air temperature while the average temperature of the concrete has much less variation. Concrete bridges have much greater thermal mass and so they do not fully adapt to short term temperature changes as does steel. Direct radiation of the sun may cause daily local temperatures which greatly exceed the air temperature for both steel and concrete. Steel that is exposed to this direct radiation may quickly assume a similar temperature throughout the section because of the conductivity and relatively low thermal mass of the steel. Concrete bridge decks are commonly exposed to direct solar radiation and this affects their daily temperature cycle. However, the average temperatures of the bridge deck seldom approach the ambient temperatures because of the thickness of the deck.

Daily temperature movements are somewhat erratically related to the average bridge temperature. The erratic nature is caused by the slip-stick action caused by friction and other resistance in bearings and expansion joints. The frictional resistance prevents movements until the internal forces are large enough to overcome it, and then a sudden step like movement will occur. The movement will then remain constant until there is an adequate temperature change to overcome the resistance again.

The second part of the thermal movements is caused by the annual temperature cycle. This component is usually considerably larger than the movement due to the daily cycle. Concrete bridges will experience smaller annual movements than steel bridges, because the extreme high and low annual temperatures are of short duration. The mass of the concrete bridge prevents it from responding to very short duration temperature changes, but the relative difference between the annual cycle movements for concrete and steel bridges is much smaller than the relative difference between the daily temperature cycle movements. Movements in concrete bridges are dependent upon a smaller temperature range such as a three day running average of the air temperature.

Experiments have shown that the direction of thermal movement is not always clearly defined. This is particularly true for skewed and curved bridges. Field observations have shown that curved bridges have thermal movements which are neither tangential nor are they on the chord. In some cases the radial component of movement is of similar magnitude to the chord or tangential movement. Field observations have shown that skewed bridges sometimes display transverse movements as well as the longitudinal movements for which they are designed.

A survey of state bridge engineers was made to determine if similar discrepancies between the predicted and actual thermal movements in bridges were noted in the US. The initial response of most bridge engineers was that they observed no problems with temperature movements in bridges, but many of these respondents quickly pulled back from this position after a few moments thought. These engineers noted that they had occasional problems with anchorage pull-out failure, spalling of girders, piers or abutments, and bearing failures. After some thought, they indicated that many of these problems could be related to thermal effects. This initial reaction of bridge engineers represents one of the major difficulties in assessing the thermal movement problem. When bridge engineers note damage in a bridge, their first reaction is to repair it. This leads to an assessment that a component was too weak or defective. Once this assessment has been made, bridge engineers frequently do not consider the cause of the large forces which produced the damage. Only a few engineers directly noted that they had observed temperature movements which were unusual. When these observations were combined, it was clear that the majority of these bridges were sharply skewed or curved bridges. A few typical examples will be discussed in this paper.

CASE STUDIES OF TEMPERATURE MOVEMENTS

Sharply skewed bridges are one area where serious temperature related structural problems sometimes are noted. Figure 2 shows a photograph of a sharply skewed bridge in Richmond, VA. This bridge has 3 spans with simply supported prestressed concrete T-beams. The bridge is approximately 49° from the orthogonal. The beams rest on a bearing pad, and they are set into a recess (approx. 1.5" deep) which restricts the thermal movement to the longitudinal direction. The ends of the simply supported beams were cast into a diaphragm with an expansion gap between adjacent diaphragms.

This particular bridge was built in 1938 and served for a number of years with no observable problems. In the 1960's large transverse movements (in the order of 3" to 6" or 75 to 150 mm) occurred at each interior support and caused severe spalling of the support piers when the girders were forced from the guided path. Figure 3 is a photograph which shows some of the repaired spalled areas of this bridge. Inspection of the bridge showed that dirt had filled the expansion gap between the diaphragms, and the summer expansion of the bridge had caused large internal forces. The granular material developed forces in compression rather than shear and so a large transverse component of force developed as shown in Fig. 4, where f_n is the normal force and f_t is the transverse force. This caused the damage and transverse movement noted in Fig. 3.

FIGURE 2 Photograph of 3 span skewed concrete bridge

FIGURE 3 Repaired spalled concrete bridge piers

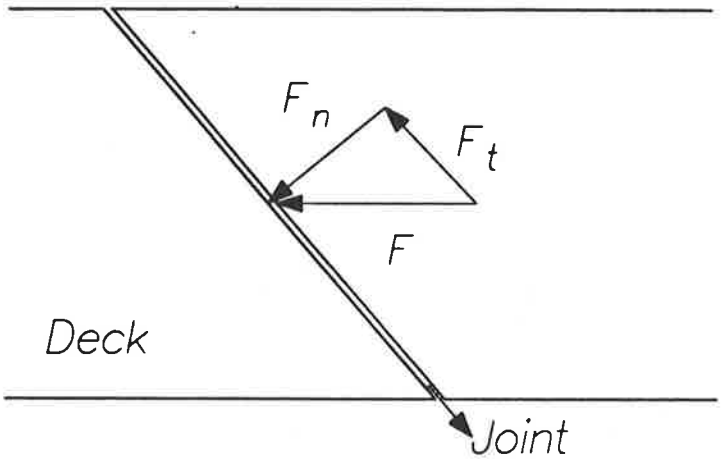

FIGURE 4 Transverse component of force in restrained skew bridges

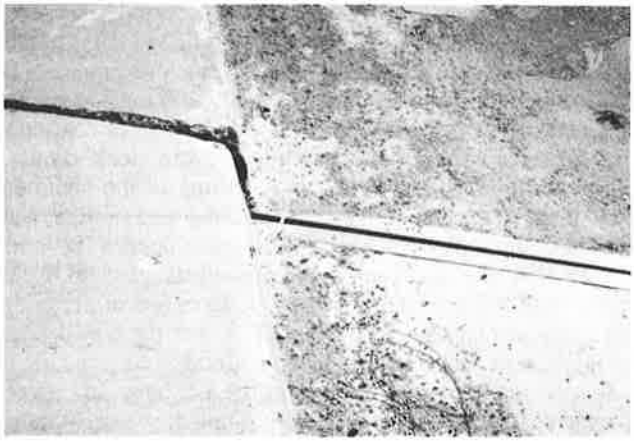

FIGURE 5 Misaligned deck panels due to thermal movement

FIGURE 6 Minor spalling of concrete at piers due to transverse thermal movement

FIGURE 7 Misalignment of curb due to transverse movement of skew bridge

The bridge was repaired by replacing the spalled concrete and by making the deck continuous across the gap. Steel ties also were placed across the gap to transfer the large transverse force between adjacent girders and to prevent the transverse movement and develop the required component of transverse force.

A similar situation can be observed with another sharply skewed bridge in Helena, Montana. This bridge is a 5 span precast concrete girder bridge with simple spans. The bridge deck was replaced with precast deck panels several years ago, and there are small gaps between adjacent panels to accommodate thermal expansion. Each of these panels is misaligned by approximately 1 inch (25 mm) as shown in the photograph of Fig. 5, because of the transverse movements caused by the forces depicted in Fig. 4. The total transverse movement is quite large (6" to 8 " or 150 to 200 mm) over the length of the bridge, but the damage is slight because it is spread over many locations. Nevertheless, there is some minor spalling of the concrete at the piers and supporting elements as shown in Fig. 6. It is possible that this damage may increase if an extremely hot summer occurred.

The Casper Creek Bridge in Wyoming (10) is another sharply skewed bridge with large transverse movements. The transverse movements are more than 8" (200 mm) at the east (fixed) end of the bridge. The bridge has 3 spans of continuous steel girders, and it has sustained severe deck damage, anchorage failure of supports, and spalling of the abutments due to these transverse movements as illustrated in Figs. 7 and 8. This bridge has been analyzed in some detail (10), and it appears that the transverse movement is caused by the expansion of the approach slab into the fixed end of the bridge. This again develops large transverse forces of the type depicted in Fig. 4, and has resulted in considerable damage to the bridge. Numerous other examples of large transverse movements in skewed bridges could be noted.

Curved bridges may also exhibit unusual thermal movements. The Sutton Creek Bridge shown in Fig. 9 in northwest Montana is a sharply curved 3 span continuous steel girder bridge with rocker bearings placed on the tangent of the arc. The bridge was constructed in the early 1970's. The total length of the 3 spans is approximately 577.5 ft (176 m) and so the thermal expansion should be significant. However, an inspection of the bridge bearings in 1988 showed that the bearings were in good condition and unlikely to be frozen, but there was evidence that the rocker bearings over the more slender piers had moved very little if any. This movement was accommodated by the bending of the piers. On the other hand, state inspectors observed that some of the bridge bearings had lifted approximately .25 in. (6 mm) above the piers amid great creaking and groaning on a very hot summer day shortly after the bridge was constructed. This movement is clearly unusual, and it represents a dramatic redistribution of load within the bridge since the bridge girders are 12 ft (3.5 m) high and are quite heavy. This bridge is being analyzed in detail, but the detailed results are not yet finished. However, the preliminary results indicate that the radial movements of the bridge are comparable to the tangential movements and they increase with increase in the internal resistance of the bearings to tangential movements. The results also suggest that the flexibility of the bridge piers is an important factor in the observed movements. This is an important observation, in that bridge engineers seldom consider the deflections of the piers and abutments when designing bridge bearings and expansion joints.

There is other evidence that curved girders frequently experience radial movements. Long curved bridges frequently use finger joints to accommodate expansion and contraction of the deck. The geometry of these joints is well suited for tangential movement, but is poorly suited for differential radial movements. A number of curved bridges in the US have had locked finger joints due to radial movements as illustrated in the photograph of Fig. 10. This locking action has resulted in considerable damage to some bridges (11). Guideways for bridge bearings have sustained similar damage due to unexpected movement in both skewed and curved bridges. Figure 11 shows a guideway that has lost its guiding key and has become misaligned due to these unexpected movements.

There are examples of unexpected temperature movements in straight, orthogonal bridges, but these examples are relatively less common than those for skewed or curved bridges. Figure 12 shows the spalling of a concrete pier produced by thermal shortening of a single span steel bridge girder. The girder rests on an elastomeric bearing with an anchor bolt in a slotted hole. The length of the slotted hole should accommodate the thermal movement. However, it appears that the slot was either of inadequate length or improperly positioned during construction, and spalling has occurred due to pull-out of the anchor bolts. This bridge has a very slight skew (well under 10°), but the skew does not appear to be a contributing factor. Straight, orthogonal bridges have sustained transverse movements due to orientation of the bridge or unusual local conditions. For example, an east-west oriented bridge in a northern latitude exhibits transverse movement due to the low angle of the sun causing direct radiation to the south steel girder. North-south oriented bridges at lower latitudes have exhibited similar problems due to morning or evening sun. There are also a large number of straight and curved bridges with bearing damage where the bearing damage can at least be partially attributed to thermal movements. These transverse movements place severe demands on the bridge bearings and expansion joints, and the demands clearly are not considered in their design. These observations indicate that thermal movements are a significant aspect of bridge behavior, and they cause serious problems if not adequately considered in the design and maintenance of the bridge.

PRELIMINARY ANALYSIS

A series of analyses are being performed to examine thermal movements. Some of the analyses are directed to specific bridges but others are being used for parameter studies. The analyses are not complete and they will be discussed in detail in a later paper. However, some preliminary results will be presented with this paper.

The first step in the analysis of thermal movement is the determination of the temperatures within the bridge as a function of time. Temperature calculations are based on 3 basic heat flow components, radiation, convection, and conduction. Radiation heat transfer consists of long distance transfer of heat from a hot body to a colder one. The sun heats the bridge on sunny days, and the bridge transmits radiant heat to the environment on cold nights. Convection is the transfer of heat from a solid (the bridge) to moving air or fluid. This

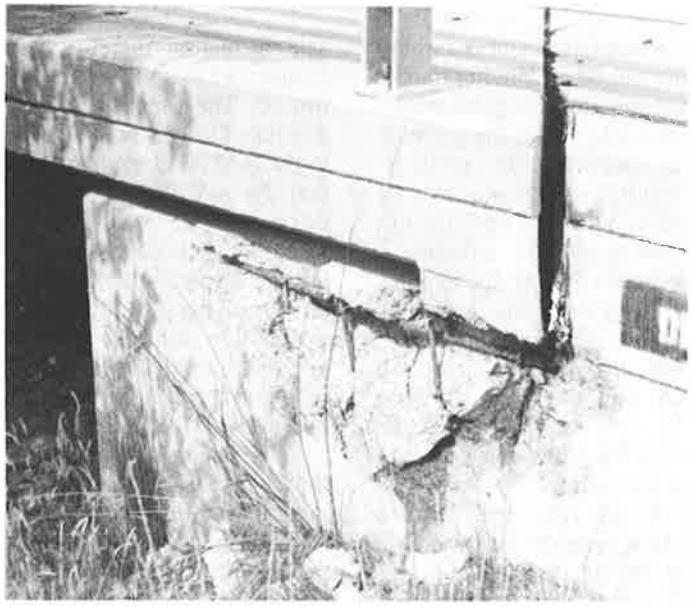

FIGURE 8 Severe spalling of concrete at abutment due to transverse thermal movement

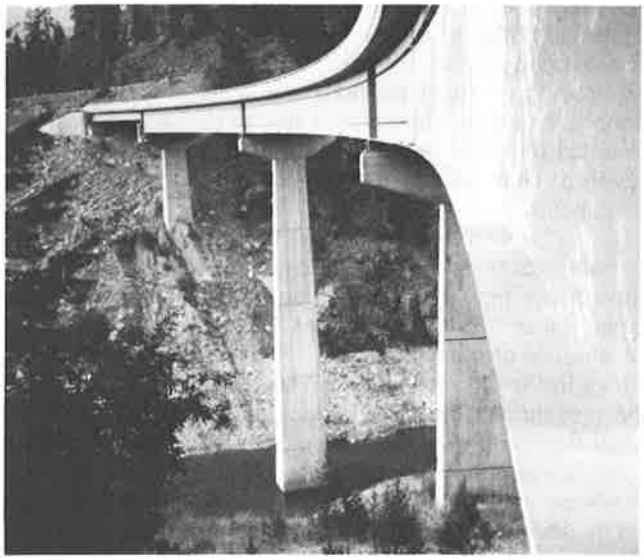

FIGURE 9 Curved steel girder bridge

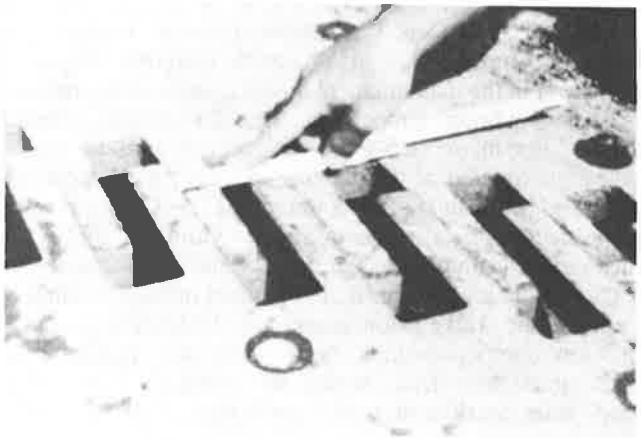

FIGURE 10 Locked finger joints on a curved bridge

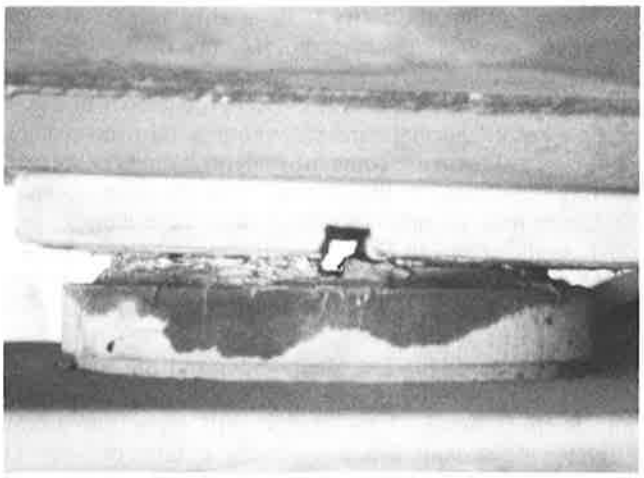

FIGURE 11 Misaligned guideway in a pot bearing due to transverse movement

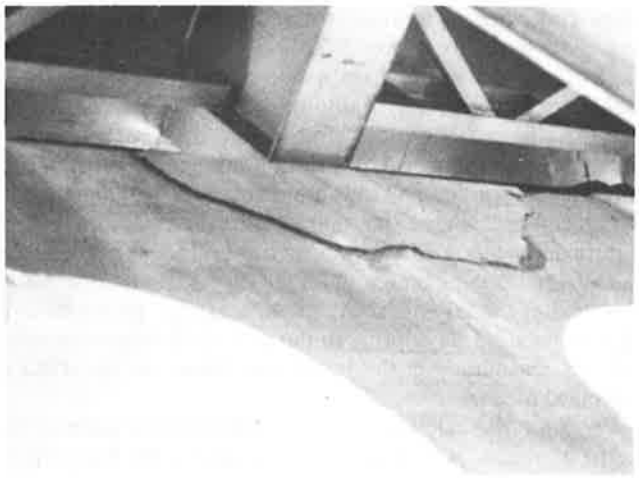

FIGURE 12. Spalling of a concrete pier due to thermal shortening of a steel girder

heat flow is influenced by the air temperature and is largely driven by the wind or by air currents caused by moving traffic. Convection tends to reduce the extreme high temperatures of the bridge during the summer, and it may lower the extreme low temperatures which occur during cold winters. Conduction is the flow of heat within the bridge, since all solid bodies are moving toward a uniform equilibrium temperature in the absence of other outside influences. Accurate determination of the temperature of the bridge requires consideration of all 3 components of heat flow, and it requires other information including the cloud cover, air temperature, wind speed, the angles of the sun, the orientation of the structure with respect to the sun, and the geometry and materials of the bridge.

The horizontal movements of the bridge are primarily related to the average bridge temperature. This average temperature is an integration of the true temperature distribution over the total bridge at a given time. The true distribution may have a minor effect on the thermal movements, but it has a major influence on the temperature dependent deflections and rotations of the bridge girders and the thermal stress in the structure. A series of temperature studies were performed for different bridge types at different locations to evaluate thermal movements. The bridge types included concrete box girders, multiple girder bridges with concrete T-beams, and steel girder bridges with composite deck slabs. The temperature distribution within the bridge may vary significantly with each of these different bridge types. Different bridge types also require different degrees of refinement in the mathematical model to accurately predict the differences in bridge temperature. One dimensional models are adequate for many slab-girder bridges. Figure 13 shows a typical distribution of temperature in a steel girder-composite deck bridge during a hot summer day. The steel girder experiences very little temperature variation through its thickness or depth unless there are unusual circumstances such as the sun shining on a portion of a girder or local shading of a portion of the bridge. Concrete box girder bridges or concrete girder bridges with thick beam webs may require a two dimensional heat flow model to accurately estimate the temperature distribution within the bridge. The more refined model is required since the heat lost by convection from the webs is neglected in a one-dimensional analysis, which results in the prediction of higher bridge temperatures. The air cell in a box girder acts as an insulator and little heat transfer occurs between the inner surface of the webs and the air cell. Hence, the bridge temperatures on a hot summer day are slightly higher for a box girder bridge than a concrete girder bridge. Figure 14 shows a typical temperature distribution within a concrete box girder bridge during a hot summer day. Three dimensional heat flow models are required only in very unusual circumstances where the temperature is expected to vary significantly along the length of the bridge. The heat flow calculations are dependent upon the initial conditions, and the time history analysis sometimes must be performed for approximately 3 days prior to the period of interest to assure that any inaccuracy in the initial conditions do not affect the computed results.

Similar calculations were performed for summer high temperatures and winter low temperatures for the three types of bridge at 11 different locations in the United States. The known air temperature, cloud cover, and local wind speed for the location of interest (12) were used for these conditions. The calculations therefore considered high and low temperature periods where good data was available rather than extreme limits. The ranges of the mean bridge temperatures were computed for the high and low conditions and were compared to the AASHTO temperature range. The comparison suggests that the AASHTO temperature range for steel bridges was fairly similar to that computed for the composite bridge elements. The composite steel girder bridge invariably had a larger temperature range than the concrete bridges, but the difference between the steel and concrete bridge temperature was often smaller than suggested by the AASHTO Specification. The calculations suggest that the AASHTO temperature ranges may be a bit small for some concrete bridges.

After the temperatures are defined, the movements in the bridge can be computed. A wide range of mathematical models were used in these calculations. Simple calculations, such as Equation 1, with the mean bridge temperature provided reasonable accuracy for many simple bridges. However, more refined models were needed in some cases. These more refined models considered factors such as the 3-dimensional deformation of the bridge, the stiffness of piers and abutments, the directional restraint and internal resistance of expansion joints and bridge bearings, the geometry of the bridge and the true temperature distribution. Skewed or curved bridges required the refined methods much more frequently than straight, orthogonal bridges. A few of the typical results will be noted for these bridges, and these results will be used to develop some general conclusions regarding thermal movements.

Skewed bridges frequently have more complex thermal movements and an elementary discussion of these movements may help understand the problem. Thermal expansion as defined in Equation 1, occurs in all directions in the absence of outside restraint. This is depicted for a skew bridge in Fig. 15. This figure shows that the idealized fixed end restraint acts only in the longitudinal direction, and as a result there is horizontal movement in all directions. In this unrestrained condition, there are no thermal forces, and the transverse movements are often of the same magnitude as the longitudinal movement. The greatest movement is across the long diagonal. Unfortunately the fixed end of a real bridge is nearly always restrained in both directions, and bearings at moveable supports are usually guided in the longitudinal direction. Further, the fixity is invariably applied at several points, and so these restraint points may work against one another in restricting thermal movement. These practical restraints prevent some of the movements shown in Fig. 15, and as a result thermal forces develop within the structure. The forces may increase some movements by concentrating the resulting movement to the location with the least resistance. The forces may become very large and cause damage to the bridge as illustrated in Figs. 3-8. It should be noted that the movements increase dramatically once damage initiates, because the bridge no longer has the elastic stiffness to restrain this component of movement.

Skew bridges are often wide, and the unrestrained movements are directly proportional to the bridge dimensions. Thus a short, wide skew bridge will have unrestrained transverse movements which are nearly as large or larger than the longitudinal movement considered in the bridge design, yet they are transverse to the normal bearing placement. Under these conditions the refined theoretical models predict

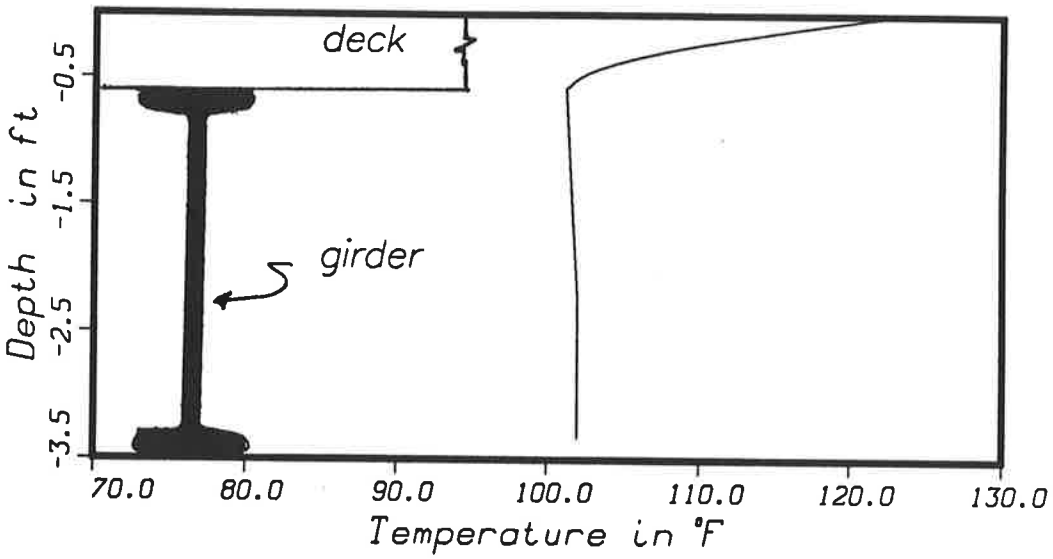

FIGURE 13 Computed temperature distribution on a composite steel girder bridge on a hot summer day

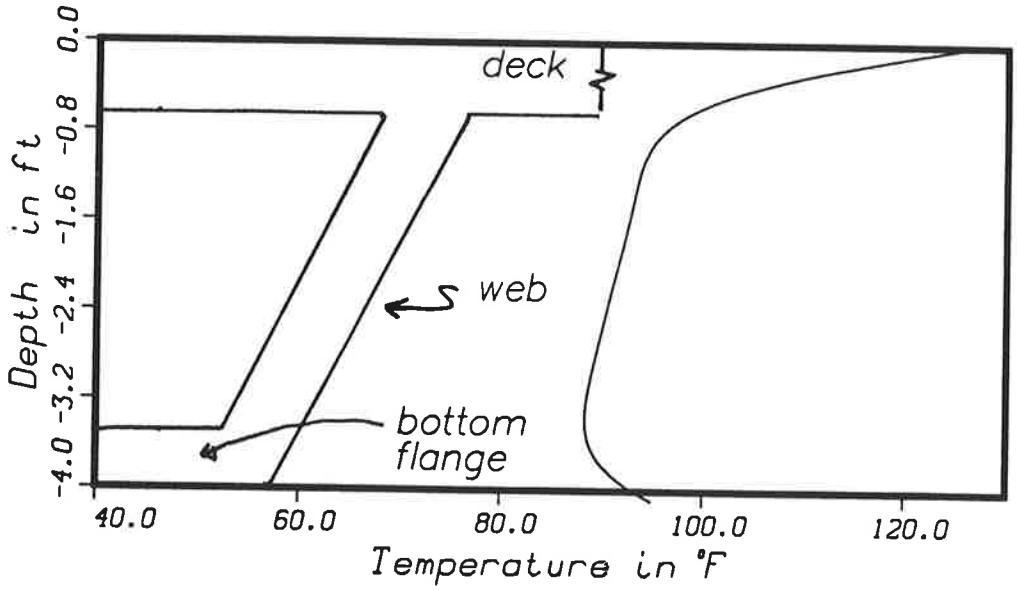

FIGURE 14 Computed temperature distribution on a concrete box girder bridge on a hot summer day

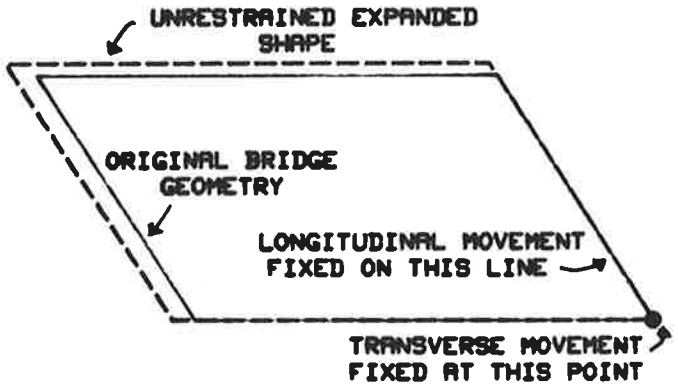

FIGURE 15 Thermal movement in an unrestrained skew bridge

considerable twisting of the bridge girders as illustrated in the lower part of Fig. 16 and an unexpected transverse movement of the bridge as illustrated in the upper part of Fig. 16. If the bridge has stiff diaphragms between girders, the torsional deformation of the girder will be prevented, and the transverse effects will move to other parts of the structure such as the piers or bearings. Increased stiffness results in increased restraint forces and this increases the transverse force component at all interfaces as depicted in Fig. 4. Unfortunately, these forces sometimes find a weakest link in the bridge. This transverse force is the driving mechanism in the damage to skew bridges in earlier figures. When the bearing resistance to longitudinal movement increases, the transverse movement in skewed bridges also increases.

Curved bridges may also illustrate a similar phenomenon. However, they have an additional complication in that engineers do not have a uniform way of placing the bearings. If the curved bridge is a line element with uniform temperature and rigidly fixed at one location, theoretical calculations show that the movement at free supports will be on the chord from the fixed point. However, theoretical calculations show that real bridges often do not obey this simplistic relation. Curved bridges always have at least two girders, and they cease to behave as a line element when this occurs. In addition, the fixed location of the curved girders is often at a pier which is not rigid, and as a result it may have thermal deflection which complicates the direction of movement. The net effect of these observations is that any directional guiding devices at moveable bearings of a curved bridge are almost certain to be oriented in a less than optimal direction. A study conducted on a three span, four girder curved bridge predicted the thermal movements shown in figure 17. The dashed outline in figure 17 is the undeformed shape of the bridge. This figure shows that there is considerable movement of the bridge even at the "fixed" support due to deflection of the piers. The radial movements that would be obtained by orienting the bearings along the chord of this bridge were slightly larger than those obtained by orienting the bearings along the tangent. Thus, guiding devices on curved bridges must be relatively strong or the piers and supporting elements must be relatively flexible if all damage is to be avoided.

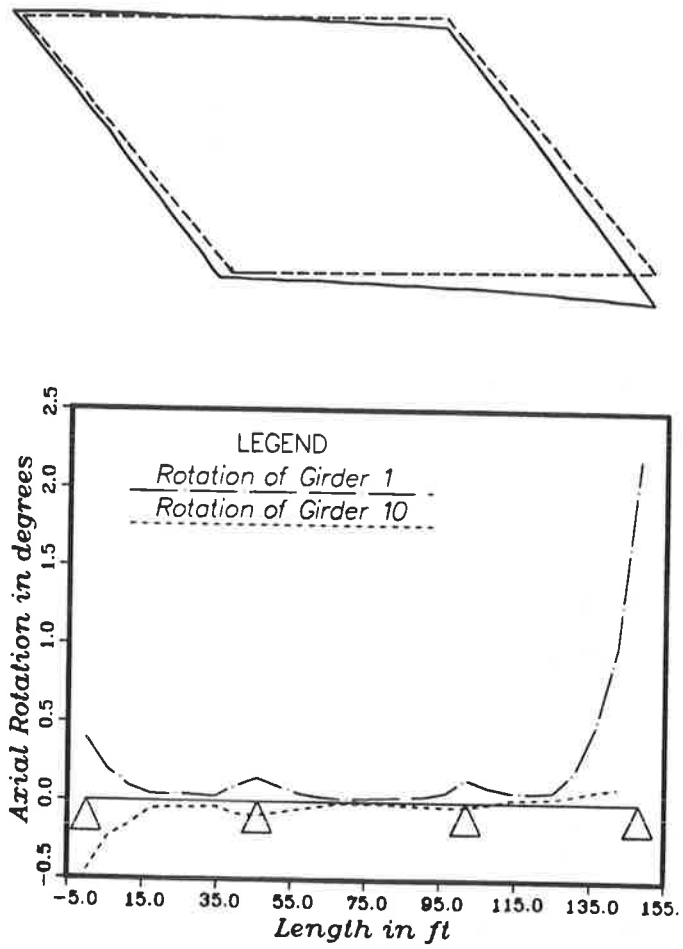

FIGURE 16 Transverse displacements in a skew bridge

PRACTICAL IMPLICATIONS

This paper has provided a brief review of thermal movements observed in real bridges, and it has summarized the results of theoretical studies to examine this behavior. The results are not complete, but a few preliminary observations which have real practical significance can be noted.

1. The present AASHTO temperature ranges for thermal movement calculations appear to be calculated annual temperature range for steel bridges, but they may be a bit small for some concrete bridges. However, concrete bridges are usually designed for additional movements due to creep and shrinkage, and this additional movement allowance probably accounts for any deficiency in the thermal movement calculations.
2. The simple method of predicting thermal movements in Equation 1 is quite reasonable for straight, orthogonal bridges, but more refined calculation methods are needed for some special bridges such as some skewed or curved bridges.
3. Skew bridges with sharp skew angle and with a width that is relatively large compared to their length are most likely to have significant transverse movements and forces and require more refined calculations.
4. Curved bridges with a large width or a tight radius are more likely to require refined thermal movement calculations.
5. Curved bridges which behave as line elements with uniform temperature changes provide a direction of movement which is on a chord from the fixed point of the bridge. However, real curve bridges never precisely satisfy these conditions and as a result always exhibit some other additional thermal movement.
6. The direction of movement for skewed and curved bridges is an element of concern in items 3, 4, and 5, and there is some wisdom in using unguided moveable bearings wherever possible on these bridges.
7. Structural problems caused by thermal movements in bridges are frequently related to lack of maintenance of the bearings and expansion joints or to inadequate control during the construction process. These observations

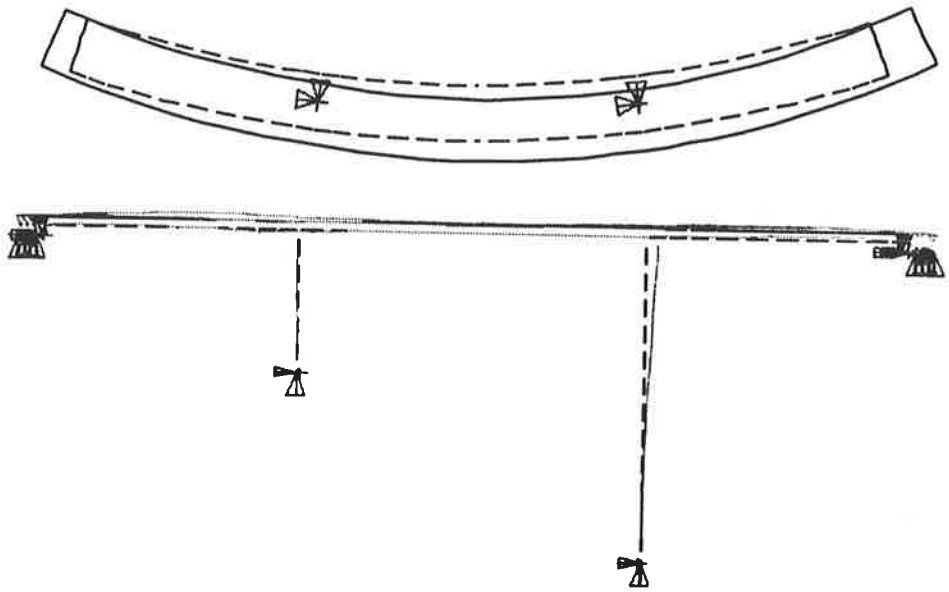

FIGURE 17 Thermal movements of a curved bridge

suggest that maintenance and construction supervision are particularly important in curved and skewed bridges.

8. The uncertainty of the direction of movement in some curved and skew bridges provides increased incentive for the engineer to use integral construction or other forms of jointless construction. However, these alternate methods are not always the panacea that they may seem to some engineers because these alternate structures are often highly restrained and they may attract much larger forces. Thus, they will not always solve the problems associated with thermal movements in complex bridges.

SUMMARY AND CONCLUSIONS

This paper has described some practical observations on thermal movement behavior of bridges. The work is in progress, and further results will be presented in a later publication. Nevertheless, this paper has some practical results which should be useful to the engineering profession. The results are based primarily on analytical studies. These analyses have been correlated to physical observations of bridge behavior, but additional experimental correlation is needed to verify the analytical results.

ACKNOWLEDGEMENTS

This research was funded by National Science Foundation Grant CES-8714894, with Dr. John B. Scalzi as the Program Manager. The authors gratefully acknowledge this support. The authors also appreciate the advice and information provided by engineers of the Montana, Wyoming, and Virginia Departments of Transportation.

REFERENCES

1. *Standard Specification For Highway Bridges, 14th Edition*, Washington. AASHTO, D.C., 1989.
2. E. Wasserman. "Jointless Bridge Decks," *Engineering Journal*, AISC, Vol. 24, No. 3, 1987.
3. L. Greimann and A. M. Wolde-Tinsae. "Design Model for Piles in Jointless Bridge," ASCE, *Journal of Structural Division*, Vol 114, ST6, June 1988.
4. R. E. Abendroth and L. F. Greimann. "Rational Design Approach for Integral Abutment Bridge Piles," TRB, *Transportation Research Record 1223*, Washington, D.C., 1989.
5. B. A. Boley and J. H. Weiner. *Theory of Thermal Stress*, John Wiley, New York, 1960.
6. H. S. Carslaw and J. C. Jeager. *Conduction of Heat in Solids*, Oxford University Press, Fair Lawn, NJ, 1959.
7. M. Emerson. "Thermal Movements in Concrete Bridges - Field Measurements and Method of Prediction," *ACI Publication Sp-70*, Vol 1. Detroit, MI, 1981.
8. M. Emerson. "Bridge Temperatures for Setting Bearings and Expansion Joints," *TRRL Report LR561*, Dept. of Transport, Crowthorne, England 1973.
9. M. Emerson. "Bridge Temperatures Estimated from Shade Temperatures," *TRRL Report LR696*, Dept. of Transport, Crowthorne, England 1976.
10. S. Moorty and C. W. Roeder. "Thermal Movements in Skewed Bridges," *Proceedings*, International Conference on Short and Medium Span Bridges, Toronto, Canada, 1990.
11. G. Busch. "Review of Design Practice and Performance of Finger Joints," *Joint Sealing and Bearing Systems*, ACI Publication 94, Detroit, MI, 1987.
12. *Climates of the States*. 2nd Edition, Gale Research Co., Detroit, MI 1974.

Finite Element Modeling, Analysis, and Design of Highly Skewed Post-Tensioned Concrete Bridges

SEETHA V. RAMAIAH, N. ALI SEYEDMADANI, AND OSCAR A. OLIDEN

Skewed bridges have been designed for many years using approximate methods. Most of these methods do not account for the high torsional moments inherent in a skewed structure. More exact methods of analysis are time consuming and the stringent budgets do not permit the design consultant the luxury of using these more elaborate and exact methods. Recently, several highly skewed post-tensioned box girder bridges have been studied and designed by Parsons Brinckerhoff Quade & Douglas, Inc. (PBQ&D) in Tempe, Arizona. The high skew angle of these highway and railroad bridges with very heavy Live Loads was caused by the restricted right-of-way limitations and necessitated the use of more exact methods and/or dependable methods of analysis for these structures. Five skewed bridges were analyzed, by conventional plane frame analysis and by two different programs, using a finite element method of analysis. Two of these bridges were compared to verify the designs based on three dimensional grid analysis. In the preliminary stage the structures were sized and preliminary forces obtained by using CaltranS "Frame System" (5) and then the finite element models were generated in order to gain a better understanding of the effect of skew bending on the deformations, stresses, support reactions, and torsional moments.

Traditionally skewed bridges were analyzed and designed considering the longest length between the supports as the actual span length. Conventional wisdom assumed that such a conservative approach would result in a very safe design. The means or the methods to do a more precise analysis and design did not exist. The advent of computers and the implementation of finite element methods of analysis, have given the means to take a closer look at the behavior of the skewed bridges.

THE BASIC DIFFERENCE - SKEW BENDING EFFECT

What makes the behavior of skewed bridges so much different than from that of non-skew bridges? To explain this, it is necessary to take a closer look at the basic geometry and framing of a skewed concrete box girder bridge.

In any bridge, the principal bending occurs along the shortest axis between the supports, which happens to be perpendicular to the axis of supports. The longitudinal axis of a bridge is defined as the axis which is directed through the centriod of the cross section, and it is usually parallel to the center of the roadway or railroad.

In a non-skewed bridge the supports are along the transverse axis which is perpendicular to the longitudinal axis of the bridge. The principal bending of the girders and the whole structure occurs about the transverse axis parallel to the supports, along the longitudinal axis. This behavior has always dictated the direction of the girders in a concrete box girder bridge to be parallel to the longitudinal axis.

In a skewed bridge, the supports are not along the transverse axis. They are located along an axis skewed to the transverse axis of the bridge. The longitudinal axis of the bridge remains the same. The principal bending occurs about an axis parallel to supports along a new longitudinal bending axis which is perpendicular to the axis of the supports. This new longitudinal bending axis is skewed to the longitudinal axis and is almost parallel to the shortest distance between the supports. Depending on the length to width ratios and the location of piers and abutment supports, this longitudinal bending axis comes close to the line joining the supports at the two obtuse corners. The bending effects caused in a skewed bridge due to the principal bending along this new longitudinal bending axis is called "skew bending" and its effects are referred to as skew bending effects. This principal bending along the new longitudinal bending axis must be carried by the girders or webs, by resolving it along the longitudinal and transverse axis of the structure.

For a proper understanding of the design requirements, it is essential that the principal bending moment along the modified longitudinal axis be resolved to a bending moment along the longitudinal axis and a torsional moment about the longitudinal axis. The torsional moments caused by skew bending effects, in turn, cause an uneven distribution of horizontal and vertical shears at a section normal to the longitudinal axis of the bridge. This uneven distribution of horizontal and vertical shears, affects the location of maximum moments, produces large variations in support reactions and the post-tensioning forces which are normally negligible in a non-skewed bridge result in uplifts at certain supports

This study indicates that besides uplift reactions at supports, torsional moments are the principal concern in the design of skewed concrete box girders because they cause diagonal tension in exterior faces of the box and uneven variation of shear and support reactions. There are large deviations in magnitude and location of maximum positive moments, which complicate the location of the post-tensioning paths. The large variations in support reactions bring out the need to pay more attention to design of bearings.

Five highly skewed bridges included in the three bridge sites listed below were part of the Aviation Project in Tucson Arizona and are the subject of this paper:

1. Southern Pacific railroad overpass at Broadway (SPRR bridge); a two span structure, with skew angles of 37 degree at the pier, 43 degrees and 51 degrees at abutment supports. Figures 5 thru 11.

2. Council/Toole Avenue bridges over Broadway. Twin two span, variable depth structures with skew angles of 53 degrees at pier supports and 66 degrees at abutment supports. Figures 12 thru 18.

3. Euclid/Park Avenue overpass structures at SR 210. Twin two span structures with skew angles of 60 degrees at pier supports and 70 degrees at abutment supports. Figures 19 thru 20.

TOOLS AVAILABLE FOR ANALYSIS AND DESIGN

The following tools were selected for a closer evaluation from the scores of material available in the professional design field.

Parsons Brinckerhoff Quade & Douglas, Engineers, Architects and Planners, Tempe, Arizona

CALTRAN Bridge Memo for Designers 15-1

This internal memo to designers (1) by California Department of Transportation, basically gives charts for increasing the shears in the girders of bridges up to 45 degree skew, beyond which it recommends a more exact analysis, by using finite element programs like CELL4 or STRUDL. This memo addresses basically increasing the shear in girders which is only one of the many problems involved in the design of skewed bridges.

Cell4 Program

It was developed at University of California, Berkeley with the cooperation of California Department of Transportation, under the supervision of Professor A.C. Scordelis (2). CELL4, based upon the finite element method, is particularly suited for the analysis of post-tensioned box girder bridges of constant depth. The finite elements used are a combination of plane stress element (Q8D11) and plate bending element (Q19). The combination of these elements with appropriate transformations can take into account curved geometry and sloping of the exterior webs. The resulting element has 5 degree of freedom (DOF) per node in the local coordination system which, when transformed to global coordinate system, becomes 6 DOF.

MDC STRUDL Program

MDC STRUDL program (3), one of the commercially available programs that is widely used across the country, was used by PBQ&D for analysis and design of the hourglass shaped urban interchange structures for 7th Street and 7th Avenue over I-10 in Phoenix.

The structural element used to model these bridges is called "PBSQ2", a four noded element with 6 degrees of freedom developed by McDonnell Douglas Architectural Engineering of Construction Systems Company. This element is capable of carrying in plane loads (plane stress) and bending loads (plate bending) and was found suitable to model the top slab and bottom slab. To model the webs, a combination of "PBSQ2" elements and structural bending members were used. This combination was needed in order to simulate the behavior of the box girder. The curved shell element "SIPQ" with five DOF could have been used in place of the combined elements for the girder. But it was not used at the time, because of prohibitive computer costs.

The 7th Street bridge model consisted of 1800 joints, 1143 elements and 337 members.

3-Dimensional Grid Analysis Program

In his book "Bridge Deck Behavior", Edmund C. Hambly (4) explains the procedure for developing a grillage grid model. The methodology seems to have limitations in simulating the torsional rigidity of the box girder. In view of this, grid analysis was not favored. However there was an opportunity to compare the results of the finite element model with those of the grid analysis, as part of a design review on Euclid/Park Structures.

COMPARATIVE TESTS

The CELL4 program was selected for use in view of the savings offered in modelling, computer time, ease of obtaining sectional forces, moments and automatic generation of equivalent loads for post-tensioning forces. In order to ascertain and validate the results of CELL4 program two identical models were tested using CELL4 and STRUDL programs. They were both skewed structures, one a single span structure and the other a two span structure. Figure 1 and 3 represent the CELL4 and STRUDL models respectively for the single span bridge. Figures 2 and 4 represent CELL4 and STRUDL models respectively for the two span bridge. Figures 1 to 4 also illustrate the Dead Load (DL) reactions.

The differences between results of the two models though not exactly the same were within reasonable limits of accuracy required for design. The maximum stresses, moments and deflections were within 5% of each other. The model in Figure 2 has a thicker pier diaphragm than the model in Figure 4, which accounts for some of the differences in the reactions. The only results that have a wide variation are the two uplift reactions at the acute corners (see Figures 1 and 3) and needs further evaluation.

The closeness of results from both the programs gave us sufficient confidence to use CELL4 on all bridges except the Council/Toole Avenue bridge, which had a variable depth. This required STRUDL program to model the Council/Toole Avenue bridges.

The CALTRANS Frame System (5) Program was used to obtain order of magnitude of the post-tensioning forces to be applied and the cable path. Various versions of this program with different names are being widely used by design consultants in the west coast.

SOUTHERN PACIFIC RAILROAD (SPRR) BRIDGE OVER BROADWAY

The SPRR bridge is a two span structure with 3 railroad tracks and one highway maintenance road. Figure 5 shows the general geometry of the bridge and the framing of the girders and centerline of the tracks.

Modeling

Having gained confidence in the results of CELL4 program, the model for the SPRR bridge was created. The finite element discretization mesh is shown in Figure 6. In order to increase the accuracy of the results in the finite element analysis, the aspect ratio of the elements was kept to 1 in critical areas and to 2 in noncritical areas. The finite element model for this structure has 1428 joints and 1818 elements.

Discussion of Results

Dead Load Reactions

Figure 7 shows the reactions due to DL at abutment supports and piers. Note the variations in reactions from one end of the abutment to the other. The variations in support reactions, location of maximum moments and the magnitude of these moments and stresses was surprising compared to what one normally expects from a conventional approach. For bridges with this span range, the Live Load (LL) from the railroad are about twice the Deal Load (DL), where as in the case of highway LL effects are about a third of the DL. Figure 8 shows the points of maximum moment. Note the fluctuations in points of maximum moment.

Maximum Moments

In a two span structure, with roller supports at each end, the points of maximum moment would usually be located at 40% of the span from the exterior roller supports. In span 1, the location of the points of maximum moments vary from 32 percent in girder 1 and to 54 percent in girder 8 (Figure 8). This effect is reversed in span 2. The location of the points at which maximum moment occurs vary from 48 percent in girder 1 to 32 percent in girder 8. These variations clearly demonstrate the skew bending behavior and the inherent torsional moment and its effect on the behavior of the structure. The situation was the same in span 2 except it was in reverse order. Note also the fluctuations in the values of maximum moments in different girders.

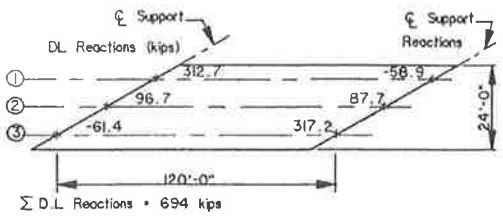

Fig. 1 Single Span CELL4 Test Model

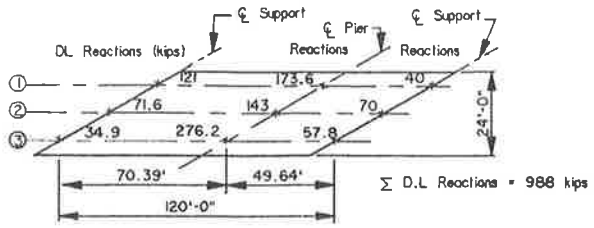

Fig. 2 Two Span CELL4 Test Model

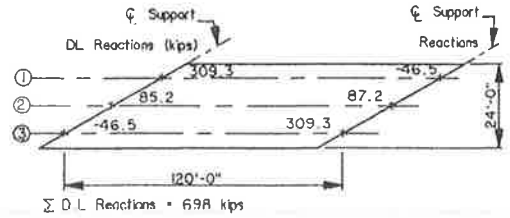

Fig. 3 Single Span STRUDL Test Model

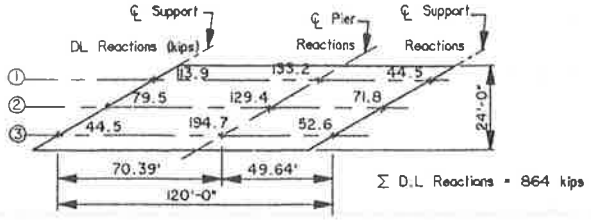

Fig. 4 Two Span STRUDL Test Model

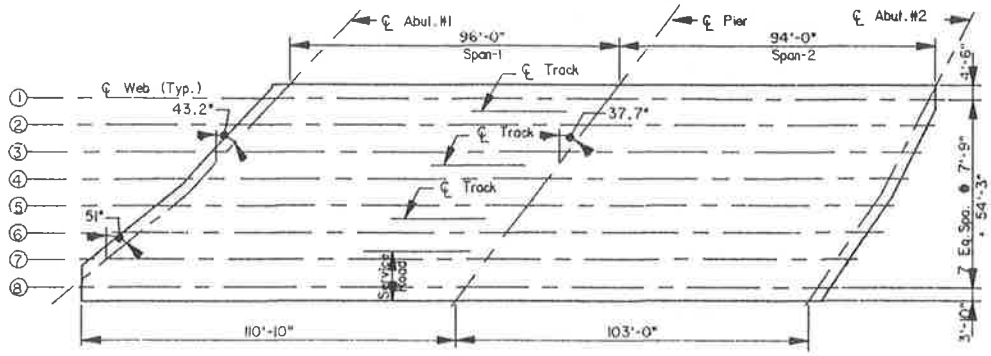

Fig. 5 Sectional Framing Plan - SPRR Bridge

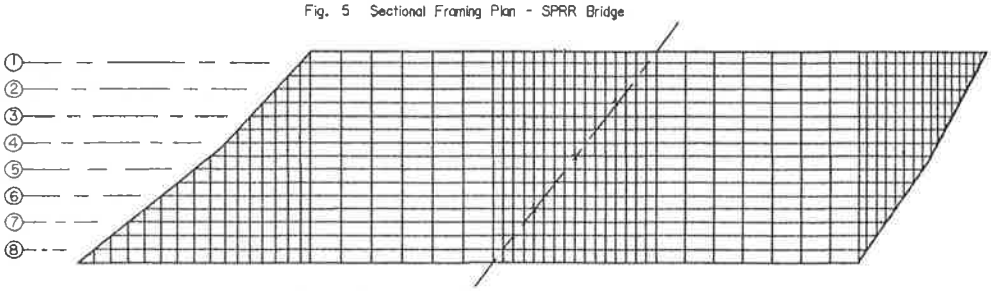

Fig. 6 Finite Element Discretization Mesh - SPRR Bridge

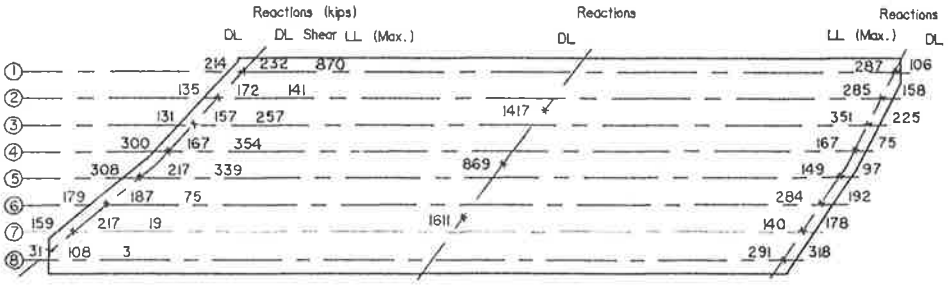

Fig. 7 Dead Load Reactions and Shears - SPRR Bridge

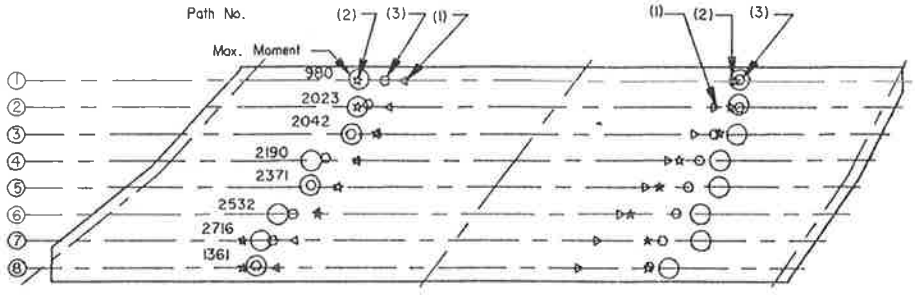

Fig. 8 Points of Max. Moments and Sags in Tendon Paths - SPRR Bridge
Max. D.L. Moments (Ft.Kips) in Span (1)

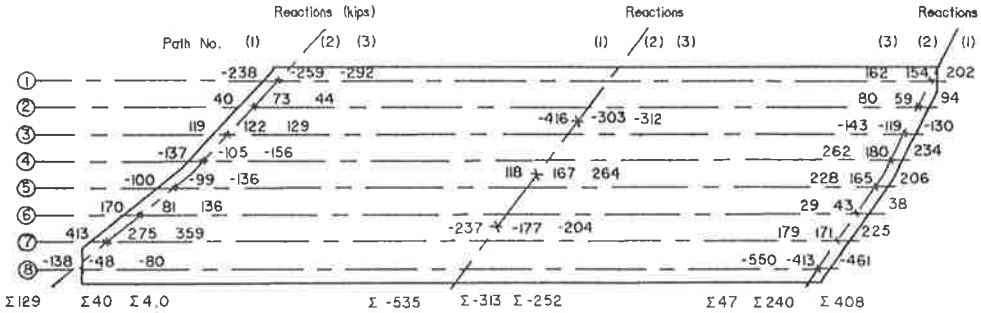

Fig. 9 Reactions Due to Alternative Post Tension (P/T) Paths - SPRR Bridge

UNBALANCED P/T REACTIONS

Σ = 2.0 (1)

Σ = -33.0 (2)

Σ = -1.0 (3)

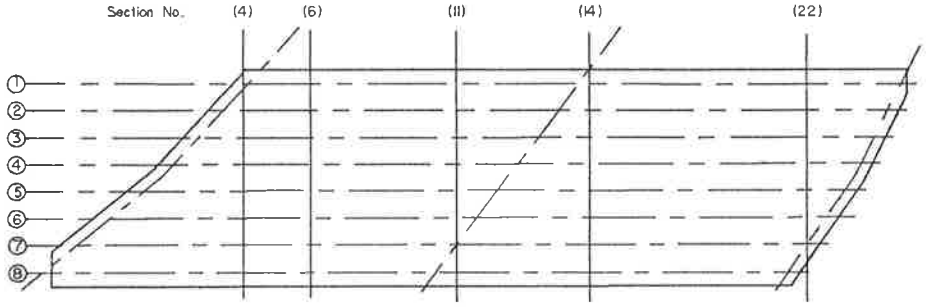

Fig. 10 Torsional Section Plan - SPRR Bridge

Table 1 Section Torsional Moment and Shear for SPRR Bridge

SECTION	4		6		11		14		22	
	Torsion	Shear	Torsion	Shear	Torsion	Shear	Torsion	Shear	Torsion	Shear
DL	-12236	-250	-12063	151	235	739	-9215	-997	-7763	538
DL+SDL	-18729	-414	-17537	168	1171	1088	-14958	-1486	-9623	756
DL+SDL+LL	-38788	-1020	-31298	-22	3768	1674	-12305	-1604	-7176	664
P_i =3910 Path 1	17327	774	21967	147	-10517	-1630	25256	2071	12488	-1011
P_i =3520 Path 2	22371	735	26315	-107	-8033	-1709	13162	1924	14948	-1084
P_i =3520 Path 3	19975	651	24566	-60	-10241	-1635	15708	1950	14945	-1010

Units Are Foot-kips and kips

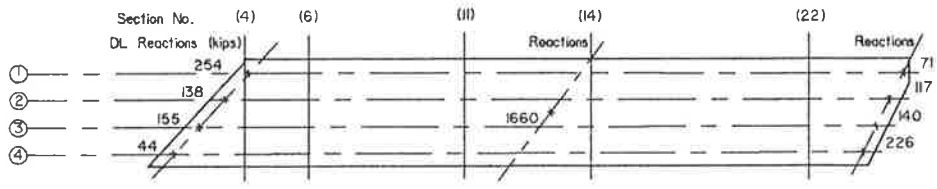

Fig. 11 Sectional Framing Plan - Half of SPRR Bridge

Table 2 Section Torsional Moment and Shear for Half of SPRR Bridge

SECTION	4		6		11		14		22	
	Torsion	Shear	Torsion	Shear	Torsion	Sheaf	Torsion	Shear	Torsion	Shear
DL	-2199	-296	-2257	-108	-2273	416	-1599	-586	-1585	169
DL+SDL	-3883	-483	-3845	-179	-3485	662	-2853	-948	-2270	266
DL+SDL+LL	-9679	-1161	-9900	-440	-8749	1280	-2281	-1043	-1709	173

Units Are Foot-kips and kips

Initially the thought was to reverse this trend by applying the equivalent upward post-tensioning forces over a longer length of girders, by varying the location of sag points. The supplemental design criteria by SPRR (6) required on having 50 psi to 200 psi compression under any loading condition. This made the location of sag points and inflection points in the tendon path more difficult, since the secondary moments due to post-tensioning are largely influenced by their locations. The skew effect made it even harder to estimate the effect of the sag and inflection points on secondary moments. Three post-tension paths were investigated, varying the sag points and are illustrated in Figure 8.

Post Tensioning Cable Path

Path No. 1: Initially path No. 1 was tried, to determine the effect of post-tensioning. The sag point was at 50 percent in Girder No. 1 and varied linearly to 60 percent at Girder No. 8. We anticipated this path to help lift girders 1 and 2 in span 1. It did not give the anticipated results. Instead it resulted in large tension stresses in the bottom slab near the piers.

Path No. 2: The tendon paths were moved to coincide with the location of points of maximum moments in girders 1, 2, 7, and 8 and was kept the same in the remaining girders. The results of path No. 2 showed an improvement over path No. 1, with some small compressive stresses (150 psi) in the bottom slab near the pier support.

Path No. 3: Finally path No. 3 was tried with a view to obtaining higher compressive stresses near the pier supports. Note the location of sag points vary from 41 percent at girder 1 to 54 percent at girder 8. This path gave the required results with compressive stresses in the bottom slab near the pier exceeding 250 psi.

Figure 9, shows the support reactions induced by the three paths. Note the reversals in support reactions at certain locations. This did not happen with the DL of the structure. This in a way indicates that the concept of load balancing method may not eliminate the problems of torsion and the large variations in support reactions induced by the DL and LL on the structure.

Note the post-tensioning reactions (Figure 9) exceed the DL reactions (Figure 7) at the exterior supports and result in uplift. The bearings at these locations were designed for uplift capacities. The critical section for torsion is section 4 Figure 10. The post-tensioning force does have the beneficial effect of reducing the torsion due to DL and LL as evidenced by figures in Table 1. Note also the reversal in torsion for certain LL conditions at other non-critical sections.

Torsional Moments and Effect of Width/Length Ratio

Figure 10 shows the location of the five sections used for computing torsional moments and shears. The torsional moments obtained due to DL, LL, and the three different post-tensioning paths are shown in Table 1. Note that the DL torsion moments are huge and are almost constant between the closest edges of the abutment and pier supports. It was thought that one of the reasons for this huge torsional moment might be the large width of the structure, causing skew bending effects. So the structure was cut by half and a finite element model was run using CELL4 program. The results of this model are shown in Figure 11 and Table 2. Comparison of results in Table 1 and Table 2 indicate that the total torsion was reduced to 35 percent of the full bridge. The corresponding section resisting torsion was reduced to 38 percent of the full bridge. Also the torsion capacity of the structure was reduced to 32 percent of the full bridge.

The steel required for torsion based on Thomas T. C HSU (7), ACI building code (8), (9) and ACI - analysis of structural systems for torsion (10) was found to be the same for both bridges. This indicates that the length to width ratios have practically very little effect on the amount of torsion steel required in a skewed box girder bridge. Since there was no apparent gain in cutting the structure by half, it was decided not to break the structure and to use the full model for verifying the LL and post-tensioning loads.

COUNCIL/TOOLE AVENUE BRIDGES

The extremely tight vertical clearances imposed by the roadway profiles, dictated the use a two span structure with a variable depth. The skews at the abutment and pier supports for the east bound (EB) and west bound (WB) lanes varied by a large amount and introduced a kink in the pier diaphragm. As a result it was decided to have two separate structures, one for east bound and the other for the west bound. Both the structures were analyzed separately and the results of the east bound (EB) structure are presented here.

Figure 12 shows the geometry and framing of girders for the EB structure. Note the extremely high skews varying from 45 degrees to 66 degrees. Figure 13 shows the typical longitudinal section, with the parabolic haunch.

Modelling

Since CELL4 program did not have the capability of analyzing variable depth box girders, it was decided to model this structure using the MDC STRUDL program. The finite element called "SIPQ", available in McAuto STRUDL library, was used in this model. The "SIPQ" is a quadrilateral curved element with four corner nodes and four midside nodes with five degrees of freedom (DOF), three of which are linear DOF and two are rotational DOF about a nodal local axis. This model had a total of 1482 elements and 4119 joints. The aspect ratio was kept to 1 in critical areas and to 2 in other areas. The design of SPRR bridge was slightly ahead of this bridge, which enabled to use the experience gained and avoid some of the iterations we went through earlier on.

Discussion of Results

Reactions and Moments

In Figure 14 are shown the locations of points of maximum moment and the DL support reactions. The support reactions are more than 100 percent different at certain locations. Note the heavy reactions at the top left hand corner and the bottom right hand corner supports. The line joining these points, almost coincides with one of pier supports. Though it is not perpendicular to the lines of support, it seems to act like the principal longitudinal bending axis of the structure. The reaction at this pier is more than twice the reaction at the other pier and greatly affects the design of the cantilever pier diaphragm. The effects of skew bending and torsion are again very evident, as illustrated in Table 3. As in the SPRR bridge, Figure 14 illustrates the enormous fluctuations in the location of points of maximum moments. The distance from the center of abutment to these points varies from 25 percent of span for girder 1 to 55 percent for girder 5, which is very different than the usual 40% of span for a two span structure with roller supports at the ends.

Cable Path

Two post-tensioning paths were tried. The first one was with sag points of cable path coinciding with the location of maximum moments. This path did not help in balancing the stresses due to DL and LL. Also the required upward deflection in span 1 was not obtained.

The second post-tensioning path was modified as shown in Figure 15, locating all the sag points at 40 percent of the span from the abutment in span 1 and at 30 percent of the span from abutment in span 2. The span 2 being shorter, the amount of sag in span 2 was smaller than in

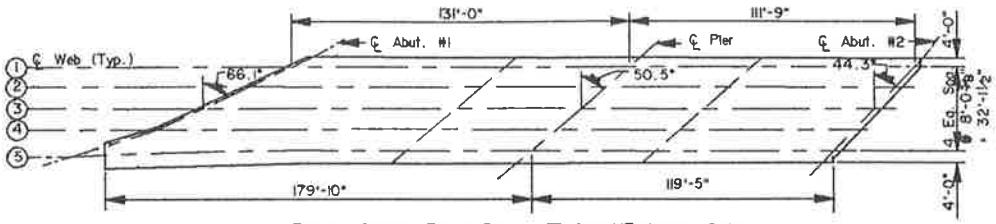

Fig. 12 Sectional Framing Plan for EB Council/Toole Ave. Bridge

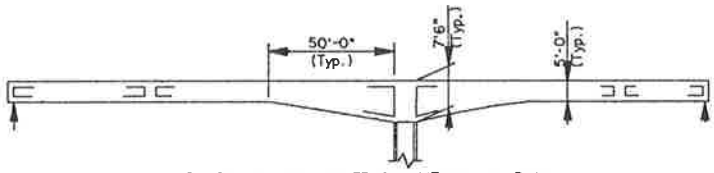

Fig. 13 Typical Section for EB Council/Toole Ave. Bridge

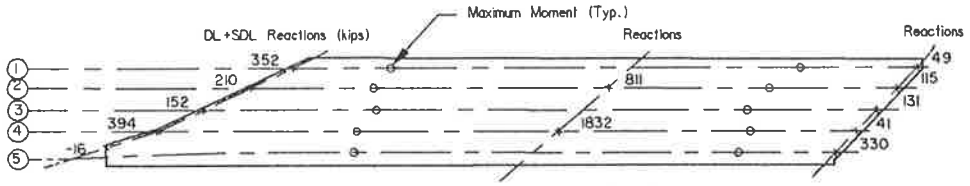

Fig. 14 Dead Load Reactions and Points of Max. Moments for EB Council/Toole Ave. Bridge

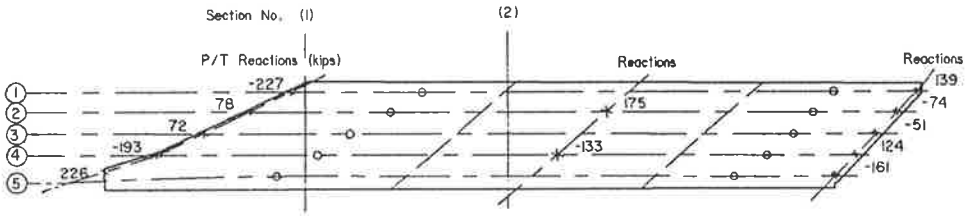

Fig. 15 Points of Max. Sags in Tendon Paths for EB Council/Toole Ave. Bridge

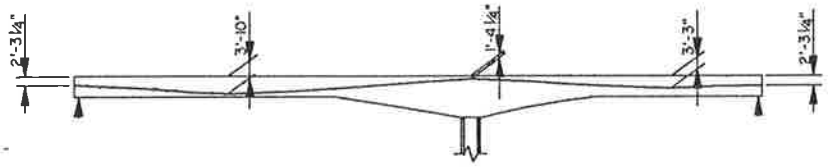

Fig. 16 Typical Tendon Path for EB Council/Toole Ave. Bridge

Table 3 Section Torsional Moments for EB Council/Toole Ave. Bridge

SECTION	1	2
DL	-7370	-7585
DL+SDL	-9167	-9435
DL+SDL+LL	-11563	-11893
P/T	6210	4994

Units Are Foot-kips

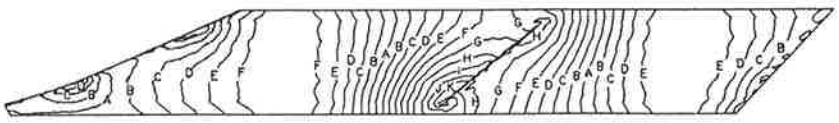

Units Lbs/In^2

A 0.000E+00
B 7.806E+01
C 1.561E+02
D 2.342E+02
E 3.122E+02
F 3.903E+02
G 4.683E+02
H 5.464E+02
I 6.245E+02
J 7.025E+02
K 7.806E+02
L 8.586E+02
M 9.367E+02

Fig. 17 Stress Contours Top Slab (DL) - EB Council/Toole Ave. Bridge

Units Lbs/in^2

A 0.000E+00
B 1.174E+02
C 2.348E+02
D 3.522E+02
E 4.696E+02
F 5.870E+02
G 7.044E+02
H 8.218E+02
I 9.392E+02
J 1.057E+03
K 1.174E+03
L 1.291E+03
M 1.409E+03

Fig. 18 Stress Contours Bottom Slab (DL) - EB Council/Toole Ave. Bridge

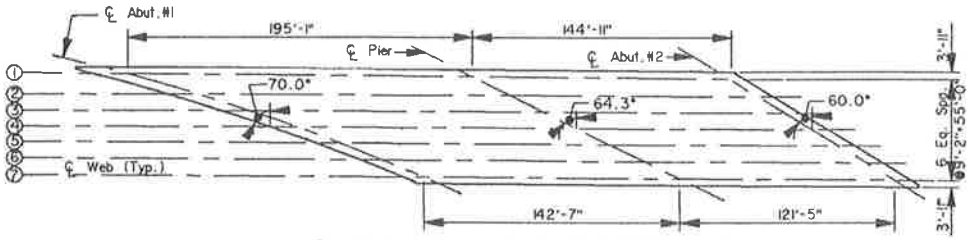

Fig. 19 Sectional Framing Plan for WB Euclid/Park Ave. Bridge

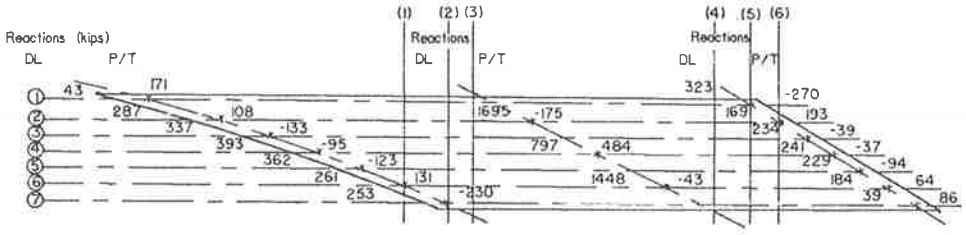

Fig. 20 Sectional Framing Plan for WB Euclid/Park Ave. Bridge

Table 4 Section Torsional Moments for WB Euclid/Park Ave. Bridge

SECTION	1	2	3	4	5	6
	Torsion	Torsion	Torsion	Torsion	Torsion	Torsion
DL	10640	21828	21971	16780	16653	7085
DL+SDL	12690	26058	26209	19900	19757	8323
DL+SDL+LL	15396	31694	31632	24403	24397	10324
P/T	-11273	-23392	-17097	-13341	+18965	-8340

span 1. Figure 16, illustrates the cable path with reduced eccentricity in span 2, to help lift off span 1. This was done with a view to help the upward deflection in span 1. The reactions due to post-tensioning force are shown in Figure 15 and the torsional moments are listed in Table 3. These results have a pattern similar to the ones obtained for the SPRR bridge using CELL4.

Stress Contours

Stress contours were plotted for several cases of loadings, DL, LL and post-tensioning forces. Figure 17 shows the stress contours in the top slab and Figure 18, the stress contours in the bottom slab for the DL of the structure. Note the concentration of stress contours at the bottom left hand edge and top right hand edge of pier support line. These stress contours really helped us to evaluate the critical points for checking the stresses and to arrive at details of the post-tensioning path for each girder.

EUCLID/PARK STRUCTURES

These are two highway bridges with large skews varying from 60 degrees to 70 degrees, similar to Council/Toole Avenue bridges. Parsons Brinckerhoff was involved in the review of final design for these two structures. The design was based on a 3-dimensional grid analysis. CELL4 program was used for the design verification. The basic geometry of one of the structures is shown in Figure 19. The finite element model consisted of 1,116 joints; and 1,370 elements. The aspect ratio of elements was 1 in critical areas and 2 in less critical areas.

The DL reactions and post-tensioning reactions are shown in Figure 20.

Load Balancing Method

The load balancing method is explained in design of prestressed concrete structures by T.Y. Lin (11). By load balancing, the moments due to post-tensioning are made equal the maximum moment due to DL and LL. In load balancing the axial stress effect of the post-tension force is neglected. As such, this method yields uneconomical design resulting in excessive post-tensioning force.

The design of this structure was based on the assumption that by using the load balancing method for post-tensioning, the skew bending effects of DL and LL will be reversed, leaving the structure without any torsional moments. Table 4 gives the sectional torsional moments from CELL4 model for DL, (DL + SDL), (DL + SDL + LL) and the post-tensioning force used for load balancing. For location of these sections see Figure 20.

By inspection of results in Table 4, it can be seen that the post-tensioning force does not offset the torsional moments due to (DL + LL + SDL). In view of this it would be erroneous to assume load balancing as a cure for eliminating torsional moments and to assume that there is no need for a more exact method of analysis.

Dependability of Grid Model

In the initial stages, there were wide variations of reactions and moments between the results of the 3-dimensional grid and finite element models. With some iterations in the development of properties for the grid model, the gap was narrowed down and the final reactions from grid model were close to the ones from finite element model. However the torsional moments as furnished for the grid were much lower than those given by the finite element model. This is a major drawback for dependability of the grid methodology for the analysis of highly skewed bridges.

INTERMEDIATE DIAPHRAGMS

The model for the SPRR bridge was tested with and without intermediate diaphragms. There was negligible difference in moments,

stresses and support reactions between the two models. No transfer of loads to other girders were observed. The differences noticed were attributable to the additional DL added by the introduction of the intermediate diaphragm.

CONCLUSIONS AND RECOMMENDATIONS

• Analysis and design of highly skewed bridges requires careful evaluation of skew-bending effects.

• Finite element models, with proper aspect ratios, provide the best means to evaluate the behavior of highly skewed bridges.

• Support reactions are unpredictable by conventional procedures.

• Torsional moments induced by the high skews need to be addressed in the design. The torsion capacity of the post-tensioned concrete box girders was not adequate to resist the total torsions induced on the structures. Torsion steel was required in all the five bridges.

• The load balancing procedure does not offset all the skew bending effects in a post-tensioned concrete structure. The post-tensioning force required for load balancing is much higher than what is required for balancing the stresses.

• Three dimensional grid analysis does not give a true account of the behavior of the highly skewed structure. The results are very sensitive to the torsional rigidity of the members assumed in a grid model and the comfort level for dependability of results is low.

• Intermediate diaphragms do not have any noticeable effect on the Behavior of the box girder structure or the re-distribution of loads.

• Structures with skews greater than 25 degrees should be avoided if an accurate method of analysis like finite element methodology is not used for analysis. Otherwise it seems imperative to use a more exact method of analysis like finite element methodology to assure the structural design integrity.

Based on the numerical results of the models, there is a need for further study of the effects of skew bending of concrete box girder bridges. The study should include second order analysis and inclusion of time and creep factors and non linear effects in concrete. Also, the numerical results should be correlated with experimental data for future recommendations of design guidelines.

References

1. California Department of Transportation (CALTRANS).Bridge memo to designers 15-1, Sacramento, California, January 1986.
2. A.C. Scordelis, E.C. Chan, M.A. Ketchum, D.D. Van Der Walt; Computer programs for prestressed concrete bridges, Department of Civil Engineering, University of California, Berkeley, March 1985.
3. Macdonald Douglas: MDC STRUDL program, release 5.4, October 1986, Architectural, Engineering and Construction Systems Company, Saint Louis Missouri.
4. Edmund C. Hambly: Bridge Deck Behavior, Chapman and Hall, London, 1976.
5. California Department of Transportation: "Frame System", Sacramento, California, 1983.
6. Southern Pacific Transportation Company (SPRR): Supplement to American Railway Engineering Association, Manual of Recommended Practice, Chapter 8, Concrete Structures and Foundations, San Francisco, California, April 1972.
7. Thomas T.C. HSU: Torsion of Reinforced Concrete, Van Nostrand Reinhold Company, New York, 1984.
8. ACI: Building Code Requirements for Reinforced Concrete (ACI 318-83).
9. ACI: Commentary on Building Code Requirements for Reinforced Concrete (ACI 318-83).
10. ACI: Analysis of Structural Systems for Torsion, ACI publication SP-35.
11. T.Y. Lin: Design of Prestressed Concrete Structures, Third Edition, John Wiley and Sons, New York, 1981.

Cracking, Serviceability, and Strength of Concrete Bridge Decks

JOHN H. ALLEN

Cracking and global load effects are as important as behavior under a single, fixed load in the strength and serviceability of bridge decks. Shrinkage and flexural cracking dramatically affect load response of bridge slabs. The strength enhancement due to "arching-action" is a "post-yield" phenomena which does not aid service load performance. Evidence from field observation indicates that the flexural response of lightly reinforced isotropic decks may not provide adequate long term serviceability.

Maximum negative flexural moments over the girders under service loads are significantly less than the service load positive moments. Confining the reinforcing bars to the bottom layer only offers the greatest structural efficiency and promises dramatically improved deck performance. A better design criterion for satisfactory deck performance is based on yield strength in the positive moment region.

An understanding of the true behavior of bridge decks is not limited to the understanding of the structural system. The material behavior and the loading system must also be understood. The structural behavior of a bridge slab is dominated not only by local effects but also by global effects. The cracking response of bridge decks is an important element in both the strength and serviceability behavior of the deck. The load system consists not of a single fixed load but of a multiplicity of concentrated loads in the form of pneumatic tires which are moving across the structure. The behavior of the structure under this complex system is dramatically different than the behavior of reduced scale specimen structures subjected to fixed loads.

The purpose of this paper is to present an unusual insight into the behavior of bridge decks which is supported by observational evidence and original analysis of the recent research by others related to bridge decks. These insights lead to novel conclusions that differ from the conclusions of the research work cited. The arguments in this paper apply only to concrete bridge decks continuous over multiple beams and may not apply to decks supported on torsionally stiff members such as concrete and steel box girders. The following points will be made:

1) Shrinkage cracking in bridge decks significantly affects the flexural behavior of the deck.
2) The cracking strength of typical bridge decks is an important parameter in the performance of the deck.
3) Compression membrane action is a post-yield phenomenon.
4) Strength enhancement due to compression membrane action does not improve service behavior.
5) Test results indicate that service loads may cause flexural cracking in the positive moment region of lightly reinforced isotropic decks.
6) The current AASHTO service-live-load design positive moment roughly corresponds to the cracking moment of typical bridge decks.
7) The maximum negative moment over the interior girders under service loads is much less than the cracking strength of the deck.
8) The measured reinforcing bar stresses in experimental isotropic decks do not correspond to the observed cracking.
9) The field performance of isotropic bridge decks shows that reliance on the strength enhancement due to compression membrane action adversely affects the serviceability of these decks.
10) Field observations of isotropic decks show that they exhibit extensive longitudinal cracking in the positive moment region.
11) Cracking in the positive moment region of some isotropic decks has propagated through the deck.

12) Longitudinal cracking in the negative moment region above the girders was not observed in isotropic decks in the field.
13) Cracked behavior of isotropically reinforced bridge decks validates the current AASHTO service-live-load design positive moment.
14) The orthotropic arrangement of reinforcing is more efficient than the isotropic pattern of reinforcing.
15) The most efficient reinforcing arrangement is a single-layer-bottom-only-orthotropic pattern designed for the positive moment specified by AASHTO.

These points are discussed in five major sections of this paper. The first four sections lead to the novel conclusions developed in the last section.

CRACKING

An understanding of the cracking behaviors of bridge decks is absolutely essential to a thorough understanding of the "true behavior" of bridge decks from both the serviceability and the strength aspects. Two facets of cracking are important: shrinkage cracking and flexural cracking strength.

Shrinkage Cracking

Cracking patterns in bridge decks are changing. This was the subject of a recent presentation by the author [15] to which the reader is referred for additional information. Many recently built bridges experience crack frequency, width, and depth unlike that previously experienced. This cracking could have adverse consequences for bridge deck durability. Observations of bridge deck cracking in several states show that the change in cracking experience is widespread. Many of these bridges now exhibit transverse cracking which extends through the deck. Where these cracks occur, they are typically spaced about 4-8 feet on center and are fairly wide--on the order of 1/32 to 1/64 inch (.015" - .03"). Leaching makes these cracks readily visible on the bottom of bridge decks. This transverse-through-shrinkage cracking did not occur in bridges built 20 or more years ago and dramatically alters the load distribution behavior of the bridge deck.

The transverse shrinkage cracks are so wide that load is transferred across the crack, not through flexure, but through dowel action. This writer conjectures that this action could lead to premature failure of bridge decks. This failure mechanism is not the subject of this paper. Wide shrinkage cracks alter the stiffness of the deck. The deck stiffness in the longitudinal direction is dramatically reduced. Load is no longer distributed in two directions but in one direction.

Cracking is often discounted by structural engineers who claim that reinforced concrete structures are expected to crack. That is why reinforcing is used! However, before blithely dismissing cracking as an expected phenomenon, one should first seek to understand whether the actual cracking observed has or does not have functional consequences. The assumption that cracking of reinforced concrete is not significant harkens back to concepts about the behavior of reinforced concrete beams which may no longer apply to slabs.

It is important to distinguish slab behavior and beam behavior. Shrinkage cracks in beams do not alter the distribution of load, therefore they do not affect the load-carrying capacity of the beam. Transverse shrinkage cracks in the top of beams reduce the stiffness, causing greater deflection under load as the shrinkage cracks close.

The presence of wide transverse shrinkage cracks through the thickness of the deck dramatically reduces the stiffness in the longitudinal direction whereas the stiffness in the transverse direction is not diminished. Thus the presence of transverse shrinkage cracks in bridge decks dramatically alters the load response. As a result the deck slab behaves like a series of discrete panels rather than a monolithic plate.

Flexural Cracking

The second important aspect of cracking in bridge decks that must be thoroughly understood is the flexural cracking

strength of concrete bridge decks. The cracking strength of concrete can be expressed by the following equation:

$$fr = K\sqrt{fc'} \qquad \text{[Eqn. 1]}$$

where: K = 7 to 13

The modulus of rupture of concrete is significantly affected by the size of the concrete member. Where the rate of change of strain is small in relation to the depth of the member, the modulus of rupture approaches that of concrete in direct tension (K = about 7). For this reason a K of 7.5 is used for determining the cracking modulus of prestressed concrete in the AASHTO Specification for the Design of Highway Bridges [1]. For thin members such as pavements, or bridge slabs, the cracking strength is much higher.

Table 1. Range of Concrete Cracking Modulus

K	fc'(psi)	fr(psi)
7.5	4500	503
13	4500	872
13	6000	1007

Table 1 shows the variation in expected cracking modulus for the range of K and specified versus approximate obtained concrete strength. As shown, the cracking modulus of the typical deck concrete can vary from 500 to 1,000 PSI for a typical bridge deck.

Table 2. Cracking Moment for Plain Concrete Deck Slabs of Various Thicknesses

	CRACKING MOMENT (ft-lb)				
	Slab Thickness				
fr(psi)	7"	7.5"	8"	8.5"	9"
500	4080	4690	5330	6020	6750
1000	8170	9380	10670	12040	13500

Table 2 illustrates the cracking moment for plain concrete slabs varying in thickness from 7 - 9 inches for the range of rupture strength. The minimum cracking strength of the typical eight-inch bridge deck is 5,300 ft-lbs/ft. The AASHTO design live-load moment for a bridge deck with an effective span of 8.0 feet is 5,460 ft-lbs/ft, including continuity and impact factors. Comparing the AASHTO live-load design moment to the cracking moment of the deck reveals that the cracking strength of a plain concrete bridge deck is roughly the same as the conventional design live-load bending moment. This is an extremely important point. Flexural cracking in the positive moment region between the girders has been observed by the author in many experimental isotropic bridge decks, and is discussed in greater detail later in this paper. Cracked behavior directly relates to both the strength and serviceability of bridge decks.

Summary

Many bridge decks experience extensive through-deck-shrinkage cracking. This cracking causes bridge decks to behave orthotropically. The flexural cracking strength of typical bridge decks is similar to the AASHTO service-live-load design moment.

STRENGTH OF ISOTROPIC BRIDGE DECKS

Isotropic bridge decks typically have two layers of nominal reinforcing with a reinforcement ratio of .3% by volume in each direction and each layer. Isotropic decks are lightly reinforced decks which rely on the reserve strength from "compression membrane action" or "arching action". This strength enhancement from "arching action" is the basis for the "Empirical Design Method" first adopted in Ontario, Canada and currently being used on an experimental basis in several states of the U.S. Figure 1 shows the assumed deck behavior with compression membrane action that has been proposed by others. For detailed background on the theory and practice of isotropic decks, the reader is referred to Perdikaris [4] or Fang [18] for the relevant references.

Strength enhancement from what is now called "compression membrane action" of

bridge floors is not a new concept. Professor Turneaure describes this phenomenon in his 1907 textbook Principles of Reinforced Concrete Construction [2]. Likewise, Newmark, in his famous 1948 paper on I-beam bridges, recommends using slab design moments which are 30% lower than the theoretical design moments calculated in his research because of this additional reserve strength. They recognized that the strength enhancement due to compression membrane action occurred only after yield and that eventual collapse took the form of punch-out shear. Compression membrane action occurs only after a complete yield mechanism has formed.

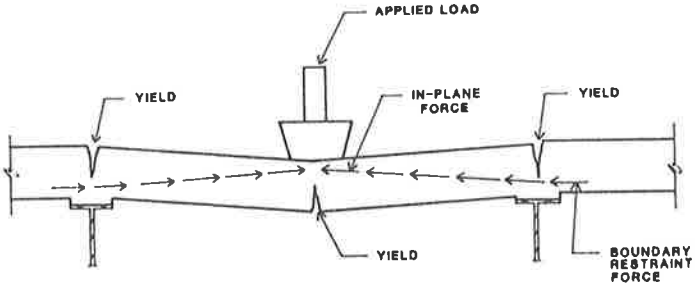

Figure 1. Compression Membrane Action

Strength enhancement due to compression membrane action is a "post-yield" phenomenon. The research by Professor Burns and his colleagues at the University of Texas will be discussed to illustrate this view.

Isotropic Bridge Testing

Burns et al. tested a full scale specimen bridge deck (Texas Test Bridge, [7] & [18]). Half the bridge had a cast in place slab; the other half of the bridge had pre-cast, pre-stressed panels with a cast-in-place topping. The purpose of this research was to demonstrate that precast panels with isotropic reinforcing in the top of the slab were as strong as a cast-in-place deck with both top- and bottom-layers of isotropic reinforcing, and that the strength of both the CIP and panel decks were sufficient to support the AASHTO wheel load.

Figure 2 shows the plan and cross section of the Texas Test Bridge. Compared to much of the other research related to isotropic decks, Burns' research is unique in that it used a full-scale model bridge specimen, which eliminated scale effects. Other work by this writer [16] has clearly shown that strength of a bridge deck is sensitive to the scale of the specimen. Burns' work is also significant in that the load was applied at four positions simultaneously. Thus the global effects due to multiple wheels on the structure and flexibility of the girders and the test specimen were included.

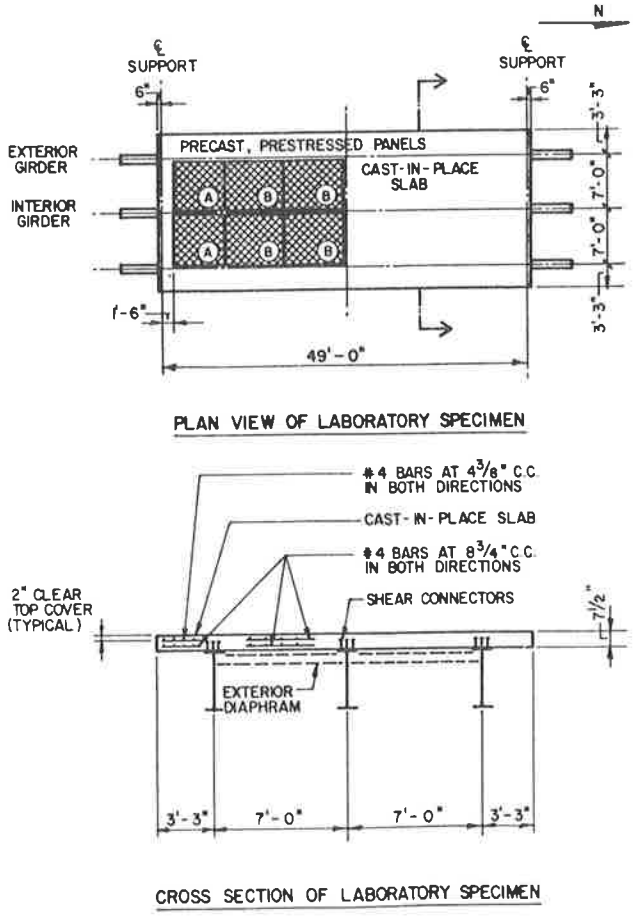

Figure 2. Plan and Cross Section of the Texas Test Bridge [after Burns, et al., ref. 7]

Cracking in the Texas Test Bridge

Figure 3 [excerpted from Burns etal, ref.7] shows the deck cracking before and after fatigue loading. The first bottom crack occurred at a load of 38 kips/actuator. Longitudinal cracking on the top of the deck was not observed until the load had reached 55 kips/actuator, an increase of 45%. It is interesting to note that this figure also shows a longitudinal crack in the top of the deck near the

loads at the CIP end. After initial cracking, several million load cycles at 26 kips/actuator were applied. It is extremely interesting to note that the cracks grew significantly in the positive moment region under this load but no crack growth was noted in the negative moment region. A slight extension of the bottom cracks could be accounted for by fatigue-induced cracking of concrete. But crack propagation about ten feet from the load position is startling. Particularly considering that Loftus [12] shows that when the load is only four feet from the gage position, the stress is less than 50% of the peak stress. The lack of transverse cracking indicates that the longitudinal moments are much less significant than the transverse moments, suggesting an orthotropic pattern of load distribution.

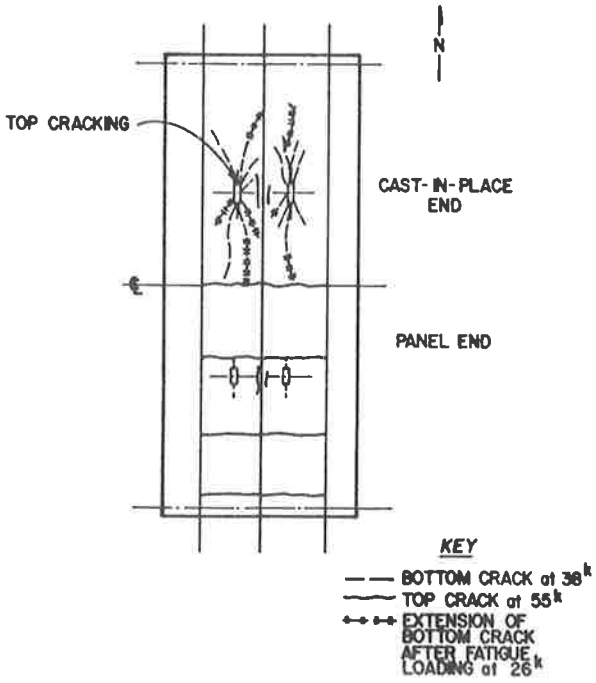

Figure 3. Deck cracking before and after fatigue loading of the Texas Test Bridge [7].

The pattern of cracking indicates that yield has occurred. However, the maximum measured reinforcing stresses for this test structure were well below the yield strength of the reinforcing bars. The stress behavior of the reinforcing is discussed later. For the continuing discussion, I am assuming that yield has occurred based on the cracking observed in the test structure.

Transverse Membrane Forces

Earlier the point was made that the compression membrane strength enhancement is a post-yield phenomenon; the research by Burns clearly illustrates that this is the case.

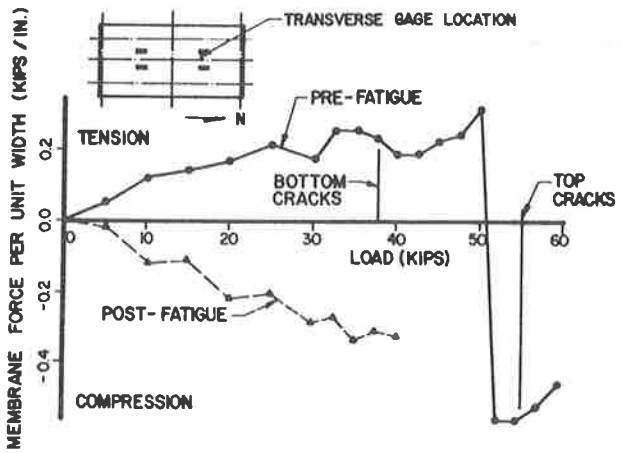

Figure 4. Transverse membrane force versus load, CIP end of Texas Test Bridge [7]

Figure 4 is taken from Burns [7] and plots load vs. transverse membrane force in the CIP deck. One can see that there is no compression membrane force until cracking and yielding has occurred in the negative moment region over the girders. It should also be noted that yield in the positive region occurs in both isotropic and conventional decks prior to yield in the negative moment region.

By superpositioning the plan view of the cracking (from Figure 3), one can see that there is a significant relationship between the cracking pattern and the development of compression transverse membrane force as shown in Figure 5. Extensive flexural cracking has occurred in the positive moment region where the membrane forces are in compression.

Further, Burns' work can also be used to illustrate the hypothesis that yield in the positive moment region is a prerequisite for the development of compressive transverse membrane forces. Figure 6 shows the development of transverse mem-

brane force in the panel deck. Because the pre-cast panels were heavily reinforced, little cracking was experienced in the positive moment region. The transverse membrane force remained in tension under the test load regime. For the panel end, load-stress relationships show that yield was not experienced in either the positive or negative regions. This is additional evidence that compression membrane forces are a "post-yield" phenomenon. That the membrane force is in tension rather than compression prior to yield has not been not discussed by any researchers and this behavior deserves discussion.

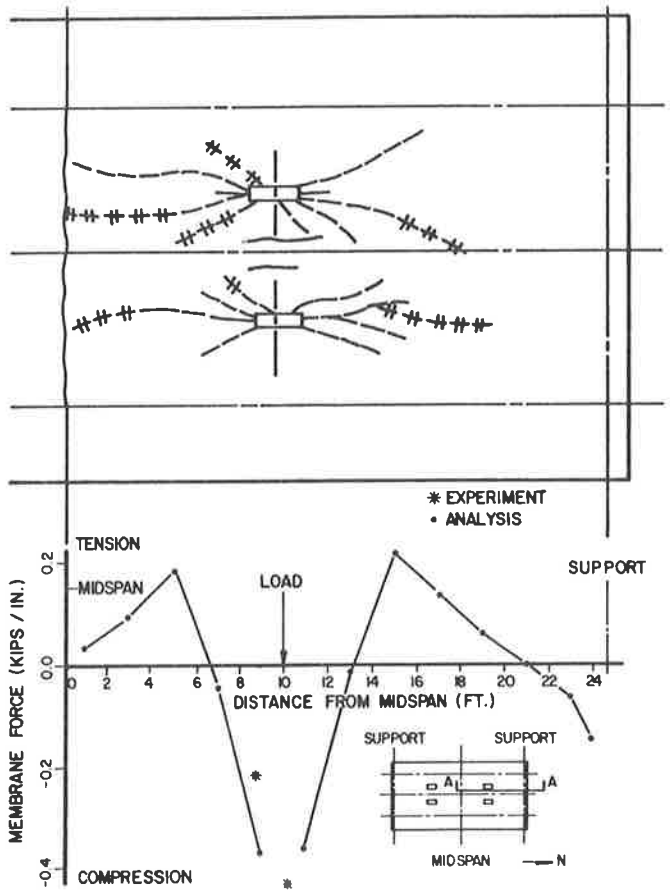

Figure 5. Distribution of transverse membrane force along the center girder, CIP end [7].

An interesting observation can be made from the behavior of the panel portion of the deck on the Texas Test Bridge. Because of the strength of the panels on the Texas Test Bridge, cracking in the positive moment region did not appear until after cracking in the negative moment region appeared. Fine cracks in both negative and positive moment regions were first noted at loads of 55 kips and 60 kips per actuator, respectively. For the panel portion of the deck, the reinforcing stress in the transverse direction both near the load point and over the interior girder remained essentially linear up to the maximum applied load of 60 kips. The Texas research indicates that "global effects" dominate the development of membrane forces. It appears that these forces are tensile until cracking occurs in both the positive and negative moment regions.

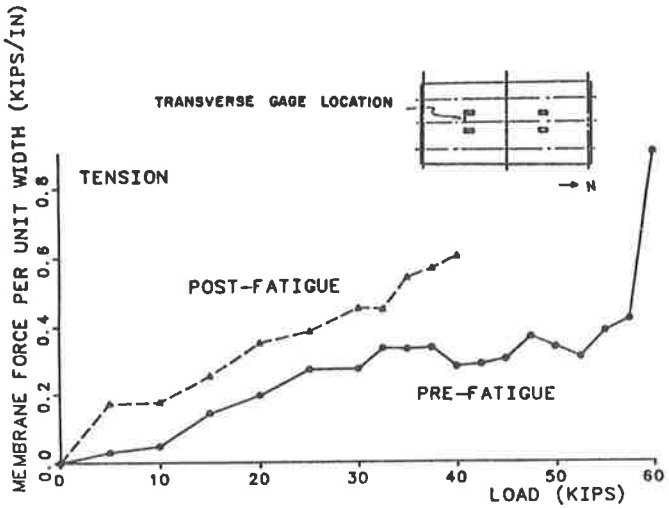

Figure 6. Transverse membrane force versus load, PANEL END of Texas Test Bridge [7].

For the Texas test bridge, the compression membrane force developed only after "yield-mechanism" formation in the positive moment region. A mechanism has been formed when yielding has occurred in the positive moment regions of adjacent bays. This type of mechanism formation is unusual in that hinging in the negative moment region is normally expected to occur before hinging in the positive moment region. This is not how bridge deck slabs behave, however. In fact the strength enhancement offered by the compression membrane force does not require any top reinforcing at all, which Professor Turneaure recognized in 1907.

The reliance on the strength enhancement due to compression membrane action for slabs is like reliance on strain hardening in steel beams. Eventual punch-out failure of bridge deck slabs should be thought of as "collapse".

Summary

Compression membrane action is a "post-yield" phenomenon that does not increase the flexural strength nor improve bridge deck performance at service load levels. Fatigue loading at service-load levels resulted in extensive crack growth in the bottom of the isotropically reinforced test bridge. Orthotropic behavior is indicated by the lack of transverse cracking in the test bridge.

SERVICE BEHAVIOR OF ISOTROPIC DECKS

The Texas test results provide a valuable source for understanding the service behavior of both isotropic and conventional bridge decks.

Table 3. Deck Parameters for the Texas Test Bridge.

Deck: 7.5" w/2" top cover
s = 7.0'-0.5' = 6.5'
#4 @ 8.75" isotropic reinforcing
As = .27 sq-in/ft
= .003

Cracking Strength

The average compressive strength for the concrete in the Texas Test Bridge was 4240 psi. Using a modulus of rupture of 500 psi based on 4500 psi concrete from table 1, the Texas test bridge flexural moment cracking strength is:

$$Mcr = Fr*T^2/6 \quad \text{[Eqn. 2]}$$

$$= 500 * (7.5)^2/6$$

$$= \underline{4690}\ \underline{ft\text{-}lb/ft}$$

After cracking the flexural load strength in the positive moment region is provided by the reinforcing. The post-crack flexural strength of the isotropic reinforcing for the Texas Test Bridge is only 7140 ft-lbs/ft, or 152% of the nominal cracking strength of the bridge deck. If bridge decks crack under service loads, then isotropic bridge decks do not meet the AASHTO specification for the resistance to be at least 217% of the service-live-load moment. Thus, the observation of flexural cracking in isotropic decks at service loads means such decks have deficient flexural strength.

There is more cover on the upper reinforcing than the lower reinforcing of typical bridge decks. Hence, the post-crack flexural strength in the negative moment region is significantly lower, only 5950 ft-lb/ft or 127% of the cracking strength. This barely meets the AASHTO minimum reinforcing requirement that the strength be at least 1.2 times the cracking moment. If the actual service-live-load is close to the cracking load, then the flexural resistance would need to be about 217% of the cracking load. The isotropic reinforcing of the Texas Test Bridge provides less than 60% of the required strength when service-load moments are near the cracking load.

Flexural cracking in isotropic decks must be unlikely at service loads, otherwise isotropic decks have insufficient reserve flexural strength after cracking. Hence the cracking strength of a concrete bridge deck is an extremely important element in assessing the performance of lightly reinforced bridge decks. Cracking behavior has a demonstrable size effect. The size effect cannot safely be ignored in testing bridge decks.

Service Load Moments

The design service-live-load moment equation in AASHTO is based not on a 16 kip wheel from the HS20 vehicle but upon the tandem 12 kip wheels of the military load [13]. The AASHTO design moment for the Texas test bridge (with impact) is:

$$Mlli = .8x1.3x\frac{[16x(6.5+2)]}{32} \quad \text{[Eqn. 3]}$$

$$= 4420 \text{ ft-kips/ft}$$

Newmark [3] recommends the following design moments for the positive moment region between girders:

$$\text{spans to 60':}\quad M = \frac{Pw}{3 + 10\ c/b} \qquad \text{[Eqn.4]}$$

Newmark recognized that the effects of other wheels on the bridge became more significant as span length increased. Consequently, he proposed a formula to account for these effects:

$$\text{spans over 60':}\quad M = \frac{Pw}{3 + 10\ c/b} + \frac{Pw(L-60)}{1000} \qquad \text{[Eqn. 5]}$$

where: Pw = wheel load, pounds
L = span length, feet
c = wheel width, 1.25'
b = beam spacing, feet

Newmark's made a recommendation for the design bending moment that was only about 70% of the maximum positive slab bending moments predicted from his research. He did not propose that the full design moment be used for slab design because of the inherent high reserve strength of bridge slabs.

For the Texas test bridge Newmark's recommendation for the design live-load moment with impact is calculated:

$$M = 1.3 \times \frac{16{,}000\#}{3 + 10(1.25/6.5)} \qquad \text{[Eqn. 6]}$$

$$= 4230 \text{ ft-lb/ft}$$

For shorter spans, Newmark's recommended design moment is similar to current AASHTO practice. Using Equation 5 for a 100 ft. span, the design positive moment according to Newmark would be 5060 ft-lb/ft. Likewise, with the 24 kip wheel for the Military Load, the Newmark design moment becomes 6380 ft-lb/ft (taking c=2.0). Considering "global effects," Newmark's equation yields moment values significantly higher than AASHTO. Newmark's pioneering work has been ignored by researchers promoting the isotropic decks.

A recent study by Jackson [19] in the U.K., calling the effects of beam flexibility and multiple wheels "global effects", has discovered that the "global effects" more than double the "local" flexural moments (those due to a single wheel). Jackson found that the "reinforcement required to resist these global transverse moments exceeded the total required by Ontario rules". Under global load effects failure occurred at only "55% given by the approach of Kirkpatrick, et al. and Hewitt & Batchelor." This is consistent with my analysis of the work of Lybas and Burns reported elsewhere [16].

Solving Newmark's Equation (4) to find the wheel load at the cracking moment gives a load of 23 kips, which is roughly 60% of the applied load at which cracking was first observed. This might mean that Newmark's equation overestimates the bending moment. Or it could mean that the actual cracking strength is much higher than the nominal cracking strength of the deck. In the discussion of cracking, it was shown that the cracking strength can be much higher. For this case, the Newmark bending moment for the cracking load results in an extreme fiber bending stress of only 823 psi, well within the expected range of flexural strength of concrete.

The flexural strength of the Texas isotropic deck is only 117% greater than Newmark's recommended design service-live-load moment for a 100' span and 24kip wheels, inadequate by the current AASHTO specification [1] requiring the strength to be at least 217% of the service-live-load moment. If Newmark's slab design recommendations are representative of real bridge deck behavior, then some isotropic decks can be expected to exhibit flexural cracking.

Figure 7, taken from Burns et al., shows the post-fatigue transverse moment distribution with an applied load of 20 kips/actuator. In the Texas Test Bridge, the load actuators were spaced six feet apart and symmetrically placed about the interior beam. This position should cause the largest negative moments. By conventional-rigid-girder theory, the negative moments over the interior girder would be expected to equal or exceed the positive moments. Yet, as shown in the figure, the maximum negative moments are only about 1/5 of the positive moment. Even more importantly, the maximum negative moment is only 17% of the cracking strength! This explains why longitudinal cracking over the interior girders is not normally

observed, and in fact, has only been observed under extremely unusual conditions.

However, the design wheel load is more appropriately taken as 24 x 1.3 = 31.2 kips (including impact), approximately 50% greater than the 20 kip wheel load take to represent the AASHTO design wheel. A 30 kip wheel load moment curve has been developed by amplifying the 20 kip moment curve by 50%. This curve corresponds to the AASHTO service-live-load and should be compared to the AASHTO design moment. Newmark's recommended design moments for a 16 kip wheel, a 24 kip wheel and 100 foot span have also been shown for further comparison. The cracking strength, as well, has been plotted on Figure 7 to graphically illustrate the relationship of the test load to the cracking load and service-live-load design moments.

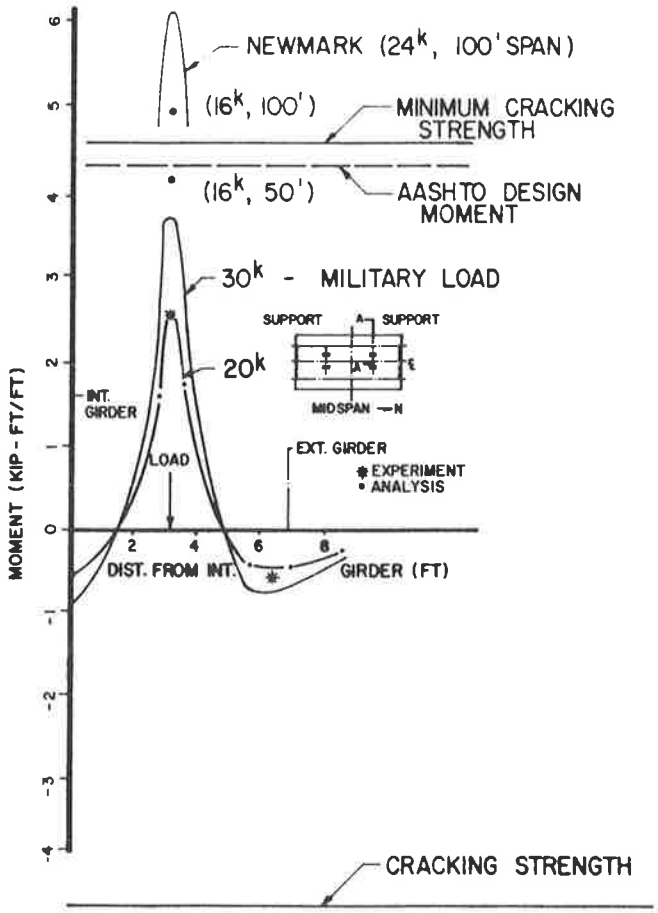

(1) For a 16 kip wheel with impact.
(2) For a 24 kip wheel with impact.

Figure 7. Transverse moment distribution across the load for the Texas Test Bridge [7].

The AASHTO design moment and the cracking moment are both only slightly greater than the experimental moment for a 30 kip load. It is also interesting to note that the AASHTO design positive moment is slightly less than the nominal cracking strength of the Texas Test Bridge. In fact the cracking moment would not be exceeded at service-live-load levels unless one considers the "global effect" of beam flexibility according to Newmark for spans of 100 feet or more. Therefore, the cracking load is more likely to be exceeded for bridges of longer span.

Another significant observation from this figure is that the negative moment cracking strength is several times greater than the maximum negative moments even for the 30 kip load. The significant observation from this comparison is that the AASHTO design positive moment is only slightly less than the nominal cracking strength of the bridge deck. It should be noted that Figure 7 is based on the post-cracking transverse moment distribution.

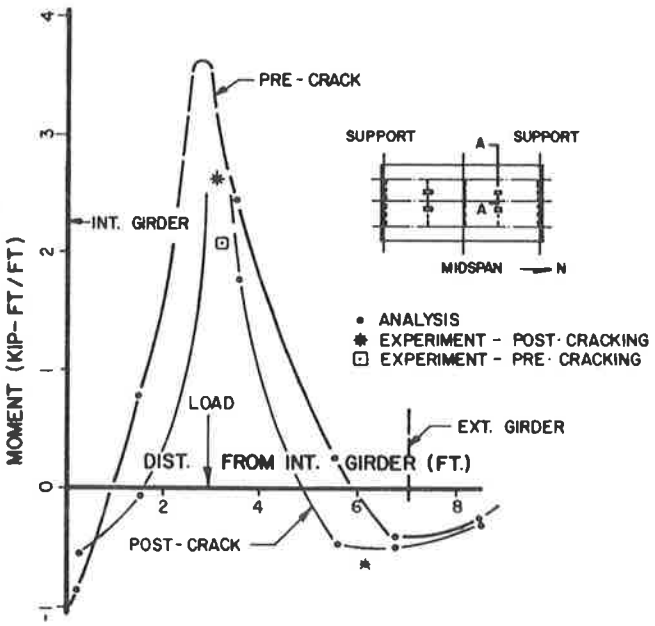

Figure 8. Transverse moment distribution before and after cracking for the Texas Test Bridge [7].

Burns et al., also calculated the distribution of transverse moment prior to cracking. It is interesting to compare the magnitude of the pre-cracking moments of Figure 7 and the post-cracking moments, shown together in Figure 8. The maximum

positive pre-cracking moment, shown as a dashed line, has been projected by this writer from the analytical results of the Texas researchers. Before cracking, the transverse moments were larger than after cracking, increasing the likelihood that the flexural moments would exceed the cracking strength under normal vehicle loads in the positive moment region of longer spans. The approximate maximum pre-crack moment is 3500 ft-k/ft at a twenty kip load, and the corresponding cracking moment is 6560 ft-k/ft. A moment that is significantly higher than the nominal cracking strength calculated in Equation 2. In spite of this, the fatigue testing showed significant crack propagation at a load level significantly less than the nominal cracking load of the deck. This is a significant observation.

As shown in Figure 8, both the maximum positive moment and maximum negative moment before cracking are greater than the post-cracking moment. This clearly shows the distribution of stress is dependent upon cracking and, further, it shows that the stress in the reinforcing is lowered after cracking because the load distribution is greater. I propose, however, that this additional load distribution is peculiar to a load that is applied in a fixed position. Peak stresses and strains under rolling loads could be expected to be much greater, significantly reducing fatigue life.

Fatigue

The fatigue behavior of the Texas Test Bridge may be more like that due to legal trucks rather than an overload truck as suggested by the Texas researchers. They neglected the global effects of the other wheels on the bridge, and believed that the fatigue loading of 26K was 25% greater than the presumed design wheel of 16 kips with 30% impact (20.8k). As previously noted, the proper AASHTO design wheel is 24 kips (31.2 kips with impact). In fact, considering all wheels, total applied load on the bridge was only slightly greater than a standard HS20 truck (72 kips) allowing for 30% impact.

$$\frac{4*26}{1.3} = \frac{104}{1.3} \text{ kips} = 80 \text{ kips} \quad \text{[Eqn. 7]}$$

Highway bridges with frequent truck traffic can experience in excess of one hundred million wheel load cycles in a fifty year period. The several million load cycles which the Texas Test Bridge underwent represented less than 10 years of high volume truck traffic. The duration of the fatigue test for this bridge was insufficient to predict adequate service performance for a 50 year life expectancy.

This testing indicates that, once cracked, isotropic decks have too little flexural strength to prevent flexural crack propagation even under fixed position loads. Field observations of isotropic decks confirm this behavior.

Perdikaris' research [4] shows a substantial reduction of fatigue life for a moving load compared to a fixed pulsating load--on the order of 100 fold. Thus the crack growth experienced in Burns' testing under fixed pulsating loads might occur in real structures subjected to rolling loads in only a few tens of thousand of truck passages. Most primary system highway structures will experience this number of load cycles in less than a year and will exhibit a substantial positive moment cracking. This is not merely conjecture but supported by observational evidence. The relevancy of these arguments will be made clear in the discussion of field observations of isotropic bridges later in this paper.

Reinforcing Bar Stresses

Some interesting observations regarding the stresses in the reinforcement under load can be drawn from Burns' research. Figure 9 shows the reinforcement stress in the bottom transverse bars in the positive moment region with respect to applied load. The load level at which first cracking was observed in the positive and negative moment regions has been added to the figure. The reader should note that the stress did not return to zero upon unloading but a residual stress of about 6 ksi remained upon unloading. Presumably this indicates that the bars had experienced yield, since bond slip would be unlikely to occur at such low stress levels. Bond slip, if it did occur should result in a residual compressive stress in

the bar rather than tensile stress. Neither can slab dead load on the cracked section account for this magnitude of residual stress. Similarly, in the negative moment region, the top transverse bar stress after unloading was almost 4 ksi (Figure 10).

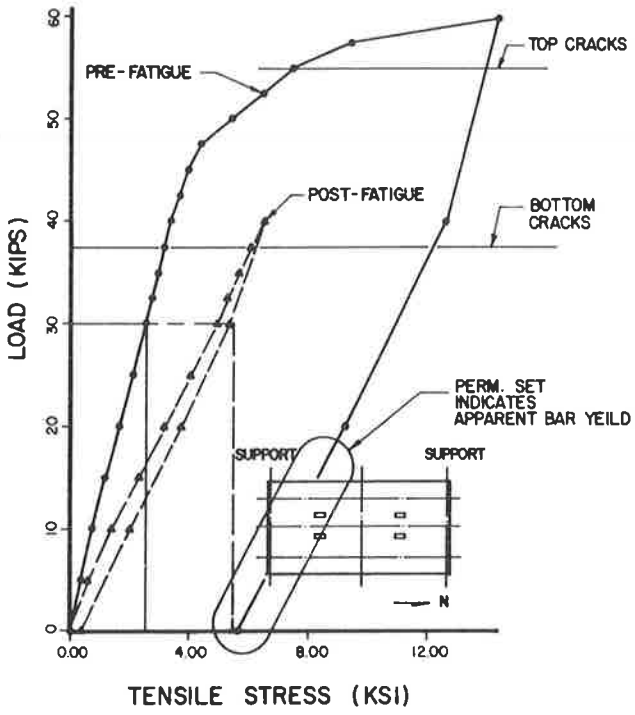

Figure 9. Reinforcement stress in transverse bottom bars near load point, Texas Test Bridge [7].

Two other observations need to be made regarding the reinforcing stresses in both the positive and negative moment regions pre- and post-cracking. Rather than using the measured bar stress however, in this comparison the calculated bar stress based on the maximum transverse moments post-fatigue will be used. At the maximum transverse moment of 3800 ft-lb/ft for the 30 kip load from Figure 7, the calculated bar stress is 30,000 psi in the bottom bars on the cracked section. This is much greater than the measured bar stress of 5.5 ksi at the same load level. As shown earlier, membrane action is not in compression at these low load levels. The calculated reinforcing stress greatly exceeds the allowable stress range of 21,000 psi. Since isotropic decks do not conform to the current AASHTO design specification, the exemption for deck slabs should not apply.

In the top reinforcing, for the same load, the calculated maximum stress on the cracked section would be only 8000 psi, well within the tensile strength and fatigue stress range of the reinforcing bars. It should be noted that the load required to cause cracking in the top was nearly double the design load.

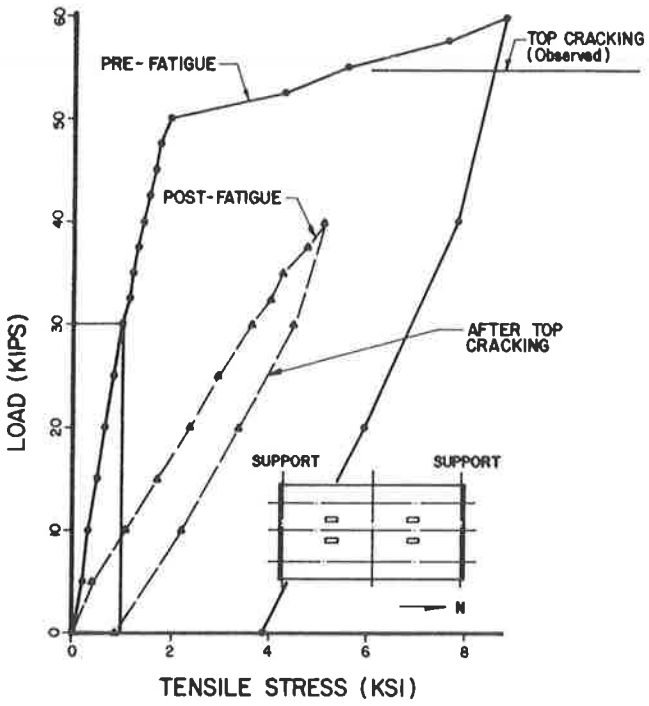

Figure 10. Reinforcement stress in transverse top bars above interior girder, Texas Test Bridge [7].

After cracking, the Texas researchers measured the crack width at a load of 20 kips per actuator to be .008" in the bottom of the deck. The measured post-fatigue stress at this load, from Figure 9, is less than 4 ksi. Using the Gergely-Lutz equation to calculate crack width at this stress, including the sized factor adjustment for the depth of the slab, the expected crack width would be only .0014", or 17% of the measured crack width. Inversely, a crack width of .008" corresponds to a reinforcing bar stress of 20 ksi, five times the measured stress. The crack width also corresponds to the bar stress calculated from the bending moment obtained from Figure 7 for a 20 kip load. Because I doubt that the Gergely-Lutz

equation adequately accounts for the size effects of thin slabs, I am not showing the calculations, but am leaving it to the readers to perform their own calculations.

I draw the conclusion from this observation that the bars at the location of maximum moment may have undergone yield. The lower stress under subsequent reloading is likely to be the result of load redistribution as evidenced by the extensive propagation of cracking under cyclic load. A rolling load, then, would be a much more severe load because each bar would be subjected, in turn, to the peak stress as cracking fully develops and load redistribution ceases.

One must consider these observations in light of the fact that none of the numerous experimental isotropic bridge decks with strain gages have reported such high bar stresses. There can be several explanations:

- o The slabs are uncracked because the short span keeps flexural moments below the cracking moment or because the flexural cracking strength of the deck is very high.
- o Bar coatings reduce bond therefore the full flexural stress in the bar is not developed.
- o The gage is poorly located with respect to the position of maximum positive moment.
- o The service loads on the bridge being tested are low.
- o The normal path of traffic is not situated to cause the maximum positive moment.
- o Strain gages are at the center of the bridge and the longitudinal cracking progresses from the ends of the bridge to the center, rather than the reverse, so testing has ceased before cracking has propagated to the gage locations, and the measured stresses reflect uncracked behavior.

In recording the bottom reinforcing stresses in an isotropic deck near Albany, New York, Loftus [6] reported that the maximum recorded stress increased every year. Progression of cracking may account for the growth in stress range. This deck has both AASHTO reinforced and isotropic reinforced portions. Figure 11 shows that stress growth has been experienced in the isotropic portion of the deck but not in the AASHTO portion of the deck.

Summary

Are these arguments unfounded or are they supported by evidence? Let us consider the principle arguments presented:

1) The flexural cracking strength of a bridge deck is approximately the same as the conventional AASHTO live-load design moment.
2) The flexural strength of isotropic decks after cracking is only slightly greater than the flexural cracking load.
3) The "global effects" increase the positive moments such that the stress in the reinforcing at service loads exceeds the allowable stress range for isotropic decks.
4) The maximum positive moment in bridge decks is much greater than the maximum negative moment.
5) The maximum positive moment exceeds the cracking strength of the bridge deck but the peak negative moment over the interior girders is well below the flexural cracking strength.

If these arguments are valid, evidence of positive moment cracking should be apparent among the many experimental isotropic decks constructed in the United States.

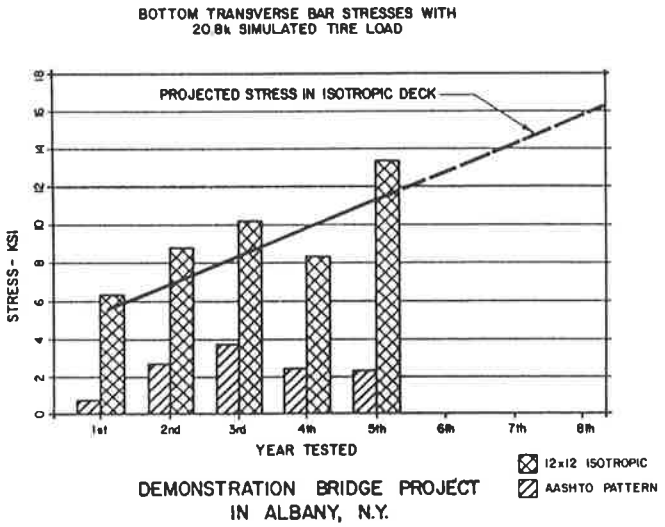

Figure 11. Maximum reinforcing stresses in bottom transverse top bars for the Albany Bridge [6].

OBSERVATION OF CRACKING IN ISOTROPIC BRIDGE DECKS

Very few isotropic decks have been built in the United States, yet several exhibit significant detrimental cracking. Though they were recently built, periodic observation of the cracking in these bridges reveals the cracking is getting progressively worse. The cracking observed in these bridges validates the stated concerns regarding the service behavior of isotropic decks.

The writer has visited many experimental isotropic bridge decks built in North America, including: New York, Wyoming, Texas, Wisconsin and Ontario, Canada. At least twenty isotropic bridge decks have been observed by the writer. Nearly every isotropic bridge exhibited more cracking than a typical AASHTO reinforced deck. These observations are not consistent with the published reports by researchers studying isotropic decks. These observations of the bridges in the U.S. are particularly important for two reasons: first, some of these decks are thinner than the structures built in Ontario, and secondly, the extent of cracking in the bridge deck is directly related to the cracking strength of the bridge deck. The flexural load required to cause cracking of a 9" deck is more than 40% greater than the flexural cracking load of a 7.5" deck. Therefore, it is reasonable to expect that thicker isotropic bridge decks may never experience service-loads sufficient to cause cracking and thus may be deemed to perform satisfactorily. Of the twenty structures that I have seen, at least 50% exhibit significant signs of flexural cracking. In this discussion I will show only two. In a sample of only twenty structures, finding even two with significant flexural cracking is serious and very significant, especially when other researchers have reported no such problems.

NY 104 over Hard Road, Rochester, New York

New York has built an experimental isotropic bridge on NY 104 over Hard Road near Rochester, NY. This route NY 104 is a limited access facility designed to interstate standards, carrying a high volume of heavy traffic. The twin bridges have both been built with isotropic decks. Although the bridges have only been open to traffic less than five years, Loftus reported [12] that longitudinal cracking between the girders was occurring and getting progressively worse. Because the extent of longitudinal cracking was not well described, I elected to make my own observations. What I found is startling and noteworthy.

These twin bridges are single-span steel plate girder structures, over 100 feet long, with a composite, isotropically-reinforced concrete deck. The girders are spaced at about 9-10 feet on center. The second interior girder bay coincides with the righthand driving lane. The cracking observed was similar for both bridges.

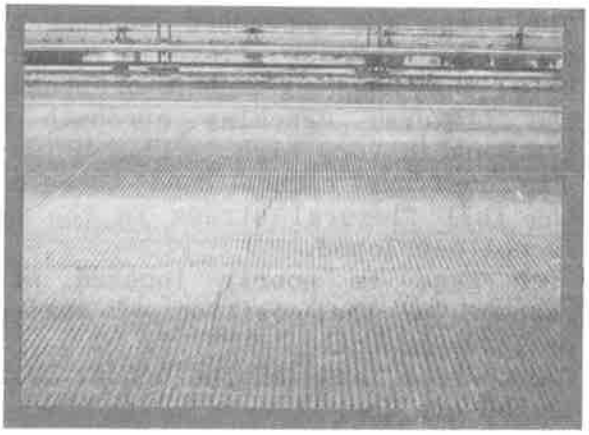

Figure 12. Top deck cracking at midspan.

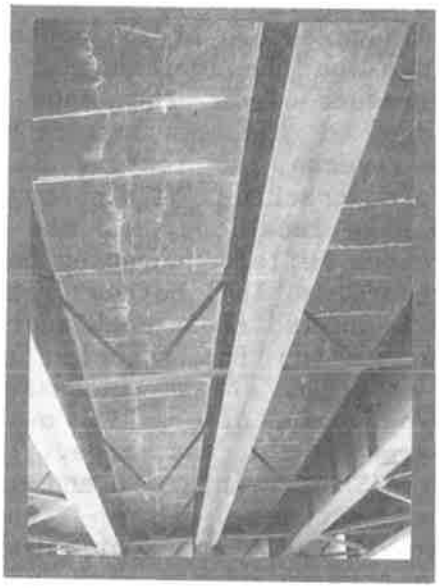

Figure 13. Bottom deck cracking at midspan

Extensive through-transverse-shrinkage cracking is spaced between 4-8 feet on center. There is extensive longitudinal cracking between the girders, running nearly the full length of the structure beneath the righthand lane on both the eastbound and the westbound bridges. The longitudinal cracking is visible in the top (Figure 12) of the deck as well as in the bottom of the deck (Figure 13). It appeared that a second longitudinal crack was forming in the westbound structure (Figure 13).

Figure 14. Top deck cracking at end.

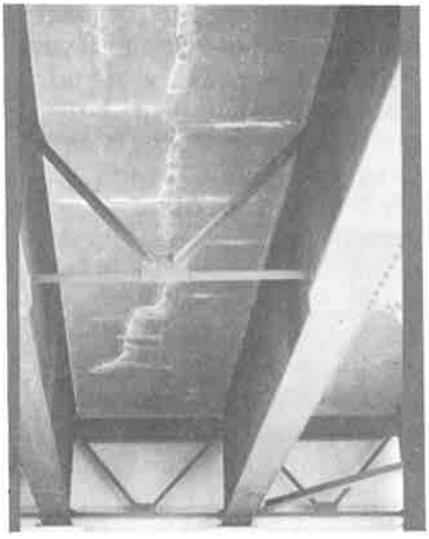

Figure 15. Bottom deck cracking at end.

At both ends of the bridge underneath the driving lane there are diagonal cracks extending from the ends of the girder toward the center of the deck in both the top (Figure 14) and the bottom (Figure 15). The diagonal cracks then join near the center of the panel and continue longitudinally for the length of the bridge. These cracks are readily visible and exhibit efflorescence, leading to the conclusion that they extend through the deck. This cracking is typical of yield mechanism formation in the positive moment region and does not bode well for long-term durability of this bridge under service loads. It is important to note that no longitudinal cracking was visible in the top of the deck over the girders, in spite of the extensive flexural cracking apparent in the positive moment region. Compare the pattern of cracking in figures 12-15 to the cracking of the Texas Test Bridge, Figure 3.

The deck of this bridge is believed to be at least 8.5" thick and should have a cracking strength exceeding the AASHTO service-live-load design moment. Accordingly, such extensive and rapid crack growth in a structure less than five years old would not be expected. However, since the span exceeds 100 feet, then the service-live-load moments predicted by Newmark would likely result in flexural cracking and the extensive cracking that has been observed would be expected. Thus the observation of this cracking in this bridge would seem to corroborate Newmark's theory.

US 30 over Sand Creek, Cheyenne, Wyoming

Two years ago I visited the experimental isotropic bridges that had been built in Wyoming. One of them, I-80 over the Union Pacific Railroad, had been instrumented by Dr. Puckett [14]. The other one is in Cheyenne, WY, and has not been instrumented and is the subject of discussion. This bridge is a three span continuous I-beam structure. The deck is probably non-composite.

This bridge on US 30 in Cheyenne, WY also exhibits extensive transverse through cracking with efflorescence. In June, 1988, I visited this bridge for the first time and observed diagonal cracking starting at the ends of the exterior three girders at each corner. No longitudinal cracking was apparent. Because of my observations of the bridge in Rochester, NY, I returned to Cheyenne to look at this bridge again in February, 1990, to see if the cracking was any different. A pattern

of longitudinal cracking is developing and the diagonal cracking appears more extensive.

On my first visit, the diagonal cracks on top of the deck were hard to see, so pictures were not taken. Now the diagonal cracking in the top of the deck is readily apparent and easy to photograph as shown in Figure 16. Furthermore, faint longitudinal cracks are now visible in the top of the deck, but are too fine to be readily photographed from the edge of the road.

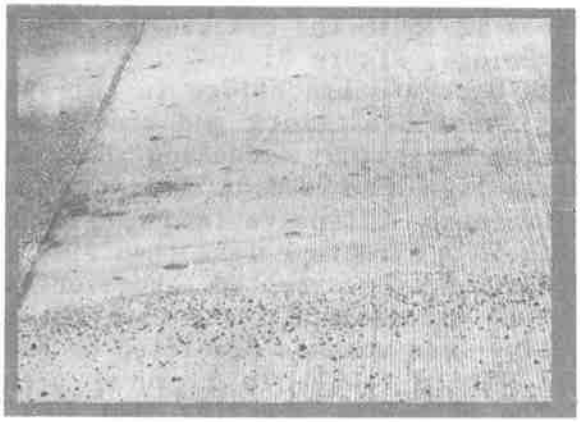

Figure 16. Diagonal cracking in top at end of isotropic deck.

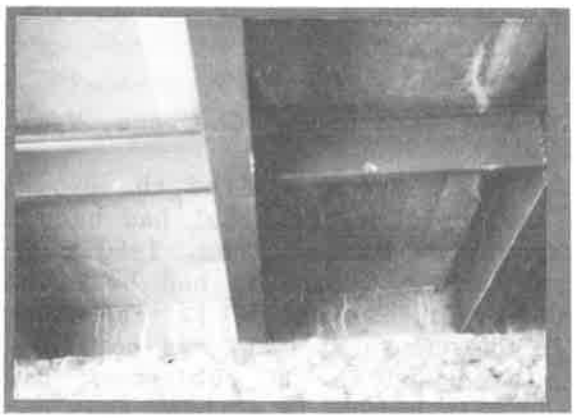

Figure 17. Diagonal cracking in bottom at end of isotropic deck.

In the bottom of the deck, more diagonal cracking with efflorescence is also visible (Figure 17). The extensive efflorescence indicates that moisture is migrating through the crack and that the crack extends to the upper surface. Longitudinal cracking in the bottom of the deck is now evident, as shown in Figure 18. The transverse through cracking visible in the figure was present at the time of the first visit. Since the longitudinal cracking was not observed during the first visit, the onset of flexural cracking is time and load dependent.

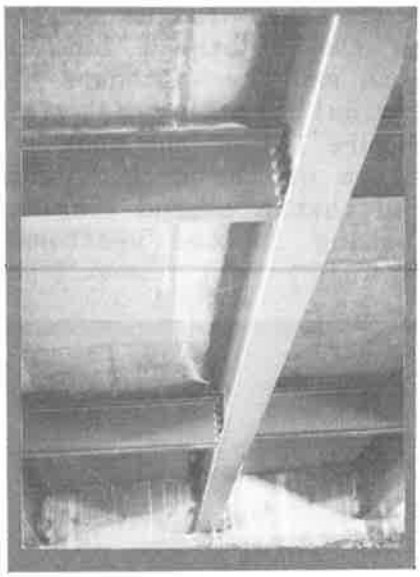

Figure 18. Longitudinal cracking in bottom of isotropic deck

Other Isotropic Bridges

Similar cracking has been observed in isotropic bridges built in Wisconsin, Texas and Ontario; however, the cracking and efflorescence was not as extensive. The bridges included both steel beam and concrete girder structures. In Texas, an asphalt-wearing surface prevented observation of the top of the deck, but hairline diagonal and longitudinal cracks were apparent at the ends of two of four bridges.

In Wisconsin, two of the three isotropic decks exhibited longitudinal cracking near the end of the bridge. The cracks were only visible for the first twenty to thirty feet at the end of the bridge. They were visible in the top of the deck as well and exhibited faint efflorescence. No transverse-through-shrinkage cracking was observed in these decks. In Wisconsin, an adjacent deck, perhaps twenty or thirty years older, exhibited no signs of transverse or longitudinal cracking nor efflorescence in the bottom of the deck.

Several experimental isotropic bridges have been built in New York in addition to the one cited. I have visited many of them. Most had stay-in-place forms pre-

venting observation of cracking in the bottom of the deck, including the one in Albany (Figure 11). Some had signs of either longitudinal or transverse cracking in the top of the deck. Many were lightly traveled rural road bridges or city streets, therefore no conclusions related to the performance of these bridges should be drawn.

Several isotropic bridges were visited in Ontario. Some were known to be isotropic because they were the early experimental bridges. Others were assumed to be isotropic decks because of their obvious recent construction. In no case was cracking observed as extensive as that in the New York or Wyoming bridges. But some diagonal and longitudinal cracking with signs of efflorescence was evident in the bottoms of the decks. The Conestoga River Bridge is an exception, but this bridge was an experimental structure and has had test loads applied, therefore its cracking will not be discussed except to say that longitudinal cracking was observed between the girders and that this longitudinal cracking apparently extended through the deck.

Conclusions from Cracking in Isotropic Decks

The observation of extensive longitudinal cracking in the bottoms of isotropic bridge decks indicates that they are experiencing flexural cracking loads under normal vehicular traffic. As shown earlier, the flexural-cracking moment for a typical bridge deck is close to the AASHTO design service-live-load moment, therefore the observation of flexural cracking in isotropic decks indicates that the AASHTO design moment is representative of normal truck traffic. But even more startling, and totally unexpected, is the observation that the longitudinal cracks in the positive moment region have propagated through the deck. The propagation of these cracks through the deck indicates that an unusual yield/collapse mechanism is forming.

The occurrence of transverse-through-shrinkage cracking, as noted in the New York bridge, severely diminishes the longitudinal stiffness of an isotropic deck and is likely to have played a major role in the rapid progression of cracking on this deck. Because longitudinal-through-flexural cracking has been observed in isotropic bridges without transverse-through-shrinkage cracking, the occurrence of shrinkage cracking is not a prerequisite for flexural cracking in isotropic bridge decks.

In spite of extensive longitudinal cracking in the positive moment region, no such cracking has been noted in the negative moment region over the girders as of yet. This is further evidence that the flexural moments over the girders are not significant.

Migration of moisture through the crack will only accelerate deterioration. Eventually, cracking will develop over the girders and then actual collapse will ensue. The isotropic decks are becoming unserviceable long before they reach actual collapse. The observational evidence indicates that the progression of cracking and ultimate life expectancy for isotropic decks is proportional to the number of load cycles (truck passages) to which the deck is subjected.

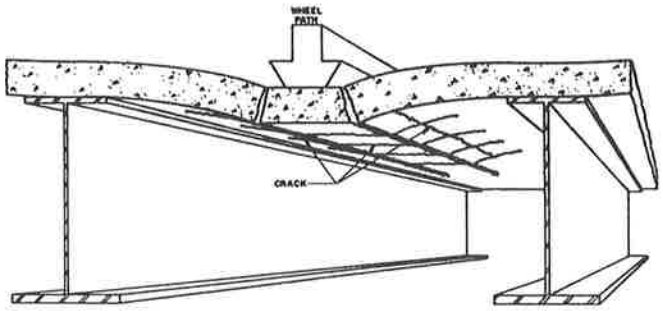

Figure 19. Observed cracking behavior of isotropic decks.

The development of extensive positive moment cracking in isotropic bridge decks confirms the importance of flexural behavior of bridge decks. Flexural strength, not "punch-out" strength, should be the governing design criterion. Decks designed in accordance with the flexural requirements of AASHTO are deemed satisfactory for shear, and have proven satisfactory performance in both flexure and shear. The evidence presented herein shows that the performance of empirically-designed-isotropic bridge decks based on punch-out shear strength are not performing well.

SERVICEABILITY OF CONCRETE BRIDGE DECKS

The control of cracking in the positive moment region is essential for durability of bridge decks. Hence, the observation of positive moment cracking in isotropic decks is important because it indicates that the traffic-applied moments on the deck exceed the cracking moment of the deck. It was shown earlier that the cracking moment of the deck is approximately the same as the design live-load moment based on the current AASHTO practice. Therefore, because cracking has been shown to develop in the positive moment region under normal traffic, it can be inferred that deck moments under normal traffic are similar to the AASHTO design moment. Hence, the AASHTO design positive moment is not overly conservative! In fact, considering the work of Newmark and the extensive cracking that has been observed in the positive moment regions of isotropic decks, it may be slightly under the actual service-load moments.

The presence of an adequate amount of bottom deck reinforcing to control positive moment cracking may be the most important factor in minimizing positive moment cracking. Because the strength of the concrete in flexure is variable, most of the deck can be expected to have sufficiently high cracking strength to prevent flexural cracking. Some portions of the deck will not have sufficient flexural cracking strength and fine, short flexural cracks will occur. With an adequate amount of bottom reinforcing bars, such as required by AASHTO, these cracks are arrested.

Lightly reinforced isotropic decks do not have sufficient flexural reinforcing to arrest crack growth. Positive moment cracks propagate from weaker regions through stronger regions, getting longer and wider under repeated load applications.

Serviceability problems arising from corrosion of the top reinforcing bars is well documented and generally understood, therefore no added discussion is needed herein.

STRENGTH OF CONCRETE BRIDGE DECKS

The two important aspects for bridge deck performance are strength and serviceability. The serviceability of a bridge deck is related to the cracking strength and flexural yield strength of the deck. A serviceable deck can, and should, be designed by current AASHTO practice for the bottom mat of reinforcing. The cracking experience of isotropic decks is observational evidence that the positive design moments given by the AASHTO code are reasonable.

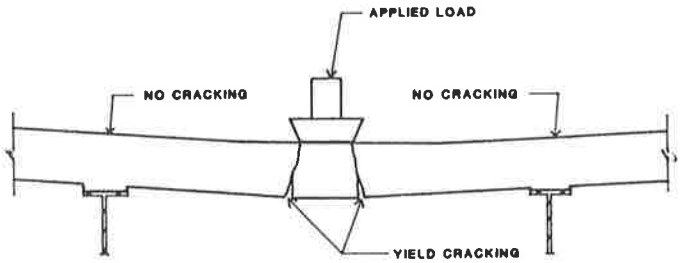

Figure 20. Yield mechanism formation.

Flexural strength is governed by yield in the positive moment region. Yielding in the positive moment region of adjacent bays results in the formation of a partial mechanism. The positive moment yield load is the load at which this mechanism forms. As shown earlier, the positive moments are greater than the negative moments and yielding occurs first in the positive moment region, therefore this is the first mechanism to form, which we are calling the yield mechanism.

Collapse flexural strength is governed by the formation of a full flexural mechanism in both the positive and negative moment regions. It has been shown that membrane forces are in tension until hinge formation occurs below the load and over the girders. A collapse flexural mechanism occurs prior to any strength gain from compression membrane action. The collapse reserve strength after full yield mechanism formation is not likely to be affected by the amount of reinforcing in the zone of yielding, but higher volumes of reinforcing in the bottom layer will enhance the boundary restraint. The more bottom reinforcing, the higher the total collapse load.

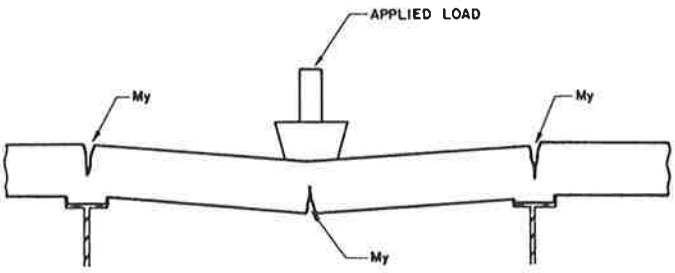

Figure 21. Collapse mechanism formation.

Two new "limit-states" have been defined: yield mechanism and collapse mechanism. Both are flexural limit states. No investigations have been made to define the flexural limit states nor to determine what load factors should govern these limit states to insure satisfactory service load performance. For bridge decks, the positive moments are much greater than the negative moments. For this case, the limit state for the collapse mechanism is never less than the limit state for the yield mechanism, as defined.

There are many proponents of an empirical deck design procedure based on the "punch-out" limit state. Obviously, decks having an adequate punch-out strength may not have satisfactory flexural strength. For these decks, rapid propagation of flexural cracking is likely and they may become unserviceable at an early age. The punch-out strength of bridge decks is so high that it is unlikely that a bridge deck meeting flexural strength requirements would fail to have satisfactory punch-out strength. The AASHTO bridge design specifications [1] have long recognized this fact. Therefore, the limiting state of yield mechanism formation should be used to insure both adequate strength and, with appropriate load factors, assure satisfactory serviceability.

For the most economical bridge deck, the placement and orientation of a given volume of reinforcing that produces the highest yield strength and collapse strength should be determined. This can be done by comparative analysis. A comparative analysis of an orthotropic deck (AASHTO) to an isotropic deck with a .003 reinforcement factors follows based on these assumptions:

1) Transverse flexural moments govern.
2) Longitudinal moments can be ignored.
3) The yield strength of the top reinforcing is 75% that of the bottom.
4) Yield in the positive moment regions precedes flexural cracking over the girders.
5) Flexural cracking strength is assumed to be equal to the negative moment yield strength of a lightly reinforced isotropic deck.
6) The structural efficiency of the alternative deck designs will be compared to a typical AASHTO deck assigning it a value of 1.00.
7) The orthotropic deck (AASHTO) has three times the transverse reinforcing of the isotropic deck in the top and bottom layers. Two-thirds of the transverse reinforcing is used in the bottom longitudinal direction and one-third longitudinal top.

The first two and the fourth assumptions correspond to the cracking behavior that was observed on the Texas Test Bridge. The third assumption accounts for the reduction in structural depth that occurs due to the increased cover provided for the top reinforcing. The fifth assumption is based on the calculated cracking moment and flexural strength for the Texas Test Bridge. The seventh assumption is typical for a standard 8.5" thick AASHTO deck with #6 bars at 6". These assumptions mean that the yield strength is controlled by the amount of bottom transverse reinforcing only. The total amount of the top and bottom reinforcing determines the collapse strength.

Table 4. Comparison of strength and economy of different reinforcing patterns.

	REINFORCING		STRENGTH		
PATTERN (1)	TRANSVERSE RATIO (2)	TOTAL RATIO (3)	YIELD (4)	COLLAPSE (5)	EFFICIENCY RATIO[a] (6)
Two layer					
ISOTROPIC	.003	.012	My	1.75*My	0.75
ORTHOTROPIC	.009	.027	3*My	5.25*My	1.00
Bottom Only					
ORTHOTROPIC	.009	.015	3*My	3.75*My	1.29
			1.5*My[b]	3.0*My	1.03

[a] Efficiency ratio is the ratio of the collapse strength over the reinf. ratio ((5)/(3)) to that ratio for the two-layer orthotropic deck.

[b] Cracking occurs in top at 150% of yield strength of isotropic decks.

Based on these assumptions, Table 4 has been developed. This table shows that a two-layer orthotropic deck has significantly greater yield and collapse strength

than the isotropic decks. Since no transverse flexural cracking was observed in the Texas Test Bridge (Figure 3), even after yield mechanism formation, the ratio of longitudinal to transverse reinforcing of 2/3 in accordance with AASHTO practice is probably reasonable. Comparing structural efficiency of the orthotropic and isotropic patterns reveals that an orthotropic pattern is 33% more efficient than an isotropic pattern.

The most revealing comparison is that of an orthotropic deck with reinforcing in the bottom layer only. The bottom-layer only deck provides the same yield strength of an standard orthotropic deck using less than 60% as much reinforcing. The total volume of reinforcing is only slightly greater than that of a lightly reinforced isotropic deck but provides up to three times the yield strength and more than twice the collapse strength. Even if flexural cracking over the girders occurs, the collapse strength of the bottom-layer only orthotropic deck is greater. In this case, it is 71% stronger than the isotropic deck but requires only 25% more reinforcing, for an efficiency ratio 37% greater. It is also more efficient that a two-layer orthotropic deck. Based on either yield or collapse strength, the bottom-only orthotropic pattern is the most efficient.

Many researchers who have tested bridge decks with a single reinforcing layer near mid-depth of the deck and have found these decks did not perform any better than unreinforced decks [20]. What these researchers failed to observe was that cracking occurred first in the positive moment region and that yield in the positive moment region did indeed occur prior to yielding in the negative moment region. A single layer of bars near the center of the deck does not provide the post-cracking ductility provided by a bottom layer. According to the flexural behavior of bridge decks, no significant improvement should have been expected. Therefore, the lack of improved behavior for a single-centroidal-layer of reinforcing is evidence that flexural behavior of bridge decks should be the controlling criterion. If these researchers had tried placing the reinforcing at the bottom of the deck this writer believes they would have realized significantly improved performance.

Decks without top reinforcing bars avoid the problem of deck deterioration from corrosion of these bars. A bridge deck with flexural reinforcing in the bottom only can provide sufficient flexural strength. It is the most efficient placement of reinforcing because the reinforcement arrangement more closely conforms to the bending moments on the deck.

CONCLUSIONS

1) High collapse strength, or punch-out strength, of a bridge deck does not assure adequate serviceability.

2) Isotropic decks which have transverse-through-shrinkage cracking exhibit serious serviceability problems.

3) Vehicle loads are sufficient to cause flexural cracking in many isotropic or conventional bridge decks.

4) Strength of isotropic bridge decks after cracking is not adequate.

5) The load regime under moving loads is more severe than fixed position loads.

6) Flexural moments in the negative moment region over the interior girders are well below the flexural cracking strength of the concrete.

7) Decks with full flexural positive moment reinforcing according to AASHTO provide satisfactory strength.

8) A bottom-layer only AASHTO deck will not suffer degradation from corrosion of top reinforcing bars and can be expected to have superior durability compared to two layer decks with either isotropic or AASHTO reinforcing.

9) The greatest efficiency and economy of reinforcement placement for a specified strength is achieved when reinforcing is confined to the bottom mat.

ACKNOWLEDGEMENTS

This paper is a result of unfunded research by John H. Allen, P.E. Portions of this paper are the subject of allowed U.S. patent application serial number 299618 and allowed international patent application serial number WO 89/11003.

REFERENCES

1. STANDARD SPECIFICATIONS FOR HIGHWAY BRIDGES, 14th ed., AASHTO, Wash, D.C., 1989.
2. Turneaure, F.E. and Maurer, E.R., Principles of Reinforced Concrete Construction, John Wiley & Sons, New York, 1907.
3. Newmark, N. M., "Design of I-Beam Bridges", a part of "Highway Bridge Floors, A Symposium", Transactions, ASCE, vol 114, pp. 979-1072, 1949.
4. Perdikaris, P. C., and Beim, S., "RC Bridge Decks under Pulsating and Moving Load", Journal of the Structural Division, ASCE, Vol. 114, No. 3, March, 1988.
5. Allen, J. H., "Proposed Research Program for Improving Bridge Deck Construction and Rehabilitation", Presented to the Concrete Bridge Subcommittee of the AASHTO Bridge Subcommittee, Atlanta, GA, May, 1988.
6. Loftus, Michael J., Isotropic Reinforcement: Field Experience Through 1987, Engineering Research & Development Bureau, New York State DOT, March, 1988.
7. Fang, I.K., Worley, J.A., Burns, N.H. and Klingner, R.E., "Behavior of Ontario-Type Bridge Decks on Steel Girders", Research Report 350-1, Center for Transportation Research, Univ. of Texas, Austin, TX, Jan., 1986.
8. Elling, C.W., Klingner, R.E., and Burns, N.H., "Distribution of Girder Loads in a Composite Highway Bridge", Center for Transportation Research, U. of Texas, Austin, TX, Dec., 1985.
9. Tsui, C.K., Burns, N.H. and Klingner, R.E., "Behavior of Ontario-Type Bridge Deck on Steel Girders: Negative Moment Region and Load Capacity", Research Report 350-3, Ctr. Trans. Research, U. of Texas, Austin, TX, Jan., 1986.
10. Kim, K.H., Dominguez, J.M., Klingner, R.E., and Burns, N.H., "Behavior of Ontario-Type Bridge Decks on Steel Girders", Research Report 350-4F, Center for Transportation Research, Univ. of Texas, Austin, TX, Jan., 1988.
11. C.O. Hays, J.M. Lybas and J.O. Guevara, "Test of the Punching Shear Strength of Lightly Reinforced Orthotropic Bridge Decks", Engineering and Industrial Experiment Station, University of Florida, Gainesville, FL, August, 1988.
12. Loftus, Michael J. and Pezze, Frank P., "1988 Visual Inspection of Isotropic Bridge Decks," Client Report 44. May, 1988.
13. Minutes of AASHTO Bridge Subcommittee, Federal Highway Administration files, 1957-1961.
14. Puckett, J.A. and Naiknavare, R.D., "A Review of bridge Deck Design Specifications Based on Recent Research Findings: project No. 38717, Addendum to the Final Report", Department of Civil Engineering, University of Wyoming, Laramie, WY, May, 1989.
15. Allen, J.H., "Cracking in Bridge Decks", presented at ACI Spring Convention, Toronto, Canada, March, 1990.
16. Allen, J.H., "Isotropically Reinforced Bridge Decks--A Different Look", presented at 1990 ACI Spring Convention, Toronto, Canada.
17. Allen, J.H., "Bridge Decks Without Top Bars--An Innovative Approach", presented at ACI Spring Convention, Toronto, Canada, March, 1990.
18. Fang, I.K., Worley, J.A., Burns, N.H. and Klingner, R.E., "Behavior of Isotropic R/C Bridge Decks on Steel Girders", Journal of Structural Engineering, ASCE, Vol. 116, No. 5, March, 1990, 659-678.
19. Jackson, P.A., "The global and local behaviour of bridge deck slabs", The Structural Engineer, Vol. 68, No. 6, March, 1990, 112-116.
20. Beal, David B., Reinforcement for Concrete Bridge Decks, Research Report 105, Engineering Research and Development Bureau, NYDOT, Albany, NY, July, 1983.

Heavy Loads on Prestressed Girders: The Probability of Flexural Cracking

VERNE A. GEIDL

Bridge engineers often need to determine the maximum safe load that may be allowed to pass over a prestressed concrete bridge. Frequently the need for the load to pass is urgent, requiring a swift but accurate evaluation of safety. Many times the maximum load is governed by flexural cracking, and the bridge must be analyzed to find the cracking moment capacity of the girders. A conventional bending analysis uses deterministic strength properties even though properties such as concrete strength and prestress force are random variables. Because of this, a conventional load capacity analysis cannot reveal the probability of failure (i.e., by flexural cracking) associated with the passage of an extreme load. Therefore, bridge engineers have been forced to try to account for the probability of failure by a combination of experience and engineering judgement. This approach is sometimes disquieting for those engineers required to set load limits, issue overload permits, or approve large temporary construction loads. A computer program was written to use a very accurate analytical model and probabilistic methods to calculate a population of cracking moment capacities, rather than a single, deterministic value. Using this data and information about the extreme load moment, the engineer can calculate an associated probability of cracking failure. This result along with other information can be used to help the engineer in making a final decision about the safety of the passage of an extreme load.

PROBABILISTIC CAPACITY ANALYSIS TOOL

Introduction

A research study (1), for the U.S. Department of Transportation through the TRANSNOW Northwest Transportation Center and in cooperation with the Idaho Transportation Department, produced a computer program to do probabilistic bending analysis of prestressed girders. The program is called Probabilistic Capacity Analysis Tool (PROCAT) and produces a population of cracking moment capacities (See Figure 1). The results of the program can be used to find the probability that a heavy load will cause flexural cracking. PROCAT can accept several standard cross-sections or any section made up of a combination of rectangular and triangular areas. The probabilistic analysis uses a very exact, analytical model that employs the non-linear stress-strain relationships for concrete. The model also accounts for the fact that live-load strains in the prestressing steel cause an
increase in the prestressing force (and moment capacity). In addition to PROCAT, a program called STEP1 was written to prepare input for the analysis.

Department of Civil Engineering, University of Idaho. Moscow, Idaho 83843

The Input Program

STEP1 is an interactive program that prepares the necessary input files for the analysis program. The entire input process usually takes only a few minutes. The user has the option of selecting one of several standard shapes or a nonstandard shape. The standard shapes include bulb-tees and AASHTO I-girders. To fit the needs of a particular agency, more standard shapes can be easily added to the program by creating the appropriate data files.

For nonstandard shapes, the user subdivides half of the cross

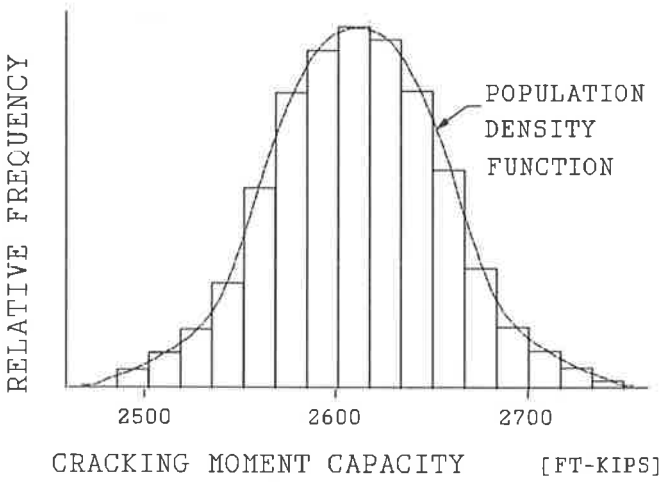

FIGURE 1 Sample population.

section into rectangular and triangular areas; the program assumes the shape has a vertical axis of symmetry (Figure 2). The maximum number of areas allowed in the half-section is 50. Each area has seven attributes: width; height; type (i.e., rectangle or triangle); vertical position (i.e., distance from the top of the girder to the top of the area); cast-in-place indicator (1 for cast-in-place, 0 for precast); class (i.e., whether the area is above or below the clear web (See Figure 2)); and 28-day concrete compressive strength. The "class" attribute is needed to deal with the random variation in girder dimensions during Monte Carlo simulation.

The user enters the specific weight of the concrete, not including the weight of any imbedded reinforcing steel or other dead

load. Because the girder dimensions are random values, the analysis program automatically calculates the girder dead load, including all longitudinal reinforcing steel (both prestressed and non-prestressed). The program also requests the value for the additional dead load that acts on the precast section, not including the dead load of the precast concrete and any imbedded longitudinal mild steel or prestressing steel. The user also enters the number, and locations of mild steel reinforcing bars and prestressing steel. One-half-inch, seven-wire, 270 ksi strand and Grade 60 mild steel reinforcing are assumed. The mild steel and prestessing steel are used in the calculation of the cracking moment capacity as explained later.

Analysis Options and Features

Probabilistic Analysis

PROCAT, will perform either a probabilistic analysis or a deterministic, mean-value analysis; both solve for the flexural cracking moment. The probabilistic analysis is accomplished by simulating a random sample of prestressed girders. The user selects the size of the sample (i.e. the number of girders to be simulated). The program uses Monte Carlo simulation to produce the sample; the Monte Carlo simulation procedure is discussed in detail later in the paper. The total cracking moment capacity of each girder in the sample is found using a very exact analytical model. The calculation of these moment capacities results in a corresponding sample (or population) of cracking moment capacities.

Important Features

Some important features of the analysis program are as follows:

- The maximum sample size that can be specified is 1000 girders.
- For a probabilistic analysis, the user must enter two numbers to be used as the seed values for the random number generator. This assures that all probabilistic analyses will be done with different series of random numbers.
- Because prestress losses are often a point of disagreement, the program offers maximum flexibility in this area. The user has the choice of specifying either a deterministic loss value (even though all other variables are randomly simulated) or the mean and standard deviation of the losses. For both options, default values are available (4).
- For the probabilistic analysis, the output consists of the mean and standard deviation of the total cracking moment capacity. In addition, the entire sample of cracking moment capacities is saved for statistical evaluation by the user. The input data are also included for user verification.
- For the mean-value analysis, the output consists of the mean cracking moment capacity of the girder and all of the input values for the girder (for user verification).

Mean-Value Analysis

As the name implies, the mean-value anaylsis finds the cracking moment capacity of the girder using the mean values for all properties and dimensions. Since, in this case, all properties and dimensions are single-valued (i.e., deterministic), this analysis produces only a single-valued result, rather than a population. However, there may be situations where the user simply wants to do a mean-value analysis, since this represents the expected value of the moment capacity. The expected value represents the location of the centroid of the area under the population curve. For symmetrical distributions, such as the normal distribution, the expected value is also the most likely value (i.e, the mode). For unsymmetrical distributions, such as the Weibull, the expected value does not coincide with the mode.

Software Standards and Portability

Both PROCAT and STEP1 are very portable. Both programs have been compiled and run on IBM PC/AT and compatible microcomputers. The analysis software also accommodates batch or interactive runs and has been

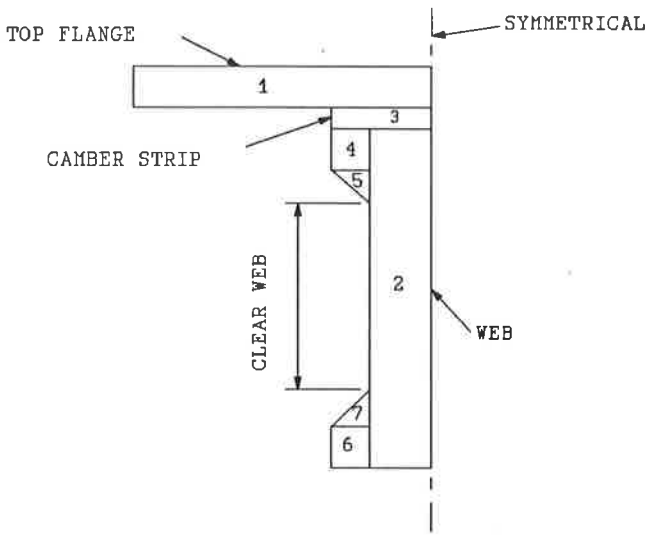

FIGURE 2 Typical cross section for input.

TABLE 1 RANDOM VARIABLE RESISTANCE PARAMETERS

RANDOM VARIABLE	DISTRIBUTION TYPE	MEAN	STANDARD DEVIATION	REFERENCE
Top Flange Width	Normal	+5/32* in.	1/4 in.	[7]
Top Flange Depth	Normal	0.0* in.	3/16 in.	[7]
Web Thickness	Normal	0.0* in.	3/16 in.	[7]
Girder Depth	Normal	+1/8* in.	5/32 in.	[7]
Effective Depth to Mild Steel	Normal	+1/8* in.	11/32 in.	[7]
E of Mild Steel	Normal	29000 ksi	957 ksi	[6]
F_y of Mild Steel	Log Normal	66.8 ksi	5.5 ksi	[6]
Initial Prestress	Normal	189 ksi	2.8 ksi	[8]
Prestress Loss	Normal	36 ksi	5.75 ksi	[8]
Prestress Ultimate Stress	Normal	281 ksi	7.0 ksi	[8]
Prestress Ultimate Strain	Normal	0.05	0.0035	[8]
Prestress E	Normal	28400 ksi	568 ksi	[8]
Depth to Prestressing	Normal	0.0* in.	1/16 in.	[8]

*Deviation from nominal dimension.

compiled and run on IBM 4300 series computers under VM/CMS and MVS/XA2.2 operating systems. The original programs, which were the basis for this software, have also been run on VAX, Prime, and Cray computers. Both PROCAT and STEP1 are written in ANSI Fortran 77

MONTE CARLO PROCEDURE

Simulation of Properties and Dimensions

For a probabilistic analysis, the random properties (6)(7)(8) (Table 1) of a sample girder are produced by Monte Carlo simulation. The statistics of the random concrete properties (i.e., compressive strength, modulus of elasticity, and flexural tensile strength) depend on the specified 28-day compressive strength and are calculated as outlined in reference (2). The user can easily change or customize the statistical parameters if desired.

Random values for the material properties and dimensions are produced in the following way. I use the term property to represent either a material property or a dimension. For each property, a random number generator produces a random number from the appropriate distribution type. For example, if the property is normally distributed, the random number generator produces random values that are normally distributed. Also, for a normal distribution, these random values have a mean of zero and a standard deviation of one and are between negative and positive infinity.

The simulated random property is computed by algebraically adding the product of the random number and the standard deviation of the property to the mean value of the property. The random number represents a random number of standard deviations from the mean. In this example, since the random numbers have a mean value of zero, as the sample size is increased, the mean value of the simulated property will approach the mean value of the property. That is, the mean plus zero equals the mean. In other words, the simulated property accurately represents the actual property. Each sample girder has a unique set of random values, simulated in this way, for its properties.

Finding the Cracking Moment Capacity

Selecting a Trial Curvature

The analytical model used in PROCAT was first developed by Hognestad(2), was later used by Mirza et al.(4) and Ellingwood et al.(5), and recently was applied to prestressed bulb-tee

girders (3). The process of using the analytical model to find the cracking moment can be summarized as follows. Once the properties of a girder are determined, an arbitrary curvature, ϕ, is imposed on the girder. That is, we specify that the girder is deflected downward. The curvature represents the slope of the strain distribution on the girder cross section, however we do not know the moment that caused the curvature. The equilibrium moment that corresponds to that curvature must be found.

Selecting a Trial Top-of-Girder Strain

Since the curvature only represents the slope of the strain distribution, we need to assume the strain at some point in the section to completely define a unique strain distribution. Therefore, a trial value for the top-of-girder strain (Figure 3) is

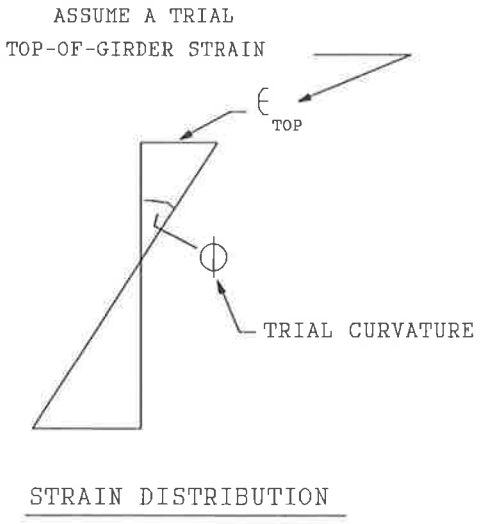

FIGURE 3 Strain distribution on cross section (precast deck).

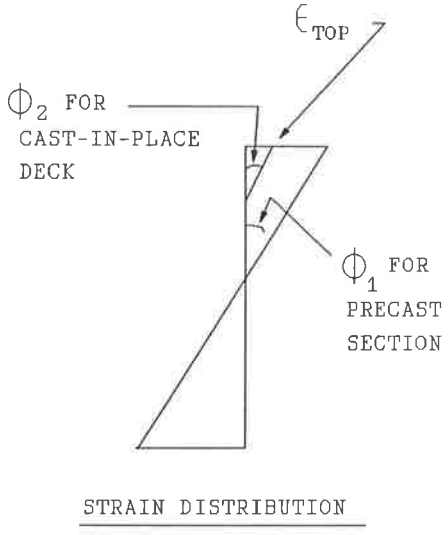

FIGURE 4 Strain distribution on cross section (CIP deck)

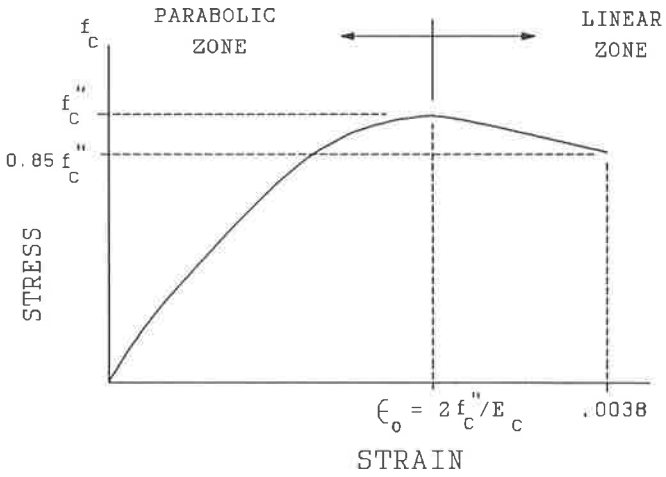

FIGURE 5 Concrete stress vs. strain.

assumed in order to establish a trial strain distribution. For a girder with a cast-in-place deck, the strain distribution is slightly more complicated (Figure 4). However, there is a fixed difference between the curvature of the precast girder and the curvature of the cast-in-place deck. There is also a fixed difference between the strain at the top of the precast girder and the strain at the bottom of the cast-in-place deck.

The Equilibrium Strain Distribution

Using the trial strain distribution and the stress-strain relationships (Figures 5 and 6) for the materials (2)(4), the total tensile and compressive forces, T and C, on the cross section are found. For the mild steel forces, the program uses an elastic-perfectly-plastic stress-strain curve using the mild steel

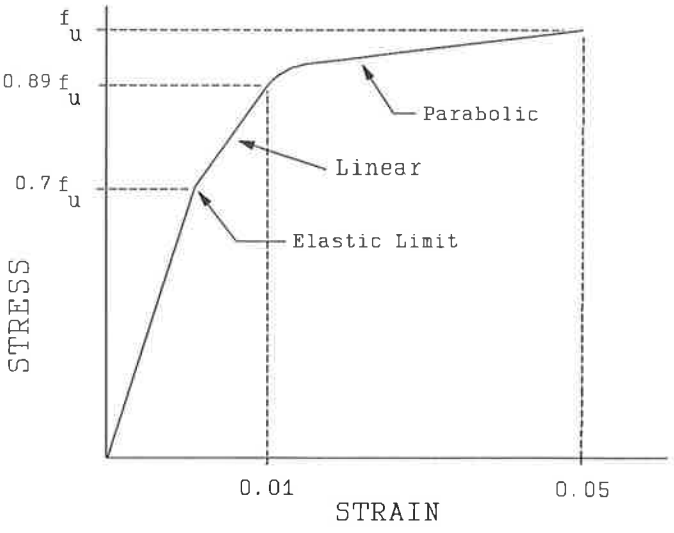

FIGURE 6 Prestressing steel stress vs. strain.

properties listed in Table 1. The current model assumes planes remain plane under bending (i.e., a linear strain distribution). Creep and shrinkage effects are only included by way of the prestress losses. If, after the force calculation, the net force (T - C) is not zero, a new trial value for the top-of-girder strain is selected and the process repeated. This process of varying the top-of-girder strain shifts the strain distribution (Figure 7). For example, if T is greater than C, then the strain distribution should be shifted to the right to increase C and decrease T. If T is less than C, the strain distribution should be shifted to the left. If T is
equal to C (i.e., the net force is zero), the equilbrium value for the top-of-girder strain has been found (Figure 8). The corresponding equilibrium moment for the trial value of ϕ is then calculated using the tensile and compressive forces on the section.

The Cracking Moment

Once equilibrium is found, PROCAT checks to see if the equilibrium moment is also the cracking moment. The equilibrium stress at the bottom of the girder is compared to the flexural cracking strength of the concrete. If the equilibrium stress is not equal to the cracking stress, a new trial curvature is selected and the process is repeated. For example, if the equilibrium stress is less than the cracking strength, a larger curvature would be tried. If the two stresses are equal, the equilibrium moment is the cracking moment capacity of the sample girder (Figure 9).

This process is repeated for each sample girder. Because the properties for each sample girder have unique values, the cracking moment capacities will also be unique. If the sample consists of, say, 100 girders, this Monte Carlo procedure computationally represents the building and testing of 100 individual girders.

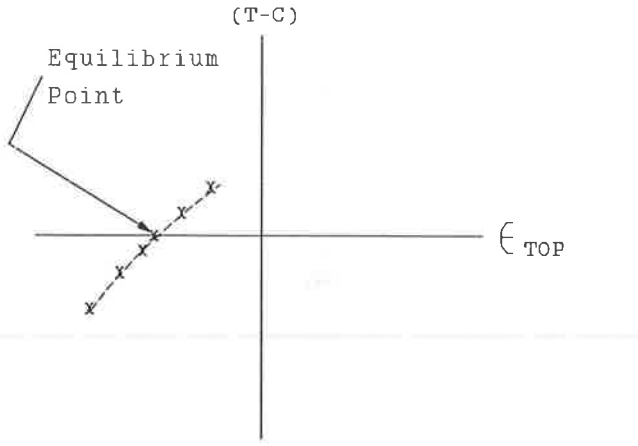

Figure 8 Schematic of search for equilibrium moment.

USING PROCAT OUTPUT

The Parent Distribution

The probabilistic analysis produces a sample population of cracking moment capacities for the subject girder. It is desirable to be able to describe that population mathematically. There are many known theoretical distribution types (for example, the normal distribution and the Weibull distribution) that can be considered to represent the sample population. The distribution that best represents the sample is known as the parent distribution and can be found using standard statistical methods. Once a parent distribution type is chosen, this implies that we believe our sample came from a larger population distributed according to the parent distribution. Previous studies (9) found that the population of moment resistances for

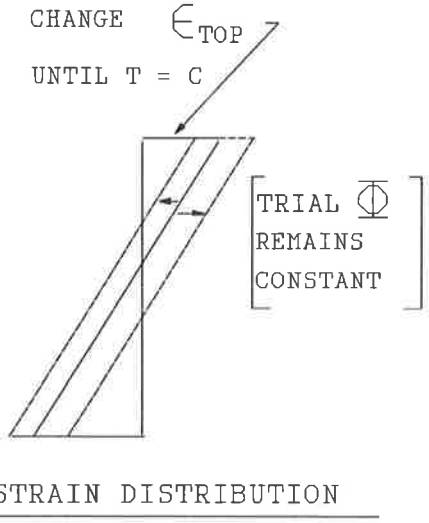

FIGURE 7 Shifting strain distribution for equilibrium.

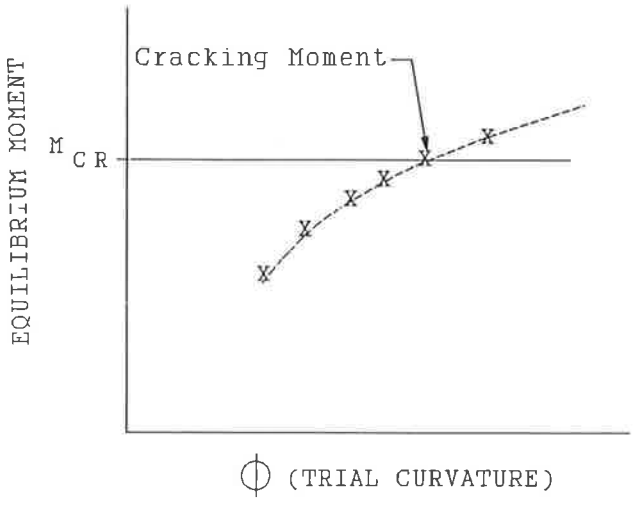

FIGURE 9 Schematic of search for cracking moment.

bulb-tee girders could usually be represented by a normal distribution. No attempt is made here to recommend a parent distribution type for cracking moment resistances of prestressed bridge girders. Since nearly all of the random properties are normally distributed, it is reasonable to assume that the moment capacity might also be normally distributed. However, for a given girder, the sample population produced by PROCAT should be statistically evaluated to determine a parent distribution.

Finding the Probability of Failure

Given adequate information about the load moment, the probability of failure can be calculated using the cumulative distribution function for the parent distribution. For example, suppose the population of moment resistances for a bridge girder turns out to be normally distributed (Figure 10). Further, suppose an extreme load needs to pass over the bridge and that the load will result in a total moment of 2500 ft-kips in the girder. Assume the extreme load is carefully controlled so that the 2500 ft-kip moment can be taken to be deterministic (i.e., not random). Using the mean, μ=2610 , and the standard deviation, σ=35.6, of the cracking moment capacity, we first calculate the standard normal variable, z, and get

$$z = (2500 - \mu)/\sigma = -3.09 \quad (1)$$

where

z = number of deviations from the mean,
μ = mean cracking moment capacity, and
σ = standard deviation of cracking moment capacity.

The probability that the girder will have a moment capacity, M, less than 2500 ft-kips is

$$P[M \leq 2500 \text{ ft-kips}] = \Phi(z) = .001 \quad (2)$$

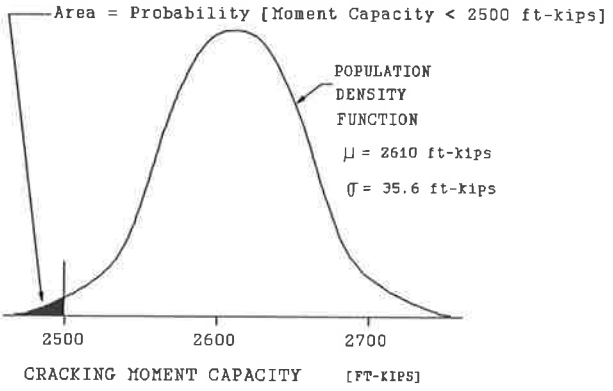

FIGURE 10 Population of cracking moment capacities.

where

Φ = the standard normal cumulative distribution function.

Values for the standard normal cumulative distribution are available in tables and on many hand-held calculators. Physically, this probability represents the area in the tail of the population curve below a value of 2500 ft-kips (See Figure 10). This result indicates that there is a 1/1000 chance that the load would cause flexural cracking in the girder.

An alternative to the use of a parent distribution, such as Φ above, is to use the actual, discrete cumulative distribution of the sample. Other methods are also available as outlined in reference (10). In any case, using normal methods of reliability theory, a probability of failure can be calculated for either a deterministic extreme load or a probabilistic extreme load.

Realistic Application of Results

Some discussion of how to apply the results obtained by PROCAT is in order. It is important to note that PROCAT only produces information about the cracking capacity of a girder. Information about the load moment must come from other sources. As suggested in the example, the load moment is also a random variable. Its variability must be either minimized or quantified in some way in order to calculate a meaningful probability of failure. Often engineers choose to minimize that variability by weighing each axle of the load, carefully controlling the location of the wheel lines on the bridge, limiting the speed of the load (e.g., 5 mile-per-hour maximum), prohibiting shifting of gears, and maintaining a constant speed (i.e., no braking or acceleration). The engineer may also use finite element analysis or methods such as those presented by Bakht and Jaeger (11) to calculate a more accurate load moment. In any case, one should attempt to minimize the uncertainty associated with the load moment analysis. By carefully controlling the load and the moment calculation, it is often reasonable to establish a deterministic value for the load moment. This may affect the theoretical purity of the resulting probability of failure, but not necessarily its practical usefulness. Individual agencies may well choose not to calculate a probability of failure, but they can still use the knowledge about the variability of the cracking moment capacity to aid the process of dealing with extreme loads.

The statistical results that PROCAT provides are a valuable source of **additional information.** The engineer can use this additional information to **help** make a decision about the passage of the extreme load. That is, **the information provided by using PROCAT should not be seen as a substitute for engineering judgement, but rather as an additional aid to that judgement.** The situation is similar to the way finite element techniques are used to help in this same area. The intention is that PROCAT will help the engineer to make better decisions about the safety of the passage of extreme loads.

CONCLUSIONS

Probabilistic analysis is a powerful tool to aid the engineering

decision-making process. The computer program PROCAT, introduced in this paper, is written specifically for finding the probabilistic, flexural cracking strength of prestressed concrete girders; it does not find the statistical parameters of the applied load moment. The cracking strength statistics provided by the software is important, additional information to help in assessing the safety of extreme loads on prestressed concrete structures. By providing the strength information needed to calculate a probability of failure, PROCAT contributes to a more rational process for dealing with load limits, overload permits, and construction loads.

ACKNOWLEDGEMENTS

The author appreciates the funding provided by the TRANS-NOW Northwest Transportation Center in cooperation with the U.S. Department of Transportation and the significant funding provided by the Idaho Transportation Department.

REFERENCES

1. V. A. Geidl and S. Saunders. Calculation of Reliability for Time-Varying Loads and Resistances. In *Structural Safety*, Elsevier, Amsterdam, Vol. 4, 1987, pp.285-292.
2. E. Hognestad. *A Study of Combined Bending and Axial Load in Reinforced Concrete Members*. Bulletin No. 399, Engineering Experiment Station, University of Illinois, Urbana, 1951, 128 pp.
3. B. Khafagi and V. A. Geidl. Reliability of Cracked, Prestressed Girders. In *Proceedings: ASCE Confer ence on Probabilistic Mechanics*, Blacksburg, VA., 1988, pp. 309-312.
4. S. Mirza, D. Kikuchi and J. MacGregor. Flexural Strength Reduction Factor of Bonded Prestressed Concrete Beams. In *Journal of the American Concrete Institute*, July-Aug., 1980, pp. 237-246.
5. B. Ellingwood, T. V. Galambos, J. G. MacGregor and C. A. Cornell. *Development of a Probability Based Load Criterion for American National Standard A58*. NBS Special Publication 577, National Bureau of Standards, June 1980.
6. S. A. Mirza and J. G. MacGregor. Variability of Mechanical Properties of Reinforcing Bars. In *Journal of the Structural Division*, ASCE, Vol. 105, No. ST5, Proc. Paper 14590, May, 1979, pp. 921-937.
7. S. A. Mirza and J. G. MacGregor. Variations in Dimensions of Reinforced Concrete Members. In *Journal of the Structural Division*, ASCE, Vol. 105, No. ST4, Proc. Paper 14495, April, 1979, pp. 751-766.
8. S. A. Mirza, M. Hatzinikolas and J. G. MacGregor. Statistical Descriptions of Strength of Concrete. In *Journal of the Structural Division*, ASCE, Vol. 105, No. ST6, Proc. Paper 14628, June, 1979, pp. 1021-1037.
9. V. A. Geidl. *Structural Reliability Assessment of AASHTO Limit States Design for Prestressed Concrete Bulb-Tee Bridge Girders*, Department of Civil Engineering, University of Idaho, Moscow, Idaho, May, 1985.
10. P. Thoft-Christensen and M. J. Baker. *Structural Reliability Theory and Its Applications*. Springer-Verlag, New York, 1982.
11. B. Bakht and L. G. Jaeger. *Bridge Analysis Simplified*. McGraw-Hill, New York, 1985.

Code Predictions Versus Small Scale Bridge Deck Model Test Measurements

PHILIP PERDIKARIS AND MICHAEL PETROU

This paper presents the test results of eight 1/6.6 bridge deck models of an 8.5 in. thick and 50 ft long prototype concrete bridge deck supported on four simply supported steel girders spaced at 7 ft or 10 ft and subjected to a static concentrated wheel-load. The effects of the lateral restraint, girder spacing and amount of reinforcement on the behavior of the deck is determined and discussed. In addition to the enhancement of the ultimate load carrying capacity of the deck, membrane compressive forces present in the deck may shift the primary failure mode from a flexural type to that of punching shear. The effect of this arching action mechanism on the bridge deck response explains the differences between the observed ultimate strength values and the shear strength predictions by the ACI 318 and the European CEB Code. The shear capacity code predictions are conservative (down to about 28% of the measured ultimate strength values). The level of restraint (deck continuity) in a non-composite bridge deck affects the arching action mechanism considerably higher than the amount of reinforcement specified by the AASHTO and Ontario design approach and the girder spacing used in existing highway concrete bridge decks (7 to 10 ft).

The improvement of the current AASHTO design approach for reinforced concrete bridge decks (1) is the major objective of an on-going research project at Case Western Reserve University. Non-composite, reinforced concrete bridge deck models (1/6.6 scale) supported on steel girders are tested under static, fixed pulsating and moving wheel-loads (2 to 4). A prototype girder spacing of either 7 ft or 10 ft (2.13 m or 3.05 m) is assumed corresponding to a lower and upper girder spacing limit, respectively, for highway reinforced concrete bridge decks built in North America. This paper focuses on the effects of reinforcement ratio, girder spacing and lateral restraint on the load-deflection response and failure mode of reinforced concrete highway bridge decks subjected to a static concentrated wheel-load.

The reinforced concrete deck models are tested at nine specified locations to study the influence of the deck continuity level (lateral restraint). The failure mode (flexural or punching shear) for each restraint level and girder spacing is determined. Selected deck panels simply supported on adjacent steel girders are also tested to determine a lower limit of the compressive membrane action which enhances the load-carrying capacity of the decks (5, 6). It is apparent that, although eventually all the decks punched through, the punching shear mode is more prevalent for the orthotropically reinforced decks with girders spaced at 7 ft (2.13 m). For the decks with a girder spacing of 10 ft (3.05 m) failure occurred in a combined flexural-shear type mode. Finally, the ultimate strength values from the physical model tests are compared with the flexural capacity of the deck predicted by the yield-line theory (7) and the shear capacity of the deck predicted by the ACI 318 (8) and the European CEB Code (Comite Euro-International du Beton) (9).

Department of Civil Engineering, Case Western Reserve University, Cleveland, Ohio 44106

BEHAVIOR OF BRIDGE DECKS - DISCUSSION OF MODEL TEST RESULTS

Tests are performed on 1/6.6 scale non-composite concrete deck slab models (see Fig. 1) on steel girders reinforced according to the AASHTO (ρ_t = 0.7% top and bottom transversely and ρ_ℓ = 0.35% top and bottom longitudinally) and the current Ontario Highway Bridge Design Code (ρ = 0.3% top and bottom in both transverse and longitudinal directions)(10). The testing program is presented in Table 1. Only the results of the tests performed under a static load are presented in this paper. The assumed prototype structure is a 50 ft (15.24 m) long, simply supported, non-composite highway bridge with an 8.5 in. (216 mm) thick reinforced concrete deck on four W36x150 steel girders spaced at either 7 ft (2.13 m) or 10 ft (3.05 m). Details regarding the model concrete and steel used and instrumentation can be found in Refs. 2 to 4. The measured ultimate strength values, V_{exp}, of the deck models (B series) subjected to a static concentrated wheel-load with a prototype contact area of 10 in. (longitudinal) x 24 in. (transverse) (254 x 610 mm) are shown in Tables 2 and 3.

The load-deflection curves for all bridge deck models are presented in Fig. 2. The curves with a distinct nearly horizontal plateau, indicating extensive steel yielding and a ductile response, correspond to the deck panels that failed primarily in flexure. All the specimens with a ductile response eventually punched through. The presence of a compressive membrane action in the deck delays the opening of the flexural cracks and stressing of the tension reinforcement. This may shift the primary failure mode from flexural to punching shear. The reinforced concrete deck models that failed primarily in shear exhibited a brittle behavior.

Representative load-deflection curves in terms of non-

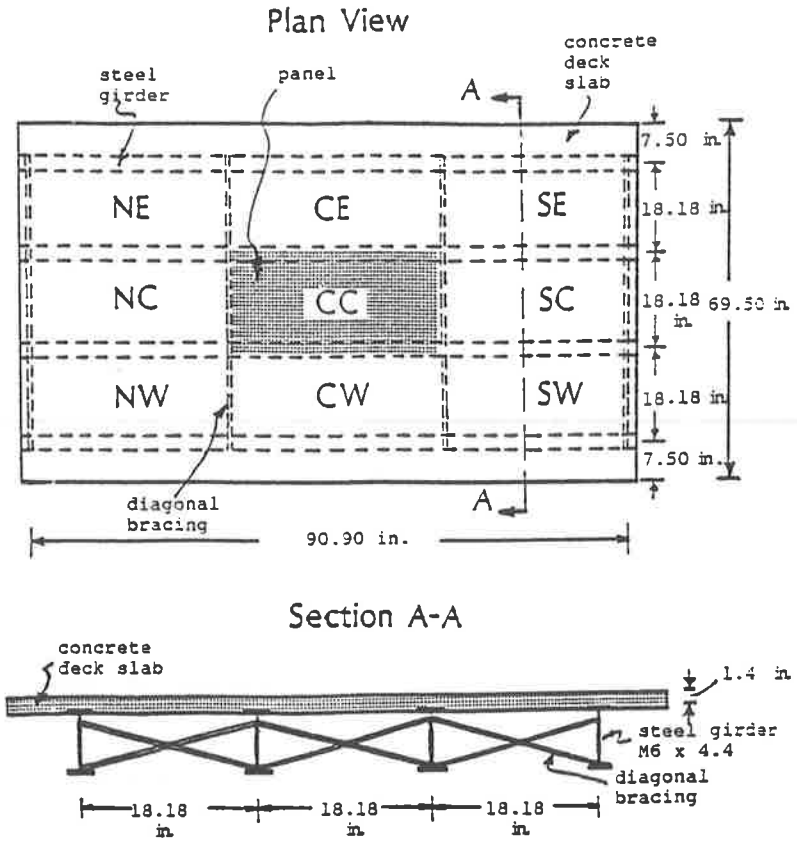

FIGURE 1 Dimensions for the 1/6.6 scale bridge deck model with a prototype girder spacing of 10 ft simply supported over a 50 ft span (1 in = 25.4 mm; 1 ft = 0.3 m).

dimensional parameters are presented in Fig. 3. The applied load to ultimate strength ratio is plotted as a function of the net load-point deck deflection to thickness ratio for two reinforcing patterns (AASHTO and Ontario design), two prototype girder spacings (7 and 10 ft) and two extreme deck boundary conditions (full and no deck continuity). The ultimate net deck deflections never exceeded 50% of the deck thickness. A much narrower peak deflection range of about 0.3h to 0.45h (h = deck thickness) was observed for the isotropically reinforced decks (Fig. 3b) compared to that of 0.08h to 0.46h for the AASHTO deck design (Fig. 3a). The decks reinforced according to the AASHTO Code showed considerably higher influence of girder spacing and lateral restraint on the type of failure mode than in the case of the "Ontario" decks. It is apparent that the response of the lighter reinforced decks (Ontario design), is really independent of girder spacing for prototype values between 7 and 10 ft, at least for the boundary conditions present in non-composite "concrete slab - steel girder" type bridge decks.

The concrete strains on the top deck surface in the transverse direction (perpendicular to the traffic direction) measured next to the loaded area and the steel strains in the transverse tension steel measured at the center of selected deck specimens are presented in Fig. 4 as a function of the applied load to ultimate strength ratio. Results are shown for the simply supported deck panel BO-10S (no deck continuity) and a partially continuous (higher level lateral restraint) deck panel of BO-10C with orthotropic reinforcement (AASHTO) and 10 ft prototype girder spacing. For the concrete strain measurements, data point A (BO-10S) and for the steel strain measurements, data points B (BO-10S) and C (BO-10C) correspond to the largest strain values recorded before the malfunction of the gages. The shape of the load-strain curves, the peak compressive concrete strain value and the load level at which concrete strain peaks and reinforcement yields are closely related to the mechanics of the arching mechanism and the type of failure mode. As indicated in Fig. 4, in the case of BO-10C (punching shear mode rather dominant) the top transverse concrete strain measured next to the applied load peaks closer to the ultimate load level with a lower peak value than that measured in specimen BO-10S, where the primary mode of failure is flexural. Initially, both top surface concrete and bottom steel strains increase at more or less the same rate up to the first flexural cracking. Beyond this point, the transverse tension steel strains at the bottom of the deck increase much faster than the compressive concrete strains at the top of the deck (neutral axis moves upwards). It is important to note that while the transverse tension steel starts yielding (at 2000 to 2500 $\mu\epsilon$) the rate of increase in the transverse concrete strain

TABLE 1 EXPERIMENTAL PROGRAM FOR THE 1/6.6 SCALE BRIDGE DECK MODEL SPECIMENS WITH A GIRDER SPACING OF 10 AND 7 ft (1 psi = 6.9 kPA; 1 in = 25.4 mm)

Deck Model	Boundary Cond.	h (in.)	Reinforcing Pattern	Number of Static Load Tests	Average Compressive Strength, f'_c (psi) (2 x 4 in. Cyl.)
BI-10C	cont.[a]	1.40[c]	isotropic[d]	6	7,259
BO-10C	cont.	1.40	orthotropic[e]	6	7,011
BI-10S	s.sup.[b]	1.40	isotropic	1	6,497
BO-10S	s.sup.	1.40	orthotropic	1	6,907
BI-7C	cont.	1.30	isotropic	5	6,685
BO-7C	cont.	1.30	orthotropic	5	5,783
BI-7S	s.sup.	1.30	isotropic	1	6,917
BO-7S	s.sup.	1.30	orthotropic	1	6,917

Notes:

[a] cont. = continuous bridge deck model (see FIGURE 1)

[b] s.sup.= simply supported deck panel model (see FIGURE 1)

[c] h = deck thickness

[d] ρ_ℓ = 0.003 and ρ_t = 0.003 (top and bottom)-Ontario design

[e] ρ_ℓ = 0.0035 and ρ_t = 0.007 (top and bottom)-AASHTO design

(ℓ = longitudinal; t = transverse)

TABLE 2 STATIC ULTIMATE STRENGTH OF CONTINUOUS BRIDGE DECK MODELS (1 lb = 4.45 N)

Deck Model	Ultimate Strength of Each Panel (lb)								Average Ultimate Strength (lb)
	NW	NC	NE	CW	CC	CE	SC	SE	
BI-10C[1]	-	5,994	5,200	-	7,600	6,079	5,188	5,125	5,864
BO-10C[1]	-	8,289	7,751	-	10,608	9,009	8,350	7,397	8,567
BI-7C[2]	8,514	8,070	8,563	-	8,858	7,874	-	-	8,376
BO-7C[3]	-	-	11,811	13,091	16,142	-	13,484	12,106	13,327

Note:

Sequence of testing:
1. CC - NC - CE - NE - SC - SE
2. NE - CE - NW - NC - CC
3. NE - SE - SC - CW - CC

TABLE 3 STATIC ULTIMATE STRENGTH OF SIMPLY SUPPORTED DECK PANEL MODELS (1 lb = 4.45 N)

Deck Model	Ultimate Strength (lb)
BI-10S	3,934
BO-10S	5,350
BI-7S	4,761
BO-7S	6,885

decreases and eventually it may even decrease. This means that as the ultimate strength level is approached the compressive resultant force carried by the concrete is decreasing and therefore a compressive membrane force should exist for equilibrium to be satisfied.

For a constant loaded area and deck thickness, the arching action mechanism in the deck, and as a result its load-deflection response and failure mode, is affected by the amount of reinforcement, girder spacing (deck slenderness) and lateral restraint. The lateral restraint is provided by the part of the deck slab surrounding the loaded area and by the deck supports.

Reinforcement ratio

The amount of reinforcement for an orthotropically reinforced deck panel (AASHTO design) is 130% and 17% higher in the transverse and longitudinal direction, respectively, than for an isotropically reinforced deck panel (Ontario design). The ratio of the measured ultimate strength values to the yield-line theory predictions, V_{exp}/V_J, are shown in Fig. 5 for both AASHTO and Ontario designs and different boundary conditions. The three levels of continuity C0, C1 and C2 correspond to the cases of a simply supported panel, an edge panel and a central panel of the continuous deck slab, respectively. As indicated in Fig. 5, while for the orthotropically reinforced decks (BO-10) the observed ultimate strength ranges between 1.4 (simply supported) and 2.7 (central panel of BO-10C) times the Johansen load (assuming a concentrated applied load), for the isotropically reinforced deck (BI-10) varies between 1.7 (simply supported) and 3.3 (central panel of BI-10C) times the Johansen load. The bottom reinforcement ratio for values equal to or higher than 0.3% seems to have a very small effect on the arching action for specimens with a span to thickness ratio equal to 13 (prototype girder spacing of 10 ft and deck thickness of 8.5 in.). In the case of a span to thickness ratio of about 9 (prototype girder spacing of 7 ft and deck thickness of 8.5 in.) the effect of reinforcement on the effectiveness of the arching mechanism is even smaller.

Girder spacing (deck slenderness)

The load-carrying capacity of all deck models increased with decreasing slenderness, as shown in Fig. 2. The effect of slenderness on the deck's ultimate deflection is considerably higher for the orthotropically reinforced model decks (AASHTO design), as can be seen in Fig. 2. As shown in Fig. 5, the influence of girder spacing on the enhancement of the deck's ultimate strength due to the arching mechanism is considerable, especially for those decks designed according to the current AASHTO Code. The fully restrained deck panels (central panel) with a prototype girder spacing of 7 ft (2.13 m) exhibited a load-carrying capacity increase over the Johansen load of about 2.2 and 1.5 times that measured in similarly restrained deck panels supported on steel girders spaced at 10 ft (3.05 m) for the AASHTO and Ontario design, respectively.

Lateral restraint

It is clear from Fig. 5 that the arching action mechanism becomes more prevalent with increasing rotational and translational transverse restraint in the deck. It appears that the enhancement of the deck's load carrying capacity is more sensitive to increasing lateral restraint for the AASHTO than the Ontario design independently of the girder spacing. The degree of influence of deck continuity on the arching action for the two reinforcing patterns (AASHTO and Ontario design) is considerably higher compared to the influence of girder spacing and amount of reinforcement.

CODE PREDICTIONS VS. TEST RESULTS

The ratio of the measured load-carrying capacity, V_{exp}, to the nominal shear strength according to the ACI 318 (1989) Code,

$$V_{ACI} = (2 + 4/\beta_c)\ b_o d\sqrt{f_c'} \le 4\, b_o d\sqrt{f_c'} \text{ (lb)} \quad (1)$$

where the cylinder compressive strength of concrete f_c' is

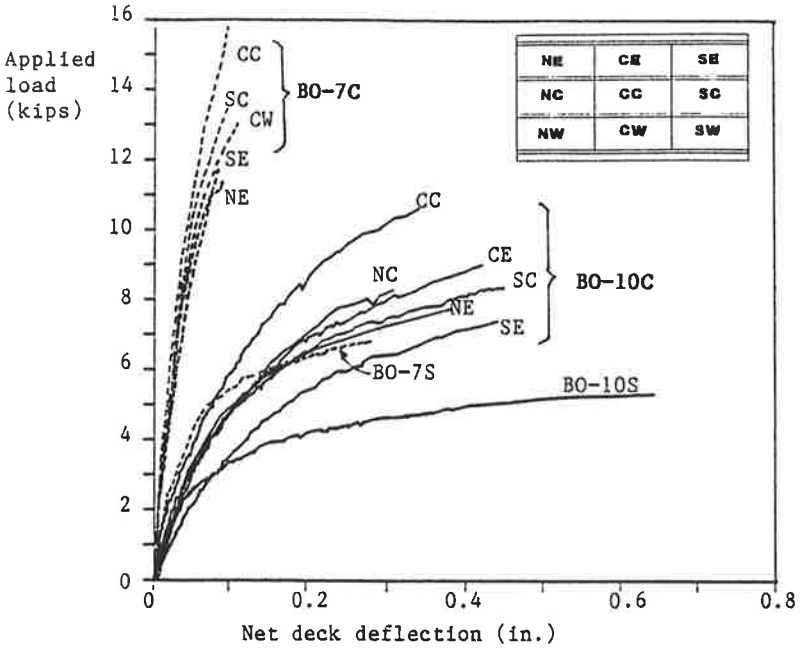

a) Orthotropic reinforcement (AASHTO design).

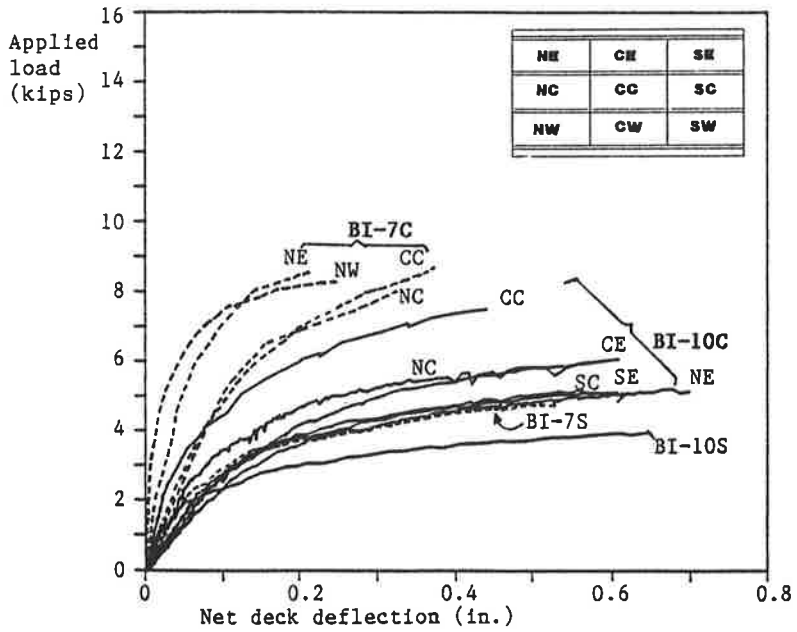

b) Isotropic reinforcement (Ontario design).

FIGURE 2 Experimental load-deflection curves under a static concentrated wheel-load for the 1/6.6 scale model bridge decks (girder spacing of 7 and 10 ft).

in psi, $\beta_c = 2.4$ is the ratio of the long-to-short side of the loaded area and b_o (in.) the perimeter of the critical section equal to the perimeter of the load area plus four times the effective depth d (in.), is shown in Fig. 5. Eq. 1 is unable to predict the shear capacity of laterally restrained slabs. It takes into account only the compressive strength of concrete, effective depth of the deck and the assumed perimeter of the critical section. The compressive membrane action enhances not only the flexural capacity of the deck but also its shear capacity. Hence, the ultimate strength of a highly restrained deck such as BO-7C, is considerably greater than the ACI Code shear strength prediction, as can be seen in Fig. 5. The ultimate strength of all panels for the isotropically reinforced deck model BI-10C (except that of the central panel CC) and all the non-continuous deck panels (simply supported) are very close to the ACI Code predictions (see Fig. 5). These specimens appear to have failed in flexure.

The shear resistance of a reinforced concrete slab according to the European CEB-FIP 1990 Model Code is

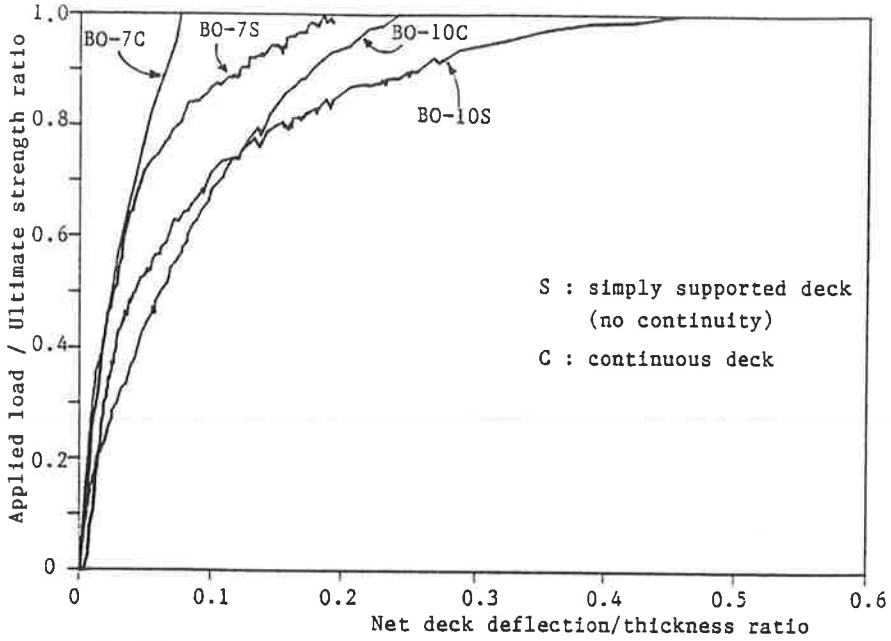

a) Orthotropic reinforcement (AASHTO design).

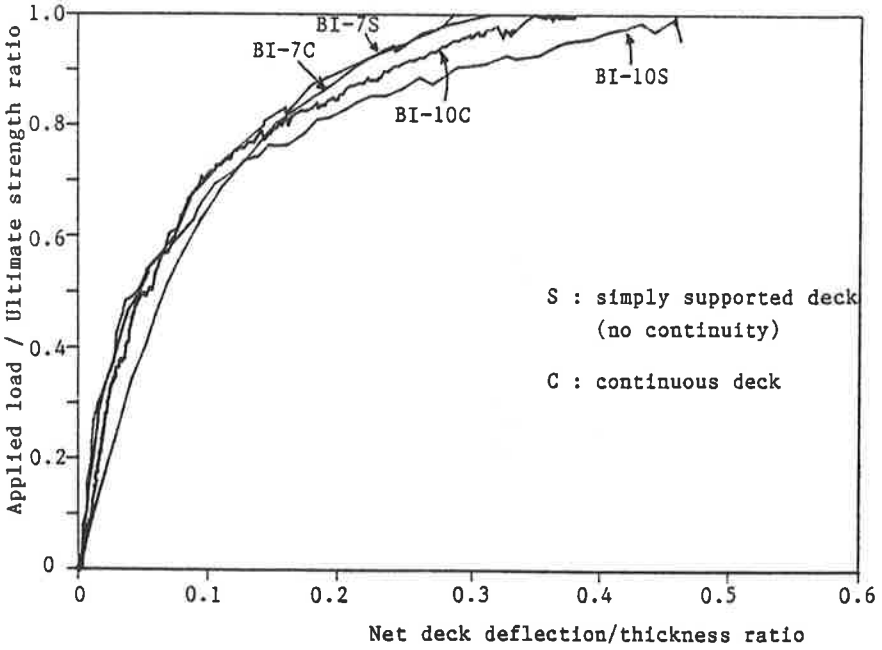

b) Isotropic reinforcement (Ontario design).

FIGURE 3 Non-dimensional load-deflection curves under a static concentrated wheel-load for two levels of deck continuity (S and C) and two girder spacings (7 and 10 ft).

given by the equation

$$V_{CEB} = 0.12\ \xi\ (100\ \rho f_{ck})^{1/3}\ ud \quad (N) \qquad (2)$$

where $\xi = 1 + \sqrt{200/d}$ (d in mm), u (in mm) is the perimeter of the critical section equal to the perimeter of the load area plus $4\pi d$(mm), ρ the average reinforcement ratio in the two orthogonal directions and f_{ck} the characteristic cylinder compressive strength of concrete (MPa). The CEB-FIP Model Code takes into account the effect of the flexural reinforcement on the shear capacity of the deck slab but it does not consider other important parameters, such as lateral and rotational restraint in the deck and deck slenderness. The CEB predictions, at least for the parameter values studied, appear to be either very similar to or slightly more conservative than the ACI predictions. For all non-continuous deck panels (simply supported) both ACI and CEB codes give predictions very close to the experimental findings, as expected,

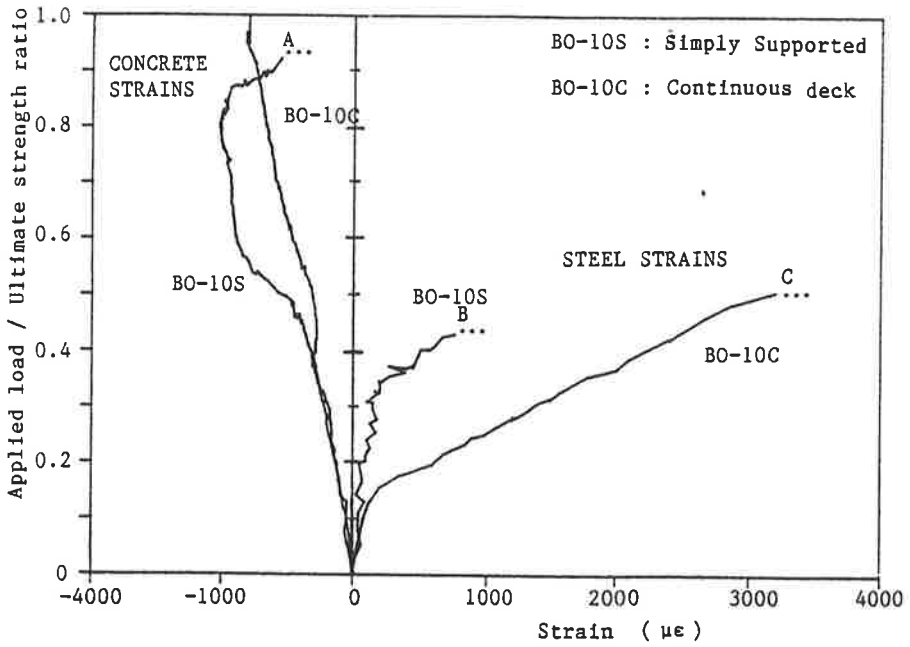

FIGURE 4 Measured transverse steel and concrete strain at the bottom midspan rebar and top deck surface next to the loaded area, respectively, for two levels of deck continuity (S and C) and a girder spacing of 10 ft as a function of the level of applied load.

independently of girder spacing and reinforcing pattern.

CONCLUSIONS

1. A given level of lateral restraint in the deck for the Ontario design has a higher influence on the effectiveness of the arching mechanism in enhancing its ultimate strength above the Johansen load than for the AASHTO design.
2. The enhancement of the deck's load carrying capacity appears to be more sensitive to increasing lateral restraint for the AASHTO than the Ontario design independently of the girder spacing.
3. At least for girder spacings between 7 and 10 ft and deck thickness of 8.5 in. (deck slenderness between 9 and 14) the level of lateral and rotational restraint (deck continuity) in a non-composite bridge deck affects the arching action mechanism considerably more than the decrease of girder spacing (from 10 ft to 7 ft) or increase of reinforcement (adopting AASHTO vs. Ontario design).
4. Although some of the decks, such as those designed according to the Ontario Design Code and supported on girders spaced at 10 ft, failed primarily in flexure, all of the decks eventually punched through with a maximum net deflection always less than 50% of the deck thickness. Those decks designed according to the AASHTO code (with either 7 or 10 ft girder spacing) exhibited a rather brittle response and a primary failure mode of punching shear.
5. The CEB-FIP (1990) shear strength predictions are either very similar to or slightly more conservative than the ACI predictions.
6. For all non-continuous deck panels (simply supported) both ACI and CEB codes give predictions very close to the experimental findings independently of girder spacing and reinforcing pattern.
7. Both ACI and CEB codes are more conservative in the case of decks with isotropic reinforcement (Ontario design).

ACKNOWLEDGMENTS

The model tests for highway bridge decks were performed at the Structures Laboratory of Case Western Reserve University. Aidong Wang, graduate research assistant in the Department of Civil Engineering, has performed part of the experimental work presented. Funding for this research program was provided by the Ohio Department of Transportation (ODOT) and the Federal Highway Administration. Any opinions, findings and conclusions expressed in this paper are those of the writers and do not necessarily reflect the views of ODOT and FHWA.

REFERENCES

1. AASHTO Standard Specification of Highway Bridges (1989), 14th Ed., American Association of State Highway and Transportation Officials, Washington, D.C.
2. Perdikaris, P.C., and Beim, S. (1986), "R/C Bridge Decks Under Pulsating and Moving Load," Journal of Structural Engineering, ASCE, 114(3), March, pp. 591-607.

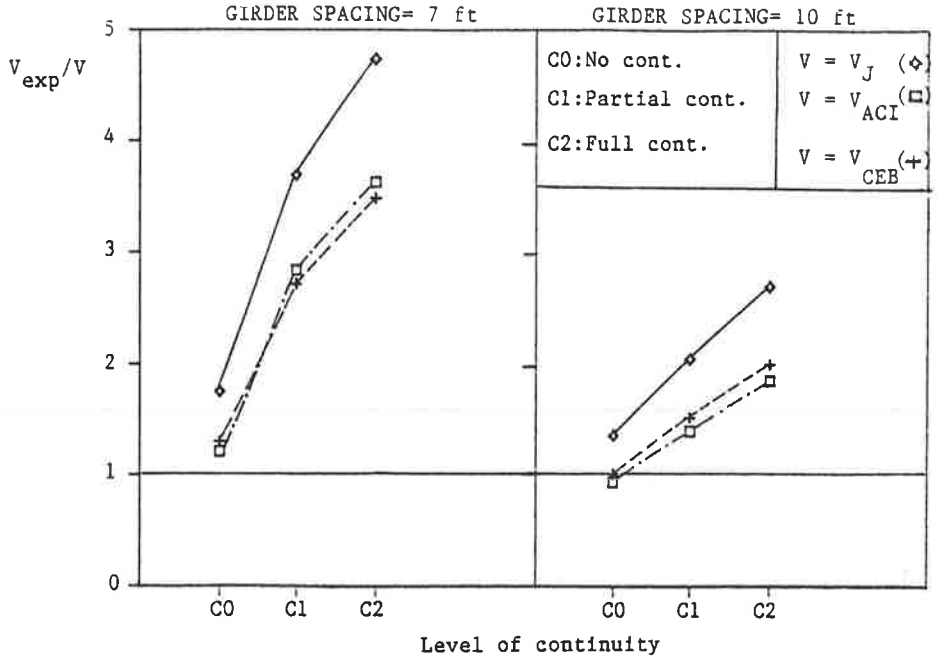

a) Orthotropic reinforcement (AASHTO design).

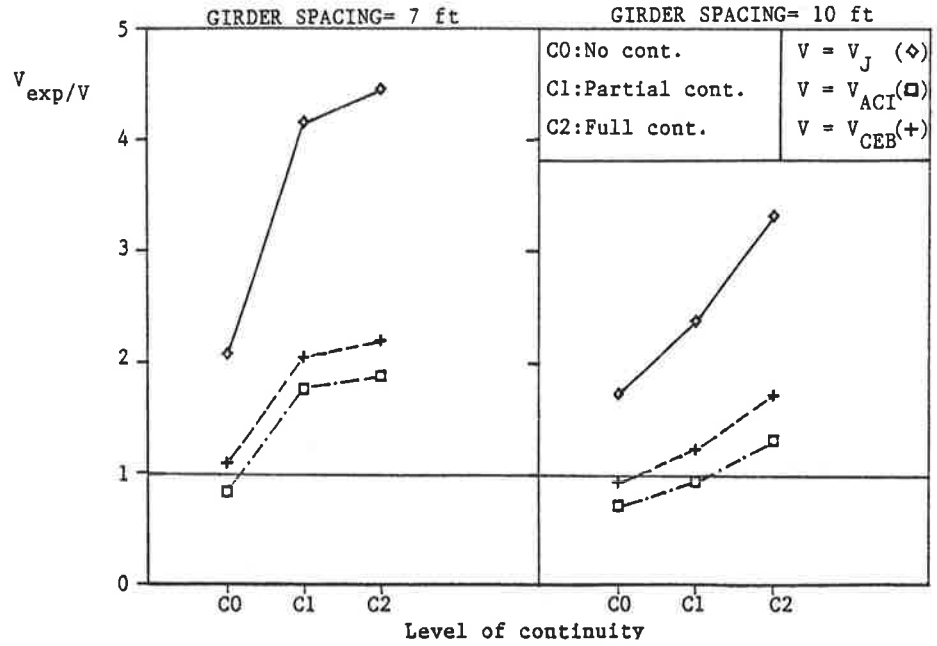

b) Isotropic reinforcement (Ontario design).

FIGURE 5 Comparison of experimental static ultimate strength values with yield-line theory and ACI, CEB code predictions.

3. Perdikaris, P.C., Beim, S., and Bousias, S. (1989), "Slab Continuity Effect on Ultimate and Fatigue Strength of R/C Bridge Deck Models," ACI Structural Journal, 86(4), July-August, pp. 483-491.
4. Petrou, M.F., and Perdikaris, P.C. (1990), "Small Scale Model Tests: Arching Action in Reinforced Concrete Bridge Decks;" 3rd International Conference on Short and Medium Span Bridges, Toronto, Canada, August.
5. Hewitt, B.E., and Batchelor, B. deV. (1975), "Punching Shear Strength of Restrained Slabs," Journal of the Structural Division, ASCE, 101(ST9), pp. 1837-1853.
6. Csagoly, P., Holowka, M., and Dorton, R. (1978), "The True Behavior of Thin Concrete Bridge Slabs," Transportation Research Record No. 664, Transportation Research Board, pp. 171-179.
7. Johansen, K.W. (1962), Yield-line Theory, Cement and Concrete Association, London.
8. ACI Committee 318 (1989), "Building Code Requirements for Reinforced Concrete and Commentary," American Concrete Institute, Detroit,

Michigan.
9. CEB-FIP Model Code (1990), First Draft, Bulletin No. 196, Comite Euro-Internationale du Beton, Lausanne, Switzerland, September.
10. Ontario Highway Bridge Design Code (1983), 2nd Ed., Highway Engineering Division, Ontario Ministry of Transportation and Communications, Downsview, Ontario, pp. 357.

Design of a Staged, Two-Rib Reinforced Concrete Arch Bridge

LAURIE G. MCGINNIS

A replacement bridge was needed across the Mississippi River between Minneapolis and St. Paul, in an area where the river valley is lined with natural limestone bluffs. There was strong support to replace the existing deck arch structure in kind, so design proceeded on a steel and concrete alternate. The concrete arch alternate consists of two arch spans, each 555 feet in length. Each span has two ribs; each rib is a twin-cell, conventionally reinforced concrete box. Staged construction was necessary to maintain traffic on the existing bridge. This meant one arch rib would be completed and in service for more than a year before the second rib is completed.

The first design challenge was analyzing the structure. The analysis included time-dependent loads in order to predict the magnitude of creep stresses and deflections in the arch ribs. An in-house computer program was utilized which indicated that the crown of the arch rib would deflect downward about 12 inches over time. This large deflection induces large moments in the arch at the fixed supports, so AASHTO's serviceability criteria for flexural members were applied to the section. No. 9 bars at 6 inches at each face satisfied all design criteria.

The second design challenge was predicting the magnitude and evaluating the effects of differential creep due to staged construction. The program predicted that the stage one arch will have deflected 2 inches more than the stage two arch at the time of closure. After closure, the stage one arch restrains deflection in the stage two arch and changes are accommodated by torsional creep. No. 6 stirrups at 12 inches are adequate for these torsional forces.

The third design challenge was preparing adequate construction plans. The plans define the shape of the arch by giving coordinates for the dead load polygon and values for vertical and horizontal camber to offset deflections. The plans also provide pedestal elevations for the spandrels which differ for each stage. The elevation difference accounts for the differential creep due to staged construction.

One of the first crossings of the Mississippi River in the Twin Cities connected Lake Street in Minneapolis with Marshall Avenue in St. Paul. This 100 year old wrought iron and steel deck arch could not be economically rehabilitated. A structural analysis which examined the existing bridge revealed that, in each of the four wrought iron arches, a total of 74 of the 106 main members needed replacement, either due to insufficient member size or the number of fatigue cycles. In addition, approximately 63% of the pins and pin plates of this pin-connected-arch truss were found to be overstressed. But due to its historical significance, the Minnesota Department of Transportation and FHWA agreed that the replacement bridge should be aesthetically pleasing to compliment the river valley and natural limestone bluffs. The surrounding communities preferred to replace the bridge with another deck arch so design proceeded on a steel and concrete alternate.

The concrete arch alternate consists of two arch spans, each 555 feet in length (see Figure 1). Each span has two ribs; each rib is a twin-cell, conventionally reinforced concrete box. A cast-in-place concrete box was chosen over a precast segmental concrete box for the following reasons:

- The box varies in height from the spring to the crown so there was little opportunity to realize the economy of repetitive castings.
- Precast elements would need to be match cast which increases the cost.
- The flat shape of the arch resulted in significant tension in the box at the supports. The amount of prestress needed to overcome this tension would be large

FIGURE 1 Rendering of two-ribbed concrete arch bridge.

Howard Needles Tammen & Bergendoff, 6700 France Avenue, Minneapolis, Minnesota 55435

and would possibly increase the required concrete area to keep compressive stresses within allowable limits.

- The tight construction schedule would require winter construction and heating of concrete elements for epoxy joints is difficult and expensive for a large number of joints. Joints also introduce the possibility of leakage.

The design of this arch presented many challenges but one of the most significant problems was accommodating staged construction. The existing bridge is a key link in the metropolitan area infrastructure. It carries about 20,000 vehicles per day and is a primary bus route. The DOT decided to leave the existing bridge essentially intact to maintain traffic during construction. In addition, the bridge connects two long-established neighborhoods with homes, businesses and parks along the approach roadway, so it was necessary to minimize right-of-way acquisition. In order to accommodate these requirements, the bridge needed to be stage constructed on an alignment as close as possible to the existing one.

The new bridge deck will be more than twice as wide as the existing deck and will carry four lanes of traffic, so it is well suited for staged construction (see Figure 2). The north half of the new bridge will be built first with only 2'-10" of clearance between the new and old bridge decks. After traffic is switched to use two lanes of the new bridge, the old bridge will be removed and the south half of the new bridge constructed. Then the two halves will be connected with closure pours at the spandrel caps and the decks.

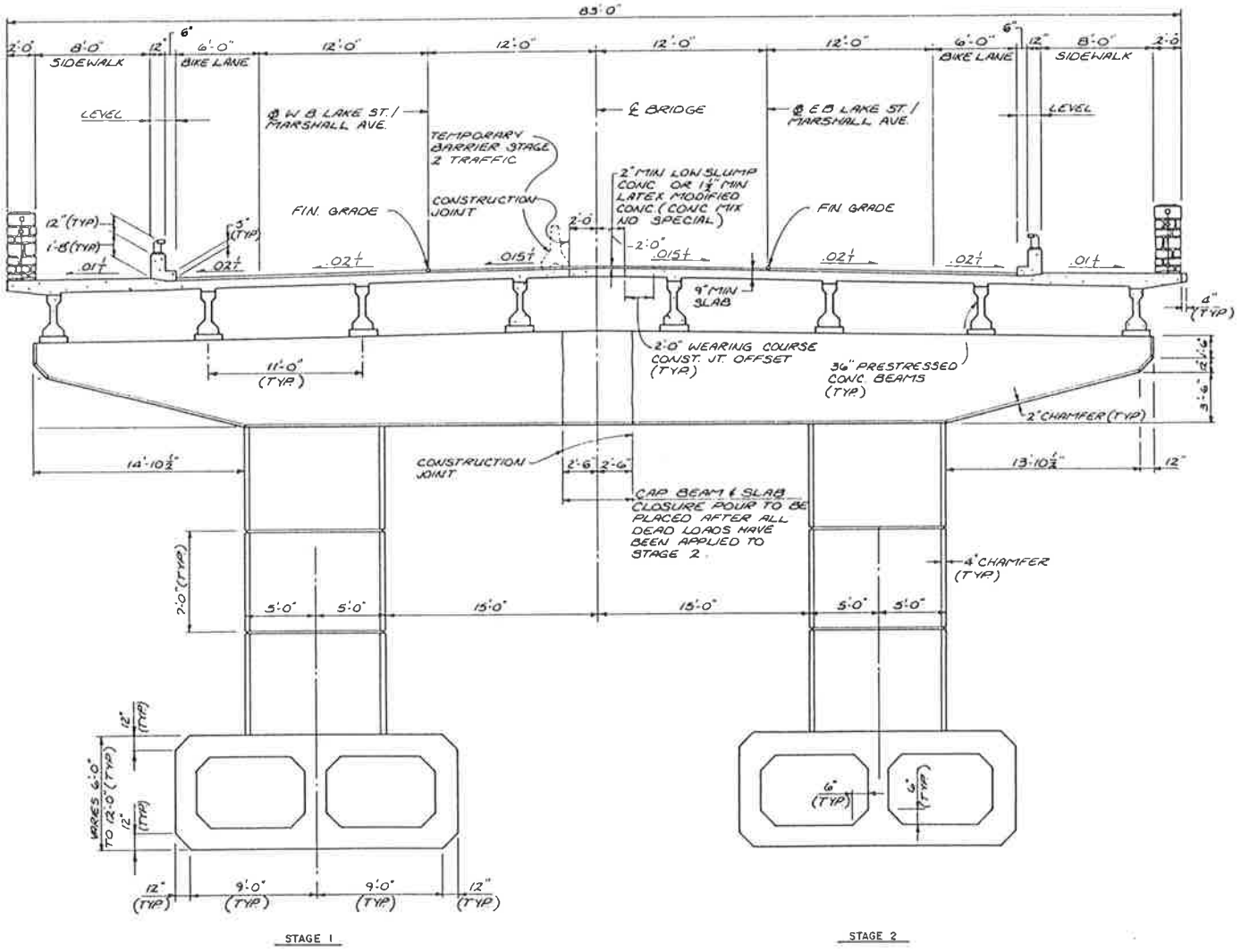

FIGURE 2 Transverse section indicating staged construction.

Staged construction adds complexity and interest to bridge design, be it steel or concrete construction. This project was no exception. One arch rib will be completed and in service for more than a year before the second rib is completed. This created three key challenges during design:

- Predicting the magnitude of time-dependent creep deflections for the arch ribs.
- Evaluating the effects of differential creep on the arch ribs and spandrels after connecting the two stages.
- Preparing plans which would ensure that the decks from both stages would be at the same elevation for closure.

ANALYZING THE STRUCTURE

Creep deformations in concrete structures can be significant, particularly when compressive stresses are high. For this concrete arch structure, creep deflections were expected to be large due to the relatively flat geometry of the arch rib. It was essential to know the magnitude of the deflection so that the arch rib and the deck could be cambered appropriately. But it was also necessary to know the difference in creep deflections between the stage one and stage two arch ribs at the time the closure pours would be made.

The means for obtaining the needed deflection information was available through an in-house computer program. The program is a matrix structural analysis program based on the direct stiffness method which can model and analyze any stable frame. It also has the capability to analyze time-dependent loads on concrete structures. The structure can be built member by member using the Erection Mode feature with creep, shrinkage, relaxation and elastic stresses and deflections accumulated at selected time intervals. Erection Mode models time-dependent losses for concrete based on procedures from the Precast Segmental Box Girder Bridge Manual, published by the Post-Tensioning Institute and the Prestressed Concrete Institute, which in turn are taken from the CEB-FIP bulletin d'information No. 111. Plots of concrete strains versus age and duration of loading were plotted and matched to published curves in order to validate the algorithms.

The arch model was initially developed two-dimensionally. The arch shape would need to match as closely as practical the dead load polygon for this arch. The spring and crown elevations had been determined in the preliminary design phase along with the dimensions of the twin-cell box. To determine the dead load polygon, the arch was modelled as a beam using the structural analysis program. The arch dead load was applied uniformly and the remaining superstructure dead loads were applied as joint loads at the spandrel locations. The resulting output for beam deflections became the coordinates for the centerline of the arch.

Both spans of the arch rib and all the spandrels were modelled as frame members. The concrete deck and prestressed concrete beams were modelled together as truss members with three deck joints for longitudinal movement. Initially, all joints in the model between the spandrels and the beams were fixed due to the planned use of fixed bearing assemblies. Under this condition, the stresses in the short, stiff spandrels near the crown were excessive under dead load. To reduce the large stresses, it was decided that the beams on top of spandrels near the crown would rest on expansion bearing assemblies. This allowed the spandrel to move independently of the superstructure where needed. Wind, temperature, seismic and live loads were applied to this final version of the model.

Dead load and time-dependent loads were applied to the concrete arch as it was "built" using the Erection Mode feature of the program. Age is a key variable in the determination of time-dependent stresses and deflections, so an accurate estimate of the age of each member at loading is important input to the analysis. To assist in developing a reasonable construction sequence and schedule for estimating member ages, discussions were held with a contractor. Based on these discussions, a schedule was assumed which loaded members at a young age so that the results for creep stresses and deflections would be conservatively maximized.

At this point, the model went three-dimensional. The Erection Mode feature provided the capability of building the stages independently, connecting them at the appropriate point in time and analyzing the behavior of the newer rib and the older rib together over time. The stage one structure was built by adding members and accumulating stresses in the following order: construct arch rib and remove falsework; add spandrels near springs; add spandrels near crown; add beams and diaphragms; add deck; add railings and overlay. After an appropriate time interval for demolishing the old bridge and constructing foundations, the stage two structure was built in a similar manner. Then the two halves were connected and aged for almost 30 years, the point when time-dependent changes are essentially complete.

The results produced by the Erection Mode analysis indicated that total dead load and creep deflections at the crown of the arch rib would be over 12 inches downward. The results also indicated that the stage one arch will have deflected 2 inches more than the stage two arch at the time of closure.

DESIGNING THE ARCH

The most significant impact of the dead load and creep deflections was large moments induced in the arch at the fixed supports. A temperature fall of 45°F also induced large moments at the support, which resulted in AASHTO's Load Group IV controlling the design.

The longitudinal reinforcement in the arch was designed per AASHTO's criteria for compression members and

flexural members. Based on the criteria for compression members, the cross-sectional area required one percent reinforcement steel. But, the moments produced under dead load, creep and temperature loading cause the arch to behave like a beam and, in fact, result in a cracked section. For this reason, AASHTO's serviceability criteria for flexural members were applied. Nearly twice as much reinforcement steel was required to meet the serviceability requirements. The final bar arrangement was No. 9 bars at 6 inches at each face for a total of 260 bars in cross-section (see Figure 3).

In evaluating the effects on the arch ribs and spandrels of connecting the two stages, the program output indicated that there would be no significant problems. The total long-term deflection of the stage two arch rib is estimated to be slightly less than that of the stage one rib. As the arches creep at different rates, changes are accommodated by the structure through torsional creep and minor cap and deck rotations. Torsional forces doubled at the quarter point of the stage two arch rib as its deflections are restrained by the stage one rib, but No. 6 stirrups at 12 inches are still adequate. Moments increase slightly in the spandrel caps as a result of differential creep but, again, not enough to alter the reinforcement.

PREPARING CONSTRUCTIBLE PLANS

Following the completion of the arch design, effort was concentrated on preparing plans which would accurately and adequately communicate the necessary information for building the structure. Most of the key decisions related to the issue of deflections: total long term deflections and differential deflections between stages one and two.

Two types of information needed to be communicated for constructing the arch: coordinates to define the shape and cambers to offset deflections. The decision was made to define the shape of the arch in the plans by giving the coordinates for the dead load polygon. Coordinates were more accurate and more useful than an equation since the arch would actually be built to the cambered shape. Coordinates were provided to the centerline of the arch at each spandrel location by giving a horizontal distance from an origin and a vertical distance above a base elevation (see Figure 4).

The arch rib will be cambered during construction for the total dead load and creep deflection, so the final deflected shape will approximate the dead load polygon after 30 years. The values for vertical and horizontal camber were obtained from the program output and were

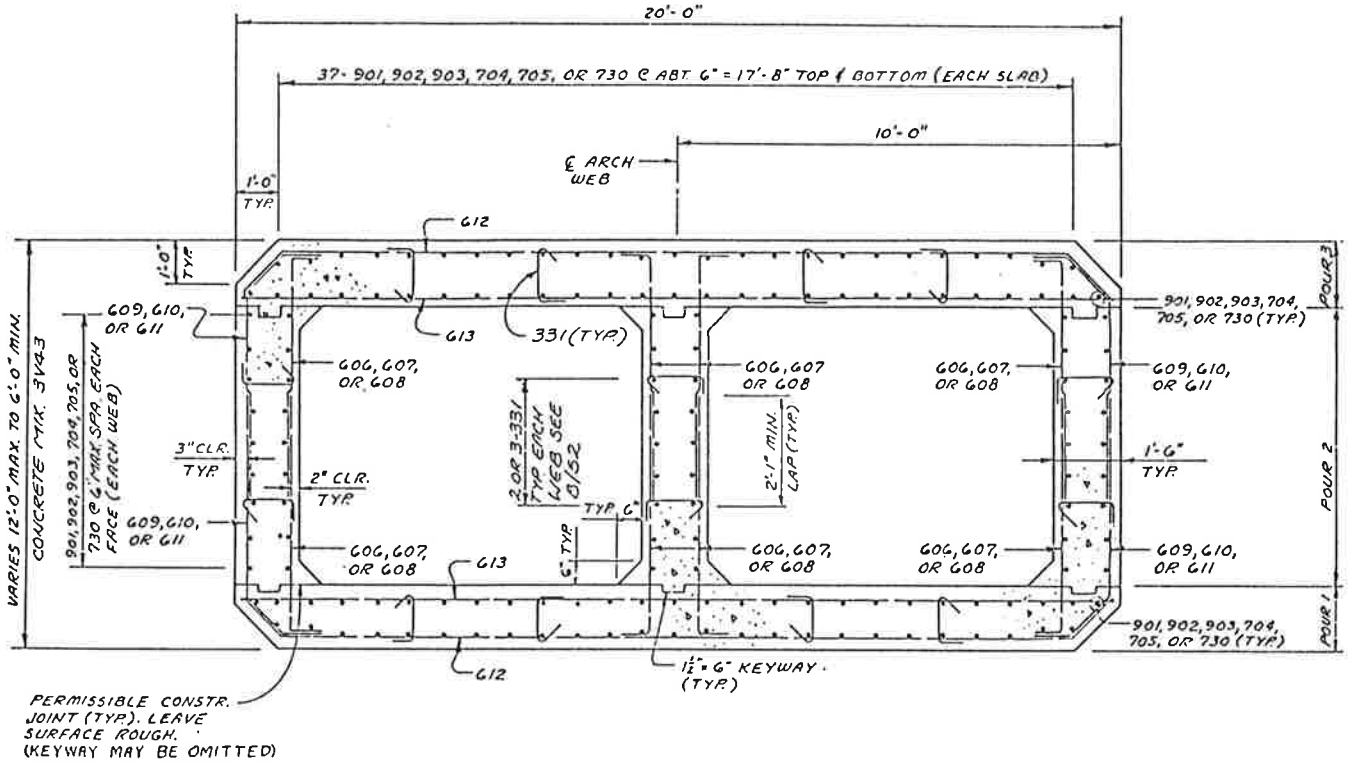

FIGURE 3 Cross-section through twin-celled concrete arch rib.

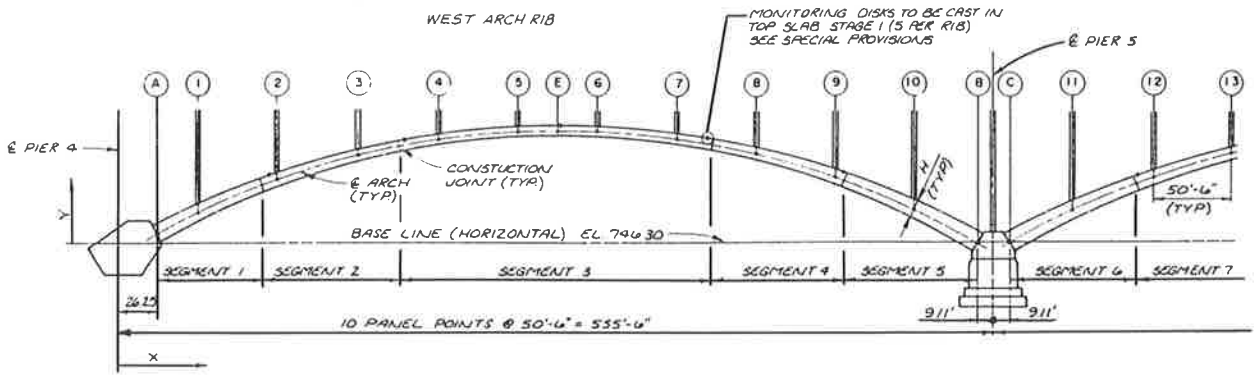

PANEL POINT DIMENSIONS

PANEL POINTS	A	1	2	3	4	5	6	7	8	9	10	B	C	11	12	13
Y	9.18	21.00	41.41	56.17	65.71	70.38	70.38	65.71	56.17	41.41	21.00	0.00	0.00	21.00	41.41	56.17
H	11.62	11.09	9.96	8.83	7.70	6.56	6.56	7.70	8.83	9.96	11.09	12.00	12.00	11.09	9.96	8.83
ΔY	0.000	0.045	0.248	0.517	0.783	0.983	1.040	0.906	0.657	0.369	0.109	0.000	0.000	0.109	0.363	0.639
Δ X	0.000	0.011	-0.014	-0.044	-0.048	-0.011	0.046	0.090	0.088	0.052	0.004	0.000	0.000	-0.003	-0.048	-0.081

DEAD LOAD DEFLECTION

ARCH	0	1/8"	1/2"	1"	1 1/8"	1 3/8"	1 1/2"	1 5/8"	1 3/4"	1 5/8"	1 3/8"	1 1/8"	0	0	1/4"	3/4"	1 1/8"
SPANDREL	0	0	1/8"	3/8"	3/4"	1"	1 1/4"	1 3/8"	1 1/4"	1"	3/4"	1/2"	0	0	1/2"	3/4"	1 1/8"
BEAMS	0	1/8"	1/8"	1/4"	3/8"	1/2"	5/8"	3/4"	7/8"	1"	1 1/8"	0	0	0	0	1/4"	1/4"
DECK	0	0	1/4"	1/2"	3/4"	1"	1"	7/8"	3/4"	1/4"	1/8"	0	0	0	1/4"	1/2"	3/4"
DEAD LOAD 'B'	0	0	3/4"	1/2"	1/2"	3/4"	3/4"	1/2"	3/4"	1/2"	0	0	0	0	1/4"	1/4"	
TOTAL	0	1/4"	1 1/8"	2 1/8"	3 1/8"	4 1/8"	5 1/8"	4 3/8"	3 1/4"	2 1/8"	1 1/8"	0	0	1/4"	2"	3 1/8"	

Y VERTICAL DISTANCE ABOVE SPRING LINE AFTER ULTIMATE DEAD LOAD DEFLECTIONS HAVE OCCURRED

ΔY TOTAL VERTICAL CAMBER FOR CREEP, SHRINKAGE, AND RIB SHORTENING

ΔX TOTAL HORIZONTAL CAMBER FOR CREEP, SHRINKAGE AND RIB SHORTENING

DEAD LOAD 'B' INCLUDES 2" WEARING COURSE, PEDESTRIAN RAILING AND TRAFFIC BARRIER

VARIABLES USED IN ESTIMATING CREEP, SHRINKAGE AND RIB SHORTENING:

CONCRETE STRENGTH = 5000 psi
MODULUS OF ELASTICITY = 4,280,000 psi
AVERAGE ANNUAL HUMIDITY = 68 PERCENT

FIGURE 4 Coordinates and camber data for constructing arch rib.

shown in the plans as delta Y and delta X at each spandrel. A construction note explained that the arch rib shall be cambered by delta Y and delta X to compensate for ultimate dead load deflections.

Over half of the ultimate deflection will take place after the deck has been placed. This results in the deck profile dropping about seven inches at the crown of each arch span over many years. The planned profile includes a crest vertical curve over the center pier between arches with approach grades over two percent. This type of profile could accommodate a future sag without significant aesthetic or drainage impacts but the final decision was to minimize potential impacts by cambering one half of the anticipated sag into the deck profile. This was called rideability camber.

The final phase of construction will connect the decks and the spandrel caps of the two stages. Specific information needed to be provided in the plans to ensure that the two decks would be at the same elevation for closure, somehow accommodating the 2 inch differential in deflections between the arches.

Two potential solutions existed for this problem. One solution was to camber the stage two arch differently than the stage one arch so they would be at the same elevation at closure. The drawback to this solution was that the contractor would have to develop a new equation and new construction data for the stage two arch.

The second, and preferred, solution compensates for the differential creep by varying the height of the concrete pedestals on which the prestressed concrete beams rest. For stage one construction, the pedestals will be about four inches high and for stage 2 construction, they will be a maximum of 2 inches shorter. This allows construction of the arch ribs, spandrel columns and spandrel caps to be identical for both stages.

The pedestals will be constructed to an elevation given in the plans. These elevations were calculated by taking the profile grade elevation, subtracting structure depth, adding rideability camber and adding the anticipated arch dead load deflections due to beams, deck and railings. Stage two pedestal elevations were then obtained by subtracting the value for differential creep at that spandrel location.

PARTICIPATING DURING CONSTRUCTION

The plans and special provisions state that the contractor must submit a construction sequence and schedule for the arch ribs, spandrels, beams and deck for the engineer's review. Part of the intent of the requirement is to enable the designer to compare assumptions with the planned construction. If necessary, the Erection Mode analysis can be rerun using the actual sequence and schedule and revised camber values can be provided to the client and contractor.

In an effort to monitor actual dead load and creep deflections, five disks will be placed in the top slab of both stage one arch ribs. During construction, elevations will be recorded at each disk weekly and converted to deflections. These deflections can then be compared to the estimated stage one deflections which are given in the plans. If necessary, the stage two pedestal elevations can be adjusted up or down during construction to result in a better fit at closure.

The Minnesota Department of Transportation is planning to continue to record deflection data after construction is complete. The availability of this data will provide an excellent means for comparing actual and predicted values of time-dependent deflections. The information obtained from this comparison will assist future designers in their efforts to accurately and practically account for time-dependent deflections.

Secondary Load Paths in Bridge Systems

ROLA L. IDRISS AND KENNETH R. WHITE

Abstract

Although most structural systems are designed as a series of individual elements, they will in fact respond to load as a rather complex integration of these elements. The load is transmitted through a combination of members which resist loads in proportion to their relative stiffness. These types of structures are said to have multiple load paths. Redundant load paths have not been normally considered in the design of structures. However, the consideration of secondary load paths can be a major factor in the assessment of the load carrying capacity of a damaged structure. This paper takes a further look at the reserve strength present in a multi-girder bridge system, and investigates the behavior of a damaged superstructure, the redistribution of loads, and the secondary load paths along which the load is transmitted when a damage occurs in the structure. Limit analysis was used to predict the overload behavior of a simply supported concrete slab-steel girder highway bridge system. The bridge superstructure was modeled as grid and grid framework elements. The experimental results from tests to failure on four large scale bridge models were used to verify the computer approach.

In order to study the response of a distressed bridge, a mathematical model consisting of four girders was analyzed. Three different finite element models were used to investigate the following conditions:

1. No damage in the superstructure.
2. Localized flange losses in a girder.
3. Crack in a girder.

Results are given in terms of load deflection curves for the three models.

Introduction

Evaluation of the load capacity of existing bridges is a major concern for highway agencies throughout the united states. A very important factor in the evaluation of a bridge is the determination of it's load carrying capacity. Bridge engineers are increasingly concerned about the overloading of highway bridges, due to the fact that many of these bridges are loaded beyond levels for which they were originally designed. Another difficult situation arises when a structure is rated deficient, and the decision has to be made concerning posting it, closing it, or replacing it.

Although most structural systems are designed as a series of elements, they generally behave as a system in which loads are transferred through a combination of members that resist loads in proportion to their relative stiffness. These types of structures are said to have multiple load paths. The proportion of load carried by each path is a function of the load location and intensity, as well as the relative stiffness of the various paths. Redundant load paths have not been normally considered in the design of structures. However the consideration of secondary load paths can be a major factor in the assessment of a damaged superstructure.

Typical steel stringer bridges are rather highly redundant structures. The reason for this is that although the girders are designed as line elements, they are continuously connected to a common concrete deck and to each other at close intervals with rather strong diaphragms, as well as bottom flange bracing in many instances. None of these elements are specifically recognized in the typical design calculations for live load.

Information on the behavior of a damaged structure is scarce; the influence of redundancy on the load capacity of such a structure has not been quantified yet. In this paper we further investigate the reserve strength present in a multi-girder bridge system, and the effects of deterioration on such a structure. To study the effects of deterioration, different types of damages are modeled into the structure, the reserve strength assessed, and the load redistribution and structural response of the bridge monitored.

Analytical Approach

To perform the analysis, limit analysis by the displacement method was used. Limit analysis by the displacement method was first introduced by Wang (1); this technique is simple, yet effective for the study of large systems in bending; it combines matrix displacement method and plastic analysis; plastic hinges are accounted for by modification of the members stiffness matrices.

The general procedure is as follows:

- An elastic analysis of the structure subjected to a given set of proportionate loads is made. The allowable load factor at each member end is computed as the ratio of the plastic moment capacity at the point to the end moment caused by the proportionate loads. The smallest of all the allowable load factors thus computed is the first stage load factor for the entire structure, and the location of the first plastic hinge.
- A second analysis of the modified structure, in which there is now one plastic hinge, is made for the proportionate loads. The point by which the second stage load factor is controlled is the location of the second plastic hinge. These processes are repeated until an unstable structure is encountered. The ultimate load factor is the sum of the load factors in all stages. The end moments are determined in the same manner.

Analytical Model

The beam and slab bridge superstructure is modeled by a system of grid and grid framework elements, as shown in figure 2. Grid framework elements were first investigated by Yettram and Hussain (2), and later applied by Traina (3) to the study of large flat plate structural systems in bending. The deflections and moments obtained by use of these models were found to converge to the exact mathematical solution as the mesh was refined. The concrete slab is modeled by equivalent grid plate elements, while the steel girders and diaphragms are modeled by grid elements. These compatible finite elements are connected thru their common nodes. This technique and analytical model were used successfully in previous studies by McCarthy (4) and Melhem (5) to predict the elastic-plastic response of concrete slab steel girder bridges. The results of the analytical study were checked against a number of failure experiments on bridge models . The analytical results compared well with the experimental data.

The limit analysis by the displacement method was further refined to accommodate full scale bridge modeling, including dead load, live load as well as impact. Dead load is applied gradually, and live load is applied as a set of concentrated proportional loads simulating a truck loading with the truck wheel configuration but only a fraction of the actual weight; this set of concentrated live loads is then incremented in the limit analysis, and live load factors are given at every cycle along with all the system flexural response: deflections, rotations, and plastic hinge formation.

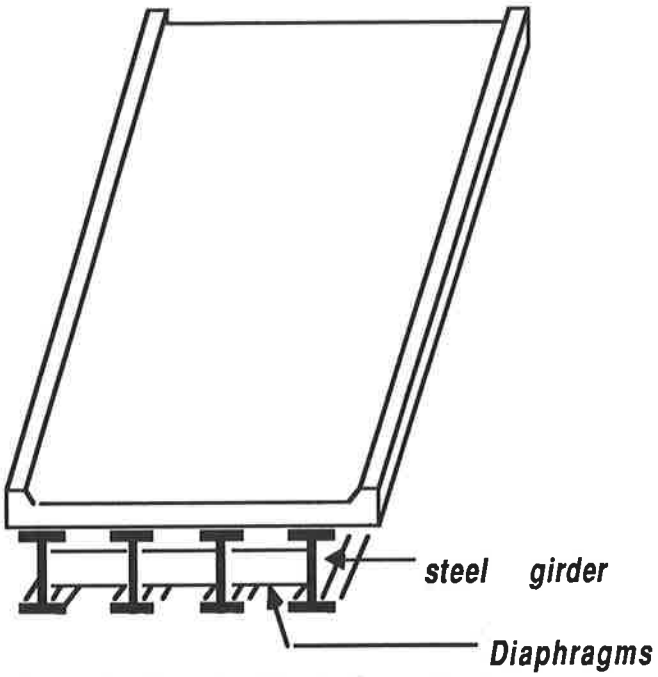

Figure 1. Typical I-Beam Superstructure

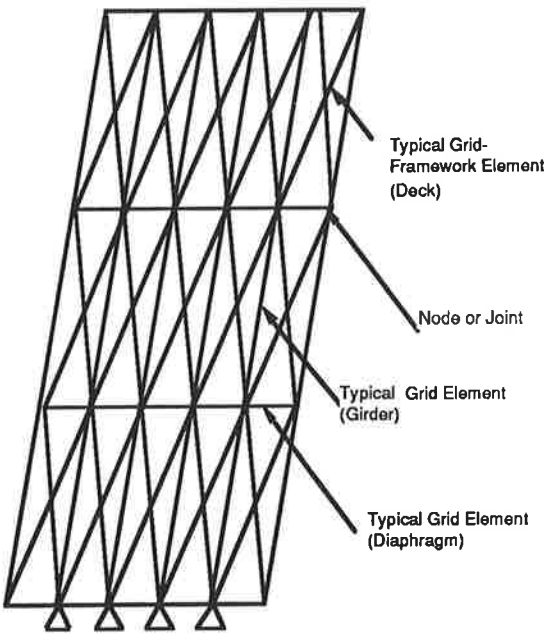

Figure 2. Typical Finite Element Arrangement .

Analytical vs Experimental Results

Analytical results were compared to experimental results from tests to failure on four bridges from the AASHTO road test (15) conducted in the early 60s. Four bridges were studied: 1A, 9A, 9B, and 3B. The first three were non composite bridges, while the last one was composite.

The four bridges had similar geometry; but differed in the beam sizes, the length and presence or absence of cover plates; each bridge superstructure consisted of three identical beams; the nominal sizes of the rolled sections and the length of the cover plates are given in table 1. The beams were simply supported, had a 50 ft span and carried a reinforced concrete slab 6.5 in thick and 15 ft wide.

Table 1. AASHTO Bridges beam sizes.

Bridge		Beam size	Length of cover plates (centered about midspan)	
Designation	Type		Top	Bottom
1A	Non Composite	18WF55		20 ft 6 in
9A,9B	Non Composite	18WF96	17 ft 0 in	17 ft 0 in
3B	Composite	18WF60		18 ft 6 in

Tests to failure were carried out with increments of loads applied with several overload vehicles. Permanent deformations accumulated rapidly with each increment of load after the load causing the first large permanent set.

In the computer simulation, each bridge was loaded with a proportionate set of concentrated live loads. These loads simulate the overload vehicle that caused first large permanent set in the bridge, with the same wheel configuration, but only a fraction of the actual weight. The truck was positioned to cause maximum bending moment at midspan. Analytical and experimental curves as shown in figures 3, 4, 5 and 6 compared very favorably up to the load that caused the first large permanent set (load factor of 1).

The analytical simulation was successful in predicting the plastic flow in the bridges; for bridges 1A, 9A, and 9B heavy yielding in the girders at sections near the ends of the cover plates, with full plastic hinges forming in these locations at failure. Composite bridge 3B showed excessive cracking in the slab and yielding of the girders at the ends of the cover plates that later formed plastic hinges. The analytical simulation for bridge 3B shows the slab reaching its plastic moment capacity first near the ends of the cover plates, then towards midspan of the bridge, which would be in agreement with the extensive cracks observed in the slab, and the formation of plastic hinges at the ends of the cover plates.

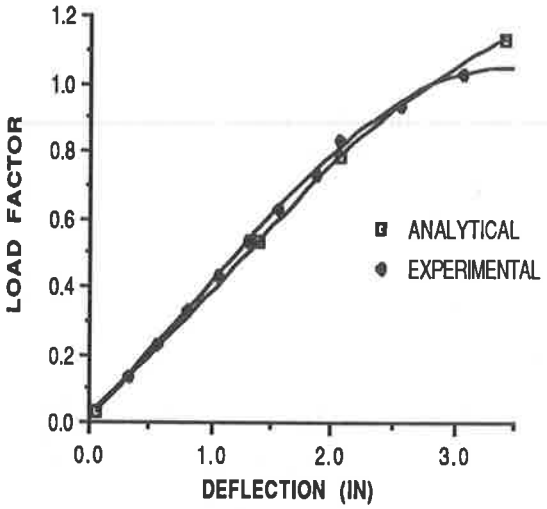

Figure 3. AASHTO Bridge 1A. Analytical vs experimental load-deflection curves.

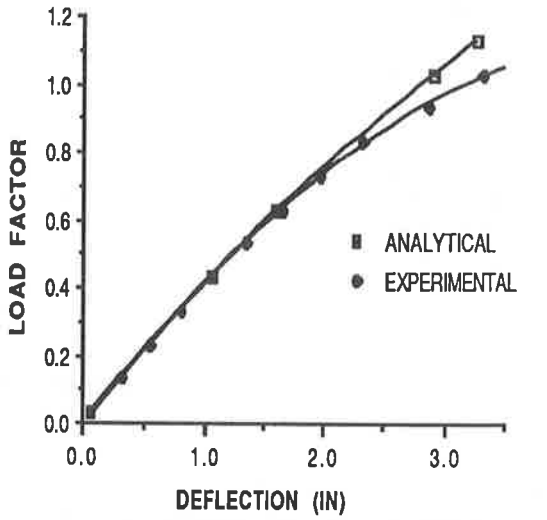

Figure 4. AASHTO Bridge 9A. Analytical vs experimental load-deflection curves.

The analytical simulation and actual experimental results showed good agreement in predicting load-deflection response up to the load that caused the first large permanent set; the analytical simulation was able to predict quite accurately the plastic flow in the structure. Experimental and analytical results disagreed when we compared the rate at which the deflection increased after the first large permanent set.

After the load that caused the first large permanent set (or decrease in stiffness), the actual structure showed a much greater deflection than the analytical model did.

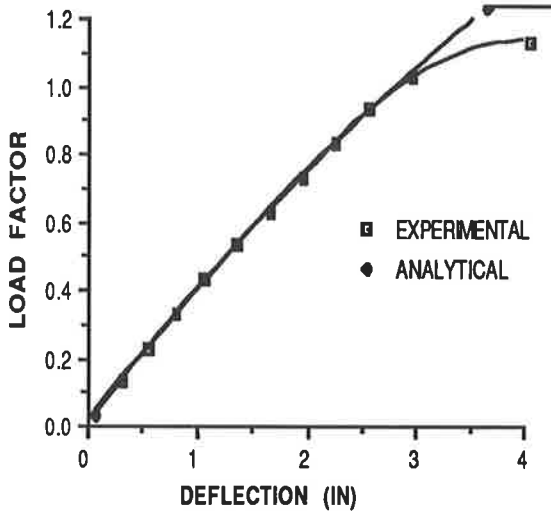

Figure 5. AASHTO Bridge 9B. Analytical vs experimental load-deflection curves.

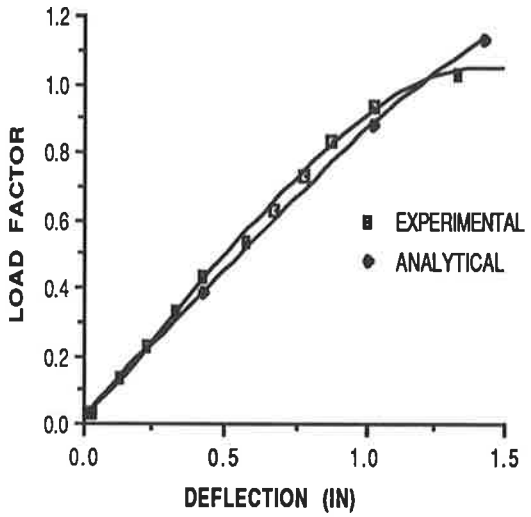

Figure 6. AASHTO Bridge 3B. Analytical vs experimental load-deflection curves.

Effects of deterioration:

In order to assess the effects of deterioration on the behavior of a concrete slab, multi-girder bridge superstructure, two multi-girder systems were examined. They consist of four main longitudinal girders, with diaphragms at ends and midspan. The roadway is a 28 ft wide, 8 in thick reinforced concrete deck; figure 7 shows a typical bridge cross section; girder sizes for span length of 50 ft and 180 ft are shown in table 2.

Table 2. Beam sizes, 50 ft and 180 ft simple span bridges.

Bridge		Beam Size
Span	Type	
50 ft	Non Composite	W36X182
180 ft	composite	Top Flange: 5/8 X 14 Web: 1/2 X 125 Bottom Flange: 1 1/4 X18 (for the72' midspan section) and 15/16 X 18 (for the two 54' endspan sections)

The 50 ft span bridge is non composite, while the 180 ft bridge is composite .

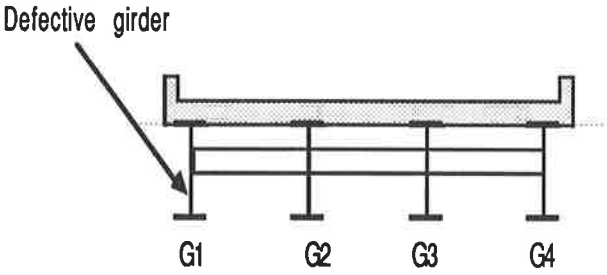

Figure 7. Typical Cross Section.

Three types of defects were modeled:

- Flange losses: 50% and 100% lower flange section losses, with a length of 5-6 ft, centered about the centerline of the beam. The reduced flange section at the location considered is uniform across the section and along the beam; the reduced section modulus is used for this portion of the beam.

- Crack at midspan in the bottom flange extending upward thru the full depth of the web plate. At that location a small element of the beam was assigned a zero moment of inertia and a negligible moment capacity.

The defects were modeled at midspan of one of the exterior girders. In addition to the dead load, two lanes of AASHTO HS20 truck loading with impact are used. The trucks are located in the same longitudinal position that would be used in normal design to compute the maximum bending moment at midspan of the girder. The dead load is applied gradually, and the truck loading is simulated by concentrated loads having the same wheel truck configuration, but only a fraction of the actual weight. This initial live loading is then incremented in the limit analysis, (a load factor of one corresponding to an HS20 loading plus impact).

Analytical Results:

50 ft span, non composite bridge : figures 8, 9, 10, and 11 show the load-deflection response of the bridge; the load deflection behavior of the defective girder G1 is shown in figure 8; the load deflection curves for the other girders , adjacent interior girder G2, interior girder G3 and exterior girder G4 are shown in figures 9, 10, and 11 respectively.

We can see that when a defect occurs in exterior girder G1, the other three girders respond to it by an increase in deflection, due to redistribution of the load; the more severe the defect, the greater the shedding of load to the other girders; we can also note that the closer the girder is to the defect the greater the distribution of load to it.

when a 50% flange loss was modeled in girder G1, a plastic hinge occurs at the midspan of the defective girder at a load factor of 2.3; at that point we observe the following response of the structure: the slab adjacent to the defect assumes an increasing amount of load until it reaches its plastic moment capacity, in the process of redistributing the load to the adjacent girder G2; a plastic hinge occurs at midspan of girder G2 at a load factor of 4.

A 100% flange loss in girder G1 caused a plastic hinge to occur in that girder at a load factor of 0.6; again the same redistribution pattern was observed: the slab adjacent to the defect picking up the load, yielding and redistributing to the other girders, mainly the closest one, interior girder G2; girder G2 develops a plastic hinge at midspan at a load factor of 3.0.

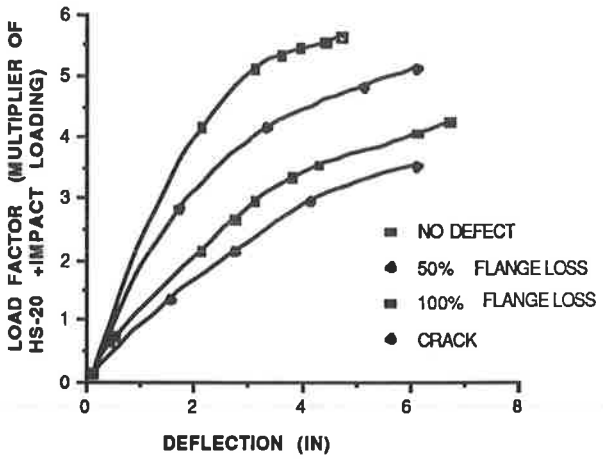

Figure 8. 50 FT Span Bridge. Load deflection curves for the defective girder G1.

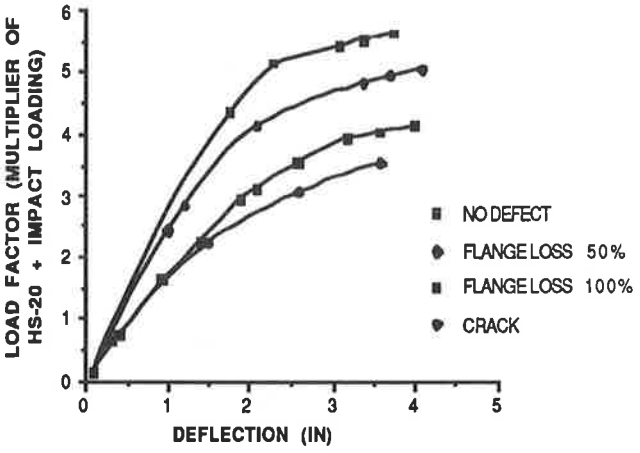

Figure 9. 50 FT Span Bridge . Load-deflection curves for interior girder G2.

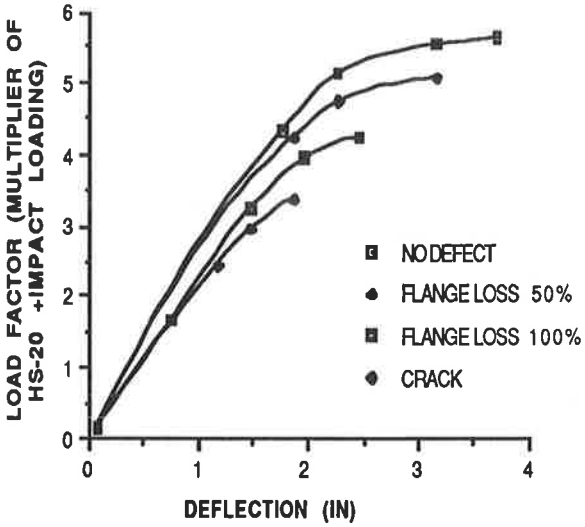

Figure 10. 50 FT Span Bridge. Load-deflection curves for interior girder G3.

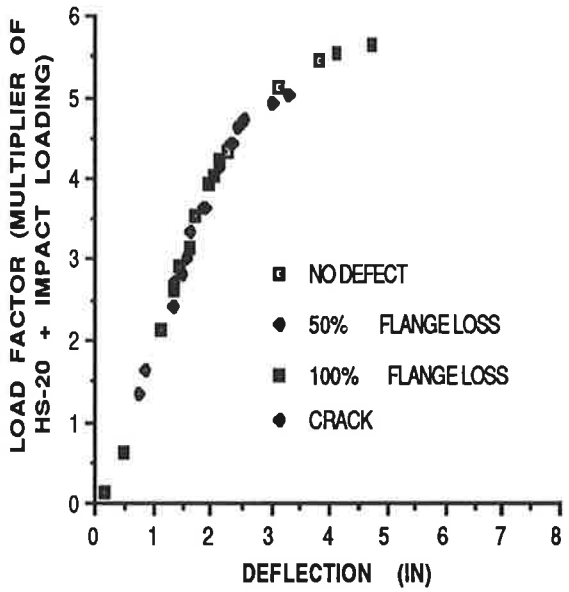

Figure 11. 50 FT Span Bridge. Load deflection curves for exterior girder G4.

A crack in girder G1 causes yielding of the adjacent slab , a first plastic hinge at midspan of adjacent girder G2 at a load factor of 2.5 , followed by a second plastic hinge in girder G2 at a load factor of 3.4 .

180 FT Span composite Bridge

The load deflection response of the bridge is shown in figures 12, 13, 14 and 15; we can see that when a defect occurs in one of the elements, in this instance girder G1, the bridge behaves as a system, and the other girders respond to the defect by assuming more load ; the more severe the defect, the more redistribution and shedding of loads to the other girders.

A 50% flange loss had little effect on the stiffness, but the reserve strength diminished; the first plastic hinge formed at midspan of the defective girder at a load factor of 2.4; this was followed by yielding and a plastic hinge forming in the diaphragm at the location of the defect; next there was formation of two plastic hinges in the adjacent girder, slab yielding at midspan near the defect location and another plastic hinge forming at midspan of girder two, at a load factor of 5.

With a 100% flange loss, the load redistribution followed the same pattern as with the 50% reduction, but with heavier yielding of the diaphragms, and further reduction in the reserve capacity.

When a crack was modeled at midspan of the exterior girder, the dead load deflection at the crack increased to 6.0 in; we observed yielding of the diaphragms and the slab in the vicinity of the crack; at a load factor of two, the adjacent girder G2 had already developed three hinges at three different locations at midspan and at the two sections where the lower flange reduces in size.

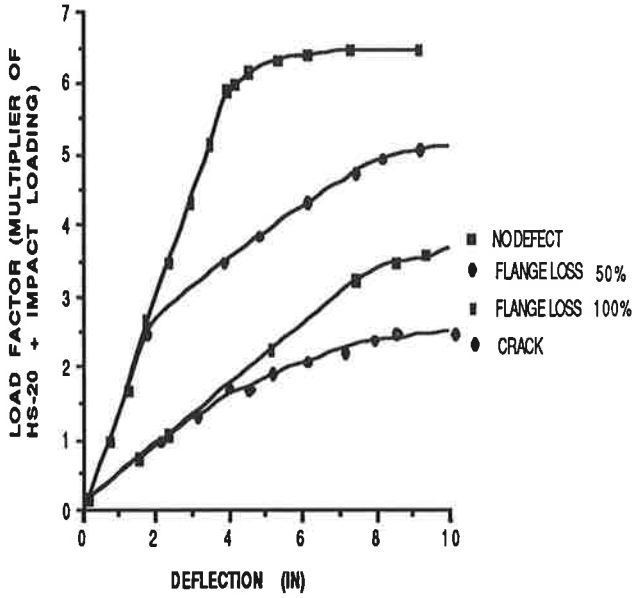

Figure 12. 180 FT Span Bridge. Load deflection curves for exterior defective girder G1.

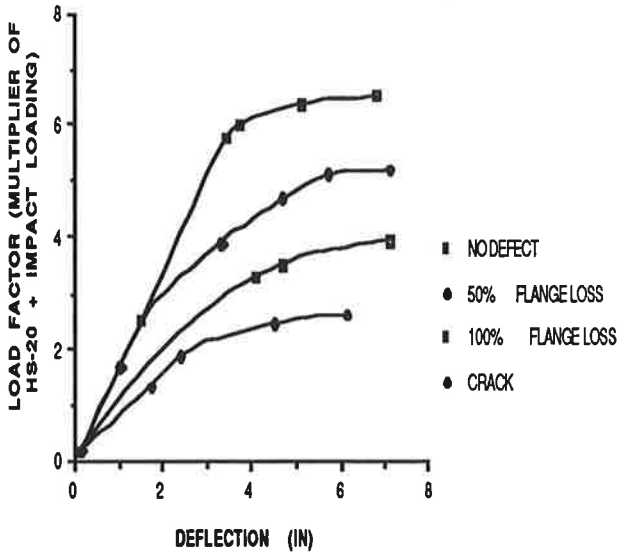

Figure 13. 180 FT Span Bridge. Load deflection curves for interior girder G2.

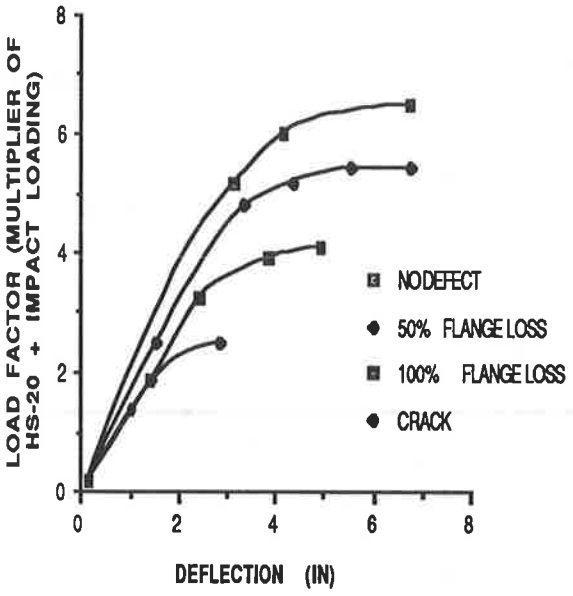

Figure 14. 180 FT Span Bridge. Load vs deflection curves for interior girder G3.

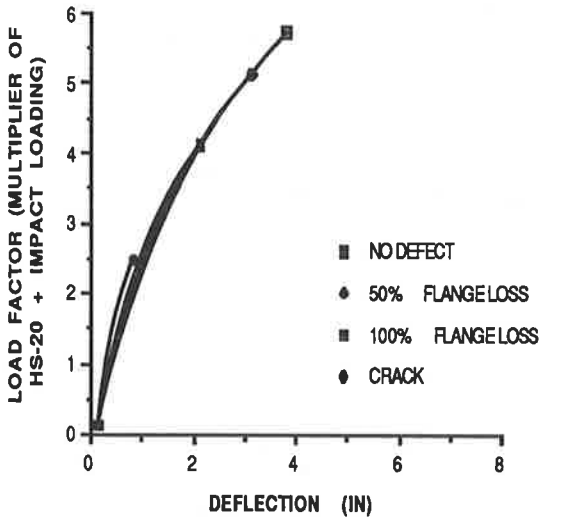

Figure 15. 180 FT Span Bridge. Load vs deflection curves for exterior girder G4.

Table 3. Maximum capacity of the 50', and 180' simple span bridges.

BRIDGE	NO DEFECT	50% FLANGE LOSS	100% FLANGE LOSS	CRACK
	LOAD FACTOR (MULTIPLIER OF HS20 + IMPACT LOADING)			
50' SPAN	5.0	4.11	3.1	3.0
180' SPAN	6.6	5.0	3.4	2.0

Summary and Conclusions

This study took a closer look at multi-girder bridge systems, their reserve capacity, and the secondary load paths present in these structures. When analyzing the overload response of the bridges studied, several conclusions could be drawn:

1. When no defect was present:
   a. The girders assumed the load, and failure occurred when all the girders had reached their ultimate capacity.
   b. The plastic flow mechanism was as follows: plastic hinges formed at first in the most stressed girders, followed by hinges occuring in the other girders.

2. When a defect was introduced:
   a. There was a change observed in the response of the bridge to load. The signs of distress in the bridge originated at the defect location in the girder, and spread first to the slab and diaphragm at the vicinity of the defect, and next to the adjacent girders; the closer the girder to the defect, the more shedding of load to it.
   b. The plastic flow pattern observed when a localized flange loss was introduced at midspan of a girder was as follows: excessive yielding and a plastic hinge forming in the girder at the defect location, followed by yielding of the slab and diaphragms at the vicinity of the defect, and then yielding and plastic hinges forming in the adjacent girders.
   c. The more extensive the defect, the more widespread and extensive the yielding was in the slab, diaphragms and girder at the vicinity of the defect. Therefore, the more severe the defect, the more load was assumed by the slab, diaphragms and adjacent girders.
   d. The multi-girder bridges considered exhibited a large reserve strength when no defect was present, several times an HS-20 truck loading. When a defect was modeled in the bridges, they still demonstrated a large reserve strength as shown in Table (3). Even when a near full depth crack was modeled at midspan of one of the main girders, the maximum capacity was 1.5 to 3.0 times an HS-20 truck loading.

References

1. Wang, C. K. "Matrix Methods of Structural Analysis", Second Edition, American Publishing, Madison, Wisconsin, 1970.

2. Yettram A.L. and Hussain H. M., " Grid-Framework Method for Plates in Flexure," Journal of the Engineering Mechanics Division, ASCE Proc.,Vol. 91, June 1965, No. EM3.
3. Traina L. A. , "Matrix Analysis of Plate Structures in Bending", Ph.D. Thesis, University of Wisconsin, Madison, 1968.
4. McCarthy W. C., "An Elastoplastic Plate Bending Finite Element with Applications to Bridge Structures", Final Report, Engineering Foundation, December 1982.
5. Melhem A. Q. "Elastic-Plastic Analysis of Composite Steel Concrete Superstructures", Ph.D. Thesis, New Mexico State University , 1986.
6. ASCE-AASHTO Task Committee " State of The Art Report on Ultimate Strength of I-beam Bridges", Journal of Structural Division, ASCE, Vol.101, May 1975,pp. 1085-1096.
7. Transportation Research Board, " Correlation of Bridge Load Capacity Estimates with Test Data", Report 306, June 1988.
8. Heins, C.P., Kato H., " Load Redistribution of Cracked Girders", Journal of Structural Engineering, ASCE, Vol.108, August 1982, pp.1909-1915.
9. Halls, J.C., Kostem,C.N. "Inelastic Analysis of Steel Multi-Girder Highway Bridges", Fritz Engineering Lab Report No.435.1, Lehigh University, Bethlehem, Pennsylvania,1980.
10. Schwendeman L. P. , Hedgren A. W. Jr. , "Bolted Repair of Fractured I-79 Girder",Journal of the Structural Division, ASCE, Vol. 104, No. ST10, Proc. Paper 14083. Oct., 1978, pp. 1657-1670.
11. Standard Specifications for Highway Bridges, AASHTO Code, 13th ed.,American Association of State Highway and Transportation Officials,1983.
12. Daniels, J.H., Kim, W., and Wilson, J.L., "Recommended Guidelines for Redundancy Design and Rating of Two-Girder Steel Bridges", NCHRP Report 319 (1989).
13. Heins,C.P., Hou,C.K., "Bridge Redundancy: Effects of Bracing", Journal of the Structural Division, Vol. 106,No. ST6, June, 1980, pp. 1364-1367.
14. Burdett,E.G., AND Goodpasture, D.W., "Full Scale Bridge Testing: An Evaluation of Bridge Design Criteria", University of Tennessee, December 1971.
15. Highway Research Board, "The AASHTO Road Test: Report 4, Bridge Research", Highway Research Board Special Report 61D, 1962.

High-Strength Bolts for Steel Bridges

KRISHNA K. VERMA AND FRED R. BECKMANN

ABSTRACT

The manufacture and use of substandard, mismatched or bogus bolts have been, and continue to be, a major concern to bridge owners in the U.S. Based on FHWA-sponsored research at the University of Texas, supplemental specifications were developed and issued modifying fastener manufacturing, testing and installation procedures.

Nearly all bridge bolts are designed for dynamic loading. They are designed to resist either tension forces and/or shear forces. Fatigue concerns govern bolts designed for cyclic tension forces. Cyclic shear forces require slip critical connections. Both loading conditions require bolts to be installed to a minimum preload.

The FHWA recommendations were developed in order to assure the ability of bolts to achieve this preload. Minimum nut strength is increased, maximum bolt strength is reduced, thread fit tolerance is reduced, additional rotational-capacity testing is required, and additional testing, documentation, handling and shipping requirements are imposed. The rationale for these new FHWA provisions are discussed.

Finally, slip critical joints depend upon friction between faying surfaces to develop strength. Values of slip resistance or coefficient of friction for various paints and coatings must be determined by testing. Bolt design parameters depend upon minimum values of tested coatings.

Improperly manufactured and installed and poorly inspected high strength fasteners can precipitate structural failures. The behavior of bolted joints depends on a large number of variables many of which are rather difficult to predict. Depending on the usage, and concerns for protection from the environment, different materials and acceptance requirements have been specified by the users depending on their current knowledge. In spite of over 30 years of experience with high strength fasteners, there continue to be problems in ensuring that fasteners are of adequate quality and are installed properly. There are concerns that bolted connections in many bridges built over the past 10 years or so might not meet acceptance criteria if they were subjected to test requirements of today. The October 1989 issue of the Civil Engineering Journal reported (p.61-62) that the Industrial Fastener Institute (IFI) claims that billions of substandard, mismatched or counterfeit products may have entered the country's supply line, threatening the reliability of industrial and consumer products. Besides not meeting the stricter U.S. Engineering Standards, the lower priced foreign manufactured fasteners flooding the market are helping to drive U.S. bolt and nut manufacturers out of business according to IFI.

Welding Engineer, Federal Highway Administration
Director of Bridges, American Institute of Steel Construction

Numerous problems have been identified. These include the fact that mismatched fasteners made abroad have been sold in the U.S. market and may have the potential to cause failure and possible serious consequences to the travelling public particularly if these bolts are used in joints subject to tensile or reversible forces. These concerns can be eliminated when fasteners are manufactured to code requirements and subsequent quality control testing is done by the fastener manufacturers, acceptable installation procedures are practiced by the installers, followed by a reliable quality assurance (QA) and traceability program by the owner.

FASTENER REQUIREMENTS AND RATIONALE

Researchers, owners, code writing organizations and the fastener industry have been attempting to constantly improve the quality of fasteners and fastener installation practices to produce a better end product. To ensure that only those fasteners which meet the minimum quality standards are used, the Federal Highway Administration (FHWA) initiated an extensive experimental research program with the Department of Civil Engineering of the University of Texas at Austin to evaluate the performance of both black and galvanized high strength bolts for steel bridge structures. The study was done using ASTM A325 hot dipped or mechanically galvanized bolts and A325/A490 black bolts. Only normal size fasteners commonly used in steel bridge superstructures were tested. Research findings were reported in the FHWA publication FHWA/RD-87/088 "High Strength Bolts for Bridges." Recognizing the need to underscore the various recommendations made in the report and to implement them, the recommendations were compiled, modified in consultation with the researcher and the fastener industry, and later distributed to the field offices via an FHWA memorandum. The objective of the FHWA memorandum was to allow the AASHTO (American Association of State Highway and Transportation Officials) bridge owners to incorporate these high strength bolt specifications in the state standard specifications or contract documents without duplicating the effort of sorting out the recommendations from the report. A copy of the FHWA supplemental specifications contained in the memorandum is included in the appendix. The rationale behind the pertinent specifications is discussed in this paper. The supplemental specifications were written for AASHTO M164 (ASTM A325) bolts but it is recognized that similar specifications are needed for A490 bolts and other alternate fasteners. The supplemental specifications for A325 bolts were

written first because those bolts are used most commonly for bolted connections of bridge members.

The following background information should be helpful in understanding the rationale for the various requirements in the memorandum.

Essentially clamping force is needed to prevent fatigue failure of bolts subjected to cyclic tension and to prevent slip and increase fatigue strength in shear connections. Fatigue failure of threaded fasteners is well known. It can be traced to points of stress concentrations such as those locations where there are abrupt geometric changes, a notch or a nick, or locations where the material may have poor fracture toughness. The torque applied to the fastener assembly is not uniformly distributed over the engaged length because fastener materials are not inelastic and there are manufacturing tolerances resulting in less than perfect matching of bolt and nut threads over the engaged length. However, failure in threaded fasteners is often located at the washer face of the nut, at the thread runout or at the junction of the bolt head and shank. This is primarily because of probable high stress concentrations at these locations, although the average stress levels in the body of the bolt may remain well below the endurance limit of the material. Furthermore, cyclic external forces applied to the bolt can reduce the life of the fasteners by fatigue.

As the torque is applied to the nut, a portion of it is resisted by friction between the nut and the gripped material; the remainder is resisted by friction at the thread interface resulting in torsional stresses in the bolt shank. The bolt is thus subjected to a combined torque-tension stress condition. Load deformation characteristics of bolts subject to direct tension compared to torque-tension reveal that specimens subject to torque-tension are less ductile[2] and have strength levels reduced between 5 and 25 percent.

Clamping force is an important consideration if a bolted joint must function as a slip resistant joint. In such a joint the external load component parallel to the faying surface(s) is resisted by the frictional resistance which is dependent on the clamping force of the bolt and the coefficient of friction at the faying surface. In a bearing type connection, slip is allowed and movement stops as the material bears against the bolt. In such joints the critical factors are the permissible bearing stress on the connection material, the axial stress on the net section and the shear stress of the fasteners - not the initial preload of the bolt. Comparative studies of bolts subject to shear stresses under tension or compression show that shear stress deformation characteristic of A325 bolts and A490 bolts are similar; however, A490 bolts have a lesser ability to deform than A325 bolts under similar conditions, and the maximum shear stress experienced by A490 bolts (of higher strength material) is greater than that in A325 bolts. The research also suggests that when the same type of bolt (A325 or A490) is subjected to shear test in tension or compression jigs, samples in tension jigs show lower shear strength, (a tension jig is preferred for testing shear strength of bolts because it produces the lower range of the shear value.) Available data also demonstrate that the shear strength of A325 or A490 bolts is approximately 62 percent of the tensile strength. It is significant to note that unlike bolts subject to tensile loads, the clamping force has no significant effect on the ultimate shear strength of the bolt. Thus, for slip critical joints subjected to dynamic loads, it is apparent that not only should initial preloads as high as practicable be applied to fasteners, but it is also critical that the desired preload is indeed in the bolt after it is installed.

Until 1985, the practice in North America had been to provide as high a preload as practical regardless of whether or not the joint was slip critical and whether or not tensile forces were applied. Though the apparent objective was to achieve uniformity and simplicity in bolt installation, there were inherent economic disadvantages in attempting to accurately preload bolts where preloading was not even necessary. However, since 1985 the requirement has been that high strength fasteners in slip critical joints and connections subject to direct tension or reversible loads need to be preloaded to a predetermined level. Snug tightening in many situations is adequate for bearing type fasteners though generally not used for bridges.

Obviously, an adequate preload is essential within certain tolerances for dynamically loaded structures such as steel bridges. Proper preloading of fasteners in such structures an important critical task faced by bridge engineers and inspectors. There are, however, numerous related problems and issues and hence the need to specify adequate control. Material specifications, e.g., ASTM Specifications, AASHTO Materials Specifications and other specifications provide necessary controls during the manufacturing process. Installation of fasteners for bridges is addressed by AASHTO, in Division II of the "AASHTO Standard Specifications for Highway Bridges;" in addition, AASHTO bridge owners may have their own special requirements and preferred practices.

The FHWA memorandum cited earlier supplements AASHTO Specifications based on the research findings reported in the reference No. 1 "High Strength Bolts for Bridges." It should be understood that except for the proposed supplemental specifications, other ASTM Specifications and AASHTO Material Specifications remain valid. The memorandum amends or revises AASHTO Material Specifications, but does not replace them. These modifications also ensure the strength of the bolts, nuts and washers during manufacturing and cover issues pertaining to testing of fasteners and fastener assemblies, needed documentation, shipping and installation at the job site. As an example, the FHWA supplemental specifications take some exceptions to AASHTO Material Specifications for tensile strength and hardness requirements and modify related specifications.

Some of these are:

1. A325 bolts are available as type 1, 2 and 3 fasteners. These require a minimum strength of 105 ksi for 1 1/8 inch to 1 1/2 inch diameter bolts and 120 ksi minimum strength for 1/2 inch to 1 inch diameter bolts. Though A325 bolt specifications provide a range of hardness, the upper bound of tensile strength is not included in the ASTM or AASHTO Material Specifications. The hardness can generally be converted to an equivalent tensile strength using conversion tables such as those in ASTM Specifications (A370) or other references. Current AASHTO Material Specifications and ASTM Specifications require matching nuts for A325 bolts. These include heat treated nuts as well as non-heat treated nuts with hardness values as low as 78 HRB (Hardness, Rockwell B). Similarly, A490 bolts are available as type 1, 2 and 3. These bolts have required material strength ranges from 150 ksi to 170 ksi with matching nuts of hardness greater than 24 Rc (Rockwell C) which is much greater than 89 HRB. For A490 bolts non-heat treated nuts are not permitted by either ASTM Specifications or AASHTO Material Specifications. An examination of these two specifications reveals an inconsistency in fastener specifications. As noted above, current specifications allow manufacturing A490 bolts with a minimum tensile strength 150 ksi and hardness value of approximately 33 Rc, but these A490 bolts are not permitted to be galvanized. However, using current ASTM Specifications or AASHTO Material Specifications, A325 bolts can be manufactured with hardness as high as 35 Rc which is equivalent to 156 ksi tensile strength, well into the A490 strength range. The current AASHTO Material Specifications and ASTM Specifications do allow galvanizing A325 (M164) bolts. Thus comparing the two situations it does not seem logical to allow galvanizing A325 bolts of 35 Rc hardness when galvanizing A490 bolts of 33 Rc hardness is prohibited. The FHWA supplemental specifications include modified requirements to correct this inconsistency.

2. Thread stripping is controlled by (a) bolt and nut strength and (b) fit of threads at the interface. Prevention of stripping requires proper fit of bolt-nut assemblies and often requires that heat treated nuts be specified. Non-heat treated nuts with lower hardness values have potential for nut stripping. In previous years, AASHTO had been allowing the use of non-heat treated nuts which could have a minimum hardness as low as 78 HRB. The FHWA supplemental specifications require that the minimum hardness of the nut should be 89 HRB to prevent possible stripping of nuts. The need for this minimum hardness can be explained by Alexander's model[1] which was developed based on experimental data. It is illustrated in Figure 1 below:

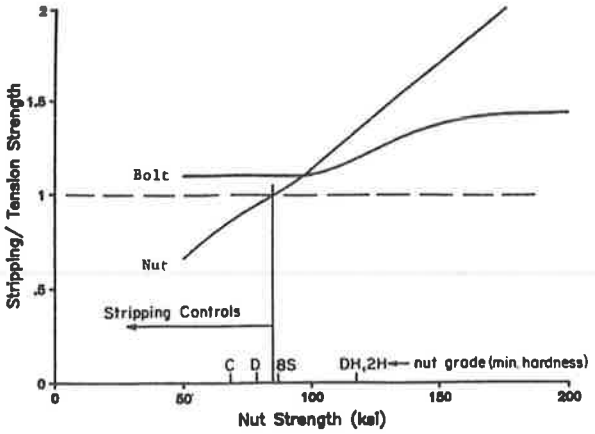

Effect of nut strength on bolt and nut stripping.

Figure No. 1
(Reproduced from Reference No. 1)

Curves have been plotted for 7/8" diameter bolts of tensile strength 156 ksi (equivalent to 35 Rc hardness). In Figure 1, the ratio of the stripping strength of nut (or stripping strength of bolt) to the tensile strength of the bolt has been plotted against the nut strength. The dotted horizontal line represents those assemblies which have stripping strength equal to the tensile strength of the bolt. Points on the curve which are below this horizontal dotted line are subject to possible failure by thread stripping only. Those above the dotted line will fail by tension in the bolt rather than stripping of threads. From Figure No. 1, it is evident that for those assemblies which have nut strength greater than 87 ksi, neither the bolts nor the nuts will strip since the corresponding points lie above the horizontal dotted line. Since 87 ksi tensile strength is approximately equivalent to 89 HRB hardness, the FHWA supplemental specification requires hardness of nuts not less than 89 HRB. On the abscissa, in Figure No. 1, nut strength and various nut designations have been shown. These nut representations indicate lowest permissible strength (or hardness) as permitted by the current ASTM/AASHTO Material Specifications. From this figure, it is possible to infer that heat treated nuts, 2H, DH, and DH3, have minimum hardness well above 89 HRB, the suggested minimum hardness to prevent nut stripping. However, non-heat treated nuts, if manufactured with minimum hardness as permitted by ASTM and AASHTO Material Specifications, will be prone to nut stripping. The suggested minimum hardness 89 HRB is within the upper and the lower limits of hardness permitted in those

specifications. Nut stripping in non-heat treated nuts can be prevented if such nuts are manufactured to a hardness not less than 89 HRB.

A limited study[1] of comparable fasteners produced in accordance with ASTM specifications using traditional U.S. units of measurement with fasteners produced in accordance with ASTM specifications using metric units of measurement seems to suggest that metric fasteners with loose fit and minimum hardness of 89 HRB are less prone to stripping, whereas other fasteners with tighter thread fit tolerances and minimum hardness of 78 HRB are prone to stripping. The study revealed that fasteners made using the metric standard with slightly greater nut strength (approximately 2 percent), as evidenced by hardness numbers, are more forgiving, even with a loose fit. It is important to recognize that failures resulting from thread stripping must be avoided because such failures could go undetected during the service life of the bridge, resulting in possible failure of bridge members and related consequences to the travelling public. However, it may be noted that even though the minimum hardness requirement of 89 HRB for non-heat treated nuts 2, C, C3 and D is specified in the FHWA supplemental specifications, stripping failure can still occur if there are only a few threads in the grip. For that reason it is desirable to ensure that a minimum 3 to 5 complete threads are in the grip. Bolts with more threads in the grip have greater ductility and lower apparent tensile strength.

3. Some of the test requirements for bolts, nuts, washers and fastener assemblies have also been modified by the FHWA supplemental specifications. Proof load testing of bolts and nuts is required. Proof load is the tension applied load which the fasteners must resist without evidence of any permanent deformation. This test provides a check on the yielding behavior of the material since the elongation is measured during testing. If galvanized fasteners are used, proof load testing is required after galvanizing. Wedge testing of bolts and hardness testing of washers is also required, but in the case of galvanized fasteners these tests are required after galvanizing. For galvanized fasteners, zinc thickness measurements are also needed. Zinc thickness measurements on bolts and nuts are important for proper fit and to control overtapping. Performance capability of these fasteners together in an assembly is checked via rotational-capacity testing for either black or galvanized units. Rotational-capacity testing is required prior to shipping as well as at the job site. Job site testing is important but only a minimal amount is needed. Rotational-capacity testing prior to shipping can be done either by the manufacturer or the distributor, as appropriate.

The purpose of the rotational-capacity testing is to verify the torque tension relationship in order to ensure (a) efficiency of lubrication, (b) adequate installation ductility and (c) adequate resistance to stripping. Essentially the rotational-capacity test requires measurement of the bolt tension at the specified minimum rotation (twice the amount of the required installation rotation) from a snug tight condition; and also torque tension values in a Skidmore-Wilhelm Calibrator, at any point above installation rotation, to satisfy the following requirement:

$$\text{Torque (Foot-Pounds)} \leq 0.25 \times P \text{ (Bolt Tension-Pounds)} \times D \text{ (Bolt Dia. Feet)}$$

The FHWA supplemental specification does not allow rotational-capacity testing of long bolts in a steel joint as currently permitted by both ASTM Specifications and AASHTO Material Specifications. Testing in a steel joint does not allow direct measurements of bolt tension during rotational-capacity testing. A Skidmore-Wilhelm Calibrator or similar device is required by the FHWA supplemental specification because such a device allows direct measurement of bolt tension as the rotational-capacity test is performed. The torque-tension relationship curves for these two situations have different slopes at the lower levels of bolt tensioning, but then the curves level out, merge and form a horizontal plateau prior to sloping downwards as the bolt tension is increased. Because the values of tension and torque from this somewhat horizontal portion of the curve are used for acceptance or rejection of the rotational-capacity test, and for determination of the maximum tension in the bolt, the values obtained using a steel joint or a Skidmore-Wilhelm Calibrator will be the same for all practical purposes.

In the case of short bolts which cannot be installed in a Skidmore-Wilhelm Calibrator, the FHWA supplemental specification does not require measurement of the actual maximum tension for the turn test. Anticipated turn test tension as tabulated in the FHWA supplemental specifications, is used to calculate torque using the equation noted above. This calculated torque can then be compared with the measured torque.

4. In addition to job site rotational-capacity tests, calibration tests are also required. This is because for a given tension there can be large variation in bolt torque as measured in the laboratory prior to shipping to the job site and that obtained in the field. Hence, it is required that calibration tests be performed after fasteners are received at the job site using a Skidmore-Wilhelm

Calibrator or an acceptable equivalent tension measuring device to ensure compliance with the minimum installation pretension.

SLIP RESISTANCE OF FAYING SURFACES

As previously noted, the intent of the FHWA supplemental specification is to ensure that the washer/nut/bolt combination functions as a matched unit. It is appropriate to consider the influence of surface preparations and coatings on the faying surfaces in achieving slip critical joints using high-strength fastener assemblies.

The design of a bolted connection may be governed by bearing on the connected material, shear in the shank or thread plane of the fastener or the slip resistance of the contact surfaces of the connection. In nearly all bridge design, because of dynamic loading, slip resistance of the joint is the critical criterion. Bolts are seldom used in tension in bridge structures.

Slip resistance of the contact of faying surfaces is a function of the surface condition. The design specification recognizes three classes of surface conditions:

- Class A - Clean mill scale surfaces and surfaces coated with a Class A coating.
- Class B - Blasted surfaces and surfaces coated with a Class B coating.
- Class C - Galvanized and roughened surfaces.

The most economical joint design generally occurs using Class B surfaces. These are either uncoated blasted surfaces or surfaces coated with a Class B coating. Where the structure is to be unpainted, it makes sense to specify uncoated blasted surfaces. Where the structure is to be painted, the structure should be designed with painted faying surfaces using Class B coatings.

Coatings are classified as Class A or B based on slip coefficient testing performed in accordance with Appendix A of the Specification for Structural Joints Using ASTM A325 or A490 Bolts. The essential variables for the test are paint formulation, cure time, dry film thickness and thinner used. Actual coating application procedures that deviate from the essential variables beyond certain limits require retesting. Because there are many combinations of essential variables, choosing the proper values when performing the test is very important.

Part of the test lasts 42-days; to retest is costly and can delay a project.

As of the summer 1990, very little testing of candidate class B coatings has been performed. Since bridges are currently being designed using the Class B coatings, it is important that testing proceed at a faster rate. Steps are currently underway to increase the number of paints that have been tested. Hopefully, by the spring of 1991, the situation relative to the testing will improve and designers will be using the higher slip values with the full knowledge that there are an adequate number of paints available to meet the need.

REFERENCES

1. J. A. Yura, K. H. Frank, D. Polyzois. High Strength Bolts for Bridges. Publication No. FHWA/RD-87/088. U.S. Department of Transportation. Federal Highway Administration.
2. G. L. Kulak, J. W. Fisher, and J. H. A. Struik. Guide to Design Criteria for Bolted and Riveted Joints. A Wiley-Interscience Publications. John Wiley and Sons, New York.
3. J. H. Bickford. An Introduction to the Design and Behavior of Bolted Joints Marcel Deckker Inc. New York.
4. J. A. MacDonald. For Want of Bolt. Civil Engineering, October 1988.
5. FHWA Memorandum. High Strength Bolts, November 1989.

APPENDIX

November 1989

SUPPLEMENTAL CONTRACT SPECIFICATIONS FOR PROJECTS WITH AASHTO M164 (ASTM A325) HIGH-STRENGTH BOLTS

A. Scope

A1. All AASHTO M164 (ASTM A325) high-strength bolts, nuts and washers shall be furnished in accordance with the appropriate AASHTO Materials Specifications as amended and revised herein.

Additional requirements for field or shop installation of AASHTO M164 (ASTM A325) high-strength bolts are also included. These additional requirements supplement AASHTO Division II, Section 10.

B. Specifications

B1. All bolts shall meet the requirements of AASHTO M164 (ASTM A325) and these revisions.

B2. All nuts shall meet the requirements of AASHTO M292 (ASTM A194) as applicable or AASHTO M291 (ASTM A563) and these revisions.

B3. All washers shall meet the requirements of AASHTO M293 (ASTM F436) and these revisions.

C. Manufacturing

C1. Bolts

1. Hardness for bolt diameters 1/2 inch to 1 inch inclusive shall be as noted below:

Hardness Number				
Bolt Size, In.	Brinell		Rockwell C	
	Min.	Max.	Min.	Max.
1/2 to 1 inch	248	311	24	33

C2. Nuts

1. Nuts to be galvanized (hot dip or mechanically galvanized) shall be heat treated grade 2H, DH, or DH3.

2. Plain (ungalvanized) nuts shall be grades 2, C, D or C3 with a minimum Rockwell hardness of 89 HRB (or Brinell hardness 180 HB), or heat treated grades 2H, DH, or DH3. (The hardness requirements for grades 2, C, D and C3 exceed the current AASHTO/ASTM requirements.)

3. Nuts that are to be galvanized shall be tapped oversize the minimum amount required for proper assembly. The amount of overtap in the nut shall be such that the nut will assemble freely on the bolt in the coated condition and shall meet the mechanical requirements of AASHTO M291 (ASTM A563) and the rotational-capacity test herein (the overtapping requirements of AASHTO M291 [ASTM A563] paragraph 7.4 shall be considered maximum values instead of minimum, as currently shown).

4. Galvanized nuts shall be lubricated with a lubricant containing a dye of any color that contrasts with the color of the galvanizing.

C3. Marking - All bolts, nuts and washers shall be marked in accordance with the appropriate AASHTO/ASTM Specifications.

D. Testing

D1. Bolts

1. Proof load tests (ASTM F606 Method 1) are required. Minimum frequency of tests shall be as specified in AASHTO M164 (ASTM A325) paragraph 9.2.4.

2. Wedge tests on full size bolts (ASTM F606 paragraph 3.5) are required. If bolts are to be galvanized, tests shall be performed after galvanizing. Minimum frequency of tests shall be as specified in AASHTO M164 (ASTM A325) paragraph 9.2.4.

3. If galvanized bolts are supplied, the thickness of the zinc coating shall be measured. Measurements shall be taken on the wrench flats or top of bolt head.

D2. Nuts

1. Proof load tests (ASTM F606 paragraph 4.2) are required. Minimum frequency of tests shall be as specified in AASHTO M291 (ASTM A563) paragraph 9.3 or AASHTO M292 (ASTM A194) paragraph 7.1.2.1. If nuts are to be galvanized, tests shall be performed after galvanizing, overtapping and lubricating.

2. If galvanized nuts are supplied, the thickness of the zinc coating shall be measured. Measurements shall be taken on the wrench flats.

D3. Washers

1. If galvanized washers are supplied, hardness testing shall be performed after galvanizing. (Coating shall be removed prior to taking hardness measurements).

2. If galvanized washers are supplied, the thickness of the zinc coating shall be measured.

D4. Assemblies

1. Rotational-capacity tests are required and shall be performed on all black or galvanized (after galvanizing) bolt, nut and washer assemblies by the manufacturer or distributor prior to shipping. Washers are required as part of the test even though they may not be required as part of the installation procedure.

   The following shall apply:

   a. Except as modified herein, the rotational-capacity test shall be performed in accordance with the requirements of AASHTO M164 (ASTM A325).

   b. Each combination of bolt production lot, nut lot and washer lot shall be tested as an assembly. Where washers are not required by the installation procedures, they need not be included in the lot identification.

   c. A rotational-capacity lot number shall be assigned to each combination of lots tested.

   d. The minimum frequency of testing shall be two assemblies per rotational-capacity lot.

   e. The bolt, nut and washer assembly shall be assembled in a Skidmore-Wilhelm Calibrator or an acceptable equivalent device (note - this requirement supersedes the current AASHTO M164 (ASTM A325) requirement that the test be performed in a steel joint). For short bolts which are too short to be assembled in the Skid-more-Wilhelm Calibrator, See Section D4.1i.

   f. The minimum rotation, from a snug tight condition (10% of the specified proof load), shall be:

      240° (2/3 turn) for bolt lengths < 4 diameters

      360° (1 turn) for bolt lengths > 4 diameters and < 8 diameters

      480° (1 1/3 turn) for bolt lengths > 8 diameters

      (Note that these values differ from the AASHTO M164 Table 8/ASTM A325 Table 6 Specifications).

   g. The tension reached at the above rotation shall be equal to or greater than 1.15 times the required installation tension. The installation tension and the tension for the turn test are shown below:

Diameter (In.)	1/2	5/8	3/4	7/8	1	1 1/8	1 1/4	1 3/8	1 1/2
Req. Installation Tension (kips)	12	19	28	39	51	56	71	85	103
Turn Test Tension (kips)	14	22	32	45	59	64	82	98	118

   h. After the required installation tension listed above has been exceeded, one reading of tension and torque shall be taken and recorded. The torque value shall conform to the following:

      $\text{Torque} \leq 0.25\ PD$

      Where

      Torque=measured torque (foot-pounds)
      P=measured bolt tension (pounds)
      D=bolt diameter (feet).

   i. Bolts that are too short to test in a Skidmore-Wilhelm Calibrator may be tested in a steel joint. The tension requirement of Section D4.1g need not apply. The maximum torque requirement of Section D4.1h shall be computed using a value of P equal to the turn test tension shown in the table in Section D4.1g.

D5. Reporting

1. The results of all tests (including zinc coating thickness) required herein and in the appropriate AASHTO specifications shall be recorded on the appropriate document.

2. Location where tests are performed and date of tests shall be reported on the appropriate document.

D6. Witnessing

1. The tests need not be witnessed by an inspection agency; however, the manufacturer or distributor that performs the tests shall certify that the results recorded are accurate.

E. Documentation

E1. Mill Test Report(s) (MTR)

1. MTR shall be furnished for all mill steel used in the manufacture of the bolts, nuts, or washers.

2. MTR shall indicate the place where the material was melted and manufactured.

E2. Manufacturer Certified Test Report(s) (MCTR)

1. The manufacturer of the bolts, nuts and washers shall furnish test reports (MCTR) for the item furnished.

2. Each MCTR shall show the relevant information required in accordance with Section D5.

3. The manufacturer performing the rotational-capacity test shall include on the MCTR:

   a. The lot number of each of the items tested.

   b. The rotational-capacity lot number as required in Section D4.1c.

   c. The results of the tests required in Section D4.

   d. The pertinent information required in Section D5.2.

   e. A statement that MCTR for the items are in conformance to this specification and the appropriate AASHTO specifications.

   f. The location where the bolt assembly components were manufactured.

E3. Distributor Certified Test Report(s) (DCTR)

1. The DCTR shall include MCTR above for the various bolt assembly components.

2. The rotational-capacity test may be performed by a distributor (in lieu of a manufacturer) and reported on the DCTR.

3. The DCTR shall show the results of the tests required in Section D4.

4. The DCTR shall also show the pertinent information required in Section D5.2.

5. The DCTR shall show the rotational-capacity lot number as required in Section D4.1c.

6. The DCTR shall certify that the MCTR are in conformance to this specification and the appropriate AASHTO specifications.

F. Shipping

F1. Bolts, nuts and washers (where required) from each rotational-capacity lot shall be shipped in the same container. If there is only one production lot number for each size of nut and washer, the nuts and washers may be shipped in separate containers. Each container shall be permanently marked with the rotational-capacity lot number such that identification will be possible at any stage prior to installation.

F2. The appropriate MTR, MCTR or DCTR shall be supplied to the contractor or owner as required by the Contract Documents.

G. Installation

The following requirements for installation apply in addition to the specifications in AASHTO Division II, Section 10 when high-strength bolts are installed in the field or shop.

G1. Bolts shall be installed in accordance with AASHTO Division II Article 10.17.4. During installation, regardless of the tightening method used, particular care should be exercised so that the snug tight condition as defined in Article 10.17.4 is achieved.

G2. The rotational-capacity test described in Section D4 above shall be performed on each rotational-capacity lot prior to the start of bolt installation. Hardened steel washers are required as part of the test although they may not be required in the actual installation procedures.

G3. A Skidmore-Wilhelm Calibrator or an acceptable equivalent tension measuring device shall be required at each job site during erection. Periodic testing (at least once each working day when the calibrated wrench method is used) shall be performed to assure compliance with the installation test procedures required in AASHTO Division II, Article 10.17.4.1 for Turn-of-Nut Tightening,Calibrated Wrench Tightening, Installation of Alternate Design Bolts and Direct Tension Indicator Tightening. Bolts that are too short for the Skidmore-Wilhelm Calibrator may be tested using direct tension indicators (DTIs). The DTIs must be calibrated in the Skidmore-Wilhelm Calibrator using longer bolts.

G4. Lubrication

1. Galvanized nuts shall be checked to verify that a visible lubricant is on the threads.

2. Black bolts shall be "oily" to the touch when delivered and installed.

3. Weathered or rusted bolts or nuts not satisfying the requirements of G2 or G3 above shall be cleaned and relubricated prior to installation. Recleaned or relubricated bolt, nut and washer assemblies shall be retested in accordance with G2 above prior to installation.

G5. Bolt, nut and washer (when required) combinations as installed shall be from the same rotational-capacity lot.

Corrosion and Its Influence on Strength of Steel Bridge Members

JOHN W. FISHER, BEN T. YEN, AND DAYI WANG

INTRODUCTION

Extensive corrosion damage is often observed in girders, floor beams, and stringers of steel girder bridges and in the truss members and their floor system of truss bridges. The loss of material often results in complete corrosive penetration of the plates or rolled components. Figures 1 to 3 show examples of complete penetration of a built-up hanger, batten plate on a chord and the web of a girder. Significant reductions in cross-section areas are possible as a result of active corrosion cell activity[1].

Severe notches in the flanges can develop, particularly where dirt and debris accumulate and create an active corrosion cell. This type notching will occur in all steel materials. Figures 4 and 5 show corrosion notched flange angles of riveted girder members. In Figure 4, dirt and debris accumulated under a diaphragm, and this provided an active corrosion cell site.

The rusting process of steel (or iron) is two-fold involving the chemical change of iron to iron oxide and secondly the electrical process of current flow. Hence, it is an electrochemical process similar to the conditions that develop in a battery[1,2].

The corrosion battery requires oxygen and an electrolyte. For the corrosion conditions generally observed at bridge members, the electrolyte is a solution in water of salts or other chemical compounds, which are capable of conducting electrical current. The current carrying capacity of the electrolyte is due to the presence of electrically charged particles called ions. Ions are formed by the splitting of salts or caustic chemical dissolved in water into mobile, electrically charged fragments. These electrically charged fragments are present in great numbers, and readily conduct current. Ions cannot carry current under dry conditions, so the presence of water is essential for the corrosion battery to function.

Figure 6 shows a schematic representation of an active corrosion battery. It represents a magnified portion of the steel surface. Tiny adjacent areas act as anode and cathode on and adjacent to the surface where water contains ions and serves as the electrolyte. Gaseous oxygen is dissolved in the electrolyte and is available to the metal surface. As the schematic shows, the external circuit is provided by the electrolyte and the internal circuit by the metal.

As the corrosion battery operates, atoms of metallic iron are converted to iron ions which react with the water and oxygen to form rust. As the iron anode is eaten away, a growing deposit of rust forms. Although the iron cathode is not attacked, it serves as a site for oxygen reaction. This process will continue until all of the iron is converted to rust or until the battery circuit is broken. The perforations and notches shown in Figures 1 to 5 are examples of active corrosion cell activity.

Crevices or pockets exist at the edge of the angles used to connect end connections and flange angles to the girder web. Crevices have a tendency to corrode at a far faster rate than the adjacent flat metal areas. Figure 7 shows a schematic of the corrosion battery that tends to develop at the crevice between the angle and web interface. The essential elements of the corrosion process of oxygen, water and ions must be present. Crevices generally trap dirt, salt and rust, and with water, promote galvanic corrosion with the anode provided by the web at the crevice and with the cathode of the steel adjacent to the crevice. The steel in the crevice is an oxygen starved area, acts as the anode, and becomes corroded. Both the web plate adjacent to the connection and crevices in the connection are anodes. However, the corrosive attack is greatest where the anodic and cathodic regions meet as

shown in Figure 3. When the angles are more flexible, the corrosion cell can extend into the joint.

Pitting corrosion results in an extremely localized electrochemical process that produces local holes. It occurs when a small area of the metal surface becomes anodic to the rest of the surface. An anode will often form at a point where oxide film or paint coating breaks occur, so that the external electrolyte comes in contact with a small area relative to the larger surrounding cathodic area. Mill-scale is a form of iron oxide created during the steel rolling process. It is a hard brittle film that adheres to the steel surface, is fragile, and is subject to cracking and spalling. Mill-scale is also cathodic with respect to the steel surface and can accelerate galvanic corrosion. The failure resulting from painting over mill-scale is shown schematically in Figure 8. When the coating is applied over mill-scale, small bare steel areas may exist. After cracking of the coating occurs, a corrosion battery will be set up and the small bare areas will be subject to attack from the large cathodic areas. As the pitting and rust and dirt build up, it will result in peeling, blistering and rupturing, as was illustrated in Figures 1 and 3. The oxygen concentration cell under the surface deposit and coating creates an accelerated galvanic corrosion reaction. When dirt and debris are not present, pitting can develop at the surface, as illustrated in Figure 9.

The rate of corrosion is related to the aggressiveness of the electrolyte. In industrial and marine atmosphere the rate of pitting penetration can be up to 100 times faster than the general corrosion rate[1].

Under general atmospheric exposure, structural steels experience an average corrosion penetration, as illustrated in Figure 10. This shows a plot developed by Horton in 1965 comparing the corrosion of plain carbon, copper-bearing and Mayari R steel (A588) in the Pittsburgh area[3].

The effects of corrosion on the strength and performance of steel members are the areas of concern. A common assumption is that the net area strength will be governed by yielding. However, the corrosion notch may result in fatigue cracking. Corrosion notches may provide a substantial reduction in fatigue resistance, as was demonstrated in References 4 and 5. Cracks developed in the gross section at the notches with little or no influence of rivet holes.

Figure 11 shows the cracks that developed in the heavily corroded flange angle and web plate of the built-up section from a bridge member. It can be seen that the flange angle crack was not influenced by the rivet holes.

The ultimate strength of the corroded riveted section, and the fatigue resistance of corroded riveted member will be examined from the available experimental data.

FATIGUE STRENGTH OF CORROSION NOTCHED MEMBERS

The corrosion notches shown in Figures 4, 5 and 12, resulted in fatigue cracking, as illustrated in Figures 11 and 13. The fatigue resistance of corrosion notched riveted sections has been examined with full scale tests on riveted members with regions of corrosion reduced flange angle thickness, as was illustrated in Figures 4, 5 and 12[4,5]. In Reference 4, five members with corroded sections failed at a corrosion-reduced section. In Reference 5, three members with corroded sections resulted in fatigue cracking. These test results are summarized in Figure 14. All of the cracks initiated in corrosion notched flange angles of the eight test girders. The degrees of reduction in the flange angle cross-section, however, were quite different and varied from 5 to 40% of the angle leg area. The angle leg thickness reduction was the principal influence on the fatigue strength of the detail. In three cases there was also a reduced width. These effects resulted in significant stress concentration at the corroded section. The stress elevations resulted from the notches on the rough irregular surface. No convenient measure of quantifying this was found. Figure 4 shows the reduced section of beam 1 which lost about 60% of its thickness. Cracking was observed to initiate at multiple sites in the region near the edge of the angle, where the thickness was minimal. No cracking was observed in the corroded region of members when the maximum thick-

ness reduction was less than half the original thickness. In those cases cracks developed at rivet holes.

The most severely corroded angle evaluated in Reference 4 is shown in Figure 5. The angle leg was about 40% corroded away. After cracking developed at the corroded section, this detail was retrofitted by drilling a hole at the crack tip and splicing the section. The crack had propagated to near the mid-depth of the web at the time of retrofit, as can be seen in Figure 11.

The fatigue test data of the corroded flange angles are plotted in Figure 14. The stress range is based on the net section of the corroded section. The stress range at the corroded net section varied from 8.3 ksi (57.2 MPa) to 14.1 ksi (97.2 MPa). Also plotted in Figure 14 are the results of the three girders that developed fatigue cracks at corrosion notches in Ref. 5. These three members were subjected to higher stress range levels at the corrosion "net area." The stress range varied from 12 ksi (82.7 MPa) to 18 ksi (124.1 MPa). All three girders had cover plates, as can be seen in Figs. 12 and 13. One of the girders cracked at the end of a cover plate. The other two girders developed cracks in the cover-plated section where the corrosion notches in the sections were severe.

The mechanism of crack formation in the corroded area proceeded as follows. First, several small cracks formed in the rough surface at the deeper notches close to the flange tip. These cracks coalesced and formed a long, shallow surface crack. This surface crack then propagated through the flange thickness at the tip and became an edge crack. Small cracks continued to form in the corroded surface and coalesced with the edge crack. The crack length measured at the bottom surface of the angle leg always lagged behind the length at the corroded top surface.

The test results plotted in Figure 14 demonstrate that the most severely corroded section provides a fatigue resistance comparable to Category E. Three of the test girders provided fatigue lives bounded by the Categories D and E AASHTO and AREA resistance curves. Those girders with a loss of thickness equal to about 50% of the flange thickness approached the lower bound resistance curve provided by Category C.

STRENGTH OF CORRODED HANGERS

Two hangers with severe corrosion loss (39 to 41%) were removed from the Grand Narrows Bridge in Nova Scotia. This structure had experienced severe and rapid corrosion penetration in a large number of the truss and floor system members. In 1983 it was decided to stop maintaining the structure, because of the possibility of constructing a new structure jointly with the Highway Authority[6]. Inspections were carried out yearly between 1979 and 1987[7]. Extensive pitting and crevice corrosion was observed in most of the bridge members. The structure is in a severe marine environment and experienced an acceleration in pitting corrosion in most of its members, as illustrated in Figures 1 and 2. These local pitting holes quickly enlarged and resulted in complete loss of the outstanding leg in local areas. Figure 15 shows how the ratio of remaining net area to the original net area changed at the corroded region for the period between 1982 and 1987. An examination of samples by CN Rail verified that pitting corrosion had indeed developed. With the aggressive marine atmosphere at Grand Narrows, the rate of pitting penetration can be up to 100 times faster than the general corrosion rate. Hence, unprotected 3/8 in. plate could be perforated in less than three years. The local effect is not quite as severe on the total cross-section, as can be seen in Figure 15.

The hangers were tested to failure in a static test in order to assess the residual strength and evaluate the adequacy of the limit state model.

The test specimens were 20 ft. (6.10 m) long, cut from the lower end of the 30 ft. -8 in. (9.35 m) long hangers. End plates were bolted to the flanges for anchorage and load application. Figure 16 is a photograph of the pin-connections at the ends of the hanger. Thus, the hangers were subjected to axial loads only, without end moments.

The corroded portions of the hangers were placed at the lower end of the test setup to simulate the actual orientation of the hangers in the structure.

Six strain gages were mounted on each specimen near midheight: one gage on each of the angles and two on the web. Also attached to each specimen were four LVDT's for the measurement of overall elongation and elongation of the corroded portion. Both specimens failed by excessive elongation and local cracking of the angles at the corroded region. Figure 17 shows the load-elongation plots from the LVDT data. The overall elongation at maximum load was about 1.75 in. (44.5 mm). At termination of the test, the deformation was about 2 in. (50.8 mm) for the 16 ft. (4.9 m) measurement length of the specimens. Figures 18 and 19 are examples of the cracked flange angles of specimens No. 1 and 2. Testing was continued until the applied load dropped substantially below the maximum load. The maximum applied loads, P_{max}, are listed in Table 1, together with the computed reference forces and the section properties.

At the maximum applied load, strains at some of the gages were close to the yield level. One gage was subjected to very high strain because it was adjacent to the corroded area and sensitive to bending. The hangers were severely corroded in the region just above the floor beam connection. Measurement of remaining thickness of the components indicated a measured net cross-section area, A_{nm}, of 11.3 in.^{2} (7290 mm^2) and 10.8 in.^{2} (6968 mm^2) for hangers No. 1 and 2, respectively (Figure 20). Based on these net areas and the average measured ultimate strength of the hanger components, the predicted ultimate net section tensile strength would be 666 kips (2960 kN) and 610 kips (2711 kN), respectively. The corresponding maximum applied test loads were 638 kips (2836 kN) and 584 kips (2596 kN). These values are compared in Table 1.

The maximum applied loads corresponded to slightly less than the computed ultimate tensile strength. The non-uniform corrosion introduces a "shear lag" effect and reduced capacity by about 5%. The hangers did not fail by sudden fracture but exhibited ductile behavior.

The experiments demonstrated that the corroded section was capable of developing the tensile capacity of the remaining net area. The effect of the corrosion on the member strength and ductility was similar to the behavior of mechanically fastened tension members[8]. The local bending which resulted from the lack of symmetry at the severely corroded sections did not deteriorate the tensile strength a significant amount.

SUMMARY

The effects of significant corrosion loss on the strength and performance of riveted members has been examined by full scale tests on members removed from bridge structures.

It is important to note that in actual structures, cracks are seldom observed at the corrosion notched section until significant loss in the total section has occurred. This appears to result from the fact that the rate of corrosion in actual structures often exceeds the rate for fatigue damage thus preventing the development of cracks. Any local damage from cyclic loading appears to be removed by the ongoing corrosion process. Cracks only form when the corrosion loss becomes extensive and causes a substantial increase in the cyclic stress.

When cracks are initiated at a corrosion notched element, the fatigue tests have demonstrated that the corrosion notch effect can be as severe as Category E of the AASHTO and AREA specifications. The results discussed here indicated that the thickness of the corroded riveted member must be reduced by about 50% before the corrosion notch becomes more severe than the rivet holes. The riveted member then provides a fatigue resistance corresponding to Category C. As the thickness reduction increased beyond 50%, the corrosion notch effect became more severe creating its own fatigue initiated detail. Seldom did the resulting fatigue crack intersect a rivet hole. More often it propagated in the gross section of the riveted member.

The ultimate strength tests on corrosion damaged hangers demonstrated that the hangers were able to resist maximum axial loads about equal to the tensile strength on the net section at the corroded area. Hence, the use of an effective net area using the combined corrosion reductions and the hole pattern permitted a reasonable estimate of the limit state.

Both hanger specimens failed in a duc-

tile manner. The corroded region did not significantly reduce the ductility of the material.

ACKNOWLEDGMENTS

This paper was prepared with the support of the NSF Engineering Research Center, Advanced Technology for Large Structural Systems (ATLSS) at Lehigh University. It draws extensively on experimental work carried out at Fritz Engineering Laboratory under sponsorship of the National Cooperative Highway Research Program and the Federal Highway Administration, Department of Transportation during the 1970-1988 period.

Thanks are also due the Canadian National Railroad for the opportunity to examine and evaluate the behavior and characteristics of bridge structures subject to corrosion deterioration.

REFERENCES

(1) "Failure Analysis and Prevention of Corrosion Failures," pp. 168-204, Metals Handbook, Vol. 10, 8th Ed., 1975.

(2) Dismuke, T. D., Coburn, S. K. and Hirsch, C. M.; HANDBOOK OF CORROSION PROTECTION FOR STEEL PILE STRUCTURES IN MARINE ENVIRONMENTS, AISI PI 072-581-5M-EP, 1981.

(3) Horton, J. B., "The Rusting of Low Alloy Steels in the Atmosphere," Presented at the San Francisco Meeting, AISI, Nov. 18, 1965 (see also Bethlehem Steel Booklet 2385-A).

(4) Out, J. H., Fisher, J. W. and Yen, B. T., FATIGUE STRENGTH OF WEATHERED AND DETERIORATED RIVETED MEMBERS, Final Report DOT/OST/P-34/85/016, U.S. DOT, Oct. 1984.

(5) Fisher, J. W., Yen, B. T., Wang, D. and Mann, J. E., FATIGUE AND FRACTURE EVALUATION FOR RATING RIVETED BRIDGES," NCHRP Report 302, Dec. 1987.

(6) Sweeney, R. A. P., Director Structures Design, C. N. Rail, Personal Correspondence to J. W. Fisher, Jan. 1987.

(7) Oommen, G., Engineer, C. N. Rail, Personal Correspondence to J. W. Fisher, Jan. 13, 1987.

(8) Kulak, G. L., Fisher, J. W. and Struik, J. H. A., GUIDE TO DESIGN CRITERIA FOR BOLTED AND RIVETED JOINTS, John Wiley and Sons, 2nd Ed., 1987.

TABLE 1
CROSS-SECTIONAL AREA AND AXIAL LOADS

		Hanger 1	Hanger 2	
Original	An	18.4	18.4	($in.^2$)
Area	Ag	20.6	20.6	
Measured	Anm	11.3	10.8	
Material	Fu	58.9	56.5	(ksi)
Strength	Fy	33.7	32.9	
Computed	AnmFu	666	610	(kips)
Capacity	AngFy	694	678	
Test	P_{max}	638	584	

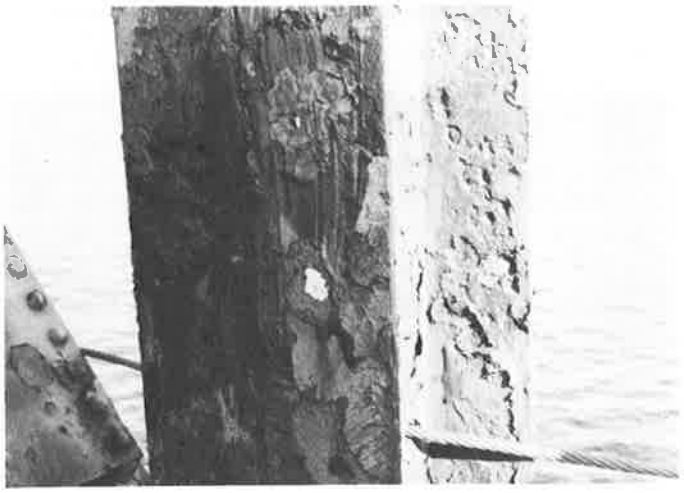

Figure 1 Corrosion Penetration of Riveted Hanger Components

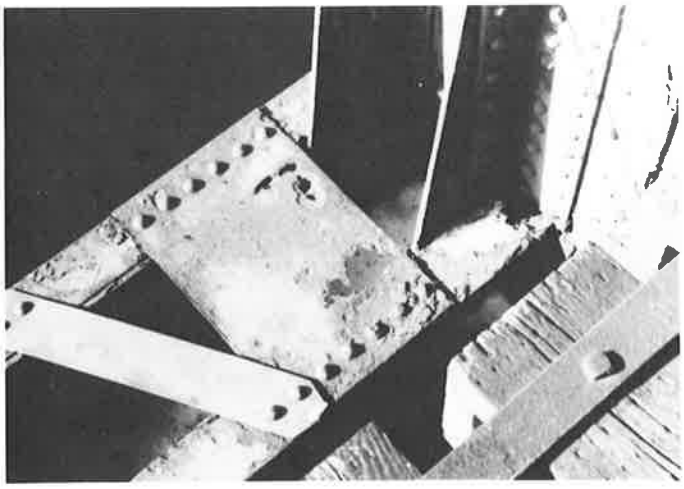

Figure 2 Local Corrosion Penetration of Batten Plate and Chord Components

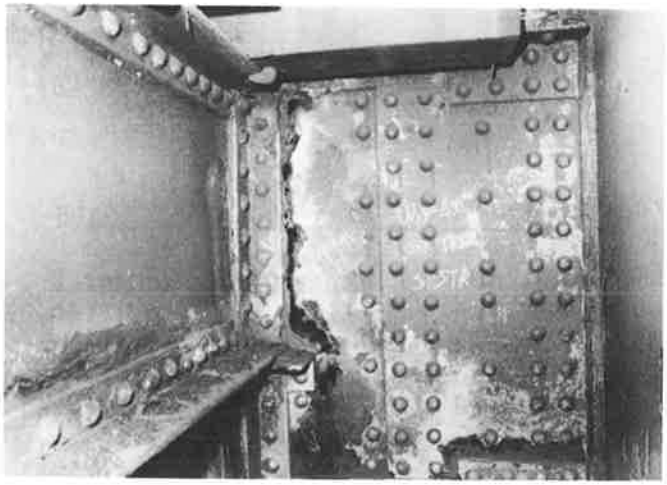

Figure 3 Corroded Web Penetration Along Vertical Angle Legs of Stringer End Connection to Floor Beam

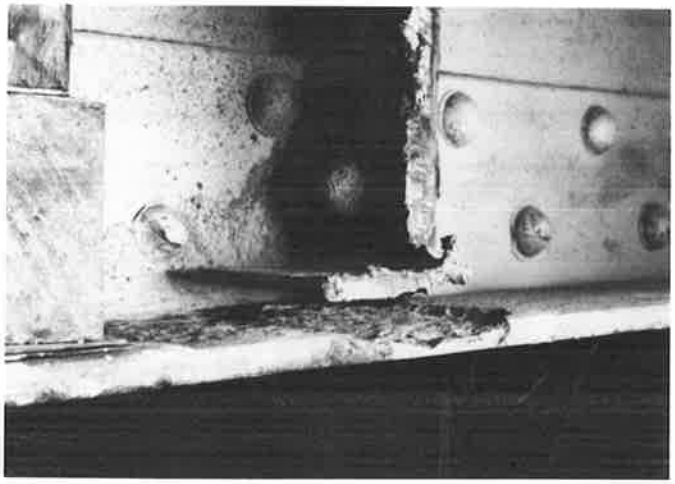

Figure 4 Corrosion Notched Flange Angle Below Diaphragm Where Dirt and Debris Accumulates

Figure 5 Severe Corrosion Notching of Flange Tip

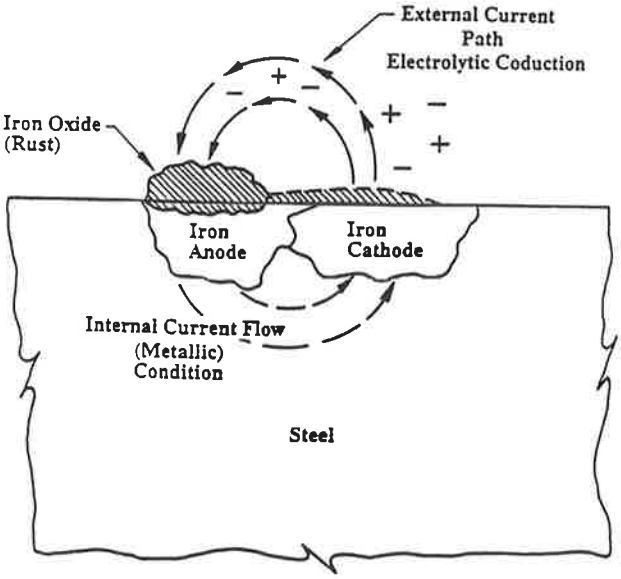

Figure 6 Schematic of Corrosion Cell (Battery)

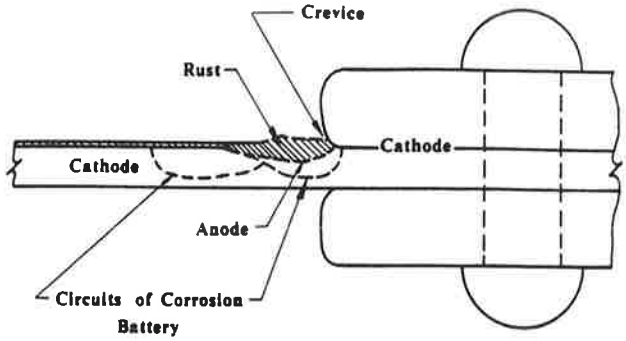

Figure 7 Crevice Corrosion Cell Created at Web-Connection Interface

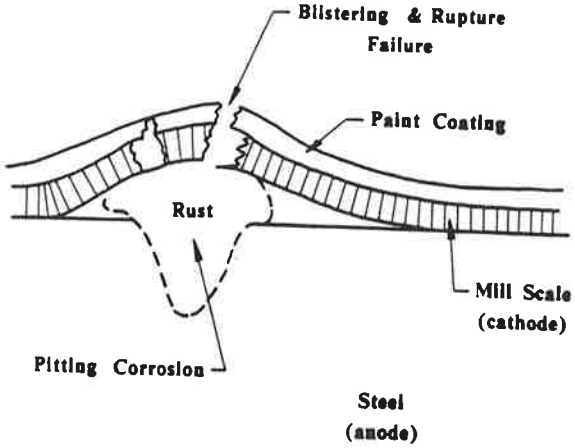

Figure 8 Corrosion Cell at Break in Mill Scale

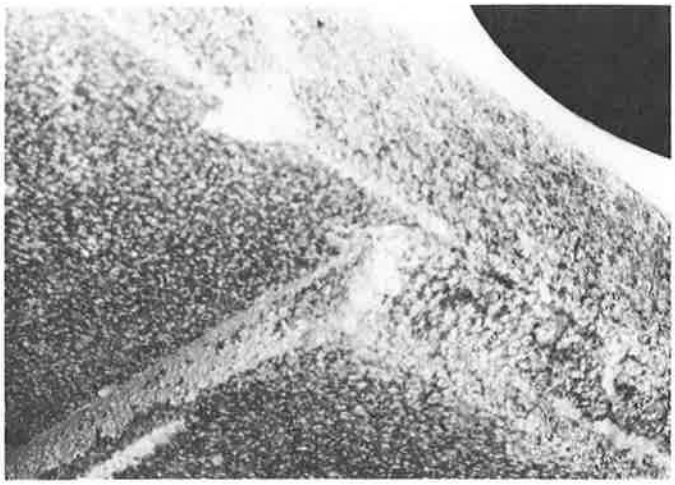

Figure 9 Corrosion Pitting of Beam Flange and Welded Coverplate

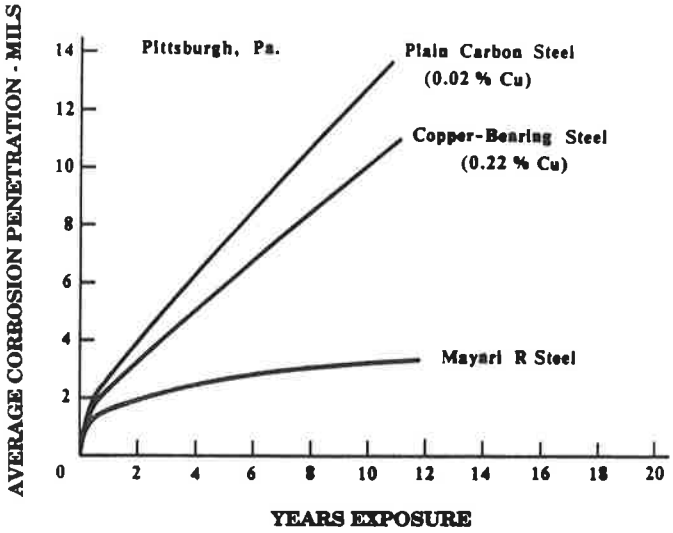

Figure 10 Corrosion of Steels in Industrial Atmosphere

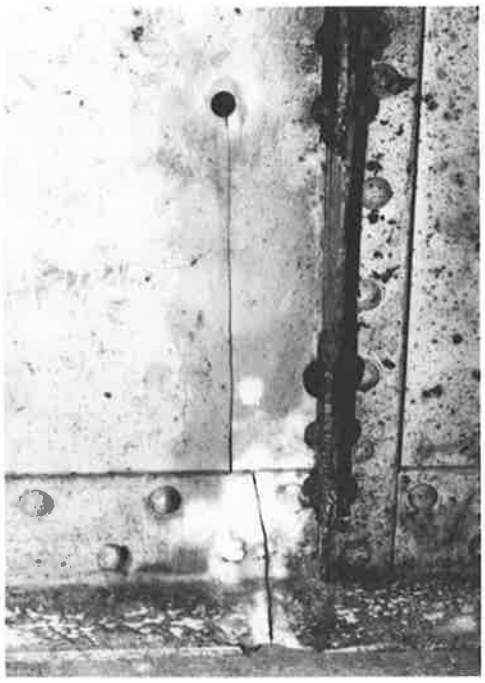

Figure 11 Cracked Components in Corrosion Notched Member

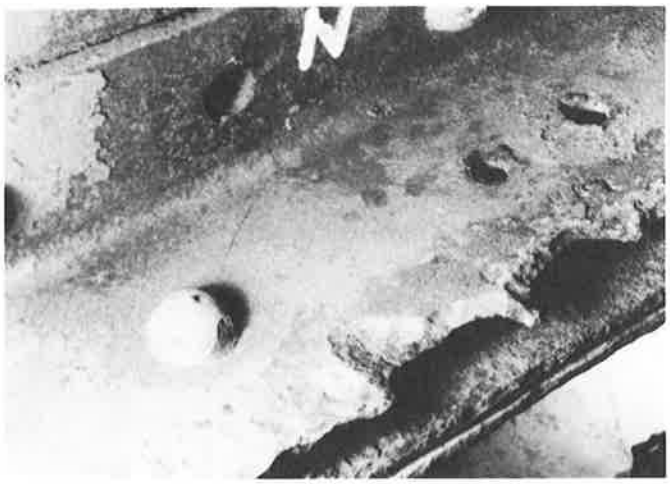

Figure 12 Extensive Corrosion Loss of Tension Flange

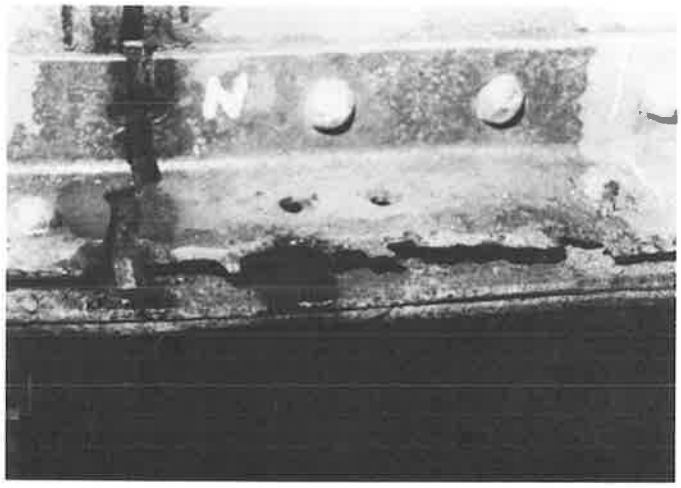

Figure 13 Fatigue Crack Initiated From Corroded Flange Angle

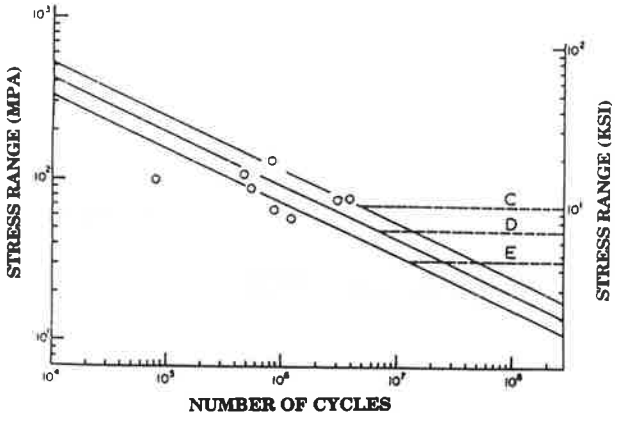

Figure 14 Fatigue Strength of Corrosion Reduced Element

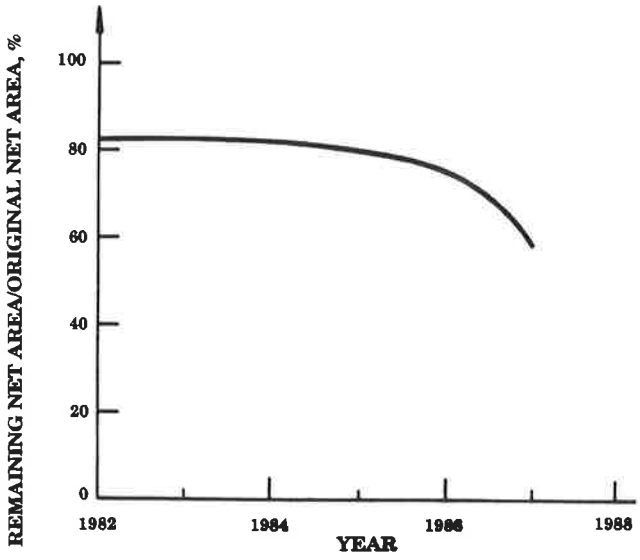

Figure 15 Ratio (%) of Remaining Net Area to Original Net Area as Function of Exposure Time

Figure 16 Corroded Hanger Specimen with Bolted End Fixtures

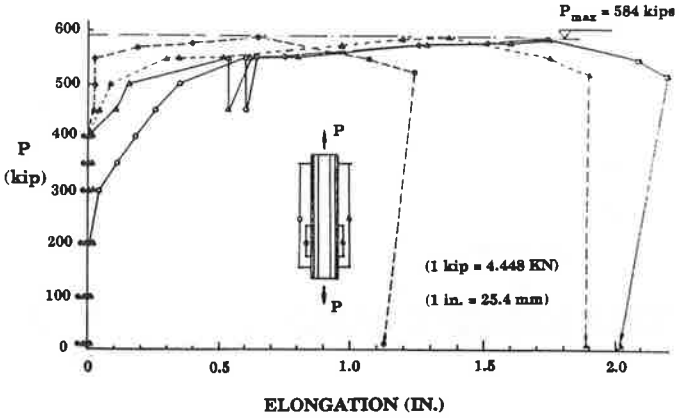

Figure 17 Load-Displacement Relationship of Hanger No. 2

Figure 18 Crack in Flange of Hanger No. 1

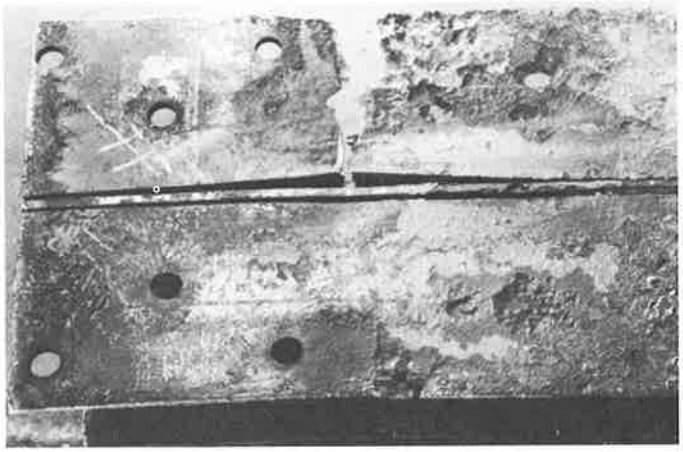

Figure 19 Crack in Flange of Hanger No. 2

Cross-section of Hanger No. 1

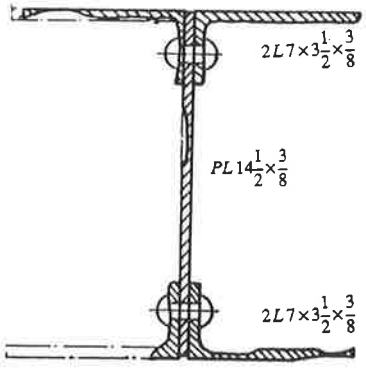

$A_g = 20.6\ in.^2$
$A_n = 18.4\ in.^2$
$A_{nm} = 11.3\ in.^2$

Cross-section of Hanger No. 2

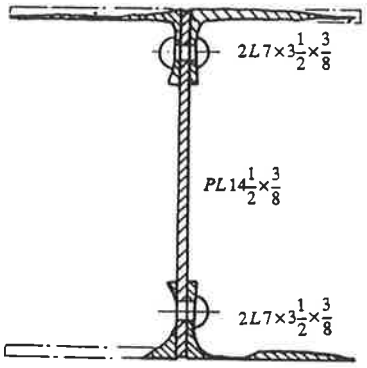

$A_g = 20.6\ in.^2$
$A_n = 18.4\ in.^2$
$A_{nm} = 10.8\ in.^2$

Fig. 20 Remaining Cross-Sectional Area

Fatigue Crack Growth Rates in Bridge Steels

WILLIAM J. WRIGHT[1] AND PEDRO ALBRECHT[2]

This paper presents the results of fatigue crack growth rate measurements for three commonly used bridge steels under conditions that simulate those occurring in highway bridges. Three different types of loading were investigated to eliminate any effect of crack closure on the measurements. It was found that the rate of crack propagation is dependent on the dead load stresses present in a structure. One equation should be used for fatigue life prediction in locations experiencing low dead loads, and another for locations with high dead loads.

The main factor limiting the useful life of steel bridges, other than material degradation such as corrosion, is metal fatigue. The process of metal fatigue may be divided into the two stages of crack initiation and propagation. Many load cycles are required to initiate a fatigue crack and propagate it to a size at which the crack can be readily detected with nondestructive inspection methods. Once an inspector has detected a fatigue crack, the engineer must determine how fast the crack will propagate to failure of the component and when the bridge will become unsafe and require repair.

The greatest part of the fatigue life of steel bridge details is spent growing cracks at low values of stress intensity factor range, at both short crack lengths and small stress ranges. Once the crack becomes longer, the crack growth rate accelerates and the remaining fatigue life is rapidly shortened. Therefore, it is of interest to measure crack growth rates at low values of stress intensity factor range.

The rate of fatigue crack propagation is defined as the change in crack length divided by the corresponding number of load cycles (da/dN). This rate can be determined as a function of the fracture mechanics parameter ΔK (the stress intensity factor range at the crack tip). In general, ΔK can be calculated from a formula of the following form where $\Delta\sigma$ is the stress range perpendicular to the crack, a is the crack length, and F_g is a parameter that depends on the detail and crack geometry:

$$\Delta K = \Delta\sigma \sqrt{\Pi a} \quad F_g \qquad (1)$$

1) Federal Highway Administration, Turner-Fairbank Highway Research Center, 6300 Georgetown Pike, McLean, VA 22101.

2) Department of Civil Engineering, University of Maryland, College Park, MD 20742.

Crack growth rates are commonly plotted as shown in figure 1 (*1*). Such data plots reveal three distinct types of behavior corresponding to regions I, II, and III. In region I da/dN approaches a threshold, ΔK_{th}, below which the crack does not propagate and in region II the straight line behavior is described by the power law equation where C and n are material constants.

$$\frac{da}{dN} = C\ \Delta K^n \qquad (2)$$

Finally, in region III, da/dN increases asymptotically as K_{max} approaches the fracture toughness, K_{Ic}. Again, region I and the lower part of region II are of most interest for application to bridges.

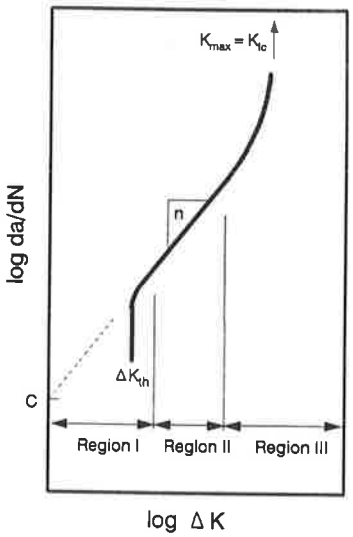

FIGURE 1 Crack growth rate example plot.

Once a fatigue crack has initiated in a structure, the remaining life can be predicted by rearranging and integrating equation 2 between the limits of initial and final crack lengths a_i and a_f

$$N = \int_{a_i}^{a_f} \frac{da}{C\ \Delta K^n} \qquad (2a)$$

The final crack length is determined as the point where $K_{max} = K_{Ic}$, the plane strain fracture toughness of the material. The calculation of ΔK and fatigue life for

various types of structures has been addressed elsewhere (*2*), and are beyond the scope of this paper.

EXPERIMENT DESIGN

Fatigue crack growth rates were measured for the following three types of steel: ASTM A572 grade 50 high-strength, low-alloy steel; A588 grade B high-strength, low-alloy weathering steel; and A852 quenched and tempered, low-alloy weathering steel. The A572 and A588 steels are commonly used in highway bridge construction, and the steel A852 is new. The measured yield strengths were 361, 417, and 582 MPa (52.4, 60.4, and 84.4 ksi) for the A572, A588 and A852 steels respectively (*3*).

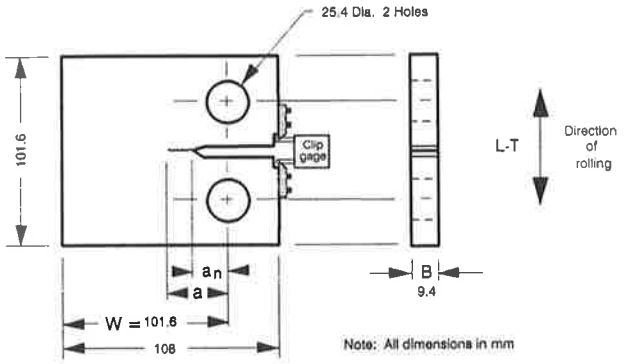

FIGURE 2 2T-C(T) specimen.

Compact tension specimens of dimensions shown in figure 2 were fabricated from 9.5 by 915 by 6,100 mm (3/8 by 36 by 240 in.) rolled plates. The specimens were oriented so that the crack propagated transversely to the direction of rolling in the plate.

TABLE 1 TEST MATRIX

Load Spectrum	Type of Loading	Type of Steel		
		A 572	A 588	A 852
Constant amplitude	R = 0.1	CC3	BC3	AC4
	R = 0.5	CC2	BC2	AC3
	K_{max} = 35.2 ($MPa\sqrt{m}$)	CC1	BC1	AC2

The test matrix, shown in table 1, consisted of 9 specimens arranged in a two-way factorial with three load cases and three types of steel. One specimen was tested in each cell. All specimens were tested at the U.S. Naval Academy in Annapolis with a computer-controlled MTS servo-hydraulic system, using software originally written by Professor James Joyce, USNA, and later modified by the authors to suit the needs of the present study. All testing was conducted in accordance with the requirements of the ASTM specification E647 (*4*).

LOADING PLAN

The loads were applied to the specimen according to three different plans. In two plans the load ratio ($R = P_{min}/P_{max}$) was kept constant at R = 0.1 and 0.5, and in the third plan the maximum stress intensity factor was kept constant at K_{max} = 35.2 $MPa\sqrt{m}$ (32 $ksi\sqrt{in}$). The R = 0.1 and R = 0.5 tests will simulate locations in structures where the dead load is 10 and 50 percent of the total load, respectively. The constant K_{max} test is designed to eliminate any effect of crack closure on da/dN as would be the case for cracks growing in regions of high residual tensile stresses near weldments.

Figures 3, 4, and 5, show the variation in ΔK throughout each test. In stage A, a fatigue crack initiated from the machined notch and propagated about 4 mm (0.16 in.) before crack growth rates were measured. In stage B the crack propagated under load shedding, with ΔK gradually decreasing in small steps according to the formula (*4*):

$$\Delta K_i = \Delta K_{i-1} \exp[-2(a_i - a_{i-1})] \qquad (2b)$$

where a_{i-1} and a_i are the crack lengths in two successive steps. There were about 190 load shedding steps in stage B, making the load shedding essentially continuous. The tests were ended when either the crack stopped growing as ΔK approached the threshold or ΔK reached a value of about 4.4 $MPa\sqrt{m}$ (4.0 $ksi\sqrt{in}$). The load shedding tests lasted between 6 and 10 million cycles. In stage C the crack propagated

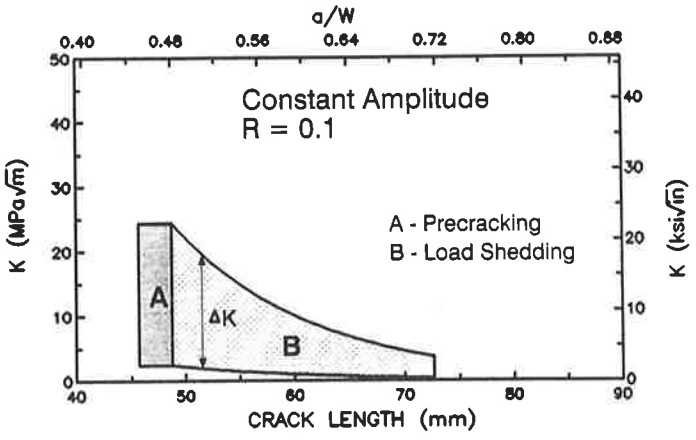

FIGURE 3 Test plan for R = 0.1.

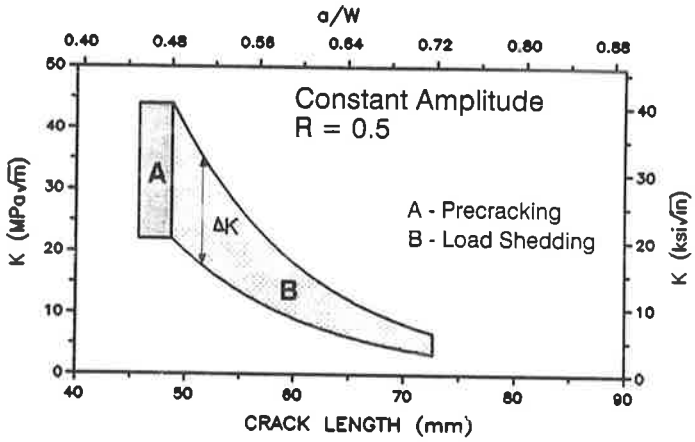

FIGURE 4 Test Plan for R = 0.5.

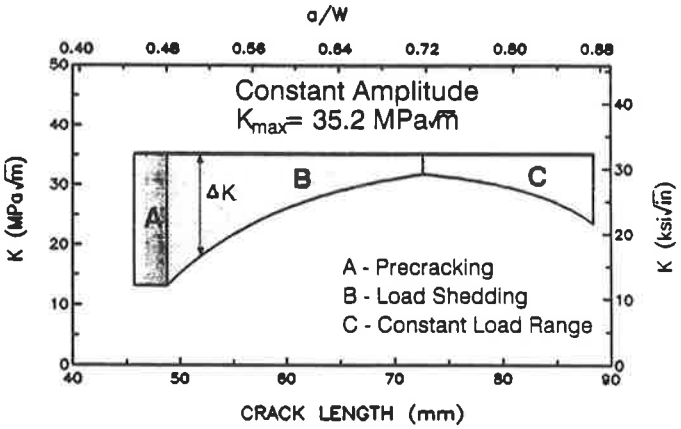

FIGURE 5 Test plan for K_{max} = 35.2 MPa $\sqrt{m}$.

under constant load range with ΔK increasing. This was done in one constant K_{max} test (figure 5) to confirm that cracks propagated at the same rate under load shedding (ΔK decreasing) and constant load range (ΔK increasing).

CRACK CLOSURE

Under certain loading conditions, the plastic deformations at the crack front can induce residual compressive stresses in the wake of the advancing crack, thereby keeping the crack closed until the applied load is high enough to overcome the residual stresses. Recognizing that the proportionality between da/dN and ΔK is only valid when the crack is fully open, Elber recommended the use of an effective stress intensity factor range, ΔK_{eff}, corresponding to the load range above the crack opening load (*5*).

In this study, the crack closure load, P_{cl}, is defined as the point where the compliance of the specimen changes. This point is determined from the intersection of the upper and lower lines in the load-displacement plot shown in figure 6. Measurements of displacement near the crack tip have shown that the crack closes at higher loads than is predicted with measurements of displacement remote from the crack tip (*6*). However the former

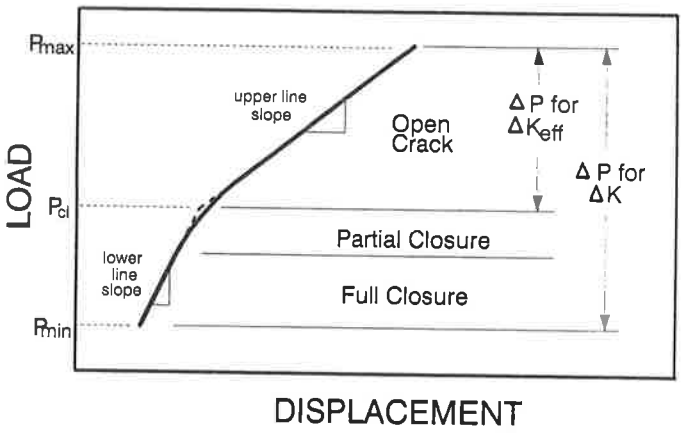

FIGURE 6 Definition of crack closure.

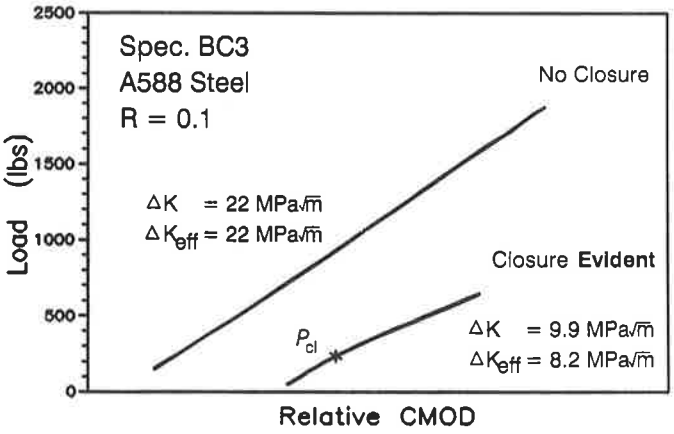

FIGURE 7 Typical compliance data showing effect of crack closure.

approach was followed in this study because it is better suited for real-time closure measurements of propagating fatigue cracks.

Figure 7 shows a typical plot of load versus crack mouth opening displacement (CMOD) data from a test with R = 0.1. Each line consists of 128 data points recorded over two cycles of loading. The upper line, recorded at ΔK = 22 MPa$\sqrt{m}$ (20 ksi$\sqrt{in}$), is straight, meaning that the crack did not close. Therefore, the values of ΔK_{eff} and ΔK are equal. The lower line, recorded at ΔK = 9.9 MPa$\sqrt{m}$ (9.0 ksi$\sqrt{in}$), exhibits a change in slope at the load at which the crack tip closed.

As an example of the effect of crack

closure, the growth rates measured in a R = 0.1 test are plotted in figure 8 against both ΔK and ΔK_{eff}. In this specimen tested under load shedding, the crack did not close at values of $\Delta K > 13.2$ MPa$\sqrt{m}$ (12 ksi$\sqrt{in}$). But, crack closure below that value caused ΔK_{eff} to become smaller than ΔK by up to 2 MPa$\sqrt{m}$ (1.8 ksi$\sqrt{in}$) at the threshold.

Crack closure generally will not occur in typical fatigue cracks in highway bridge members. If crack growth rate data that contains closure effects are used to make fatigue life predictions, it will predict slower crack growth and thereby overestimate the remaining life of the structure. This is especially true in the threshold region, where data containing closure effects will predict much higher thresholds. To remove the effect of closure, all crack growth rate data presented in this paper were plotted in terms of da/dN versus ΔK_{eff}.

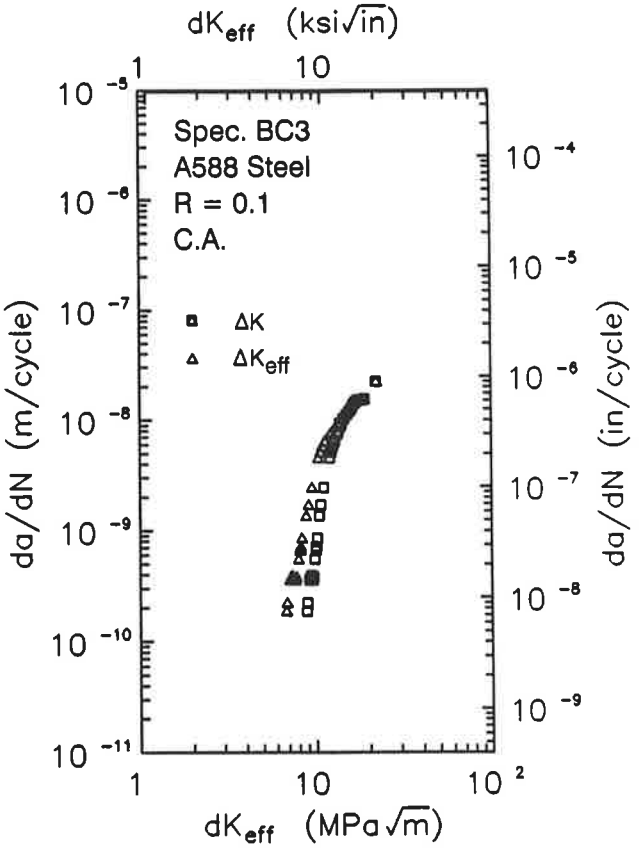

FIGURE 8 Effect of crack closure.

CRACK GROWTH RATE RESULTS

Figures 9, 10, and 11 show the data for all steels tested under R = 0.1, 0.5, and constant K_{max} loading, respectively. As can be seen for each type of loading, the data from all three steels correlated very well, suggesting that type of steel had no apparent effect on crack growth rate under constant amplitude cycling. The crack growth rates measured at R = 0.5 and constant K_{max} (figures 10 and 11) were comparable in both regions I and II. The constant K_{max} loading resulted in a constantly varing R ratio starting at about 0.4 at high ΔK values and increasing to a maximum of 0.9 at low ΔK values. It can therefore be concluded that tests conducted at high R-ratios of 0.4 and above should give similar crack growth rates. Therefore, the two sets of high R-ratio data were combined in figure 12.

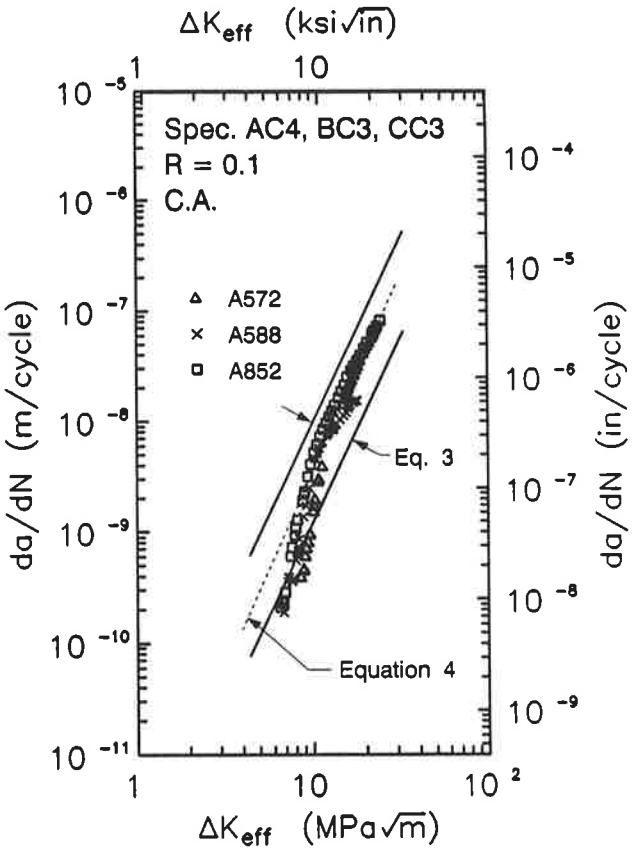

FIGURE 9 Comparison of crack growth rate for all steels at R = 0.1.

Figures 9, and 12 compare the low and high R-ratio data with the bounds at two standard deviations above and below the mean crack growth rates (*7*)

$$\frac{da}{dN} = 1.537 \times 10^{-12} (\Delta K_{eff})^{3.344} \times 10^{\pm 2 \times .2258} \quad (3a)$$

$$\frac{da}{dN} = 8.291 \times 10^{-11} (\Delta K_{eff})^{3.344} \times 10^{\pm 2 \times .2258} \quad (3b)$$

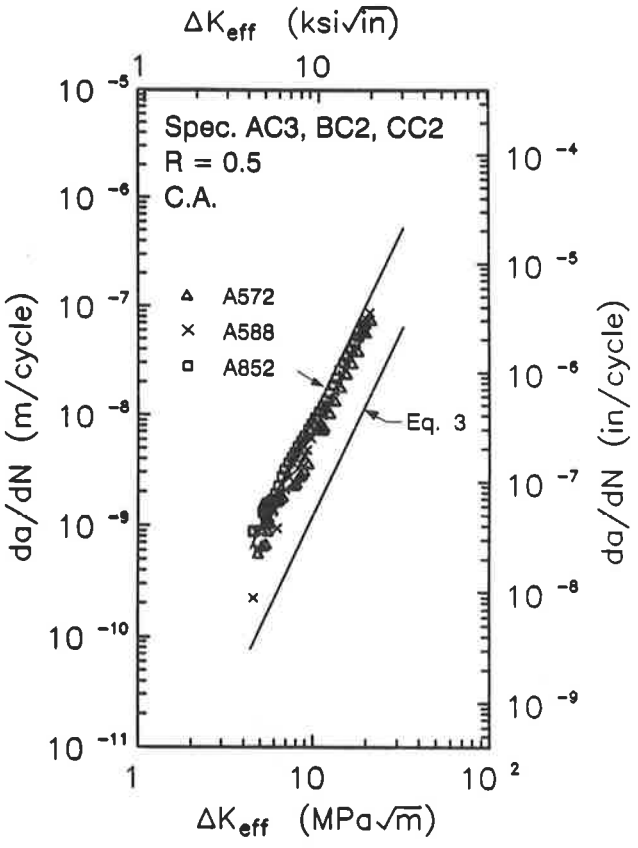

FIGURE 10 Comparison of crack growth rate for all steels at R = 0.5.

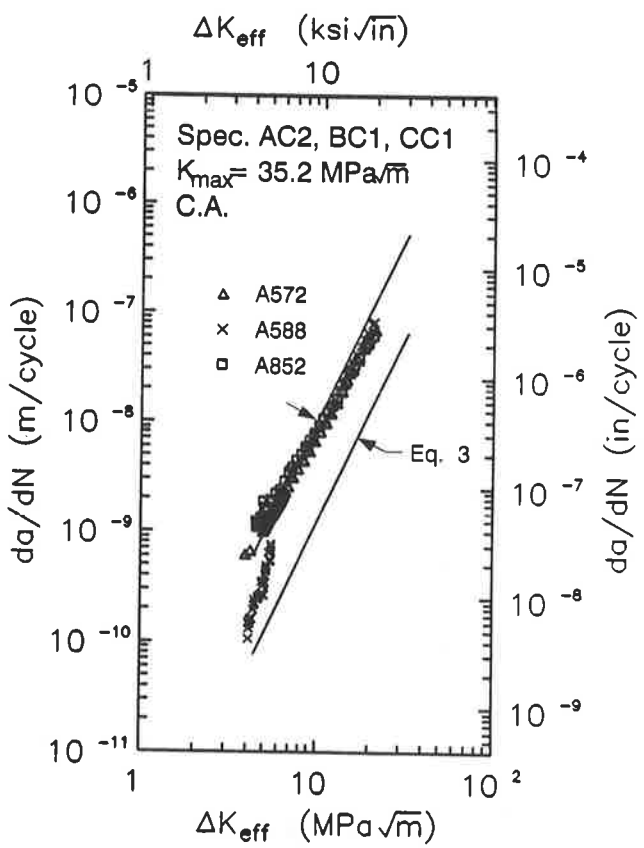

FIGURE 11 Comparison of crack growth rate for all steels at K_{max} = 35.2 MPa$\sqrt{m}$.

reported by Yazdani and Albrecht for mild and HSLA steels tested in air mainly at low R-ratios. The units for ΔK_{eff} and da/dN are MPa$\sqrt{m}$ and m/cycle in subequation (a) and ksi$\sqrt{in}$ and in/cycle in subequation (b). As would be expected, the low R-ratio data from the present study fell about half-way between the upper and lower bounds while the high R-ratio data fell along the upper bound. Clearly, cracks grow faster at R > 0.4 than at R = 0.1, even when ΔK is calculated with the load range above crack closure only. The R = 0.1 data will be considered separately from the R = 0.5 and constant K_{max} data in further analysis.

Threshold behavior was observed in five of the nine constant amplitude tests performed in the present study. In the high R ratio tests, the value of ΔK approached a threshold of about 4.0 MPa$\sqrt{m}$ (3.6 ksi$\sqrt{in}$) for A588 steel, but the threshold could not be determined for the A572 and A852 steels. In contrast, the R = 0.1 tests showed a much higher average threshold of ΔK_{th} = 6.5 MPa$\sqrt{m}$ (5.9 ksi$\sqrt{in}$). Again, the difference between low and high R ratios is apparent.

CRACK GROWTH RATE EQUATIONS

Equations were fitted to the crack growth rate data from the low and high R-ratio tests. Only the points falling along a straight line in region II were included in the regression analysis. The units for ΔK_{eff} and da/dN are MPa$\sqrt{m}$ and m/cycle in the sub-equations "a" and ksi$\sqrt{in}$ and in/cycle in the sub-equations "b". The resulting equation for the mean crack growth rate at low R-ratio:

$$\frac{da}{dN} = 1.03 \times 10^{-12} (\Delta K_{eff})^{3.528} \quad (4a)$$

$$\frac{da}{dN} = 5.65 \times 10^{-11} (\Delta K_{eff})^{3.528} \quad (4b)$$

is shown as a dashed line in figure 9. Although it is only valid for $\Delta K_{eff} \geq 10$

MPa$\sqrt{m}$ (9.1 ksi$\sqrt{in}$), equation 4 was extended to lower values of ΔK_{eff} in figure 9 for ease of comparing it with the data bounds from previous tests.

The equation for the mean crack growth rate at high R-ratio

$$\frac{da}{dN} = 7.17 \times 10^{-12} (\Delta K_{eff})^{3.019} \quad (5a)$$

$$\frac{da}{dN} = 3.75 \times 10^{-10} (\Delta K_{eff})^{3.019} \quad (5b)$$

is shown as a dashed line in figure 12. Clearly, cracks grow faster at high than at low R-ratios.

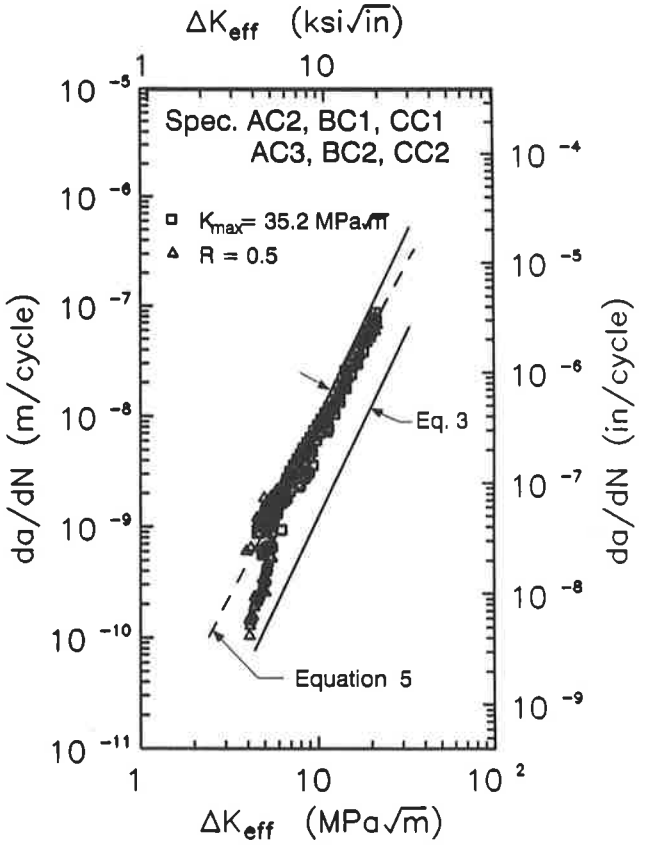

FIGURE 12 Eqution for crack growth rate data for all steels at high R-ratios.

CONCLUSIONS

Under constant-amplitude cycling, cracks were found to grow significantly faster at high R-ratios than at low R ratios. Accordingly, equations 4 or 5 should be used in predictions of fatigue life of a structural detail depending on whether the R-ratio under the combined dead, live, and residual stresses is low or high. The more severe effect of high R-ratio was also observed in the threshold region, with the high R-ratio data showing a lower threshold than the low R-ratio data (4.0 versus 6.5 MPa$\sqrt{m}$). This finding agrees with the results of S-N tests reported by Albrecht and Liu (*8*) in which the fatigue limit of a transverse stiffener detail was shown to be lower the higher the R-ratio.

Type of steel -- A572, A588, and A852 -- had no effect on crack growth rates under constant amplitude cycling.

RESEARCH IN PROGRESS

The authors are currently analyzing crack growth rate data from tests they have performed under variable-amplitude cycling. The variable-amplitude load spectrum is

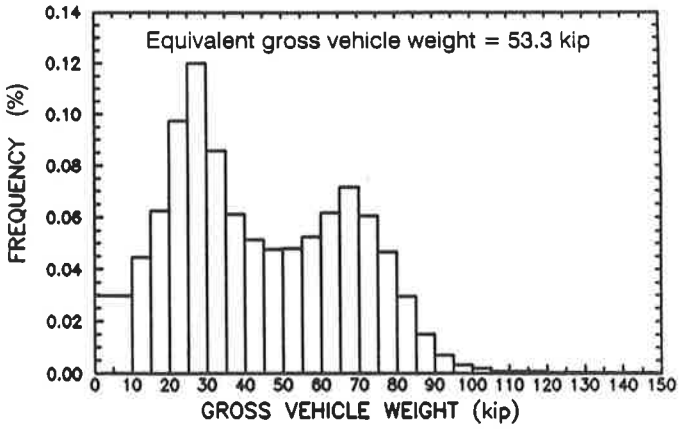

FIGURE 13 GVW Histogram.

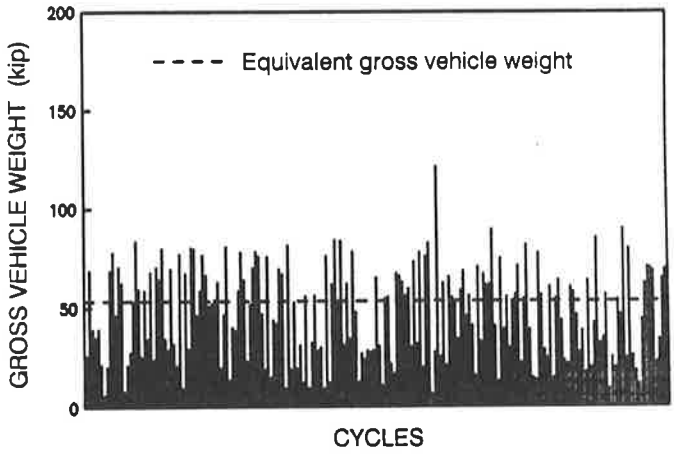

FIGURE 14 200-cycle segment of the random spectrum.

proportional to the gross vehicle weight (GVW) distribution of trucks reported in an extensive weigh-in-motion study sponsored by the FHWA. Figure 13 shows the resulting frequency distribution of GVWs for 27,513 trucks that were weighed at 31 sites in seven states (*9*). The equivalent root-mean-cube GVW is (*10,11*)

$$W_e = \{\sum \alpha_i W_i^3\}^{1/3} = 237 \text{ kN} \quad (53.3 \text{ kip}) \qquad (6)$$

where α_i is the frequency of occurrence of the GVWs W_i.

The variable-amplitude load spectrum used in the crack growth rate tests consisted of 10,000 individual cycles of amplitudes proportional to the GVWs. The cycles within the 10,000-cycle spectrum were arranged in random order to simulate the random passage of trucks over a bridge. Figure 14 shows a representative block of 200 cycles taken from the spectrum.

Crack growth rates under variable-amplitude cycling were measured for the same steels and at comparable R=ratios as those under constant-amplitude cycling. The analysis performed to date is showing no signs of a threshold for the variable-amplitude crack growth rate data at values of equivalent stress intensity factor range as low as ΔK_e = 2.7 MPa$\sqrt{m}$ (2.5 ksi$\sqrt{in}$). Until crack growth rate data become available at lower ΔK_e values, no threshold should be assumed to exist for variable amplitude cycling.

Also in progress is research to measure fatigue crack growth rates in full scale bridge members. Special gages are being attached to large beams being tested at the Turner-Fairbank Highway Research Center to measure the rate of growth of cracks. These results should provide an excellent confirmation of the small specimen test results reported in this paper.

ACKNOWLEDGEMENT

This report is part of the ongoing research project "Variable Amplitude Load Fatigue", sponsored by the Federal Highway Administration at the Universities of Pittsburgh and Maryland under contract number DTFH-86-C-00036. The authors wish to thank Dr. James Joyce, who contributed his valuable experience and the use of laboratory facilities at the United States Naval Academy.

REFERENCES

1. Paris, C. and Erdogan, F., "A Critical Analysis of Crack Propagation Laws," Transactions of the ASME, Journal of Basic Engineering, Series D, 85, No. 3, 1963.
2. Albrecht, P. and Yazdani, N., "Risk Analysis of Extending the Service Life of Steel Structures", Report No. FHWA/MD-84/01, Maryland State Highway Administration, Baltimore, Maryland, 1984.
3. Albrecht, P., "Variable Amplitude Load Fatigue - Quarterly Progress Report", Contract No. DTFH61-86-C-00036, University of Maryland, January 1989.
4. "Standard Test Method for Measurement of Fatigue Crack Growth Rates," ASTM Designation E647-88, Annual Book of Standards, Volume 03.01.
5. Elber, W. "Significance of Crack Closure," Damage Tolerance in Aircraft Structures, ASTM STP 486, American Society for Testing and Materials, Philadelphia, 1971.
6. Hudak, S.J. and Davidson, D.L., "The Dependence of Crack Closure on Fatigue Loading Variables," Mechanics of Closure, ASTM STP 982, J.C. Newman, Jr. and W. Elber, Eds., American Society for Testing and Materials, Philadelphia, 1988, pp. 121-138.
7. Yazdani, N. and Albrecht, P., "Crack Growth Rates of Structural Steels in Air and Aqueous Environments," Journal of Engineering Fracture Mechanics, Volume 32, No. 6, 1989, pp. 997 - 1007.
8. Albrecht, P. and Liu, H.J., "Quarterly Progress Report - 10/1/89 through 12/31/89," Contract No. DTFH61-86-C-00036, University of Maryland, January 1990.
9. Snyder, R.E., Likins, G.E., and Moses, F., "Loading Experienced by Bridge Structures in the United States," Report FHWA/RD-85/012, Bridge Weighing Systems, Inc., Warrensville, OH, February, 1985.
10. Yamada, K., "Fatigue Behavior of Structural Components Subjected to Variable Amplitude Loading," Ph.D. Dissertation, Department of Civil Engineering, University of Maryland, College Park, Maryland, 1975.
11. Schilling, C. G., "Variable Amplitude Load Fatigue - Task A Literature Review", Volume I - "Traffic Loading and Bridge Response", Report No. FHWA/RD-87/059, Federal Highway Administration, Washington, D.C., March, 1987.

Evaluation of Fatigue Life and Retrofitting on the Benicia-Martinez Bridge

JOHN M. HANSON, MICHAEL J. KOOB, AND JOHN W. FISHER

An evaluation of the fatigue life of the Benicia-Martinez Bridge was undertaken in anticipation of the widening of the bridge. This 1.2 mile long, high level crossing includes ten steel deck-truss spans up to 528 ft in length. Welded built-up H sections of T-1 and ASTM A242 steel were used for the truss members. Stay plates were also fillet welded to the flanges of the H-sections at the joints, apparently to offset the loss of section due to bolt holes.

Cracking had been found at several fillet weld terminations of the stay plates prior to the evaluation. Subsequent examination during the course of the evaluation confirmed that fatigue crack growth had occurred, even though most of the previously-observed cracking was related to fabrication.

A state-of-the-art evaluation of the fatigue life was made using strain data recorded under normal traffic. This evaluation revealed that, on a conservative basis, the fatigue life was nearly exhausted. Details to remove the fatigue-sensitive conditions were developed and subsequently implemented.

INTRODUCTION

The Benicia-Martinez Bridge, located thirty miles northeast of San Francisco, carries Interstate Highway 680 across the Sacramento River. This 1.2 mile long, high-level crossing consists of ten steel deck-truss spans ranging in length between 330 ft and 528 ft and eight steel plate-girder approach spans. A photograph of the bridge, looking south, is presented in (Figure 1).

The bridge was designed by the California Department of Transportation (CalTrans) in the late 1950s and has been in continuous service since it was opened to traffic in 1963. The design was based on AASHO and CalTrans specifications in effect at that time, using welded built-up steel H-sections for the truss members and bolted connections. The H-sections were fabricated using both T-1 and ASTM designation A242 plates. The T-1 plates conform to the current ASTM A514 specification. Stay plates were welded to the flanges of the H-sections at the joints in the truss members, apparently to offset the loss of section due to the bolt holes. A photograph of one of these locations is shown in (Figure 2).

An evaluation of the fatigue life of the main truss members of the bridge was undertaken in preparation for widening of the roadway. The evaluation was to have been based mainly on strain data and traffic records made by CalTrans. However, fatigue cracks were found at the ends of and along the fillet welds connecting the stay plates to the flange tips of the chord members. It was evident that retrofitting of this condition was desirable. Procedures for this retrofitting were developed and implemented which would allow the widening to proceed as planned. This paper describes the work carried out for this evaluation.

REVIEW AND INITIAL INSPECTION

The structural system consists of two parallel trusses joined by top and bottom plane lateral bracing and diagonal sway bracing. An elevation of a typical suspended and continuous span is shown in (Figure 3), and a typical cross-section in (Figure 4).

The so-called continuous span trusses are simply supported on the piers, and have 99-ft end cantilevers extending into the adjacent spans. The suspended span trusses are simply supported on the end cantilevers of the adjacent continuous span trusses. Dummy members are used at the ends of the suspended trusses. Each of the parallel truss systems is statically determinate.

Typically, the H-shaped sections were fabricated by fillet welding a web plate to two flange plates. The web and flange plates contain transverse groove welds, where there may be either a change in thickness or a change in the grade of steel. Top and bottom chord members are continuous between the five-member joints (i.e., continuous through the T-joints). The truss members are connected at the joints by gusset plates bolted to the flanges of the members. Additional "stay plates" were fillet welded to the tips of the flanges in the joint regions.

Mill reports for the 1-in.-thick flange plates indicated that five heats of steel had an ultimate tensile strength exceeding the limit of 130 ksi for A514 steel. The highest reported strength was 134.6 ksi. The yield strengths of these five heats ranged from 120.8 ksi to 125.3 ksi. The location in the bridge of steel plates from these heats, as well as mill information on plates thicker than 1 in., was not available. According to CalTrans, all groove welds were radiographed to assure that standards then in effect were met.

In accord with the current AASHTO specifications (1)*, the fillet welds connecting the web plate to the flange plates and the groove welds in the flange plates are Category B conditions. The fillet welds connecting the stay plates to the tips of the flange plates are also Category B along their length, becoming a condition between Category E or E' at their terminations. For this fatigue evaluation, it is reasonable to consider the detail to be a Category E' condition.

Since there are only two main trusses in the superstructure, the bridge is classified as nonredundant. Furthermore, in accord with the Guide Specifications for Fracture Control of Nonredundant Steel Bridge Members (2), the tension members in these trusses are fracture critical members, because their failure could result in collapse of the bridge.

The concrete roadway is supported on stringers which frame into transverse beams that are supported on the top

* Numbers in parentheses refer to references listed at the end.

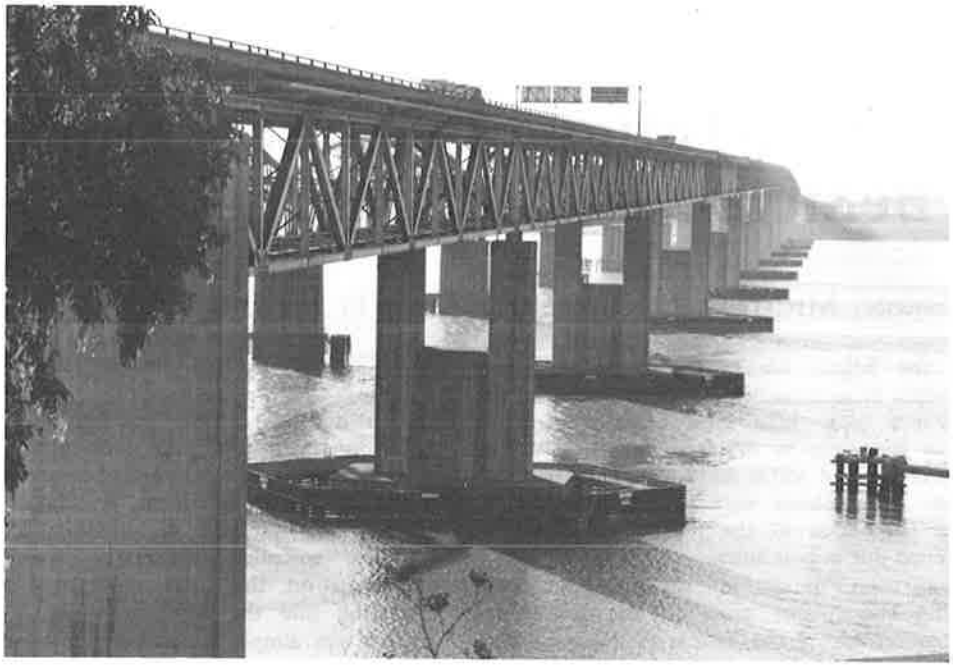

FIGURE 1 View of west side of bridge.

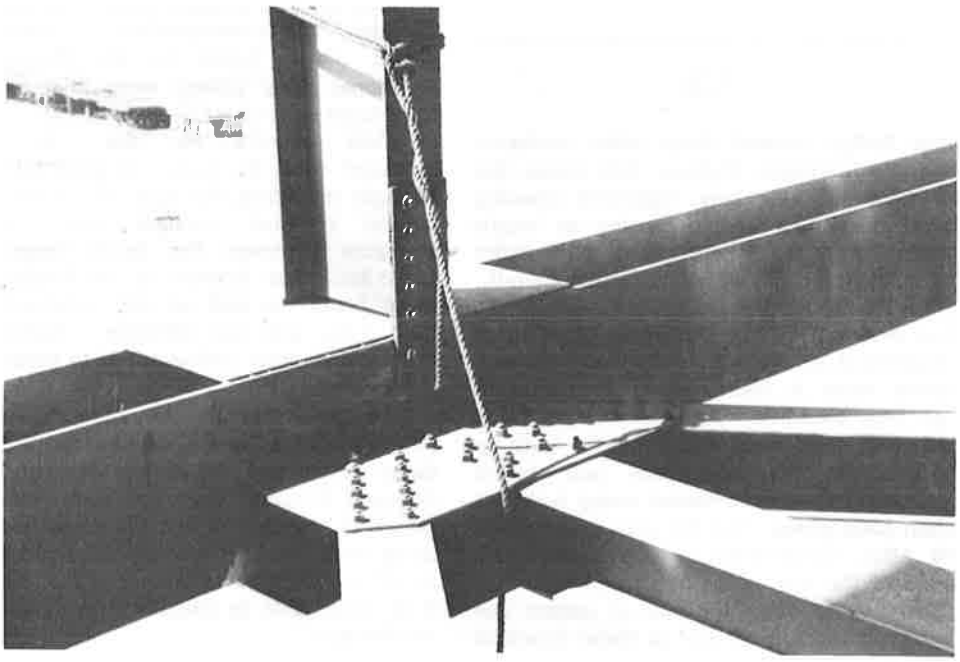

FIGURE 2 Stay plate welded to flange, at a T-joint.

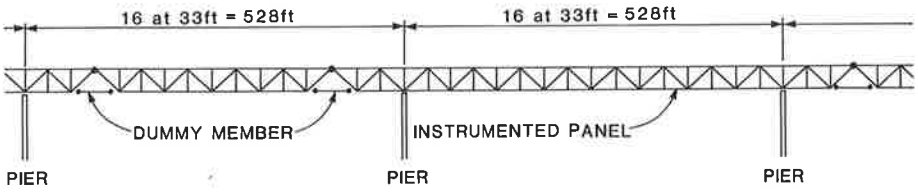

FIGURE 3 Continuous and suspended spans.

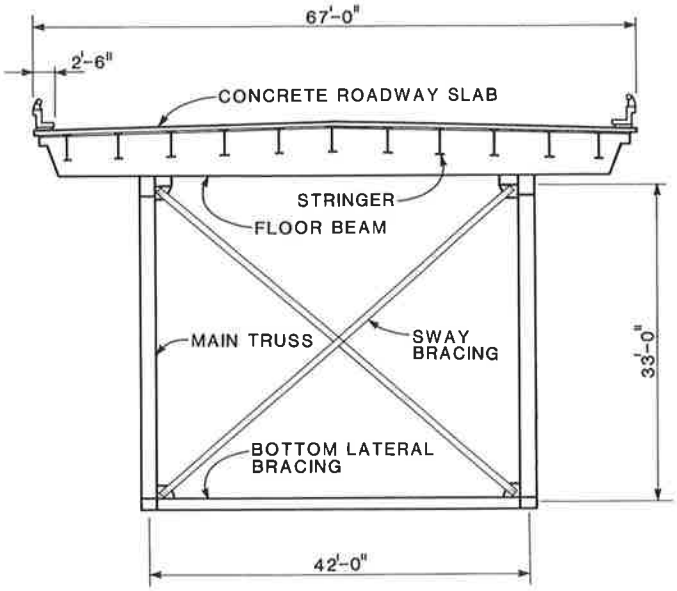

FIGURE 4 Typical cross section.

chord joints of the trusses. The evaluation of fatigue life did not include the welded connections in these members.

Structural analyses were performed by CalTrans based on two-dimensional and three-dimensional models of the bridge. The analyses showed that, under a moving truck load, members located at the approximate point of bending moment inflection under dead load in each continuous span are subject to the highest stress range. These members are subject to relatively small axial forces under dead load and are therefore of relatively small cross-sectional area. Under a moving truck load, however, they are subject to a significant axial force range.

An initial inspection of the bridge was made to gain first-hand familiarity with the fatigue-critical conditions. The quality of the welding was observed to vary from span to span. The fillet welds connecting the stay plates to the edges of the flanges were particularly uneven with indications of discontinuities, possibly because they were made in the field and also because some of the welds were made in the overhead position. The geometry of the wrap-around welds at the termination of the fillet welds varied considerably in shape, frequently appearing to be susceptible to cracking. Information provided by CalTrans indicated that cracks had previously been found at five locations. However, the nature of these cracks was not indicative of fatigue.

Several locations were observed where it appeared that there was overlapping in the fillet welds connecting the web plate to the flange plates, or where repairs had been made. At these locations, the weld profile was such that the fatigue strength might approach a Category E condition.

The roadway was to be widened from 62 ft-0 in. to 74 ft-0 in. by extending the transverse floor beams and the concrete deck slab. According to a three dimensional stress analysis made by CalTrans, when a single truck is located over one truss, 40 percent of the load is distributed by the bracing to the other truss. On this basis, stress due to a single truck will increase by approximately 5 percent after the widening is completed. As subsequently discussed, a stress range increase of this magnitude was recognized in the evaluation of fatigue life.

COLLECTION OF STRAIN HISTORY AND TRAFFIC DATA

From May 14, 1987 through June 3, 1987, strain data under general traffic loading were recorded by CalTrans on truss members in Span 5, a 528 ft span of the bridge. Data were recorded simultaneously from each gage for approximately 325 hours. During the collection of the strain data, the number of northbound vehicles crossing the bridge per day

was recorded by CalTrans for each of several vehicle weight classes.

Strains were also recorded by CalTrans for four separate round trips of a permit vehicle crossing the bridge, in the absence of all but a few other relatively small vehicles. These strain data were recorded in the early morning of June 27, 1987. The permit truck was a 9-axle tractor-trailer weighing 204,000 lb. travelling at a speed of approximately 20 mph.

Locations of Instrumentation

Strain gages were installed at six locations in the top chord (U12-U13) and bottom chord (L12-L13) in the fifth panel from the north end of both trusses in Span 5. The locations of these 24 gages are shown schematically in (Figure 5).

Gages 3, 4, 9, and 10 in the west truss and gages 15, 16, 21, and 22 in the east truss were located at the mid-lengths of the chords and at the mid-widths of the flanges. Strains measured at these locations should not be influenced by bending moment or local strain concentration. Gages 5, 6, 7, and 8 in the west truss and gages 17, 18, 19, and 20 in the east truss were located on the flange tips, approximately one inch from the ends of the stay plates. At these locations the strains may be affected by both bending due to restraint of end-rotations and strain concentration at the ends of the stay plates. The gusset plates at the T-joint are relatively small and do not extend to the locations of the strain gages along the member. Gages 1, 2, 11, and 12 in the west truss and gages 13, 14, 23, and 24 in the east truss are located near the ends of the members and at the tips of the flanges, approximately one inch from the ends of the stay plates. However, they are also located slightly inside the edge of the gusset plates. Consequently, the strain at these locations may be reduced due to transfer of force in the member to the gusset plates, and may be affected by moment and strain concentration.

Traffic Records

During the recording of the strain data under general traffic loading, records were kept at the toll booths of the volume of northbound bridge traffic. Total daily bridge traffic in both directions was estimated as double that in the northbound direction. This traffic was in the range of 35,000 to 42,000 vehicles on week days, and 31,000 to 37,000 vehicles on weekend days.

The daily records include the number of vehicles in each of several different weight classifications. The largest stress cycles are associated with either trucks or heavy trucks. Heavy trucks are those having five or more axles. About 2700 trucks crossed the bridge each week day. On weekend days, only about one quarter as many trucks crossed the bridge. Fifty five percent of the total truck traffic was in the heavy truck classification.

Interpretation of Strain Records for the Permit Vehicle

Records of strain under the permit vehicle loading showed that the strain along the length of the instrumented tension chords had different amplitudes but nearly identical variations over time (time signatures), regardless of whether the permit vehicle was traveling northbound or southbound. For twelve of the gages, the maximum stress

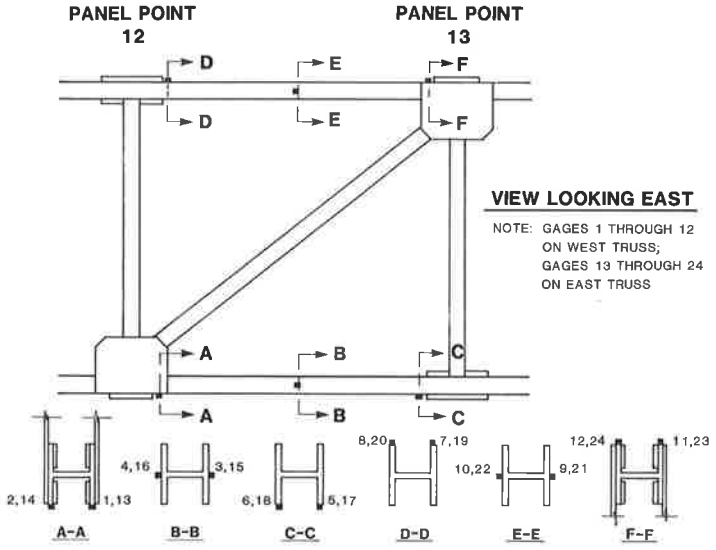

FIGURE 5 Stress gage locations.

ranges were computed. These ranges are given in Table 1. The reasonable agreement of the stress range for pairs of gages at a particular section indicates that the effect of out-of-plane and torsional distortions in these members under a heavy loading is small compared to the primary effect.

A simple pin-jointed truss analysis predicts that strain under load is constant over the length and width of a member. Table 1 shows that the recorded strains and derived stresses vary between the instrumented locations. The stresses are lowest at the gages near the five-member joints, and highest at the gages at the T-joints.

Several factors apparently interact and contribute to the variation of stress between the different gage locations:

1. Influence of strain concentration near the ends of the stay plate welds, which cause an increase in the stresses at these locations.
2. Bending at the ends of the members, which causes either an increase or decrease in the stresses at the tips of the flanges.
3. Overlapping of the gusset plates with the gages at the five-member joints.
4. Torsional deformation due to the location of the permit vehicle relative to the center of the bridge.

These factors are considered in the assessment of the stress range histograms.

DEVELOPMENT OF STRESS RANGE HISTOGRAMS

Stress range histograms were developed from the strain data using computer hardware and software especially developed for this purpose. The hardware consisted of a Compaq 386 desktop computer connected to peripheral devices. These devices included an EMI 7000C 28-channel tape recorder for reading the analog data from the tapes supplied by CalTrans, a DASH IV stripchart recorder for output of the strain records, and a Kyowa 116B Analog/Digital converter.

Previously written software for developing histograms from short segments of strain records was modified to allow continuous analyses of the strain records. The software performed a point-by-point analysis of the data from each channel, using a modified one-pass rainflow algorithm (3). In this algorithm, the cycle count in each stress range is accumulated as local maxima and minima are encountered in the strain data, and data that are not local maxima or minima are discarded. This algorithm does not retain the digitized data record.

The histograms were output in a form suitable for post processing with standard micro-computer software. Effective stress ranges and numbers of cycles for each strain data record were computed using Lotus 1-2-3(c) spreadsheet templates.

A total of 20 stress range intervals each 500 psi wide were used for the histograms, from zero to 10,000 psi. This selection was made on the basis of a visual examination of the recorded data and a desire for four to eight

TABLE 1 - MAXIMUM STRESS RANGES IN TENSION CHORD MEMBERS UNDER THE PERMIT VEHICLE LOADING

(a) Chord L12-L13 (West Truss)

Run	Direction	Channel 1	2	3	4	5	6
		Stress Ranges, in ksi					
1	Northbound	2.18	2.12	4.18	4.20	5.89	5.34
	Southbound	2.87	2.93	5.60	5.48	8.32	7.48
2	Northbound	2.58	2.55	4.96	4.84	6.84	6.26
	Southbound	3.25	3.31	6.32	6.24	9.37	8.41
3	Northbound	3.07	2.99	5.57	5.54	7.74	7.16
	Southbound	3.07	3.10	6.03	5.95	8.96	8.03
4	Northbound	2.55	2.49	4.76	4.61	6.50	5.92
	Southbound	2.99	2.99	5.54	5.74	8.56	7.74

(b) Chord L12-L13 (East Truss)

Run	Direction	Channel 13	14	15	16	17	18
		Stress Ranges, in ksi					
1	Northbound	2.55	2.64	4.47	4.47	6.93	6.47
	Southbound	2.70	2.50	4.29	4.32	6.12	5.77
2	Northbound	3.25	3.05	5.39	5.39	8.29	7.60
	Southbound	3.22	3.07	5.25	5.16	7.40	6.84
3	Northbound	3.63	3.48	5.96	6.06	9.31	8.47
	Southbound	2.90	2.73	4.70	4.76	6.67	5.86
4	Northbound	3.13	3.10	5.34	5.37	8.27	7.48
	Southbound	2.78	2.58	4.47	4.52	6.35	5.86

intervals containing a significant number of cycles. The data tapes were read on the EMI 7000C tape recorder at a tape speed of 15/16 inches per second, which helped to minimize noise contamination. A digitizing rate of 100 Hz provided adequate detail of the higher frequency components of the data, and allowed the computer to process the data in real time.

Sixteen of the 24 data channels on each tape were selected for processing. The selected channels are noted with asterisks in (Figure 5). All six data channels in each bottom (tension) chord member were processed, since these members are subject to fatigue crack growth. The remaining four channels were selected in the top (compression) chord members, consisting of one mid-length gage (gage 10) in the west truss and one gage at each of the three member cross sections (gages 19, 22, and 23) in the east truss.

Production of Stress Range Histograms

During processing of the strain data tapes, measures were taken to detect and reduce possible noise contamination. An electronic air cleaner was used to remove dust. The heads of the tape recorder were cleaned before processing each tape to remove accumulated dust or tape residue. Also, processing was stopped a few minutes before the end of the data in order to avoid processing random noise after the end. Each histogram represented 297.7 hours of strain measurements. Data for selected histograms is given in Table 2. A histogram for channel 5 is shown in (Figure 6).

Effective Stress Range and Fatigue Cycles

For each of the 16 strain gages for which data were processed, the effective stress range and the number of equivalent stress cycles were determined from the stress range histograms. The effective stress range S_{re} was calculated using Miner's Rule (4):

$$S_{re} = [\Sigma_i \alpha_i S_{ri}^3]^{1/3} \quad (1)$$

where the summation is over all stress range intervals in the histogram, α_i is the fraction of the total number of stress range cycles that occurs within the i^{th} stress range interval, and S_{ri} is the average stress range for stress range interval i.

The corresponding number of equivalent stress cycles N_e was calculated from expression:

$$N_e = \Sigma_i N_i \quad (2)$$

where the summation is over all stress range intervals in the histogram, and N_i is the number of cycles counted for stress range interval i.

In both of the above summations, data for the lowest stress range interval (0 - 500 psi) and data above 10,000 psi were excluded. Stress ranges below 500 psi contribute very little to the effective stress range. Stress ranges above 10,000 psi were infrequent and did not have a significant effect on the effective stress range. Many appeared to be due to noise in the data from spurious signals.

The resulting equivalent stress ranges and numbers of cycles from these calculations are shown in Table 3 for each of the 16 strain gages for which data were processed.

Interpretation of Results

Several observations were made by studying the stress range histograms, the effective stress ranges, and the numbers of equivalent stress cycles for the different strain gage locations. First, both the effective stress range and the number of equivalent stress cycles vary over the length of the chord members. The variation in stress range is similar to that observed for the stress ranges under the permit vehicle loading. Second, both the effective stress range and the number of equivalent stress cycles vary appropriately with respect to location. This indicates that the data are reliable and relatively free of noise contamination. Third, both the effective stress range and the number of equivalent stress cycles are lower at the locations in the top (compression) chord members than they are in the bottom (tension) chord members. This probably is due to the larger cross sectional area and possibly some composite action of the top chord members with the deck. It should be recognized that fatigue crack growth is not critical when a member is in compression, because the growth will stop outside of any region of residual tension.

The variation in the effective stress ranges over the length of the chord members is consistent with the data recorded under the permit vehicle loading: the lowest stress ranges are at the five-member joints (Channels 1, 2, 13, and 14) and the highest stress ranges are next to the T-joint (Channels 5, 6, 17, and 18). Also, stress ranges from the gages at the mid-lengths of the chords (Channels 3, 4, 15 and 16) fall between those at the ends.

The number of equivalent stress cycles over the lengths of the members varies similarly. The relatively higher stress ranges from Channels 5, 6, 17, and 18 result in fewer cycles falling into the 0 to 500 psi stress range interval, which was neglected in the summations, resulting in a larger number of equivalent stress cycles for these channels. Just the opposite is true for Channels 1, 2, 13 and 14, resulting in a smaller number of equivalent stress cycles for these channels. For Channels 3, 4, 15 and 16, at the mid-length of a chord, the equivalent stress cycles fall between those for the two ends.

The variation in stress ranges and number of equivalent stress cycles over the lengths of the compression members follows the same trends discussed above for the tension members.

The procedure used for estimating the fatigue life of the welded connections is based on the nominal stress range, including axial force and moment components, but neglecting effects of strain concentration caused by the weld. None of the gage locations precisely meet these requirements. The gages near the mid-length of the chords are not influenced by bending, while the gages near the ends of the chords are influenced by strain concentration caused by the welds. Gages 5, 6, 17 and 18 best approximate the critical conditions. The strain concentration caused by the weld may slightly increase the effective stress range at these locations. On this basis, nominal values of S_{re} = 2.0 ksi and N_e = 71,000 were judged to best represent

TABLE 2 DATA FOR SELECTED STRESS RANGE HISTOGRAMS

Strain Gage No.			3	4	5	6	15	16	17	18
Bin Number	Stress Levels From: (ksi)	To: (ksi)								
0	0.00	0.50	4E+07	3E+07	4E+07	3E+07	4E+07	3E+07	4E+07	3E+07
1	0.50	1.00	20952	20284	41536	38001	21608	18830	42784	37396
2	1.00	1.50	7984	7828	10205	10218	7875	7561	9348	9126
3	1.50	2.00	5460	5491	5931	5822	5405	5234	5748	5595
4	2.00	2.50	4180	4034	4200	4274	3807	3597	4159	3961
5	2.50	3.00	1961	1768	3299	3414	1461	1140	2948	3034
6	3.00	3.50	534	494	2643	2638	424	357	2343	2511
7	3.50	4.00	238	227	2136	1435	171	138	2001	1329
8	4.00	4.50	82	77	1016	500	60	47	913	469
9	4.50	5.00	32	24	412	256	28	16	379	229
10	5.00	5.50	18	17	217	131	19	12	183	97
11	5.50	6.00	11	6	104	65	4	9	97	49
12	6.00	6.50	6	5	52	36	3	4	53	32
13	6.50	7.00	4	9	26	15	5	4	27	16
14	7.00	7.50	4	7	18	12	4	2	14	7
15	7.50	8.00	5	5	8	6	3	4	14	12
16	8.00	8.50	2	2	6	5	2	1	15	6
17	8.50	9.00	3	4	3	6	6	3	1	2
18	9.00	9.50	5	4	4	4	3	3	9	3
19	9.50	10.00	2	1	7	3	3	1	5	1
20	10.00	and over	30	13	44	74	13	10	62	39

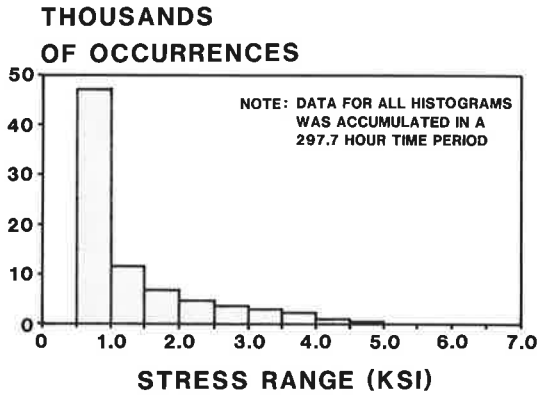

FIGURE 6 Stress range histograms for channel 5.

TABLE 3 EFFECTIVE STRESS RANGES AND NUMBERS OF CYCLES

Gage No.	Effective Stress Range, Ksi	No. of Cycles	Location
West Truss			
1	1.66	24909	behind gusset
2	1.35	23969	behind gusset
3	1.70	41483	mid-length
4	1.69	40287	mid-length
5	2.04	71823	at T-joint
6	1.93	66841	at T-joint
7	Not determined		
8	Not determined		
9	Not determined		
10	1.36	18291	mid-length of top chord
11	Not determined		
12	Not determined		
East Truss			
13	1.21	24945	behind gusset
14	1.25	23475	behind gusset
15	1.63	40891	mid-length
16	1.61	36963	mid-length
17	2.00	71041	at T-joint
18	1.90	63875	at T-joint
19	1.34	31910	top chord T-joint
20	Not determined		
21	Not determined		
22	1.56	27138	top chord mid-length
23	1.22	13770	top chord behind gusset
24	Not determined		

the critical stress range and corresponding number of cycles for the bridge. As discussed earlier, CalTrans' analysis indicates that live load stress ranges will increase by about 5 percent after the bridge is widened. Therefore, S_{re} = 2.1 ksi was used for the critical stress range in the widened condition.

ESTIMATION OF PAST AND FUTURE LIVE LOAD EFFECTS

In order to estimate past and future live load effects, it is assumed that the histogram and associated effective stress range represents a stationary process that does not vary over time, and that the cumulative number of equivalent fatigue cycles at any given gage location increases over time in linear proportion to the cumulative number of trucks estimated to have crossed the bridge since its opening in 1963.

Two measures of truck traffic were considered in the analysis. The first measure was the number of trucks with 5 or more axles, denoted as heavy trucks. The second measure was the total number of trucks, regardless of size, number of axles, or weight. This alternative measure could be more directly related than the first to the more frequent but lower amplitude stress ranges experienced by the bridge components.

The correlation between fatigue cycles and truck traffic volume was assessed by plotting the number of trucks that crossed the bridge during the time encompassed by each data tape against the number of equivalent fatigue cycles computed for the data tape. Although the number of fatigue cycles increased with increasing truck traffic, the data were widely scattered.

Based on these assumptions, past and future live load effects were incorporated into the fatigue life estimate using the following procedure:

1. An estimate was made of the total number of trucks that crossed the bridge while the strain data was collected. This number of trucks, denoted as T_{meas} was 51,860 for total truck traffic and 28,650 total heavy truck traffic.
2. Two-way average annual daily traffic (AADT) data for different vehicle classes was available for the years 1971 through 1985. An average of 6.2 percent of total vehicle traffic was trucks, and an average of 3.4 percent of total vehicle traffic was heavy trucks. These percentages were used to estimate total truck traffic and total heavy truck traffic from 1963 through 2010. This cumulative number of trucks was denoted as T_{TOT}.
3. For each strain gage, the cumulative number of fatigue cycles N_{TOT} experienced in each year was estimated from $N_{TOT} = N_e \times S.F.$ where N_e is the number of equivalent uniform amplitude fatigue cycles computed for the strain gage location (shown in Table 3) and S.F. is a scale factor relating the cumulative number of trucks having crossed the bridge by a given time to the number of trucks which crossed the bridge during the strain recording, expressed as $S.F. = T_{TOT}/T_{meas}$.
4. For each gage, two curves of the cumulative number of fatigue cycles N_{TOT} as a function of time were plotted, one in which only heavy truck traffic volumes are used for computation of T_{meas} and T_{TOT}, and the other in which all truck traffic volumes are used. The difference between the cumulative cycle curves provides an indication of the uncertainty in this aspect of the fatigue life estimate.

Using the procedure outlined above, the cumulative number of cycles vs time were tabulated. Plots of these results are shown in (Figure 7) for selected gage locations. It may be seen that the cycle curves developed from the total truck traffic are slightly higher than those based on heavy truck traffic. Therefore, cumulative cycles based on all-truck traffic were used to estimate fatigue life.

INSPECTION AND TESTING

The inspection was limited to Span 5 (east and west trusses) and Spans 9 through 12 (east truss) and, within these spans, primarily to horizontal chord members that are in tension. Attention was directed mainly to the fillet weld terminations at the ends of the stay plates, and to indications of discontinuities in the fillet welds along their length. The procedure generally included the following steps:

1. A visual examination was made for indications of cracking or discontinuities.
2. Where the examination revealed potential discontinuities, light grinding was performed to remove paint and clean up the weld toe.
3. After grinding, the surface was cleaned with a solvent.
4. Magnetic dry-particle testing was performed using an articulated-leg magnetic yoke and 110 volt, 60 Hz alternating current, in general accordance with ASTM E-709.
5. Where crack-like indications were found, light grinding was continued to verify that they extended into the base metal (i.e., the flange tip of the chord member). Some indications were removed in the grinding process.

A total of 242 stay plate welds at 35 connections were inspected. Ground areas were repainted. Cracks that extended into the base metal were found at four locations. The cracks occurred at either weld terminations or at a transverse discontinuity that was observed in the weld along the length of a stay plate.

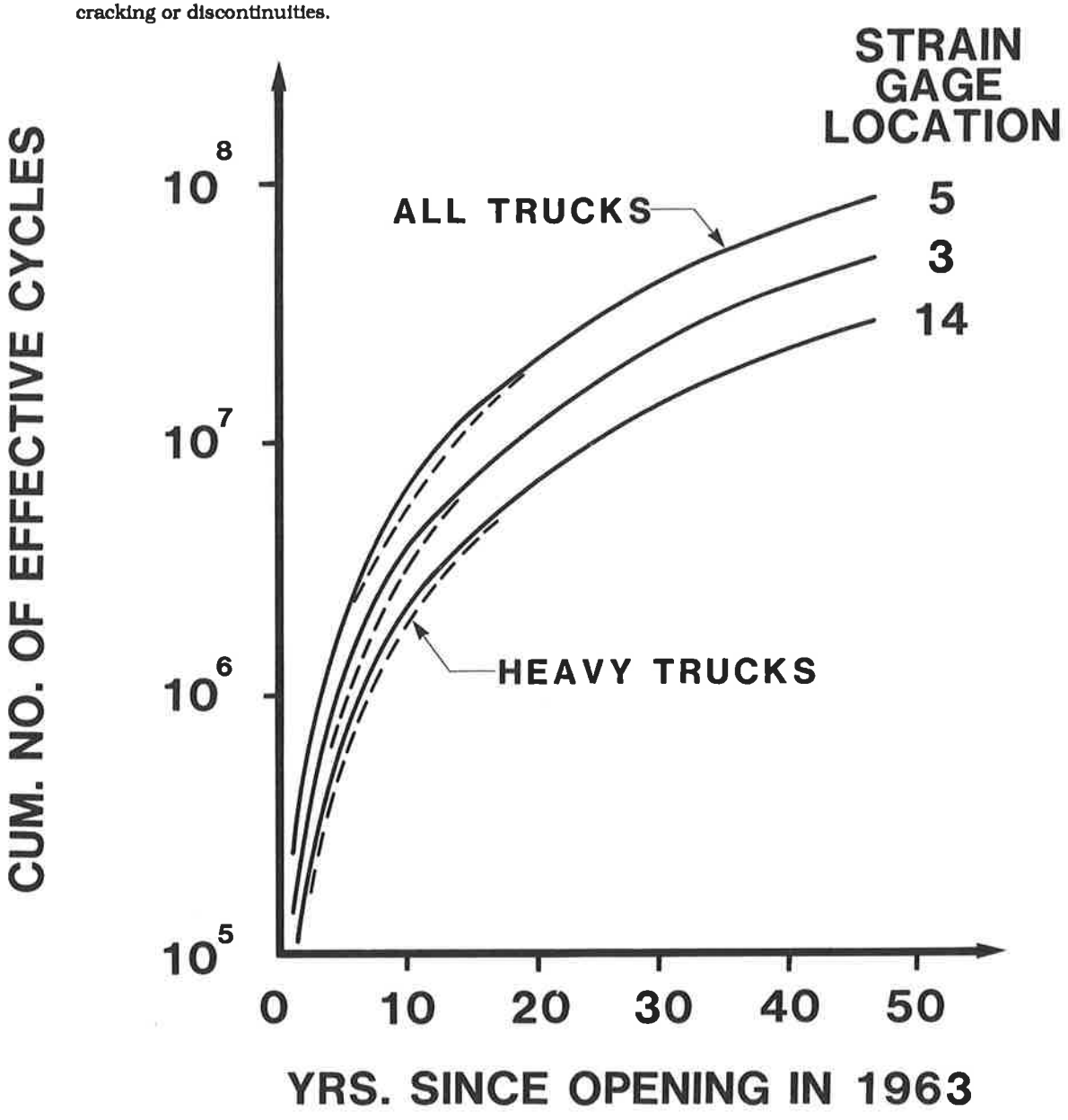

FIGURE 7 Cumulative cycle estimates.

Fractographic Examination of Cracks

All four indications of cracks or discontinuities were removed by coring. Metallographic and fractographic examinations indicated that fatigue crack growth had occurred at all four locations. Cracks at weld terminations had a length of about 3/8 inch. The examinations indicated that the crack growth rate was near the threshold level. The transverse crack through the fillet weld is believed to have started during fabrication as a hydrogen-related crack.

Additional cracks were also found emanating from the roots of the fillet welds, which appeared to have occurred during fabrication due to hydrogen. These cracks also appeared to have extended due to fatigue.

Tests on Cores Extracted from Bridge

A total of 20 cores were extracted by CalTrans. The core locations were selected to range over the entire length of the bridge, since steel heats would have varied within different regions of the bridge. They were also selected to be taken from flanges of compression members whose thicknesses best represented the range of flange thicknesses for the tension chord members. The cores had a diameter of 4 in.

All of the Charpy V-notch (CVN) tests were performed by CalTrans. The average of the three test results at each temperature level for each core are plotted in (Figure 8). It is apparent that the material from Core No. 8, which was from the east truss of Span 11, had a lower fracture toughness than material at the other locations. This is the only result that did not meet the minimum AASHTO requirement (1) of 35 ft-lbs at 0 deg F for A514 steel in a Zone 1 or Zone 2 service application.

The compact tension tests were made by Materials Research Laboratory, Inc. of Glenwood, Illinois. They were performed at 0 deg F in accordance with ASTM E399-83, except that the loading rate was approximately one second to failure. This loading rate is more representative of the conditions associated with bridge loadings than the dynamic rate given in E399. The cores were machined to obtain a test specimen with W equal to 3 in. The thickness of specimens from Core Nos. 7B and 8A was 1.5 in. The thickness of the other cores was reduced by machining only enough to clean the surface.

Results of the tests are given in Table 4. All test results were invalid according to ASTM E399 criteria, as anticipated, because the thickness of the flanges from which the cores were extracted was less than required by the test method, and also because the toughness of the material was higher than for brittle materials for which the test method was intended. However, the values of K_Q are considered to be a conservative estimate of K_{Ic}. The average of the four test values is 103 ksi sq root in.

An estimate of K_{Ic} was also made from the result of of the CVN tests, using the following upper-shelf correlation equation from Barsom and Rolf (5):

$$(K_{Ic}/\sigma_{ys})^2 = 5\,[(CVN/\sigma_{ys}) - 0.05] \quad (5)$$

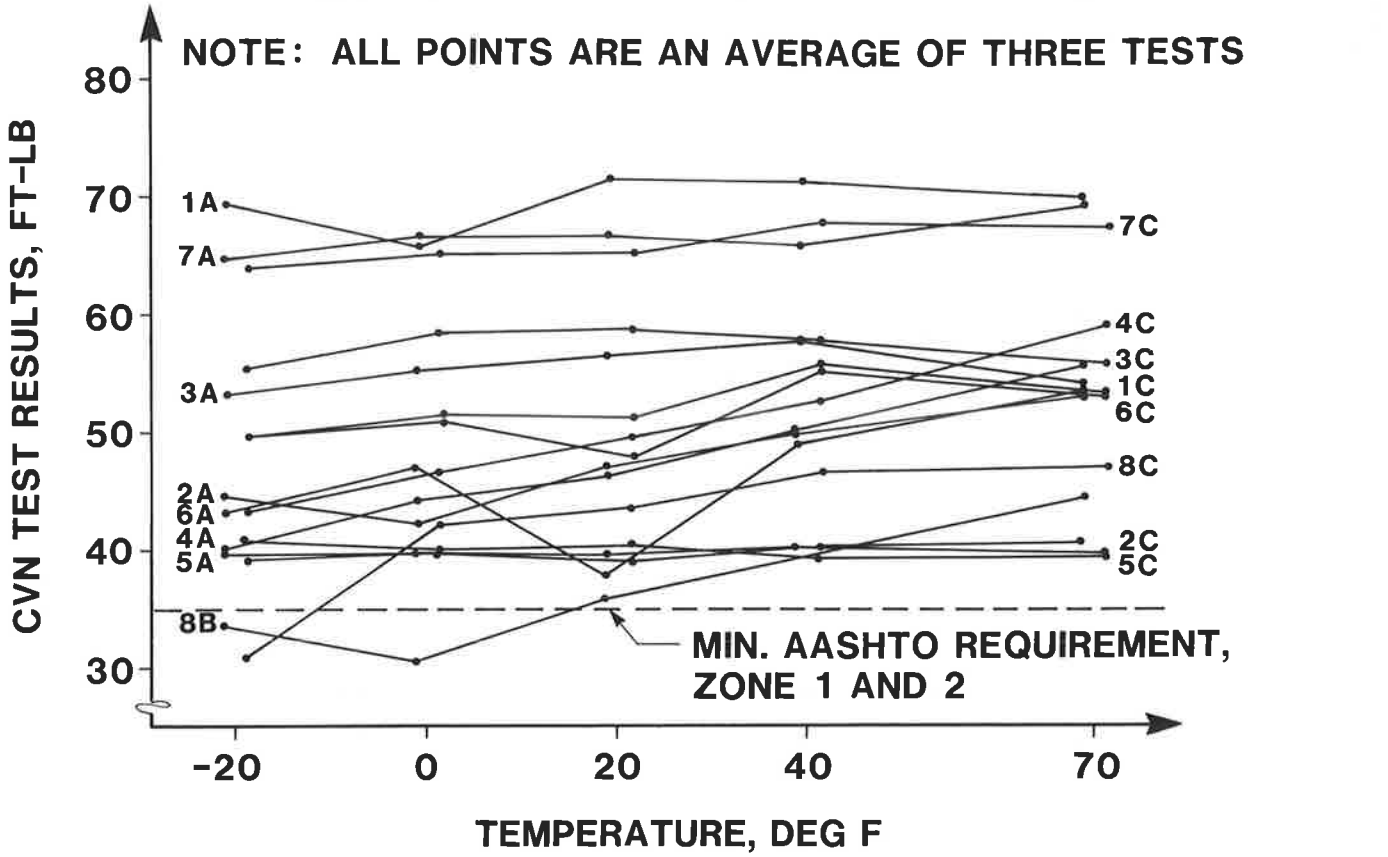

FIGURE 8 Charpy V-notch test results on cores of A514 steel.

TABLE 4 COMPACT TENSION TEST RESULTS

Core No.	By MRL K_Q (a) ksi$\sqrt{in.}$	By MRL R_{sd}	By Fisher J Integral in. kip/in.^{2}	By Fisher K_J (b) ksi$\sqrt{in.}$
1B	99.1	1.87	3.393	319
3B	102.2	1.85	2.290	262
7B	111.6	2.02	2.483	273
8A	100.8	1.72	2.020	246
Average	103.4	1.87	2.546	275

NOTES: (a) K_Q was computed as if there was no plastic yielding.
(b) $K_J = (EJ)^{1/2}$

Assuming that the yield strength, σ_{ys}, is equal to 100 ksi and the CVN is equal to 30 ft-lbs, the minimum value obtained in the test program at 0 deg F, K_{Ic} is equal to 112 ksi sq root in. Taking σ_{ys} equal to 125 ksi, the highest value from the mill test reports, K_{Ic} is equal to 122 ksi sq root in. These values are comparable with the value of K_Q equal to 103 ksi sq root in. obtained from the test program.

It was concluded that K_{Ic} equal to 150 ksi sq root in. was reasonable for an evaluation of the fracture resistance of the bridge. However, in view of the uncertainties with respect to the steel properties, the possibility for K_{Ic} as low as 100 ksi sq root in. was considered.

EVALUATION OF REMAINING FATIGUE LIFE

The estimate of the remaining fatigue life of the bridge was based on the following assumptions:

1. Through 1988, the time of this evaluation, the critical condition has been a Category E' detail at the termination of the fillet welds connecting the stay plates to the flange tips. This condition has been subject to an effective stress range of 2.0 ksi.
2. From 1989 on, the effective stress range should be increased to 2.1 ksi, to reflect the as-widened condition.
3. The cumulative number of effective cycles at any time under recorded and projected traffic is proportional to the total number of trucks crossing the bridge. The critical Category E' detail had accumulated 29,386,500 cycles through 1988, corresponding to 21,450,000 trucks crossing the bridge.

S-N curves, which relate the stress range S to the number of cycles N which can be resisted, have been established by AASHTO (1). However, recent tests and a review of all available data have led to new S-N curves published in NCHRP Report 286 (6). These curves were used for this evaluation. They are nearly the same as the AASHTO curves, and they were derived to expect with 95 percent confidence that 95 percent of the data would survive.

In NCHRP 286, S-N curves are given for both redundant and nonredundant load path structures. The curves for redundant structures are based on test data, while the ordinates of the curves for nonredundant structures are reduced by approximately 20 percent for additional conservativeness. The trusses in the Benicia-Martinez bridge are nonredundant. However, since an evaluation of the fatigue life is desired, the S-N curves derived directly from the test data were used. These curves are shown in (Figure 9).

In evaluating the fatigue life of the weld termination at the ends of the stay plates, the fatigue life cutoff given in NCHRP 286 was not used, because the existence of a fatigue limit below which no fatigue crack propagation occurs is considered to be assured only if all of the stress range cycles do not exceed the constant amplitude fatigue limit. This is not the case for the histograms developed in this analysis. The fractographic examination also showed that crack growth was occurring because some stress ranges were exceeding the crack growth threshold.

The NCHRP 286 S-N curves are compared directly in (Figure 9) to the assumed effective strength of 2.0 ksi and the accumulated number of equivalent stress cycles of 29,386,500 for the critical Category E' detail. It is apparent that the intersection of the two lines representing these conditions is close to the curve for the Category E' condition.

Two sources of uncertainty were recognized. The first is the uncertainty in the cumulative cycles, which is due mainly to the extrapolation of the data collected over a limited time interval to incorporate past and future life load effects over several decades. This uncertainty was accounted for by arbitrarily providing a $\pm$25 percent band around the cumulative truck traffic curve which was used for the evaluation. The second source of uncertainty is in the assignment of a fatigue category to the stay plate weld terminations. As pointed out earlier, the condition is believed to be between Category E and E', but was taken as Category E' to be conservative.

It may be seen from (Figure 9) that there is very little uncertainty associated with the predicted higher stress range of 2.1 ksi in the widened bridge. The narrow cross-hatched region represents the effective stress range before and after widening. The effect of the widening should be within the band, provided that the widening does not change the dynamic response of the bridge in a manner that would cause an amplification in the predicted stress range.

An iterative procedure was used to estimate the year in which the number of cycles and the combined stress ranges reaches the fatigue life corresponding to a Category E or E' condition. On this basis, the fatigue life is reached in 1995 for the Category E' condition, as illustrated in (Figure 10). Similarly for the Category E condition, the fatigue life is reached in 2018. Taking into account the

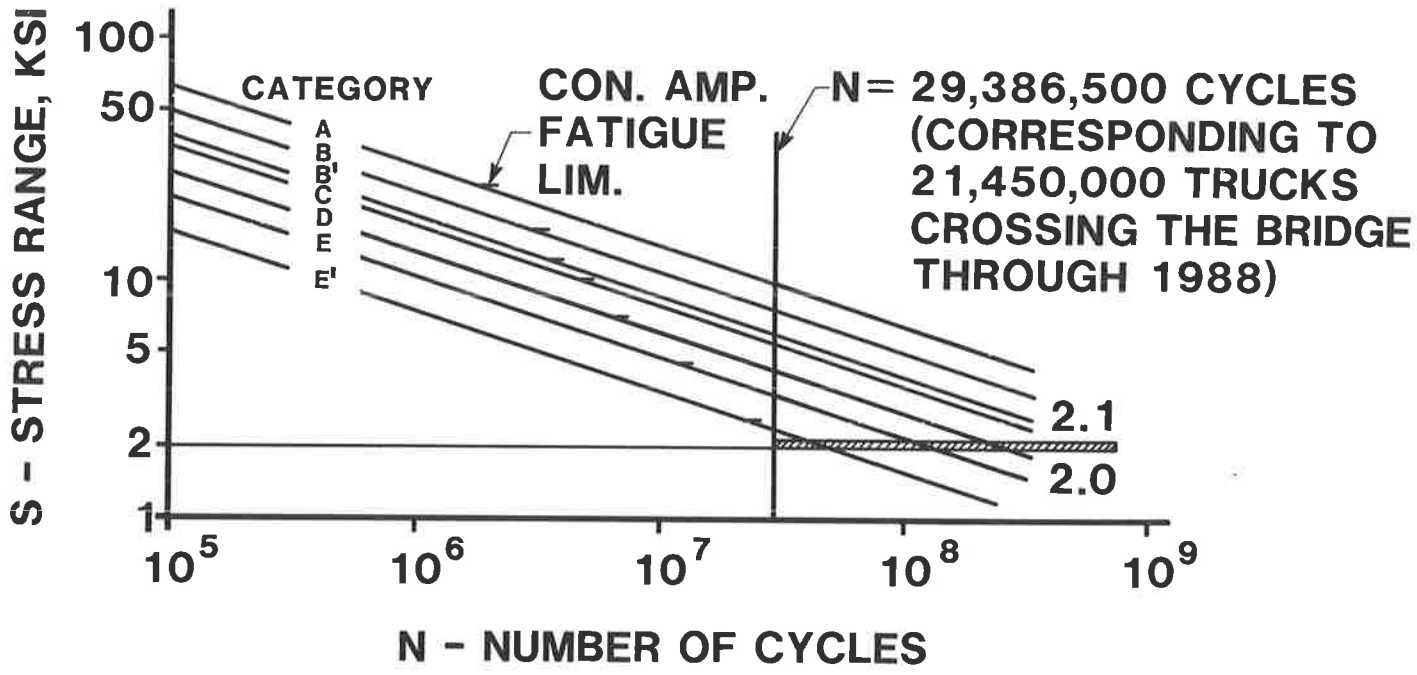

FIGURE 9 Estimated cycles compared to NCHRP 286 S-N curves.

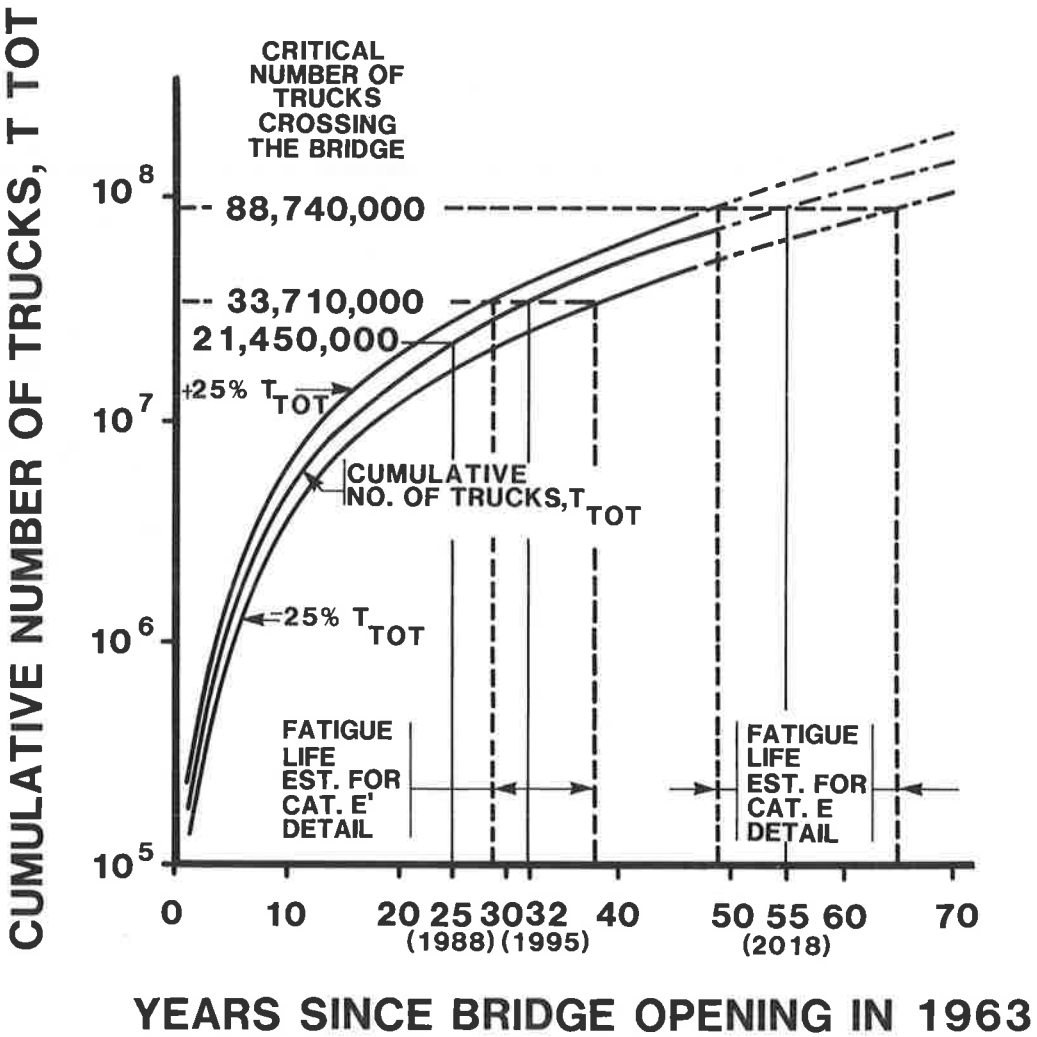

FIGURE 10 Fatigue life estimates.

uncertainty in the cumulative cycles, the estimated fatigue life for a Category E' condition is approximately 28 to 37 years, which corresponds to calendar years 1991 to 2000. In other words, taking a conservative position, the fatigue life of the bridge condition could be regarded as nearly exhausted. For a Category E instead of E' detail, the estimated fatigue life is much longer. The fatigue life for this case falls past the end of the traffic projections in 2010, but the fatigue life range could be extrapolated as 49 to 65 years, corresponding to calendar years 2012 to 2028.

Discussion

It is important to recognize that the state-of-the-art does not lead to a precise evaluation of fatigue life. There is uncertainty in the selection of the category for the wrap-around, fillet weld terminations on the stay plates. There is also uncertainty in the traffic estimates, in the correlation of the number of cycles associated with the effective stress range with the traffic estimate, and in the determination of the effective stress range.

It should also be recognized that the S-N curves on which the evaluation is based are lower bound estimates and represent a 95 percent level of probability that 95 percent of the conditions would achieve longer fatigue lives. Failure in a fatigue test is loss of load carrying capacity. Failure in a bridge may be fracture. Therefore consideration must also be given to the critical crack sizes that may cause a fracture.

For the Category E' condition at the termination of the fillet welds on the stay plates, it will be assumed that a fatigue crack will grow as a shallow semi-elliptical crack across the flange tip, becoming an edge crack condition as the crack advances. The stress intensity factor for a semi-elliptical surface crack is given by (5):

$$K_I = 1.12\,\sigma\,\sqrt{\pi a/Q}\,M_K \qquad (3)$$

where

K_I = stress intensity at the crack tip, ksi sq root in.
σ = in situ stress close to the crack tip, ksi
α = crack depth, in.
Q = flaw-shape parameter
M_K = correction factor, say 1.0

From (Figure 2.13) of Ref. 5, Q will be about 1.0 for the condition being considered. Then

$$K_I = 1.12\,\sigma\,\sqrt{\pi a} \qquad (4)$$

which is the equation for an edge crack condition.

The relationship between a and σ as expressed by Eq. (4) is plotted in (Figure 11) for K_I equal to 100 ksi sq root in. and 150 ksi sq root in. As discussed earlier, K_I equal to K_{Ic} of 100 ksi sq root in. is considered to be the worst possible condition. K_I equal to K_{Ic} of 150 ksi sq root in. is considered to be a more probable representation of the toughness of the steel.

Crack tips are often located in regions of high residual stress, in which case σ may be equal to the yield stress of the steel. The only information on yield strength came from the mill reports for 1-in.-thick steel plate. These yield strengths ranged from 108 to 125 ksi. As indicated in (Figure 11), a crack that is approximately 0.15 in. deep could induce a fracture (under a dynamic vehicular loading) if σ was 125 ksi and K_{Ic} was 100 ksi sq root in. However, it is more likely that the critical crack size will be of the order of 0.35 to 0.5 in. deep, corresponding to K_{Ic} equal to 150 ksi sq root in. Considering the small size of the fillet welds, even a 0.15-in.-deep crack is probably outside of the region of high residual stress. Taking σ equal to an assumed maximum in situ stress of say 40 ksi, it may be seen from (Figure 11) that the critical depth of crack should be at least approximately 1.5 in., and more likely about 3.5 in.

In view of the limited extent of the inspection of the fillet weld terminations, it would not be surprising if cracks that are 0.15 in. deep exist at some locations in the bridge. The crack growth threshold for the fillet weld terminations on the stay plate is about 2 ksi, and hence growth should be expected. While it is probable that a crack at these locations would need to grow to a depth of at least 1.5 in. to be critical, as noted in the previous paragraph, the view that the fatigue life could be close to exhausted is reasonable with respect to the observed conditions. Consequently, it is believed to be highly advisable to remove these potentially critical Category E' conditions from all of the fracture-critical members in the bridge, or to provide reinforcement across a potential crack location.

For the Category E condition corresponding to a transverse crack through a fillet weld along the edge of the stay plate, the fatigue crack will also grow as a semi-elliptical crack from the junction of the weld and the flange tip. Thus Eq. 3 should approximately represent the condition. However, at shallow depths, Q should be greater than one, because crack growth into the flange tip will initiate from the region of the weld. Hence K_I is reduced, and it seems likely that the crack would have to grow out of the region of high residual stress before becoming critical. At greater depths, the condition will be the same as that at the termination of the weld at the end of the stay plate.

Although crack growth from a transverse crack through a fillet weld along a stay plate should be less critical than for the weld terminations, the potential for a critical condition developing should be recognized. Therefore it was deemed advisable to provide reinforcement through the T-joints in order to provide an alternate load path in the event of a fracture. The gusset plates at the five member joints may provide an acceptable alternate load path, without through joint reinforcement. It was recommended that these welds should be ground and inspected in an effort to locate and remove the discontinuities, irrespective of whether the joints are reinforced.

For the fillet welds connecting the web plate to the flanges of the chord members, and for the groove welds in the flanges, the condition is more complex. Because of the larger size of these welds, any defect or crack must be regarded as being in a zone of high residual stress equal to the yield strength. Experience indicates that K_I for any internal crack growing from an embedded flaw should be penny-shaped, and therefore K_I can be approximated from (5):

$$K_I = 2\alpha\,\sqrt{a}\,/\,\sqrt{\pi} \qquad (5)$$

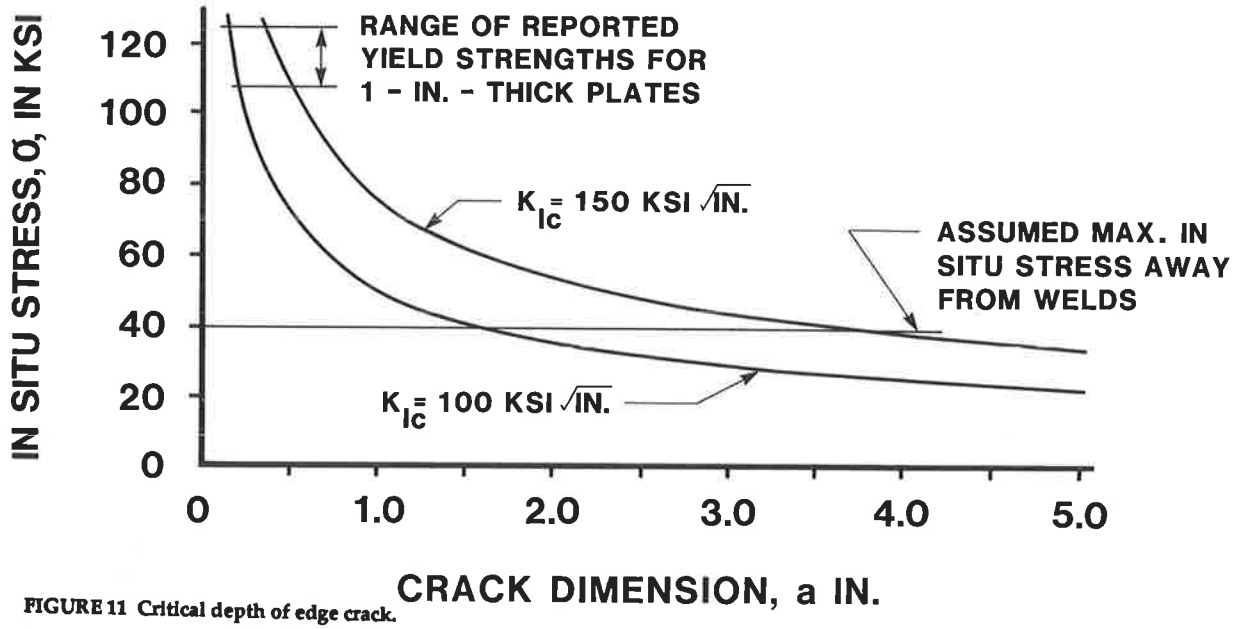

FIGURE 11 Critical depth of edge crack.

where a = the radius of a circular approximation of the internal crack.

Taking K_I equal 100 ksi sq root in. and σ equal to 125 ksi, a is equal to 0.5 in. Thus such an internal crack should have an overall size of about 1 in. and should also extend into base metal in order to have the potential for causing a brittle fracture. A crack growing from a surface defect should also reach the same overall size before becoming critical, because it will grow radially from the initiating defect.

In view of the lack of information about the fillet welds connecting the web plate to the flanges of the truss members and to the groove welds in the flanges, further examinations were deemed to be advisable. In particular, locations where there are irregularities in the fillet weld profiles or where repairs may have been made should receive close scrutiny by means of magnetic particle or dye penetrant inspection. Some percentage of the groove welds should be examined ultrasonically, and the results of this testing should be used to decide whether further examinations are needed. If an indication of crack growth is found, the region should be removed by coring and the indication should be exposed for fractographic examination.

CONCLUSIONS AND RECOMMENDATIONS

An evaluation of the remaining fatigue life of the Benicia-Martinez Bridge was made that indicates that the fatigue life should be regarded as close to being exhausted for the fillet weld terminations at the ends of the stay plates. In view of this finding, it was recommended that the fatigue-sensitive conditions associated with the stay plates located on the tension chord members be retrofitted, as subsequently discussed in this chapter.

It was also recommended that further examinations and testing be conducted on the groove welds in the flanges and on the fillet welds connecting the web plate with the flanges in the tension chord members. If indications of defects are found, samples of the defects should be extracted by coring for fractographic examination of the defects.

It was also recommended that a three-dimensional nonlinear analyses of the bridge be made in an effort to predict whether the loss of a tension member in a truss would lead to a collapse, or whether there are alternative load paths in the deck and bracing that could sustain the bridge.

Proposed Retrofitting

It is believed that the fatigue life of the bridge can be extended considerably by retrofitting the fatigue-critical conditions at the stay plates in fracture-critical tension chord members. Several retrofit measures are recommended, both to remove the critical Category E' conditions at the terminations of the fillet welds and to also add reinforcement that provides an alternate force path at all tension chord member T-joints. While the addition of reinforcement will reduce the stress range, the capability of that reinforcement to prevent a fracture will depend on the size of the initial defect and the accumulated fatigue damage. Thus the extension of fatigue life is uncertain, particularly for the defects along the fillet welds.

Core holes at stay plate weld terminations

The Category E' condition at the terminations of the fillet welds connecting the stay plates to the tension chord flanges are probably the most fatigue-critical details in the trusses. These details can be largely shielded from any stress range by drilling a partial core hole at these locations and then finishing the surface by grinding. The core holes should remove any existing cracks which may be subject to fatigue crack growth, but this should be verified by nondestructive examination. A detail of the recommended procedure is shown in (Figure 12).

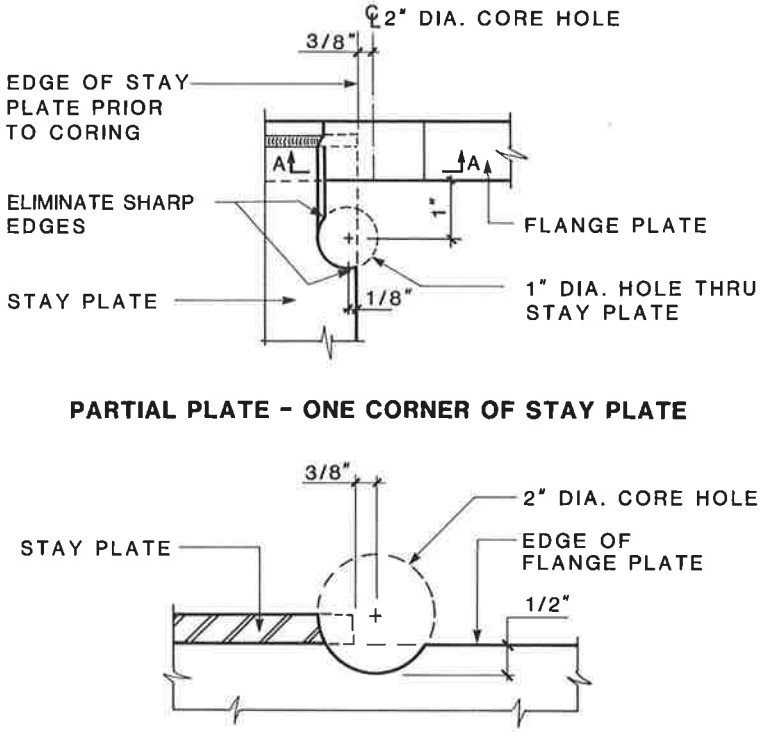

NOTES:

1. At locations of lateral gusset plate connections, a small portion of the lateral connection plate and some bolts from the vertical gussets will have to be removed in order to core through end of stay plate.
2. Grind cut surface of stay plate to remove any irregularities. Finish all ground surfaces to a surface roughness (R_A) of 500.
3. Clean exposed steel surface to remove any contaminants and paint.

FIGURE 12 Retrofitting detail for T-joints.

Strap plates at joints in tension

A discontinuity along the length of the stay plate fillet welds is a Category E condition, and is thus subject to fatigue crack extension. This condition cannot be shielded by coring. Therefore, an alternative redundant load path should be available in case of a fatigue failure initiated by such a discontinuity. Steel strap plates across the joints would provide an alternate load path. They would also reduce the subsequent stress range, reducing the likelihood of a fatigue failure. Strap plates should prevent a failure if a fracture occurs in the chord, but it still may be necessary to repair damage associated with the fracture. The accessible fillet welds should be ground in an effort to locate and remove the discontinuities, even though strap plates are installed.

At the five-member joints, the large gusset plates may possibly provide an acceptable alternate load path. It is recommended that a special analytical investigation of these joints be made in order to confirm that the load path provided by the gussets is acceptable. Otherwise these joints should also be reinforced.

At the T-joints, which have much smaller gusset plates, an alternate load path does not exist. At these locations, strap plates can be bolted to either the webs of the members or to the flanges. The strap plates must be effective beyond the ends of the stay plate welds in order to function as required.

Fatigue Life After Proposed Retrofitting

The fatigue life of the Benicia-Martinez Bridge will be extended substantially by the proposed retrofitting procedures. All of the Category E' details at the weld terminations at the ends of the stay plates on the tension chord members of the trusses should be eliminated.

The next most severe condition is the potential discontinuities in the fillet welds along the stay plates. These could be Category E conditions. Where they can be inspected, the discontinuities can be eliminated by grinding. Further, the fatigue life at the location of a discontinuity that cannot be eliminated may be increased because the stress range will be reduced by the strap plates or the gusset plates. While it appears that the increase should be substantial, the magnitude is difficult to assess.

The fatigue life of the fillet welds connecting the web to the flanges of the chord members and of the groove welds in the chords should be very high, and possibly without limit if the stress ranges are below the crack growth threshold. However, this expectation absolutely requires that there not be defects in these welds which will cause crack growth under cyclic loads.

Finally, it is important to keep in mind that the Benicia-Martinez Bridge is a very large structure. Unless the bridge can sustain without collapse the loss of a main load-carrying member in tension, even one undiscovered defect of critical size has the potential to cause a collapse. As previously discussed, further evaluation of this bridge is recommended, including additional material testing, inspection and nondestructive testing of the Category B conditions, and analysis of alternate load paths. Such evaluation will give greater assurance for the long range, safe use of the bridge.

IMPLEMENTATION OF THE RETROFITTING

The recommended retrofitting was subsequently included in the construction work for widening of the bridge. The prime contractor was Kiewit Pacific Company. With the approval of CalTrans, WJE undertook the coring work at the stay plate weld terminations as a subcontractor to Kiewit Pacific. This work was accomplished in the first half of 1989.

In total, about 1800 weld terminations were retrofitted. No effort was expended to examine the coring remnants for fatigue cracks, as this would have required further sectioning and testing. However, cracks extending from the root of the fillet welds were observed frequently.

Retrofitting of the stay plates was accomplished by coring a partial depth hole using a drilling template. This template was clamped to the flange. Magnetic base drill presses were used for the work.

The A514 material and weld metal used in the bridge was found to be very hard with poor machinability. Carbide tipped cutters were used. It was found that carbide tools cut approximately 10 times more holes than cutters made from high speed steel. Removing material by milling was also attempted on a trial basis. Again it was determined that high speed steel cutters did not perform in this material.

ACKNOWLEDGEMENTS

The authors wish to recognize and extend their appreciation to all of the people who assisted with and contributed to this evaluation. Personnel of CalTrans, including particularly Lee Everett, Bill Crozier, Richard White, Mark Seyed and Roger Caudle, were very helpful and supportive. Abolhassan Astaneh-Asl at the University of California at Berkeley and John O'Donnell at Materials Research Laboratory, Inc. provided valuable assistance. Other WJE staff that contributed substantially to the project included Stuart Werner, Dirk Heidbrink, Conrad Paulson, Roger Pelletier and Victor Monroy.

REFERENCES

1. American Association of State Highway and Transportation Officials (AASHTO). *Standard Specifications for Highway Bridges, Thirteenth Edition 1983 as Amendment by Interim Specifications - Bridges*, Washington, D.C., 1984, 1985 and 1986.
2. American Association of State Highway and Transportation Officials (AASHTO). *Guide Specifications for Fracture Control of Nonredundant Steel Bridge Members*, Washington, D.C., September 1978, updated 1986.
3. Downing, S. J. and Socie, D. F. Simple Rainflow Counting Algorithms. *Int. J. Fatigue*, January 1982.
4. Brockenbrough, R. L. and Johnston, B. G. *USS Steel Design Manual.* Pittsburgh: United States Steel Corporation, 1981.
5. Barsom, J. M. and Rolfe, S. T. *Fracture and Fatigue Control in Structures.* Second Edition, 1987.
6. Keating, P. B. and Fisher, J. W. Evaluation of Fatigue Tests and Design Criteria on Welded Details. *National Cooperative Highway Research Program (NCHRP) Report 286*, Washington, D. C. Transportation Research Board of National Research Council, September 1986.

Field Test of a Cable-Stayed Bridge

F. W. BARTON, T. T. BABER, P. S. DUEMMEL, AND W. T. MCKEEL, JR.

This paper describes the results of a field test on a cable stayed bridge subjected to vehicle loads. The test was conducted as part of an extensive research program concerned with the overall field response of a cable stayed bridge under a variety of loading conditions. The test structure is a concrete twin box-girder bridge with a 630-foot main span and two approach spans on either side supported by a single plane of stay cables. The vehicle loading was applied by placing a heavily loaded truck at specific locations in both the interior and exterior lanes of the main span and adjacent spans of the bridge. Response information was obtained from an extensive array of electrical resistance strain gages mounted on dummy reinforcing bars imbedded in the concrete and placed within selected deck segments. Data from the electrical resistance strain gages were automatically recorded using a data acquisition system. Results from these load tests are presented and discussed. The response information is also compared with that predicted from a detailed finite element model of the structure.

INTRODUCTION

Segmentally erected post-tensioned box girders and cable-stayed construction are two relatively recent developments in bridge technology which can lead to aesthetically pleasing and economical structures. In spite of their clean exterior lines and pleasing form, structures using these technologies are challenging to analyze and design. Much about the behavior of these complex structures in service environments is still unknown. Determining the response under load requires consideration of multi-point and multi-stage post-tensioning, cable stay connection and support, time-dependent creep and shrinkage deflections, cable stay nonlinearity, variation in residual stress and cable preload throughout the structure, and complex live and thermal loadings.

Considerable effort has been expended in developing suitable techniques for the analysis of segmentally prestressed and cable stayed bridges [1]. Present computational and modelling capabilities permit the development of sophisticated and detailed finite element models of complex bridge structures from which a wealth of behavioral information can be easily generated. However, the response information obtained from these computer models is only as good as the model representation of the actual bridge. In addition, response information of a local nature such as transverse shear lag in the deck elements, load transfer through cable connecting mechanisms, and local stress concentrations is generally unavailable from finite element analysis, even when large complex models are employed. To understand the actual behavior of cable stayed bridges under vehicle loadings and to provide response information to assist in the development of more reliable computer models, field testing of large complex bridge structures employing new and innovative design concepts is essential.

Beginning in the summer of 1986 and continuing until the present time, a research team from the University of Virginia and the Virginia Transportation Research Council has undertaken an ambitious and extensive

F. Barton, T. Baber and P. Duemmel, Department of Civil Engineering, University of Virginia, Charlottesville, Va. 22903.
W. McKeel, Jr., Virginia Transportation Research Council, Charlottesville, Va. 22903.

program involving the field testing of one segmental, cable-stayed, box girder bridge in Virginia in which construction was recently completed. These field studies have utilized an extensive array of strain gage instrumentation on a number of key elements in this bridge along with an automated data acquisition system for recording response information resulting from a variety of loadings. Previous studies reported elsewhere [2,3] have been concerned with bridge behavior during the construction phase and with the dynamic characteristics of the structure.

The objective of the study described in this paper was to measure and evaluate the response of this completed cable-stayed bridge when it was subjected to a known vehicle load placed at locations along the main and approach spans. The response data was obtained from a series of strain gages placed in several deck segments of the main span. In addition, analytical response data was also provided from a detailed finite element model of the bridge. Comparison of the measured and predicted response data facilitated evaluation of the measured response and also made it possible to better define the format of future field tests on this bridge.

The structure which was the subject of this investigation is a segmentally erected, precast, post-tensioned, cable-stayed box girder bridge which carries Interstate 295 over the James River near Richmond, Virginia. The bridge consists of 28 individual spans including the approach spans. That portion of the structure which is the focus of this particular phase of the overall investigation consists of the central seven-span continuous section of the bridge which includes the 630-ft. main span over the river and the three approach spans on either side. The approach span segments are 20 ft. long and weigh approximately 145 tons, while the main span segments are each 10 ft. in length and weigh approximately 70 tons. An elevation sketch of the bridge is shown in Fig. 1.

As indicated in the figure, the middle five spans of the bridge including the main span are supported by a total of 52 cable stays arranged in a single plane harp configuration and emanating from two pylons, one on either side of the river.The forces from the cable stays are transferred to the twin box girders through a series of precast delta-frame assemblies located between the girder segments at each stay location as shown in the cross-section sketch of Fig. 2. The main span over the river was constructed as two cantilevers extending from piers located adjacent to the pylons and made continuous by a midspan closure pour. Posttensioning consisted of two parts, temporary post-tensioning bars used during construction, and permanent strand post-tensioning located inside the box segments after the erection was completed. Construction of the bridge was completed in April 1990 and it was opened to traffic in July 1990.

EXPERIMENTAL PROGRAM

Instrumentation and Data Acquisition

Instrumentation utilized in this particular study consisted of an extensive array of electrical resistance strain gages installed in three deck segments of the main span. These

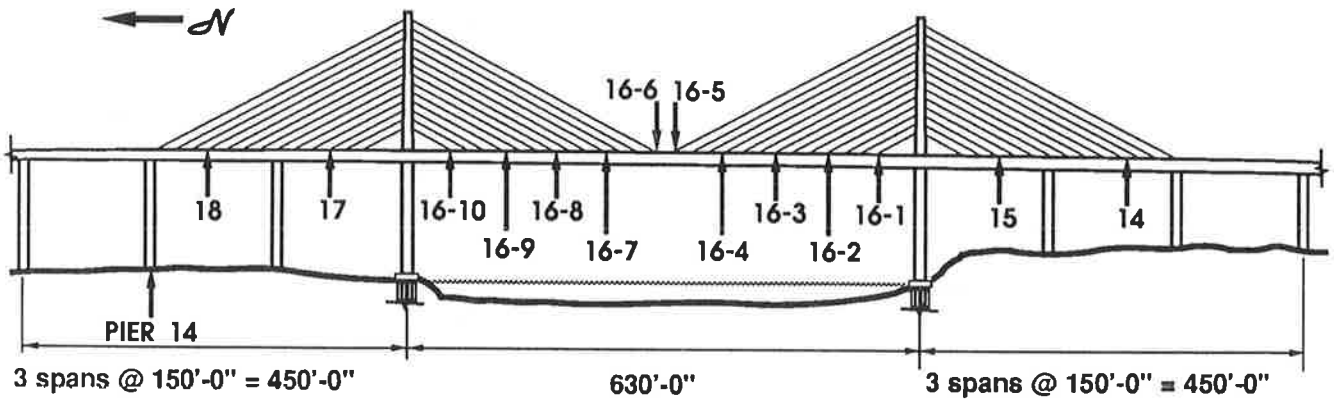

FIG. 1 ELEVATION VIEW OF THE I-295 BRIDGE SHOWING LONGITUDINAL LOCATIONS OF TEST VEHICLE

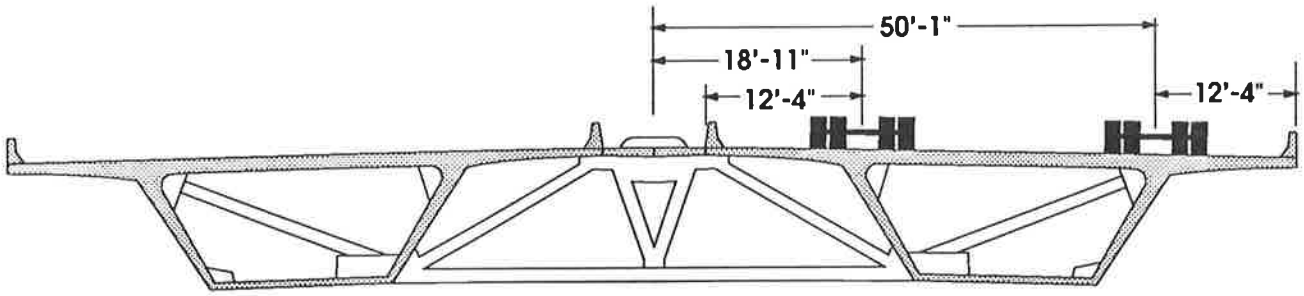

FIG. 2 CROSS SECTION OF TWIN BOX GIRDER SHOWING TRANSVERSE LOCATIONS OF TEST VEHICLE

strain gages were placed in six different deck segments on the south side of the main span corresponding to three different longitudinal locations along the roadway. Specifically, sections corresponding to the north and south bound lanes in segments 33, 48 and 62 in the main span, span 16, were instrumented with gages installed either as single gages or in a rosette configuration. Segment 33 is adjacent to the south pier, segment 48 is approximately at quarter-span and segment 62 is at midspan. The locations of the strain gages within each of the segments is shown in Fig. 3. Each of the gages and rosettes are identified with a number in the figure to facilitate discussion of the measured strains in a subsequent section of this paper.

During installation, each of the gages was mounted on four-foot lengths of reinforcing bar. The gaged reinforcing bars were then placed in the reinforcing cages of the deck segments during the period between cage construction and placement of the cage in the precasting forms. The gaged bars were tied to one of the reinforcing bars in the cage and the lead wires were run along the cage to a block-out in the wall of the box segment. After casting and placement of the segment, the lead wires were retrieved and run directly to a data acquisition system located in one of the box segments in the vicinity of the instrumentation.

The data acquisition system is a unit manufactured by the John Fluke Company. This system uses a Helios main controller to communicate with a number of individual remote scanning units each of which is located near an instrumented segment. The data is then transmitted from the scanning units to the main controller in digital form and from there to a personal computer where the data is recorded and stored on a hard disk. This data is periodically retrieved and transferred to a computer in the laboratory in spreadsheet format for subsequent analysis and manipulation. The personal computer in the field and the main controller unit are located in a specially designed and fabricated cabinet which is provided with complete environmental controls.

Loading

Loading was applied to the bridge during the field test by means of a heavily loaded dump truck which was loaded to the legal maximum. The total weight of the truck was determined to be approximately 49,720 pounds with 16,820 pounds on the front axle and 32,900 pounds on

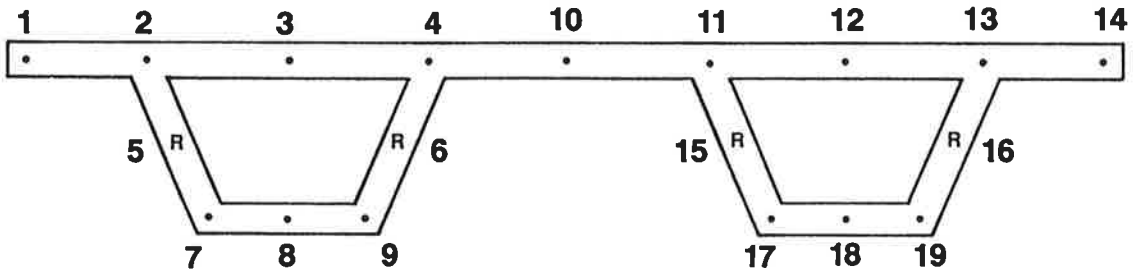

FIG. 3 LOCATION OF STRAIN GAGES IN INSTRUMENTED SEGMENTS

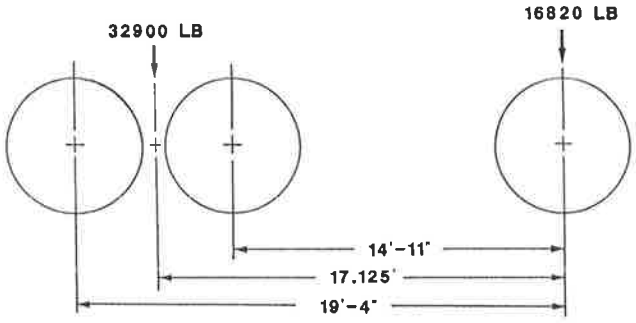

FIG. 4 TEST VEHICLE DIMENSIONS AND LOADS

the rear tandem axle. The axle loads and dimensions between front and rear wheels are shown in Fig. 4. The truck was placed at a variety of locations along the main span and the two adjacent approach spans on either side of the main span. A total of fourteen longitudinal locations were selected along the bridge, one in each of the approach spans and ten in the main span. These longitudinal load locations are identified in Fig. 1 where the number of each longitudinal load position corresponds to the span number and, within the main span, to a position along the span. As indicated in the figure, each load position along the deck also corresponded to the location of a cable stay connection to the deck segments through a delta frame assembly. For each load position, the truck was placed such that the centerline of the rear axles was at the load point with the truck always headed in the southerly direction.

As noted, there were fourteen different longitudinal load locations along the span. At each longitudinal position, there were also four different transverse load positions. These transverse positions, shown in the sketch in Fig. 2, correspond approximately to the two traffic lanes in each of the north and south bound lanes of the bridge. Also, as shown in the figure, these transverse positions place the test vehicle over the webs of the box sections. Thus, during this field test, the test vehicle was located at a total of 56 different positions on the bridge.

At each load position, at least two complete sets of strain data were recorded. Zero readings, with the test vehicle completely off the bridge, were also recorded before the beginning of the test, at the completion of the test, and at six approximately equal intervals during the test. This procedure was adopted to ensure a reliable zero reference for use in calculating strain increments due to the application of the load. Because of temperature variation during the test procedure, the zero readings did vary slightly and it was assumed that the small variation was linear between readings.

The strains produced by the load application were calculated as the difference between the recorded strain and the zero reading at the time of each test load. Since all strain readings were recorded in spreadsheet format, this calculation of strain due to load application was a straightforward procedure. Stresses corresponding to load application could then be calculated using a modulus of the concrete of approximately 4.5 million psi and also assuming the strains in the top and bottom flanges were predominantly uniaxial in nature.

Results

A careful evaluation and analysis of the recorded strain data indicated several data values that had to be discarded. For example, an apparently defective board in the data acquisition system controlled the majority of data input from segment 33. Consequently, only the strain gages in the bottom flanges of this segment were able to record reliable strain data. Also, analysis of the complete set of data recorded at the quarter-span of the bridge at segment 48 indicated an almost random oscillation of strains even though the data appeared to be consistent between gages. Thus, since reliable strain data was available from two segments, segment 33 and segment 62, the response information from segment 48 was not included in this discussion.

In the discussion that follows, only strain data obtained from segments 33 and 62 are presented and discussed. Also, since data patterns were similar for loads in the north and south bound lanes, only the northbound lane loadings are discussed. It should be noted here that the test loading applied, a tandem-axle dump truck loaded to the maximum legal limit, is a loading of relatively small magnitude compared to the self weight of the bridge. The total vehicle weight was approximately 50,000 lbs while the weight of each of the 124 single segments making up the main span was approximately 135,000 lbs. The corresponding strains and stresses produced by this load were also small in absolute magnitude. For example, maximum

strain values recorded, due to the application of the test load, were on the order of 5 to 10 microinches per inch. Although small, the reliability of these values is attested to by the fact that the readings were reproduced with little error under repeated load applications and recorded values of strain were consistent between different gages and different locations.

As noted, only the strain gages in the lower flanges of segment 33 were operative. Recorded strains from gages 17, 18 and 19, which are located in the lower flange of the northbound lane of segment 33 (see Fig. 3), are presented in Figs. 5 and 6 for loads in the exterior and interior lanes respectively. The strains are plotted as a function of vehicle location where the distance denoting the vehicle position is measured from pier 14. This reference point for location of the test load was chosen arbitrarily and represents the origin of the first span in which the load was placed. Thus, the first load point, at midspan of span 18, is plotted at a distance of 75 ft. From Figs. 5 and 6, it may be observed that the recorded strains are essentially negligible until the vehicle enters the main span. The strain responses, which are similar for all three gages shown, are of the form that would be expected since segment 33 is located adjacent to the south pier in the negative moment region of the continuous span. Relative to the reference point for the distance parameter, the gages in segment 33 are located approximately 920 ft from pier 14. For the vehicle in the exterior traffic lane, the maximum strain recorded was on the order of 8.0 microin./in. corresponding to a

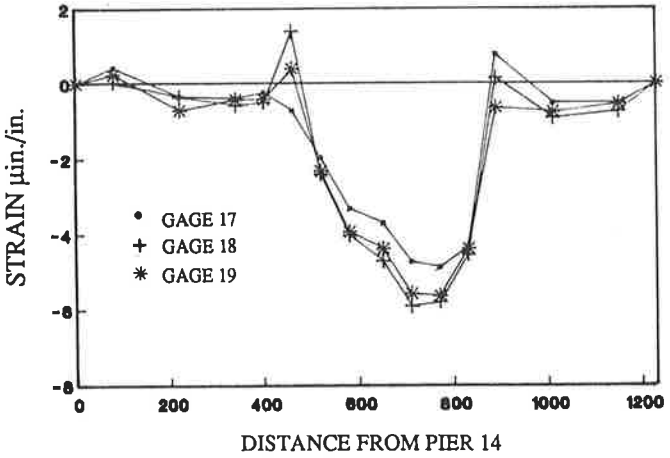

FIG. 6 LOWER FLANGE STRAINS, SEG 33 (NBL), FOR VEHICLE LOCATIONS IN INTERIOR LANE

stress value of approximately 36 psi. With the load in the interior lane, the variation of strain as a function of load position is the same but the maximum strain value recorded is approximately 6 microin./inch.

Strains measured in the top flange, or deck region, of segment 62 are shown plotted in Figs. 7 through 10. Figure 7 represents strain response for gages 1 through 4 of segment 62 for the load in the exterior lane while Fig. 8 provides the same data from gages 11 through 14. Figures 9 and 10 show strain data for the same gages as Figs. 7 and 8 respectively, but for the load traversing the interior lane. There appears to be considerable scatter in these plots but the actual strain values plotted are small and variations are actually less than 1.0 microin./inch. These gages are located longitudinally within a few feet of midspan and the results as shown in the figures

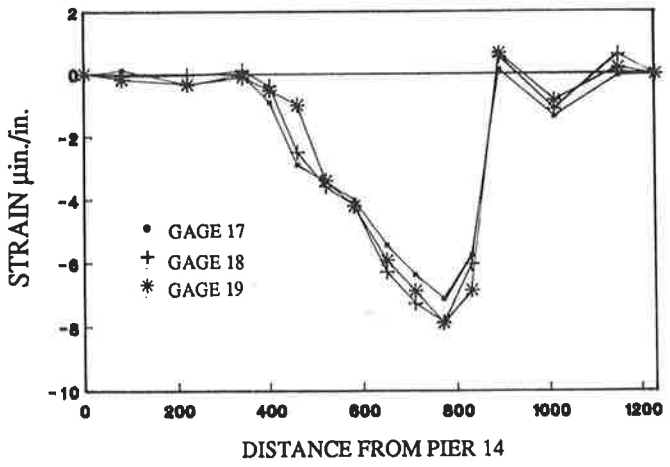

FIG. 5 LOWER FLANGE STRAINS, SEG 33 (NBL), FOR VEHICLE LOCATIONS IN EXTERIOR LANE

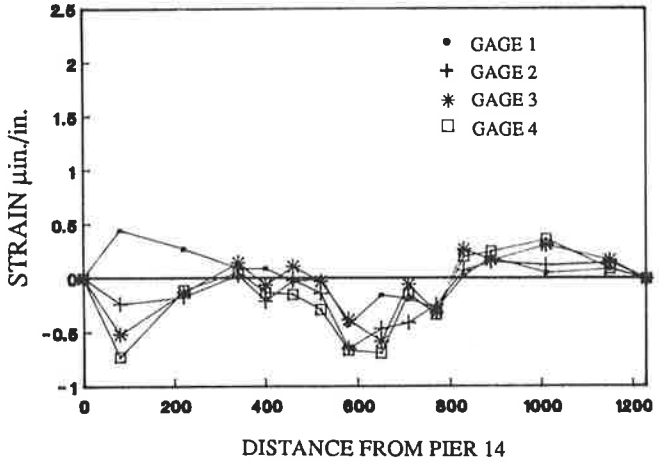

FIG. 7 UPPER FLANGE STRAINS, SEG 62 (SBL), FOR VEHICLE LOCATIONS IN EXTERIOR LANE

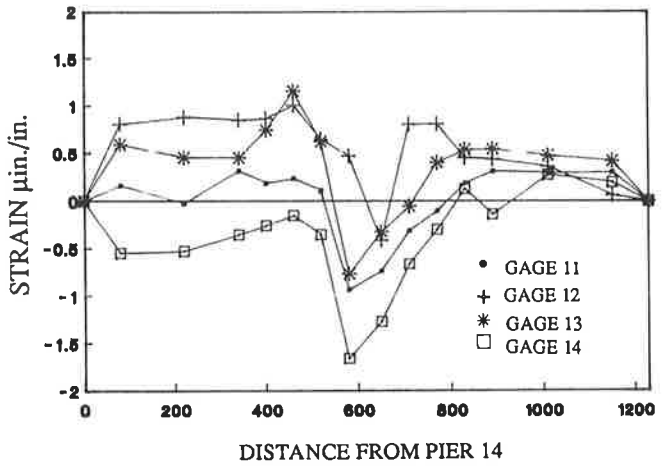

FIG. 8 UPPER FLANGE STRAINS, SEG 62 (NBL), FOR VEHICLE LOCATIONS IN EXTERIOR LANE

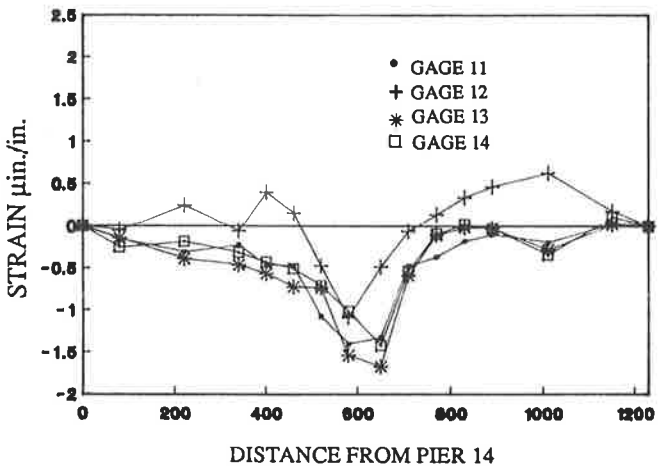

FIG. 10 UPPER FLANGE STRAINS, SEG 62 (NBL), FOR VEHICLE LOCATIONS IN INTERIOR LANE

indicate small compressive strains for the load at midspan as expected. The neutral axis for the box segments in the deck is located much closer to the top flange and hence the measured strains would be expected to be smaller than those observed in the lower flange. The maximum compressive strains recorded are on the order of 1.0 to 1.5 microin./in, even less than might be expected. This apparent anomaly is considered further in the next section. Although there is somewhat more scatter in these data than in those observed in segment 33, the trends are the same and the values are relatively consistent.

Strain data from gages located in the lower flange of segment 62 are plotted against longitudinal load position in Figs. 11 through 14. Figures 11 and 13 provide strain data recorded from gages 8 and 9 in the southbound portion of the segment as a result of loading in the exterior and interior lane respectively. Figures 12 and 14 provide the same data from gages 17, 18 and 19 located in the lower flange of the northbound portion of segment 62. It may be seen that all of these plots have the same general character with compressive strains recorded for the load in the approach spans and larger tensile strains recorded for the load in the main span. For gages 8 and 9, located in the unloaded side of the segment, maximum strains of approximately 2.0 to 2.5 microin./in. were observed while gages 17, 18 and 19 recorded maximum strains of approximately 2.5 to 3.0 microin./inch. This would indicate that although slightly more load is carried by the section on which the load is placed, there is

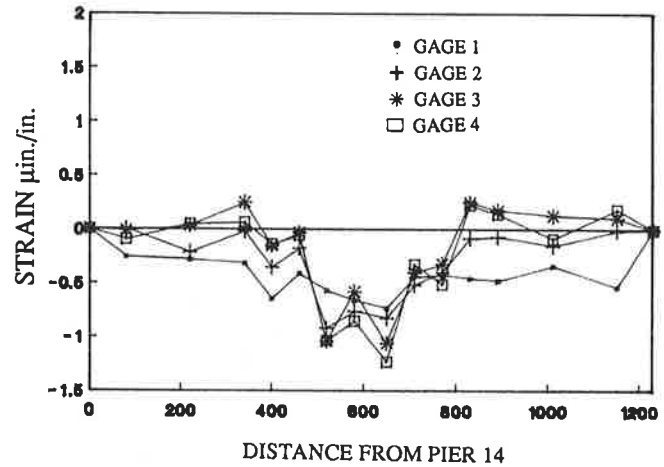

FIG. 9 UPPER FLANGE STRAINS, SEG 62 (SBL), FOR VEHICLE LOCATIONS IN INTERIOR LANE

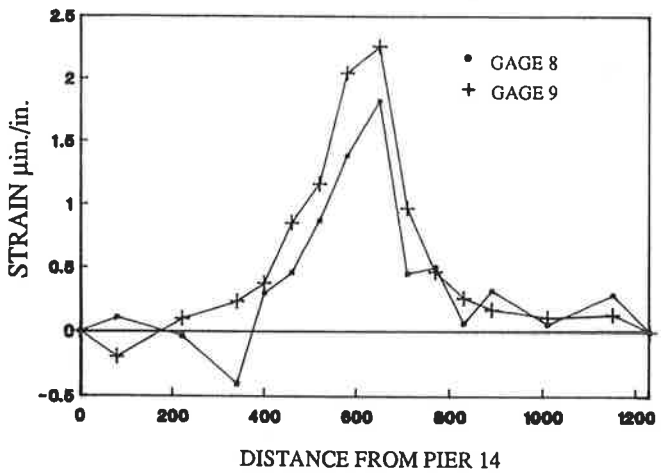

FIG. 11 LOWER FLANGE STRAINS, SEG 62 (SBL), FOR VEHICLE LOCATIONS IN EXTERIOR LANE

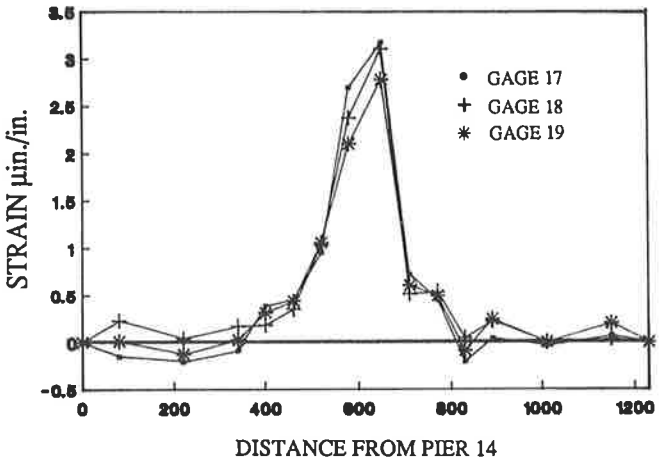

FIG. 12 LOWER FLANGE STRAINS, SEG 62 (NBL), FOR VEHICLE LOCATIONS IN EXTERIOR LANE

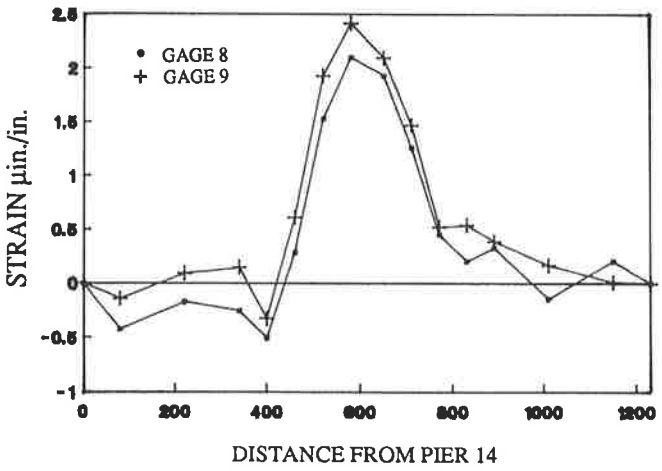

FIG. 13 LOWER FLANGE STRAINS, SEG 62 (SBL), FOR VEHICLE LOCATIONS IN INTERIOR LANE

almost uniform lateral distribution of the load throughout the segment. For all of these gages, the strain behavior is similar regardless of load or gage location.

Considerable strain data was obtained from these tests and this data provides a basis for predicting the behavior of this complex structure due to a single vehicle load. Nevertheless, field testing for every possible loading condition is not possible and it would be desirable to have a computer model to predict such stresses. In addition, there is definitely a need to validate the strain values measured during the field tests described. For these reasons, an analytical study was undertaken to develop a finite element model which could be used to validate field test data as well as provide a mechanism for predicting response under other more complex loadings.

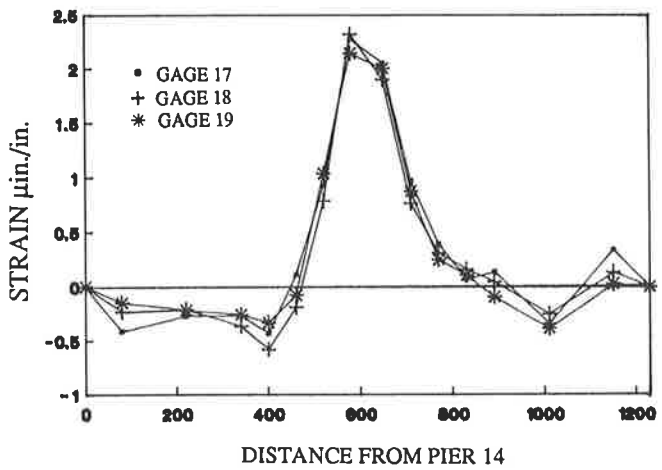

FIG. 14 LOWER FLANGE STRAINS, SEG 62 (NBL), FOR VEHICLE LOCATIONS IN INTERIOR LANE

ANALYTICAL STUDY

The emphasis of this paper was on presentation and discussion of experimental response. Consequently, only a brief description of the analytical model and limited results will be provided here. A more detailed description of the finite element model may be found elsewhere in the study by Lissenden [3]. The finite element model used in this study, primarily for validation purposes, was a three-dimensional model in which the deck segments were represented in a two-dimensional sense as a series of beam elements. Loadings were applied to the model as concentrated loads and moments at the locations corresponding to the actual position of the vehicle. The magnitudes of the model loads were calculated to represent the wheel loads of the test vehicle. Properties of the cross section of the deck segments were used to define the element properties and stresses in the top and bottom fibers of the beam elements, corresponding to the top and bottom flanges of the box segments, were calculated for all positions of the test load.

Stresses in the top and bottom flanges of the deck segment in the finite element model are plotted as a function of load position in Figs. 15 and 16 The magnitudes of the plotted stresses represent the average stress in the top and bottom flange for segments 33 and 62. For segment 33, the maximum tensile stress in the top flange was calculated to be approximately 8 psi while the maximum compressive stress in the bottom flange was approximately 28 psi. For segment 62, the

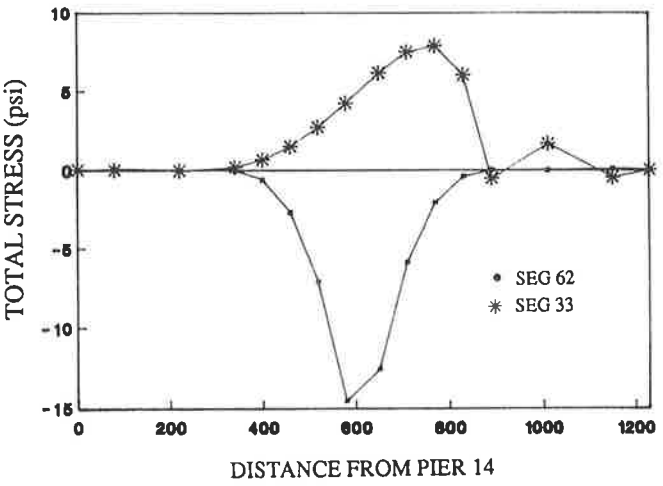

FIG. 15 UPPER FLANGE STRESSES FOR FINITE ELEMENT MODEL, SEGMENTS 33 & 62

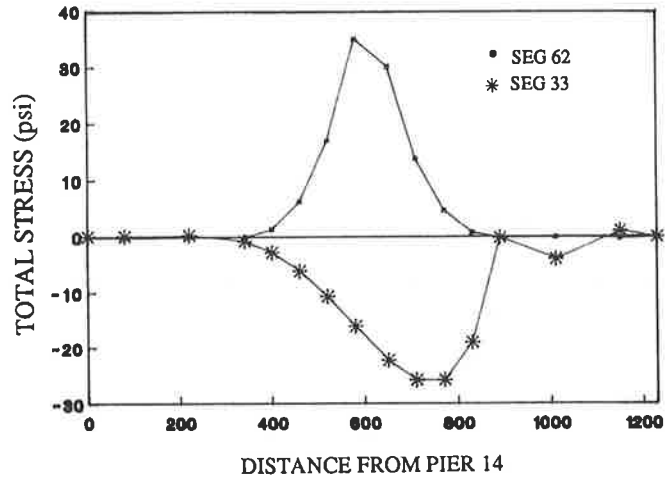

FIG. 16 LOWER FLANGE STRESSES FOR FINITE ELEMENT MODEL, SEGMENTS 33 & 62

corresponding stresses were calculated to be approximately 15 and 37 psi respectively. For the midspan location, stresses were determined to be essentially zero for the load anywhere in the approach spans while small stresses were produced in the location corresponding to segment 33 for the load in the spans adjacent to the segment.

For validation purposes, it is of interest to compare the stresses determined from the strains measured during the field test with those stresses predicted from the finite element model. In Figs. 5 and 6, the variation in strain in the bottom flange of segment 33 is plotted as a function of load position. The corresponding values of stress predicted by the analytical model are plotted in Fig. 16. Comparison of the two figures indicate close agreement in terms of the overall shape and magnitudes of the response. Both measured and predicted response are essentially zero for load positions from zero to approximately 350 feet when the load enters the main span. Similar variations in response are also observed for distances greater than approximately 900 feet when the load traverses the final two approach spans. Furthermore, the maximum stress as determined from the experimental strain data was approximately 30 psi while the predicted maximum for the same loading was 28 psi, extremely close agreement.

Comparisons between measured and predicted stresses in the vicinity of the bridge midspan may be made by examination of Figs. 7, 8, 11 and 12 for measured data and Figs. 15 and 16 for analytical data. These comparisons raise some interesting questions that have yet to be satisfactorily answered. Data measured in the top flange of segment 62 as shown in Figs. 7 and 8 show some scatter but an average value of maximum compressive stress may be estimated to be on the order of 4 to 6 psi. The corresponding value of stress predicted by the finite element model was calculated to be 14.5 psi as indicated in Fig. 15. These measured and predicted values of maximum stress differ by a factor of approximately 3. Similar differences were observed to exist between measured and predicted stresses in the lower flange of the box segments at midspan. From Fig. 11, the value of maximum tensile stress as determined from the measured strains in segment 62 was found to be approximately 12 psi while the corresponding stress value predicted by the model was calculated to be 37 psi, as shown in Fig. 16. Again, the measured and calculated values of response differ by a factor of approximately 3.

A careful review and evaluation of the experimental procedure for measuring and recording strains have indicated no source of error in the experimental data. Likewise, the finite element model appears to be a reasonable representation of the bridge according to the plans. If, in fact, both measured and predicted response values are to be accepted, this would suggest the possibility that there is some difference in the behavior of the actual structure that is not adequately represented in the finite element model. For example, one factor under consideration is the possibility that complete continuity does not exist at midspan of the

bridge. This main span was constructed as two cantilevers from either side of the river and these two sections were then joined by a closure pour at midspan. The subsequent post-tensioning was intended to render the completed span continuous but there is the possibility that the continuity may not be complete. This could lead to lower stresses at midspan. This and other possible factors which could lead to differences between measured and predicted values of stress are currently being investigated.

In spite of certain differences that exist, the similarities between the stresses predicted by the finite element model and those measured in the field test indicate that finite element models can be a useful analysis tool for predicting the behavior of complex structures such as cable stayed bridges. However, care should be taken that the models used in the analyses accurately represent the actual structure as built. This can only be achieved through the use of carefully controlled and monitored field tests.

SUMMARY AND CONCLUSIONS

A load test of a cable stayed bridge was conducted by placing a known vehicle load at various positions on several spans of the structure and measuring the response from strain gages imbedded in deck segments at three different locations of the main span. Variations in strain as a function of load position were plotted for strain gages in the top and bottom flanges of the segments. Similar response data was calculated from a finite element model developed as a part of the study. Comparisons of measured and calculated response were made as a means of validating the computer model and to provide credibility to the experimental data collected and the system used to collect and record the data.

Results from the field test provided considerable data regarding the behavior of the bridge under a specific vehicle load. For example, the study indicated that reliable experimental strain data can indeed be measured even when the applied load is only approximately 0.5 percent of the self weight of the bridge. The measured strain data, when plotted as a function of load position, was found to vary in a manner generally consistent with expected response. Results from the analytical study indicated that maximum values of stress in the vicinity of the pier varied from approximately 8 psi in tension to 28 psi in compression. At midspan of the bridge, maximum values of stress were found to vary from 13 psi in compression to approximately 38 psi in tension. Comparison between measured and calculated stresses indicated close agreement with regard to overall trends and magnitudes in most regions of the bridge but differences on the order of a factor of 3 were observed at midspan. Various explanations for this apparent anomaly are currently under study.

ACKNOWLEDGEMENT

The work reported herein was supported by the Virginia Transportation Research Council through HPR funds and oversight was provided by the Federal Highway Administration. Mr. James W. French provided invaluable assistance during the conduct of the field tests.

REFERENCES

1. A.M. Abdel-Ghaffar. An Analysis of the Dynamic Characteristics of a Suspension Bridge by Ambient Vibration Measurements. Report No. EERL 77-01, Earthquake Engineering Research Laboratory, California Institute of Technology, Pasadena, CA, 1977.
2. F.W. Barton, T. T. Baber, R. D. Ramsey and W. T. McKeel, Jr. Measured Stresses in the Deck Segments of a Cable Stayed Bridge. Proceedings, ASCE Structures Congress, Baltimore, MD, 1990.
3. C. J. Lissenden, III. *Dynamic Modeling of a Cable-Stayed Bridge During Construction.* M.S. Thesis. University of Virginia, Charlottesville, VA, 1986.

Evaluation and Load Testing of a 100-Year-Old Elevated Steel Transit Structure

S. G. PINJARKAR, R. W. KRITZLER, R. A. ROLSING, AND P. O. MCCARTHY

Full-scale diagnostic load tests were performed on a typical single-span structure as part of a pilot test program for the Engineering Condition Assessment of the Chicago Rapid Transit System. The purpose of the load testing was to evaluate the actual behavior of a 100-year old elevated steel structure under train loading. Measured static and dynamic responses to train loads were used to evaluate impact loading, and to establish methodology for fatigue life assessment. Tests were also performed to evaluate longitudinal braking forces at the support columns, and recent modifications made to the stringer bracing system. The Chicago Transit System includes approximately 40 miles of elevated steel structures and bridges. The results of the pilot test program were used to develop an expanded test program for an overall condition assessment of the entire elevated transit support system.

The static load tests were performed by stopping a test train at known positions along the track structure. Strains and deflections were measured at critical locations in the stringers, columns and cross-bracing members. The dynamic tests were performed by moving a test train across a test span at crawl speed and at various operating speeds. Strains were measured in the stringers during movements of the test train and in-service trains. Dynamic tests were also performed by braking the moving test train to evaluate the effects of both normal and emergency braking.

The test data showed the average measured impact loading to be 5 to 10 percent, as compared with the code design impact of 55 percent. The braking and stopping of the test train caused bending stresses in the columns approximately equal to the column axial stress. The new stringer cross-bracing was found to be effective in distributing train loads from one track to all four stringers supporting both tracks, causing significant uneven distribution to the two stringers supporting the loaded track.

INTRODUCTION

Full-scale nondestructive diagnostic load testing was conducted on the elevated steel structure located on the Southside Main Line of the Chicago Rapid Transit System. The load tests were performed as part of a pilot program for the overall Engineering Condition Assessment of the Chicago Rapid Transit System, which includes approximately 40 miles of elevated steel structures and bridges. The original foundations and elevated steel structures were designed and built during the early 1890's for the 1893 Chicago Columbian Exposition. The transit trains were originally powered by small steam locomotives. The system was later converted to lighter electric-powered cars.

S. G. Pinjarkar and R. W. Kritzler, Raths, Raths & Johnson, Inc., Willowbrook, Illinois
R. A. Rolsing, McDonough Associates, Inc., Chicago, Illinois
P. O. McCarthy, H. W. Lochner, Inc., Chicago, Illinois

Diagnostic load testing was used to supplement the engineering analyses and rating calculations made to evaluate behavior of the steel structure supporting the tracks. Static and dynamic load tests were conducted using a special test train and also normal in-service train movements. Load testing reduced the uncertainties in the assumptions made for analytical rating by measuring the actual response of the structure to static and dynamic train loads. The diagnostic type of nondestructive load test is generally performed to determine response characteristics of a structure. These characteristics are then used to determine the load rating by analytical methods, as described in Reference [1].

Description of Test Program

The load testing was conducted on a typical single span located between Bents 595 and 596 just north of 45th Street (*Figures 1 through 4*). The test span consisted of four simple-span, open-deck stringers, with bottom end bearing on steel bents 53 feet-6 inches center to center, supporting two standard-gage tracks on timber ties. The stringers had been recently retrofitted with new flange angles fastened to the original web with high-strength bolts. In addition, the stringer bottom lateral system had been removed and vertical cross-bracing installed (*Figure 4*) between all four stringers. In general, all tests were

Figure 1. View of Elevated Structure, Test Span Left of Center

Figure 2. View of Tracks Along Test Area

Figure 3. View of Static Load Test

performed using an empty four-car test train which represented approximately 80 percent of the total train load including passenger loading. The empty test train was found to be more suitable for calibration because of known axle weights.

The static load test was performed by stopping an empty four-car test train at known positions along the track structure. Stresses (strains) were measured at critical locations in the stringers, columns, and cross-bracing members (*Figure 5*). Vertical deflections were measured at the span center for each stringer.

The dynamic tests were performed by moving the test train across the test span at crawl speed and at various operating speeds. Strains were measured in the stringers to evaluate dynamic load effects (impact factor) and to determine actual variable amplitude stress cycles for fatigue evaluation. Dynamic tests were also performed by stopping the moving test train on the test span to determine the effects of braking, and to compute the approximate magnitude of longitudinal forces caused by braking action. Additional dynamic tests were performed by monitoring strains during normal in-service train movements across the test span. The tests were conducted on Sunday afternoon, during off-peak hours, to evaluate the test methods. Future in-service testing will be performed during peak traffic hours.

Figure 4. View from Below Test Span Structure

The measured strains (converted to stresses) and deflections were plotted to evaluate the track structure response under train loading. Test results were reviewed for consistency and symmetry, and compared with calculated values. The results of this pilot test program were used as a basis for developing an expanded load testing program for use in the overall condition assessment of the entire elevated transit support system.

STATIC LOAD TEST

The static load testing consisted of measuring and recording strains and deflections for a four-car test train stopped at seventeen known positions along the east and west tracks of the elevated structure (*Figure 3*). An empty four-car test train was provided by the Chicago Transit Authority (CTA) (*Figure 6*). A single empty test car weighed approximately 54,400 pounds, with an approximate axle load of 13,600 pounds, and an overall length of 48 feet (*Figure 6*). The test train positions were established to locate the centerline of the car axle groups over the test span quarter points, midspan, and end support bent. The train lead axle was used to stop the train at pre-selected positions along each track.

Instrumentation

Eighteen 1-inch long electrical resistance strain gages were installed on the test span and bent (*Figure 5*) to monitor

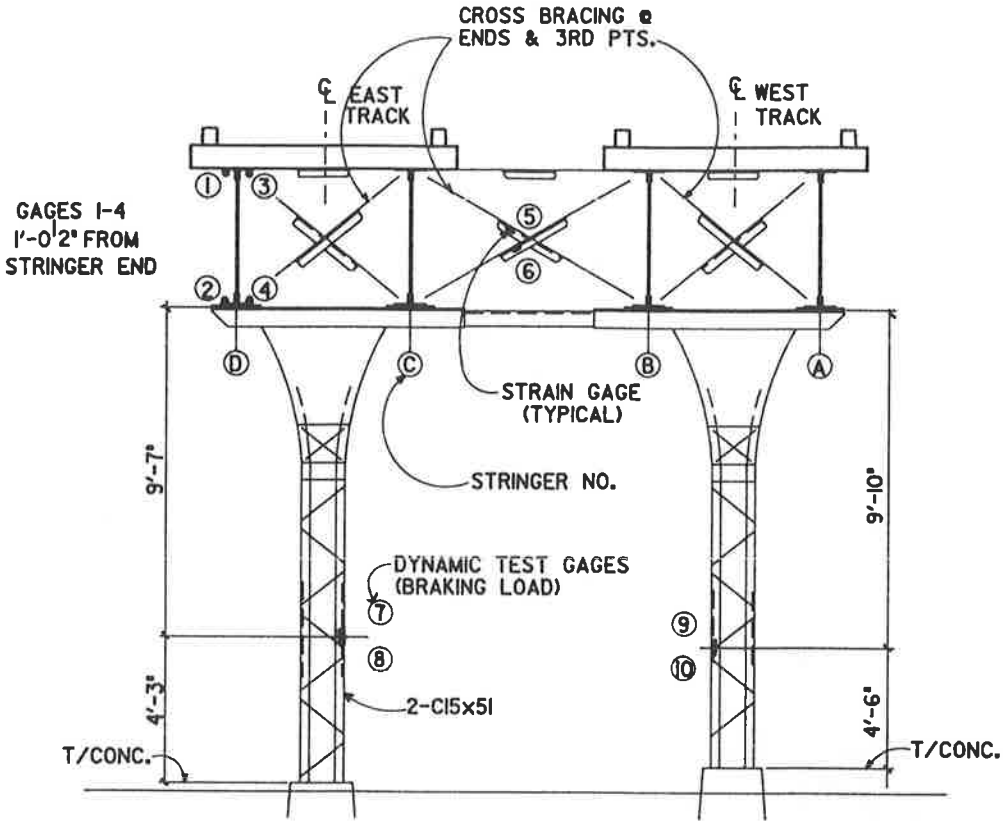

CROSS SECTION AT BENT 595

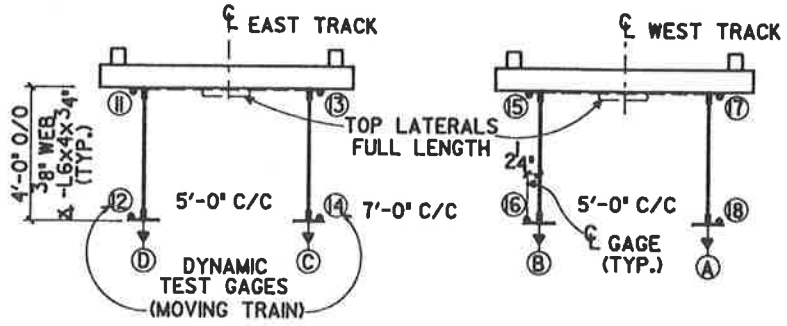

CROSS SECTION AT MIDSPAN 595-596

- DENOTES LONGITUDINAL STRAIN GAGE
- DEFLECTION MEASURED W/ SUSPENDED TARGET

Figure 5. Instrumentation

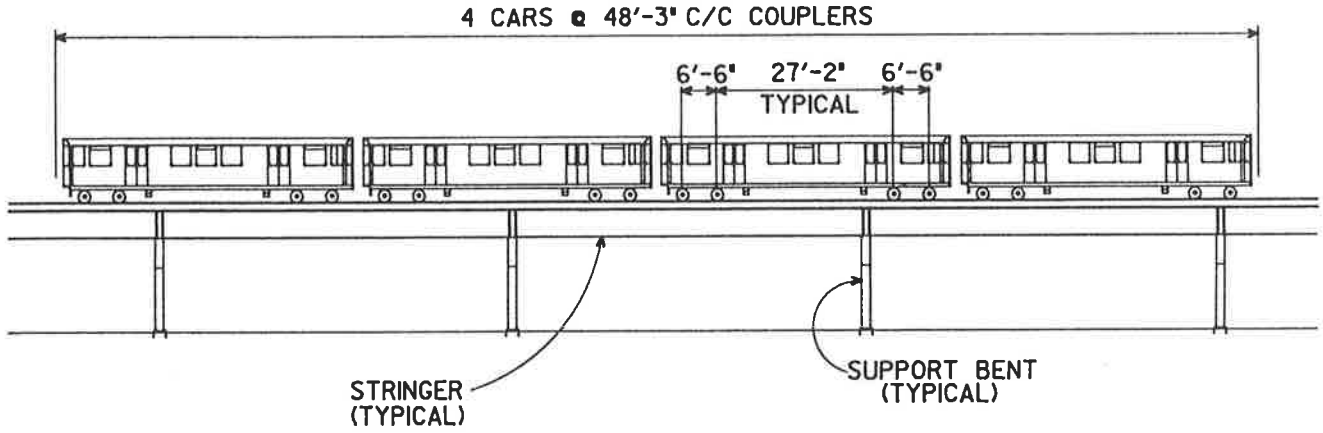

Figure 6. Elevation of Four-Car Test Train

structural behavior during the load test. Strain gages were installed to measure maximum bending stresses at midspan (top and bottom flange) of the stringers and also at the ends of the stringers. In addition, strain gages were installed on two of the columns and on several cross-bracing members.

The strain gages were wired to eighteen completion circuits, a DC power supply, and a scanning digital voltmeter. The eighteen channels were read and recorded using an automatic data acquisition system, composed of a scanner and a portable computer. Measured strains were converted to equivalent stresses, printed out on paper, and recorded on magnetic diskette for each test train position.

Vertical deflections were measured at midspan for all four stringers, for each train position, using suspended targets and a precision level. The recorded stress and deflection data were later plotted for study and evaluation.

Results

A.1. The maximum bottom flange bending stress in the outside stringer, at midspan under static loading of the test train, was found to be in the range of 3.9 to 5.3 ksi. The corresponding maximum bottom flange bending stress in the interior stringer was found to be in the range of 2.4 to 3.2 ksi. The maximum stresses were recorded when groups of axles at the car ends were located at midspan. As shown *(Figure 7)*, the maximum recorded midspan bending stress was 5.3 ksi when the third axle group, composed of the second car rear axles and the third car front axles, was located at midspan.

A.2 The calculated maximum stress in the track stringers, based on measured cross-section and equal load distribution to the two loaded stringers, was 4.1 ksi. The calculated maximum stress in the outside stringer was 4.5 ksi, based on load distribution to the stringers by rigid body rotation of the four-stringer group. A comparison of measured and calculated stresses is summarized for Test Train Position 11 *(Table 1)*.

A.3 The midspan deflection measurements made during the static testing were consistent with the flexural behavior of the stringers *(Figure 8)*. As shown, the maximum recorded deflection of the outside stringer was 0.28 inch. The corresponding maximum deflection, at the interior stringer was 0.22 inch. The calculated maximum deflection in the outside stringer is 0.28 inch. A comparison between measured and analytically-predicted deflections showed good correlation *(Table 2)*.

A.4 The cross-bracing between the stringers was found to be effective in distributing loads from one track to all four stringers. Both the strain and deflection test data showed the four stringers to rotate (twist) as a unit under load from one track *(Tables 1 and 2)*. The behavior of the four stringers, as one unit, caused significant uneven distribution of train load to the two stringers supporting the loaded track. In addition, there were significant shifts in the load distribution to the stringers between each static and dynamic test train run.

A.5 The measured live load bending stresses in the outside stringer were generally 25 to 40 percent greater than the interior stringer for the static and dynamic tests. One static test (East Run A) indicated the measured stress in the outside stringer was 110 percent greater (5.3 ksi versus 2.5 ksi) than the interior stringer *(Figure 7)*. Evaluation of the bottom flange stresses for this test showed consistently higher load distribution to the outside stringer, and lower load distribution to the inside stringer than other static and dynamic test runs *(Table 1 and Figures 9 and 10)*. The variation in load distribution may be attributed to residual stresses caused by (i) connection slippage, (ii) stringer bearing restraint, and (iii) foundation movement.

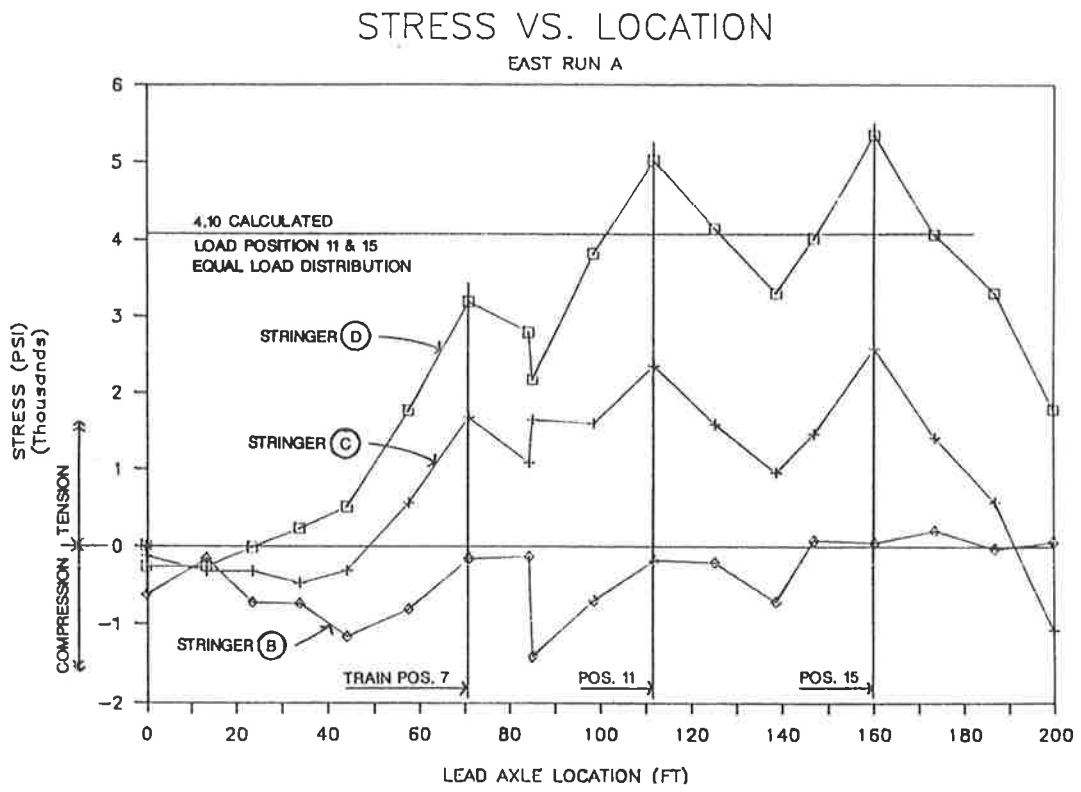

Figure 7. Test Train Static Testing
Stringer Bottom Flanges at Midspan

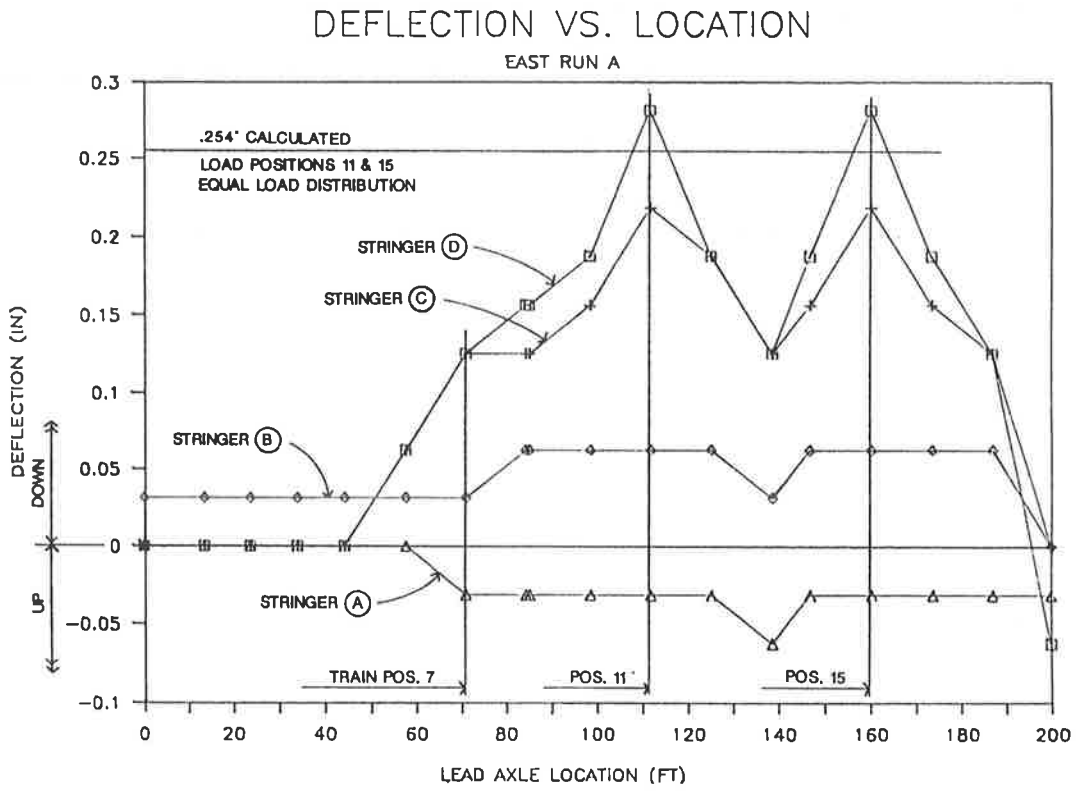

Figure 8. Test Train Static Testing
Stringers at Midspan

TABLE 1
COMPARISON OF CALCULATED AND MEASURED STRESS
STRINGER BOTTOM FLANGES AT MIDSPAN - TEST TRAIN AT EAST TRACK POSITION 11

Stringer	D	C	B	A	Avg. D & C
Calculated Stress					
Equal Load Distrib. to East Track Stringers	4.1	4.1	0.0	0.0	4.1
Load Distrib. by Rigid Body Rotation of 4-Stringer Group	4.5	3.1	1.0	-0.4	3.8
Measured Stress					
Before East Run A	3.9	3.1	0.3	*	3.5
East Run A	5.0**	2.4	-0.2	*	3.7
East Run B	4.1	3.2	0.0	*	3.6
East Run C	4.4	3.2	*	*	3.8

* Test data incorrect due to bad gage circuit or local two-way radio noise.
** Maximum stress of 5.3 ksi measured at Position 15.

TABLE 2
COMPARISON OF CALCULATED AND MEASURED DEFLECTION
STRINGERS AT MIDSPAN

Stringer	D	C	B	A
Test Train at East Track Position 11				
Calc. Deflection (in.):				
Equal Distrib. - 2 Stringers	0.25	0.25	0.00	0.00
Load Distrib. - 4 Stringers (1)	0.28	0.19	0.06	-0.03
Measured Deflection (in.)	0.28	0.22	0.06	-0.03
Test Train at West Track Position 11				
Calc. Deflection (in.):				
Equal Distrib. - 2 Stringers	0.00	0.00	0.25	0.25
Load Distrib. - 4 Stringers (1)	0.03	0.06	0.19	0.28
Measured Deflection (in.)	-0.06	0.06	0.25	0.31

(1) Load distributed by rigid body rotation (twist) of 4-strtinger group.

A.6 The measured axial stresses in the stringer center cross-bracing, located above the end support bent (*Figure 1*), indicated resistance to the rotation of the four-stringer group. The maximum measured stress was 2.4 ksi, and occurred when the train car axle groups were centered at midspan.

DYNAMIC LOAD TEST

The dynamic load testing included three parts. The first part consisted of recording stringer bottom flange stresses during test train movements across the test span at various speeds: 3.0, 7.4, 21.1 and 33.7 miles per hour (mph). The second part consisted of recording column flange stresses during test train braking and stopping while moving across the test span. The train was stopped using normal braking by the motorman, and then was stopped using full emergency braking (including track brake). The third part consisted of recording stringer bottom flange stresses during two in-service train movements across the test span at 27 and 41 mph. The results of dynamic tests performed for stringer bending stresses are summarized in *Table 3*.

Instrumentation

Instrumentation to measure dynamic response included two strain gages wired to two completion circuits, a DC power supply, a two-channel digital oscilloscope, and a portable computer. The two channels were read and recorded using the oscilloscope and computer. Measured strain records for each train movement were recorded on magnetic diskette and also by Polaroid photographs of oscilloscope screen plots. The measured strains were converted to equivalent stresses, and later plotted for study and evaluation (*Figures 9 through 12*).

Results

B.1 The impact factor was measured to be approximately 5 to 10 percent for the test train movements and in-service train movements recorded. The maximum stringer bottom flange stress, under the moving test train, was 4.5 ksi and, under two moving in-service trains, was 4.6 ksi *(Table 3)*.

B.2 The impact factor is considered to be the increase in stringer flexural stress due to the dynamic effect of moving train loads. Several definitions have been used in various

TABLE 3
DYNAMIC TESTING
SUMMARY OF MEASURED DYNAMIC EFFECTS
GAGE 12 - OUTSIDE STRINGER, BOTTOM FLANGE AT CENTER SPAN

Train Type (1)	Train Speed (1a)	Max. Approx. Static Stress (2) (KSI)	Peak Dynamic Stress (3) (KSI)	Measured Percent Impact (4) (%)	Max. Dyn. Response Amplitude (5) (KSI)	Percent Impact (6) (%)
Test	0.0	3.9	3.9	-	-	-
Test	7.4	4.1	4.1	0.0	0.0	0.0
Test	3.0	4.1	4.1	0.0	0.0	0.0
Test	21.1	4.2	4.5	7.1	0.25	6.0
Test	33.7	4.2	4.4	4.8	0.39	9.3
Test	0.0	4.2	4.2	-	-	-
Normal	27	4.1	4.4	7.3	0.35	8.6
Normal	41	4.4	4.6	4.5	0.14	
					0.18	
					0.32 (total)	7.3

(1) Test denotes 4-car test train; Normal denotes normal in-service train movements (both 4-car trains).
(2) Maximum value of static response curve fit to median values of dynamic response (Figure 11).
(4) [(3) - (2)] / (2) * 100 definition of impact by peak dynamic response.
(5) Maximum dynamic amplitude of stress oscillations along peak segments of dynamic response (Figure 11).
(6) (5) / (2) * 100 definition of impact by dynamic oscillation.

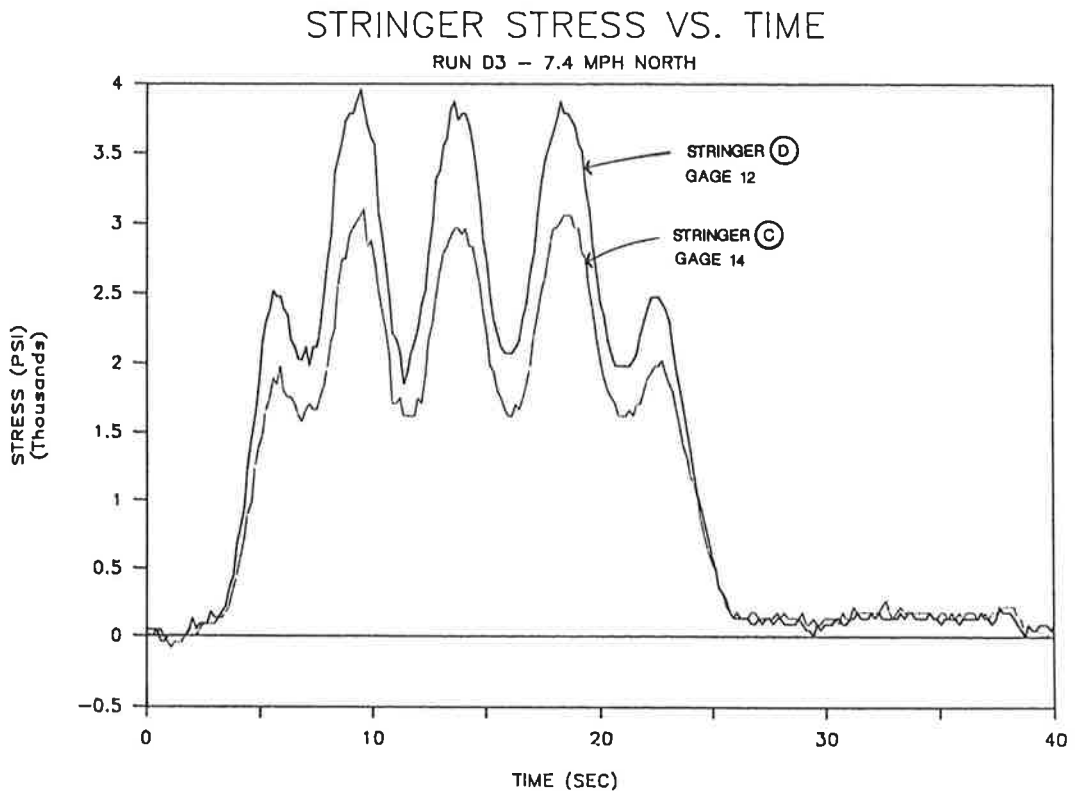

Figure 9. Test Train Dynamic Testing
Train Moving at Crawl Speed

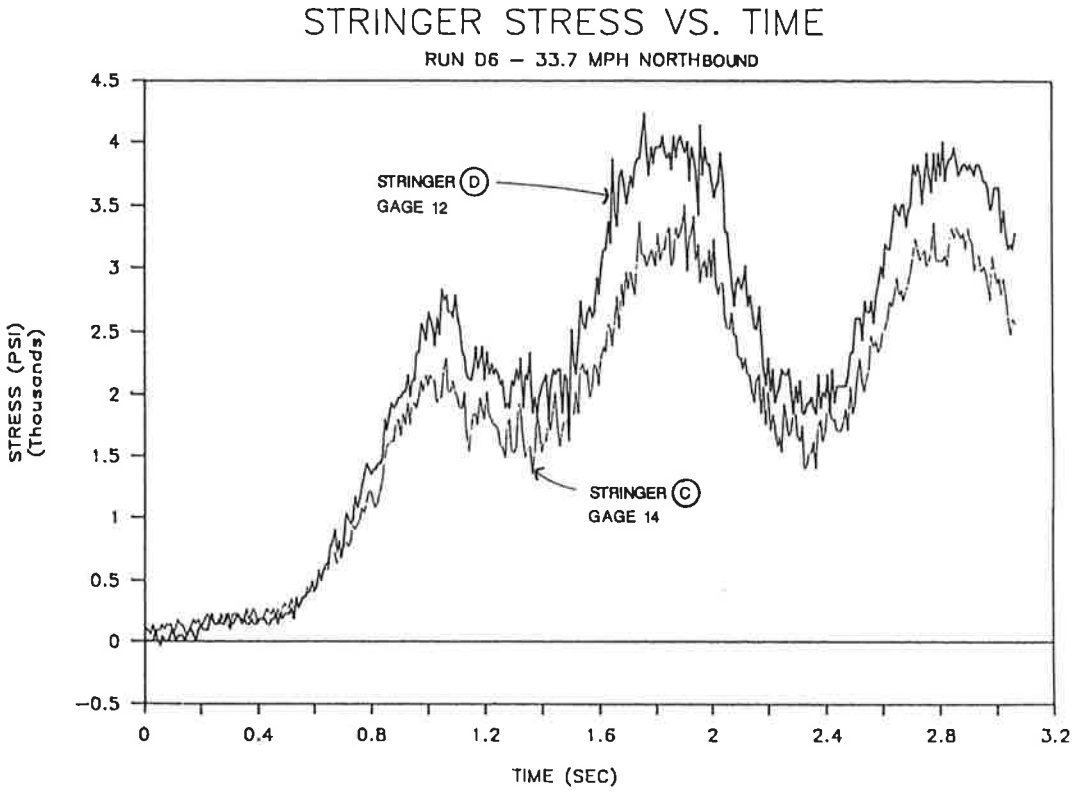

Figure 10. Test Train Dynamic Testing

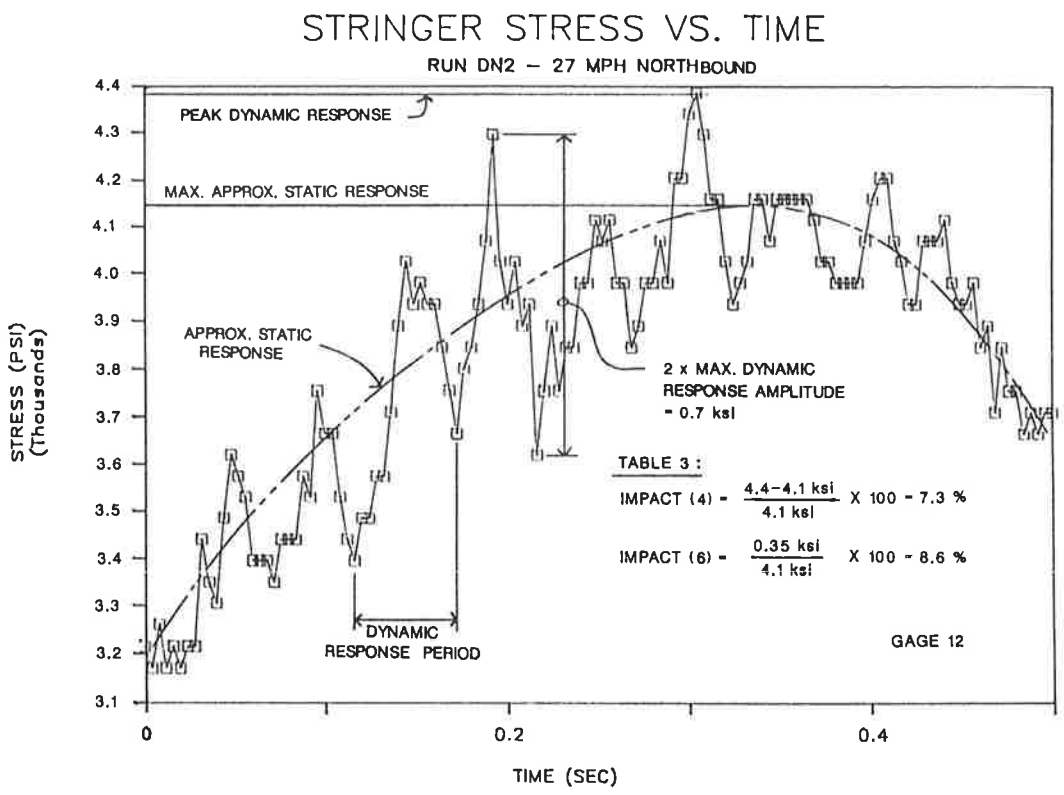

Figure 11. In-Service Train Dynamic Testing

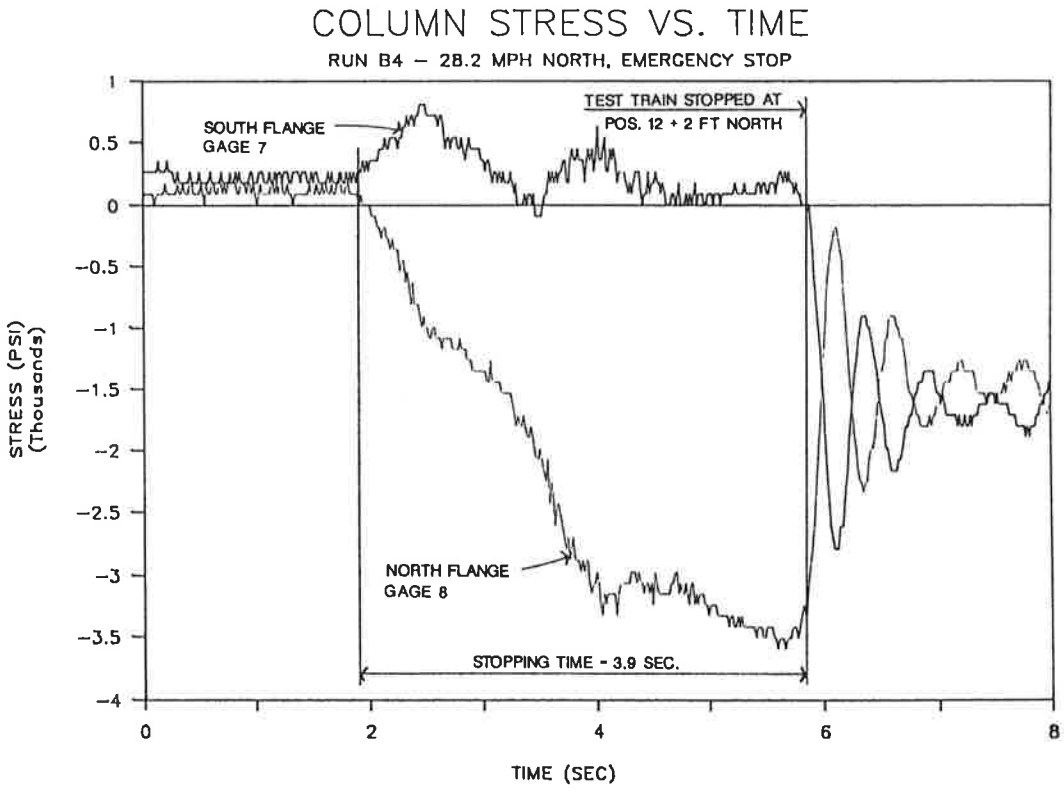

Figure 12. Test Train Longitudinal Force Testing

recent technical literature [2]. Impact is usually defined as the increase in peak response from a moving load over the maximum response from a static load. However, the maximum response from static train loading on this CTA track structure was found to vary considerably between each test run (*Table 1*). The impact factor was therefore determined from the dynamic response curve for each test (*Table 3 and Figure 11*). *Figure 11* illustrates the variables summarized in *Table 3* to calculate impact. *Table 3* shows measured impact calculated using two different equations. Column (4) shows measured impact as the increase in the peak dynamic response over the approximate maximum static response. The approximate static response was determined by fitting a curve to the median values of the dynamic response *(Figure 11)*. *Table 3*, Column (6), shows measured impact as the maximum amplitude of stress oscillations along the peak segments of the dynamic response curve. Both methods of calculating measured impact should be used where the measured maximum static response is not available for a given train load. The measured impact should then be reported as the greater of the two calculated values.

B.3 The braking of the train applies longitudinal forces to the elevated structure, causing bending of the support columns. The test data did not indicate a significant difference in maximum column flange stresses caused by braking and stopping the train using normal brakes or using emergency brakes (including track brake).

The braking and stopping of the test train caused a maximum flange tensile stress of 0.8 ksi and a maximum flange compressive stress of 3.6 ksi (*Figure 12*). The maximum column bending stress occurred at 0.2 ksi flange tensile stress, and 3.6 ksi flange compressive stress, equivalent to 1.7 ksi column compressive axial stress and 1.9 ksi bending stress. The measured compressive axial stress in the column for the test train stopped at this position, during the static testing, was 1.7 ksi. The calculated axial compressive stress in the column for the test train emergency stop position was 1.9 ksi. A calculation to determine the approximate magnitude of longitudinal force caused by braking indicated a force of 1.8 kips per column.

RECOMMENDATIONS

C.1 The maximum train live load stress for the outside stringers of this test span would be approximately 5.3 ksi plus allowance for train passenger load plus 10 percent average impact load.

C.2 Fatigue Assessment - The fatigue damage in the outside stringer bottom flanges of this test span, caused by passage of a typical empty four-car train, can be calculated from the dynamic test response plots (*Figures 9 and 10* are examples). These response plots show the variable amplitude complex stress cycle of the stringer bottom flange. Using the "rain-flow" type method [3] of counting cycles, the complex stress cycle can be expressed as an equivalent number of simple stress cycles causing the same amount of damage.

Using the stress response plot for the in-service train traveling at 41 mph and neglecting all dynamic stress oscillations, the equivalent variable simple cycles are as follows:

1 - Cycle 4.5 ksi
2 - Cycles 2.6 ksi
2 - Cycles 1.6 ksi

Cumulative fatigue damage rules, as outlined in A.R.E.A. Manual, Chapter 15, Section 7.3.4.2.e [4], are used to relate fatigue damage under variable loading to known behavior under constant amplitude loading. The effective or equivalent stress range of constant amplitude, calculated as the root-mean-cube (RMC) of all variable cycle stresses, produces the same degree of fatigue damage as the variable amplitude fatigue damage.

Effective RMC Stress Range = 3.0 ksi
Total Fatigue Damage = Five 3.0 ksi cycles

Using the equation for the fatigue strength curves of the form $N = A/S_R^3$, where N equals the minimum number of constant stress cycles to failure and S_R is the corresponding fatigue stress range, the above fatigue damage of five 3.0 ksi cycles is also equivalent to one and one-half 4.5 ksi cycles, and also to one 5.1 ksi cycle.

This methodology can be applied to rush-hour loaded cars by approximately factoring the above stresses for the increased passenger load. These results can then be applied to determine the total cumulative fatigue damage to the stringers, caused by the past and future loadings of this type of transit car.

C.3 The magnitude of impact loading measured for this test span (5 to 10 percent) was significantly lower than the A.R.E.A. Manual design impact value of 55 percent. Additional dynamic load testing is planned, as part of the overall condition assessment of the entire elevated transit support system, to verify and determine actual impact loading for:

a. Rush-hour, in-service loaded trains
b. Different spans, especially shorter spans
c. Elevated spans without stringer cross-bracing
d. Stringer spans with riveted flange angles
e. Variations of train speed and track alignment

C.4 Additional static load testing was recommended to evaluate and establish adequate long-term performance of the stringer cross-bracing system recently installed on the test span. This modification to the stringer bracing was being installed extensively along the Southside Main Line

elevated structure. This static load testing indicated significant non-linear behavior and shifting of train load distribution to the stringers, believed at this time to be caused by connection slip and residual end bearing forces. In order to equalize stringer loads, it was recommended to consider omitting the center diagonal cross-braces at all locations except at the bents. However, additional load testing should be conducted to evaluate dynamic response without the center cross-bracing.

C.5 Additional longitudinal-force brake testing is planned for the assessment of this type of structure throughout the entire elevated transit system. The additional testing is to determine the contribution of support bents at various distances from the braking train.

CONCLUSIONS

Static and dynamic diagnostic load tests were conducted to evaluate actual behavior of a 100-year old elevated steel structure. Load tests were conducted as part of a pilot test program for the condition assessment of the Chicago Rapid Transit System. Tests indicated a significant difference in the load distribution between the stringers, and the average measured impact factor was found to be much less than required by A.R.E.A. design specifications. A methodology was established to evaluate impact factors and fatigue life, and to determine the load rating using diagnostic load tests. The pilot program was successful and is currently being used as a guide for conducting more comprehensive system-wide testing of the Chicago Rapid Transit System.

ACKNOWLEDGEMENTS

The authors appreciate the cooperation and assistance provided by the Chicago Transit Authority in conducting the load tests. Also, the authors express gratitude to the Regional Transportation Authority for providing funding for the condition assessment of the Rapid Transit System.

REFERENCES

[1] Pinjarkar, S. G., Guedelhoefer, O. C., Smith, B. J., and Kritzler, R. W., "Nondestructive Load Testing for Bridge Evaluation and Rating", NCHRP Project 12-28(13), Final Report, (February, 1990).

[2] Bakht, B. and Pinjarkar, S. G., "Dynamic Testing of Highway Bridges - A Review", Transportation Research Record 1223, TRB, National Research Council, Washington, D.C., (1989), pp. 93-100.

[3] Schilling, C. G., "Stress Cycles for Fatigue Design of Steel Bridges", Journal of the Structural Division, ASCE, Vol 110, No. 6, (June, 1984), pp. 1222-1234.

[4] A.R.E.A, "Manual for Railway Engineering", American Railway Engineering Association, Washington, D.C. (1989).

Field Observation of Steel Pier Caps

DALE E. POORMAN

INTRODUCTION

When faced with designing a complex interchange, problems with vertical and horizontal clearances between roadways and overhead bridges often occur. The steel pier cap has been a frequently used solution to this problem. It is not uncommon to find one or more steel caps supporting a bridge superstructure at an interchange. However, due to the difficulty of traffic control and access, hands-on inspection of these pier caps are performed infrequently.

The Ohio Department of Transportation realized this problem and in 1989 authorized Burgess & Niple, Limited (B&N) to inspect 24 bridges with steel pier caps. The bridges are located in Cincinnati, Columbus, and Dayton, as well as other small municipalities and rural locations within Ohio. A total of 58 caps were inspected that have dimensions up to 14 feet deep and 110 feet long. Forty-four of these caps are boxes and 14 are girders.

Figure 1. Elevation View of Typical Pier Cap

INSPECTION

B&N was responsible for coordinating traffic control with city and state traffic officials, railroads, and contractors for paving projects. The project consisted of a hands-on inspection of each cap. For box members, this included an interior inspection. Fatigue prone details were nondestructively tested (magnetic particle) at random locations.

Burgess & Niple, Limited, Engineers and Architects, 5085 Reed Road, Columbus, OH 43220.

Access to the caps was provided by using a manlift or ladder where a cap is over roadways. An underbridge inspection crane was used where a cap spanned railroads and waterways. Traffic control, also provided by B&N, typically consisted of closing a single lane, either above or below the bridge depending upon the means of access. Traffic control consisted of an arrow board, warning signs, and safety cones. A majority of the bridge sites involved multi-lane divided highways, however, several of the sites involved two-lane roadways which required flaggers. Off duty police or highway patrol officers were also employed to assist with the set up and tear down of the traffic control. Bridges over railroads required the use of railroad flaggers.

A subcontractor was used to remove and replace the access hatches. Many of the bolts were frozen or broke during removal. Also the access hatch covers typically do not have lifting rings making the covers difficult to handle when removing and replacing.

The exterior of the caps were inspected from a manlift, underbridge inspection crane, ladder, or by using rock climbling techniques. The interior of the box caps were inspected by climbing through the cap. In caps where the depth measured 10 to 14 feet deep, rope ladders and rock climbing techniques were necessary to inspect the inside. Only one hatch was opened on each cap due to the difficulty of traffic control and removing the cover. A portable gas monitor capable of detecting oxygen content and toxic gases was used to assure air quality. Although the air quality was always within the acceptable range, the trapped paint fumes from construction typically were uncomfortable. To provide adequate ventilation, a fresh air blower was used. The blower pumped air into the cap by means of a 2 inch diameter hose pulled along by the inspectors.

Other equipment used included a generator to run the magnetic particle yolk, an air compressor and small sand blasting unit, and helmet-mounted light similar to those used by miners. Two way radios were also used as echos inside the cap made it difficult to communicate.

OBSERVATIONS

Deficiencies observed during the inspection are separated into the following categories:

- Welded Details
- Cracks and Distortions of the Cap
- Miscellaneous Deficiencies

Figure 2. Cap Web Seal Weld Around Girder Lower Flange.

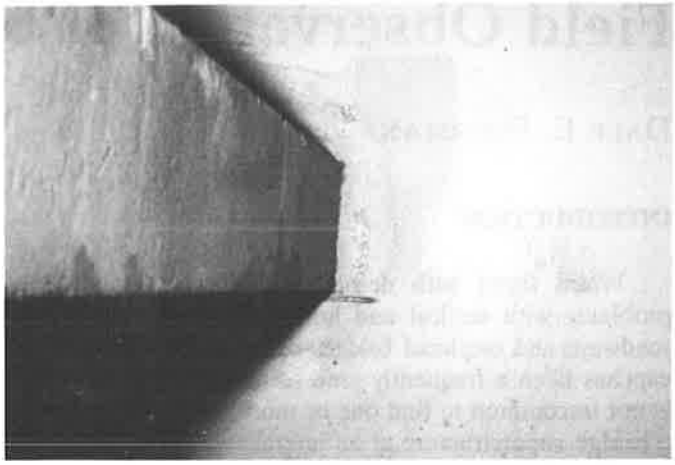

Figure 3. Opening in Cap Web for Girder Lower Flange Inside Box Cap Member

Welded Details

Seal Weld Between the Girder Lower Flange and the Tension Region of the Cap Web.

A seal weld is commonly made around the girder lower flange where the flange frames through the cap web (see Figure 2). The seal welds produce an abrupt change in the cap cross section as the girder lower flange becomes part of the cap. This change in cross section creates a fatigue prone detail in the cap. Triaxial welds also are common at the girder lower flange connection to the cap.

The seal welds typically were made around the girder lower flange on both sides of the cap web. However, on box cap members the seal weld was often omitted where the girder flange is not easily accessible inside the cap. At these locations, the weld material from the exterior seal weld has run through to the inside of the cap. The openings cut in the cap web for the girder lower flange typically has square corners and overcuts at the corners (see Figure 3). Backing bars tack-welded to the cap web were also used to back up the exterior seal weld at some locations. These uneven weld contours, sharp corners, and the tack welds all create fatigue prone details in the cap.

Retrofit details were suggested where the girder bottom flange frames into the tension zone of the cap. The detail typically consisted of making sawcuts through the web around the sides of the girder flange. Holes are drilled at the end of the cuts.[1] Bolts are placed through the holes and the sawcuts are caulked to seal the cap.

Girder Lower Flange Splice Plate or Fill Plate is Stitch-Welded to the Bottom of the Cap Lower Flange.

At locations where the girder lower flange splice plate exists below the cap lower flange, the splice plate or a fill plate has been stitch welded to the cap lower flange to aid erection (see Figure 4). Typically, the stitch welds were used to hold the plates in place until bolts could be installed. The stitch welded plates produce a fatigue prone detail in the cap lower flange similar to a partial length cover plate.

The stitch welds were recommended to be removed and ground flush with the cap lower flange. Carefully grind away fill or splice plate until all fused area with the cap is removed.

Girder Web is Welded to the Top and Edge of the Cap Upper Flange.

The girder web is welded to the cap upper flange where the girders are continuous through the cap (see Figure 5). This abrupt change in cross section of the girder web at the edge of the cap flange produces a fatigue prone detail in the girder.

The girder web welded to the top flange and web of the cap is retrofitted by making vertical saw cuts in the girder web. The cuts are adjacent to the cap flange and terminate in holes, drilled above and below the cap flange.[1]

Figure 4. Fill Plate Between Cap and Girder Lower Flange is Stitch Welded to the Cap Lower Flange

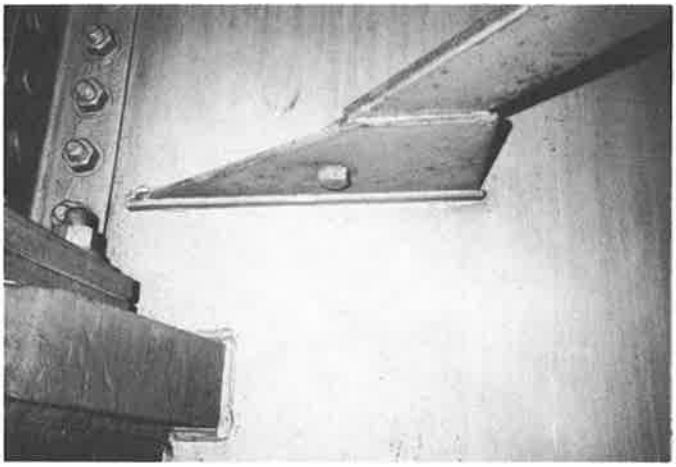

Figure 6. Lower Lateral Bracing Gussett Plate Welded to Cap Web

Figure 5. Girder Upper Flange and Web are Continuous Over the Cap Upper Flange.

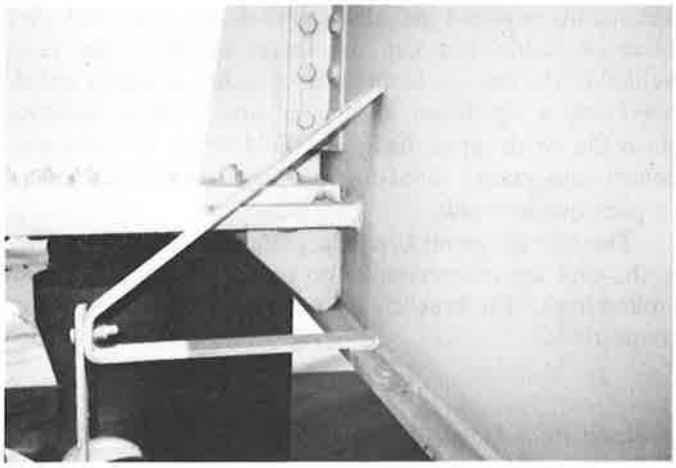

Figure 7. Roadway Drainpipe Welded to Cap Lower Flange

Lateral Bracing Gusset Plate is Welded to the Cap Web in the Tension Zone of the Cap.

The abrupt change in cross section of the cap produces a fatigue prone detail. Backing bars tack welded to the cap web were commonly used (see Figure 6). The gusset plates were attached at the girder web connection to the cap on several bridges. At these locations, the gusset plates are welded to the cap and girder web forming a triaxial weld. The gusset plates typically are located just above the girder lower flange making inspection of the seal weld difficult.

The lower lateral bracing welded to the cap web in the tension zone is recommended to be removed from the cap and the weld material ground flush. The bracing is reattached using bolts. Where the bracing is welded to the cap in the compression zone and to the cap web, a triaxial weld exists. The triaxial weld is cored from the opposite face of the girder to remove a portion of the gusset plate to girder web weld.

Roadway Drainpipe Bracket, Miscellaneous Structural Sections, Plates, Nuts, and Bolts are Welded to the Tension Zone of the Cap.

These items were welded to the cap during fabrication of the cap or erection of the bridge (see Figures 7 and 8).

Figure 8. Angle and Bolt Welded to Inside of Box Cap Member

Figure 9. Diaphragm Stiffener Inside Box Cap Member is Welded to the Cap Lower Flange

The details were not included in the design plans and often occurred inside box cap members. Typically, the items welded to the cap are less than four inches in length and do not cause a significant change in cross section. However, since the welds most likely are field welds or temporary connections, cracks could develop due to insufficient preheat or poor quality welds.

The miscellaneous brackets, plates, and sections welded to the caps are recommended to be removed and the welds ground flush. The brackets are to be reattached using bolted connections.

Welded Partial Length Cover Plates and Vertical Diaphragm Stiffeners are Welded to the Cap Flanges in the Tension Zone.

The cover plates and stiffeners cause an abrupt change in cross section of the cap and create fatigue prone details. The bottom cover plates typically are easily accessible for inspection. However, top cover plates in negative moment regions often cannot be inspected if the cap top flange is cast in the deck. Inspection of top cover plates is therefore limited to nondestructive testing or during deck replacement. The vertical diaphragm stiffeners were noted inside several of the box cap members (see Figure 9). They typically are triangular plates positioned longitudinally with the cap and are welded between the transverse diaphragms and cap flange. The stiffeners cannot be examined during routine inspections if the inspectors do not enter the box cap members.

Welded cover plates should be retrofitted with bolted splice plates across the ends of the cover plate. A horizontal saw cut also should be made in the web near the flange and centered over the cover plate termination. The saw cuts terminate in drilled holes.[1]

The diaphragm stiffeners are recommended to be removed and the weld material ground flush with the cap flange.

Backing Bars Typically are used at the Web-To-Flange Connections of Box Cap Members.

The cap web to cap flange connections were made by external groove welds due to space and ventilation limitations inside the cap. The backing bars used inside the cap typically were tack welded to the web and flange to hold the components in place during fabrication (see Figure 10). The stitch welds are susceptible to cracking due to insufficient cross section and lack of penetration. These welds were most likely made without preheating the base metal. The welds therefore would cool very quickly due to the chilling effect of the thick flange. At several locations, the backing bars were not welded together where they are spliced (see Figure 10). The bars are butted together creating a notch or stress riser where a crack could propagate from. The backing bars are bent away from the flanges or webs at numerous locations (see Figure 11). This allowed weld material from the web-to-flange groove weld to flow between the backing bar and cap web or flange. The temperature of the molten weld material alone is insufficient to thoroughly fuse with the cap web or flange. The weld is most likely cracked due to rapid cooling. These factors combined with the nonuniform weld contour create locations where cracks can form.

The stitch welds were recommended to be removed and the base metal ground 1/16 inch deep where the weld was

Figure 10. Backing Bars Inside Box Cap Member is Tack Welded to Cap Web and not Welded Together at Splice

Figure 11. Backing Bar Inside Box Cap Member is Bent Away from Cap Web

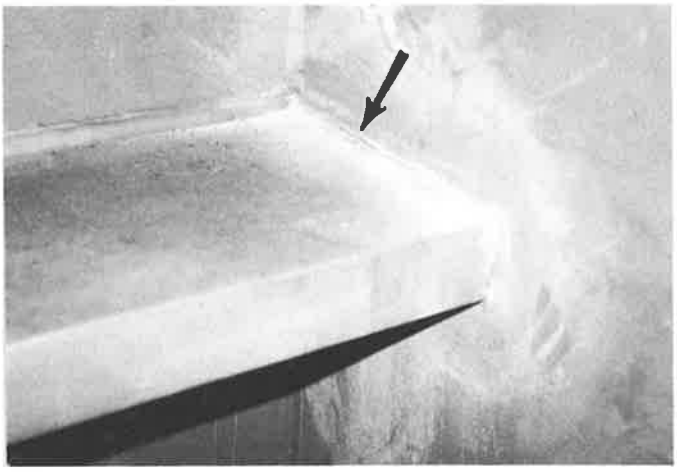

Figure 12. Crack in Seal Weld on Inside Face of Web of Box Cap Member

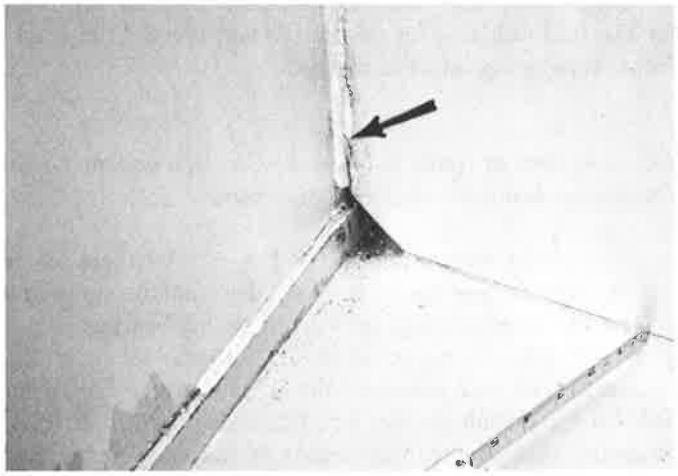

Figure 13. Crack in Vertical Weld Between Cap Web and Diaphragm Inside Box Cap Member

removed. The backing bar splices are to be beveled and groove welded together. Where the backing bars are bent, the retrofit detail consisted of removing the bent bars and tapering the ends of the remaining bars. The root of the groove weld between the cap web and flange is then gouged out and rewelded.

Cracks and Distortions of the Cap

Cracks in the seal weld around the girder lower flange.

Hairline cracks were noted in the seal welds around the girder lower flange where the girders frame through the cap. The cracks were noted only in the weld and did not propagate into the web of the cap. Magnetic particle testing was used to determine the extent of cracking (see Figure 12). At several locations, the crack had followed the seal weld along the bottom or top of the flange and turned to continue along an adjacent side. The cracks were noted in either the interior seal or the exterior seal weld of a girder flange, but not in both welds. Cracks in the interior seal weld had been painted over and the paint had not cracked. From these findings, the cracks appear to have occurred during fabrication, possibly due to cooling or the making of the other seal weld on the interior or exterior of the cap web.

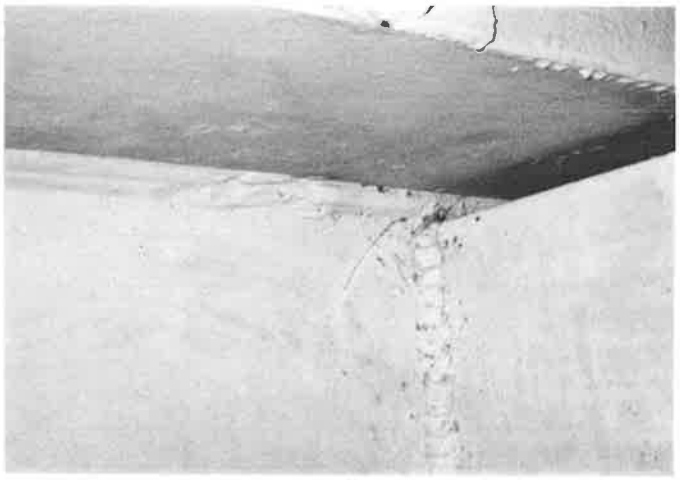

Figure 14. Crack Through Web of Girder "T" Type Pier Web Connection of the Center Beam.

Figure 15. Crack in Weld Between Vertical Stiffener and Cap Upper Flange of Girder "T" Type Pier.

Seal weld cracks are retrofitted the same as suggested for the seal welds. The saw cuts would prevent the cracks from propagating into the cap web.

Cracks in Vertical Welds Between the Cap Web and the Girder Diaphragm Inside the Box Cap Members.

The cracks were noted in two box cap members where the caps extend past the edge of the deck and are supported at its ends. The bearings are curved sliding bearings which allow the caps to rotate about its longitudinal axis. The vertical cracks were noted in the bottom of the diaphragm welds at the outside girders (see Figure 13). The cracks exist on both sides of the diaphragms at both cap webs. The cracks appear to be caused by torsion of the cap. The live load on the bridge causes the girders to deflect and rotate the cap. Friction between the curved sliding surfaces of the bearings produce torsional stresses in the cap.

The diaphragm is recommended to be welded to the cap lower flange to decrease secondary bending and improve torsional resistance. The vertical cracks are to be rewelded.

Crack in Cap Web of Girder "T" Type Pier.

The crack exists at the top of the welded beam web connection above the pier stem. The crack propagates down along both sides of the beam web and extends through the cap web (see Figure 14). Holes were drilled through the cap web at the ends of the crack to stop the crack growth.

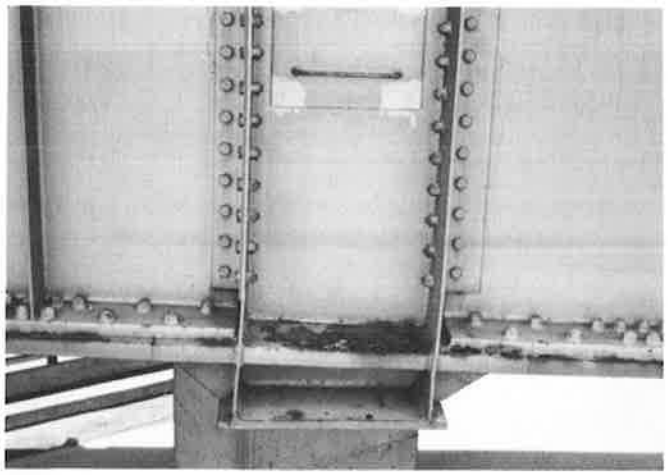

Figure 16. Cap Webs Bent at Cantilevered End of Box Cap Member

Crack in the Weld Between the Vertical Stiffener and the Upper Flange of a Girder "T" Type Pier.

The crack initiates at the girder web and propagates towards the edge of the flange (see Figure 15). The vertical stiffener appears to have been cut too short causing a gap between the top of the stiffener and the cap upper flange. As the weld between the flange and stiffener cooled and contracted, tension forces developed in the weld causing the cap flange to be bent downward. The tension force is greatest at the cap web where the flange is most difficult to deflect.

The top of the stiffener was recommended to be trimmed and the weld on the cap upper flange be ground flush.

Figure 17. Cap Web Bowed at Web Splice Weld

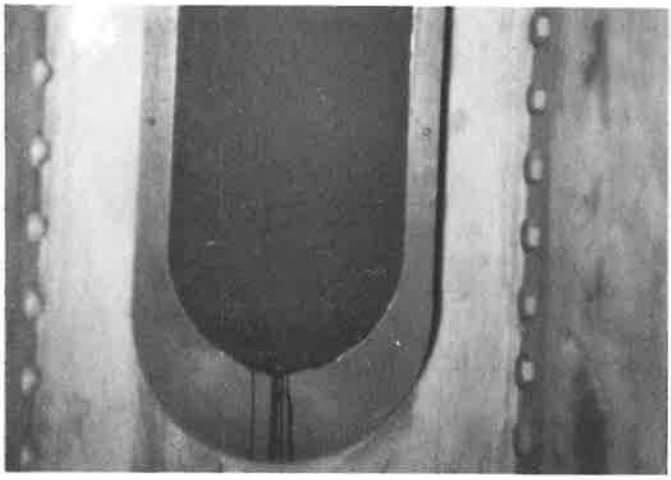

Figure 18. Access Hatch Gasket Inside Box Cap Member Beginning to Deteriorate

Cap Webs are Bent Where the Outside Girder Frames into the Cantilevered End of the Box Cap Member.

This condition appears to have occurred during erection of the superstructure. The cap was not bent at the other girder connections and no signs of distress were noted in the deck, superstructure, or substructure. The cap webs appeared to be bowed approximately two inches (see Figure 16).

Cap Webs are Bowed at the Welded Web Splices.

The splices were noted to be bowed out a maximum of 5/16 inch over a 12-inch length (see Figure 17). The splices most likely were bent during fabrication and were noted in several box cap members.

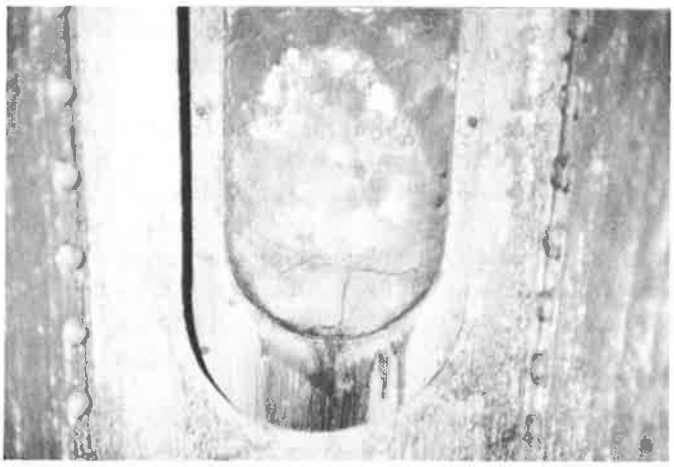

Figure 19. Access Hatch Gasket Inside Box Cap Member in Advanced Deterioration Stage

Miscellaneous Deficiencies

Access Hatch Covers on Box Cap Members Leak Due to Deteriorated Gaskets and Insufficient Bolt Spacing.

The gasket materials encountered in this project consisted of asphalt impregnated felt or an elastomeric sheet. Although leaking access hatch covers were noted with both types of gaskets, the asphalt impregnated felt gaskets typically were deteriorated. Deterioration begins by the presence of a tar-like substance running down the inside of the cap from the bottom of the access hatch (see Figure 18). As the gasket continues to deteriorate, increasing amounts of water and decreasing amounts of the tar would be noted running from the hatch. The gasket would begin to tear, crack and wrinkle, exposing the corroded surface of the access cover (see Figure 19). It is uncertain whether the deterioration of the gasket caused the hatch to leak or if the leaking hatch caused the gasket to deteriorate. However, a significant amount of the hatches using asphalt impregnated gaskets allowed water to enter the cap. The hatches using elastomeric gaskets also had cases of leakage; the leakage is due to lack of a proper seal, and not from deterioration.

The leaking gaskets allow water and roadway drainage to pass into the cap. This condition also promotes corrosion between the hatch cover and the cap. The corrosion causes the hatch cover to bow and further funnel more water into the cap (see Figure 20). Once inside the cap, the moisture

Figure 20. Access Hatch Cover Bowing Due to Corrosion

Figure 21. Condensation on Inside of Box Cap Member

causes high humidity, condensation, ponding water, corrosion and peeling paint (see Figure 21). Ponding water in one cap measured a maximum of 1/2-inch deep (see Figure 22).

Temporary utility lines at a construction site were attached to the handles of the access hatch cover. The tension in the utility lines has bowed the access cover away from the cap allowing moisture to enter the cap.

The access hatches were repaired by adding additional bolts to decrease bolt spacing. Elastomeric gaskets and caulking were also used to seal the caps. The utility lines were recommended to be removed from the hatch cover.

Openings for Utilities and Retrofit Details in Webs of Box Cap Members Allows Birds, Moisture, and Debris to Enter the Cap.

Holes and sawcuts made through the cap webs to prevent crack growth at fatigue prone details and openings cut in the webs for a water main were observed (see Figure 23). The openings allow birds, debris, and moisture to enter the cap. These conditions have caused peeling paint and corrosion of the cap. The bird droppings and nesting material deteriorates the paint and holds moisture.

Nesting material inside one cap measured 18 inches deep (see Figure 24). This debris inhibits inspection inside the cap.

The Interior of the Box Caps Typically Have Only a Primer Coat of Paint.

The primer coat does not adequately protect the steel if moisture enters the cap. Mill scale on the interior face of the steel is typical. The paint is peeling or easily removed at

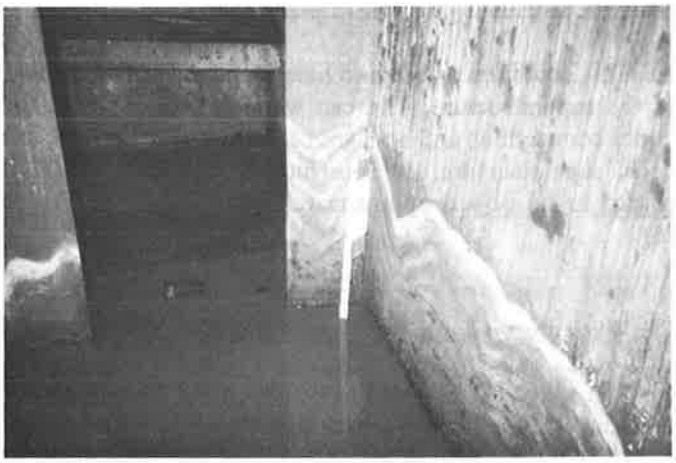

Figure 22. Water Accumulated Inside Box Cap Member Due to Leakage of Access Hatch Cover.

these locations. The primer paint also does not reflect light well, making inspection inside the cap more difficult. Areas of burned and blistered paint are typical on the inside of the cap where welds were made to the cap exterior.

Cap Bearings are Not as Shown on the Design Plans.

A multi-span bridge composed of continuous steel girders is supported over several piers using steel box pier caps. The girders frame through the pier caps. The center pier has fixed bearings between the cap and concrete columns, while the remaining caps were designed to have sliding bearings. During our inspection, it was discovered

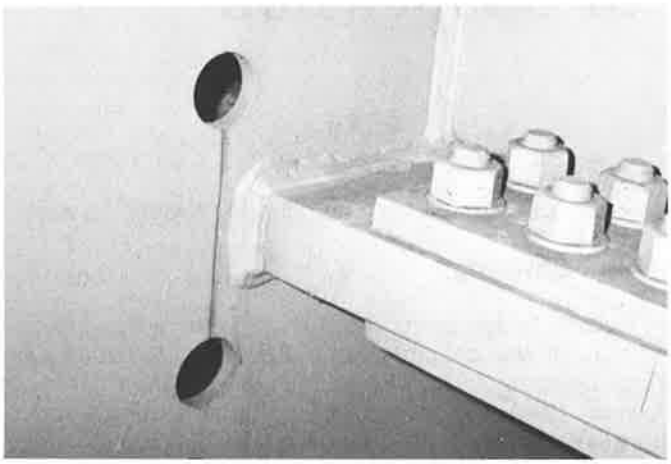

Figure 23. Retrofit Detail Cut in Cap Webs of Box Cap Member

Figure 24. Nesting Material Inside Box Cap Member

that two caps actually had fixed bearings. The expansion of the bridge between the fixed bearings has caused the bearings to slide on top of the concrete columns. Movement of the base plate is evident by the unpainted and corroded areas adjacent to the anchor bolts. These unpainted areas at one time were under the anchor nuts.

A similar condition was noted on another bridge. The pier cap was designed to have the only fixed bearing of a series of continuous spans. However, during the inspection it was discovered that a sliding bearing had been installed at the cap and no fixed bearings existed between expansion joints.

SUMMARY

This project has shown some of the defects and problems encountered with steel pier caps. The clearance restrictions imposed on these members have caused the caps to be compacted within the bridge superstructure. For this reason, the caps typically contain many fatigue prone details. Although some details were included by design, some additional details and poor workmanship were a result of space and ventilation restrictions during fabrications. These details typically exist inside box cap members and cannot be inspected from the outside of the cap. Inspection of the cap interior is also impared by the same space limitation making a close visual examination difficult but necessary.

REFERENCE

1. *Fatigue and Fracture in Steel Bridges: Case Study.* John W. Fisher, 1984.

Studies on the Longevity of Suspension Bridge Cables

PETER SLUSZKA

Man has been building suspension bridges for at least 2,000 years; the earliest recorded example going back to 65 A.D. in China. Throughout the centuries, the main tension elements have evolved from primitive organic rope materials to iron chain, eyebars, and finally, wire. Since the first iron-wire cable suspension bridge (built in 1816 at Fairmount, Pennsylvania), the materials, design, and construction procedures have been refined to today's state of the art. We are still learning how well our design and construction methods for these structures will stand up over time. Recent in-depth inspections of three of New York's major suspension bridges have provided valuable information to compare the effects of variations of materials and construction details on the durability of parallel wire cables. The Brooklyn Bridge, possessor of the world's first steel wire cables, is now undergoing rehabilitation that will allow it to continue in service for its second century. The Williamsburg Bridge, which narrowly escaped demolition after a recent study to determine its fate, will have its cables cleaned, oiled, and rewrapped at an estimated cost of more than 60 million dollars. The Mid-Hudson Bridge, youngest of the three, will undergo a detailed study and testing program after strong evidence of stress corrosion cracking was found during a 1987 inspection and confirmed by observations made by Steinman engineers in 1989.

THE BRIDGES AND THEIR CABLES

The following paragraphs provide a brief description of each bridge. Detailed cable information is provided in table 1.

Brooklyn Bridge

The Brooklyn Bridge, which spans New York's East River, connecting Manhattan with Brooklyn Heights, is the most famous of John A. Roebling's suspension bridges. Completed in 1883, the bridge is now a national monument. The exact number of wires in each of the main cables is not known because Roebling called for the addition of supplemental wires after discovering that an unscrupulous contractor had tricked the engineers into spinning some inferior wire into the cables. After spinning, the cables were compacted, coated with a thick paste of white lead, and then tightly wrapped with galvanized steel wire. This was then sealed with several coats of paint.

Williamsburg Bridge

The Williamsburg Bridge, completed in 1903, is within sight of the Brooklyn Bridge, and spans the East River between Manhattan and the Williamsburg section of Brooklyn. Its designer, Lefferts L. Buck, took it as a personal challenge to construct the bridge with a greater main span length than Brooklyn Bridge and to do it in a shorter time at less expense. The cable wire was drawn and cables were spun by John A. Roebling's sons. Buck decided to depart from usual practice where instead of galvanizing the cable wires and wrapping them with wire, the cables were coated with a mixture of graphite and oil, wrapped in cotton duck impregnated with an asphaltic compound, and then covered with sheet steel. By 1921 the sheet steel covering had corroded so badly that it was removed and replaced with galvanized wrapping wire.

Mid-Hudson Bridge

Mid-Hudson Bridge spans the Hudson River at Poughkeepsie, N.Y. It was constructed in 1929-30 by the American Bridge Company. The wire for the cables was supplied by American Steel and Wire Company, a sister organization. This was one of the earliest contracts of bridge wire manufacture and cable spinning undertaken by these companies, a fact that may prove to be significant in the ultimate fate of the bridge. The cables were compacted, painted with red lead, wrapped with soft galvanized wire, and finally coated with three coats of lead-based paint.

TABLE 1. CABLE INFORMATION

CHARACTERISTIC	BROOKLYN BRIDGE	WILLIAMSBURG BRIDGE	MID-HUDSON BRIDGE
Main Span	1,595.5 ft (486 m)	1,600,ft (488 m)	1,500 ft. (457m)
Side spans (2)	933 ft. (285m)	596.5 ft (182m)	750 ft. (229m)
No. of Main Cables	4	4	2
Wires per cable	~ 5,434	7,696	6,080
Wire Diameter	0.180 in (4.57 mm) 0.184 in (4.67 mm) [after galvanizing]	0.192 in (4.88mm)	0.192 in (4.88 mm) 0.196 in (4.98 mm) [after galvanizing]
Compacted Cable Diameter	15.75 in (400 mm)	18.75 in (476 mm)	16.75 in (425 mm)
Average tensile strength of wire	160,000 psi (1,100 MPa)	218,000 psi (1,500 MPa)	215,000 psi (1,480 MPa)
Average 2% offset yield point	106,000 psi (730 MPa)	191,000 psi (1,310 MPa)*	Not Available
Average recovered elongation in 10 inch gage length	2.88%	2.6%	2.5%**
Average reduction in area at fracture	15.6%	20%	23%**
Maximum Working Stress (Nominal)	46,000 psi (320 MPa)	56,000 psi (390 MPa)	56,000 psi (390 MPa)

* Based on limited tests, 1988
** Based on limited tests, 1989

INSPECTION, SAMPLING AND TESTING

Brooklyn Bridge

Inspection of the Brooklyn Bridge cables was performed in two distinct parts: wrapped areas between the anchorages and the unwrapped individual strands within the anchorage chambers. The four cables were visually inspected end to end. Based on conditions observed, an in-depth investigation was programmed.

Wrapped Portions

Two sections of the cable in the main span and one section in the Manhattan side span were unwrapped and split open with oak wedges. Because cable bands are located every 7.5 feet (2.3 meters), it was first necessary to remove the suspender and cable band (or cable post in areas where the cable passes below the floorbeams) to provide enough free cable to penetrate with the wedges. Unlike modern practice, the cable bands were installed over the wire wrapping. It was found that the wrapping wire beneath the cable bands had begun to corrode significantly due to the tendency for moisture to lay between the ribbed surface of the wrapping and the smooth inner surface of the cable bands. The outer layer of main cable wires immediately below the wrapping and cable bands had corroded sufficiently to consume most of the zinc galvanization, and rusting of the wires had occurred. One wire broke after losing more than 75 percent of its cross section. The remainder exhibited localized loss of material that is commonly referred to as "pitting" although in the strict technical definition no real pits were present (a pit is a defect that is at least as deep as its width at the surface). At the areas between the cable bands, the surface wires were still in excellent condition. Dried white lead paste covered most of the surface, but in occasional spots powdery zinc oxide from the galvanizing coated the exposed wires. Oak wedges were driven between the wires at four radial points (one point at a time) and the cable was penetrated approximately 6 inches (15 cm), or almost to its center. It was found, even under the cable bands, that all corrosion had been limited to the outside layer of wires. From the second layer in, the original galvanizing was still in near-perfect condition.

Fifty-seven wire samples were cut from the cables at various locations and sent to Columbia University's Carleton Laboratory for testing. The cut wires were replaced with lengths of new wire spliced in using a combination of pressed-on and threaded ferrules. The results indicated that the typical corroded wires had not lost measurable strength as compared to the uncorroded wires, but it was apparent that the original material was not uniform and was of considerably lesser quality than modern bridge wire. Carbon content varied from 0.55 to 0.91 percent, whereas modern wire is generally in the range of 0.78 to 0.82 percent. Average tensile strength was 160,000 psi (1,100 MPa), and the 2 percent offset yield point was approximately 106,000 psi (730 MPa). The most significant finding was that the original wire was of low ductility: reduction of area varied from practically 0 to 26.5 percent, averaging 16 percent (reduction of area for modern galvanized bridge wire is typically 35 percent).

The samples and results of these tests were evaluated by various materials experts, including faculty members of Columbia University and bridge wire specialists at Steinman. While the small reduction of area values indicated low ductility, it was concluded that the wire had not suffered any degradation from its original condition. Fracture surfaces indicated failure by microvoid coalescence originating within the wire. The low ductility was attributed to the coarse pearlite grain structure.

It is interesting to note that Roebling had originally specified that each cable be comprised of 6,308 wires of No. 8 Birmingham Gauge, which would have a diameter of 0.165 inch (4.19 mm), but the cables are actually made of 0.184 inch (4.67 mm) wire. It appears that the larger size wire was obtained by drawing the rolled rod through one die, rather than drawing twice, as would be necessary to produce the smaller wire. The "underdrawing" is considered the primary reason for the coarse grain structure. It is believed the wire size was changed due to difficulties encountered in drawing the smaller wire.

Fatigue testing results and microscopic examination of longitudinally sectioned wires provided the assurance that there was no evidence of stress corrosion cracking in the wires.

Cables at Anchorages

The initial inspection in the anchorages revealed conditions of serious concern. Here, the cables changed their configuration from a single, large, tightly wrapped cylinder to 19 individual, unwrapped strands of 286 (the generally accepted number) wires each. Each strand further separated into two halves before looping around the strand shoes that are pinned to an eyebar chain buried in the masonry. At the point of transition from one cable to 19 strands, the cable was clamped by a forged steel splay band. Serious corrosion and numerous broken wires were found between the splay band and strand shoes as well as at the back of the shoes, where concrete had been placed in contact with the wires. The confined space of the anchor chambers had barely enough room for a man to pass between the strands and the chamber walls. Therefore, it was impossible to determine the full extent of corrosion damage at the shoes or within close proximity to the splay band. Extraordinary measures would be necessary in order to fully examine and evaluate the conditions at the anchorages. The possibility existed that entire strands were damaged beyond repair. It was therefore decided to develop procedures and equipment to splice entire strands concurrently with developing a detailed program to continue investigation.

First, the anchor chambers would need to be enlarged to provide working space; second, the existing splay bands would need to be removed to allow spreading of the strands for inspection at the splay points; and third, repair details for various possible conditions needed to be developed. With the assistance of Carleton Laboratory, a mock-up of a typical anchor chamber and splayed cable was constructed. Clamps, sockets, and jacking equipment were designed for the worst-case scenario, in which entire strands would need to be cut, socketed, and reanchored in the field, something never done before. New splay bands and strand spreader frames were also designed. Working in the mock-up, methods were tested for zinc-socketing of the strands in the horizontal, rather than the usual vertical, position. This was achieved by inserting the cleaned strand into a cast steel socket, "brooming" the wires within the socket's conical cavity, and then filling the cavity with molten zinc. To provide working room, the existing anchor chambers would need to be enlarged in width and

height by approximately 3 feet (1 m). Tests on the temporary strand, hold-back clamps, and the poured zinc sockets showed that the strand replacement scheme was practical.

The next step was to enlarge the chambers, relocate the cable splay points, and, if needed, to cut and replace the deteriorated strands. It was decided to start at Cable B in the Brooklyn Anchorage. After the chamber had been modified, two temporary splay bands were installed spanward of the existing band, and the old band was removed. In a series of "leap frog" moves, the two temporary bands were moved up along the cable until they reached the location of a new permanent splay band about 12 feet (4 meters) from the original splay. Horizontal and vertical spreader frames were placed between the strands and the strands were gradually spread apart using specially designed hydraulic equipment. The placement of the new splay was such that the total length of each strand would be unchanged after the splay relocation was completed. Strain gauges were used to monitor stresses in the anchor eyebars as the strands were spread. Upon completion of the strand spreading and removal of concrete behind the strand shoes, a detailed inspection was made strand by strand. Fortunately, the serious corrosion and breaks were primarily confined to surface wires. Most of the wires were slightly corroded or uncorroded, although much of the galvanizing zinc had been consumed by oxidation. The operation proceeded on to the remaining seven anchorages and similar conditions were found. All in all, several hundred broken or seriously corroded wires were found, but these were repairable by splicing in new sections of wire, and no full strands needed to be replaced. Test results on wire samples from the anchorages were essentially identical to the results obtained from the wrapped cable, indicating no insidious degradation, such as hydrogen embrittlement or stress corrosion cracking. This work was completed in early 1987.

Williamsburg Bridge

Williamsburg Bridge has had a long, troublesome reputation as one of the few remaining suspension bridges in the U.S. with bright (ungalvanized) wire cables. Historical records indicate that hundreds of broken wires had been repaired over its life and several attempts had been made to pour various oils into the cables to stem corrosion. One study conducted in the early 1980's concluded that by 1992, the cables would be unsafe to carry the heavy live loads of the combined truck, automobile, and rapid transit traffic that use the bridge. Since it was recognized that the earlier study relied heavily on theory and was not supported by sufficient hard data, Steinman was requested to perform immediate and in-depth investigations into the condition and capacity of the main cables. As in the Brooklyn Bridge project, separate approaches were developed for the wrapped portions of the cables and the unwrapped, splayed strands in the anchorages.

Wrapped Portions

A few exotic methods were used to evaluate the condition of the main cables, such as geometric survey of cable sag and photogrammetric deflection measurements under controlled live loads. These seemed to indicate that the cables were actually behaving as they should if no significant loss of strength or elastic properties had occurred. The main thrust of the investigation, however, centered around inspection, sampling, and testing of a statistically significant number of wires from the surfaces and interiors of the cables. Using procedures similar to those on the Brooklyn Bridge, five sections of four cables were unwrapped and wedged open. At each 30 to 40 foot (9 - 12 m) long site, the cable was wedged at eight radial locations, penetrating fully through the center. At each opened groove, four wire samples were cut and removed at predetermined depths. The wires were gauge-marked prior to cutting and their retractions were measured after cutting in order to estimate their actual existing tension. These tests generally confirmed that the wires were equally loaded and were under the anticipated theoretical tension.

More than 160 wires, 20 to 30 feet (6 - 9 m) long, were removed and sent to Carleton for metallurgic examination and testing. Each sample was subdivided into 18-inch (0.5 m) lengths which were inspected and graded according to the apparent degree of corrosion. After testing, the wires were cleaned by non-detrimental methods and reinspected. It was generally found that the extent of actual corrosion was difficult to assess prior to cleaning due to a mixture of oil residues that coated the wires. An apparently corroded wire often appeared in excellent condition after cleaning. A computer program was designed to randomly select samples for testing. More than 1,700 specimens were subjected to tensile tests. Their ultimate strength, recovered elongation, and percent reduction in area were recorded. Several specimens were tested expressly to plot representative stress-strain curves. The average ultimate tensile strength of the wires was 218,000 psi (1,500 MPa). The reduction of area at the fracture averaged about 20 percent. The average recovered elongation was 2.6 percent in 10 inches (254 mm). Chemical tests indicated that the carbon content of the wire varied from 0.6 to 1.1 percent. All tensile test specimens were subjected to fractographic examination and selected specimens of wires were sectioned, polished, and examined under a scanning electron microscope. Approximately 160 specimens were subjected to pulsating fatigue tests.

The conclusions drawn from the visual inspection, testing, and statistical analyses were that the cables had only suffered significant corrosion of a small portion of the wires, primarily in the segment of the bottom third of the cable cross-section, where moisture tended to collect and remain trapped. It was only these heavily corroded wires that exhibited serious loss of strength and possible damage from hydrogen embrittlement due to their proximity to the galvanized wrapping wire. A few broken wires exhibited stress corrosion-type penetration, but these wires were also so grossly corroded that they were not in any way representative of the typical wire population. There was no evidence of stress corrosion cracking or hydrogen embrittlement in the remainder of the cables. While the average recovered elongation of the cable wires was substantially lower than the original specifications, it was concluded that they were essentially unchanged from their original conditions. Historical records indicate that the steel billets, from which the wire was made, was of such variable quality that a major lawsuit ensued in which the Roebling Company sought compensation from the steel supplier for the tonnage of wasted material that was not drawable due to excessive carbon content. It is the high carbon content that is responsible for the low elongation of the wire and not environmental degradation as was once suspected. The existing stress range of the cables is well below the apparent endurance limit of the wire. The overall assessment was that

the existing cables still retain an ultimate safety factor of at least 3.5, a larger strength reserve than a modern cable would be designed for.

Cables at Anchorages

There were documented repairs to broken wires in the anchorages performed at various times during the bridge's history. At the time of Steinman's inspection, the area of greatest concern was at the Manhattan end of cable D (the northernmost cable). Between the splay casting and strand shoes, hundreds of broken wires were visible, jutting out in various directions in clusters and individually. It was clear that most of the breaks had occurred near the bellmouth of the splay casting, which was located at the outside face of the anchorage wall. The broken wire ends were, in general, grossly corroded, with some reduced to a "pencil point" at the break. Heavy leakage was getting to the wires, but since the cable and splay casting were obscured at the masonry wall, it was impossible to determine the cause or full extent of the damage. A detailed inspection revealed that strands 19 and 20 had each lost virtually all 208 of their wires.

An important goal of Steinman's cable investigation was to determine the remaining load capacity and safety factor of the existing cable system. Based on conditions observed, Cable D in the Manhattan anchorage was the obvious critical location. Because the deterioration had concentrated at some strands more than at others, it was desirable to determine the actual distribution of load in each of the 37 strands. This would permit the analysis of ultimate cable strength by modelling a sequence of progressive failure of the critically loaded strands. It was also necessary to determine the extent of damage to the cable at the splay point. A procedure to accomplish both of these goals was developed by Steinman.

The 49 eyebars, to which the strands were anchored, were equipped with strain gauges wired to a PC based scanner and data recorder. These gauges would register changes in axial force and bending in the eyebars. The dead load in each eyebar was then determined by attaching an electronic accelerometer that measured the bar's natural frequency of vibration (the bars constantly vibrate on their own), and computing the corresponding tension. Because each group of four strands was anchored to three eyebars, it was not possible to compute individual strand loads directly from the known eyebar loads. Relative loads in each strand were therefore determined by measuring the force required to deflect each strand, horizontally, a set amount. While this would not have been accurate enough to deduce the strand loads directly, it was sufficiently accurate to yield the relative loads. Using the data obtained the actual dead load was determined in each strand with a high degree of confidence.

To determine the condition of the cable at the splay required drastic steps. The anchorage wall masonry was partially removed, enlarging the cable opening to approximately 9 by 12 feet (3 by 4 m). Then at 10 PM on Friday, January 8, 1988, the bridge was closed to all transit and vehicular traffic. With temporary splay castings in place, the original splay casting was removed. By leap frogging the temporary castings in the method developed on Brooklyn Bridge, the cable was gradually spread out, enabling a detailed inspection of the wires previously hidden by the masonry and the splay casting. The eyebar-mounted strain gauges were used to continuously monitor the stresses in the eyebars and strands as the strands were spread apart and the strand shoes rotated. As more wires became visible, Steinman engineers updated the count of corroded and broken wires, and the data was fed into a PC in the anchorage that was programmed to compute the cable's factor of safety. The bridge was reopened to all traffic by noon Saturday. A total of less than 500 wires was found to be significantly corroded. Most of the damage had been confined to a local area at the downhill edge of the old splay casting where water and debris tended to collect. The safety factor of this cable was computed as 3.5.

Mid-Hudson Bridge

The cables of the Mid-Hudson Bridge were inspected in 1969 by means of unwrapping short lengths of both cables near the bridge's mid-point and the south cable near the west anchorage. This unwrapping consisted of the removal of two of the three plies of wrapping wire in order to inspect the main longitudinal wires immediately underneath. Some deterioration of the galvanized coating of the longitudinal cable wires was recorded, together with some areas of steel surface corrosion and light "pitting," primarily on the underside of the cables. The overall condition of the cables was recorded as "generally good."

In 1981 and 1982, various short lengths of wrapping wire were removed to inspect the cable wires at 10 locations. Increased deterioration of the cable wires was recorded near the midpoint of the center span, with lesser amounts of surface corrosion and "pitting" at the other locations. In 1982, approximately 6.5 feet (2 m) of cable was unwrapped between panel points 75 and 76. The cable was probed to a depth of approximately 2.5 inches (63.5 mm) by spreading with wooden wedges to view inner wires. Significant corrosion and "pitting" were recorded on the outer four layers of wire.

In 1987, at eight locations, one or two plies of the wrapping wires was removed for short lengths. At the midpoint of the center span on the south side, the cable was completely unwrapped for approximately 6.5 feet (2 m). One broken wire was discovered at this latter point, and five wires, each approximately 5.5 feet (1.7 m), were removed from the cable for observation and testing. Laboratory tests undertaken on the five wire specimens included fatigue testing at varying stress ranges, static load testing to failure, fractographic examination of the failed cable wire, and chemical analysis of corrosion product samples taken from the cable wires. Some specimens from the fatigue tests broke at obvious pre-existing crack sites, where penetration of a black corrosion product was readily visible. Microscopic examinations revealed many secondary cracks common to classic stress corrosion cracking.

In 1989, Steinman was asked to assist in a further investigation of the cables, and to provide a report on the observed conditions. The north cable between panel points 75 and 76 was the first section to be unwrapped. Two broken wires were evident in this 15-foot (4.6 m) section. Both wires were in the upper half of the cable and in the outer two layers of wires. The lower half of the cable exhibited fairly heavy corrosion, tending towards the north side lower quadrant. This corrosion was generally limited to the outer two or three layers of wire. There was also evidence of local concentrated corrosion of the main wires at all locations in the cable. This was observed in stages, from small local black corrosion products to larger areas of localized section loss, all on otherwise apparently

clean wire. The south cable at panel point 72 was the first position on the bridge to have a suspender and cable band removed. It was centered approximately 40 feet (12.2 m) west of the main span midpoint. Eight broken wires were evident in this 20-foot (6.1 m) length. The majority of these breaks were in the lower half of the cable, and in the outer two or three layers of wires; but one broken wire was recorded at approximately 3 inches (76.2 mm) into the cable (12 o'clock opening). The lower half of the cable exhibited heavy corrosion on the outer layers of wires, which penetrated the cable up to three wires deep. There was also local concentrated corrosion of the wires, from surface black marks to deep local depressions, with black corrosion products showing up in the depressions. This corrosion was present, in varying degrees, at all positions in the cable.

When the cable band was removed from the cable, a section of seizing wire (5 or 6 turns) was discovered under the center line of the cable band. The cable bands were fabricated with a groove passing all around the cable presumably to accommodate this seizing wire. However, the wires of this short section were heavily corroded, and each of the main cable wires in contact with this seizing wire had a spot of corrosion at or adjacent to the contact point. The caulking of the circumferential edges of the cable bands was originally done using lead wool. The samples of lead wool that were observed after the cable band had been removed, appeared to be porous and not fully compacted. This is conducive to the absorption of moisture by capillary action.

The north cable at panel point 125 was the third site chosen. This location is approximately at the two-thirds point of the east side span measured from the east anchorage towards the east tower. It was the last position to be inspected. The suspender and cable band were removed, the cable was unwrapped for approximately 10 feet (3 m) on either side of the suspender center line, and the cable was wedged at selected positions around the perimeter. Three broken wires were recorded. The locations of the breaks corresponded with the positions of the upper location lugs of the cable band at the downhill position. It is possible that these wires were crimped during the assembly and the tightening of the cable band. A section of seizing wire was located at the center line of the cable band, with corrosion similar to that described for the south cable, panel point 72. The main cable wires on the uphill (west) side of the cable band location were in fair condition with some moderate corrosion on the lower half of the outer layer of wires. The cable surface under the band location, and downhill from the band location, was heavily corroded over a large section of the outside surface. Corrosion was also observed in the grooves introduced by the wedges. The worst visible corrosion was on the top surface of the cable for some 8 to 10 feet downhill from the cable band location. There were no wrapping wire indentation marks in the heavy brown corrosion products that were found downhill from the cable band, which would indicate that the wrapping wire was not tight. The local concentrated corrosion, previously described for panel points at the north and south cables, was also evident at this panel point. Again, it was observed generally at all positions within the cable, but the majority of cases were adjacent to the heavy corrosion areas. Lengths of the broken wires have been removed for physical and chemical testing and fractographic analysis.

CABLE REHABILITATION PROGRAMS

Brooklyn Bridge

There were several factors that influenced the scope of rehabilitation for the Brooklyn Bridge cables. Contrary to present practice, the cables had been wire-wrapped continuously prior to installation of the cable bands and suspenders. While the original wrapping had admirably protected the cables throughout most of their length, the cable bands were trapping moisture and corrosion was taking place beneath them. The bands were also prone to slipping downhill on the cable because their design precluded a secure clamping effect. The original white lead paste was dried out and did not provide the necessary sealing between the wrapping wires. It was also found that virtually all of the wire rope suspenders were seriously corroded near their lower sockets, and would need to be replaced, as would the diagonal wire rope stays.

The cable rehabilitation contract, designed and inspected by Steinman, includes the removal of all existing wire wrapping, cable bands, suspenders, and stays. New bands of modern design and new suspenders will be installed, followed by the rewrapping and painting of the cables. The greater part of the cables will be rewrapped with galvanized wire bedded in a thick paste of red lead. At the sag points, where the cables pass near or below the roadway and are subject to splash by runoff water and deicing salts, the cables will be wrapped with 1/8 inch (3 mm) thick neoprene wrapping material. All eight anchorage chambers have been enlarged. They now provide ample space for inspection and maintenance of the strands, which will remain in their newly spread configuration. All broken and badly corroded wires have been replaced with sections of new wire, using a technique developed by Steinman. Since past experience shows that the cutting of threads on existing wires is difficult and uncertain, a length of damaged wire is first cut out and to its two ends new wires are spliced using specially designed ferrules. These ferrules consist of a mild steel cylinder, approximately 3/8 inch (10mm) in outside diameter, bored to accept a hardened helical steel wire insert of slightly larger inside diameter than the original bridge wires. After inserting the end of one old and one new wire into the ferrule, a hydraulic press crimps the ferrule onto the wire, developing a splice that is 95 percent as strong as the original wire. The two mating ends of the new wires, which have shop-cut threads, are then spliced using a ferrule with internal left- and right-hand threads. The threaded ferrules act like turnbuckles and permit the spliced wire to be stressed to a predetermined tension. After repair of the damaged wires, the cables are virtually as strong as when they were originally built.

The entire cable rehabilitation contract, including the replacement of stays and suspenders, will cost approximately $50 million, and is scheduled for completion in late 1990. It is fully expected that the rehabilitated Brooklyn Bridge will serve New York City for at least another 100 years.

Williamsburg Bridge

The Williamsburg Bridge obviously has not fared as well as Brooklyn Bridge. Unfortunate decisions made during the original design and later modifications resulted in a much less durable cable construction. The original decision to use bright

wire rather than galvanized now appears to have been "penny wise and pound foolish." Because hot dip galvanizing of bridge wire tends to lower its tensile strength by a few percentage points, Buck reasoned that he could design his cables with fewer wires and thus save money. The bright wire is also less expensive, pound for pound, than galvanized wire. While Buck's original sheet steel wrapping was a dismal failure, the error was not fully corrected when the cables were rewrapped in the 1930's. At that time, the cables were oiled, wrapped with galvanized wire, and painted. An important fact was overlooked - to be fully effective, wrapping wire must be bedded in a sealing compound such as red lead paste in order to fill the interstices between wires and to seal out moisture. Additionally, modern cable bands have grooves at their ends for the installation of caulking material and they include drainage openings to allow the escape of condensed open moisture. The cable bands of Williamsburg had no caulking grooves and no drainage openings, which let water enter, but not exit. Compounding the problem, the galvanized wrapping wire in contact with bright cable wire sets up a galvanic cell. While the zinc protects the steel from corroding, the electrochemical reaction produces hydrogen atoms at the surface of the steel, capable of penetrating into and embrittling the material.

Conditions in the anchorages varied. In the worst case (Cable D on the Manhattan side), localized corrosion had destroyed nearly all 208 wires in strand 20 and over half the wires of strand 19. Relocation of the original splay casting at this cable revealed that the damage had mainly been limited to the anchor-side strands. The wires under the wrapping, spanward of the splay casting, were found in generally excellent condition. Other anchorages contained some broken and corroded wires, but to a much lesser extent. Rehabilitation of Williamsburg's cables will require removal of all wrapping wire, cable bands, and suspenders. New properly designed bands and suspenders will be installed, after which the cables will be cleaned, oiled, and compacted. Bright steel wire wrapping, bedded in red lead paste, will be applied. The wrapping wire will be overwrapped with neoprene. This dual system will ensure that the cables remain tightly compacted and protected from water entry. Strands 19 and 20 of Cable D at the Manhattan anchorage will be cut and replaced with new strands using the procedures developed during Steinman's work on Brooklyn Bridge. The remaining deteriorated wires in all the anchorages will be repaired individually by splicing. Providing that the rehabilitation program is promptly carried out and the cables are properly maintained in the future, there is no reason that the Williamsburg will not serve for another 100 years. On the basis of our findings, the New York City and New York State Departments of Transportation have discarded two contingency plans: 1) to demolish and replace the entire bridge; and 2) to replace the main cables and rehabilitate the superstructure. The present plan to rehabilitate the cables is estimated to cost approximately $50 million, but will save more than $200 million, the amount needed to recable the bridge.

Mid-Hudson Bridge

Visual inspections of the cables indicate that the wrapping wire system on the main cables was inadequately installed, as red lead paint, instead of red lead paste, was used to coat the main cables. This has resulted in the formation of linear voids between the wrapping wire and the main cable wires which act as capillaries to absorb moisture in the event of any water getting past the wrapping wires. Existing documentation indicates that wrapping wire was installed to a tension of only 95 pounds (423 N). It is very likely that this tension relaxed significantly over time, as witnessed by the observed looseness. The caulking at the ends of the cable bands also seems to have been inadequately installed. This resulted in a spongy lead wool matrix which, contrary to the design intent, absorbs moisture through the porous lead wool instead of acting as a moisture barrier. This has been compounded by the lack of red lead paste between the cable band and cable, resulting in voids which allow the passage of moisture into the cable.

An important characteristic of the wire samples was the presence of many short transverse cracks on the inside curvature of wire No. 4 (6 o'clock position), taken from the north cable at panel point 125. This sample was stripped of its zinc coating to expose the as-drawn wire surfaces. The cracks could have been formed during wire drawing due to excessive cold working conditions, poor lubrication, or some mechanical defect on the hot-rolled rod surface. With regard to the manufacturing process of the wire, the reported practice of drawing down from a 0.625 inch diameter rod to a 0.192 inch diameter wire, a reduction of some 90 percent in area, is markedly different from accepted practice for bridge wire, which would normally be drawn from a 0.360 inch diameter rod, giving a reduction of some 72 percent. The 90 percent reduction would result in a far higher degree of cold working, giving a resultant loss in ductility. However, no figures are presently available for the wire ductility in the form of percentage elongation and cross-sectional area reduction on static load test specimens.

The preliminary conclusions concerning the cable manufacture are that the wires comprising the main cable have been subjected to excessive cold working which caused the formation of small transverse cracks on the surface of the wires. It appears that the zinc coating penetrated into the cracks during galvanizing. This would tend to embrittle the material at the crack tip. These cracks and the excessive cold working combine to make the wire distinctly susceptible to stress corrosion cracking. The present condition of the cable is a mix of galvanized wire and wire made bare by the loss of zinc due to oxidation. This mix of zinc and steel creates the potential for the formation of corrosion cells throughout the cable, which may generate hydrogen penetration into the wires. The hydrogen embrittled areas may in turn promote the stress corrosion cracks that have been found. It is suspected that each of the black spots observed throughout the cables may be a potential crack site.

This information isn't sufficient to draw definite conclusions regarding the status of the main cables, but the available evidence strongly indicates that stress corrosion is occurring. A detailed, rigorous, and methodical cable wire investigation will therefore be undertaken in order to determine the present capacity of the cables and their predicted life. The detailed investigation will include statistical wire sampling, at selected points along the cables, and a full program of laboratory testing of wires in order to establish a firm data base. The New York State Bridge Authority, along with its general consultant, began this investigation in early 1990. Steinman will continue to provide technical consultation as the work progresses.

CONCLUSION

The Brooklyn Bridge provides indisputable proof that Roebling's original cable protection system is effective when executed properly. However, the legendary degree of care and a number of other factors that went into the construction of this bridge make these cables unique. Each wire was coated with an oil/white lead mixture first in the shop, and again in the field before being loaded in the spinning apparatus. The strands were again coated prior to compacting and wrapping the cables. This formed an impervious mass that would resist moisture penetration even if the wrapping was not fully effective. Great care was then taken in compacting and wire-wrapping the cables. What little moisture did enter the cables over the past century was effectively handled by the galvanizing on the main wires. The net result is that the wrapped portions of the cables are still practically as good as new. In the anchorages, the unprotected strands had corroded. Much of the original zinc coating had oxidized and there is presently a mix of bare and galvanized wire near the strand shoes. However, the investigation has shown that the wires have not suffered any degradation of their physical properties. Although there has been the potential for hydrogen embrittlement and stress corrosion, no evidence was found. While hydrogen may well have been generated during the corrosion process, it may have dissipated over time. Since the Brooklyn Bridge wires are of relatively low strength and carry relatively low stress for bridge wire, they may not be susceptible to stress corrosion cracking nor sensitive to hydrogen penetration.

While the cables of the Williamsburg Bridge were not protected nearly as well as those of the Brooklyn Bridge, they have also survived in remarkably good condition after almost 90 years. These wires were also coated with various oils and binders during the manufacture and spinning, including lin seed oil and slushing oil mixed with graphite. The wrapping system did not effectively exclude the intrusion of water, and many wires did corrode. However, the significantly damaged wires were confined to those areas where water collected, and the oil apparently was effective in the other parts of the cables. In general, the damaged wires suffered from metal loss due to corrosion, with no embrittlement or cracking or change in physical properties. Samples of the bright wire that were in close proximity to the galvanized wrapping did appear to have lower ductility then the general population, and this is attributed to possible hydrogen embrittlement. Although this wire is nearly as strong as modern wire, its working stress is only 25 to 30 percent of its ultimate strength, a factor that would usually preclude stress corrosion cracking.

The Mid-Hudson Bridge is the most modern of the three, and the original specifications for its cable wire is very similar to present day specifications. However, the practices used in its manufacture are suspect and may have been misguided. The wire wrapping system is also similar to the system used on Brooklyn and subsequent bridges, but its execution appears to have been lacking in the application of a thick bedding compound, tightness of the wire, and caulking at the cable bands. The bridge wire received no oil or other coating over the galvanizing. Water freely penetrates these cables and the galvanizing has not been able to protect the interior bridge wires from corrosion. The surface defects created in the wire drawing compound the situation. All these factors together set the stage for stress corrosion cracking throughout the bridge's cables. Only further study will reveal the ultimate prognosis for the Mid-Hudson Bridge.

Overload Permit Checking Based on Structural Reliability

GONGKANG FU[1] AND FRED MOSES[2]

Overload permit issuance for vehicles exceeding the legal weights is a common practice in many states. Most states face increasing pressure to allow heavier and greater number of overweight truck permits. The current method of permit checking in most states adopts the concept of allowable stress with operating strengths. It does not provide uniform level of structural reliability. A rational permit checking method is therefore desired. Little research has been reported which derives a practical and rational format for permit checking. This paper proposes a format to check permit overloads based on structural reliability. Weigh-In-Motion data is used to model live load. Frequent, one-trip, and escorted permits are considered. This checking format is compatible to both load factor checking procedure of current AASHTO specifications and load and resistance factor methods under development. It can be included in a bridge structure evaluation.

1. INTRODUCTION

A large number of bridges in this country are considered structurally deficient or functionally obsolete. On the other hand, truck traffic has been growing in both volume and weight. Commercial vehicles with weights above the legal limit have frequently been observed on the public highway system. Furthermore, overweight permit issuance for vehicles exceeding the legal weights has been a common practice in many states. Increasing overweight loadings on the current U.S. highway system have been reported by FHWA to the congress [1], which provides the latest overview of the situation. The impact on bridge safety of this trend deserves careful investigation.

The passage of an overweight vehicle on bridges becomes a legitimate activity by obtaining an overload permit. Such permits are now issued by most highway agencies of the nation. In fact, it has been noticed that most states are faced with increasing pressure to allow heavier and greater number of overweight trucks to travel in the present highway network. This is because of the obvious economic advantages of heavy freight transportation and recognized conservativeness in bridge structure design. However, how much reserve strength can be used to meet the growing requests remains a critical issue. Even if vehicles utilize a greater length and number of axles which helps mitigate pavement damage, there will be questions regarding the safety of bridge structures which must carry the total loads.

The current method in most states to check the permit issuance for bridge safety uses the concept of operating strengths. This is acceptable because the current AASHTO bridge code [2] adopts this concept. Nevertheless, this method is not rational regarding bridge structural reliability for the specific issue of permit overloading. First of all, the allowable stress checking methods associated with most bridge evaluation using the operating strength do not provide uniform safety level. Secondly, bridge structural safety is sensitive to the maximum load effect by extremely heavy loadings largely affected by permit traffic. This is not covered by the current code supposedly addressing only random, mostly legal, traffic flow. A rational permit checking procedure is therefore desired, which should be based on a more realistic modeling of the permit live loads, and should provide a more uniform level of structural reliability.

Cassano and LeBeau [3] addressed the issue of permit overload in the context of design criteria. They suggested that the permit overload be included in design as an additional load case. This suggestion was based on a deterministic example of design calculation. Bakht and Jaeger [4] suggested a procedure of calculating safe permit loads, which are based on the worst combination of maximum vehicle weights that a bridge is likely to have sustained during its life time. This procedure is not generally applicable, especially in the US, as the information on the worst loading ever carried by a bridge is not usually available to evaluation engineers. Ghosn and Moses [5] were the first researchers dealing with permit overload based on the criterion of structural reliability to quantitatively cover the uncertainties. They assessed structural reliability for permit checking with the operating stress. Permit checking equations were suggested for two cases of

1 New York State Dept. of Transportation
2 Case Western Reserve University

permit vehicle presence, namely, a permit vehicle alongside another permit vehicle and a permit vehicle alongside with a normal truck. However it was unknown to evaluation engineers just how possible those extreme cases would be.

Little research has been reported which derives a practical and rational format to check the permit loads in terms of structural reliability. This paper presents a study in this direction supported by the Ohio Department of Transportation and the New York State Department of Transportation in cooperation with the Federal Highway Administration. A format to check permit overloads based on structural reliability is proposed herein for possible inclusion in a bridge evaluation code. This format is compatible to both load factor checking procedures of current AASHTO specifications [6] and load and resistance factor methods under development [7]. Different types of permits such as frequent, one-trip and escorted permits are considered. The load factors illustrated herein are for the case of steel girder bridges regarding bending moment strength checking. Nevertheless, the concept of the derivation procedure can be applied to other cases such as shear strength, concrete or prestressed concrete bridges, etc.

2. TYPES OF OVERWEIGHT PERMITS

In this study, overweight permits are considered in three categories of travel, namely I) frequent or routine trips, II) one-trip or special trip, and III) escorted or controlled trip. Accordingly, the analysis methods to select load factors vary from one category to another in order to include various levels of uncertainties especially involved with live or vehicular load.

Frequent or routine permits are those valid for unlimited passages without escort on specific routes in certain periods, varying from a few weeks to as long as 3 years. It is noted that this type of permit is the most beneficial one, in terms of redeeming the costs by reduced administration costs and added productivity for the carriers receiving the permits [1]. The presence of frequent permit vehicles on the highway system changes the live load spectrum of highway bridges from the normal traffic including illegal overloads. In turn, the probability distribution of maximum load effects experienced by these bridges is affected by these permits.

One-trip or special permits are valid only for single trip on a specific route without escort. They are usually issued for those vehicles which fit between frequent and escorted permit vehicles in terms of weight and/or size. The bridge live load in this case is analyzed herein by considering the permit vehicle plus whatever random vehicle may be alongside as needed. The maximum live load effect prediction concentrates on the possible alongside vehicle, since the permit vehicle is known with respect to its weight and configuration.

Escorted or controlled permits are issued to those overweight vehicles requiring escort. They are for passages of excessively heavy loads such as large power generators, machinery, aerospace equipment, etc. The information on those extremely heavy vehicles is usually available in terms of their axle weights and spacings. Additionally, no other vehicles will be allowed on the bridge alongside those escorted vehicles. Dynamic load impact can also be controlled by low speed if necessary. This presents the simplest case of live load modeling for permit checking.

3. PERMIT CHECKING EQUATION AND STRUCTURAL RELIABILITY

Current practice of structural strength checking in US is moving towards the use of load and resistance factors. As a matter of fact, current AASHTO bridge code [2] allows a load factor checking format evaluation. Furthermore, the format of load and resistance factors allows flexibility for adjusting those factors in order to reach a relatively uniform level of structural reliability, with respect to variation of loading distributions such as various ratios of dead to live load effects. A uniform checking format of load and resistance factors is therefore suggested for the three types of permits considered herein:

$$\phi R_n > \gamma_D D_n + \gamma_L L_p \quad (1)$$

where ϕ, γ_D and γ_L are respectively factors of resistance or capacity reduction, dead (gravity) load and live (vehicle) load, and R_n, D_n and L_p are respectively nominal values of component capacity (resistance), dead load effect and permit load effect including dynamic impact. This checking procedure is similar to load factor design (or rating) in AASHTO specifications [2,6]. Determination of the factors for checking equation (1) is a major focus herein. Structural reliability is used as the criterion to make such decisions.

Structural engineering calculations in both design and evaluation are supposed to cover uncertainties involved. This

well known fact is implicitly addressed in current and previous codes by safety factors in checking equations. Until recently those safety factors are determined by evaluation primarily based on engineering experiences. It should be noted that, therefore, these factors may not be rationally related to the uncertainties intended to be covered. Structural reliability theory quantifies these uncertainties in the context of relative probability. It therefore provides a realistic criterion for decision making in structural engineering problems. This approach is employed here.

Corresponding to the checking format using nominal values in Eq.(1) a safety margin z of a structural component being checked for permit issuance is

$$z = R - D - L \tag{2}$$

where R, D and L are respectively true values of component strength (resistance), dead load effect and live load effect in the component. A negative value of the safety margin indicates failure of the structural component. R, D and L are considered as random variables with uncertainties due to uncontrolled variations in design, construction, service condition, etc. They are assumed of lognormal distribution, and independent of each other.

The safety at component level is expressed by the so-called reliability index beta ß [8]

$$ß = m_z / \sigma_z \tag{3}$$

where m_z and σ_z are mean value and standard deviation of the safety margin z, respectively. Beta covers the uncertainties by including the scatter described by the standard deviation. An advanced algorithm [8] is used to compute the reliability index. This index is utilized as the indicator of structural safety level, and is similar to the safety indices being developed for the new AASHTO LRFD code.

It is noted that engineers use Eq.(1) for component strength checking by using nominal, instead of true, values of resistance (R), dead load effect (D) and live load effect (L). Resistance and load factors ϕ, γ_D and γ_L are applied only to those nominal values as expressed in Eq.(1). Given statistical information on load effects D and L, the mean value of random variable R of Eq.(2) varies according to the load and resistance factors used in Eq.(1), and so does reliability index ß in turn. This mechanism allows adjustment of these factors in order to reach a target reliability index ß. Determination of the relative magnitudes between dead load factor and live load factor can be made to produce relatively uniform beta over the distributions of dead and live load, which are usually span dependent.

4. MODELING OF LIVE LOAD EFFECT

Bridges are designed to safely withstand the maximum load expected over the service lifetime of the structure. It is therefore critical to have a rational prediction of the maximum live load effect L of Eq.(2) The model of maximum bending moment introduced by Moses and Ghosn [9] is employed here:

$$L = M\ g\ i \tag{4}$$

where M is total static live load moment, or shear, due to vehicle combination, g is load effect distribution factor for individual girder and i is impact factor taking dynamic response into account. They are assumed of lognormal distribution. L_p of Eq.(1) is the nominal value of L, and is accordingly computed as follows

$$L_p = M_p\ g_n\ i_n \tag{5}$$

where M_p is static moment due to the permit vehicle, g_n and i_n are code specified nominal values of girder distribution factor and dynamic impact factor, respectively.

According to Moses and Verma [10], the bias (ratio of mean value to nominal value) and coefficient of variation (COV) of lateral distribution factor g are set equal to 1.0 and 10%, respectively. The mean and COV of i are taken as 1.2 and 10%, respectively. The nominal values g_n and i_n are computed according to the simplified lateral distribution and impact formula in the AASHTO specifications [6].

Maximum bending moment M was predicted in this research by taking various factors into account, such as truck gross weight distribution (histogram), multiple presence of trucks on the bridge, traffic volume, site variation of traffic conditions, etc. The prediction is done for the three cases of permit loadings, and for various span lengths from 30 ft to 210 ft of simple and continuous span bridges. A time period of two years is covered in the prediction of maximum live load effect M for reliability assessment. This selection is consistent with the current inspection interval for bridge structures in the US.

4.1 Maximum Load Effect Prediction for Frequent Permits

Frequent permits are issued for a limited time period and a specific route. The presence of these overload vehicles has evident impact on the bridge live load spectrum. This influence is significant at the higher weight end of gross weight distribution, which in turn makes it sensitive to the structural reliability affected by maximum load effect. A simulation program is developed to find the mean and COV of maximum live load effect M for this case. This algorithm is based on the concept of convolution introduced by Moses and Ghosn [9]:

$$P[m]=\Sigma\Sigma\Sigma P[\text{weights}]P[\text{locations}]P[\text{types}] \quad (6)$$

where m is a realization of maximum moment M; P[m] is the probability of such realization, in the event of vehicle presence on a bridge; P[weights], P[types] and P[locations] are respectively the probabilities of vehicle occurrence characterized by their weights, locations on the bridge, and types with respect to vehicle configuration. These probabilities were obtained by Weigh-In-Motion data [9]. The triple summation in Eq.(6) is taken over all the combinations of weight, type and location that induce maximum moment of magnitude m. The probabilistic distribution of maximum moment due to one event of truck presence on a bridge is readily obtained by varying m in the convolution of Eq.(6). This distribution is then projected to cover the period of 2 years given traffic volume. The mean and COV of the maximum moment M are calculated based on this projected distribution.

Typical vehicle gross weight histograms based on Weigh-In-Motion data used in convolution Eq.(6) are displayed in Figs. 1a and 1b for sites of unenforced and enforced weight control, respectively. It is noted that the added permit vehicle weight histogram tail is according to statistics of Ohio Department of Transportation. For the simulation, possible locations of truck presence are depicted in Fig.2. Presence probabilities of 1, 2, 3, or 4 vehicles are based on headway statistics of several Weigh-In-Motion sites [9].

Load effects above the permit vehicle response is due to vehicles which may closely follow the permit vehicle in the same lane or more importantly be located in the adjacent lanes. The latter may especially be significant. It has been found that the effect due to permit issuance is much more significant on the sites with adequate weight control enforcement, which has few overweight vehicles in the normal traffic. The mean value and COV of maximum moment M, including site variation of live load, is contained in Table 1 for simple span bridges of various lengths. They are listed according to traffic condition. Light and heavy traffic volumes refer to average daily truck traffic (ADTT) lower and higher than 1000 trucks/day, respectively. Table 1 shows that bridges at weight control unenforced sites are expected to experience higher maximum moments than at enforced sites, as the former observe more overweight trucks. It also shows in Table 1 that heavy traffic volume increases the mean, and decreases the COV of maximum moment M. The higher the traffic volume, the higher the expected maximum moment could be, and the more certain maximum moment could be higher.

4.2 Maximum Load Effect Prediction for One-Trip Permits

Permit vehicles of one-trip without escort have much lower frequency than the frequent or routine permit vehicles to be present in the highway systems. Therefore, reliability analysis should consider only one passage instead of multiple passages as in the case of frequent permits above. The simulation for maximum load effect M is conducted with a focus on the load effect due to possible alongside vehicles, as the permit vehicle is known in terms of its weight and configuration. A simulation program similar to that for frequent permit case is also developed to obtain the mean and COV of the additional moment due to possible alongside vehicles. In this case, one of the four slots in Fig.2 is reserved for the permit vehicle. The mean and COV of the alongside vehicle induced maximum moment, including site variation of live load, is listed in Table 2 for simple span bridges of various lengths. It is noted that normal traffic volume is irrelevant in this case since an alongside vehicle of normal traffic has a very small probability to be present. This is also shown by the relatively large COV in Table 2, indicating higher uncertainty of such presence.

4.3 Maximum Load Effect Prediction for Escorted Permits

Escorted permits are usually issued to those extremely heavy overload vehicles. Speed control may be exercised to reduce dynamic effect. This makes live load simulation in the reliability assessment unnecessary, since the true maximum moment, M, is known and no other vehicles are allowed to be alongside for certain.

5. PROBABILISTIC DESCRIPTION OF DEAD LOAD EFFECT AND RESISTANCE

In addition to the statistical information on live load described above, it is also important to establish an appropriate database for dead load effect and resistance. This information is needed to assess the reliability level of bridge structures in Eq.(3). Significant work of developing such database has been done by Moses and Verma [10], and Nowak and Zhou [11].

Bias and COV of dead load effect D are respectively taken equal to 1.0 and 10% according to Moses and Verma [10]. The unbiased D indicates that dead load effect can usually be computed with relatively good accuracy. The nominal value of dead load effect D_n is estimated for the derivation by an empirical equation suggested by Hansell and Viest [12]:

$$D_n = 0.0132 \text{ SpanLength(ft)} \; M_d \; g_n \; i_n \qquad (7)$$

where M_d is design live load effect and is assumed to be that due to HS-20 vehicle of AASHTO code [6].

The uncertainties in steel member behavior are due to variation in material yield, fabrication and accuracy of strength prediction theories. The bias and COV of resistance R are set equal to 1.1 and 12%, respectively [10]. The nominal value is based on material and section properties for the component being examined.

6. LOAD AND RESISTANCE FACTORS FOR PERMIT CHECKING

Current bridge evaluation in the US is performed according to AASHTO code [2,6]. The resistance factor and dead load factor of checking equation (1) are therefore chosen equal to 0.95 and 1.20 respectively, to be consistent with AASHTO Guide Specifications for Strength Evaluation of Existing Steel and Concrete Bridges [13]. For the three cases of permit issuance discussed above, live load factors γ_L are suggested in order to reach respective target reliability values.

6.1 Load Factors for Frequent Permits

For this case a target beta ß equal to 2.3 is selected. This target value is consistent with a recent study to prepare a new version of AASHTO bridge evaluation guidelines under development [7]. This target beta ß was obtained by a calibration of current practice according to AASHTO [2] using operating stress levels for checking [14,15].

The derived live load factor is listed in Table 3 for four cases of traffic conditions. The traffic condition addresses weight control status and traffic volume. It includes cases of weight control enforced - heavy traffic, weight control enforced - light traffic, weight control unenforced - heavy traffic and weight control unenforced - light traffic. A site with unenforced weight control may observe a significant number of illegal overweight passages. This will obviously affect the safety of a bridge structure on the site by higher expected maximum moment (see Table 1). Therefore a higher live load factor is suggested (1.20). As indicated in Table 3 the traffic volume also has influence on the bridge safety, i.e. a higher traffic volume reduces structural reliability since risk is increased thereby. The traffic volume is defined by the number of ADTT. A site is considered of light traffic volume if its ADTT is lower than 1000 trucks/day, and of high traffic volume otherwise. The load factors proposed in Table 3 allows the evaluation engineer to make decisions based on information on traffic condition. In Table 3, a nominal lane load is introduced for spans longer than the length of permit vehicle + 30 ft. It reflects load effects of vehicles in the front or to the rear of the permit vehicle. This lane load is chosen such that a relatively uniform safety index is reached over span lengths.

6.2 Load Factor for One-Trip Permits

This type of permit is usually issued to those overweight vehicles heavier than frequent permit vehicles. Therefore failure implications of this type of passage may likely be more severe. At the same time the economic benefits of an infrequent permit vehicle is much lower than for high volume permit traffic. Accordingly it is suggested that the target reliability index beta ß is raised to the range of 3.0 to 3.5 for this case. This target beta level is similar to that of new bridge designed by AASHTO specifications [6], since this type of permit may exceed any previous load on the bridge structure.

Table 4 presents the derived live load factor for this type of permit. It is noted that single lane distribution factor g_n should be used as the permit vehicle is checked in loading only one lane. This factor, for example, for a steel and prestressed concrete girder is equal to girder spacing (ft) / 7 according to AASHTO code [6]. This value contrasts with the multilane distribution factor, girder spacing (ft) / 5.5, to be used for

frequent permit case. The load effect due to possible presence of other vehicles is covered herein by the suggested load factor. It should also be noted that the traffic condition (weight control and traffic volume) has negligible effect on the live load factor for this case. This is because the frequency of the permit vehicle being checked is so low that normal traffic flow may unlikely be present alongside the permit vehicle. A lane load is also prescribed in Table 4 for this case. It is consistent with that for frequent permit.

6.3 Load Factor for Escorted Permits

Table 5 proposes a live load factor for this case, based on the target safety beta ß similar to that for one-trip permits. No lane load is required here. Single lane checking should be performed as for the case of one-trip permit. This load factor is lower than that for one-trip permit above, since some of the uncertainties are eliminated. The checking is no longer influenced by uncertain traffic condition as the normal traffic will be isolated when the permit vehicle crosses the bridge. The dynamic effect is reduced as speed control can be very effective. Additionally the path of vehicle across the structure may be made to reduce member load effect, for example, by straddling girders [16].

7. EXAMPLES AND IMPACT OF PROPOSED FORMAT

This section contains examples of permit checking using the proposed format. This format is compared with currently used method, namely, AASHTO operating strength by allowable stress method [2] (referred to as current AASHTO method thereafter). It is noted that more examples are examined in [16].

Bridge:
simple span of 60 ft, 2 lanes, 6 uniform steel girders with common spacings S of 8 ft.
Analysis:
i_n=1+50/(125+SpanLength)
=1+50/(125+60)=1.27(<1.30)
g_n=S/5.5
=1.45(for multiple lane checking)
g_n=S/7
=1.14 (for single lane checking)
Dead load effect (estimated here by assumption Eq.(7)):
M_d=403 (kips-ft) (due to wheel load of HS-20)
D_n=.0132*60*403*1.45*1.27=590(kips-ft)

Checking for frequent permit:

Permit vehicle:
gross weight of 115 kips and axle configuration shown in Fig.3.
Distribution factor:
g_n=S/5.5=1.45(multiple lane checking)
Live load effect:
maximum wheel load effect M_p by the permit vehicle = 495 (kips-ft) (by moving the permit vehicle over the bridge); no lane load is needed since 60 ft (span length) < 41 (vehicle length) + 30 = 71 ft.
L_p=495*1.45*1.27=912(kips-ft)

Table 6 displays the required strengths corresponding to traffic conditions by using load and resistance factors in Table 3. It also contains the checking result by current AASHTO method for comparison. The AASHTO result is comparably expressed by plastic moment capacity assumed 13 percent higher than elastic one. It can be seen in Table 6 that the proposed method requires lower strength and allows flexibility by taking traffic condition into account.

Checking for one-trip permit:

Permit vehicle:
gross weight of 230 kip-ft and axle configuration shown in Fig.3 (100% higher than the frequent permit vehicle above).
Distribution factor:
g_n=S/7=1.14(single lane checking)
Live load effect:
maximum wheel load effect M_p by the permit vehicle = 990 (kips-ft) (by moving the permit vehicle over the bridge); no lane load is needed due to the same reason as frequent permit case above
L_p=990*1.14*1.27=1433(kips-ft)

Table 7 contains the required strength by load and resistance factors of Table 4. It also gives the result by current AASHTO method for comparison. The AASHTO result is again comparably expressed by plastic moment capacity, and requires a higher strength of members.

Checking for escorted permit:

Permit vehicle:
gross weight of 299 kips and axle configuration shown in Fig.3 (30% heavier than the one-trip permit vehicle above).
Distribution factor:
g_n=S/7=1.14(single lane checking)
Live load effect:
maximum wheel load effect M_p by the permit vehicle = 1287 (kips-ft) (by moving the permit vehicle over the bridge); no lane load is needed due to the same reason as frequent permit case above
L_p=1287*1.14*1.27=1863(kips-ft)

Table 8 contains the required

strength by load and resistance factors of Table 5, compared with the result by current AASHTO method. The AASHTO result is again comparably expressed by plastic moment capacity, and shows a higher requirement.

A general comparison of the proposed format of prescribed load factors with current AASHTO method is made as follows. A rating factor (R.F.) is used here as the indicator:

$$R.F. = (0.95\ R_n - 1.2\ D_n)/\ \gamma_L L_p \qquad (8)$$

where R_n is the plastic moment capacity assumed 13 percent higher than elastic moment capacity. If the Operating Strength requirement has been satisfied, i.e.

$$R_n = 1.13\ (D_n + L_n)\ /\ 0.75 \qquad (9)$$

R.F. can be rewritten as follows by substituting Eq.(9) into Eq.(8)

$$R.F. = [1.43(1+r)-1.2]/\gamma_L\ r \qquad \text{(Frequent Permit)} \qquad (10)$$

where r is the ratio of live to dead load L_n/D_n. R.F. indicates the times of higher load effect a bridge can take than by current AASHTO method. It is shown in Table 9 given γ_L for traffic conditions and r in an exhaustively wide range. It is seen there that at least 19 percent higher strength can be used for permit checking using the proposed format. Tables 10 and 11 provide similar information for the cases of one-trip and escorted permit based on the following relations, respectively:

$$R.F. = [1.43(1+1.27r)-1.2]/(1.55\ r) \qquad \text{(One-Trip Permit)} \qquad (11)$$

$$R.F. = [1.43(1+1.27r)-1.2]/(1.45\ r) \qquad \text{(Escorted Permit)} \qquad (12)$$

The additional factor 1.27 for r in Eqs.(11) and (12) is due to the different distribution factors specified by the proposed method and current AASHTO method (ratio of S/5.5 to S/7). Tables 10 and 11 show that generally the proposed method allows higher permit loads (R.F. greater than 1.0), and respectively at least by 17 and 25 percent.

It has been shown that the proposed method requires generally lower strength or allows higher permit loads than current AASHTO method. It is attributed to the low frequency of permit load appearance, which is taken into account here.

8. SUMMARY AND CONCLUSIONS

Overload permit issuance has become routine practice in most states of the US. Current methods for permit checking are based on the higher operating stress in the allowable stress format. This method does not contrast normal traffic flow with relatively small number of permit loads. This paper presents a method of load and resistance factors for such permit checking. The load factors are derived against the criterion of structural reliability. Permit issuance for multiple trip, single trip and escorted trip are covered. Flexibility is permitted to use the live load factors to control the safety index for such cases as nonredundant structural types or permit vehicles of extraordinary important economic consequences. This checking method also allows consideration on site traffic conditions and overall truck weight enforcement. Examples using the proposed format are included for illustration and usually higher vehicle load is allowed by this method than current one using operating strength in allowable stress. The results are suitable for inclusion in AASHTO Manual for Maintenance Inspection of Bridges [2].

9. ACKNOWLEDGEMENTS

The Ohio Department of Transportation and Federal Highway Administration sponsored the study. The support of the New York Department of Transportation in cooperation with Federal Highway Administration is acknowledged. Dr.Y.liu of Case Western Reserve University assisted in part of the calculation. The comments of reviewers on the draft version of this paper are appreciated.

REFERENCES

[1] FHWA "Overweight Vehicles - Permits and Penalties: An Inventory of State Practices for Fiscal Year 1987" FHWA-MC-89-050, Jan. 1989

[2] AASHTO Manual for Maintenance Inspection of Bridges, Washington, D.C. 1983

[3] Cassano,R.C. and LeBeau,R.J. "Correlating Bridge Design Practice with Overload Permit Policy", Transportation Research Record 664, Sept.25-27, 1978, pp.230-238

[4] Bakht,B. and Jaeger,L.G. "A Rational Procedure for Overweight Permits", Transportation Research Record 950, Vol.I, 1984, pp.59-70

[5] Ghosn,M. and Moses,F. "Calibration of A Bridge Rating Formula for Overload Permits" ASCE Structures Congress'87, Aug.17-20, 1987, Bridges and Transmission Line

Structure, Proc. (Ed.) by L.Tall, pp.15-25
[6] AASHTO Standard Specifications for Highway Bridges, Washington, D.C. 13th Ed. 1983
[7] Moses,F. and Verma,D. "Load Capacity Evaluation of Existing Bridges, Phase II", Civil Engineering Department, Case Western Reserve University, Cleveland, OH, Draft Final Report to NCHRP, July 1989
[8] Ang,A.H-S. and Tang,W.H. Probability Concepts in Engineering Planning and Design, Vol.1 and Vol.2, New York: John Wiley & Sons, 1984
[9] Moses,F. and Ghosn,M, "A Comprehensive Study of Bridge Loads and Reliability", Civil Engineering Department, Case Western Reserve University, FHWA/OH-85/005, Final Report to Ohio Department of Transportation, Jan. 1985
[10] Moses,F. and Verma,D. "Load Capacity Evaluation of Existing Bridges" NCHRP Report 301, Washington, D.C., Dec. 1987
[11] Nowak,A.S. and Zhou,J. "Reliability Models for Bridge Analysis", Dept. of Civil Engineering, University of Michigan, Ann Arbor, March 1985
[12] Hansell,W.C. and Viest,I.M. "Load Factor Design for Steel Highway Bridges" AISC Engineering Journal, Vol.8, No.4, Oct. 1971, pp.113-123
[13] AASHTO Guide Specifications for Strength Evaluation of Existing Steel and Concrete Bridges, Washington, D.C., 1989
[14] Verma,D. and Moses,F. "Calibration of Bridge-Strength Evaluation Code", ASCE Journal of Structural Engineering, Vol.115, No.6, June 1989, pp.1538-1554
[15] Ghosn,M. and Moses,F. "Reliability Calibration of Bridge Code" ASCE Journal of Structural Engineering, Vol.112, No.4, April 1986
[16] Moses,F., Fu,G. and Liu,Y. "A Reliability Analysis of Permit Loads on Bridges", Draft Final Report to ODOT, Case Western Reserve University, Cleveland, OH, Sept. 1990

Fig. 1a. TYPICAL COMBINATION VEHICLE WEIGHT HISTOGRAM (AT UNENFORCED SITES) WITH PERMIT TAIL

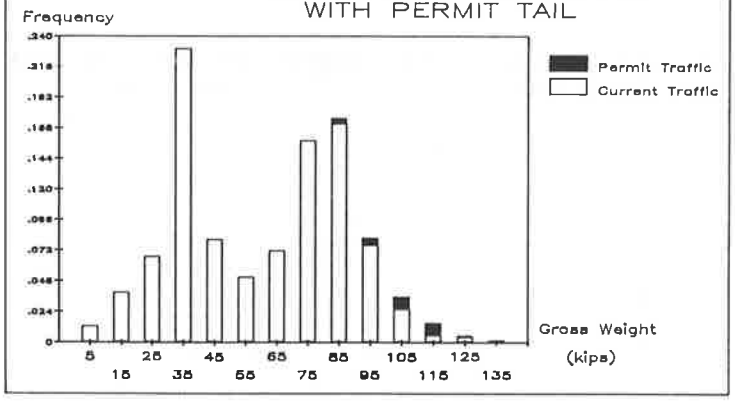

Fig. 1b. TYPICAL COMBINATION VEHICLE WEIGHT HISTOGRAM (AT ENFORCED SITES) WITH PERMIT TAIL

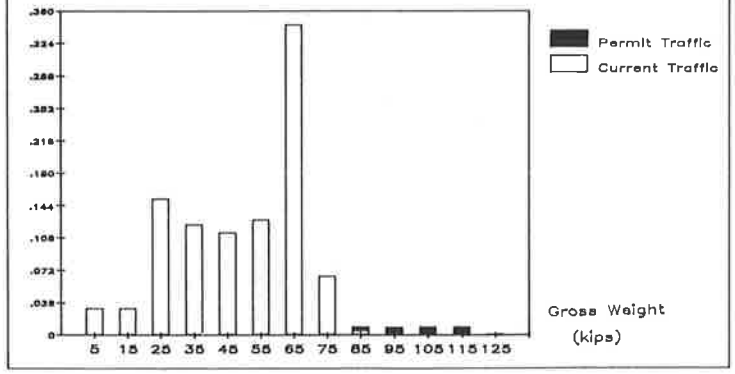

Fig. 2. VEHICLE LOCATIONS ON A BRIDGE

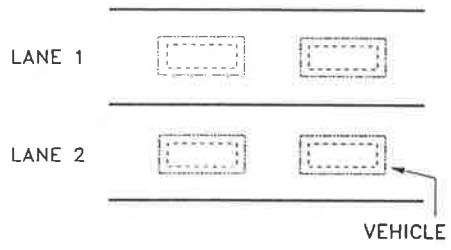

Fig.3 Example Permit Vehicles

Gross Weight = 115 kips (Frequent Permit)

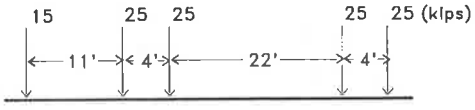

Gross Weight = 230 kips (One-trip Permit)

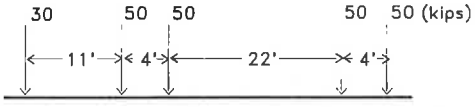

Gross Weight = 299 kips (Escorted Permit)

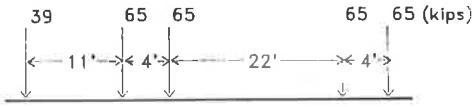

Table 1. Mean(kips-ft) and COV(%) of Maximum Moment M - Simple Spans

Span(ft)	30	60	90	120	150	180	210
Enforced Light-Traffic	641 6.2%	1758 5.4%	3307 5.1%	4890 5.4%	6499 5.6%	8244 6.7%	10085 7.9%
Enforced Heavy-Traffic	681 5.0%	1849 4.2%	3481 4.2%	5155 4.2%	6859 4.4%	8735 5.4%	10719 6.7%
Unenforced Light-Traffic	699 6.8%	1904 6.5%	3569 7.1%	5269 6.9%	6967 7.2%	8728 7.4%	10533 7.9%
Unenforced Heavy-Traffic	743 4.8%	2023 5.2%	3800 5.6%	5595 5.6%	7407 5.8%	9281 6.1%	11216 6.4%

Table 2. Mean(kips-ft) and COV(%) of Additional Maximum Moment due to Alongside Trucks (Permit Truck Effect Excluded) - Simple Spans

Span(ft)	30	60	90	120	150	180	210
Enforced	131 46.6%	358 46.9%	668 48.7%	979 49.1%	1290 49.6%	1600 49.7%	1911 49.9%
Unenforced	170 49.5%	463 49.4%	864 50.9%	1266 51.5%	1667 51.8%	2069 52.1%	2471 52.2%

Table 3. Proposed Live Load Factor γ_L for Frequent Permits
(with $\phi = 0.95$ and $\gamma_D = 1.20$ for Eq.(1))
To Be Used with Multilane Distribution Factor g_n

	Heavy Traffic	Light Traffic
Weight Control Enforced	1.15	1.10
Weight Control Unenforced	1.20	1.15

Load Effect L_n = permit vehicle load effect + lane load effect
lane load effect =
0, for span length < permit vehicle length + 30 ft
200 lb/ft, for span length > permit vehicle length + 30 ft
over as many spans as required produce maximum effect

Table 4. Proposed Live Load Factor γ_L for One-Trip Permits
(with $\phi = 0.95$ and $\gamma_D = 1.20$ for Eq.(1))
To Be Used with Single Lane Distribution Factor g_n

$\gamma_L = 1.55$
Load Effect L_p = permit vehicle load effect + lane load effect lane load effect = 0, for span length < permit vehicle length + 30 ft 200 lb/ft, for span length > permit vehicle length + 30 ft over as many spans as required produce maximum effect

Table 5. Proposed Live Load Factor γ_L for Escorted Permits
(with $\phi = 0.95$ and $\gamma_D = 1.20$ for Eq.(1))
To Be Used with Single Lane Distribution Factor g_n

$\gamma_L = 1.45$
Load Effect L_p = permit vehicle load effect

Table 6. Required Resistance (kips-ft) for Frequent Permit Issuance (Example)

by Proposed Method (Using Table 3) $0.95\ R_n = 1.2\ D_n + \gamma_L\ L_p$ (Plastic Moment $F_yZ=R_n$)			by AASHTO Operating Strength of Allowable Stress $0.75\ R_n = D_n + L_p$ (Plastic Moment $F_yZ=1.13*R_n$)
Enforced-Light	(γ_L=1.10)	1801	
Enforced-Heavy	(γ_L=1.15)	1849	1.13*2003=2263
Unenforced-Light	(γ_L=1.15)	1849	
Unenforced-Heavy	(γ_L=1.20)	1897	

Table 7. Required Resistance (kips-ft) for One-Trip Permit Issuance (Example)

by Proposed Method (Using Table 4) $0.95\ R_n = 1.2\ D_n + 1.55\ L_p$ (Single Lane $g_n = S/7$) (Plastic Moment $F_yZ=R_n$)	by AASHTO Operating Strength of Allowable Stress $0.75\ R_n = D_n + L_p$ (Multiple Lane $g_n = S/5.5$) (Plastic Moment $F_yZ=1.13*R_n$)
3083	1.13*3217=3635

Table 8. Required Resistance (kips-ft) for Escorted Permit Issuance

by Proposed Method (Using Table 5) $0.95\ R_n = 1.2\ D_n + 1.45\ L_p$ (Single Lane $g_n = S/7$) (Plastic Moment $F_yZ=R_n$)	by AASHTO Operating Strength of Allowable Stress $0.75\ R_n = D_n + L_n$ (Multiple Lane $g_n = S/5.5$) (Plastic Moment $F_yZ=1.13*R_n$)
3589	1.13*3941=4460

Table 9. Impact of Proposed Method on Frequent Permit Checking
(R.F. by the proposed method if the strength satisfies Operating Strength)

$r = L_p/D_n$	0.50	0.75	1.00	1.50	2.00	5.00	10.0	100	∞
	R.F. by the proposed method								
Enforced-Light (γ_L=1.10)	1.72	1.58	1.51	1.44	1.40	1.34	1.32	1.30	1.30
Enforced-Heavy (γ_L=1.15) and Unenforced-Light	1.64	1.51	1.44	1.38	1.34	1.28	1.26	1.26	1.24
Unenforced-Heavy(γ_L=1.20)	1.58	1.45	1.38	1.32	1.29	1.23	1.21	1.19	1.19

Table 10. Impact of Proposed Method on One-Trip Permit Checking
(R.F. by the proposed method if the strength satisfies Operating Strength)

$r = L_p/D_n$	0.50	0.75	1.00	1.50	2.00	5.00	10.0	100	∞
R.F.(γ_L=1.55)	1.47	1.37	1.32	1.27	1.25	1.20	1.19	1.18	1.17

Table 11. Impact of Proposed Method on Escorted Permit Checking
(R.F. by the proposed method if the strength satisfies Operating Strength)

$r = L_p/D_n$	0.50	0.75	1.00	1.50	2.00	5.00	10.0	100	∞
R.F.(γ_L=1.45)	1.57	1.46	1.41	1.36	1.33	1.28	1.27	1.25	1.25